Preparation of Initiators for Sustainable Polymerisation

Hancock, Stuart

Award date:
2013

Awarding institution:
University of Bath

Preparation of Initiators for Sustainable Polymerisation

Stuart Lee Hancock

A thesis submitted for the degree Doctor of Philosophy

Department of Chemistry

University of Bath

April 2013

COPYRIGHT

Restrictions

This thesis may be made available for consultation within the University library and may be photocopied or lent to other libraries for the purposes of consultation

Signed .....

Date .....

A. Contents

B. Acknowledgements

First and foremost I would like to thank Dr. Matthew Jones for his supervision and support which was fundamental in making my PhD an enjoyable experience. The opportunity to study for a PhD under his tuition was greatly appreciated.

Financial support given by the University of Bath and the EPSRC which enabled me to conduct my PhD was gratefully received.

I appreciated the assistance given by Dr. Mary Mahon and Dr. Gabriele Kociok-Köhn for their help in X-ray diffraction studies. Dr. John Lowe is acknowledged for his assistance in NMR spectroscopy and accommodating my time requirements with the spectrometers. Dr. Anneke Lubben is thanked for her help with mass spectrometry. Dr. Edit Tshuva and fellow collaborators are gratefully acknowledged for their work on stability and cytotoxicity. The collaborative work with Conrad Langridge is acknowledged for his contribution to the work conducted in chapter 4.

I wish to thank the Jones and Davidson group members, past and present. In particular I would like to thank Dr. Emma Whitelaw for passing on much of her knowledge. Special thanks goes to; Dr. Carlo Di Iulio, Rhodri Owen and Dr. Marek Lewandowski for being my office compatriots and sharing of treats. My past office companions are not forgotten I enjoyed my time with all of you. I would like to thank Tom Forder and Ben Jeffery for their fantastic chemistry discussions, which kept my desire to pursue chemistry alive. I wish to express special gratitude to Chris Ready, always by my side through continual lab and office migrations. You will all be sorely missed.

I must express my gratitude for the support of my family and friends outside of academia who have always been there for many years despite each going there own way. Finally, and importantly, thanks goes to Gemma Kilburn for sticking with me for twelve years. Without you this wouldn’t have been possible as whatever troubles I encountered however small or large you would still be there as my little constant.

C. Abstract

Current plastics are mostly derived from petrochemical sources, as it is a finite resource renewable replacements are sought after. Polymers derived from cyclic esters such as; lactide, valerolactone and caprolactone are of interest. An industrially viable method of producing stereocontrolled polylactide (PLA) from *rac*-lactide is desired. Previous work on poly(cyclic esters) is overviewed in chapter 1 with an emphasis upon PLA.

Chapter 2 reports the coordination of $Ti(O^iPr)_4$ to homo/piperazine bridged bis(phenol) (salan) ligands. Under ambient conditions bimetallic structures were produced and a steric dependent equilibrium system is discussed. Forcing conditions resulted in monometallic homopiperazine salan complexes. Their application for the ring-opening-polymerisation (ROP) of *rac*-lactide is investigated. Homo/piperazine salan titanium catecholates were synthesised and their cytotoxicity investigated by collaborators.

Chapter 3 details the synthesis of monometallic homopiperazine salan zirconium/hafnium isopropoxide complexes. Their utility for the ROP of *rac*-lactide in solution and solvent free systems are discussed. Bimetallic or tetrametallic solid state structures from attempts to coordinate Zr(IV)/Hf(IV) metals to piperazine salan ligands are also discussed.

Chapter 4 discusses the complexation of $AlMe_3$ with homopiperazine salan ligands. The resulting monometallic complexes were inactive for the ROP of lactide. Benzyl alcohol derivatives were synthesised and trialled for solvent free ROP of *rac*-lactide, δ-valerolactone, ε-caprolactone. Co-polymerisations were investigated and a tri-block polymer of poly(ε-caprolactone/δ-valerolactone/*rac*-lactide) was prepared.

Chapter 5, *trans*-1,4-DACH salen ligands were synthesised and investigated as ligands with Al(III), Ti(IV), Zr(IV), and Zn(II) metal centres. Bimetallic Al(III) and Ti(IV) structures were characterised and trialled for the ROP of *rac*-lactide. Isotactic PLA was reported for aluminium complexes, dependent upon phenoxy substituents, and these polymerisations were shown to be immortal in nature.

Chapter 6 details the synthesis of *trans*-1,2-DACH salalen ligands which were complexed to $AlMe_3$, these initiators were investigated for the solution ROP of *rac*-lactide. The further synthesis of benzyloxy derivatives is also reported and they were utilised for solution and solvent free polymerisations of *rac*-lactide. The initiator's behaviour is discussed with respect to varying amine and imine groups.

D. Abbreviations

BDI	β-Diketiminate
CHN	Carbon, Hydrogen, and Nitrogen
C_p	Cyclopentadienyl
DACH	Diaminocyclohexane
DOSY	Diffusion-Ordered Spectroscopy
EDBP	2,2'-Ethylidenebis(4,6-di-*tert*-butylphenol)
ESI	Electrospray ionisation
GPC	Gel permeation chromatography
IC_{50}	Half maximal inhibitory concentration
IR	Infrared
k_{app}	Apparent rate constant
k_{int}	Rate constant of initiation
$k_{intra.trans}$	Rate constant of intramolecular-transesterification
$k_{inter.trans}$	Rate constant of intermolecular-transesterification
k_{prop}	Rate constant of propagation
MALDI	Matrix-assisted laser desorption/ionization
M_n	Number average molecular weight
M_w	Weight average molecular weight
NMR	Nuclear magnetic resonance
PDI	Polydispersity index
PGA	Poly(glycolide)
PLGA	Poly(lactide-co-glycolide)
PLA	Poly(lactide)
P_m	Probability of isotactic enchainment
P_r	Probability of racemic enchainment
ROP	Ring-Opening-Polymerisation
RT	Room temperature
$t_{½}$	Half life
THF	Tetrahydrofuran
ToF	Time of Flight
UV	Ultraviolet
VT	Variable tempreture

E. Publications

Dalton Transactions

Cite this: *Dalton Trans.*, 2011, **40**, 2033

www.rsc.org/dalton

PAPER

Crystallographic characterisation of Ti(IV) piperazine complexes and their exploitation for the ring opening polymerisation of *rac*-lactide

Stuart L. Hancock, Mary F. Mahon and Matthew D. Jones*

Received 5th November 2010, Accepted 21st December 2010
DOI: 10.1039/c0dt01542c

In this paper a series of eight Ti(IV) piperazine based complexes have been prepared and fully characterised in the solid-state by X-ray crystallography and in solution *via* NMR spectroscopy. In the solid-state either $Ti_2(\mathbf{L})(O^iPr)_6$ or $Ti_2(\mathbf{L})_2(O^iPr)_4$ were observed depending upon the nature of the starting ligand. For complexes with less sterically demanding ligands ($\mathbf{1H_2}$ and $\mathbf{2H_2}$) an equilibrium was observed: $2\ Ti_2(\mathbf{L})(O^iPr)_6 \Leftrightarrow Ti_2(\mathbf{L})_2(O^iPr)_4 + 2\ Ti(O^iPr)_4$. The thermodynamic properties (ΔG, ΔH and ΔS) have been investigated *via* variable temperature NMR spectroscopy. With more sterically demanding ligands ($\mathbf{3–8H_2}$) the $Ti_2(\mathbf{L})(O^iPr)_6$ form was the most prevalent in the solid-state and in solution. These complexes have been tested for the production of polylactide under melt and solution conditions with high conversions being obtained.

Introduction

The preparation of homogeneous Lewis acidic complexes for the ring opening polymerisation (ROP) of cyclic esters (such as *rac*-lactide) has received considerable attention in recent years.[1] Examples of initiators for this process include groups 1–3,[2] Al(III),[3] In(III),[4] Zn(II),[2b,5] lanthanides[6] and pertinent to this study group 4 metal centres.[7] The polymers themselves have found many uses from commodity plastics to high value biomedical applications.[8] The use of amine bis(phenolate) ligands in such chemistry is ubiquitous and there are numerous examples of such initiators in the literature.[8c,7a,7d–7f] However, the use of the more conformationally strained piperazine derived ligands for this polymerisation remains limited. A notable example of work in this area is that by Yao and co-workers who have recently prepared a Yb–Li bimetallic piperazidine complex.[9] This was shown to act as a promising initiator for the ROP of L-lactide. The same group have also very recently prepared lanthanide complexes for L- and *rac*-lactide polymerisation based on piperazine ligands.[10] It has been found that *N*-substituted piperazine complexes are very versatile and can bind to either one or two metal centres.[9] Previous crystallographically characterised piperazine-phenolate complexes include Al(III),[11] Pd(II),[12] Zn(II)[13] and Cu(II).[14] For example, a series of Al(III) complexes with 1,4-bis(2-hydroxy-3,5-di-*tert*-butyl)piperazine have been prepared and in this case either monometallic or bimetallic complexes were formed in the solid-state.[11] With the same ligand Zn(II) bimetallic structures have been prepared.[13] To the best of our knowledge there are no reported examples of crystallographically characterised piperazine-phenolate complexes with Ti(IV), although the analogous 1,4-bis(2-aminobenzyl)piperazine ligand has been used by Mountford to prepare Ti(IV) imido complexes.[15] Also to the best of our knowledge there are no crystallographically characterised complexes of the methyl substituted piperazine ring systems. Crystallographically characterised complexes with the homopiperazine ligand (7 membered ring) remain limited to Fe(III),[16] Cu(II),[17] Ni(II)[17] and one example of a Ti(IV) oxo complex has been previously published.[18]

In this paper we report the preparation and characterisation of new piperazine and homopiperazine ligands. These ligands were complexed to Ti(IV) and either complexes of the form $Ti_2(\mathbf{L})(O^iPr)_6$ or $Ti_2(\mathbf{L})_2(O^iPr)_4$ have been isolated in the solid-state. Interestingly, in some cases a complex equilibrium was observed in solution between these two dimers and $Ti(O^iPr)_4$. The complexes have been tested for the ROP of *rac*-lactide with high conversions.

Results and discussion

Synthesis of ligands and complexes

The ligands were prepared *via* a modified Mannich reaction as shown in Scheme 1.[11] All ligands were characterised *via* ^1H and $^{13}C\{^1H\}$ NMR spectroscopy and HR-MS, $\mathbf{1H_2}$ was also characterised using single crystal X-ray diffraction. The complexes were prepared by the reaction of 1 equivalent of ligand with 2 equivalents of $Ti(O^iPr)_4$ in CH_2Cl_2.[7a,7d,7e] It was observed that the same products were also isolated in the solid-state with 1 equivalent of $Ti(O^iPr)_4$. For complexes with ligands $\mathbf{1H_2}$ and $\mathbf{2H_2}$ the solid-state structures are shown in Fig. 1 and selected bond lengths and angles are in Table 1.

Department of Chemistry, University of Bath, Claverton Down, Bath, BA2 7AY, U.K. E-mail: mj205@bath.ac.uk; Fax: +44 (0)1225 386231; Tel: +44 (0)1225 384908

† Electronic supplementary information (ESI) available: Full characterisation data and selected NMR data. CCDC reference numbers 800217–800225. For ESI and crystallographic data in CIF or other electronic format see DOI: 10.1039/c0dt01542c

DOI: 10.1002/ejic.201100589

Homopiperazine and Piperazine Complexes of Zr^{IV} and Hf^{IV} and Their Application to the Ring-Opening Polymerisation of Lactide

Stuart L. Hancock,[a] Mary F. Mahon,[a] Gabriele Kociok-Köhn,[a] and Matthew D. Jones*[a]

Keywords: Titanium / Zirconium / Hafnium / Ring-opening polymerization / Sustainable chemistry

In this paper we describe the preparation and characterisation, by single-crystal X-ray diffraction, of twelve Zr^{IV}/Hf^{IV} complexes based on piperazine or homopiperazine salan ligands. With the piperazine ligands, a mixture of species was observed and various solid-state structures were isolated. However, with homopiperazine salan ligands, 1:1 ligand-to-metal complexes were observed both in solution and in the solid state. Interestingly, for the homopiperazine complexes the isopropoxide ligands are *trans* to one another in the solid state, most likely because of the rigid nature of the homopiperazine backbone. All homopiperazine Hf^{IV} and Zr^{IV} complexes were tested for the ring-opening polymerisation (ROP) of *rac*-lactide. The complexes are active and produce polylactide with narrow polydispersity indices. The kinetics and living characteristics of the polymerisation have also been investigated.

Introduction

In recent years there has been an explosion of interest in the use of single-site homogeneous catalysts for the ring-opening polymerisation (ROP) of *rac*-lactide (*rac*-LA) to produce polylactide (PLA).[1] This process has been commercialised by Purac and NatureWorks, and the current catalyst used for this process is based on Sn^{II}.[2] There is currently a desire to replace tin in this system, and – as a consequence – a significant amount of work has been performed in catalyst development.[1] The polymers themselves have found extensive utility from biomedical to commodity polymer applications,[3] due to the biodegradability and biocompatibility of PLA and the fact that the monomer can be sourced from sustainable raw materials. The catalyst can have a dramatic effect on the physical properties and degradation rates of the resultant PLA.[4] For example, catalysts based on groups 1–3,[5] lanthanides,[6] Zn^{II},[1a,1b,1g] Al^{III},[7] In^{III}[8] and, pertinent to this study, group 4 metals have all been shown to have significant activity.[9] We have recently shown that Ti^{IV} salan systems with a piperazine backbone are very effective catalysts for the bulk polymerisation of *rac*-LA.[10] Kol has shown that a Zr^{IV} complex of a tetradentate phenylenediamine bis(phenolate) affords heterotactic PLA under melt conditions.[11] The same group has also shown that dithiodiolate complexes with Zr^{IV} are active for the production of hetereotactic PLA.[9h] It has been shown that dinuclear Zr^{IV} and Hf^{IV} complexes of Jacobsen's ligand are active for the controlled ROP of both *rac*-LA and β-butyrolactone.[9a] In the case of *rac*-LA, atactic PLA was formed. It has also been shown that bis(imino)phenoxide complexes of Zr^{IV} show high activities in the polymerisation.[9g]

The chemistry of group 4 metal complexes with symmetrical amine–bis(phenolate) ligands is rich and diverse, and many ligand–metal complexes are known with possible geometries shown in Scheme 1.[12] The use of bis(phenolate) ligands based on 2,2′-bipyrrolidine, *N*,*N*′-dimethyl-1,2-diaminobenzene, *N*,*N*′-dimethyl-1,2-ethylenediamine and *N*,*N*′-dimethylcyclohexane-1,2-diamine backbones forms the α-cis isomer both in the solid state and solution once reacted with $Zr(OtBu)_4$.[13] Interestingly, a search of the Cambridge Structural Database (CSD) indicates that there are no crystallographically characterised complexes of the *trans* isomer of group 4 metal complexes with amine bis(phenolate) ligands, where X = alkoxide, with the α-*cis* and β-*cis* forms being prevalent.[14] Intriguingly, Budzelaar has shown, using computational methods, that the *trans* geometry (*mer*–*mer*, where the ligand occupies the equatorial position) is the intermediate ion pair in olefin polymerisation.[15] The use of homopiperazine as a backbone for bis(phenolate) ligands remains limited with the only examples characterised in the solid state involving copper, nickel and iron.[16]

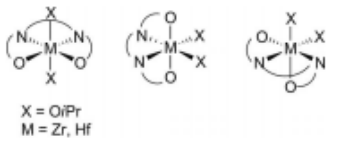

Scheme 1. Possible isomers of ONNO ligands with Zr^{IV} or Hf^{IV}.

[a] Department of Chemistry, University of Bath,
Claverton Down, Bath BA2 7AY, United Kingdom
Fax: +44-01225-386231
E-mail: mj205@bath.ac.uk

Supporting information for this article is available on the WWW under http://dx.doi.org/10.1002/ejic.201100589.

NJC

Cite this: *New J. Chem.*, 2012, **36**, 1891–1896

www.rsc.org/njc

PAPER

Al(III)–homopiperazine complexes and their exploitation for the production of polyesters†

Stuart L. Hancock, Matthew D. Jones,* Conrad J. Langridge and Mary F. Mahon

Received (in Montpellier, France) 20th April 2012, Accepted 19th June 2012
DOI: 10.1039/c2nj40300e

In this paper we report the synthesis and characterisation of a series of Al(III)–homopiperazine complexes. The *ortho* substituent has been varied from H, Me, *t*Bu to investigate the effect this has on the solid-state structures and on the catalytic activity. Aluminium–methyl complexes involving ligands $\mathbf{1H_2}$, $\mathbf{3H_2}$ and $\mathbf{5H_2}$ have been characterised in the solid-state and the aluminium centres are in pseudo trigonal bipyramidal geometries. The aluminium–methyl complexes were further reacted with benzyl alcohol to generate alkoxide complexes, which have been fully characterised by multinuclear NMR spectroscopy and elemental analysis. The alkoxide complexes were tested in the ring opening polymerisation of *rac*-lactide, δ-valerolactone and ε-caprolactone. Furthermore, triblock polyesters were also prepared with these initiators.

Introduction

Ring opening polymerisation (ROP) of lactide to produce polylactide (PLA) has received a remarkable degree of attention in recent years.[1] This is due to the biocompatibility of the final polymer and the fact that the starting lactide can be prepared from sustainable sources.[1b,d,2] This is truly making PLA a viable alternative to crude oil based polymers for commodity applications. Furthermore, PLA and its copolymers are currently being exploited for high value biomedical applications.[3] Initiators for ROP based on Al(III),[4] Zn(II),[5] lanthanides,[6] group 4 metals[7] and group 2 metals[5g,8] are prevalent in the literature. One of the most studied monomers is *rac*-lactide (a 50 : 50 mixture of the D- and L-enantiomers), this is due to the fact that different (stereoblock isotactic, heterotactic and atactic) stereo-forms of PLA can be prepared. The physical properties of the final polymer are directly related to its microstructure.[1b,2a] However, the properties of the polymer can also be varied by the copolymerisation of lactide with other monomers – such as ε-caprolactone or δ-valerolactone.[7c,9] One of the main driving forces of this approach is to produce polymers which have desirable gas/drug permeability and mechanical strength properties.[1b]

A significant number of aluminium complexes that are active for the ROP of *rac*-LA or other cyclic esters are based on either salan or salen ligands.[4c,10] One such class of salan ligands are those utilising a piperazine or homopiperazine backbone. For example, Fulton and Wang have shown that bimetallic Al(III) complexes of piperazine derived phenolates show activity for the polymerisation of ε-caprolactone.[10] Furthermore, we have previously shown that amine bis(phenolate) ligands based on homopiperazine ligands complexed to group 4 metals are active initiators for the controlled ROP of *rac*-lactide.[7b,11]

In the vast majority of aluminium examples an alkoxide initiator is generated *in situ* from the aluminium-alkyl and thus the resultant polymerisation is performed in solution.[3c,4c] However, this has a significant disadvantage in the fact that the polymerisation cannot be performed under the industrially preferred melt conditions. Therefore, in this study we have chosen to prepare a series of aluminium–homopiperazine alkoxide complexes for the application in ROP with a variety of monomers for melt polymerisation studies.

Results and discussion

Synthesis of complexes

The ligands were prepared by modified Mannich reactions and complexes were prepared *via* standard literature procedures, Scheme 1.[7b,11,12] The choice of *ortho* substituent allows us to probe the effect of steric influence on catalysis and solid-state structure. All ligands were characterised *via* multi-nuclear NMR spectroscopy and HR-MS.

The Al-methyl complexes were prepared by addition of 1 equivalent of $AlMe_3$ to 1 equivalent of ligand and it was noted that products of higher purity were isolated when the reactions were conducted at 80 °C. Complexes Al(**1**,**3**,**5**)Me were characterised by single crystal diffraction studies, see Fig. 1 for Al(**3**)Me and Table 1 for selected bond distances and angles. The aluminium centres are in a highly disordered trigonal bipyramidal geometry. For complex Al(**1**)Me a significant degree of disorder was observed in the homopiperazine ring moiety. For complexes Al(**3**)Me and Al(**5**)Me the methyl group bound to the

Department of Chemistry, University of Bath, Claverton Down, Bath BA2 7AY, UK. E-mail: mj205@bath.ac.uk; Fax: +44 (0)1225 386231; Tel: +44 (0)1225 384908

† CCDC reference numbers 877942–877944. For crystallographic data in CIF or other electronic format see DOI: 10.1039/c2nj40300e

Dalton Transactions

RSC Publishing

PAPER

View Article Online
View Journal

Aluminium salalen complexes based on 1,2-diaminocyclohexane and their exploitation for the polymerisation of *rac*-lactide†

Cite this: DOI: 10.1039/c3dt00021d

Stuart L. Hancock, Mary F. Mahon and Matthew D. Jones*

Received 3rd January 2013,
Accepted 14th March 2013

DOI: 10.1039/c3dt00021d

www.rsc.org/dalton

In this paper nine various salalen ligands have been prepared and characterised. The steric and electronic effects of both the salen and salan fragments have been varied in a systematic fashion to ascertain how this affects the selectivity for the ROP of *rac*-lactide. These were complexed to $AlMe_3$ to generate pseudo trigonal bypyramidal metal centred complexes. Upon addition of benzyl alcohol the active initiator can be easily prepared. The complexes were screened for the ROP of *rac*-lactide in solution and melt conditions. PLA with narrow molecular weight distributions (PDIs range from 1.07–1.67) could be isolated with moderate degrees of tacticity. Significantly it was found that chloro groups on the imine fragment increased the degree of heterotactic enchainment in the polymer. The kinetics for one series of salalen–Al complexes was also investigated.

Introduction

In recent years the metal catalysed polymerisation of lactide to produce polylactide (PLA) has been a "hot-topic" and will continue to be so for more years to come.[1] This is due to the favourable properties of the polymer; namely biodegradability and the fact that it can be sourced from renewable materials. Lactide can be prepared from lactic acid which in-turn is produced from fermentation of starch.[2] PLA has found utility in markets such as high value medical devices to more traditional commodity based applications.[3] Furthermore, if the racemic version of the monomer is used (*rac*-lactide or *rac*-LA) then various stereoforms of PLA can be prepared (heterotactic, atactic and stereoblock isotactic).[4] Many metal centres have been employed in the production of PLA – for example groups 1–4,[5] lanthanides,[6] Zn(II)[7] and Sn(II).[8] One of the main Lewis acid metals centres that is suitable for this polymerisation is Al(III). Pioneering work by Feijen,[9] Chisholm,[10] Nomura,[11] Spassly,[12] Coates[13] and Gibson[14] (amongst others) have shown that initiators based on Al(III) can produce controlled molecular weight PLA and are capable of inducing stereoselectivity into the final polymer.[14] Without question the two main ligands bound to the aluminium centres are based on salan or salen moieties.[9–14] These are typically symmetrical in nature, due to their preparation.

Recently, Katsuki and co-workers have prepared a series of salalen complexes for the enantioselective hydrophosphonylation of aldehydes and aldimines; and sulphur oxidations.[15] High enantioselectivities and conversions have been reported. An advantage of such systems is there is a high degree of synthetic variation possible in terms of the sterics/electronics of either phenyl ring. Kol and co-workers have recently shown that Ti(IV) salalen complexes are active for the isospecific polymerisation of 1-hexene and propylene.[16] We have previously reported the utility of group 4 salalen complexes for the polymerisation of *rac*-lactide.[17] Furthermore, we have recently shown that Al(III)–salalen complexes can produce either isotactic or heterotactic PLA depending on the nature of the substituent on the amine nitrogen centre.[18] One of the foremost Al(III) complexes prepared to date was based on Jabobsen's ligand[19] {(*R*,*R*)-(−)-*N*,*N*′-bis(3,5-di-*tert*-butylsalicylidene)-1,2-diaminocyclohexane} with highly isotactic PLA being produced.[9] In this paper we have prepared a range of salalen ligands based on the 1,2-diaminocyclohexane backbone. These have been complexed to Al(III) and tested for the ring opening polymerisation of *rac*-lactide in solution and under the industrially preferred melt conditions.

Results and discussion

Ligand and complex preparation

The ligands were prepared by modified literature procedures, as shown in Scheme 1.[15d] The *trans* form (*R*,*R* or *S*,*S*) of 1,2-diaminocyclohexane was initially mono-protected and treated with an equivalent of an aldehyde and subsequent reduction

Department of Chemistry, University of Bath, Claverton Down, Bath BA2 7AY, UK. E-mail: mj205@bath.ac.uk; Fax: +44 (0) 1225 386231; Tel: +44 (0) 1225 384908

† Electronic supplementary information (ESI) available: Full experimental details and the crystal data in the .cif format. CCDC 917781–917783. For ESI and crystallographic data in CIF or other electronic format see DOI: 10.1039/c3dt00021d

Chapter 1

1. Introduction

1. Introduction

1.1 Biopolymers

Over the last century interest in plastics has developed considerably with much focus on synthetic polyolefins derived from petrochemicals.[1] Although polyolefins have been very successful, they do have considerable drawbacks. Petrochemical derived plastics are associated with many environmental concerns, one such current issue is that petrochemical sources are being depleted and our present use of fossil fuels for plastic production is not sustainable.[2] Furthermore, petrochemical plastics are becoming a major pollutant, polyolefin plastics are not readily decomposed and when considered with our common use of disposable plastics there is an inevitable disposal problem. In recent years replacement plastic sources are becoming commercially more viable due to the rising cost of oil and public environmental concern. As a consequence of these concerns much research has been focused in the last few decades on developing biodegradable and sustainable plastics to replace petrochemical derived materials.[3, 4]

Biopolymers are polymers obtained from renewable resources which have acquired interest as replacements for petrochemical polymers, particularly within plastics. It should be noted not all biopolymers are biodegradable.[5] A variety of biopolymers have been developed over the last few decades one such example is cellulose derived polymers.[6] Cellulose is a major constituent of all plants therefore it is the most common naturally produced polymer, which is currently obtained from; wood pulp, algae and cotton.[6] Although cellulose is mass produced by nature it is difficult to extract and obtain in a form which can be easily manipulated. A critical element of cellulose research is controlling the structure and hence the properties, such examples are the ester and ether derivatives of cellulose particularly cellulose acetates used for polymer coatings.[6] Aliphatic polyesters such as polylactide (PLA) and polyglycolide (PGA) have received attention over the last few decades as suitable replacements for petrochemical polymers. Particular advantages of aliphatic polyesters include; suitable mechanical characteristics, renewable feedstocks, biodegradable, and biocompatible.[2]

Degradability is another important aspect of plastic production; there are two common methods of engineering degradable polymers, introducing degradable substituents into the polymer chain or creating the polymer from inherently degradable monomers.[7] Biodegradable monomer units can be introduced into petrochemical polymers to increase their degradability. As an example, hydrolytic degradation of poly(ethylene terephthalate) was increased by incorporation of lactide units.[8] Introduction of metal substituents into polymers propagate its degradation to smaller polymer chains, these polymers are classified as oxo-degradable. Such oxo-degradable polymers breakdown on exposure to U.V. light and oxygen, this method only break-down polymers into shorter chain oligomers at which point biological processes may decompose the shorter chains.[9-11] As stated oxo-degradation only reduces the polymers to shorter chains which still present an environmental issue. Additionally the metals incorporated in the polymer enhance the environmental issues as toxicology and metal leaching must be considered. Arguably more sought after are fully biodegradable polymers where the individual monomeric units of the polymer chain can decompose to water and carbon dioxide. Biodegradation of polymers often requires specific conditions such as; elevated heat, oxygen, and light, which are obtained in a composting facility.[12]

As stated above polylactide and polyglycolide are biodegradable, renewable and characteristically suitable replacements, within certain applications, for petrochemical derived polymers. Polylactide and polyglycolide are derived from the base components lactic acid and glycolic acid respectively. Although the direct production of PLA and PGA by polycondensation from lactic acid and glycolic acid results in polymers of low molecular weight.[2] As control over the aspects of the polymer is paramount within industry the dehydrated lactide and glycolide products are utilised to produce their respective polymers (Figure 1.01), consequently the dehydrated dimers have seen considerable attention.[2, 13, 14]

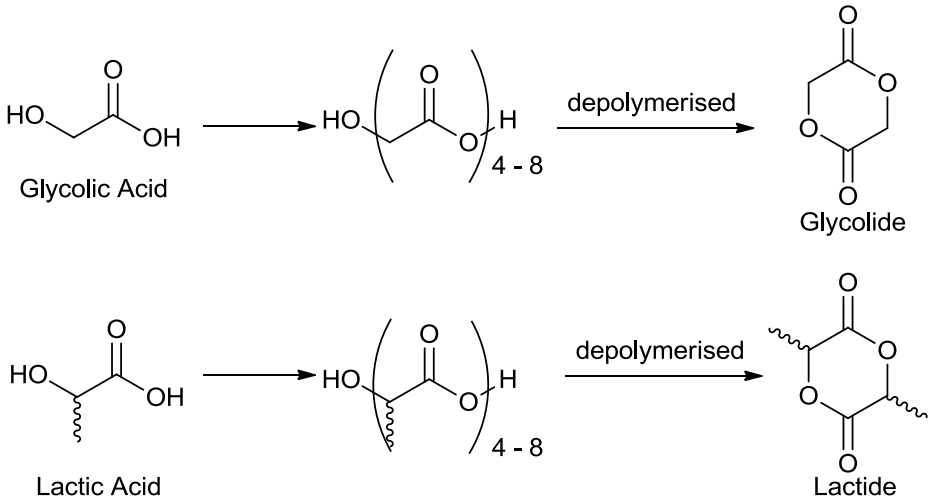

Figure 1.01: Formation of lactide and glycolide.[2, 13, 14]

PLA is not a new polymer being first observed by Pelouze in 1845 by dehydrating lactic acid.[15, 16] Within the last decade PLA has matured from a specialist chemical into an available commodity polymer. NatureWorks part of Cargill Dow LLC chemicals are the major producer of PLA with a facility in Blair, Nebraska capable of producing 140,000 tonnes of PLA per annum.[17] PLA is derived from any sugar source such as sugar beet, corn or wheat which is first introduced into a fermentation faculty to extract lactic acid. Lactic acid is partially polymerised by a condensation reaction yielding low chain length polymers due to the equilibrium nature of the direct condensation reaction and the practicalities of removing the final remnants of water (Figure 1.02).[16] *Via* use of a catalyst the oligomers are depolymerised into selective lactide units, which are sublimed before polymerisation using an organotin catalyst, in the NatureWorks process.

Since the continuous lower cost production of PLA by NatureWorks this biodegradable polymer (PLA) has become viable as a disposable material, examples include; drinking cups, yogurt pots, and cutlery.[18] Although PLA is considered as a remarkable biodegradable polymer as it is not limited to short term disposable applications, other applications include textile materials and paper coatings. Prior to large scale production of PLA its most notable use was for biomedical applications.[19, 20]

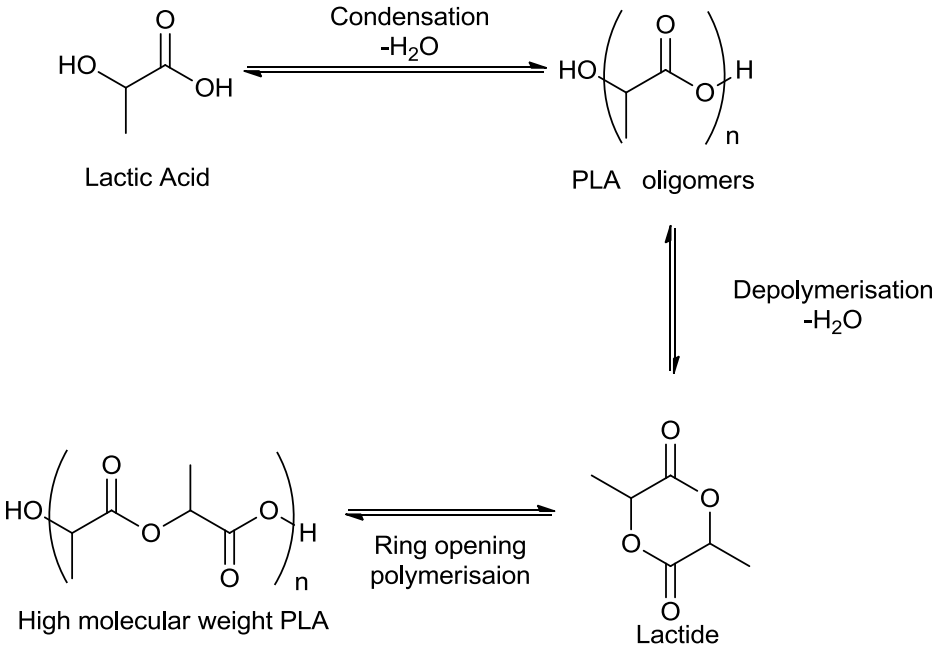

Figure 1.02: Production of Polylactide (PLA) from lactic acid.[16]

An exemplary aspect of PLA is its inherent biocompatibility attained from its base component lactic acid. Under physiological conditions PLA is hydrolysed to lactic acid, which is naturally found within the human body and consequently PLA is non-toxic. Medical applications require defined physical properties and degradation rates of polymers. Within PLA these characteristics are influenced by the steric orientation and crystallinity of the material. Fortunately lactide offers two chiral centres and by controlling the orientation of the chiral centres throughout PLA, its crystallinity, rigidity, and degradation can be tuned. Alternatively characteristics of PLA are tuned by co-polymerisation with other monomers. For example PLA and PGA co-polymer's (PLGA) are utilised for surgical sutures.[21, 22] Increasing the quantity of glycolide moieties reduces the resulting co-polymers rigidity and decreases its degradation rate. As a further example a blend of PLA and polyethylene-co-vinylacetate was investigated by Kenawy *et al*. as a media for drug delivery.[23] Kenawy *et al*. showed the co-polymer gave a stable release of the antibiotic tetracycline hydrochloride, over a period of 5 days, compared to negligible release from pure PLA.[23]

1.2 Ring-Opening-Polymerisation (ROP) of Lactide

ROP of lactide often gives good control over the resulting PLA properties. In the presence of a catalytic initiator the ROP of lactide proceeds *via* a multitude of mechanistic pathways, which are generically grouped as; anionic, cationic, or coordination insertion mechanisms.

1.2.1 Anionic mechanism

The anionic lactide mechanism is typically observed if the ROP catalyst contains a labile cationic metal such as; lithium, potassium, or magnesium. There are two mechanisms of initiation of anionic polymerisation shown in figure 1.03 and 1.04.[2, 13] The first initiation approach discussed is the direct nucleophilic attack of an ionic alkoxide to ring open lactide by acyl bond cleavage. This reaction yields a further lactide derived alkoxide unit and propagation ensues (Figure 1.03).

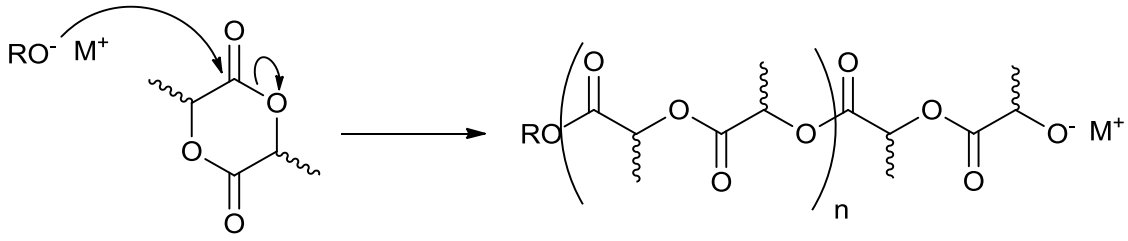

Figure 1.03: Direct nucleophilic attack of anionic ROP mechanism.[2, 13]

The alternative initiation method of anionic ROP begins with deprotonation of a lactide monomer. This deprotonated species can rearrange into a tautomeric metal-enol species (Figure 1.04).[24] Both species are capable of initiating ROP by nucleophilic attack of a lactide monomer, consequently leading to acyl bond cleavage. The propagation step is less clear. One proposition is it proceeds *via* the direct nucleophilic attack mechanism (Figure 1.03) where the ring-opened lactide, an alkoxide, becomes the nucleophilic initiator for continued propagation.[2] To elucidate the mechanism end-group analysis can be used, as the direct nucleophilic attack route will incorporate an alkoxide from the metal initiator or co-initiator.

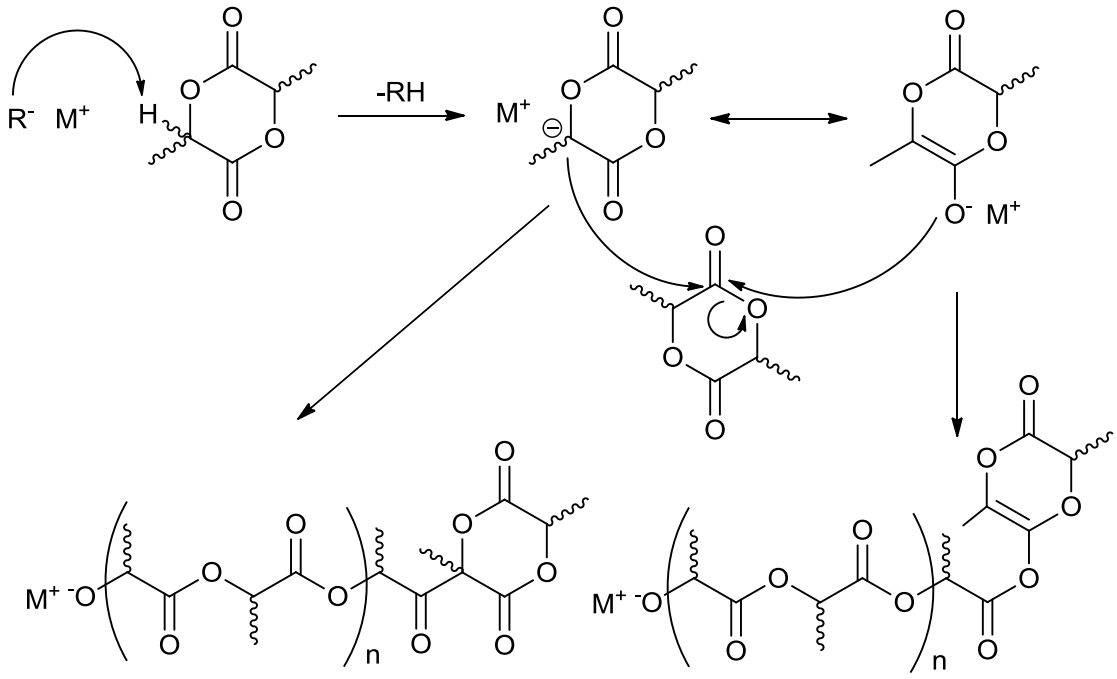

Figure 1.04: Anionic ROP mechanism, *via* the deprotonation of lactide.[2, 24]

1.2.2 Cationic mechanism

The cationic ROP mechanism is mostly observed for organic initiators and can also be referred to as a monomer-activated mechanism.[25] Cationic acid catalysed ROP of caprolactone and valerolactone was established and proceeded using HCl as the acid catalyst.[26] The polymerisation of lactide proceeds *via* a cationic mechanism utilising trifluoromethanesulfonic acid and methyl trifluoromethanesulfonate catalysts. The polymerisation initiates by cationic activation of lactide and then the triflate cleaves the alkyl oxygen, over the acyl oxygen bond, by a S_N2 style mechanism (Figure 1.05).[2, 13]

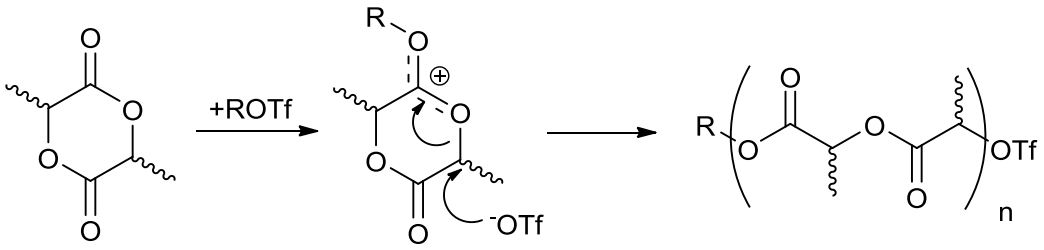

Figure 1.05: Cationic polymerisation mechanism, R = H, Me, or a growing lactide chain.[2]

A later development by Bourissou *et al.* is the cationic acid catalysis of lactide utilising a trifluoromethanesulfonic acid catalyst in the presence of a protic solvent.[27] Bourissou *et al*. proposed a mechanism based on the selective activation of a lactide unit over PLA (Figure 1.06), where the activated lactide is opened by acyl cleavage.

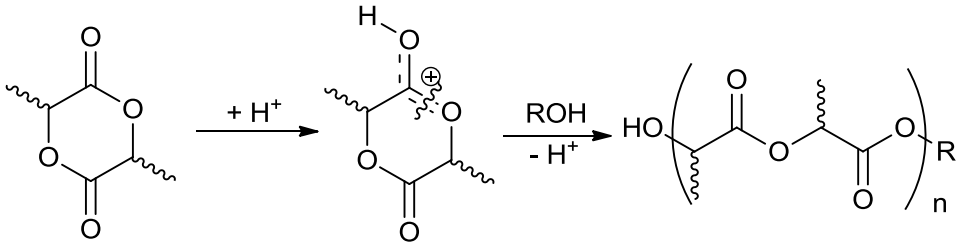

Figure 1.06: Acid catalysed ROP of lactide, adapted from Bourissou *et al*.[2, 27].

1.2.3 Coordination insertion mechanism

Throughout the literature the coordination insertion mechanism is the prevalent ROP mechanism.[2, 13, 25] The coordination insertion mechanism requires a catalytic initiator which contains an electropositive metal, where the metal does not readily dissociate as a cation. The mechanism proceeds by first coordinating the catalytic initiator, *via* the electropositive metal centre, to a carbonyl oxygen of the monomer (Figure 1.07).[2] Secondly, the monomer inserts into the metal alkoxide bond by attack of the alkoxide to the carbonyl carbon. This is followed by cleavage of the acyl bond to ring-open the monomer, leaving the metal coordinated to a newly formed lactide alkoxide bond. Formation of an alkoxide allows the polymerisation to propagate further by insertion of monomer into metal-lactide bonds. Finally the ROP reaction is quenched by saturation of the polymerisation with a proton source, typically methanol, hydrolysing the resulting metal-PLA linkage. This mechanism has been experimentally studied by Kricheldorf *et al*. in 1988[28] and further supported by Teyssié *et al*. in 1991[29] both by the study of $Al(O^iPr)_3$ as the ROP initiator.[2] Interestingly this mechanism allows the presence of a non-dissociative ligand bound to the active metal which appears to "spectate" within the reaction. This aspect of the mechanism can be exploited and the spectator ligand(s) can be used to impart control over the mechanism, inducing chirality over the metal centre. A renowned example was by Fiejen *et al*. using an Al-alkoxide initiator.[30]

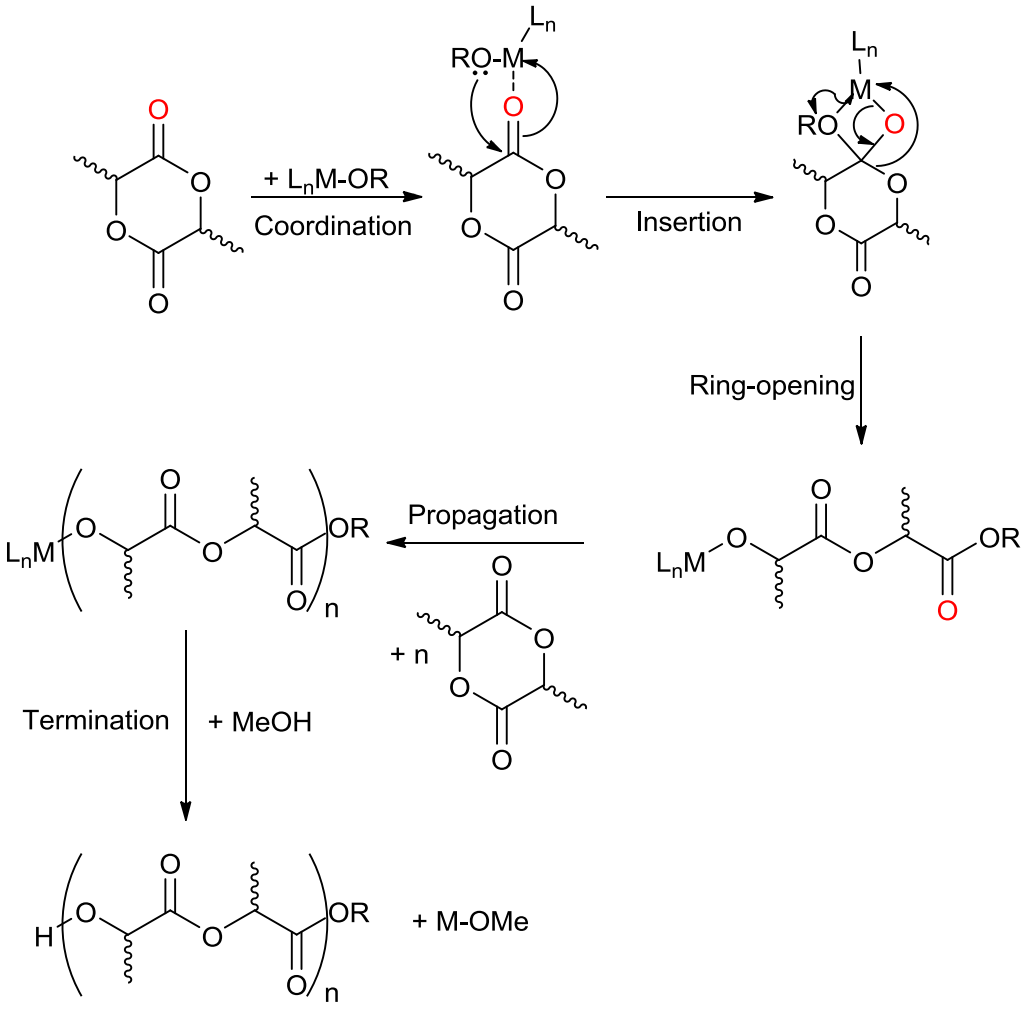

Figure 1.07: Coordination-insertion mechanism.[2]

1.2.4 Transesterification side reactions

Anionic, cationic and coordination insertion mechanism are all capable of transesterification side reactions. Transesterification is undesirable, an ester linkage within an existing polymer chain is attacked in preference to a lactide ester linkage. As a consequence transesterification reactions cause molecular weights to be lower or distributed over a larger molecular weight range. Transesterification can occur by two generic mechanisms, either intramolecular or intermolecular (Figure 1.08).[2] Intramolecular transesterification or backbiting is defined as when a growing polymer chain reacts with itself, hence reducing PLA molecular weight and forming cyclic compounds. Intermolecular transesterification is attack of one polymer to another chain thus causing wide disparity between polymer chains and high distribution of molecular weights.

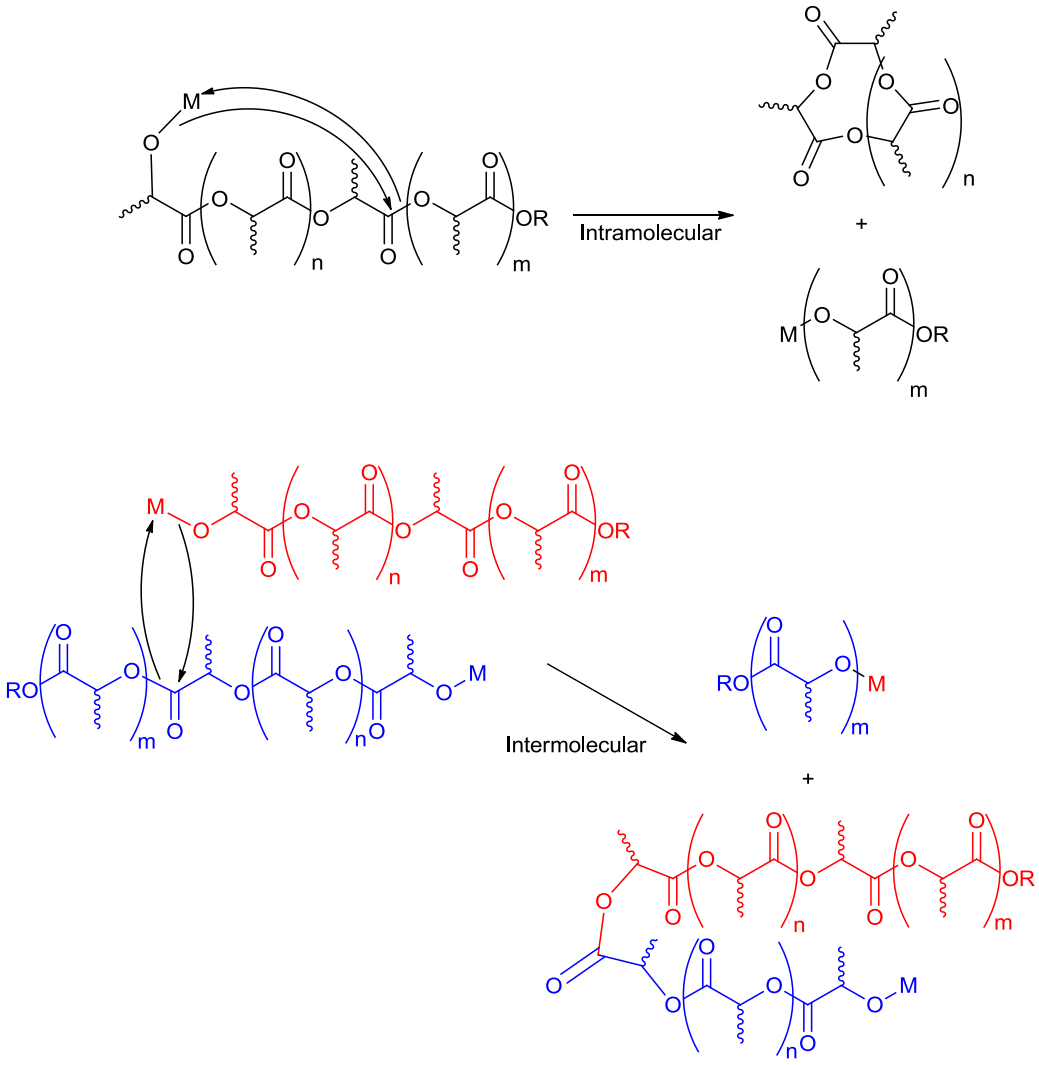

Figure 1.08: Schematic representations of intermolecular and intramolecular transesterification side reactions, within the ROP of lactide.[2]

An ideal ROP mechanistic scenario involves chain-end-control where the polymerisation proceeds by incorporating lactide monomers only at the end of a PLA chain. The chain-end control mechanism allows a tailored initiator to arrange each monomer inserted into the chain. In the circumstance that an initiator can further polymerise on addition of more monomer before quenching the polymerisation is known as "Living".[31] For a polymerisation to be considered living the above statement must be true but in addition the molecular weight of the polymer chain must coincide with the monomer-to-initiator ratio i.e. one polymer chain per initiation site. A living coordination-insertion polymerisation can be terminated by quenching of the reaction by hydrolysing the end group. In contrast immortal polymerisations cannot be quenched by addition of typical reagents, such as alcohols.

The concept of living polymerisations was first observed and introduced for ring-opening polymerisation by Inoue *et al.*[32] Immortal polymerisations share traits with living polymerisations, predominantly each reaction will continue to polymerise on addition of further monomer. As stated immortal polymerisation cannot be terminated on addition of alcohol as the polymer chains are rearranged. This rearrangement shortens the polymer chains to a degree, where the chain length is equal to the monomer:alcohol ratio.

1.2.5 Immortal ROP mechanisms

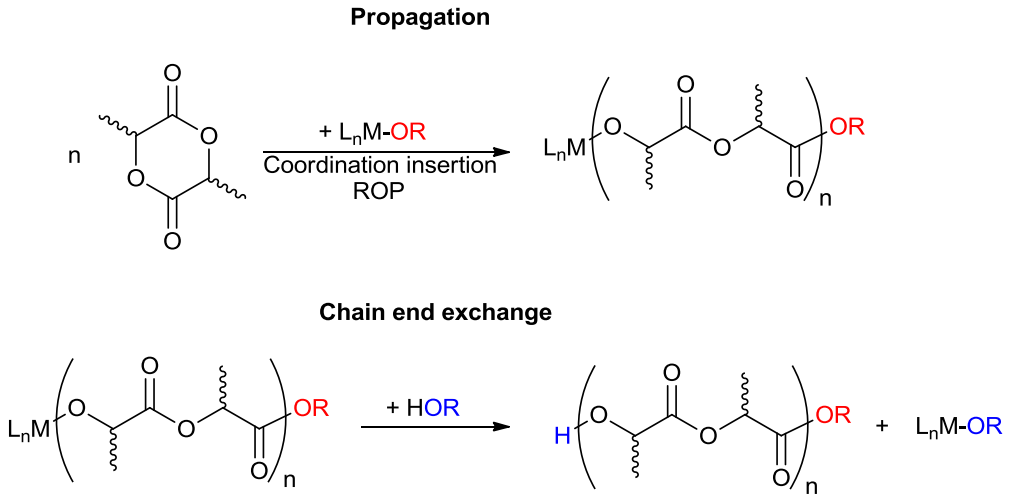

Figure 1.09: Schematic representations of the coordination-insertion based immortal mechanism for the ROP of lactide.[33]

Within the immortal ROP of lactide the polymer chains grow in a uniform manner based upon the quantity of a secondary initiator source, which is typically a protic alcohol. Two methods are discussed herein; coordination insertion with rapid chain-end exchange mechanism,[33] the second where propagation occurs *via* a transesterification method and an activated monomer mechanism.[33, 34] The coordination insertion and rapid exchange reaction propagates through a coordination insertion mechanism (figure 1.09). During the propagation, rapid proton exchange between the terminating metal and a protic co-initiator/PLA chain occurs. The proton terminated PLA chain is still available for propagation and the L_nM-OR species continues to polymerise.

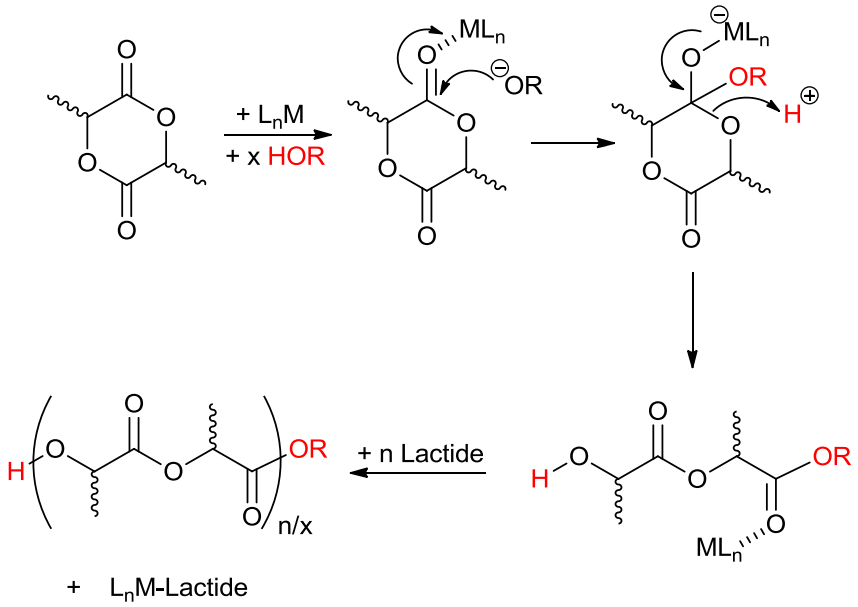

Figure 1. 10: Schematic representation of the activated monomer immortal mechanism for the ROP of lactide.[33, 34]

The activated monomer mechanism for the immortal ROP of lactide is depicted in figure 1.10.[33, 34] A lactide carbonyl coordinates to the metal complex further polarising the carbonyl bond and activating it towards nucleophilic attack. A co-initiator, typically a protic alcohol, attacks the carbonyl carbon which is followed by acyl bond cleavage. The lactide chain is terminated by a proton and the metal complex transfers from the polymer chain to a lactide monomer activating the new monomer for propagation.

1.2.6 GPC and determining polymer molecular weights

Polymers are characterised by either their physical characteristics or chemical structures. Gel permeation chromatography (GPC) can be utilised to determine structural characteristics of linear aliphatic polyesters. Herein is discussed two measurements; number average molecular weight (M_n), a measure directly related to the chain lengths within the polymer, and the polydispersity index (PDI), a measure of chain length distribution. GPC is a method of size exclusion chromatography where larger polymer chains will flow through the system at a much faster rate. The polymer must first be solubilised in a compatible solvent and the solution is then passed through a series of porous beads. Smaller polymer chains permeate the beads

while larger chains flow around (Figure 1.11). As a consequence smaller chains take a much more turbulent route directly causing a higher retention time.

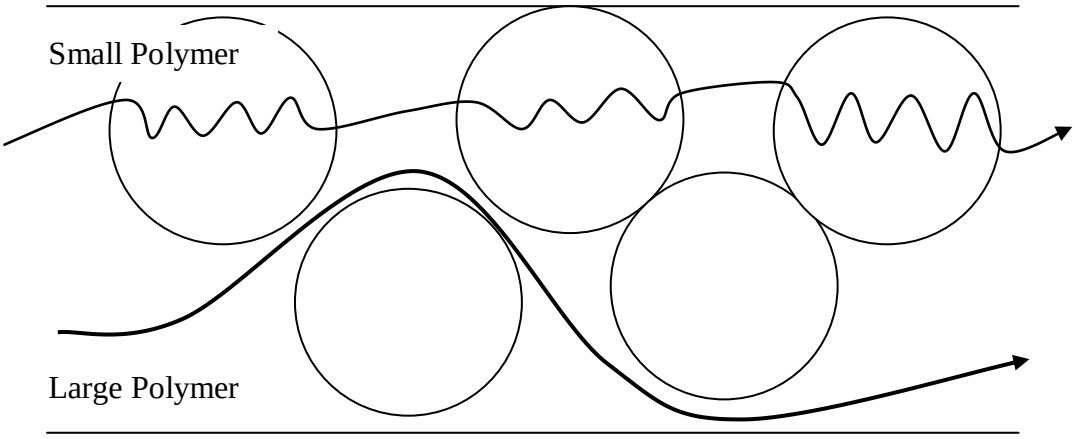

Figure 1.11: GPC diagram depicting polymer flow paths.

$$PDI = \frac{M_w}{M_n} \quad \text{Equation: 1.01}$$

$$M_n = \frac{\sum M_i N_i}{\sum N_i} \quad \text{Equation: 1.02} \qquad M_w = \frac{\sum M_i^2 N_i}{\sum M_i N_i} \quad \text{Equation: 1.03}$$

Figure 1.12: Equations relating: polydispersity index (PDI), number average molecular weight (M_n), and weight average molecular weight (M_w).

The polydispersity index (PDI) is calculated by the equation 1.01 (Figure 1.12). It is dependent on the number average molecular weight (M_n) calculated by equation 1.02 (Figure 1.12) and the weight average molecular weight (M_w) given by equation 1.03 (Figure 1.12). M_n is a measure of the mean average molecular weight, while M_w accounts for the fact that larger individual molecules account for a higher percentage of the total weight. A direct comparison of M_n and M_w is PDI, PDI = 1 indicates uniform polymer chains, PDI > 1 indicates varied polymer chain lengths. M_i and N_i values are obtained from a GPC trace (Figure 1.13) by correlating inverse retention time and relative intensity. To determine M_i from retention time a GPC instrument is calibrated to polystyrene standards. To account for the difference in hydrodynamic volume between lactide and polystyrene standards a correction value of 0.58 can be applied.[35]

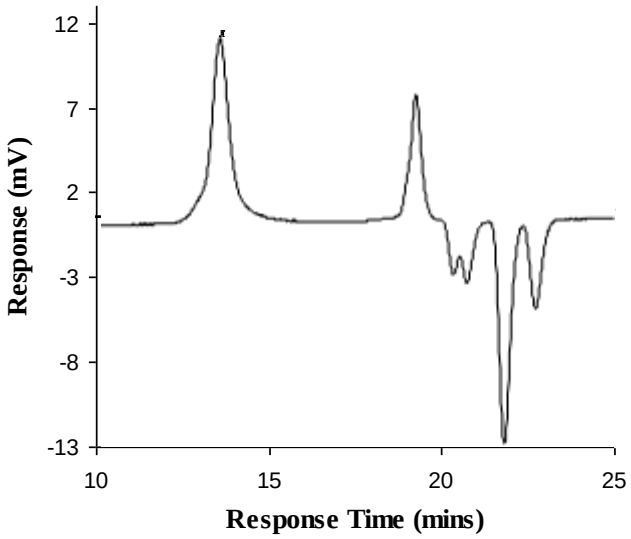

Figure 1.13: Typical GPC trace.

M_n and PDI values are related to the rates of individual mechanisms within the polymerisation. If the rate of initiation (k_{int}) >> rate of propagation (k_{prop}) the resulting polymer chains should all be uniform (PDI ≈ 1). Alternately if the opposite is true $k_{int} << k_{prop}$ a polymer chain can grow significantly before an additional chain initiates resulting in higher chain distribution (PDI >> 1). The above assumes the initiator contains one initiation site or only propagates one polymer chain. If an initiator has more than one initiation site further chain distribution will result as a consequence of multiple k_{int} values. For the coordination insertion mechanism where $k_{int} >> k_{prop}$ then the polymer chain length can be predicted from conversion of lactide by equation 1.04.

$$M_n = \frac{\text{Monomer ratio} \times \text{Conversion} \times 144.13}{\text{Initiator ratio}} + \text{End group } (M_w)$$

Equation: 1.04

Figure 1.14: Equation used to calculate theoretical molecular weight from conversion of lactide for PLA.

Molecular weight control is not limited to the rate of propagation and rate of initiation as stated previously transesterification is detrimental to uniform chain length. If $k_{prop} >> k_{inter.trans}$ (rate of intermolecular transesterification) uniform chain

growth ensues. In the case that k_{prop} >> $k_{intra.trans}$ (rate of intramolecular transesterification) controlled growth is observed, where k_{prop} << $k_{intra.trans}$ we get both high PDI and lower M_n.

Molecular weight can be determined by other methods, which can be used in addition to GPC. A valuable method is MALDI-TOF mass spectrometry which gives the repeat unit of the polymers and is highly regarded for end group analysis. Mass spectrometry has limitation due to difficulties in ionising polymer chains, limiting the polymer samples to lower molecular weights. Methods which detect polymer concentration and can work *in-situ* with GPC include; refractive index, IR, and UV absorption. Other methods which can be utilised *in-situ* with GPC or possible to get measurements directly include low angle light scattering, viscosity, and multi angle light scattering detectors.

1.2.7 Stereochemistry and characterisation by NMR spectroscopy

Lactic acid is present in the *L* and *D* forms (the *S* and *R* enantiomers respectively). As a result lactide can be isolated as a series of diastereomers. The commercially available lactide diastereomers are *L*-Lactide, *D*-Lactide, *Meso*-lactide and an mixture of *L*-lactide and *D*-lactide known as *rac*-lactide (Figure 1.15).[36] Both *L*-lactide and *D*-lactide result in isotactic PLA with their respective stereochemistry throughout the polymer. *rac*-Lactide can yield different PLA arrangements, which are determined by the initiator and reaction conditions. The resulting PLA stereoforms from *rac*-lactide are; isotactic stereoblock PLA is the arrangement of *L*-lactide units as a block of PLA followed by a corresponding block of *D*-lactide units, heterotactic PLA is an alternating arrangement of *L*-lactide and *D*-lactide, and atactic PLA is the random arrangement of lactide monomers throughout the polymer chain. *meso*-Lactide also results in different stereo arrangements of PLA and like *rac*-lactide can also yield heterotactic and atactic PLA. In contrast to *rac*-lactide *meso*-lactide can produce syndiotactic PLA where each lactic acid (or each stereocentre) adopts the opposite conformation in an alternating manner.

Each stereo-arrangement of PLA has different physical properties. Isotactic PLA derived from *L*-lactide and *D*-lactide both have similar properties; they show a higher degree of crystallinity and as such are more brittle and ridged than other stereoforms of PLA. Atactic, syndiotactic and heterotactic lactide all have similar

properties due to lack of crystallinity within the respective polymers. Isotactic stereoblock PLA results in further crystallinity within the polymer displaying similar physical properties to isotactic PLA. Isotactic stereoblock PLA exhibits a higher melting temperature than isotactic PLA derived from pure *L*-lactide or *D*-lactide. This observation has been attributed to increased intermolecular interactions between *L*-PLA and *D*-PLA chains. Isotactic stereoblock PLA can be synthesised directly from *rac*-lactide *via* the use of certain initiators.[30, 37] Blending *L*-PLA and *D*-PLA in differing quantities has been studied with the intention of mimicking isotactic stereoblock PLA with moderate success but cannot fully yield the same properties as isotactic stereoblock PLA.[18, 38]

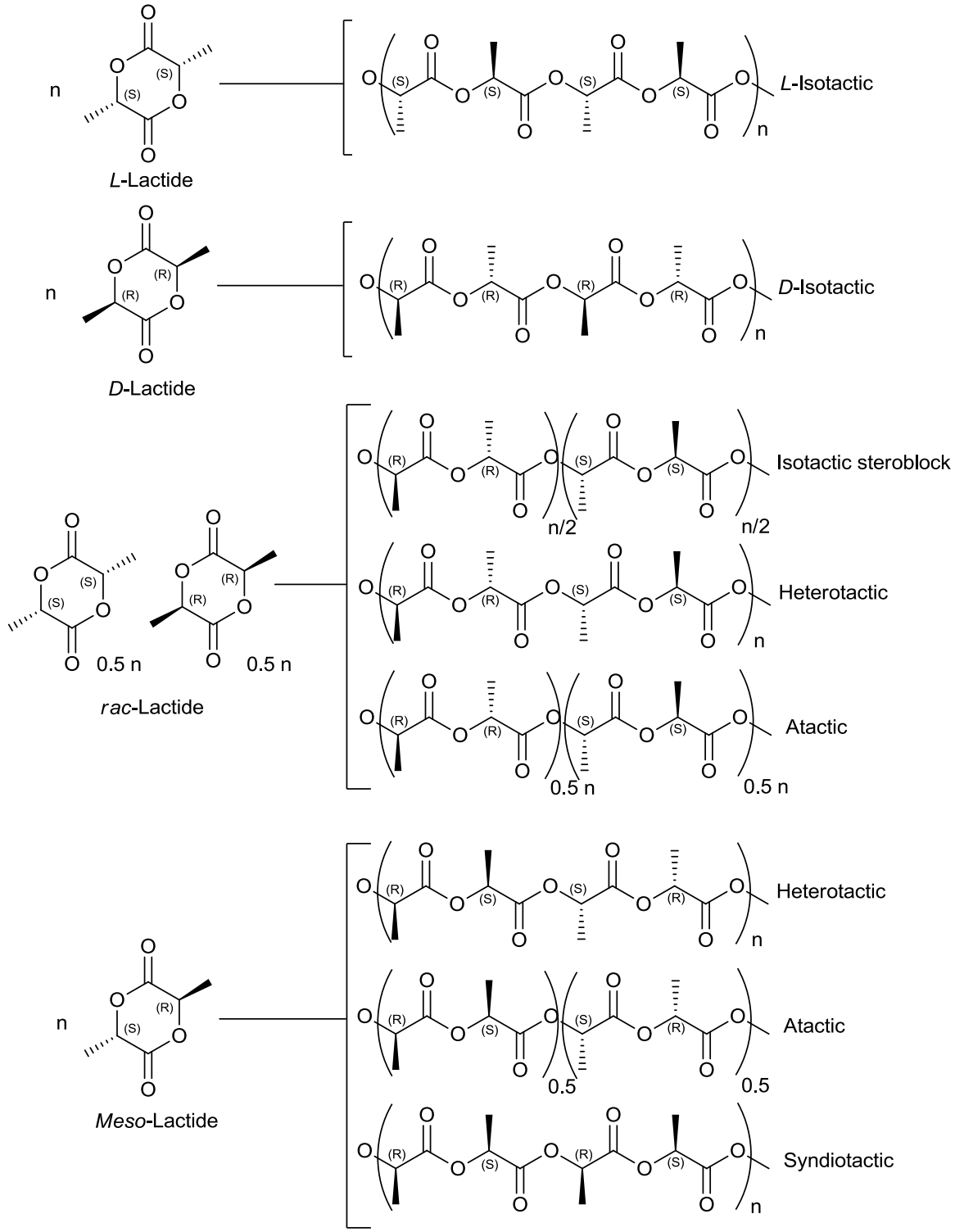

Figure 1.15: Stereoforms of lactide and resulting PLA arrangements.[36]

NMR spectroscopy is used in PLA analysis to determine conversion, tacticity, and end group analysis of low molecular weight PLA. Conversion is obtained by comparing the relative integrals of lactide methines to PLA methines by ^{1}H NMR

spectroscopy. End group analysis by NMR spectroscopy is highly dependent on the end-group in question but it generally requires higher resolution and more concentrated polymer samples. Tacticity of PLA can be determined by two methods; ^{1}H homonuclear decoupled NMR spectroscopy,[36] and ^{13}C{^{1}H} NMR spectroscopy.[39]

^{13}C{^{1}H} NMR spectroscopic method for determining tacticity was developed by Kasperczyk in 1995[39] and focused on the carbonyl region of the spectra and implemented a hexad system to determine tacticity. PLA tacticity determination by homonuclear decoupled methine region ^{1}H NMR spectroscopy was later development by Thakur *et al*. in 1997 and utilised a tetrad model.[40]

A typical spectrum of a ^{1}H homonuclear decoupled NMR spectrum of atactic PLA is shown in figure 1.16. By removing the coupling from the methine protons located at 1.62 ppm the methine region becomes five discrete resonances. The resonances are allocated to tetrad units, groups of four lactic acid units where; *i* = an isotactic linkage (*R*,*R* or *S*,*S*), and *s* = a syndiotactic linkage (*R*,*S* or *S*,*R*). Thus, it follows that the [*iii*] tetrad corresponds to an isotactic PLA tetrad with the respective lactic acid chirality of *R*,*R*,*R*,*R* or *S*,*S*,*S*,*S*. See figure 1.17.[36]

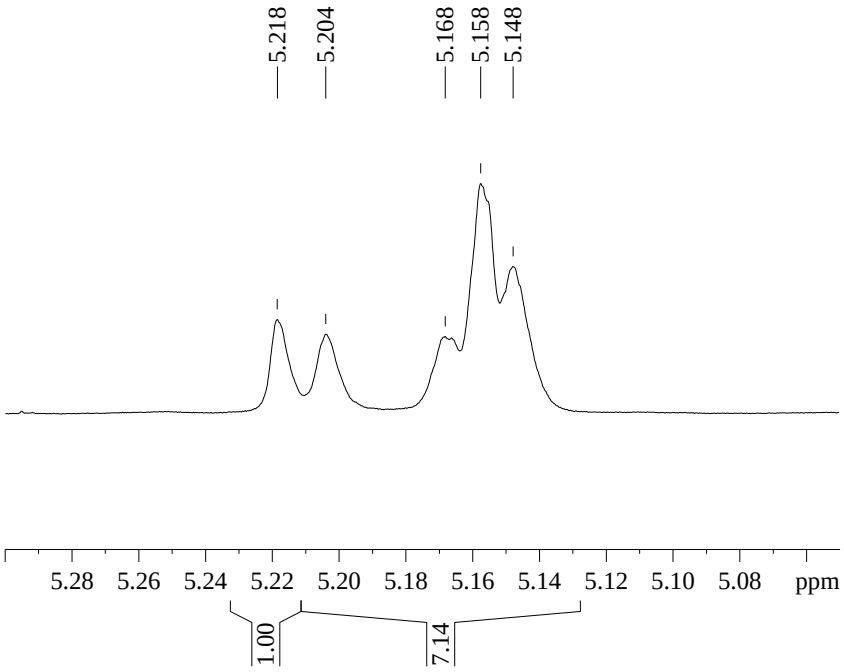

Figure 1.16: ^{1}H homonuclear decoupled NMR spectrum of the methine region from atactic PLA.

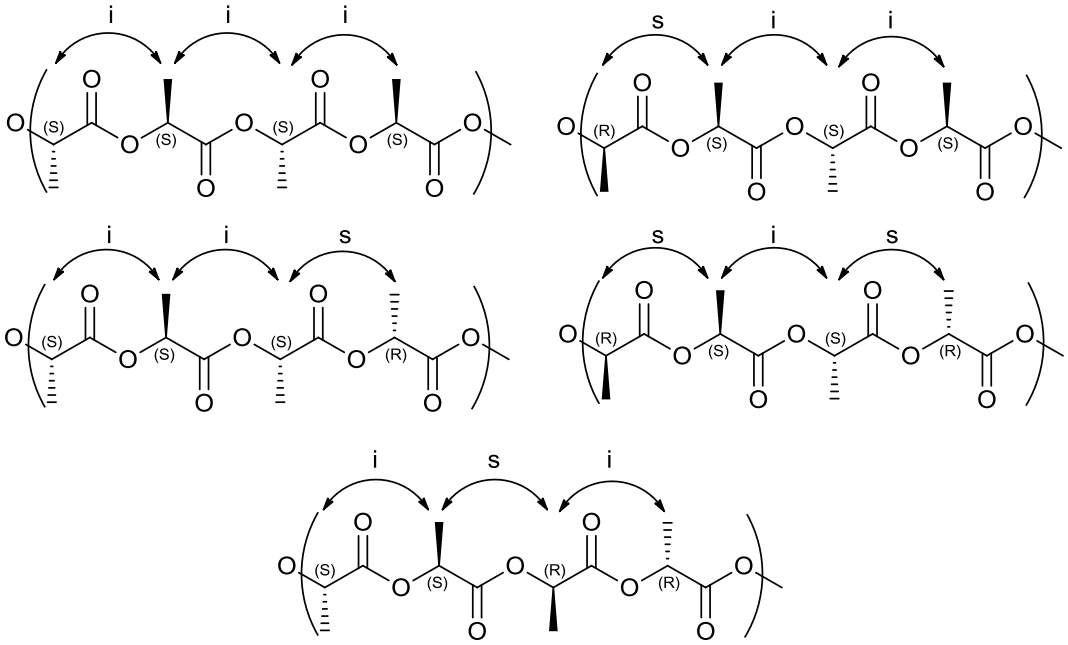

Figure 1.17: PLA tetrads derived from *rac*-lactide.

Within the decoupled ^{1}H NMR spectrum heterotactic PLA is observed as an equal combination of the [*sis*] and [*isi*] tetrads. Atactic PLA derived from *rac*-lactide yields all five tetrad possibilities (Figure 1.17). The relative integrals of the tetrad peaks within the homonuclear decoupled ^{1}H NMR spectrum are; 1[*sis*]:1[*sii*]:1[*iis*]:3[*iii*]:2[*isi*] for atactic PLA. The ratios for the eight possible tetrads are derived by Bernoullian statistics, which calculates the probability of each tetrad linkage occurring (Table 1.01). Out of the eight possibilities only five are possible for *rac*-lactide as neither *L*, or *D*-lactide units allow two adjacent syndiotactic linkages "*s*". Bernoullian statistics are also applied for PLA derived from *meso*-lactide and disallow possibilities which contain two adjacent isotactic linkages "*i*". Transesterification may cause the disallowed possibilities to occur as transesterification is not limited to lactic acid diads.

When considering *rac*-lactide the probability of racemic enchainment (P_r) is inversely proportional to the probability of isotactic enchainment (P_m) and can be calculated by rearrangement of equation 1.05 (Figure 1.18). To keep the calculations simplistic the [*sis*] relative integral is chosen to calculate P_r (Equation 1.06), which gives P_m *via* equation 1.05. P_r is a measure of the tacticity within PLA, when P_r = 1

the polymer has only racemic lactide linkages as such is heterotactic. It follows that when $P_m = 0$ there is no isotactic enchainment and the PLA is heterotactic. Therefore when $P_r = 0$ and $P_m = 1$ there is total isotactic enchainment of the PLA chains.[36]

Tetrad	Probabilities based on Bernoullian statistics	
	***rac*-lactide**	***meso*-lactide**
[*iii*]	$P_m^2 + P_r P_m / 2$	0
[*iis*]	$P_r P_m / 2$	0
[*sii*]	$P_r P_m / 2$	0
[*sis*]	$P_r^2 / 2$	$(P_m^2 + P_r P_m) / 2$
[*sss*]	0	$P_r^2 + P_r P_m / 2$
[*ssi*]	0	$P_r P_m / 2$
[*iss*]	0	$P_r P_m / 2$
[*isi*]	$(P_r^2 + P_r P_m) / 2$	$P_m^2 / 2$

Table 1.01: Tetrad probabilities based on Bernoullian statistics.[36]

$$P_r + P_m = 1 \quad \text{Equation 1.05}$$

$$\sqrt{2 \times [sis]} = P_r \quad \text{Equation 1.06}$$

Figure 1.18: Equations derived from Bernoullian statistics to calculate probability of racemic enchainment (P_r).

Determination of tacticity is not limited to ^{1}H NMR spectroscopy, differential scanning calorimetry can be used to determine tacticity in stereoregular PLA *via* melting points and crystallinity.[2] $^{13}C\{^1H\}$ NMR spectroscopy is also utilised in the determination of tacticity, the method is similar to ^{1}H homonuclear decoupled NMR spectroscopy methine analysis in that the carbonyl region is separated into a series of hexads and the probability of enchainment is calculated through equations derived from pair addition Bernoullian statistics.[39]

1.3 Ring-Opening-Polymerisation Initiators for Lactide

The ROP of lactide requires an initiator which can be either metal based or non-metal based. The initiator is the key variant of the ROP reaction in obtaining stereoselectivity from *rac*-lactide and also determines the reaction rate and resulting PLA properties. Metal initiators with simple ligands rarely impart stereoselectivity over the ROP of *rac*-lactide, although there are examples contrary to this.[41, 42] The need to control the polymerisation of *rac*-lactide has led to the use of metal complexes which utilise bulky, chelating or chiral ligands. Typical metal complex PLA initiators contain at least one or any combination of these properties. Design of metal complexes and thier associated ligand groups achieved improved stereo-control, molecular weight control and/or low PDI values, which is discussed throughout this chapter. A metal centre can control the tacticity of PLA resulting from the ROP of *rac*-lactide by chain-end-control where control over the tacticity is induced by the growing polymer chain. Another method of stereo-control involves forcing chirality over the metal centre *via* the ligand(s), referred to as enantiomorphic site control.[43]

Initiators for the ROP of lactide have been comprehensively reviewed before.[2, 4, 13, 18, 25, 44-48] Herein, selected initiators are reported for their originality in the subject, importance to the field, stereoselectivity, activity, or relevance to the study that follows. Using these criteria groups of metal based initiators (sections 1.3.1 - 1.3.7) are discussed with a short overview of organic based initiators (section 1.3.8). Following this cyclic-ester co-polymers are briefly discussed (section 1.4).

1.3.1 Tin initiators

The current industrially favoured initiator for the ROP of lactide is Tin(II) 2-ethylhexanoate or tin(II) octoate {$Sn(Oct)_2$} as it is easy to handle, commercially available, and shown to polymerise at high ratios in solvent free conditions. It was shown that $Sn(Oct)_2$) polymerises lactide at 110 °C to 98 % conversion after 24 h at very high monomer to initiator ratios.[49] Furthermore, a significant increase in ROP control and rate was observed on the addition of a protic co-initiator.[50] There was much speculation over the ROP mechanism but it has been shown that $Sn(Oct)_2$

initiates by the coordination insertion mechanism with and without a purposefully added co-initiator (Figure 1.19).[2, 51]

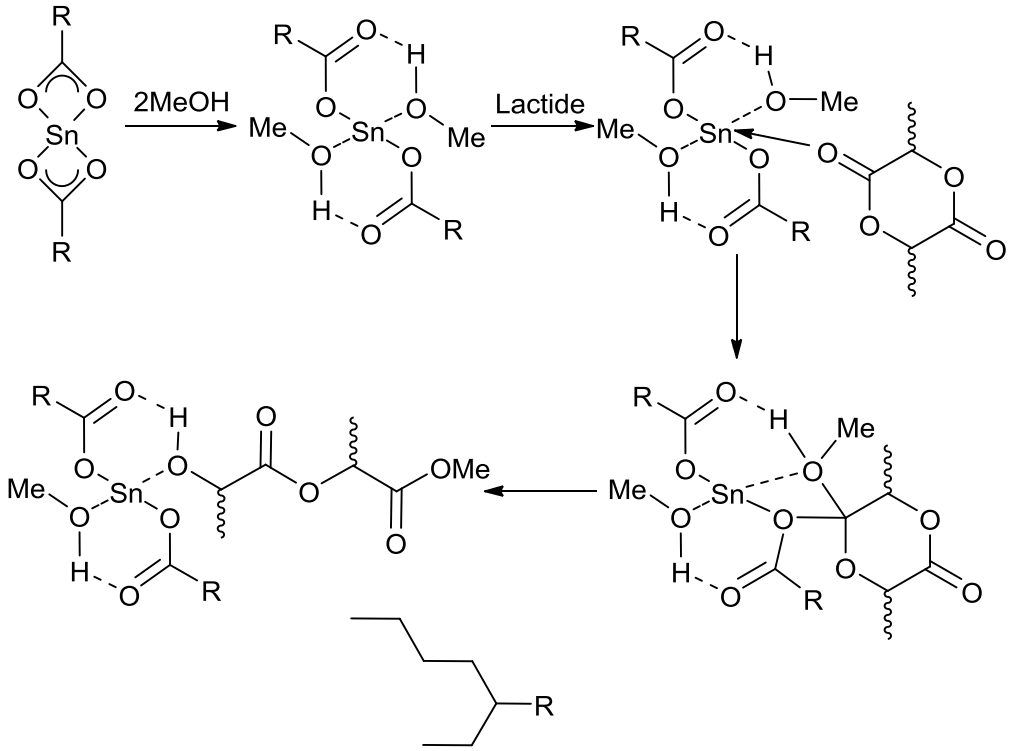

Figure 1.19: Computationally predicted mechanism of the ROP of lactide by $Sn(Oct)_2$ in the presence of a protic co-initiator. [a] Computationally derived for R = Me.[1,32]

$Sn(Oct)_2$ contains high degrees of impurities, mostly water and octanoic acid, which have a significant effect on the ROP reaction rate and resulting molecular weight (M_n) of the PLA produced. The impurities were revealed to act in a similar fashion to a protic species and form a tin-alkoxide which becomes the active initiating species.[50, 52] Although $Sn(Oct)_2$ is the industrially favoured initiator it shows no stereoselectivity and although $Sn(Oct)_2$ is non toxic, its related tin hydroxides are harmful, making them unsuitable for biomedical applications where conditions to produce tin hydroxides may occur.[53]

Gibson *et al*. has synthesised amino-phenol derived tin complexes for the polymerisation of lactide.[54] The tridentate Schiff base ligands coordinate to Sn(II) then attack of the amide to the imine occurs to yield a tetra-dentate Sn(II) complex. This amide migration is a reversible process allowing access to both tetradentate and tridentate Sn(II) complex forms (Figure 1.20).[54] This Sn(II) complex surprisingly

polymerises *rac*-lactide with a high degree of control despite its fluxional nature due to the amide migration mechanism. All the derivatives show little difference in their resulting *rac*-lactide polymerisation yielding > 90% conversion at 60 °C after 2 h at 100:1 [monomer]:[initiator] ratio. All the polymerisations show good molecular weight control with low polydispersity index values (PDI ≈ 1.2).[54] Interestingly NMR spectroscopy and MALDI-TOF mass spectrometry have both resolved the PLA end group as dimethylamide. It was suggested that the complex acts as a single-site initiator and further propagation proceeds *via* the lactide-Sn-ligand complex shown in figure 1.20.

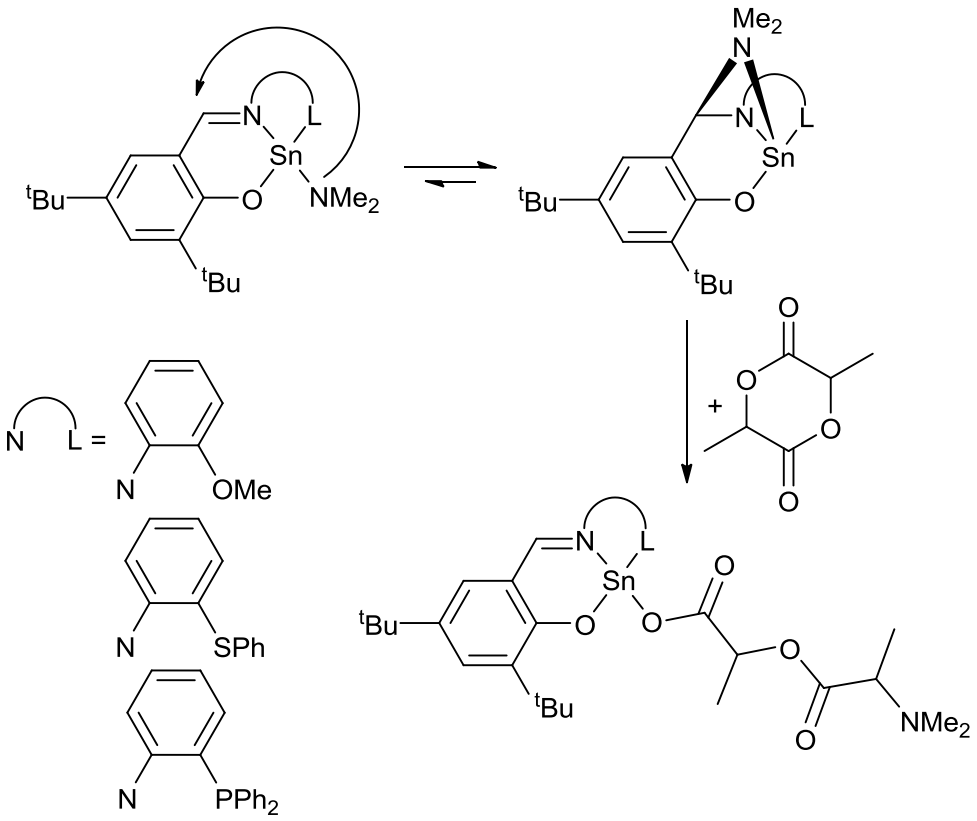

Figure 1.20: Sn(II) tridentate Schiff base complexes and amide migration to the Sn(II) tetradentate complex. Also depicted is a hypothesised polymerisation intermediate.[54]

Further work by Gibson has shown this amide migration to be present with similar ligands such as bidentate aminophenols.[55] Under similar conditions (60 °C, 100:1 [monomer]:[initiator] ratio) the bidentate aminophenol Sn(II) dimer (Figure 1.21) polymerised lactide to > 90 % conversion after 1 h. It was speculated that the dimer separates on inclusion of a lactide to produce a four-coordinate active species (Figure 1.21).[55]

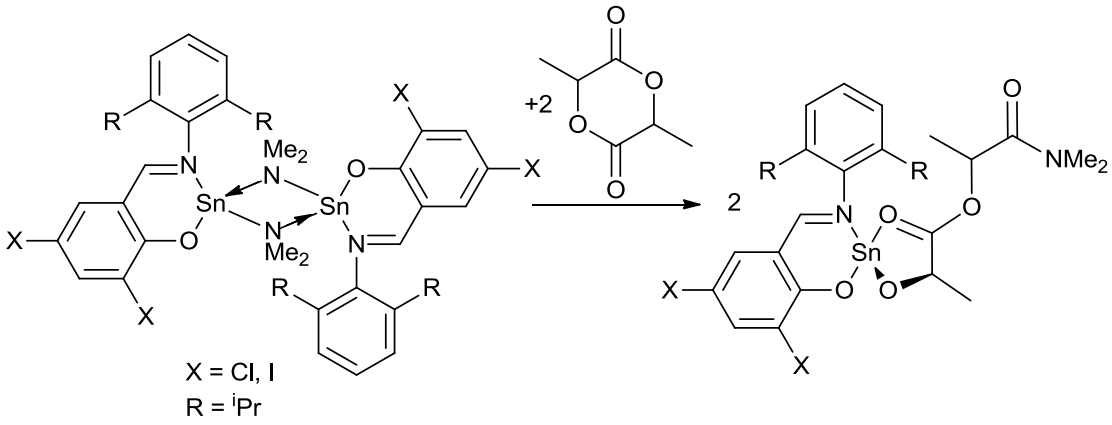

Figure 1.21: Reaction of lactide with an aminophenol Sn(II) dimer showing a hypothesised propagation species.[55]

Tin β-diketiminate complexes have been established as efficient initiators for the polymerisation of *rac*-lactide (Figure 1.22).[56, 57] Initial polymerisation studies of β-diketiminate tin complex Sn(**1**)O^{i}Pr with lactide displayed polymerisation in CH_2Cl_2 at ambient temperature to > 99 % conversion after 96 h at 100:1 [monomer]:[initiator] ratio.[56] Furthermore increasing the temperature to 60 °C (toluene) afforded an enhanced rate and achieved 85 % conversion after 4 h. Notably the higher temperature reaction yielded no loss of control over the polymerisation. Both the low and high temperature polymerisation gave good molecular weight control alongside low PDI values. All the Sn(II) complexes Sn(**1**-**4**)O^{i}Pr produced moderately heterotactic polymer from *rac*-lactide $P_r \approx 0.65$.[57] By reducing the steric bulk of the aromatic substituent the reaction rate increased. At 60 °C (100:1 [monomer]:[initiator] ratio), Sn(**4**)O^{i}Pr attained 93 % conversion of *rac*-lactide after 2 h with no loss of selectivity. Additionally the introduction of electron withdrawing substituents was shown to enhance reaction rate without selectivity loss.[57]

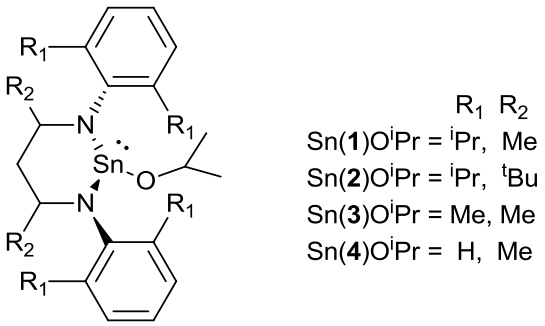

Figure 1.22: Tin β-diketiminate alkoxide complexes.[56, 57]

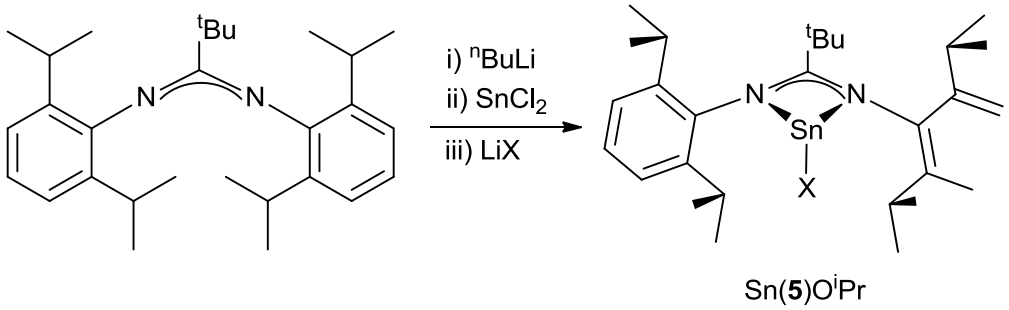

Figure 1.23: tButylamidinate tin(II) complexes for the polymerisation of *rac*-lactide.[58]

Gibson *et al*. investigated tbutylamidinate tin(II) complexes as initiators for the ROP of *rac*-lactide (Figure 1.23).[58] As a comparison the Sn(II) complex Sn(**5**)O^{i}Pr was significantly faster for the polymerisation of *rac*-lactide than its analogous β-diketiminate Sn(II) complexes {Sn(**1**-**2**)O^{i}Pr}. Under the same conditions (60 °C, toluene, 100:1 ratio) tin(II) complex Sn(**5**)O^{i}Pr afforded > 85 % conversion after 90 mins compared to 4 h for Sn(**1**)O^{i}Pr and 8 h for Sn(**2**)O^{i}Pr.[57, 58] Although tbutylamidinate tin(II) complexes proved to be faster for the propagation of *rac*-lactide they yielded PLA with a similar heterotacticity to that observed by the Sn(II) β-diketiminate. Gibson *et al*. determined that this similar behaviour for both nitrogen binding bidentate Sn(II) ligand systems can be attributed to electronic effects of the Sn(II) metal. A $5s^2$ Sn(II) lone pair plays an important role in controlling the orientation of a coordinating lactide/PLA unit and furthermore influences the control over the propagation reaction.[57, 58]

Chisholm *et al*. has reported Sn(IV) initiators for the polymerisation of *L*-lactide.[59] Tin (IV) complexes of the basic formula Ph_2SnX_2 and Ph_3SnX were synthesized and proven to be slow initiators for the polymerisation of *L*-lactide.[53] The bis(phenyl) Sn(IV) complexes were shown to be faster initiators than their tri(phenyl) Sn(IV) counter-parts with relative reaction rates; k_{prop} {$Ph_2Sn(NMe_2)_2$} = 3.8(2) × 10^{-5} s^{-1}, and k_{prop} (Ph_3SnNMe_2) = 2.8(4) × 10^{-6} s^{-1} (80°C, toluene, $[LA]_0$ = 0.084 M, $[Sn]_0$ = 1.7 mM). These Sn(IV) complexes showed a very high degree of transesterification with a significant amount of cyclic esters produced during the polymerisation, to the extent that at 50 % conversion of *L*-lactide with $Ph_2Sn(NMe_2)_2$ initiator the resulting product was mostly cyclic esters.[59] The initiating group –X was shown to have a significant impact on the

polymerisation where X = O^{i}Pr the polymerisation displayed a reduced amount of intramolecular transesterification than X = NMe_2.

1.3.2 Group 1 initiators

Group 1 metal complexes have proven to be active for the polymerisation of lactide. A notable simple initiator initially reported by Kasperczyk was LiO^{t}Bu which polymerises *rac*-lactide at room temperature in tetrahydrofuran (THF).[39] LiO^{t}Bu was shown to be a highly active initiator for the polymerisation of *rac*-lactide achieving 78 % conversion after 40 mins at 20 °C in THF at the [monomer]:[initiator] ratio of 250:1.[42] Interestingly LiO^{t}Bu yields heterotactic enriched lactide under the above conditions with reasonable control over the polymerisation. Further studies have indicated that lowering the temperature increases the heterotactic selectivity. It was also shown that heterotactic selectivity was much more significant at early reaction times and a $P_r = 0.94$ was reported at - 20 °C (THF) after 5 mins ([monomer]:[initiator] ratio of 250:1). The reduced selectivity after longer reaction times was attributed to an increasing degree of transesterification reactions as the propagation reaction proceeds.

Potassium ^{t}butoxide has been demonstrated as an active initiator for *L*-lactide polymerisation proving to be a fast initiator at ambient temperature.[60] A significant reduction in rate is observed as the reaction approaches 80 % conversion. The control potassium ^{t}butoxide exhibits over the ROP of *L*-lactide can be enhanced by the addition of 18-crown-6 ether decreasing the PDI from 1.42 to 1.17. While 18-crown-6 ether addition gives enhanced polymerisation control it also decreases the ROP reaction rate, k_{prop} (potassium ^{t}butoxide) = 5.9×10^{-3} M^{-1} s^{-1}, k_{prop} {potassium ^{t}butoxide + 18-crown-6 (1:1)} = 5.3×10^{-4} M^{-1} s^{-1}.

Lithium is renowned for forming aggregates but Lin *et al*. synthesised a lithium dimer from the addition of ^{n}BuLi and benzyl alcohol (BnOH) to 2,2'-ethylidenebis(4,6-di-*tert*-butylphenol) (EDBP-H_2).[61] In the presence of THF the {(EDBP-H)-Li(BnOH)}$_2$ dimer separates into lithium monomers with the formula {(EDBP-H)Li(BnOH)(THF)$_2$} (Figure 1.24). The {(EDBP-H)-Li(BnOH)}$_2$ dimer is a highly active initiator for the ROP of *L*-lactide at room temperature yielding > 99 % conversion after 1 h (CH_2Cl_2, 50:1 [monomer]:[initiator] ratio).

Experimental evidence suggested the dimeric species separated into monomers on coordination of an *L*-lactide moiety. The {(EDBP-H)-Li(BnOH)}$_2$ dimer is still highly active for *L*-lactide ROP at reduced temperatures albeit displaying lower activity, at 0 °C after 2 h a conversion of 91 % was obtained (CH_2Cl_2, 50:1 [monomer]:[initiator] ratio). While very active the {(EDBP-H)-Li(BnOH)}$_2$ dimeric complex also displays good control over the ROP of *L*-lactide with linear correlation between molecular weight and monomer-to-initiator ratio alongside narrow PDI values (PDI = 1.04 – 1.16). Introduction of benzyl alcohol as a co-initiator revealed a dependency of molecular weight upon the benzyl alcohol (BnOH) ratio. The monomeric species {(EDBP-H)Li(BnOH)(THF)$_2$} was also proven to be a highly active initiator for *L*-lactide polymerisation although it was shown to be less active than its dimeric counterpart {(EDBP-H)-Li(BnOH)}$_2$. Furthermore, it was speculated that THF hinders the coordination of *L*-lactide units about the lithium metal centre.[61]

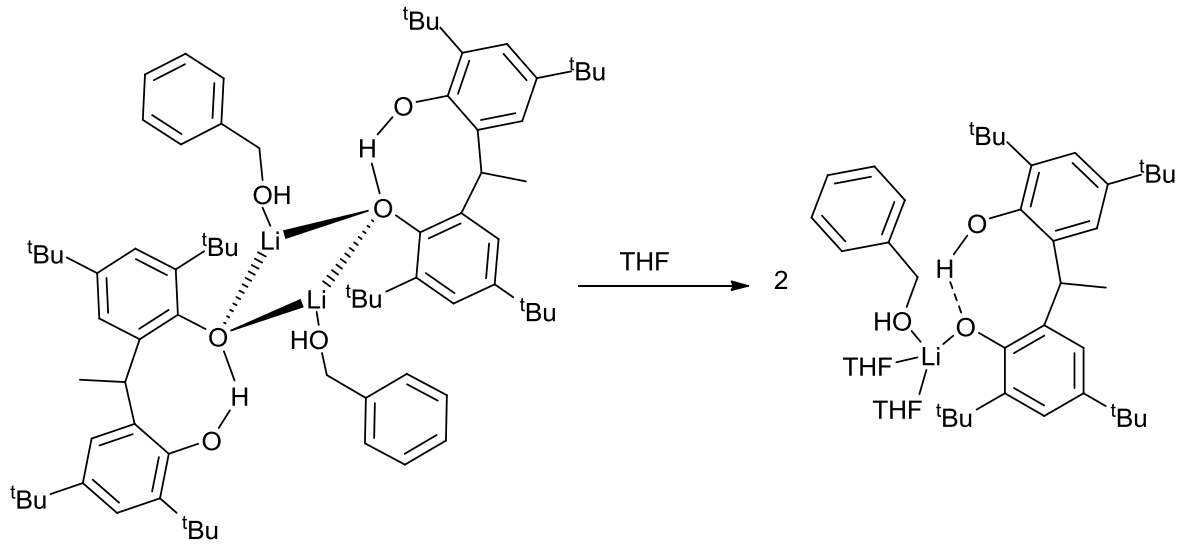

Figure 1.24: Diagram showing 2,2'-ethylidenebis(4,6-di-*tert*-butylphenol) lithium benzyl alcohol dimer {(EDBP-H)-Li(BnOH)}$_2$, and related THF derived lithium monomer {(EDBP-H)Li(BnOH)(THF)$_2$}.[61]

1.3.3 Group 2 initiators

Magnesium β-diketiminate (BDI) complexes have been thoroughly studied for the ROP of lactide by Chisholm *et al*. alongside the corresponding calcium complexes.[36, 62-65] Magnesium BDI alkoxides were obtained as dimers {Mg_2(**6**)$_2$(O^iPr)$_2$} bridged by alkoxide groups (Figure 1.25) and have been proven to

be highly active initiators for the ROP of *rac*-lactide, achieving complete conversion after 2 mins at 20 °C (CH_2Cl_2) with a 200:1 [monomer]:[initiator] ratio.[36] While the magnesium BDI complex $Mg_2(\mathbf{6})_2(^iPr)_2$ is one of the most active initiators within the literature it showed a limited degree of control, affording molecular weights ~ 2.5 times the predicted value and moderately broad PDI values of 1.59. Chisholm *et al*. speculated this reduced level of control is a consequence of a slow initiation rate compared to the rate of propagation.[36] Interestingly the addition of a catalytic equivalent of 2-propanol significantly enhances the molecular weight control within the polymerisation giving lower PDI values of 1.29 under the same conditions. The dimeric magnesium BDI complexes do not exhibit stereocontrol over the ROP of *rac*-lactide.

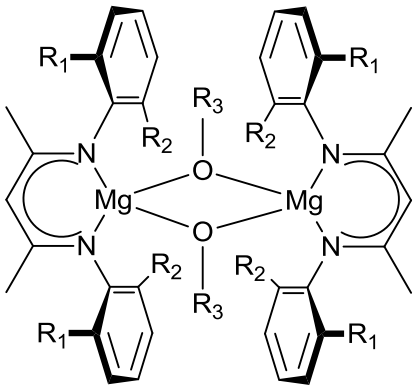

$Mg_2(\mathbf{6})_2(O^iPr)_2$ $R_1 = R_2 = {}^iPr$, $R_3 = {}^iPr$
$Mg_2(\mathbf{7})_2(O^iPr)_2$ $R_1 = O^iPr$, $R_2 = H$, $R_3 = {}^tBu$

Figure 1.25: Magnesium BDI complexes for the ROP of lactide.[36, 62]

Magnesium BDI complexes are still active for the ROP of *rac*-lactide upon variation of the aromatic groups, a notable variation is the introduction of ether groups on the aromatic ring $\{Mg_2(\mathbf{7})_2(O^iPr)_2\}$ (Figure 1.25).[62] Structurally the magnesium BDI complex $Mg_2(\mathbf{7})_2(O^iPr)_2$ is a dimer like $Mg_2(\mathbf{6})_2(^iPr)_2$, NMR spectroscopic evidence suggests the ether groups are in a fluxional coordination state with the magnesium metal centre. Magnesium BDI complex $Mg_2(\mathbf{7})_2(O^iPr)_2$ was less active than $Mg_2(\mathbf{6})_2(^iPr)_2$ achieving 91 % conversion after 20 mins at 20 °C (CH_2Cl_2) with a 100:1 [monomer]:[initiator] ratio. While less active there is also a decrease in molecular weight control, yielding ~7.5 times higher molecular weight than predicted with a high PDI value (PDI = 2.23). Although poor molecular weight control was observed with $Mg_2(\mathbf{7})_2(O^iPr)_2$ it displayed enhanced stereoselectivity control over the ROP of *rac*-lactide (P_r = 0.61). Changing the solvent has a profound

effect upon the ROP of lactide.[62] Using THF as the solvent lowered the activity of the reaction {90 % conversion, 90 mins, 20 °C (THF) with a 100:1 [monomer]:[initiator] ratio}, while also enhancing molecular weight control and heterotactic stereoselectivity (P_r = 0.90) Ether and THF affect the ROP of lactide by reversibly coordinating to the magnesium metal, this creates a competitive coordination environment for lactide monomers. Due to coordinating THF or ethers the magnesium metal is less accessible thus creating stereoselective demands for a coordinating lactide.

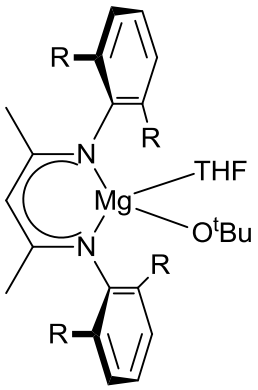

Mg(**8**)O^{t}Bu.THF R = ^{i}Pr

Figure 1.26: Magnesium BDI complexes with coordinated THF.

Chisholm also isolated monomeric magnesium BDI complexes with coordinated THF, one such is complex Mg(**8**)O^{t}Bu.THF (Figure 1.26).[63, 64] The active propagation species within the ROP of *rac*-lactide is a dimeric species {Mg(**8**)(lactide)}$_2$ similar to the complex Mg$_2$(**6**)$_2$(O^{i}Pr)$_2$. As a result of the labile THF and the nature of the active propagation species the ROP of *rac*-lactide by Mg(**8**)O^{t}Bu.THF did not significantly vary from Mg$_2$(**6**)$_2$(O^{i}Pr)$_2$. If THF was used as the solvent a noteworthy increase in stereoselectivity was observed (P_r = 0.93). THF also decreased the activity of the polymerisation of *rac*-lactide yielding 95 % conversion after 5 mins at 20 °C at 100:1 [monomer]:[initiator] ratio.

β-diketiminate ligands were also complexed to calcium and trialled as *rac*-lactide ROP initiators. NMR spectroscopic evidence suggests the calcium BDI complex {Ca(**8**)N(SiMe$_3$)$_2$.THF} (Figure 1.27) is unstable as a monomer and a plethora of species are present in solution. The complex was still shown to be highly active towards the ROP of lactide yielding atactic PLA up to 90 % conversion after 2 h at room temperature (THF) with a 200∶1 [lactide]:[initiator] ratio.[66]

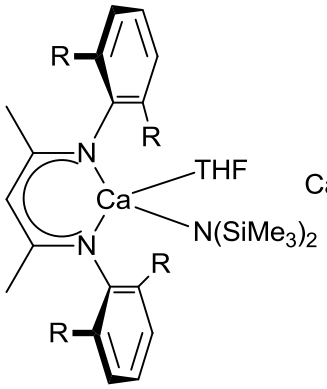

Ca(**8**)N(SiMe$_3$)$_2$.THF R = ^{i}Pr

Figure 1.27: Monometallic BDI calcium complexes with coordinated THF.

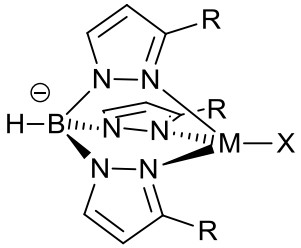

Mg(**9**)OEt R = ^{t}Bu
Ca(**9**)N(SiMe$_3$)$_2$ R = ^{t}Bu
Ca(**9**)O-2,6-^{i}Pr$_2$C$_6$H$_3$ R = ^{t}Bu
Ca(**10**^{a})O-2,6-^{i}Pr$_2$C$_6$H$_3$ R = ^{i}Pr

Figure 1.28: Group 2 tris-pyrazolyl borate complexes for the ROP of lactide.

A tris(3-*tert*-butylpyrazolyl)borate magnesium alkoxide complex {Mg(**9**)OEt} (Figure 1.28) was investigated for the ROP of lactide and has proven to be a highly active initiator, akin to other magnesium initiators.[67, 68] The magnesium tris-pyrazolyl borate complex Mg(**9**)OEt resulted in 90 % conversion of *L*-lactide after 1 h (20 °C, CH_2Cl_2, 500:1 [monomer]:[initiator] ratio). While a highly active initiator Mg(**9**)OEt also displayed good molecular weight control exhibiting linear relationship of M_n with conversion, a PDI value of ~1.2 is maintained up to a 1000:1 [monomer]:[initiator] ratio.[67] Mg(**9**)OEt showed a significant preference towards the ROP of *meso*-lactide over *rac*-lactide. A chiral tris-pyrazolyl borate magnesium complex was also synthesised and determined to give a 25 % preference for syndiotactic PLA from *meso*-lactide.[68]

Chisholm *et al*. have utilised tris-pyrazolyl borate ligands for complexation to calcium and further investigated these complexes for the ROP of *rac*-lactide.[65, 66] Both the tris-pyrazolyl borate calcium complexes Ca(**9**,**10**)O-2,6-^{i}Pr$_2$C$_6$H$_3$ were isolated as five coordinate metal complexes (Figure 1.28), with THF completing the coordination sphere. With prolonged heating and reduced pressure the coordinated

THF was removed to yield the four coordinate complex Ca(**9**)O-2,6-$^{i}Pr_2C_6H_3$ (Figure 1.28). This calcium complex is highly active towards the ROP of *rac*-lactide achieving 90 % conversion within 1 min (RT, THF, 200:1 [monomer]:[initiator] ratio). Introduction of an amide {Ca(**9**)$N(SiMe_3)_2$} as the initiating group did not have a detrimental effect on the rate of propagation for *rac*-lactide, under the same conditions. Initiators Ca(**9**)$N(SiMe_3)_2$, and Ca(**9**,**10**)O-2,6-$^{i}Pr_2C_6H_3$ are all highly active initiators for *rac*-lactide ROP but they exhibited moderate molecular weight control (PDI = 1.61 – 1.74). Both of these calcium initiators showed a high degree of heterotactic stereoselectivity in THF at room temperature (P_r > 0.93). The stereoselectivity was influenced by the steric demands of the HB(3-^{t}Bupz)$_3$ ligand as introduction of less sterically demanding groups, demonstrated by Ca(**10**)O-2,6-$^{i}Pr_2C_6H_3$, afforded atactic PLA under the same ROP conditions.

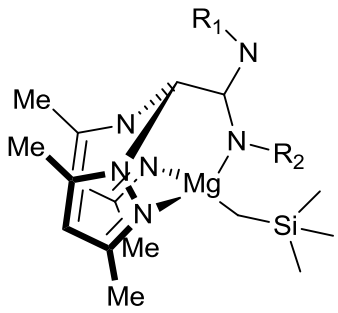

Mg(**11**)CH_2SiMe_3 $R_1 = R_2 = {}^{i}Pr$
Mg(**12**)CH_2SiMe_3 R_1 = Et, $R_2 = {}^{t}Bu$

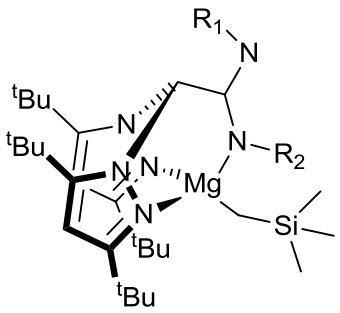

Mg(**13**)CH_2SiMe_3 $R_1 = R_2 = {}^{i}Pr$
Mg(**14**)CH_2SiMe_3 R_1 = Et, $R_2 = {}^{t}Bu$
Mg(**15**)CH_2SiMe_3 $R_1 = {}^{t}Bu$, R_2 = Et

Figure 1.29: Magnesium Scorpionate complexes used as initiators for the ROP of lactide.[69, 70]

Magnesium scorpionate complexes were investigated for the ROP of *rac*-lactide by Sánchez-Barba *et al.*[69, 70] Mg(**12**)CH_2SiMe_3 was identified as the isomer (Figure 1.29), while the analogous complexes {Mg(**14**,**15**)CH_2SiMe_3} are isomers of each other. The less sterically bulky magnesium scorpionate complexes undergo a rearrangement at high temperature (90 °C, 4 days) to form "sandwich" complexes with two scorpionate ligands per metal.[69] The methyl substituted magnesium scorpionate complexes Mg(**11**,**12**)CH_2SiMe_3 are significantly less active towards the ROP of *rac*-lactide than other reported magnesium complexes Mg_2(**6**,**7**)$_2$(^{i}Pr)$_2$, Mg(**8**)O^{t}Bu.THF, and Mg(**9**)OEt {Mg(**11**)CH_2SiMe_3, 42 %, 72 h, 70 °C, toluene, 100:1 [*rac*-lactide]:[initiator] ratio, PDI = 1.09}{Mg(**12**)CH_2SiMe_3,

31 %, 72 h, 70 °C, toluene, 100:1 [*rac*-lactide]:[initiator] ratio, PDI = 1.09}. Although less active for the ROP of lactide both magnesium complexes Mg(**11**,**12**)CH_2SiMe_3 gave good control over the polymerisation showing molecular weights (M_n) close to predicted values and low PDI values (PDI = 1.09), also an experiment with *L*-lactide revealed no epimerisation of the PLA chains. Addition of a catalytic equivalent of isopropanol as a co-initiator enhanced the activity of Mg(**12**)CH_2SiMe_3 (54 %, 48 h) under the same conditions, while slightly broadening the resulting PLA molecular weights (PDI = 1.13). These less sterically bulky magnesium scorpionate complexes {Mg(**11**,**12**)CH_2SiMe_3} afforded no stereoselectivity. It should be noted that magnesium complexes {Mg(**11**,**12**)CH_2SiMe_3} were also very active initiators for the ROP of caprolactone.[69]

The more sterically bulky magnesium scorpionate complexes Mg(**13-15**)CH_2SiMe_3 investigated by Sánchez-Barba *et al.*[70] proved more stable in solution than Mg(**11**,**12**)CH_2SiMe_3 complexes,[69] with no evidence of ligand rearrangement into "sandwich" complexes. As noted above Mg(**14**,**15**)CH_2SiMe_3 are isomers with each other and were synthesised with a relative isomeric ratio of 3:7, where the magnesium isomer Mg(**15**)CH_2SiMe_3 was the dominant product. Isomers Mg(**14**,**15**)CH_2SiMe_3 were individually isolated before investigation for the ROP of lactide and alongside magnesium complex Mg(**15**)CH_2SiMe_3 were revealed as highly active initiators for the ROP of *rac*-lactide. Magnesium complexes Mg(**13**,**15**)CH_2SiMe_3 achieved 49 % - 51 % conversion after 2 minutes (0 °C, THF, 100:1 [*rac*-lactide]:[initiator] ratio) with excellent molecular weight distributions (PDI < 1.03), additionally polymerisation of *L*-lactide showed no epimerisation was. The sterically bulky magnesium scorpionate complexes {Mg(**13-15**)CH_2SiMe_3} yielded heterotactic PLA from *rac*-lactide (P_r = 0.70 – 0.79). Reducing the temperature slightly increased the selectivity, the isomer Mg(**14**)CH_2SiMe_3 afforded the highest selectivity with P_r = 0.79 at 0 °C.

The hybrid scorpionate/cyclopentadienyl magnesium complex shown in figure 1.30 was trialled for the ROP of *L*-lactide and *rac*-lactide.[71] This hybrid scorpionate/cyclopentadienyl magnesium complex was an active initiator for the ROP of *L*-lactide affording 97 % conversion after 2.5 h (90 °C, toluene, 200:1 [monomer]:[initiator] ratio), with good molecular weight control and low PDI values

(PDI = 1.05), and no epimerisation occurs. The ROP of *rac*-lactide was revealed to be less active under the same conditions yielding 59 % conversion after 8 h for the ROP of *rac*-lactide. Similar molecular weight control (PDI = 1.12) and a very slight heterotactic bias was reported. The hybrid scorpionate/cyclopentadienyl magnesium complex was tested for the "bulk" ROP of *rac*-lactide and a 41 % conversion was observed after 2 h, alongside a decrease in molecular weight control (PDI = 1.41). The hybrid scorpionate/cyclopentadienyl magnesium complex is comparable to the less sterically bulky magnesium scorpionate complexes Mg(**11**,**12**)CH_2SiMe_3,[69] but far less active than the bulky magnesium scorpionates Mg(**13-15**)CH_2SiMe_3.[70]

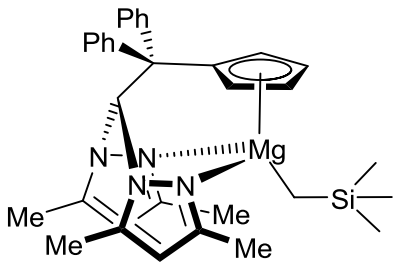

Figure 1.30: Hybrid scorpionate/cyclopentadienyl magnesium complex utilised as an initiator for the ROP of lactide.[71]

Lin *et al*. studied NNO-tridentate ketiminate magnesium complexes and demonstrated that they initiate the ROP of *rac*-lactide and *L*-lactide with high activities (Figure 1.31).[72] Magnesium complex {Mg(**16**)OBn}$_2$ afforded 90 % conversion of *rac*-lactide after 12 h, whereas the less active derivative {Mg(**17**)OBn}$_2$ afforded 96 % conversion after 25 h under the same conditions (30 °C, THF, 100:1 [monomer]:[initiator] ratio). Both initiators displayed good molecular weight control with average chain lengths consistent with each dimeric initiator propagating two PLA chains. Small variance of chain length was also observed with PDI values of 1.10 and 1.13 for {Mg(**16**,**17**)OBn}$_2$ respectively, under the conditions stated above. Magnesium NNO-tridentate ketiminate complexes displayed heterotactic selectivity, {Mg(**16**)OBn}$_2$ gave a P_r of 0.85 (30 °C in THF), complex {Mg(**17**)OBn}$_2$ gave a reduced P_r of 0.54 (30 °C in THF). Further ROP studies on {Mg(**16**)OBn}$_2$ have shown stereoselectivity is reduced upon changing the solvent to CH_2Cl_2 (P_r = 0.64). Stereoselectivity of {Mg(**16**)OBn}$_2$ was further

enhanced (P_r = 0.87) by reducing the temperature at the expense of activity (61 %, 0 °C, THF, 100:1 [monomer]:[initiator] ratio).

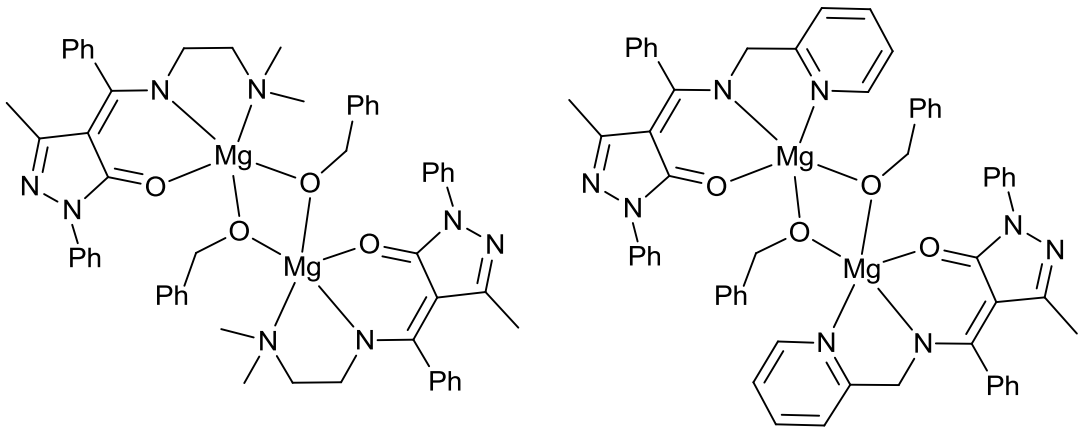

Figure 1.31: NNO-tridentate ketiminate magnesium complexes investigated as initiators for the ROP of lactide.[72]

1.3.4 Group 3 and lanthanide initiators

Group 3 and lanthanide metal complexes have been shown to initiate the ring opening polymerisation of lactide.[73, 74] Early investigation of yttrium alkoxides revealed them as highly active potential initiators. The commercially available $Y_5(\mu\text{-O})(O^iPr)_{13}$ cluster species was trialled for the ROP of lactide but it took days to obtain appreciable conversion.[73, 75] The monometallic tris(2,6-di-*tert*-butylphenoxy)yttrium species was shown to ring-open *L*-lactide, albeit comparatively slowly reaching full conversion after 10 h.[74] End group analysis of PLA resulting from tris(2,6-di-*tert*-butylphenoxy)yttrium initiation was indeterminate and no single end-group was detected, it was further speculated that impurities and solvents are mechanistically important for the ROP of lactide.[74] Tris(2,6-di-*tert*-butylphenoxy)yttrium activity towards the polymerisation of *L*-lactide is significantly enhanced in the presence of a less sterically hindered alcohol co-initiator, with an isopropanol co-initiator 100 % conversion was obtained after 2 mins at 22 °C at 50:1:0.3 [monomer]:[alcohol]:[initiator] ratio. The resulting PLA revealed well defined molecular weights (PDI = 1.24) alongside identification of isopropoxide end-groups. It was deduced that tris(2,6-di-*tert*-butylphenoxy)yttrium with isopropanol as a co-initiator proceeds *via* a fast exchanging yttrium isopropoxide

intermediate (Figure 1.32),[73, 74] which is not readily accessible to the bridging oxide yttrium cluster compound $Y_5(\mu\text{-}O)(O^iPr)_{13}$.

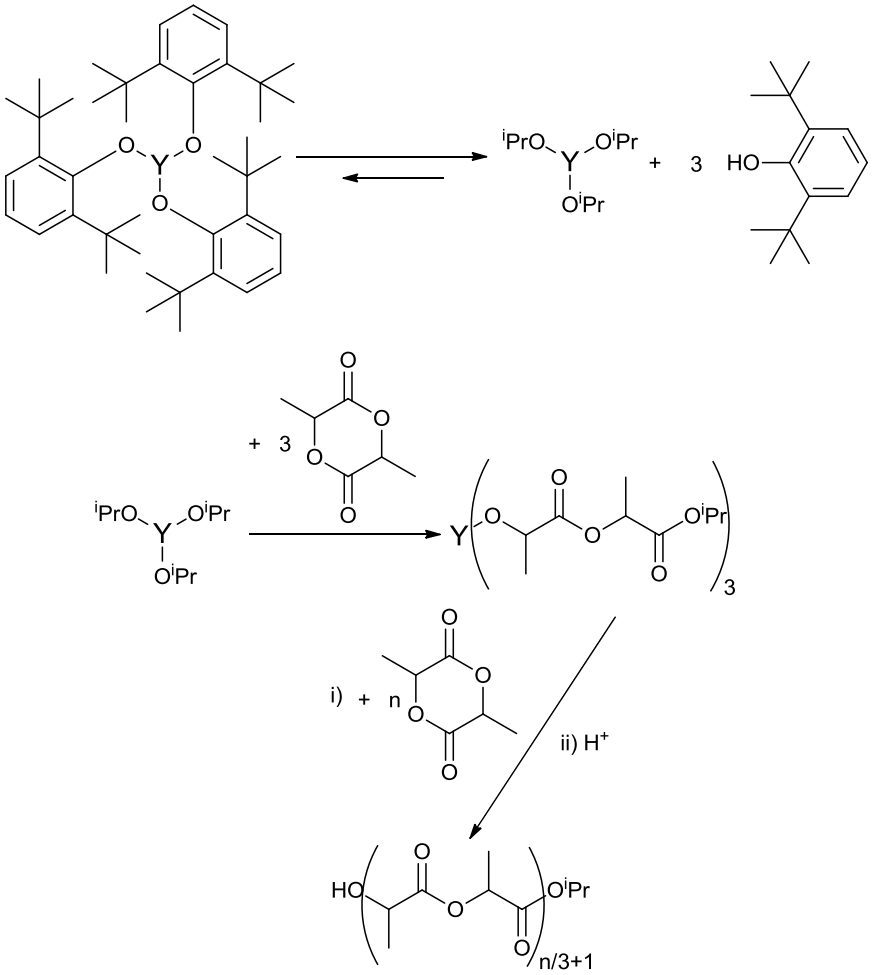

Figure 1.32: Reaction scheme depicting the ROP mechanism of lactide by tris(2,6-di-*tert*-butylphenoxy)yttrium with isopropanol as a co-initiator.[73, 74]

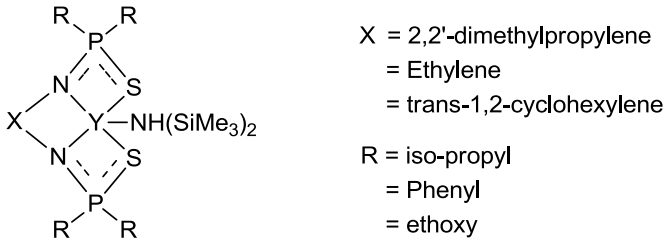

Figure 1.33: Bis(thiophosphinic amido)yttrium initiators investigated for the ring-opening polymerisation of lactide.[76]

Williams *et al*. reported bis(thiophosphinic amido)yttrium initiators as active candidates for the ROP of *rac*-lactide.[76] It was shown that the backbone (X group) had little effect on the ROP polymerisation of *rac*-lactide, whereas the phosphorus moieties (R groups) had a profound influence (Figure 1.33). Steric influence had a minimal effect on the activity of the yttrium initiator. Sterically iso-propyl and phenyl are similar but a significant difference in activity was observed (R = iso-propyl, > 90 % conversion, 3.7-6.8 mins, 25 °C, CH_2Cl_2, 200:1 [monomer]:[initiator] ratio) (R = phenyl, > 90 % conversion, 25-90 mins, 25 °C, CH_2Cl_2, 200:1 [monomer]:[initiator] ratio). It was deduced that the polymerisation reaction proceeds by a coordination insertion mechanism where the insertion step is rate limiting. An electron withdrawing phosphorus substituent increases the Lewis acidity of the yttrium metal and consequently increases the metal alkoxide bond strength, therefore hindering the insertion of a new lactide molecule. This justifies the experimental ROP activity for this series of yttrium initiators where iso-propyl > phenyl > ethoxy. ROP reactions revealed a linear relationship between molecular weight and conversion for all the bis(thiophosphinic amido)yttrium derivatives. From MALDI-TOF mass spectrometry it was determined that significant transesterification was occurring resulting in high PDI values (PDI > 1.5). A heterotactic bias was observed for bis(thiophosphinic amido)yttrium complexes with ethoxy phosphorus groups (X = ethylene, R = ethoxy, P_r = 0.68)(X = *trans*-1,2-cyclohexylene, R = ethoxy, P_r = 0.79).[76] This stereoselectivity was attributed to the hemilabile ethoxy exerting coordination geometry control over the active yttrium metal.

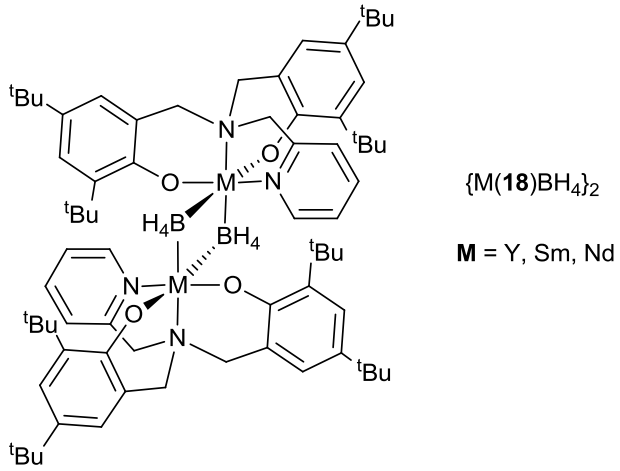

Figure 1.34: Group 3 and lanthanide diaminobis(phenoxide) borohydride complexes trialled for the ROP of *L*-lactide and *rac*-lactide.[77]

Group 3 and lanthanide borohydride complexes utilising diaminobis(phenoxide) ligands {Y(**18**)BH_4}$_2$, {Sm(**18**)BH_4}$_2$, and {Nd(**18**)BH_4}$_2$ were investigated by Mountford *et. al*. for the ROP of *L*-lactide and *rac*-lactide.[77] The complexes were identified as dimers (Figure 1.34), the Sm complex {Sm(**18**)BH_4}$_2$ has the structure depicted, the Y dimer {Y(**18**)BH_4}$_2$ contained an additional coordinated THF, and the Nd dimeric complex {Nd(**18**)BH_4}$_2$ contained two coordinated THF moieties (one THF per metal). Complexes ({Y(**18**)BH_4}$_2$, {Sm(**18**)BH_4}$_2$, and {Nd(**18**)BH_4}$_2$) were active at room temperature for the ROP of *L*-lactide and *rac*-lactide. Kinetic experiments revealed a first order dependence on *rac*-lactide concentration where the order of activity is {Sm(**18**)BH_4}$_2$ > {Y(**18**)BH_4}$_2$ > {Nd(**18**)BH_4}$_2$. Complexes {Y(**18**)BH_4}$_2$ and {Sm(**18**)BH_4}$_2$ typically polymerised *rac*-lactide to ~70 % conversion after 1 h (25 °C, THF, 200:1 [*rac*-lactide]:[initiator] ratio), whereas the neodymium complex {Nd(**18**)BH_4}$_2$ achieved 33 % conversion after 2 h under the same conditions. THF promotes the activity of these complexes, as a result using toluene at elevated temperature (70 °C) revealed a significant reduction in initiator activity for the ROP of *rac*-lactide. PLA resulting from these diaminobis(phenoxide) lanthanide complexes displayed a significant degree of transesterification with lower molecular weights than expected and broader molecular weight distributions (PDI = 1.41 – 1.59). The samarium bimetallic complex {Sm(**18**)BH_4}$_2$ displayed the greater molecular weight control. PLA resulting from initiation of *rac*-lactide by yttrium and samarium complexes ({Y(**18**)BH_4}$_2$ and {Sm(**18**)BH_4}$_2$) revealed a heterotactic bias {P_r {Y(**18**)BH_4}$_2$ = 0.87, P_r {Sm(**18**)BH_4}$_2$ = 0.72}. A significant decrease in activity of initiators {Y(**18**)BH_4}$_2$ and {Sm(**18**)BH_4}$_2$ was reported when utilised for the ROP of *L*-lactide, which is consistent with their preference in producing heterotactic PLA. The heterotactic selectivity of complexes {Y(**18**)BH_4}$_2$ and {Sm(**18**)BH_4}$_2$ was shown to be dependent on either the solvent and temperature of the polymerisation.[77]

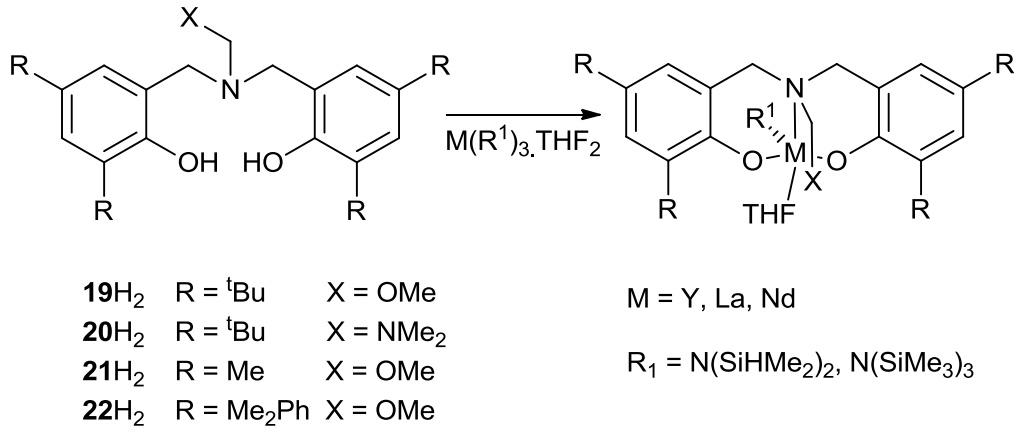

Figure 1.35: Scheme representing the synthesis of a selection of lanthanide and group 3 complexes supported by alkoxy-amino-bis(phenolate) ligands.[78, 79]

Carpentier *et. al*. synthesised a series of group 3 and lanthanide complexes derived from alkoxy-amino-bis(phenol) ligands (Figure 1.35). Furthermore these alkoxy-amino-bis(phenoxy) lanthanide complexes were investigated for the ROP of *rac*-lactide under various conditions.[78, 79] Initially the complexes Y(**19**)N(SiHMe$_2$)$_2$.THF and La(**19**)N(SiHMe$_2$)$_2$.THF were reported as highly active initiators for the ROP of *rac*-lactide, where the yttrium initiator achieved full conversion within 1 h at room temperature at a 500:1 [monomer]:[initiator] ratio.[78] The synthesised yttrium, lanthanum, and neodymium amides based on ligands (**19**-**22**)H$_2$ ROP *rac*-lactide in THF to 100 % conversion within 20 mins at 200:1 [*rac*-lactide]:[initiator] ratio.[79] Lanthanide complexes of these alkoxy-amino-bis(phenol) ligands polymerise lactide in a living manner with molecular weights consistent with one PLA chain per metal centre and narrow molecular weights (PDI = 1.19 – 1.34). The molecular weight distribution was slightly higher than expected for a truly living polymerisation, which was attributed to transesterification side reactions. Initially PLA derived from initiators Y(**19**)N(SiHMe$_2$)$_2$.THF and La(**19**)N(SiHMe$_2$)$_2$.THF revealed a heterotactic bias giving P_r = 0.80 for Y(**19**)N(SiHMe$_2$)$_2$.THF, and P_r = 0.65 for La(**19**)N(SiHMe$_2$)$_2$.THF. A solvent comparison between toluene and THF proved that THF is necessary to obtain heterotactic PLA. Substituting the methoxy group for an amide {Y(**20**)N(SiHMe$_2$)$_2$.THF} has minimal effect on the activity but a profound effect on the stereoselectivity yielding PLA with a reduced P_r = 0.60. This is to be expected as the structure of Y(**20**)N(SiHMe$_2$)$_2$.THF is ambiguous.

Y(**21**)N(SiHMe$_2$)$_2$.THF initiated the ROP of *rac*-lactide to yield PLA with a P_r = 0.56. One suggested reason for this decrease in heterotactic selectivity, was the structural ambiguity due to a formation of aggregates. Secondly, the reduction in steric bulk about the active metal centre imparts less coordination geometry control over the active metal-lactide propagating species. The highest heterotactic stereoselectivity (P_r = 0.90) for this series of complexes was achieved by the complex Y(**22**)N(SiHMe$_2$)$_2$.THF. By the same principle the bulky –Me$_2$Ph group imparts additional steric control over the yttrium metal centre enhancing coordination geometry control over the active metal-lactide propagating species. The larger metals La and Nd result in less heterotactic stereoselectivity due to less steric control, P_r {La(**19**)N(SiHMe$_2$)$_2$.THF} = 0.65, P_r {Nd(**19**)N(SiMe$_3$)$_2$.THF} = 0.49. The addition of isopropanol as a co-initiator to the ROP of *rac*-lactide by yttrium initiators {Y(**19**)N(SiHMe$_2$)$_2$.THF, Y(**22**)N(SiHMe$_2$)$_2$.THF} was shown to yield narrower PLA chain distribution (PDI = 1.06 – 1.24). Stereoselectivity was retained upon addition of isopropanol. Addition of excess isopropanol is directly proportional to the PLA average chain length. Furthermore isopropanol is an effective chain transfer agent within the polymerisation reactions as the presence of cyclic esters was not detected.

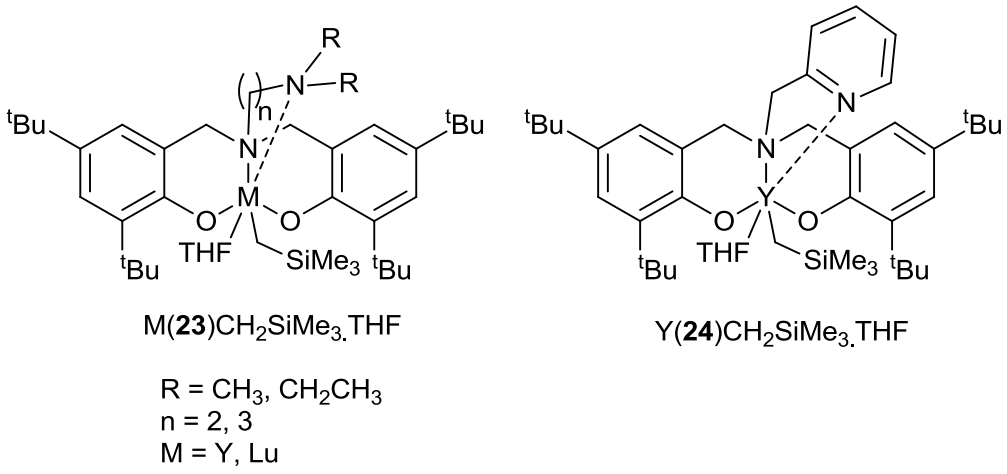

Figure 1.36: Further group 3 and lanthanide diamino-bis(phenoxy) complexes utilised for the ROP of *rac*-lactide.[80]

Following on from Mountford's[77] and Carpentier's[78, 79] work, Cui *et al.*[80] investigated further diamino-bis(phenoxy) derivatives complexed to group 3 and lanthanide metal alkys and investigated these for the ROP of lactide (Figure 1.36).

Y/Lu(**23**)CH_2SiMe_3.THF and Y(**24**)CH_2SiMe_3.THF were very active initiators for the ROP *rac*-lactide achieving > 90 % conversion after 1 h (20 °C, THF, 300:1 [monomer]:[initiator] ratio). Y(**23**)CH_2SiMe_3.THF and Lu(**23**)CH_2SiMe_3.THF displayed similar activities although by increasing the amide alkyl chain tether (n = 3) the yttrium complex became inactive for the ROP of *rac*-lactide at 20°C, showing no conversion after 6 h under the same conditions. Molecular weights showed some variance from the predicted values and moderate PDI values were obtained (PDI = 1.32 – 1.59). The yttrium and lutetium complexes {Y/Lu(**23**)CH_2SiMe_3.THF} (excluding when n = 3) yielded elevated heterotacticity, P_r > 0.94, from the ROP of *rac*-lactide. Y(**23**)CH_2SiMe_3.THF also yielded heterotactic PLA under the same conditions giving a P_r = 0.90. It was shown that THF as the ROP solvent enhances the heterotactic stereoselectivity. X-ray determined complexes Y/Lu(**23**)CH_2SiMe_3.THF (for n = 2) adopted a twisted octahedral geometry about the metal. Y(**24**)CH_2SiMe_3.THF adopted a less twisted octahedral geometry. A trend was revealed where a more twisted octahedral geometry about the metal resulted in higher activity and stereoselectivity.

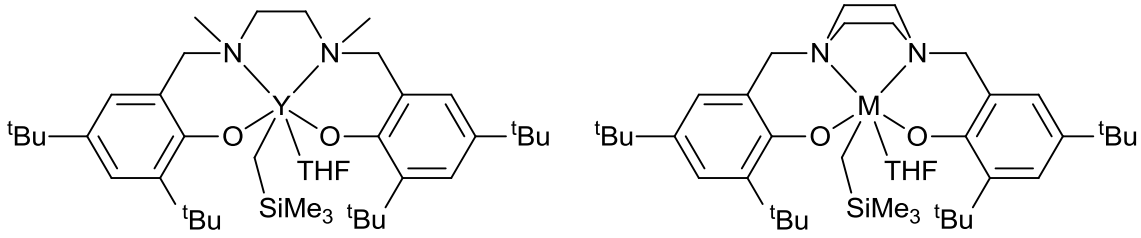

Y(**25**)CH_2SiMe_3.THF

M(**26**)CH_2SiMe_3.THF
M = Y, Lu, Yb, Gd

Figure 1.37: Group 3 and lanthanide salan[80] and piperazine salan[81] complexes investigated for the polymerisation of lactide.

The yttrium salan complex {Y(**25**)CH_2SiMe_3.THF} (Figure 1.37) was synthesised and investigated for the ROP of *rac*-lactide it was shown to be highly active resulting in > 100 % conversion after 1 h (20 °C, THF, 300:1 [monomer]:[initiator] ratio).[80] Unlike the analogous aluminium salan {see figure 1.63, Al(**90**)Me}[82] Y(**25**)CH_2SiMe_3.THF gave little polymerisation control (PDI = 1.64) and a small degree of heterotactic stereoselectivity was observed (P_r = 0.65).

Group 3 and lanthanide metals were complexed to piperazine salan ligands (Figure 1.37) and investigated for the ROP of *L*-lactide and *rac*-lactide.[81] For all the listed metals (Figure 1.37) a monometallic complex was obtained with the piperazine salan ligand (**26**H_2), where the piperazine ring adopted a boat configuration. The lanthanide complexes M(**26**)CH_2SiMe_3.THF displayed very high activity for the ROP of *L*-lactide achieving 97 % conversion within 4 minutes (70 °C, toluene, 700:1 [monomer]:[initiator] ratio). Molecular weights were consistent with one chain per metal although some deviation was reported, PDI was dependent upon the metal {PDI (Yb) = 1.12 – 1.15, PDI (Y) = 1.12 – 1.25, PDI (Lu) = 1.27 – 1.41, PDI (Gd) = 1.21 – 1.40}. Only the yttrium complex Y(**26**)CH_2SiMe_3.THF was reported for the ROP of *rac*-lactide, it was shown to ROP *rac*-lactide to 100 % conversion within 2 h (20 °C, THF, 700:1 [monomer]:[initiator] ratio). Although an active initiator towards the ROP of *rac*-lactide Y(**26**)CH_2SiMe_3.THF yielded much broader molecular weight distribution than reported for *L*-lactide, with a PDI = 1.61 for *rac*-lactide under the above conditions. Alongside broader PDI values little stereocontrol was observed, P_r = 0.48 – 0.61.

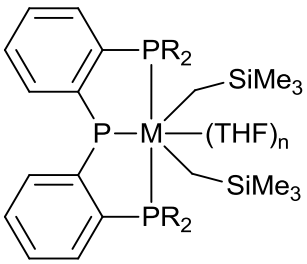

Y(**27**)$(CH_2SiMe_3)_2$.THF R = ^{i}Pr
Y(**28**)$(CH_2SiMe_3)_2$.THF R = Ph
Sc(**27**)$(CH_2SiMe_3)_2$.THF R = ^{i}Pr
Sc(**28**)$(CH_2SiMe_3)_2$.THF_2 R = Ph

Figure 1.38: Group 3 complexes bound to phosphido-diphosphine pincer ligands used as initiators for the ROP of lactide.[83]

Complexes of group 3 metals utilising phosphido-diphosphine pincer ligands have been reported as initiators for the ROP of lactide (Figure 1.38).[83] The yttrium initiator displayed a high activity towards the ROP of lactide at room temperature. The yttrium initiator Y(**27**)$(CH_2SiMe_3)_2$.THF achieved 65 % conversion after 15 mins (THF) at 20 °C with a 200:1 [monomer]:[initiator] ratio. By introducing less electron donating substituents to the phenyl ring {Y(**28**)$(CH_2SiMe_3)_2$.THF} the yttrium metal becomes more Lewis acidic. This caused an enhancement in activity where initiator Y(**28**)$(CH_2SiMe_3)_2$.THF gave a conversion of 92 % after 15 mins

under the same conditions. The scandium initiators were much slower with Sc(**27**)(CH_2SiMe_3)$_2$.THF achieving 38 % conversion after 20 h under the same conditions, this was attributed to scandium being a smaller metal hindering lactide coordination and further lactide insertion. Despite two possible initiation sites per metal it was revealed that at room temperature phosphido-diphosphine complexes of group 3 metals propagate one PLA chain per metal centre. They displayed good control over molecular weight being almost a controlled living polymerisation. Molecular weight distributions of the resulting polymers were relativity low with PDI values between 1.20 - 1.28 for initiators Y(**27**,**28**)(CH_2SiMe_3)$_2$.THF and Sc(**27**)(CH_2SiMe_3)$_2$.THF under the above conditions. The deviation from a controlled living polymerisation (PDI < 1.10) was acknowledged as transesterification side reactions. PLA resulting from the ROP of *rac*-lactide by the yttrium initiators Y(**27**,**28**)(CH_2SiMe_3)$_2$.THF was identified as having a heterotactic bias, with respective P_r {Y(**27**)(CH_2SiMe_3)$_2$.THF} = 0.63, P_r {Y(**28**)(CH_2SiMe_3)$_2$.THF} = 0.64. Scandium initiators {Sc(**27**)(CH_2SiMe_3)$_2$.THF and Sc(**28**)(CH_2SiMe_3)$_2$.THF_2} revealed a heterotactic bias, with respective P_r {Sc(**27**)(CH_2SiMe_3)$_2$.THF} = 0.60 and P_r {Sc(**28**)(CH_2SiMe_3)$_2$.THF_2} = 0.62. Solvent free conditions (130 °C) complicated the ROP of lactide, typically showing broader PDI values and as each yttrium metal propagated two PLA chains at the highly elevated temperature.

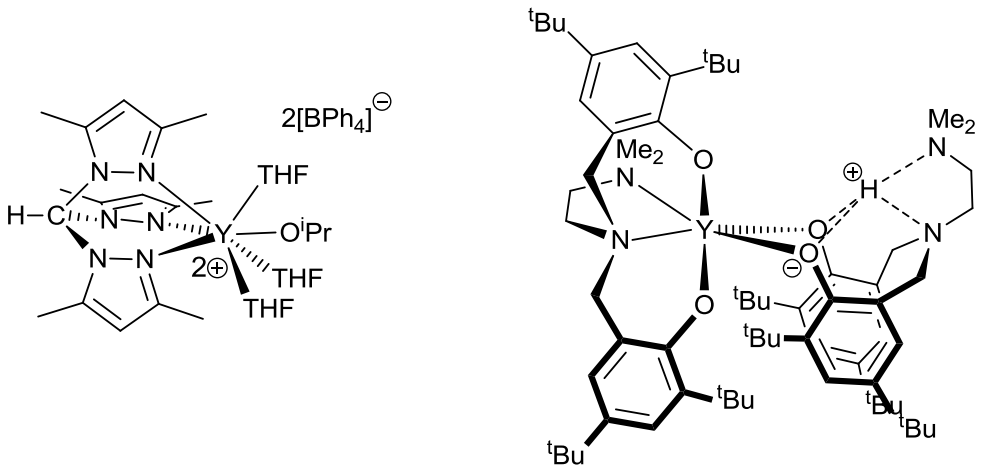

$[Y(\mathbf{29})O^{i}Pr.THF_3]^{2+}$ 2[BPh]$^{-}$ $Y(\mathbf{30})_2H$

Figure 1.39: A dicationic yttrium complex and a zwitterionic yttrium complex synthesised and trialled for the ROP of *rac*-lactide.[84]

Dicationic and zwitterionic yttrium complexes were synthesised by Mountford *et. al.*[84] who investigated their properties as initiators for the ROP of *rac*-lactide (Figure 1.39). The dicationic yttrium complex {$[Y(\mathbf{29})O^{i}Pr.THF_3]^{2+}$ 2[BPh]$^{-}$} was moderately active towards the ROP of *rac*-lactide yielding high conversions after 12 h (70 °C, 100:1:5 [monomer]:[initiator]:[co-initiator]). The direct polymerisation of *rac*-lactide by $[Y(\mathbf{29})O^{i}Pr.THF_3]^{2+}$ was shown as a living polymerisation system. Furthermore addition of 5 eq. of co-initiator (^{i}PrOH or $BnNH_2$) resulted in proportionally lower molecular weights, consistent with an immortal polymerisation system. Analysis of the resulting PLA revealed an atactic microstructure. The zwitterionic yttrium complex $Y(\mathbf{30})_2H$ was shown as highly active for the ROP of *rac*-lactide resulting in high conversion after 20 mins (RT, THF, 100:1:5 [monomer]:[initiator]:[BnOH]). While $Y(\mathbf{30})_2H$ is a neutral complex it possesses a Lewis acid yttrium centre and a Brønsted acidic proton, both are capable of coordinating or enhancing the coordination of lactide. The zwitterionic yttrium complex was also identified as an immortal initiator for the ROP of lactide resulting in very controlled molecular weights and low PLA chain distribution (PDI = 1.17, for the above conditions). Additionally the resulting PLA was highly heterotactic (P_r = 0.93) and negligible transesterification was observed.

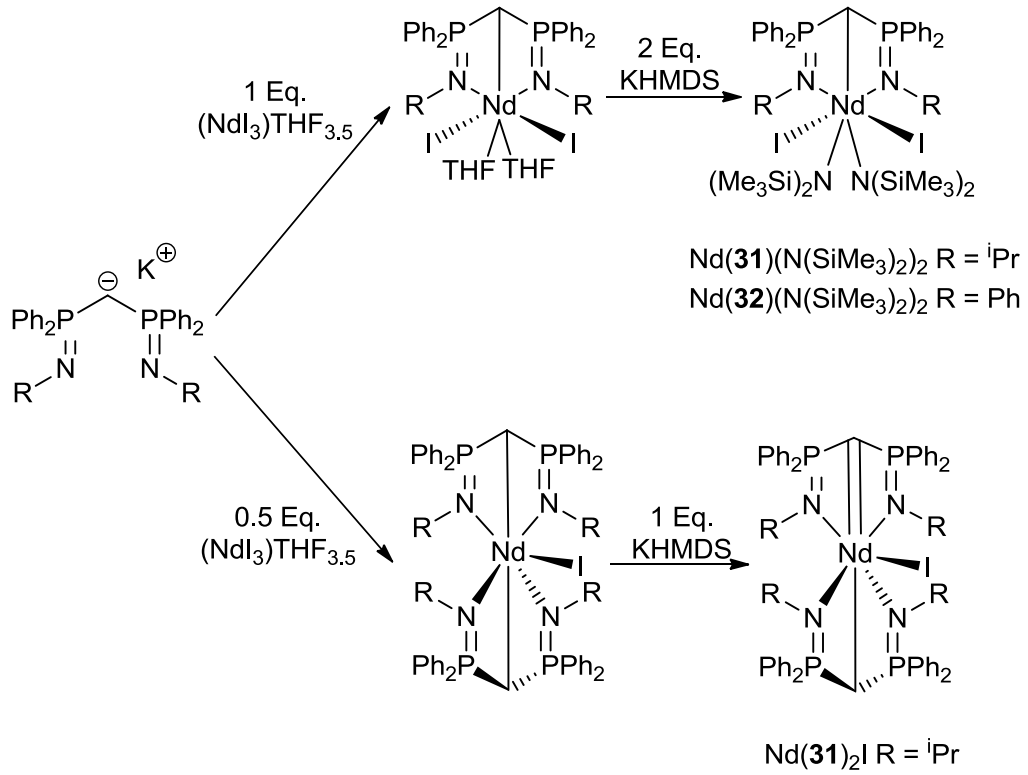

Figure 1.40: Iminophosphorane neodymium(III) Complexes investigated as initiators for the ROP of lactide.[85]

Monometallic iminophosphorane neodymium(III) amide complexes Nd(**31**,**32**)$(N(SiMe_3)_2)_2$ were shown to be highly active initiators for the ROP of lactide (Figure 1.40).[85] The monometallic neodymium(III) complexes {Nd(**31**,**32**)$(N(SiMe_3)_2)_2$} both yielded > 95 % conversion of *rac*-lactide within 5 mins (25 °C, THF, 200:1 [monomer]:[initiator] ratio). A linear molecular weight increase proportional to conversion was observed with moderate chain length distribution (PDI ~1.3), although molecular weights were about 10 times the expected value implying only 10 % of initiators were active. Furthermore, intermolecular transesterification was indentified by MALDI-TOF, alongside amido and hydroxyl end groups. An analogous bis(alkoxide) of Nd(**32**)$(N(SiMe_3)_2)_2$ was synthesised from the neodymium(III) bis(phosphorus-amide) and further shown to decompose after 2h, following this polymerisation experiments were conducted by adding ^{i}PrOH *in-situ* as a co-initiator. The *in-situ* generated alkoxide derivatives of Nd(**31**,**32**)$(N(SiMe_3)_2)_2$ achieved > 95 % conversion after 6 mins (25 °C, THF, 200:1:2 [monomer]:[initiator]:[^{i}PrOH] ratio). The *in-situ* polymerisation displayed molecular weights consistent with 2 PLA chains from each metal, also very low

molecular weight distributions were observed (PDI = 1.05 – 1.07). Furthermore, the resulting polymer displayed a slight heterotactic bias (P_r = 0.57 – 0.60). Treatment of iminophosphorane potassium complex with 0.5 Eq. of neodymium (III) iodide resulted in a bis(iminophosphorane) neodymium (III) iodide complex, further addition of a base produced the neodymium (III) carbene complex Nd(**31**)$_2$I (Figure 1.40). Formation of bis(iminophosphorane) neodymium (III) iodide was dependent on steric bulk of the nitrogen substituents. The Nd (III) carbene complex Nd(**31**)$_2$I was investigated for the ROP of *rac*-lactide but it was proven to be inactive. Addition of ^{i}PrOH to Nd(**31**)$_2$I resulted in the decomposition into neodymium (III) alkoxides and free ligand, which consequently produced PLA, albeit with a lack of control. Interestingly addition of ^{i}PrOH or KOEt to a mixture of Nd(**31**)$_2$I and *rac*-lactide resulted in the moderately fast polymerisation (^{i}PrOH = 81 %, KOEt = 0.85 %, 60 mins, RT, THF, 200:1:1 [monomer]:[initiator):[^{i}PrOH/KOEt]), molecular weights were consistent with one polymer chain per neodymium and low chain length distributions (PDI = 1.05 – 1.11) were observed. A monomer activated mechanism was proposed,[85] where neodymium activates the monomer for alcohol/alkoxide attack. After the polymerisation reaction reaches completion the alcohol/alkoxide terminated polymer chains proceed to attack the neodymium complex to yield free ligand. Chain length could not be controlled by addition of excess ^{i}PrOH as the additional alcohol decomposed the neodymium initiator.

1.3.5 Group 4 initiators

Group 4 metal complexes are successful initiators for the ROP of lactide, of particular note due to their relevance to this study are the salen, salan, and salalen (-ONNO-) group 4 complexes. Tris-phenolates and other C_3 symmetric group 4 complexes have been investigated for the ROP of lactide and yielded a high degree of stereo-selectivity. Although titanium is the most prominent throughout the literature zirconium and hafnium initiators are often more active, or more stereoselective than their titanium counterparts.

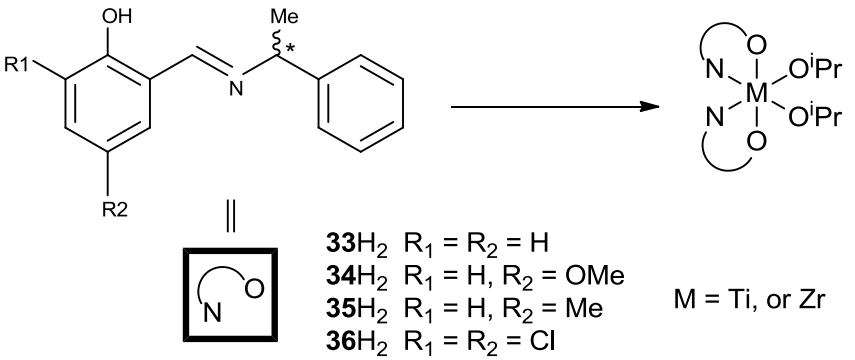

Figure 1.41: Scheme depicting chiral Schiff bases complexed to Ti(IV) and Zr(IV) alkoxides investigated for the ROP of *rac*-lactide.[86]

Chiral Schiff base ligands (**33**-**36**)H_2 were complexed with Ti(IV) and Zr(IV) isopropoxides by Davidson *et al.* and investigated as initiators for the ROP of *rac* lactide (Figure 1.41).[86] Pure chiral *R,R* and *S,S* complexes were synthesised alongside racemic mixtures (*S,R* and *R,S*), NMR spectroscopic analysis showed the complexes were fluxional in solution at room temperature. All the Ti(IV) Schiff base complexes {Ti(**33**-**36**)$_2$(O^iPr)$_2$} were inactive in solution at 80 °C, whereas the Zr(**33**-**36**)$_2$(O^iPr)$_2$ initiators ring opened *rac*-lactide with moderate activities achieving 45 – 69 % conversion after 24 h (20 °C, 100:1, [*rac*-lactide]:[initiator] ratio). Under these conditions Zr(IV) Schiff base complexes {Zr(**33**-**36**)$_2$(O^iPr)$_2$} displayed good chain length control (PDI < 1.12) and resulted in heterotactic biased PLA (P_r = 0.68 – 0.76). Ti(IV) Schiff base complexes {Ti(**33**-**36**)$_2$(O^iPr)$_2$} were active for the ROP of *rac*-lactide in solvent free conditions (130 °C, 30 mins, 300:1 [*rac*-lactide]:[initiator] ratio) and afforded good molecular weight control but yielded atactic PLA. Utilising melt conditions the Zr(IV) Schiff base initiators gave a reduced degree of chain length control (PDI = 1.39 – 2.49) but retained their heterotactic bias (P_r = 0.68 – 0.73). These Schiff base initiators were shown to have a degree of tolerance to water and impurities, and were capable of the polymerisation of lactide under such conditions.

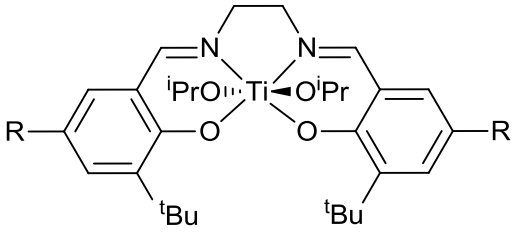

Ti(**37**)(O^iPr)$_2$

R = OMe, H, ^{t}Bu, I, Cl

Figure 1.42: Salen supported titanium (IV) bis(alkoxide) complexes trialled for the ROP of *rac*-lactide.[87]

Salen supported titanium(IV) bis(alkoxide) complexes {Ti(**37**)(O^iPr)$_2$} (Figure 1.42) were shown to be moderately active initiators for the ROP of *rac*-lactide.[87] The salen complexes {Ti(**37**)(O^iPr)$_2$} adopted a solution stable *trans* octahedral geometry. As initiators for the ROP of *rac*-lactide they achieved between 66 - 97 % conversion after 24 h (70 °C, toluene, 100:1 [*rac*-lactide]:[initiator] ratio). The variance in activity was dependent upon the *para*-substituent, where the more electron withdrawing substituents resulted in lower activities. A significant induction period before the propagation stage of the polymerisation was observed and the authors speculated that the initial metal-lactide coordinated species is relatively stable towards propagation. Although two likely alkoxide initiation sites are present in the titanium salen complexes {Ti(**37**)(O^iPr)$_2$} only one PLA chain per metal was observed alongside well defined molecular weights (PDI = 1.15 – 1.21), the resulting PLA was atactic.

Further 1,2-diaminocyclohexane (1,2-DACH) salens were complexed to titanium, yielding a monomeric species {Ti(**38**)(O^iPr)$_2$}, and zirconium/hafnium resulted in bimetallic complexes {Zr_2(**38**)(O^iPr)$_6$, Hf_2(**38**)(O^iPr)$_6$} (Figure 1.43).[87, 88] Unlike the related Ti(**37**)(O^iPr)$_2$ structures the titanium DACH salen {Ti(**38**)(O^iPr)$_2$} adopted an α-*cis* octahedral structure. Titanium DACH salen {Ti(**38**)(O^iPr)$_2$} was less active than its analogous Ti(IV) salen {Ti(**37**)(O^iPr)$_2$} achieving 57 % conversion after 24 h (70 °C, toluene, 100:1 [*rac*-lactide]:[initiator] ratio). Although slightly less active towards the ROP of *rac*-lactide, slightly lower molecular weight distribution was observed (PDI = 1.11) whilst atactic PLA was obtained.

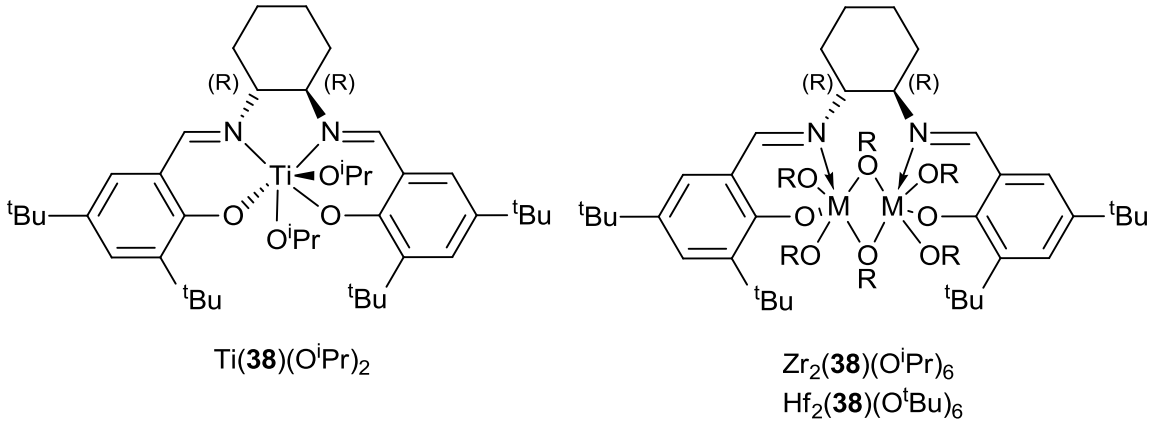

Figure 1.43: Group 4 alkoxide complexes supported by *R,R*-DACH salen ligands trialled for the ROP of *rac*-lactide and cyclic esters.[87, 88]

The bimetallic Zr(IV)/Hf(IV) *R,R*-DACH salens {Zr_2(**38**)(O^iPr)$_6$, Hf_2(**38**)(O^iPr)$_6$} were trialled for the ROP of *rac*-lactide in solvent free conditions, reaching completion after 48 mins {Zr_2(**38**)(O^iPr)$_6$}, and 66 mins {Hf_2(**38**)(O^iPr)$_6$} (140 °C, 200:1 [*rac*-lactide]:[initiator] ratio).[88] Very good molecular weight control was observed for both Zr(IV) and Hf(IV) initiators {Zr_2(**38**)(O^iPr)$_6$, Hf_2(**38**)(O^iPr)$_6$} resulting in PDI = 1.02 and molecular weights consistent with one PLA chain per bimetallic complex. Although atactic PLA was obtained the ROP of *rac*-lactide proceed by a living mechanism and retained molecular weight control upon addition of further monomer. Other cyclic esters including; caprolactone, valerolactone, and *rac*-butyrolactone were investigated for ROP using Zr_2(**38**)(O^iPr)$_6$ and Hf_2(**38**)(O^iPr)$_6$} as solvent free ROP initiators. The ROP of caprolactone, valerolactone, and *rac*-butyrolactone proceeded at 80 °C and retained the good molecular weight control (PDI < 1.08) observed for *rac*-lactide.

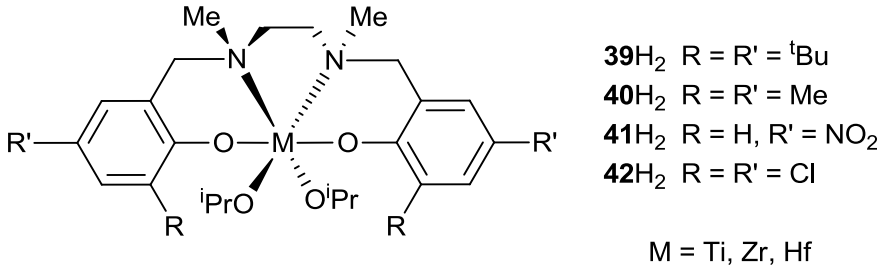

Figure 1.44: Diamine-bis(phenol) (salan) ligands complexed to group 4 metal alkoxides and utilised for the ROP of *L*-lactide and *rac*-lactide.[89, 90] *Not all combinations of complexes were synthesised.

Group 4 metal alkoxides have been complexed to diamine-bis(phenol) (salan) ligands and investigated for the ROP of *L*-lactide and *rac*-lactide by Davidson *et al*.[89] and Kol *et. al.*[90] (Figure 1.44). Titanium and zirconium salan complexes {Ti(**39**-**42**)(O^iPr)$_2$, Zr(**39**-**42**)(O^iPr)$_2$} adopt chiral (Δ, Λ) α-*cis pseudo* octahedral isomers with *pseudo* C_2 symmetry. Kol *et al*. synthesised chloro and ^{t}Bu derivatives Ti(**39,42**)(O^iPr)$_2$ and Ti(**39,42**)(O^iPr)$_2$ and reported moderate activity for the ROP of *L*-lactide under solvent free conditions.[90] Davidson *et al*. showed Zr(**40**)(O^iPr)$_2$ was the only initiator in the series to ROP *rac*-lactide in solution (> 99 %, 110 °C, toluene, 100:1 [monomer]:[initiator] ratio).[89] Titanium initiators polymerise *rac*-lactide to yield atactic lactide with 62 – 74 % conversion after 2 h under solvent free conditions (130 °C, 300:1 [monomer]:[initiator] ratio). Zr(IV) and Hf(IV) salan initiators {Zr(**39**-**42**)(O^iPr)$_2$, Hf(**39**-**42**)(O^iPr)$_2$} resulted in isotactic biased PLA under the same conditions (P_r = 0.25 – 0.30), the most selective salan derivative in this initiator series was Zr(**40**)(O^iPr)$_2$. The origin of stereoselectivity was attributed to the induced Δ, Λ chirality about the metal centre. Furthermore, back-chelation of PLA lactate units was considered to influence stereoselectivity of following lactide units. The lack of stereoselectivity observed for Ti(**39**-**42**)(O^iPr)$_2$ initiators was attributed to the inability of titanium to increase it coordination sphere to allow chelation of a lactate unit.[89]

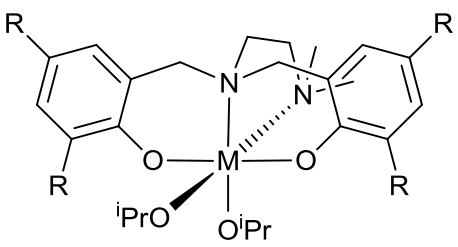

M(**43**,**44**)(O^iPr)$_2$

43 R = ^{t}Bu
44 R = Cl

M = Ti, Zr

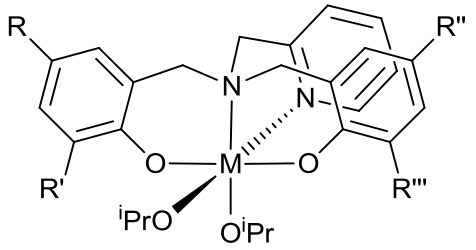

M(**45**-**47**)(O^iPr)$_2$

45 R = R' = R" = R''' = Me
46 R = R' = R" = R''' = ^{t}Bu
47 R = R' = H, R" = R''' = $C(Me)_2Ph$

M = Ti, Zr, Hf

Figure 1.45: Group 4 alkoxide complexes supported by amine−bis(phenolate) ligands utilised for the ROP of *L*-lactide and *rac*-lactide.[89, 90]

Kol *et al*. synthesised amine-bis(phenoxy) titanium and zirconium complexes with a coordinated dimethylamine side arm {Ti(**43**,**44**)(O^iPr)$_2$, Zr(**43**,**44**)(O^iPr)$_2$} (Figure 1.45), where Ti(**43**,**44**)(O^iPr)$_2$ and Zr(**43**,**44**)(O^iPr)$_2$ adopted *Cs* symmetry.[90] The Ti(IV) alkoxide complexes initiated the ROP of *L*-lactide to low conversions after an extended reaction time under solvent free conditions (130 °C, 300:1 [monomer]:[initiator] ratio). The Ti(**43**)(O^iPr)$_2$ derivative was more active than Ti(**44**)(O^iPr)$_2$ and both resulted in well defined PLA chain distributions (PDI = 1.21 - 1.28). Zr(**43**,**44**)(O^iPr)$_2$ complexes both initiated the ROP of *L*-lactide under the same conditions but revealed enhanced reactivity. The phenoxy substituents had the reverse effect upon activity where Zr(**44**)(O^iPr)$_2$ displayed a 10 fold activity increase over the related Zr(**43**)(O^iPr)$_2$ complex. Similar control over the ROP of *L*-lactide was observed for the initiator Zr(**43**)(O^iPr)$_2$ whereas initiator Zr(**44**)(O^iPr)$_2$ resulted in higher PDI = 1.56.

Davidson *et al*. synthesised amine-bis(phenol) ligands with a pyridine derived side arm and complexed them to Ti(IV), Zr(IV), and Hf(IV) alkoxides {Ti(**45**-**47**)(O^iPr)$_2$, Zr(**45**-**47**)(O^iPr)$_2$, and Hf(**45**-**47**)(O^iPr)$_2$} (Figure 1.45).[89] Solution ROP of *L*-lactide were attempted with these complexes and only Zr(**45**)(O^iPr)$_2$ was active, good activity was revealed achieving > 99 % conversion after 2 h with narrow PDI values (PDI = 1.13) (110 °C, toluene, 100:1 [monomer]:[initiator] ratio). Investigations into the solvent free ROP of *rac*-lactide were reported, Ti(**45**)(O^iPr)$_2$ was shown to be active achieving 75 % conversion after 2 h (130 °C, 300:1 [monomer]:[initiator] ratio). The Zr(**45**-**47**)(O^iPr)$_2$, and Hf(**45**-**47**)(O^iPr)$_2$ initiators were also moderately active revealing 10 – 45 % conversion under the same conditions, although the sterically bulky R = ^{t}Bu phenol substituents displayed a reduced activity requiring 24 h reaction time for low conversion. The Zr(IV) initiators Zr(**45**,**47**)(O^iPr)$_2$ resulted in PLA with an isotactic bias (P_r = 0.35 – 0.45) whereas the bulky ^{t}Bu substituents {Zr(**46**)(O^iPr)$_2$} yielded atactic PLA alongside Ti(**45**-**47**)(O^iPr)$_2$ initiators. Although PLA with an isotactic bias was observed it is less than the related Zr(IV) bis(phenoxy) complexes Zr(**39**-**42**)(O^iPr)$_2$,[89, 90] this was attributed to the non-chiral symmetry of Zr(**45**-**47**)($OiPr$)$_2$. The unsymmetrical complexes Zr(**47**)(O^iPr)$_2$/Hf(**47**)(O^iPr)$_2$ revealed no stereoselectivity enhancement over Zr(**45**)(O^iPr)$_2$/Hf(**45**)(O^iPr)$_2$ complexes with -Me phenoxy substituents.

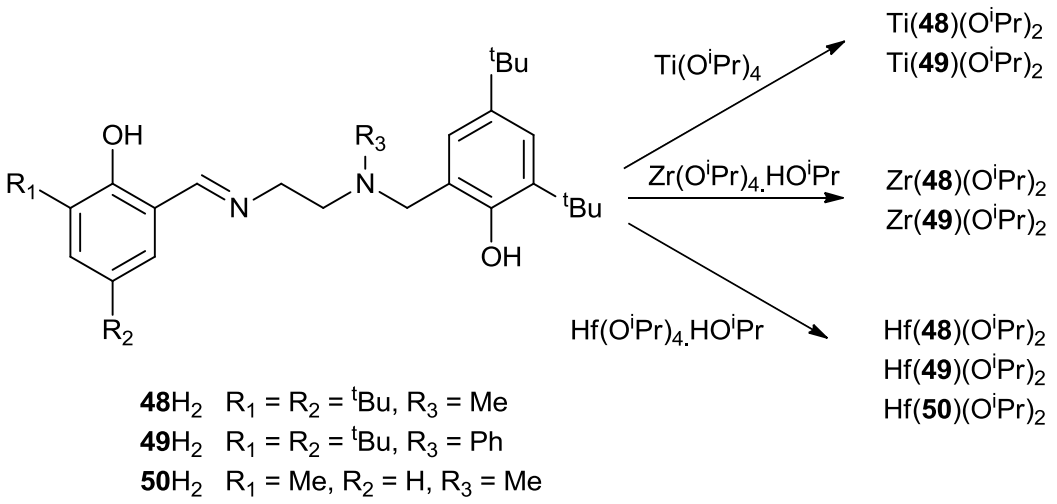

Figure 1.46: Scheme showing the synthesis of group 4 salalen alkoxides utilised for the ROP of *rac* lactide.[91]

Salalen ligands were complexed to group 4 metal alkoxides by Jones *et. al.* and utilised for the ROP of *rac*-lactide (Figure 1.46).[91] The group 4 salalen complexes were shown to adopt a *pseudo* octahedral *fac-mer* geometry by X-ray diffraction and was confirmed in solution by NMR spectroscopy, with the exception of Hf(**50**)(O^iPr)$_2$ which was shown as two isomers in solution both present in equal proportions. The salalen group 4 complexes initiated the ROP of *rac*-lactide in solution and revealed good activities achieving > 96 % conversion after 24 h (80 °C, toluene, 100:1 [monomer]:[initiator] ratio). The Zr(IV) and Hf(IV) salalen complexes typically displayed better molecular weight control over the solution ROP of *rac*-lactide (PDI = 1.07 – 1.13), while Ti(**48**,**49**)(O^iPr)$_2$ and Hf(**50**)(O^iPr)$_2$ yielded broader PDI values (PDI = 1.42 - 1.62). Ti(**48**,**49**)(O^iPr)$_2$ and Hf(**50**)(O^iPr)$_2$ resulted in atactic PLA, Zr(**48**)(O^iPr)$_2$ and Zr(**49**)(O^iPr)$_2$ resulted in a slightly heterotactic biased PLA (P_r = 0.56 – 0.60), Hf(**48**)(O^iPr)$_2$ and Hf(**50**)(O^iPr)$_2$ resulted in an isotactic biased PLA (P_r = 0.30) using the above conditions. Studies were also conducted without the presence of solvent, it was shown that Ti(IV) and Zr(IV) salalen initiators gave atactic lactide with good conversions (52 – 98 %) after 15 mins (130 °C, 300:1 [monomer]:[initiator] ratio). Hafnium initiators were slower for the ROP of *rac*-lactide in solvent free conditions with high conversion obtained after 2 days {Hf(**48**)(O^iPr)$_2$}, 1 day {Hf(**49**)(O^iPr)$_2$} and 15 mins {Hf(**50**)(O^iPr)$_2$}. Hf(**48**)(O^iPr)$_2$ and Hf(**50**)(O^iPr)$_2$ still retain their isotactic selectivity at elevated temperature in solvent free conditions. Although isotactic stereoselectivity was

observed Hf(**50**)(O^iPr)$_2$ displayed a lack of molecular weight control with lower M_n values than expected. This was attributed to the lower steric bulk about the metal allowing propagation of multiple PLA chains, also transesterification was thought to be more prevalent as a consequence of its higher activity. The ROP of *rac*-lactide using Hf(**50**)(O^iPr)$_2$ was also conducted at a lower temperature which resulted in an enhanced isotactic bias (P_r = 0.25) and 99 % conversion within 6 h (20 °C, CH_2Cl_2, 100:1 [monomer]:[initiator] ratio). Additionally more molecular weight control was observed (PDI = 1.25) consistent with one PLA chain per metal.

Group 4 complexes supported by dithiodiolate ligands {(**51**,**52**)H_2} (Figure 1.47) were trialled for the ROP of *L*-lactide and *rac*-lactide in toluene and solvent free conditions.[92] The titanium structure Ti(**51**)(O^iPr)$_2$ was isolated and characterised by X-ray diffraction and showed the complex adopts a *pseudo* α-*cis* octahedral geometry. It was reported that the complexes Ti(**51**,**52**)(O^iPr)$_2$, Zr(**51**,**52**)(O^tBu)$_2$, and Hf(**51**,**52**)(O^tBu)$_2$ are fluxional in solution inter-converting between two isomers, where the M(**52**)X_2 complexes gave greater fluxionality. The group 4 dithiodiolate complexes are very active initiators for the ROP of *rac*-lactide. The activity was more dependent upon the metal than the sulphur bridging group which, displayed minimal effect upon activity. Titanium complexes Ti(**51**,**52**)(O^iPr)$_2$ were very active initiators for the ROP of *rac*-lactide under solvent free conditions achieving high conversion within 35 and 17 mins respectively (130 °C, 300:1 [monomer]:[initiator] ratio). Zirconium initiators Zr(**51**,**52**)(O^tBu)$_2$ were more active reaching high conversion in < 4 mins under the same condition. Hafnium initiators Hf(**51**,**52**)(O^tBu)$_2$ were reported to have slightly higher activities than their zirconium analogues obtaining high conversion in < 2 mins. Furthermore the hafnium initiator Hf(**52**)(O^tBu)$_2$ was shown to polymerise *rac*-lactide to high conversion within 5 minutes at 3000:1 [monomer]:[initiator] ratio. Moderate molecular weight control was observed with a range of PDI values (PDI = 1.17 - 1.75) and molecular weights were significantly lower than expected, attributed to more than one PLA chain being propagated per metal and transesterification side reactions. Additionally under melt conditions initiators, Zr(**51**,**52**)(O^tBu)$_2$ and Hf(**51**,**52**)(O^tBu)$_2$ yielded PLA with a heterotactic bias ($P_r \approx 0.70$). By using toluene as a solvent and lowering the reaction temperature (75 °C) the stereoselectivity was enhanced, the highest heterotactic bias was obtained by Zr(**52**)(O^tBu)$_2$ (P_r = 0.89).

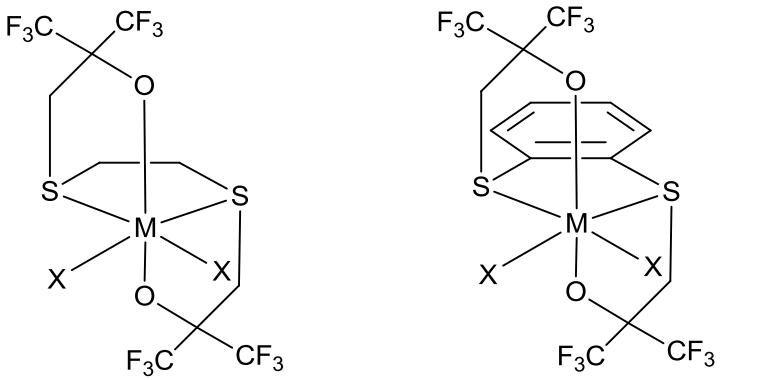

Ti(**51**)(O^iPr)$_2$ X = O^iPr
Zr(**51**)(O^tBu)$_2$ X = O^tBu
Hf(**51**)(O^tBu)$_2$ X = O^tBu

Ti(**52**)(O^iPr)$_2$ X = O^iPr
Zr(**52**)(O^tBu)$_2$ X = O^tBu
Hf(**52**)(O^tBu)$_2$ X = O^tBu

Figure 1.47: Group 4 alkoxide complexes bearing dithiodiolate ligands which were investigated as initiators for the ROP of *rac*-lactide.[92]

Titanium tetra-isopropoxide was investigated for the ROP of *L*-lactide and *rac*-lactide. Furthermore the isopropoxide moieties were substituted by chloride ligands to varying degrees [Ti(O^iPr)$_{4-x}$Cl$_x$].[93, 94] All these complexes from X = 3 though to X = 0 were active for the ROP of *rac*-lactide in solvent free conditions (130 °C) and in toluene (70 °C). Activity decreased with increasing degrees of chloride substitution although increasing chloride substitution resulted in narrower molecular weight distributions. With larger degrees of chloride substitution (X = 2, 3) the ROP of *rac*-lactide resulted in PLA with a heterotactic bias.

Bimetallic {Ti(**53**)(O^iPr)}$_2$, trimetallic Ti$_3$(**54**)$_2$(O^iPr)$_6$, and tetrametallic Ti$_4$(**55**)$_2$(O^iPr)$_{10}$ titanium complexes were investigated as initiators for the ROP of *rac*-lactide and *L*-lactide in both solution and solvent free conditions (Figure 1.48).[93, 94] The dimeric complex {Ti(**53**)(O^iPr)}$_2$ utilises triethanolamine ligands and is an active initiator for the ROP *L*-lactide and *rac*-lactide. Moderate activities were achieved 70 % conversion after 1.5 days (70 °C, toluene, 300:1 [monomer]:[metal] ratio).[94] Under these conditions {Ti(**53**)(O^iPr)}$_2$ yields PLA with very narrow molecular weight distributions with PDI values < 1.15 and molecular weights consistent with one polymer chain per-metal centre. Elevated temperature (130 °C) resulted in a higher activity but also a slight increase of molecular weight distribution (PDI = 1.35). Under solvent free conditions at the same elevated temperature (130 °C) a significant increase in molecular weight distribution was observed

(PDI = 1.69 -1.70), although at above 90 % conversion transesterification reactions are thought to further increase PDI = 2.55 – 3.68.[93]

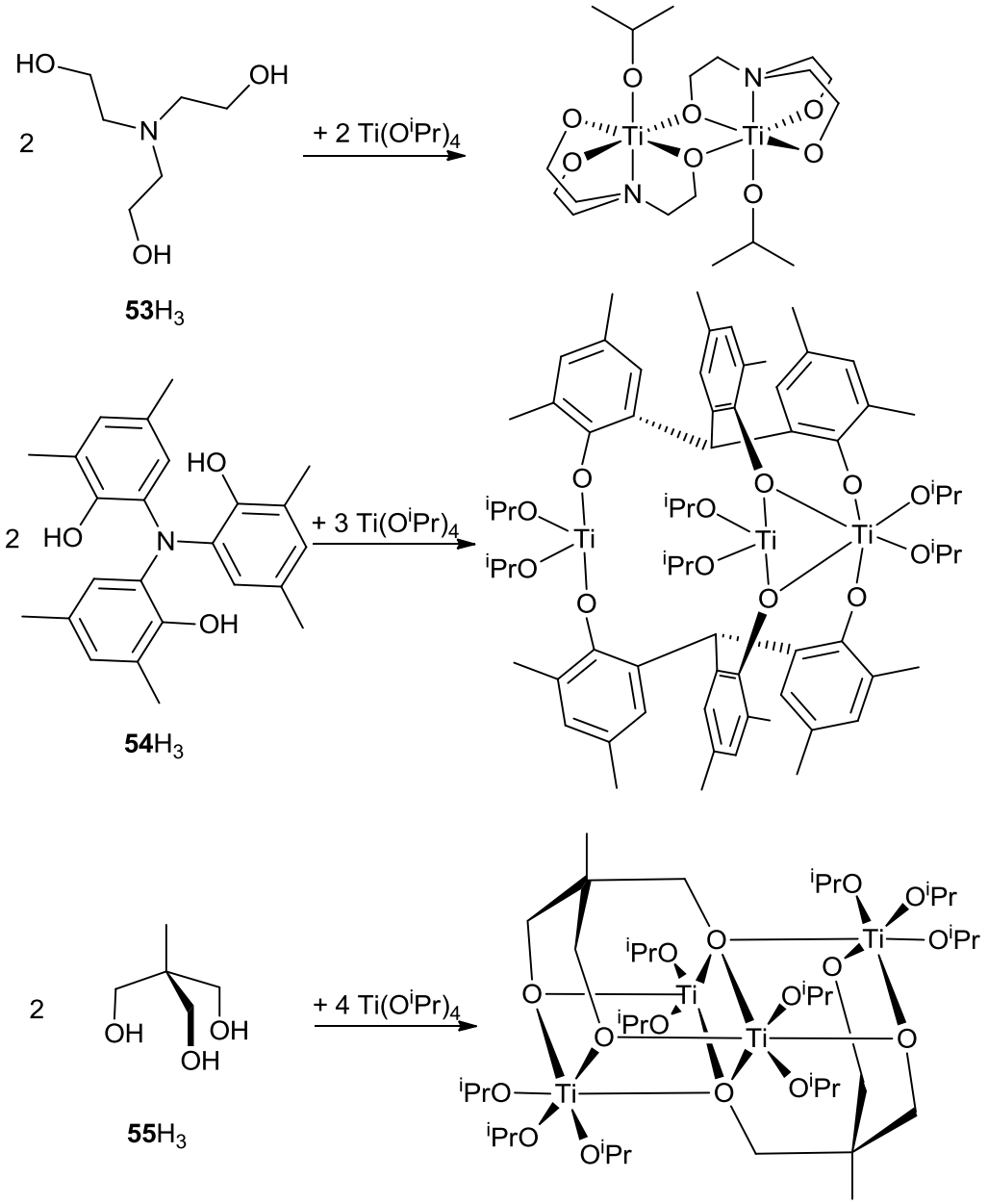

Figure 1.48: A series of bi, tri, and tetra titanium isoproxide complexes, supported by tri(alcohol) ligands, trialled for the ROP of lactide.[93, 94]

The triphenoxy supported titanium complex Ti_3(**54**)$_2$(O^iPr)$_6$ was synthesised as the kinetic and thermodynamic product. The solid state structure shown in figure 1.48 deviates slightly in solution, where the phenoxy groups do not bridge between titanium metals. The initiators were moderately active for the ROP of

lactide in toluene, achieving 95 % conversion after 12 h (130 °C, toluene, 200:1 [monomer]:[metal] ratio).[94] The ROP reaction also revealed good molecular weight control with one PLA chain being propagated per-metal and low molecular weight distributions (PDI = 1.12 – 1.36).

The tetrametallic titanium alkoxide complex $\{Ti_4(\mathbf{55})_2(O^iPr)_{10}\}$ was studied as an initiator the ROP of lactide alongside $\{Ti(\mathbf{53})(O^iPr)\}_2$ and $Ti_3(\mathbf{54})_2(O^iPr)_6$.[94] $Ti_4(\mathbf{55})_2(O^iPr)_{10}$ was shown to be relatively stable at ambient temperature although at elevated temperature it was demonstrated as slightly unstable. As an initiator for the ROP of lactide it achieved 99 % PLA yield after 24 h (70 °C, toluene 400:1 [monomer]:[metal] ratio). $Ti_4(\mathbf{55})_2(O^iPr)_{10}$ revealed good control over molecular weight with a linear increase of M_n with increasing monomer concentration, although as molecular weight increased the PDI increased in a linear relationship (PDI = 1.33 - 1.52). Unlike titanium complex $Ti_3(\mathbf{54})_2(O^iPr)_6$ which propagated one PLA chain per metal despite the presence of six potentially initiating isopropoxides. The ROP of lactide by $Ti_4(\mathbf{55})_2(O^iPr)_{10}$ resulted in PLA molecular weights consistent with a PLA chain being propagated per isopropoxide. While most of the study focused on the ROP of *L*- lactide, the ROP of *rac*-lactide by $Ti_4(\mathbf{55})_2(O^iPr)_{10}$ yielded atactic PLA.

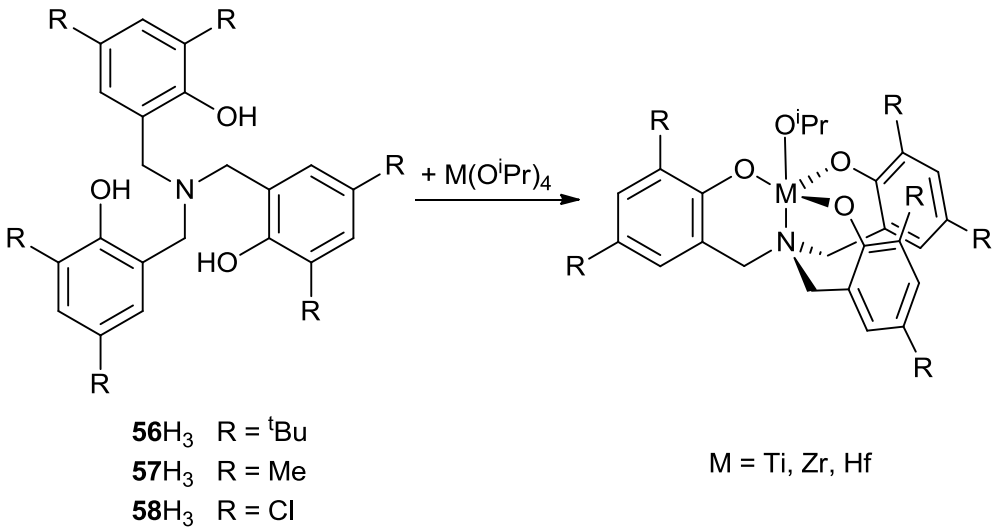

Figure 1.49: Scheme over-viewing the synthesis of group 4 trisphenolates which were investigated for the ROP of lactide.[90, 95]

Group 4 trisphenolates were first investigated by Kol *et al*. for the ROP of *L*-lactide.[90] The trisphenolate group 4 complexes adopted a chiral C_3 symmetric penta-coordinate structure (Figure 1.49). The titanium complexes Ti(**56**-**58**)O^{i}Pr were shown to polymerise *L*-lactide. Increasing the steric bulk of the phenoxy substituents was detrimental to the titanium initiators activity. Furthermore, investigation of Ti(**56**)O^{i}Pr for the ROP of *rac*-lactide resulted in atactic PLA under solvent free conditions (130 °C).[95] While Kol *et. al.*[90] demonstrated Zr(**56**)O^{i}Pr as an active initiator for the ROP of *L*-lactide, Davidson *et. al.* reported Zr(**56**)O^{i}Pr to be seven times faster for the ROP of *rac*-lactide.[95] The Zr(IV) trisphenolate {Zr(**56**)O^{i}Pr} yields strongly heterotactic PLA from the ROP of *rac*-lactide hence the ROP of *L* lactide is slower due to the inability to insert alternating enantiomers of the monomer. Both Zr(**56**)O^{i}Pr, and Hf(**56**)O^{i}Pr polymerised lactide to high conversion within 30 mins (130 °C, solvent free, 300:1 [monomer]:[initiator] ratio) and maintain control over the molecular weight (PDI = 1.19 – 1.22). The Hafnium trisphenolate Hf(**56**)O^{i}Pr also results in heterotactic PLA under melt conditions (P_r {Hf(**56**)O^{i}Pr} = 0.88, P_r {Zr(**56**)O^{i}Pr} = 0.96).[95] It was suggested that zirconium and hafnium trisphenolates control the geometric orientation of a propagating lactide by inversion of the axial chirality about the metal centre during propagation. Although it is currently unclear if the heterotactic selectivity is induced from the ligand steric bulk, *via* a chain-end control mechanism.[95]

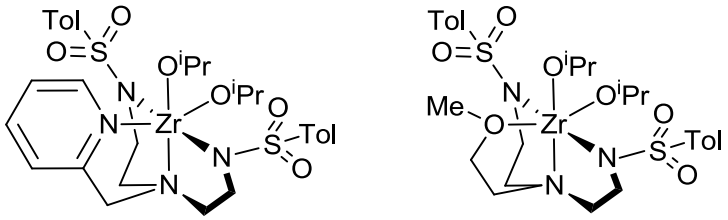

Figure 1.50: Group 4 metal alkoxide complexes supported by tetradentate bis(sulfonamide)amine ligands investigated for the ROP of *rac*-lactide.[96]

Group 4 metal tetradentate bis(sulfonamide) complexes were trialled for the ROP of *rac*-lactide by Mountford *et al* (Figure 1.50).[96] Forcing conditions were used in the coordination synthesis of the tetradentate bis(sulfonamide) ligands to group 4

metal alkoxides, requiring either elevated temperature or alcohol removal by vacuum in solvent free conditions. The resulting zirconium complexes initiated the ROP of *rac*-lactide with good activities for group 4 metals, although initiator Zr(**59**)(O^iPr)$_2$ was less active than initiator Zr(**60**)(O^iPr)$_2$. The zirconium initiator Zr(**60**)(O^iPr)$_2$ was further studied and achieved 95 % conversion within 5.5 h (70 °C, toluene, 100:1 [monomer]:[initiator] ratio). The ROP reaction was well controlled in solution and molecular weights were linear with conversion and molecular weight distributions were consistently low (PDI = 1.12 – 1.14). Conversely MALDI-TOF mass spectrometry revealed transesterification reactions were also present and NMR spectroscopy showed the resulting PLA was atactic. Studies using solvent free conditions proved initiator Zr(**60**)(O^iPr)$_2$[96] was very active and gave comparable reaction rates to group 4 trisphenolates {Zr/Hf(**56**)O^iPr}.[95] Titanium derivatives of tetradentate bis(sulfonamide) complexes Zr(**59**,**60**)(O^iPr)$_2$ were synthesised and also trialled for the ROP of caprolactone alongside the zirconium initiators Zr(**59**,**60**)(O^iPr)$_2$.[96]

Further sulphonamide group 4 initiators were synthesised by Mountford *et al*. and trialled for the ROP of caprolactone and *rac*-lactide (Figure 1.51).[97] The titanium complexes Ti(**61**,**62**)(O^iPr)$_2$ proved unstable for prolonged ROP of *rac*-lactide and the reaction was halted before full conversion was obtained. While limited conversion was obtained the titanium initiators revealed low PDI values (PDI = 1.13 - 1.22). The four coordinate sulphonamide complex Ti(**61**)(O^iPr)$_2$ exhibited little variation upon rates between R = toluene and R = Mes. The five coordinate titanium sulphonamide complex Ti(**62**)(O^iPr)$_2$ displayed higher activity for R = Me over R = Tol. Zirconium tris(sulphonamide) complexes {Zr(**63**)CH_2SiMe_3} were also investigated for the ROP of *rac*-lactide and it was found that alkoxides generated *in-situ* gave a significant activation enhancement. The five coordinate zirconium complex Zr(**63**)CH_2SiMe_3 was less active than its previously investigated six coordinate sulphonamide relative Zr(**60**)(O^iPr)$_2$. Unlike the titanium sulphonamides {Ti(**61**,**62**)(O^iPr)$_2$} the zirconium sulphonamides Zr(**63**)CH_2SiMe_3 achieved high conversion 89 - 95 % within 24 h (70 °C, toluene, 100:1 [monomer]:[initiator] ratio). Increasing the steric demands of the sulphonamide groups within Zr(**63**)CH_2SiMe_3 decreased the rate of the reaction in

the order R = Me > toluene > Ar^F. All the group 4 sulphonamides complexes reported here have resulted in atactic lactide.

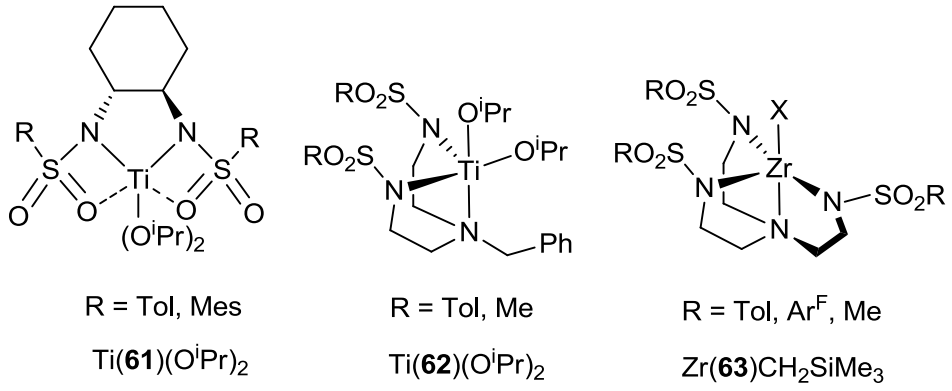

Figure 1.51: Further group 4 sulphonamide-supported complexes trialled for the ROP of cyclic esters.[97]

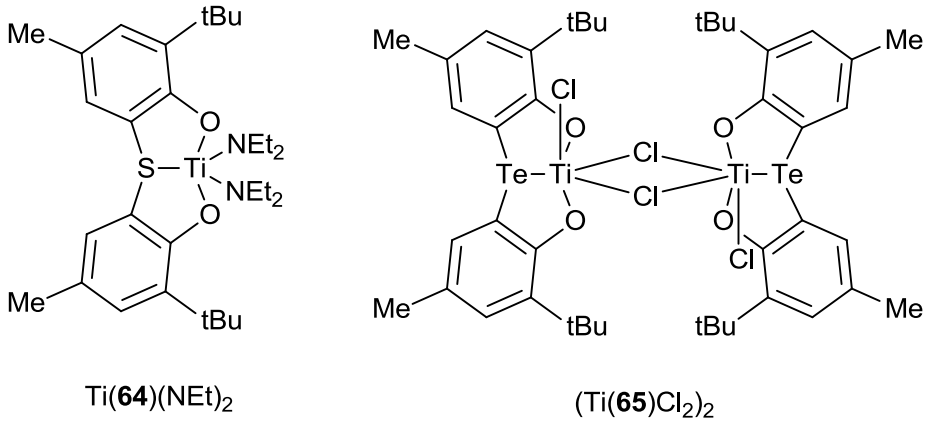

Figure 1.52: Group 4 complexes supported by sulphur and tellurium bridged bis(phenol) ligands, which were utilised for the ROP of *L*-lactide.[98, 99]

Harda *et al*. investigated titanium complexes, bridged by bis(phenol) ligands which contain a sulphur or tellurium bridging atom {Ti(**64**)$(NEt)_2$ and (Ti(**65**)$Cl_2)_2$}, for the ROP of *L*-lactide.[98, 99] Other titanium bis(phenoxy) complexes of this type were synthesised but were mainly trialled for the ROP of caprolactone and other cyclic esters. The sulphur bridged bis(phenoxy) titanium amide complex {Ti(**64**)$(NEt)_2$} (Figure 1.52) was an active initiator for the ROP of *L*-lactide although it was slow affording 96 % yield after 120 h (100 °C, toluene, 200:1 [monomer]:[initiator] ratio).[99] Ti(**64**)$(NEt)_2$ exhibited linear molecular weight growth

with conversion but a slightly linear increase in PDI was also observed, which led to speculation about the presence of transesterification/back-biting reactions.

The dimeric titanium chloride complex {(Ti(**65**)Cl_2)$_2$} containing a bis(phenol) ligand bridged by tellurium was active for the ROP of *L*-lactide without the addition of a co-initiator.[98] (Ti(**65**)Cl_2)$_2$ (Figure 1.52) achieved 98 % conversion of *L*-lactide after 48 h (100 °C, anisole, 200:1 [monomer]:[metal] ratio) with good molecular weight control (PDI = 1.04 – 1.13) throughout the polymerisation reaction. Linear growth of PLA molecular weight was observed alongside conversion and further addition of lactide to a completed ROP reaction indicating a living polymerisation. Further experiments were conducted into co-polymerisation of lactide with caprolactone.[98]

1.3.6 Zinc initiators

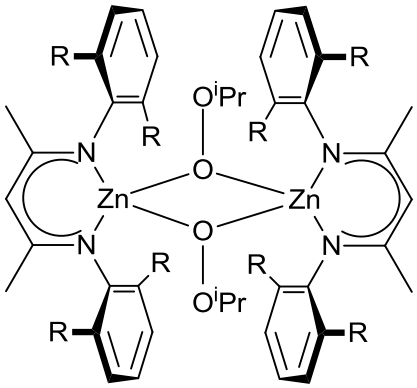

(Zn(**66**)O^{i}Pr)$_2$ R = ^{i}Pr
(Zn(**67**)O^{i}Pr)$_2$ R = Et
(Zn(**68**)O^{i}Pr)$_2$ R = ^{n}Pr

Figure 1.53: β-Diketiminate zinc complexes utilized for the ROP of *rac*-lactide.[36]

Zinc complexes have been tested for the ROP of lactide and many zinc complexes are coordinated to analogous ligands as group 2 metals. Some β-diketiminate (BDI) ligands which have been complexed to group 2 metals {(Mg(**6**)(^{i}Pr))$_2$,[36, 62] (Mg(**7**)(O^{i}Pr))$_2$,[36, 62] Mg(**8**)O^{t}Bu.THF,[63, 64] and Ca(**8**)N(SiMe$_3$)$_2$.THF}[66] were discussed earlier in this report. The BDI zinc complexes {(Zn(**66**-**68**)O^{i}Pr)$_2$} were isolated as dimers in the solid state and shown to retain their dimeric structure in solution (Figure 1.53).[36] BDI zinc complexes {(Zn(**66**-**68**)O^{i}Pr)$_2$} are active initiators for the ROP of *rac*-lactide. Substitution of the -O^{i}Pr initiating groups for -N(SiMe$_3$)$_2$, -Et, and OAc resulted in a decrease in polymerisation control. The zinc BDI complexes achieved high conversion (97 %)

within 20 mins when R = ^{i}Pr (20 °C, CH_2Cl_2, 200:1 [monomer]:[zinc] ratio). The reaction activities were dependent upon the "R" substituents where the ROP activities order follows R = ^{i}Pr > Et > ^{n}Pr, to the extent that when R = ^{i}Pr the ROP is ~33 times faster than R = ^{n}Pr. (Zn(**66**-**68**)O^{i}Pr)$_2$ complexes exhibited good molecular weight control over the ROP of *rac*-lactide (PDI = 1.09 – 1.18), furthermore the ROP has living polymerisation characteristics. The resulting PLA was revealed as heterotactic with a P_r = 0.90 for initiator (Zn(**66**)O^{i}Pr)$_2$. When substituting the aromatic substituents for -Et, or -^{n}Pr a significant decrease in selectivity was observed (P_r = 0.76 – 0.79) although the PLA was still highly biased towards heterotactic PLA.

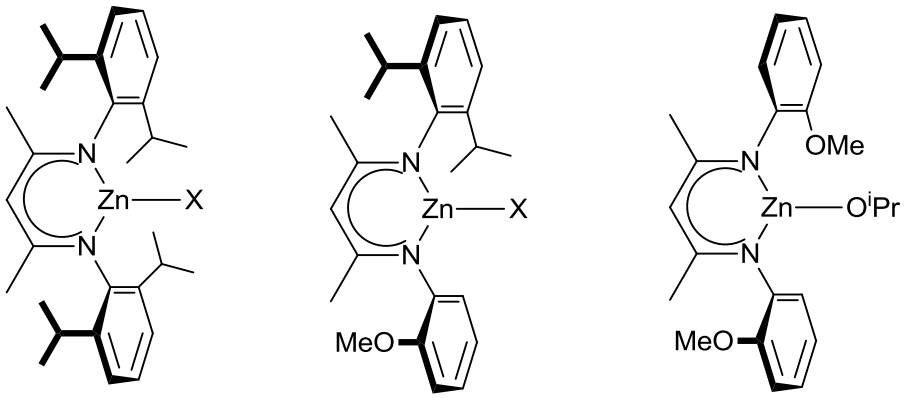

Figure 1.54: Monometallic BDI zinc complexes investigated for the ROP of lactide.[63, 64, 100]

Chisholm *et al*. isolated monometallic BDI zinc complexes {Zn(**69**)X} with bulky initiating alkoxides and amides (Figure 1.54).[63, 64] The complex Zn(**69**)O^{t}Bu resulted in 95 % conversion within 10 mins (20 °C, CH_2Cl_2, 100:1 [monomer]:[zinc] ratio) and displayed good control over the molecular weight distributions (PDI = 1.15). The mono-coordinate ligand "X" has a large effect upon the initiators activity and the degree of control the complex exhibits upon the ROP reaction. Substitution of X = O^{t}Bu to N^{i}Pr$_2$ or OSiPh$_3$ significantly decreased the activity and molecular weight control of complex Zn(**69**)X, for example when X = OSiPh$_3$ the

91 % conversion was obtained after 70 h under the same conditions. Zinc BDI complex {Zn(**69**)X} resulted in heterotactic PLA to a similar degree as the closely related zinc BDI complexes (Zn(**66**-**68**)O^{i}Pr)$_2$. Interestingly the ROP of *rac*-lactide proceeded slower in THF but the stereoselectivity observed was not affected, unlike the analogous magnesium complexes.[62-64]

Gibson *et al.* studied the zinc BDI complex Zn(**71**)O^{i}Pr, which contains two *ortho*-methoxyphenyl substituents, for the ROP of lactide.[100] Additionally Chisholm *et al*. investigated analogous zinc complexes {Zn(**70**)X} containing one *ortho*-methoxyphenyl substituent for the ROP of lactide.[62] Zn(**69**)OSiPh$_3$ achieved high conversion for the ROP of lactide in 30 h, whereas zinc complex Zn(**70**)OSiPh$_3$ reached high conversion in 30 mins under similar conditions.[64, 100] The zinc BDI initiators become more active with a higher degrees of *ortho*-methoxyphenyl substitution thus the general zinc BDI initiator activity order follows Zn(**71**)O^{i}Pr > Zn(**70**)X > Zn(**69**)X. While more active Zn(**70**)X gave a much lower degree of molecular weight control with molecular weights over four times higher than expected, although PDI remained low for Zn(**70**)X and Zn(**71**)O^{i}Pr. The resulting PLA was predominantly atactic with a slight heterotactic bias (P_r = 0.59 – 0.67).[62] While it was speculated that zinc BDI complexes Zn(**69**)X initiated the ROP of lactide by first reacting with impurities within the lactide. Analogous complexes Zn(**70**)X were shown to polymerise lactide without such impurities, furthermore -OSiPh$_3$ and -N(SiMe$_3$)$_2$ PLA end groups were identified *via* ^{1}H NMR spectroscopy. It was concluded that the *ortho*-methoxyphenyl substituents did not coordinate to the zinc metal centre. Decreasing molecular weight control could be attributed to the reduced steric demands of *ortho*-methoxyphenyl substituents over isopropylphenyl substituents.[62]

A zinc (NNO-tridentate diaminophenolate) alkoxide complex {(Zn(**72**)OEt)$_2$} was investigated for the ROP of *rac*-lactide by Hillmyer and Tolman *et al.*[101] Zinc complexed to NNO-tridentate diaminophenolate ligand (**72**H$_2$) formed a dimeric structure in the solid state (Figure 1.55), while the solution structure was identified as a monometallic species. (Zn(**72**)OEt)$_2$ is a highly active initiator for the solution polymerisation of *rac*-lactide achieving 93 % conversion after 18 mins at high monomer to initiator ratios (25 °C, CH_2Cl_2, 1500:1 [monomer]:[metal] ratio). A linear molecular weight increase with conversion was established, although the

molecular weight was lower than anticipated. This was attributed to impurities which deactivate the initiators or act as propagating chain exchange agents. Chain exchange agents were experimentally shown to reduce molecular weights by the addition of benzyl alcohol to the ROP reaction.

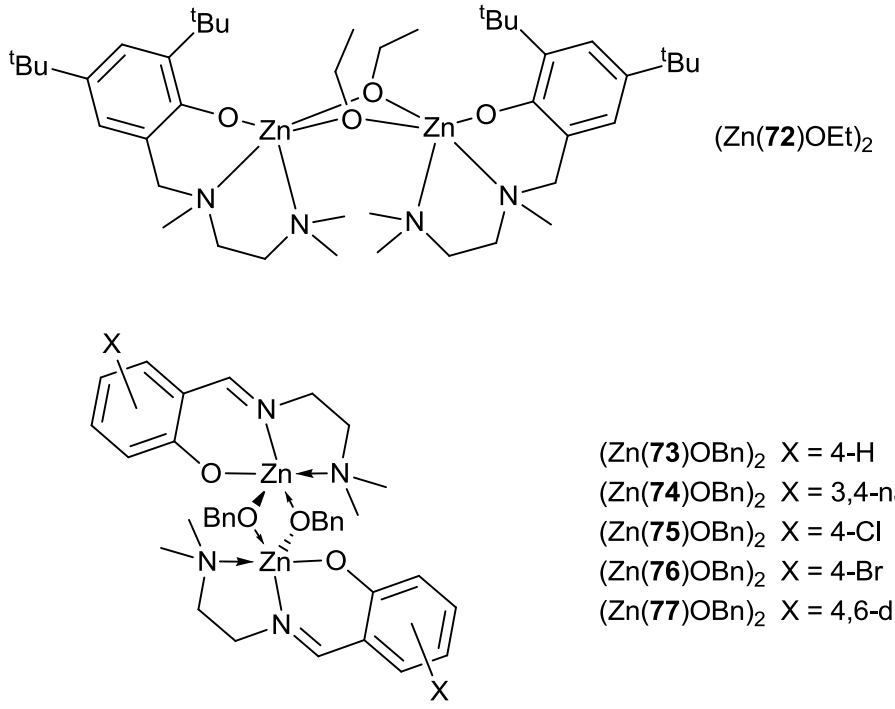

Figure 1.55: Dimeric zinc alkoxide complexes supported by a NNO-tridentate diaminophenolate ligand (**72**H_2)[101] and NNO-tridentate Schiff base ligands {(**73**-**77**)H_2}.[102]

Similar NNO-tridentate Schiff base ligands were coordinated to zinc alkyls and further reacted with benzyl alcohol to yield the zinc alkoxide complexes (Zn(**73**-**77**)OBn)$_2$ (Figure 1.55).[102] The zinc complexes {(Zn(**73**-**77**)OBn)$_2$} were demonstrated to be dimeric species in the solid state as shown in figure 1.55. The dimeric structures adopted an equilibrium in solution between three zinc complex species. Zinc complexes {(Zn(**73**-**77**)OBn)$_2$} were active initiators for the ROP of *L*-lactide and *rac*-lactide and all the phenyl substituents resulted in well controlled molecular weights with low PDI values (PDI = 1.06 – 1.26). The initiators {(Zn(**73**-**77**)OBn)$_2$} activity increased when electron donating substituents are present upon the phenoxy ring. Although the presence of steric bulk hinders lactide monomer units approach to the zinc metal and hence has a negative influence on the ROP reaction rate. A first order dependence on both lactide and the initiator was

shown and from this the authors proposed a monometallic structure as the active propagating species. The NNO-tridentate Schiff base zinc complexes (Zn(**73**-**77**)OBn)$_2$ resulted in PLA with a heterotactic bias in CH_2Cl_2 at 25 °C, the highest selectivity was obtained by the bulky 4,6-di-^{t}Bu phenyl substituents {(Zn(**77**)OBn)$_2$} (P_r = 0.74). The selectivity was increased further {P_r (Zn(**73**-**77**)OBn)$_2$ = 0.91} by cooling the reaction to -55 °C although at the expense of initiator activity.

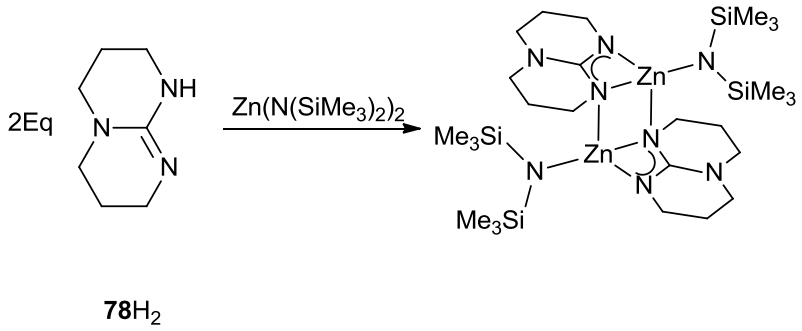

78H_2

Figure 1.56: Reaction scheme depicting the synthesis of a dimeric zinc guanidinate investigated for the ROP of lactide.[103]

A dimeric zinc acyclic guanidinate complex {(Zn(**78**)N(SiMe$_3$)$_2$)$_2$} (Figure 1.56) was investigated for the ROP of *rac*-lactide by Hitchcock and Coles.[103] The polymerisation was shown to proceed at room temperature with moderate activities achieving 95 % conversion within 2 h ($CDCl_3$, 85:1 [monomer]:[initiator] ratio). While the initiation time for –N(SiMe$_3$)$_2$ groups is often slow for the ROP of lactide, initiation for zinc complex (Zn(**78**)N(SiMe$_3$)$_2$)$_2$ proceeded rapidly. The ROP was proven as a living reaction and preceded to further polymerise lactide after completion. Atactic PLA was obtained and linear molecular weight control was demonstrated with respect to conversion.

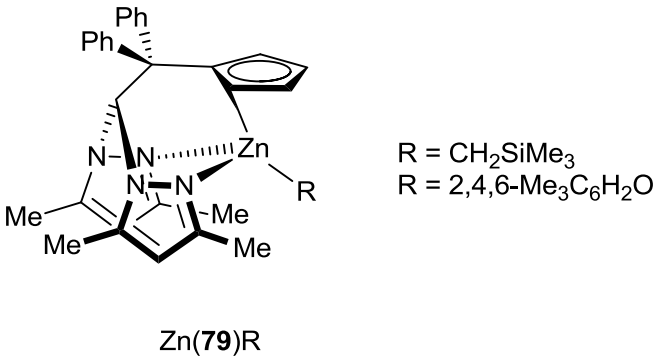

Figure 1.57: Hybrid scorpionate/cyclopentadienyl zinc complexes investigated for the ROP of lactide.[71]

The hybrid scorpionate/cyclopentadienyl ligands discussed earlier for magnesium (Figure 1.30)[71] were also coordinated to zinc {Zn(**79**)R} (Figure 1.57) and trialled for the ROP of lactide.[71] The solid-state structure is given in figure 1.57, and the solution studies have shown the η^1-cyclopentadienyl to undergo fast haptotropic exchange. The zinc complexes Zn(**79**)R were active for the ROP of *L*-lactide (92 %, 18 h, toluene, 200:1 [monomer]:[initiator] ratio, R = 2,4,6-$Me_3C_6H_2O$) albeit less active than its related magnesium initiator (Figure 1.30) (97 %, 2.5 h, toluene, 200:1 [monomer]:[initiator] ratio).[71] The zinc initiators Zn(**79**)R gave good control over the polymerisation reaction yielding one PLA chain per metal and low PDI values (PDI = 1.07 – 1.19).

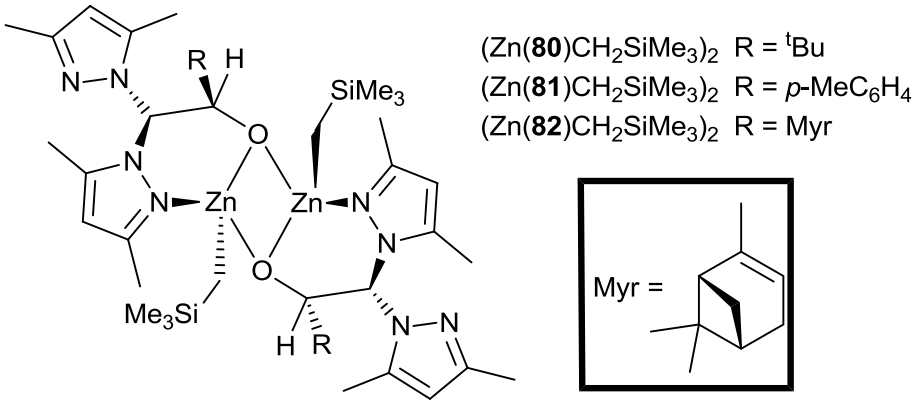

Figure 1.58: Chiral scorpionate zinc complexes investigated for the ROP of lactide.[104]

Further chiral scorpionate zinc complexes were synthesised and investigated for the ROP of both *L*-lactide and *rac*-lactide.[104] The zinc initiators

(Zn(**80**-**82**)$CH_2SiMe_3)_2$ were moderately active and were shown to achieve 85 % conversion after 3.5 h (50 °C, THF, 100:1 [monomer]:[metal] ratio). The dimeric zinc structure shown in figure 1.58 was confirmed as the solid state structure for (Zn(**80**-**82**)$CH_2SiMe_3)_2$ complexes. The solution state structure was ambiguous and a possible equilibrium process is present between monomeric and dimeric structures. Despite the ambiguity the initiators (Zn(**80**-**82**)$CH_2SiMe_3)_2$ exhibited good control over the ROP of lactide (PDI = 1.08 – 1.12). The resulting PLA was moderately heterotactic (P_r = 0.67 – 0.77) additionally increasing the reaction temperature reduced the selectivity {P_r (50 °C) = 0.77, P_r (65 °C) = 0.70}. Also the tacticity was enhanced when THF was used as the solvent over toluene {P_r (THF) = 0.72, P_r (toluene) = 0.64}. The ROP is initiated by nucleophilic alkyl attack upon the monomer, which was proven by mass spectrometry and NMR spectroscopy identification of a $(CH_3)_3CC(O)$– end group.

1.3.7 Group 13 initiators

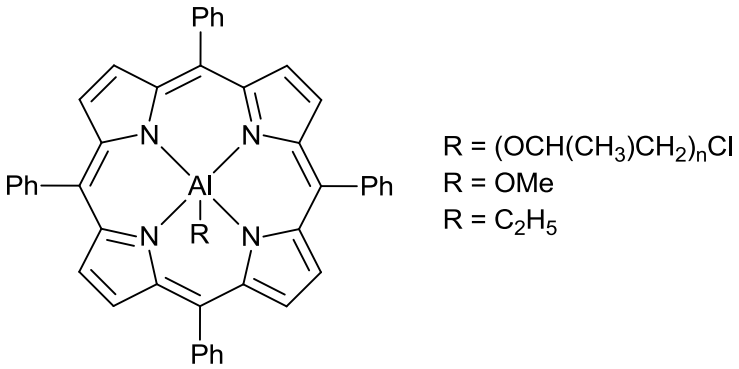

Al(**83**)R

Figure 1.59: Aluminium porphyrin initiators for the ROP of *D*-lactide.[105]

Aluminium complexes were some of the earliest initiators investigated for the ROP of lactide. One of the first reported aluminium complexes investigated for the ROP of lactide were aluminium porphyrin complexes Al(**83**)R (Figure 1.59) investigated by Inoue *et al.*[105] The ROP of *D*-lactide by the complexes of basic form Al(**83**)R were similar in ROP activity and control, their activity was relativity slow achieving 94 % conversion after 96 h {R = $(OCH(CH_3)CH_2)_nCl$ (n = 20), CH_2Cl_2, 100 °C, 100:1 [monomer]:[initiator] ratio}. While slow these aluminium porphyrin

initiators revealed living character and well defined molecular weight control (PDI ≈ 1.12). The initiator Al(**83**)R (R = Cl) was also trialled for the ROP of *D*-lactide but showed no activity.

The relativity simple aluminium complex $Al(O^iPr)_3$ proved an effective initiator for lactide polymerisation.[29, 106] Furthermore $Al(O^iPr)_3$ exists as two aggregates; a trimer $(Al(O^iPr)_3)_3$, and a tetramer $(Al(O^iPr)_3)_4$. The two aggregates were investigated independently and the trimer was found to initiate the ROP of lactide faster than the tetramer. Although, as the polymerisation proceeds, the propagation rates become equal and the propagating species for both aggregates is believed to be a monomeric compound.

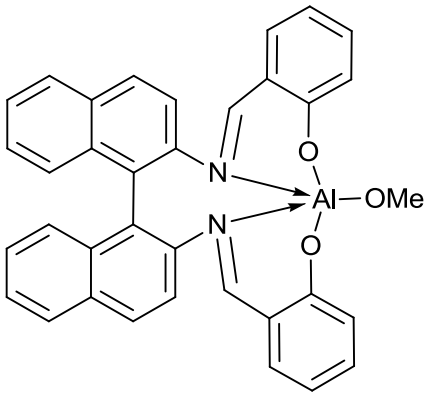

Al(**84**)OMe

Figure 1.60: Aluminium complex supported by *R*-(+)-1,1'-binaphthyl-2,2'-diamine linked bis(phenol) ligand reported for the ROP of lactide.[37]

Imine bis(phenol) ligands have been prominent throughout the ROP of lactide by aluminium complexes. Spassky *et al*. developed a *R*-(+)-1,1'-binaphthyl-2,2'-diamine linked bis(phenol) ligand coordinated to aluminium {Al(**84**)OMe} (Figure 1.60) for the ROP of lactide.[37] The aluminium complex was slow for the ROP of *rac*-lactide at 70 °C reaching 90 % conversion after 113 h (toluene 75:1 [monomer]:[initiator] ratio). Although slow the resulting PLA was isotactic with well defined molecular weight distributions (PDI = 1.10 – 1.15). A preference for the ROP of *D*-lactide was demonstrated with significant conversion up to 38 % within a relatively short time period (3.5 h). After the preferential conversion of *D*-lactide (~ 40 %) from *rac*-lactide, *L*-lactide is then polymerised as it is the prevalent

monomer remaining. Investigation of the racemic complex Al(**84**)OMe for the ROP of *rac*-lactide has shown the formation of stereoblock PLA polymer chains, where each chiral *R* or *S* binaphthyl derived aluminium initiator {Al(**84**)OMe} individually propagates a *D*-PLA or *L*-PLA chain.[107] During the ROP process an exchange process transfers the PLA chains between chiral initiators allowing the formation of stereoblock PLA chains. Additional *in-situ* investigations where chiral "*S*" binaphthyl linked bisphenol ligand and $Al(O^iPr)_3$ were used to ROP *rac*-lactide resulted in ~50 % conversion of lactide to *L*-PLA, upon which addition of the "*R*" binaphthyl linked bisphenol ligand resulted the formation of a *D*-PLA stereoblock, with an enhanced melting tempreture of 210 °C.[108] Thus, demonstrating an exchange mechanism is determining the formation of stereoblock PLA.

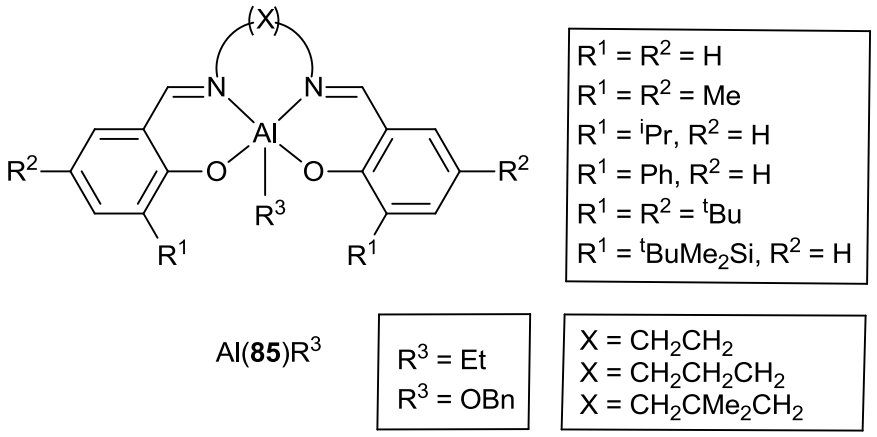

Figure 1.61: Aluminium alkyl/alkoxide complexes supported by salen ligands investigated for the ROP of Lactide. *Not all derivatives were synthesised.[109, 110]

Salen aluminium alkyl/alkoxide complexes Al(**85**)R^3 (Figure 1.61) were studied by Nomura *et al*. for the ROP of lactide.[109, 110] These aluminium salen complexes yielded PLA with an isotactic bias to varying degrees. The highest stereo-selectivity (P_r = 0.02) from this series of complexes was obtained from the initiator Al(**85**)R^3 (R^1 = ^{t}BuMe$_2$Si, R^2 = H, R^3 = OBn, X = $CH_2CMe_2CH_2$) which resulted in 96 % conversion after 14 h (70 °C, toluene, 100:1 [monomer]:[initiator] ratio). While the above binaphthyl linked bis(phenoxy) aluminium complexes {Al(**84**)R^3} exhibited stereo-control through enantiomorphic site control the salen aluminium complexes {Al(**85**)R^3} control selectivity *via* a chain end control

mechanism. Further solvent free polymerisation studies were performed using the same initiator, 97 % conversion was obtained after 1 h (130 °C, 300:1 [monomer]:[initiator] ratio). Aluminium initiator Al(**85**)R^3 still displayed isotactic selectivity to a lesser extent (P_r = 0.08 – 0.10) under solvent free conditions.

Chiral *R,R*-, *S,S*-, *rac*- diaminocyclohexane (DACH) linked salen aluminium complexes {Al(**86**)O^{i}Pr} were trialled for the ROP of *rac*-lactide by Feijen *et al*. (Figure 1.62).[30, 111] *Rac*-Al(**86**)O^{i}Pr is a slow initiator for the ROP of *rac*-lactide requiring 12 days to achieve 85 % conversion (70 °C, toluene, 62:1 [monomer]:[initiator] ratio).[30] Although slow the polymerisation was highly selective yielding isotactic PLA (P_r = 0.07) and low molecular weight distributions (PDI = 1.06). Stereoselectivity was also retained under solvent free conditions to a lesser degree (P_r = 0.12), while activity was significantly enhanced reaching 95 % conversion after 2 days (130 °C, 200:1 [monomer]:[initiator] ratio). *R,R*-Al(**86**)O^{i}Pr displayed a strong preference towards the ROP of *L*-lactide over *D*-lactide with respective rate constants k_{app} = 0.902 day^{-1} and k_{app} = 0.067 day^{-1}.[111] Furthermore the rate constant for the ROP of *L*-lactide (k_{app} = 0.509 day^{-1}) by racemic complex *rac*-Al(**86**)O^{i}Pr, as expected, was approximately half of the *R,R*-Al(**86**)O^{i}Pr *L*-lactide ROP rate constant. Stereoselectivity is controlled by an enantiomorphic site control mechanism, and similar to aluminium complexes Al(**84**)OMe a polymer exchange mechanism ensures the formation of isotactic stereoblock PLA from the ROP of *rac*-lactide by *rac*-{Al(**86**)O^{i}Pr}.[111]

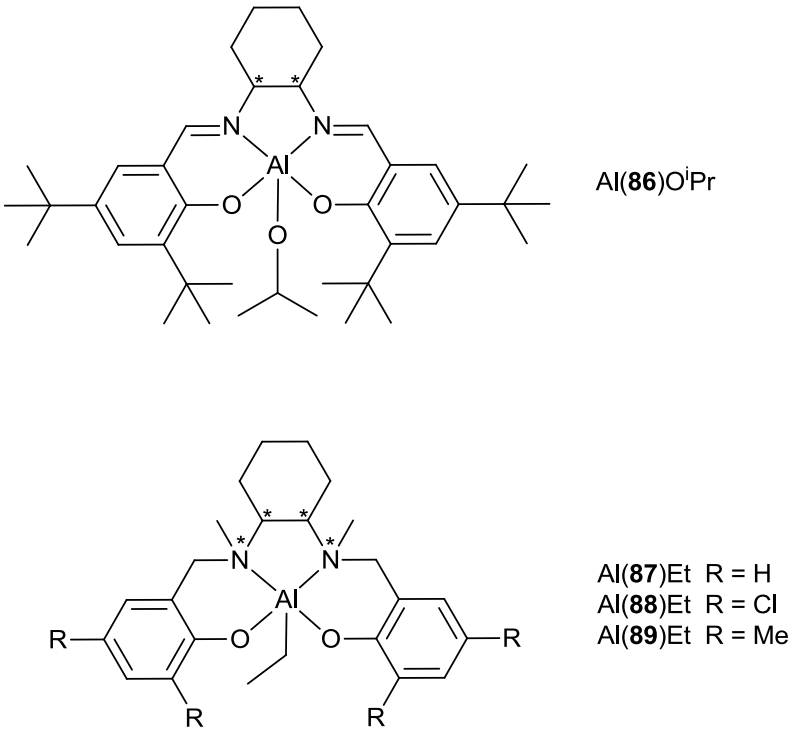

Figure 1.62: Aluminium alkoxide complex coordinated to a chiral diaminocyclohexane (DACH) linked bis(phenol) ligands, utilised for the ROP of lactide.[30, 111, 112]

Later work by Feijen *et al*. included the investigation of a similar reduced form {Al(**87**-**89**)Et} (imine to amine) of their previous DACH salen aluminium complex Al(**86**)O^{i}Pr (Figure 1.62) for the ROP of lactide.[112] The alkyl aluminium salan complexes Al(**87**-**89**)Et contained a further two chiral centres upon the nitrogen atoms, thus the proceeding complexes were present as stereoisomers. The complexes Al(**87**-**89**)Et were active initiators for the ROP of lactide with the addition of isopropoxide as a co-initiator. The activity for the ROP of *rac*-lactide was dependent upon the phenyl ring substituents, the order of activity follows; H > Cl > Me. Although slow initiators, *rac*-Al(**87**)Et achieved 89 % conversion in 9 h (toluene, 70 °C, 50:1 [monomer]:[initiator] ratio), and the polymerisation was well defined (PDI = 1.09 - 1.12). Tacticity was also dependent upon the phenyl ring substituents, isotactic biased PLA was obtained when R = H (P_r = 0.34 – 0.38), and heterotactic biased PLA was obtained when R = Cl, Me (P_r = 0.55 – 0.73). Furthermore it was demonstrated that the *R*,*R*-(DACH)-Al(**87**)Et initiator was 10.1 times more active towards the ROP of *L*-lactide over *D*-lactide. Evidence suggested these initiators proceed *via* a combination of chain exchange mechanisms and site control mechanisms.

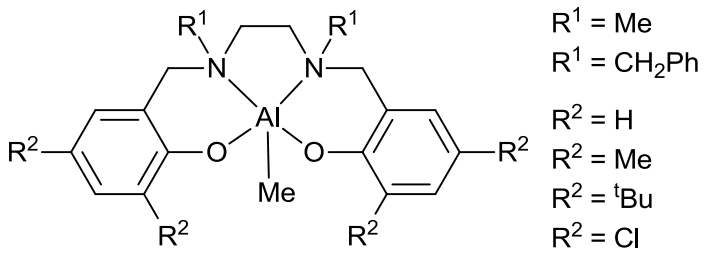

Figure 1.63: Salan aluminium alkoxide complexes investigated for the ROP of lactide.[82]

Further salan ligand systems have been coordinated with aluminium and their resulting complexes {Al(**90**)Me} investigated for the ROP of *rac*-lactide (Figure 1.63).[82] These aluminium complexes {Al(**90**)Me} were active, albeit slow initiators, for the ROP of *rac*-lactide in the presence of benzyl alcohol co-initiator. The reaction activity increased with decreasing steric influence from the phenyl ring substituents, interestingly the presence of chloro-phenyl substituents showed an enhanced rate over the methyl-phenyl substituents indicating possible electronic effects. Good molecular weight control was observed (PDI = 1.04 - 1.11), along with a varying stereocontrol. A strong isotactic bias was observed when R^2 = H (P_r = 0.21 – 0.32), when R^2 = Me, ^{t}Bu, or Cl heterotactic biased PLA was obtained (P_r = 0.61 – 0.96). The chloro-phenyl substituents yielded the highest degree of heterotactic selectivity indicating stereocontrol is not entirely sterically dependent. The amino nitrogen groups amplified any observed tacticity when the benzyl amine substituent was present (R^1 = CH_2Ph).

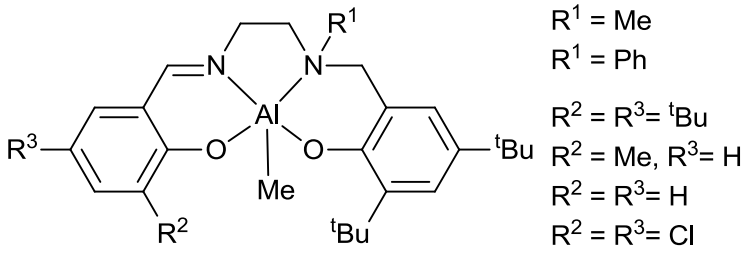

Figure 1.64: Salalen aluminium alkyl investigated for the ROP of *rac*-lactide in solution.[113]

Monometallic salalen aluminium {Al(**91**)Me} (Figure 1.64) complexes were investigated by Jones *et al*. for the ROP of *rac*-lactide in solution.[113] While active in the presence of a catalytic equivalence of benzyl alcohol the ROP reaction was slow. Well defined PLA chains were produced with molecular weights consistent with one propagating chain per metal and limited evidence of transesterification reactions occurring. In contrast to the related salan and salen aluminium initiators {Al(**85**)R^3, Al(**90**)Me} only minor-moderate stereocontrol was reported, additionally the stereocontrol exhibited was more dependent upon the amine substituents than the phenyl substituents. When R^1 = Me (except for Al(**91**)Me, $R^2 = R^3$ = ^{t}Bu) the resulting PLA was biased towards heterotactic stereoselectivity (P_r = 0.59 – 0.75), and a slight isotactic bias was observed when R^1 = Ph (P_r = 0.40 - 0.50).

In more recent years indium has been investigated for the ROP of lactide and the homoleptic complex $InCl_3$ was shown as a moderately active initiator for the ROP of *rac*-lactide achieving 96 % conversion in 5 h (25 °C, CH_2Cl_2, 203:1:1:2 monomer:initiator:BnOH:NEt_3).[41, 114] All three initiating components are required as exclusion of the $InCl_3$, BnOH, or NEt_3 renders the ROP reaction inactive. Excellent molecular weight control was reported with a linear relationship of molecular weight with varying *rac*-lactide, or varying BnOH ratio with respect to all other components. $InCl_3$ yields highly heterotactic PLA from the ROP of *rac*-lactide, this stereoselectivity was observed upon variation of initiator ratios and exposure to air. Although a very robust system an increase in temperature was detrimental to stereoselectivity and so is excess $InCl_3$ with respect to BnOH and NEt_3. The formation of an *in-situ* indium lactate complex as the active initiating/propagating species was speculated upon.

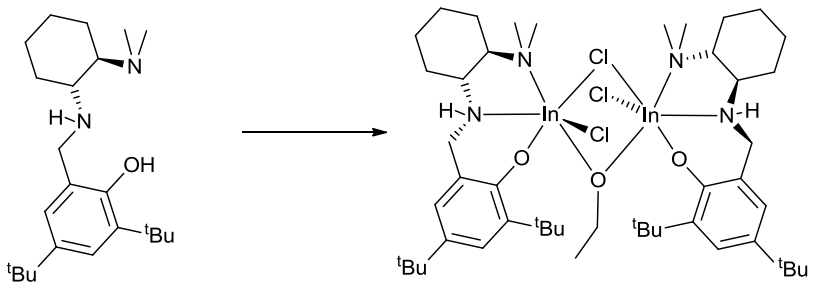

92H_2 (In(**92**)Cl)$_2$(μ–OEt)(μ–Cl)

Figure 1.65: A dimeric indium complex supported by (NNO) asymmetrically substituted *trans*-diaminocyclohexane ligands.[115]

A dimeric indium complex bearing (NNO) asymmetrically substituted *trans*-diaminocyclohexane (DACH) ligands (**92**H_2) (Figure 1.65) was the first reported example of the ROP of lactide by an indium complex.[115] The indium complex {(In(**92**)Cl)$_2$(μ-OEt)(μ-Cl)} is a dimeric structure in solution and the solid state. Moreover, the chiral DACH groups are exclusively *RR,RR* or *SS,SS* pairs within the dimer, no evidence was present to suggest an *RR,SS* or *SS,RR* dimer. The indium complex {(In(**92**)Cl)$_2$(μ-OEt)(μ-Cl)} is active for the ROP of lactide achieving 90 % in 30 mins (25 °C, CH_2Cl_2, 200:1 [monomer]:[initiator] ratio). The following ROP was living in character until high conversion was reached yielding low molecular weight distributions (PDI = 1.09 – 1.20). The resulting PLA was revealed as slightly isotactic (P_r = 0.38 – 0.47). While not dissociative at room temperature the indium complex {(In(**92**)Cl)$_2$(μ-OEt)(μ-Cl)} separates in the presence of a coordinating species, such as lactide, into the active species In(NNO)ClOEt and an inactive species In(NNO)Cl_2. There was a marked difference in the ROP activities towards *rac*-lactide between the racemic and enantiopure resolved indium structures, with respect to the DACH groups. Consequently enantiomorphic site control is thought to be significant for these indium initiators.

1.3.8 Non-metal initiators

4-Dimethylaminopyridine (DMAP) (**93**) was amongst the first non-metal based initiators reported for the ROP of lactide (Figure 1.66).[116] A protic alcohol was required as a co-initiator for the polymerisation to proceed. Furthermore the degree of polymerisation was dependent on the stoichiometric amount of alcohol utilised. Complete conversion was obtained after 50 h at 35 °C in CH_2Cl_2 at 120:1:2 [lactide]:[initiator]:[alcohol] ratio. These organic based initiators resulted in well defined molecular weight distributions (PDI = 1.08 – 1.13) and no indication of transesterification side reactions. The nucleophilic DMAP (**93**) is thought to activate the lactide monomer which allows the protic alcohol in initiate the polymerisation *via* attack of the activated DMAP-lactide species.

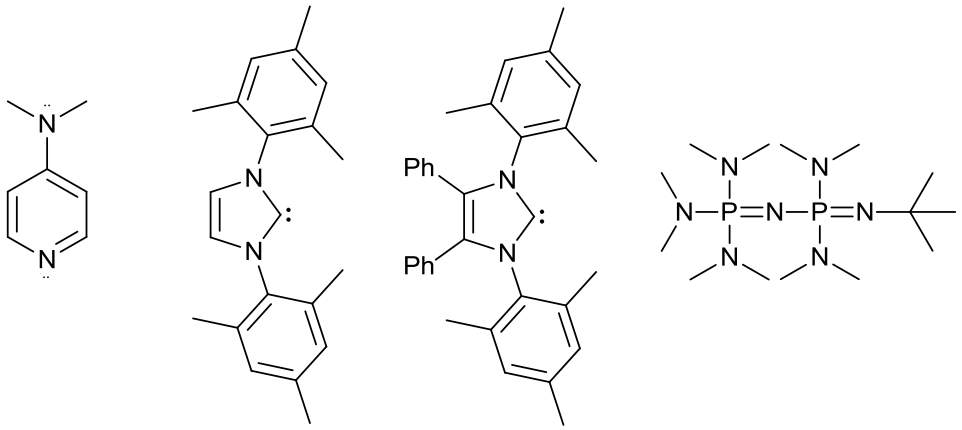

Figure 1.66: Non metallic based initiators for the ROP of lactide.[116-119]

Hillmyer and Tolman *et al*. reported the use of carbenes for the ROP of *rac*-lactide.[117] The carbene **94** (Figure 1.66) was investigated at reduced temperature (-20 °C, CH_2Cl_2) and obtained good conversion (71 %) within 20 mins at 150:1 [*rac*-lactide]:[initiator] ratio in the presence of benzyl alcohol. A moderate isotactic bias (P_r = 0.25) was observed for the reduced temperature polymerisation of *rac*-lactide by **94**. Upon increasing the polymerisation temperature (25 °C) a reduction in selectivity was observed (P_r = 0.41). Further work on carbenes was conducted by Waymouth and Hedrick *et al*. for the ROP of *rac*-lactide and *meso*-lactide.[118] The carbene **95** (Figure 1.66) was investigated at variable temperatures and resulted in a similar degree of isotacticity (P_r = 0.28) at -15 °C.[118] The polymerisation proceeded at -70 °C achieving 91 % conversion after 2 h at 100:1 [*rac*-lactide]:[initiator] ratio, under these condition a high isotactic (P_r = 0.10) bias was reported.

A dimeric phosphazene base (**96**) (Figure 1.66) was reported for the ROP of *rac*-lactide and was demonstrated to be highly active resulting in high conversion (85 %) after 3 mins with a catalytic equivalence of 1-pyrenebutanol co-initiator (25 °C, toluene, at 100:1 [*rac*-lactide]:[initiator] ratio).[119] At reduced temperature (-75 °C) the reaction required 3 h to achieve full conversion (> 99 %) and the resulting PLA was highly isotactic (P_r = 0.05). The polymerisation was controlled with no evidence of transesterification side reactions occurring at -75 °C and a low PDI value was obtained (PDI = 1.11). From experimental evidence it was postulated

that the ROP initially proceeded via activation of the alcohol by the phosphazene base (**96**).

1.4 Co-Polymers

1.4.1 Poly(lactide-co-glycolide)

The physical properties of polylactide can be tuned through co-polymerisation of lactide and glycolide. Adjusting the glycolide to lactide ratio within poly(lactide-co-glycolide) (Figure 1.67) co-polymer adjusts the physical properties, in particular the biodegradability. Both lactide and glycolide are biocompatible along with their resulting polymers as they degrade into lactic acid and glycolic acid respectively under biological conditions. Poly(lactide-co-glycolide) co-polymers have seen use within the medical industry for sutures and backbone pins.[7, 120] Surgical applications of poly(lactide-co-glycolide) co-polymers contain higher proportions of glycolide (70 % – 92 %). Co-polymer blends containing lower proportions of glycolide (20 % - 50 %) have seen use within drug delivery systems typically in the form of polymer implants.[2] The polycondensation reaction of glycolic acid and lactic acid yields low molecular weight polymers. As a consequence the dehydrated cyclic starting reagents (lactide and glycolide) procured interest. As high molecular weight polymers could be produced together with potential control over the monomer sequence. A large degree of variation is possible of the co-polymers as not only can glycolide be varied the stoichiometry of *L*-, *D*-lactide isomers can tuned.

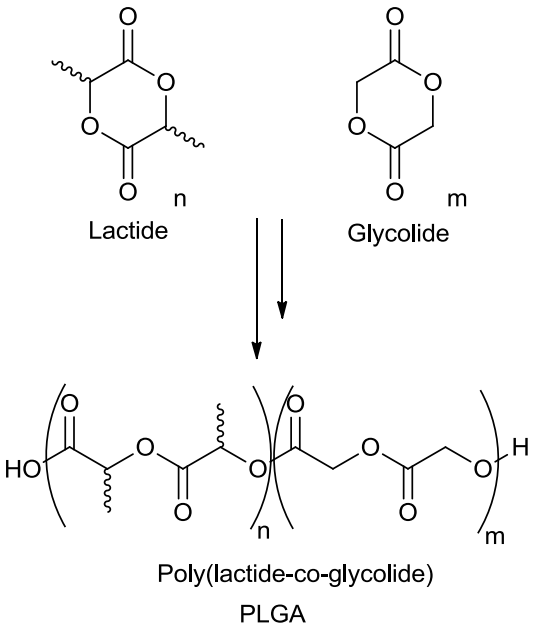

Figure 1.67: Scheme depicting the formation of poly(lactide-co-glycolide).[2]

1.4.2 Poly(lactide-co-ε-caprolactone)

Co-polymers of lactide with ε-caprolactone have been reported through the literature, each polymer has been investigated individually for medical and pharmaceutical applications.[121] The co-polymerisation of ε-caprolactone and lactide allows physical aspects of each polymer to be varied in the resulting co-polymer (Figure 1.68). Poly(lactide-co-ε-caprolactone) combines the good degradation in physiological media of PLA with the high permeability towards drug molecules that poly(ε-caprolactone) displays.[89, 121, 122] PLA has good mechanical properties and poor elasticity while poly(ε-caprolactone) has poor mechanical properties, good elasticity, and enhanced thermal properties.[89, 121, 122] The co-polymer properties can be adjusted by the; stoichiometry of the incorporated cyclic esters, molecular weight, and monomer sequence (block and random polymer).[122] Block co-polymers of poly(lactide-co-caprolactone) have been reported, Davidson *et al.* reported that the order of addition was critical to prepare a block-co-polymer. For example, caprolactone must be polymerised first, if lactide is polymerised first only a homopolymer was isolated.[89] A random co-polymer microstructure in a 1:1 ratio of lactide and caprolactone where equal proportions of each were introduced into the polymer chains was reported by Nomura *et. al.*[123]

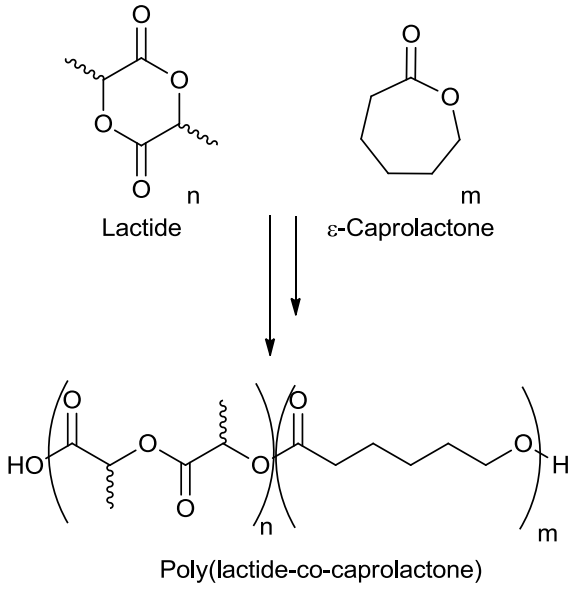

Figure 1.68: Scheme depicting the formation of poly(lactide-co-ε-caprolactone).[123]

1.4.3 Poly(lactide-co-δ-valerolactone)

Polymeric material formed from cyclic esters have been used for pharmaceutical and medical purposes for the biocompatibility and biodegradable properties of these polymers, including poly(δ-valerolactone).[121] Poly(δ-valerolactone) has similar properties to poly(ε-caprolactone) and co-polymerisation with lactide monomers can selectively vary the physical properties of the polymers. The melting point (T_m) of poly(δ-valerolactone) is 62 °C and co-polymer blends with lactide reduce the T_m of the co-polymer dependent upon the quantity of lactide introduced into the polymer, to widen the application of both polymers.[124] The microstructure of the co-polymerisation of δ-valerolactone and lactide is dependent upon the initiator.[124, 125] Where the initiator preferred the incorporation of the one monomer over the other a tapered co-polymer can be formed. The degree of polymerisation of a block of a single monomer within random poly(lactide-co-δ-valerolactone) (Figure 1.69) was dependent upon the stoichiometry of the valerolactone and lactide. The co-polymerisation of δ-valerolactone has been conducted using *L*-lactide[124] and *rac*-lactide.[125]

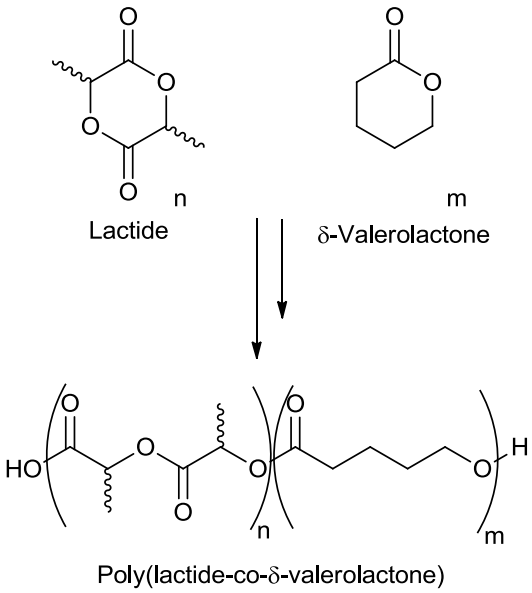

Figure 1.69: Scheme depicting the formation of poly(lactide-co-δ-valerolactone).[124]

1.5 Aims and Objectives

The development of initiators for the ROP of lactide and investigation of their behaviour is reported herein. The aim is to develop stereoselective initiators which preferably produce highly isotactic stereoblock PLA from *rac*-lactide for its enhanced thermal properties and crystallinity.[45] High activity and polymer molecular weight control is desired for applicability within industry.[44, 45] Meeting these requirement under relatively environmentally favoured solvent free conditions is desired. The initiators should use non-toxic and bio-compatible materials to fully exploit the uses of PLA.[44] Where possible abundant and cheap materials should be investigated to enhance the initiators industrial appeal.[44]

This thesis focuses upon metal based initiators around group 4 and aluminium. Piperazine/homopiperazine amine bis(phenol) ligands were complexed with group 4 and aluminium metals. Their relation to group 4 salan complexes {M(**39**-**42**)(O^iPr)$_2$}, which have previously reported moderate isotacticity led to our interest.[89, 90] Also aluminium salan complexes {Al(**90**)Me} have reported interesting stereoselectivity, which is dependent upon the phenoxy substituents.[82] Furthermore, 1,4-DACH based salen ligands were investigated, which are a derivative of the 1,2-DACH salen ligands that previously resulted in highly isotactic selective aluminium initiator

{Al(**86**)O^{i}Pr}.[30, 111] Further work was conducted with 1,2-DACH salalen aluminium initiators, as stated above, 1,2-DACH salen aluminium complexes previously resulted in high stereoselectivity. The salalen ligand system allows the systematic study of the amine and imine influence upon the ROP of lactide. Additionally aluminium salalen complexes {Al(**91**)O^{i}Pr} have previously shown promise as initiators for the ROP of lactide.[113]

1.6 References

1. A. K. Mohanty, M. Misra and G. Hinrichsen, *Macromol. Mater. Eng.*, 2000, **276**, 1-24.
2. O. Dechy-Cabaret, B. Martin-Vaca and D. Bourissou, *Chem. Rev.*, 2004, **104**, 6147-6176.
3. S. Mecking, *Angew. Chem., Int. Ed.*, 2004, **43**, 1078-1085.
4. C. M. Thomas, *Chem. Soc. Rev.*, 2010, **39**, 165-173.
5. J.-D. Gu, *Int. Biodeterior. Biodegrad.*, 2003, **52**, 69-91.
6. D. Klemm, B. Heublein, H. P. Fink and A. Bohn, *Angew. Chem., Int. Ed.*, 2005, **44**, 3358-3393.
7. W. Amass, A. Amass and B. Tighe, *Polym. Int.*, 1998, **47**, 89-144.
8. I. Acar, A. Kasgoz, S. Ozgumus and M. Orbay, *Polym.-Plast. Technol. Eng.*, 2006, **45**, 351-359.
9. G. Scott, *Polym. Degrad. Stab.*, 2000, **68**, 1-7.
10. D. M. Wiles and G. Scott, *Polym. Degrad. Stab.*, 2006, **91**, 1581-1592.
11. L. Zan, W. Fa and S. Wang, *Environ. Sci. Technol.*, 2006, **40**, 1681-1685.
12. A. A. Shah, F. Hasan, A. Hameed and S. Ahmed, *Biotechnol. Adv.*, 2008, **26**, 246-265.
13. D. Garlotta, *J. Polym. Environ.*, 2001, **9**, 63-84.
14. C. J. Frankis, PhD Thesis, 2010.
15. P. M. J. Pelouze, *Ann. Chim. Phys.*, 1845, **13**, 257.
16. P. Gruber and M. O'Brien, in *Biopolymers Online*, Wiley-VCH Verlag GmbH & Co. KGaA, 2005.
17. http://www.natureworksllc.com, 25th February 2013
18. R. Auras, B. Harte and S. Selke, *Macromol. Biosci.*, 2004, **4**, 835-864.
19. L. T. Lim, R. Auras and M. Rubino, *Prog. Polym. Sci.*, 2008, **33**, 820-852.
20. R. Datta and M. Henry, *J. Chem. Technol. Biotechnol.*, 2006, **81**, 1119-1129.
21. K. A. Athanasiou, G. G. Niederauer and C. M. Agrawal, *Biomaterials*, 1996, **17**, 93-102.
22. B. Gupta, N. Revagade and J. Hilborn, *Prog. Polym. Sci.*, 2007, **32**, 455-482.
23. E.-R. Kenawy, G. L. Bowlin, K. Mansfield, J. Layman, D. G. Simpson, E. H. Sanders and G. E. Wnek, *J. Controlled Release*, 2002, **81**, 57-64.
24. A. Bhaw-Luximon, D. Jhurry, N. Spassky, S. Pensec and J. Belleney, *Polymer*, 2001, **42**, 9651-9656.
25. M. J. Stanford and A. P. Dove, *Chem. Soc. Rev.*, 2010, **39**, 486-494.

26. Y. Shibasaki, H. Sanada, M. Yokoi, F. Sanda and T. Endo, *Macromolecules*, 2000, **33**, 4316-4320.
27. D. Bourissou, B. Martin-Vaca, A. Dumitrescu, M. Graullier and F. Lacombe, *Macromolecules*, 2005, **38**, 9993-9998.
28. H. R. Kricheldorf, M. Berl and N. Scharnagl, *Macromolecules*, 1988, **21**, 286-293.
29. P. Dubois, C. Jacobs, R. Jerome and P. Teyssie, *Macromolecules*, 1991, **24**, 2266-2270.
30. Z. Zhong, P. J. Dijkstra and J. Feijen, *Angew. Chem., Int. Ed.*, 2002, **41**, 4510-4513.
31. C. X. Song and X. D. Feng, *Macromolecules*, 1984, **17**, 2764-2767.
32. T. Aida, Y. Maekawa, S. Asano and S. Inoue, *Macromolecules*, 1988, **21**, 1195-1202.
33. N. Ajellal, J.-F. Carpentier, C. Guillaume, S. M. Guillaume, M. Helou, V. Poirier, Y. Sarazin and A. Trifonov, *Dalton Trans.*, 2010, **39**, 8363-8376.
34. E. Piedra-Arroni, P. Brignou, A. Amgoune, S. M. Guillaume, J.-F. Carpentier and D. Bourissou, *Chem. Commun.*, 2011, **47**, 9828-9830.
35. T. Biela, A. Duda and S. Penczek, *Macromol. Symp.*, 2002, **183**, 1-10.
36. B. M. Chamberlain, M. Cheng, D. R. Moore, T. M. Ovitt, E. B. Lobkovsky and G. W. Coates, *J. Am. Chem. Soc.*, 2001, **123**, 3229-3238.
37. N. Spassky, M. Wisniewski, C. Pluta and A. Le Borgne, *Macromol. Chem. Phys.*, 1996, **197**, 2627-2637.
38. H. Tsuji, *Macromol. Biosci.*, 2005, **5**, 569-597.
39. J. E. Kasperczyk, *Macromolecules*, 1995, **28**, 3937-3939.
40. K. A. M. Thakur, R. T. Kean, E. S. Hall, J. J. Kolstad, T. A. Lindgren, M. A. Doscotch, J. I. Siepmann and E. J. Munson, *Macromolecules*, 1997, **30**, 2422-2428.
41. A. Pietrangelo, M. A. Hillmyer and W. B. Tolman, *Chem. Commun.*, 2009, 2736-2737.
42. M. Bero, P. Dobrzynski and J. Kasperczyk, *J. Polym. Sci., Part A: Polym. Chem.*, 1999, **37**, 4038-4042.
43. G. W. Coates, *Chem. Rev.*, 2000, **100**, 1223-1252.
44. R. H. Platel, L. M. Hodgson and C. K. Williams, *Polym. Rev.*, 2008, **48**, 11-63.
45. X. Pang, X. Zhuang, Z. Tang and X. Chen, *Biotechnol. J.*, 2010, **5**, 1125-1136.
46. J. Wu, T.-L. Yu, C.-T. Chen and C.-C. Lin, *Coord. Chem. Rev.*, 2006, **250**, 602-626.
47. B. J. O'Keefe, M. A. Hillmyer and W. B. Tolman, *J. Chem. Soc., Dalton Trans.*, 2001, **0**, 2215-2224.
48. P. J. Dijkstra, H. Du and J. Feijen, *Polym. Chem.*, 2011, **2**, 520-527.
49. A. J. Nijenhuis, D. W. Grijpma and A. J. Pennings, *Macromolecules*, 1992, **25**, 6419-6424.
50. A. Kowalski, A. Duda and S. Penczek, *Macromolecules*, 2000, **33**, 7359-7370.
51. M. Ryner, K. Stridsberg, A.-C. Albertsson, H. von Schenck and M. Svensson, *Macromolecules*, 2001, **34**, 3877-3881.
52. A. Kowalski, A. Duda and S. Penczek, *Macromolecules*, 2000, **33**, 689-695.
53. R. H. Platel, L. M. Hodgson and C. K. Williams, *Polym. Rev.*, 2008, **48**, 11-63.

54. N. Nimitsiriwat, E. L. Marshall, V. C. Gibson, M. R. J. Elsegood and S. H. Dale, *J. Am. Chem. Soc.*, 2004, **126**, 13598-13599.
55. N. Nimitsiriwat, V. C. Gibson, E. L. Marshall and M. R. J. Elsegood, *Dalton Trans.*, 2009, 3710-3715.
56. A. P. Dove, V. C. Gibson, E. L. Marshall, A. J. P. White and D. J. Williams, *Chem. Commun.*, 2001, 283-284.
57. A. P. Dove, V. C. Gibson, E. L. Marshall, H. S. Rzepa, A. J. P. White and D. J. Williams, *J. Am. Chem. Soc.*, 2006, **128**, 9834-9843.
58. N. Nimitsiriwat, V. C. Gibson, E. L. Marshall, A. J. P. White, S. H. Dale and M. R. J. Elsegood, *Dalton Trans.*, 2007, 4464-4471.
59. M. H. Chisholm and E. E. Delbridge, *New J. Chem.*, 2003, **27**, 1177-1183.
60. L. Sipos, M. Zsuga and T. Kelen, *Polym. Bull.*, 1992, **27**, 495-502.
61. M.-L. Hsueh, B.-H. Huang, J. Wu and C.-C. Lin, *Macromolecules*, 2005, **38**, 9482-9487.
62. M. H. Chisholm, J. C. Gallucci and K. Phomphrai, *Inorg. Chem.*, 2005, **44**, 8004-8010.
63. M. H. Chisholm, J. Gallucci and K. Phomphrai, *Inorg. Chem.*, 2002, **41**, 2785-2794.
64. M. H. Chisholm, J. C. Huffman and K. Phomphrai, *J. Chem. Soc., Dalton Trans.*, 2001, 222-224.
65. M. H. Chisholm, J. C. Gallucci and K. Phomphrai, *Inorg. Chem.*, 2004, **43**, 6717-6725.
66. M. H. Chisholm, J. Gallucci and K. Phomphrai, *Chem. Commun.*, 2003, 48-49.
67. M. H. Chisholm and N. W. Eilerts, *Chem. Commun.*, 1996, 853-854.
68. M. H. Chisholm, N. W. Eilerts, J. C. Huffman, S. S. Iyer, M. Pacold and K. Phomphrai, *J. Am. Chem. Soc.*, 2000, **122**, 11845-11854.
69. L. F. Sánchez-Barba, A. Garcés, M. Fajardo, C. Alonso-Moreno, J. Fernández-Baeza, A. Otero, A. Antiñolo, J. Tejeda, A. Lara-Sánchez and M. I. López-Solera, *Organometallics*, 2007, **26**, 6403-6411.
70. L. F. Sánchez-Barba, A. s. Garcés, J. Fernández-Baeza, A. Otero, C. Alonso-Moreno, A. n. Lara-Sánchez and A. M. Rodríguez, *Organometallics*, 2011, **30**, 2775-2789.
71. A. s. Garcés, L. F. Sánchez-Barba, C. Alonso-Moreno, M. Fajardo, J. Fernández-Baeza, A. Otero, A. n. Lara-Sánchez, I. López-Solera and A. M. a. Rodríguez, *Inorg. Chem.*, 2010, **49**, 2859-2871.
72. Y. Huang, W.-C. Hung, M.-Y. Liao, T.-E. Tsai, Y.-L. Peng and C.-C. Lin, *J. Polym. Sci., Part A: Polym. Chem.*, 2009, **47**, 2318-2329.
73. W. M. Stevels, M. J. K. Ankoné, P. J. Dijkstra and J. Feijen, *Macromolecules*, 1996, **29**, 3332-3333.
74. W. M. Stevels, M. J. K. Ankoné, P. J. Dijkstra and J. Feijen, *Macromolecules*, 1996, **29**, 6132-6138.
75. W. M. Stevels, M. J. K. Ankoné, P. J. Dijkstra and J. Feijen, *Macromol. Chem. Phys.*, 1995, **196**, 1153-1161.
76. L. M. Hodgson, R. H. Platel, A. J. P. White and C. K. Williams, *Macromolecules*, 2008, **41**, 8603-8607.
77. F. Bonnet, A. R. Cowley and P. Mountford, *Inorg. Chem.*, 2005, **44**, 9046-9055.
78. C. X. Cai, A. Amgoune, C. W. Lehmann and J. F. Carpentier, *Chem. Commun.*, 2004, 330-331.

79. A. Amgoune, C. M. Thomas, T. Roisnel and J.-F. Carpentier, *Chem. Eur. J.*, 2006, **12**, 169-179.
80. X. Liu, X. Shang, T. Tang, N. Hu, F. Pei, D. Cui, X. Chen and X. Jing, *Organometallics*, 2007, **26**, 2747-2757.
81. Y. Luo, W. Li, D. Lin, Y. Yao, Y. Zhang and Q. Shen, *Organometallics*, 2010, **29**, 3507-3514.
82. P. Hormnirun, E. L. Marshall, V. C. Gibson, A. J. P. White and D. J. Williams, *J. Am. Chem. Soc.*, 2004, **126**, 2688-2689.
83. M. Mazzeo, M. Lamberti, I. D'Auria, S. Milione, J. C. Peters and C. Pellecchia, *J. Polym. Sci., Part A: Polym. Chem.*, 2010, **48**, 1374-1382.
84. L. Clark, M. G. Cushion, H. E. Dyer, A. D. Schwarz, R. Duchateau and P. Mountford, *Chem. Commun.*, 2010, **46**, 273-275.
85. A. Buchard, R. H. Platel, A. Auffrant, X. F. Le Goff, P. Le Floch and C. K. Williams, *Organometallics*, 2010, **29**, 2892-2900.
86. A. J. Chmura, D. M. Cousins, M. G. Davidson, M. D. Jones, M. D. Lunn and M. F. Mahon, *Dalton Trans.*, 2008, 1437-1443.
87. C. K. A. Gregson, I. J. Blackmore, V. C. Gibson, N. J. Long, E. L. Marshall and A. J. P. White, *Dalton Trans.*, 2006, 3134-3140.
88. T. K. Saha, V. Ramkumar and D. Chakraborty, *Inorg. Chem.*, 2011, **50**, 2720-2722.
89. A. J. Chmura, M. G. Davidson, M. D. Jones, M. D. Lunn, M. F. Mahon, A. F. Johnson, P. Khunkamchoo, S. L. Roberts and S. S. F. Wong, *Macromolecules*, 2006, **39**, 7250-7257.
90. S. Gendler, S. Segal, I. Goldberg, Z. Goldschmidt and M. Kol, *Inorg. Chem.*, 2006, **45**, 4783-4790.
91. E. L. Whitelaw, M. D. Jones and M. F. Mahon, *Inorg. Chem.*, 2010, **49**, 7176-7181.
92. E. Sergeeva, J. Kopilov, I. Goldberg and M. Kol, *Inorg. Chem.*, 2010, **49**, 3977-3979.
93. Y. Kim, G. K. Jnaneshwara and J. G. Verkade, *Inorg. Chem.*, 2003, **42**, 1437-1447.
94. Y. Kim and J. G. Verkade, *Macromol. Symp.*, 2005, **224**, 105-118.
95. A. J. Chmura, M. G. Davidson, C. J. Frankis, M. D. Jones and M. D. Lunn, *Chem. Commun.*, 2008, 1293-1295.
96. A. D. Schwarz, A. L. Thompson and P. Mountford, *Inorg. Chem.*, 2009, **48**, 10442-10454.
97. A. D. Schwarz, K. R. Herbert, C. Paniagua and P. Mountford, *Organometallics*, 2010, **29**, 4171-4188.
98. Y. Takashima, Y. Nakayama, K. Watanabe, T. Itono, N. Ueyama, A. Nakamura, H. Yasuda, A. Harada and J. Okuda, *Macromolecules*, 2002, **35**, 7538-7544.
99. Y. Takashima, Y. Nakayama, T. Hirao, H. Yasuda and A. Harada, *J. Organomet. Chem.*, 2004, **689**, 612-619.
100. A. P. Dove, V. C. Gibson, E. L. Marshall, A. J. P. White and D. J. Williams, *Dalton Trans.*, 2004, 570-578.
101. C. K. Williams, L. E. Breyfogle, S. K. Choi, W. Nam, V. G. Young, M. A. Hillmyer and W. B. Tolman, *J. Am. Chem. Soc.*, 2003, **125**, 11350-11359.
102. H.-Y. Chen, H.-Y. Tang and C.-C. Lin, *Macromolecules*, 2006, **39**, 3745-3752.
103. M. P. Coles and P. B. Hitchcock, *Eur. J. Inorg. Chem.*, 2004, 2662-2672.

104. A. Otero, J. Fernández-Baeza, L. F. Sánchez-Barba, J. Tejeda, M. Honrado, A. Garcés, A. Lara-Sánchez and A. M. Rodríguez, *Organometallics*, 2012, **31**, 4191-4202.
105. L. Trofimoff, T. Aida and S. Inoue, *Chem. Lett.*, 1987, 991-994.
106. A. Kowalski, A. Duda and S. Penczek, *Macromolecules*, 1998, **31**, 2114-2122.
107. T. M. Ovitt and G. W. Coates, *J. Polym. Sci., Part A: Polym. Chem.*, 2000, **38**, 4686-4692.
108. K. Majerska and A. Duda, *J. Am. Chem. Soc.*, 2004, **126**, 1026-1027.
109. N. Nomura, R. Ishii, M. Akakura and K. Aoi, *J. Am. Chem. Soc.*, 2002, **124**, 5938-5939.
110. N. Nomura, R. Ishii, Y. Yamamoto and T. Kondo, *Chem. Eur. J.*, 2007, **13**, 4433-4451.
111. Z. Zhong, P. J. Dijkstra and J. Feijen, *J. Am. Chem. Soc.*, 2003, **125**, 11291-11298.
112. H. Du, A. H. Velders, P. J. Dijkstra, J. Sun, Z. Zhong, X. Chen and J. Feijen, *Chem. Eur. J.*, 2009, **15**, 9836-9845.
113. E. L. Whitelaw, G. Loraine, M. F. Mahon and M. D. Jones, *Dalton Trans.*, 2011, **40**, 11469-11473.
114. A. Pietrangelo, S. C. Knight, A. K. Gupta, L. J. Yao, M. A. Hillmyer and W. B. Tolman, *J. Am. Chem. Soc.*, 2010, **132**, 11649-11657.
115. A. F. Douglas, B. O. Patrick and P. Mehrkhodavandi, *Angew. Chem., Int. Ed.*, 2008, **47**, 2290-2293.
116. F. Nederberg, E. F. Connor, M. Möller, T. Glauser and J. L. Hedrick, *Angew. Chem., Int. Ed.*, 2001, **40**, 2712-2715.
117. T. R. Jensen, L. E. Breyfogle, M. A. Hillmyer and W. B. Tolman, *Chem. Commun.*, 2004, **0**, 2504-2505.
118. A. P. Dove, H. Li, R. C. Pratt, B. G. G. Lohmeijer, D. A. Culkin, R. M. Waymouth and J. L. Hedrick, *Chem. Commun.*, 2006, **0**, 2881-2883.
119. L. Zhang, F. Nederberg, J. M. Messman, R. C. Pratt, J. L. Hedrick and C. G. Wade, *J. Am. Chem. Soc.*, 2007, **129**, 12610-12611.
120. J. C. Middleton and A. J. Tipton, *Biomaterials*, 2000, **21**, 2335-2346.
121. A.-C. Albertsson and I. K. Varma, *Biomacromolecules*, 2003, **4**, 1466-1486.
122. D. Pappalardo, L. Annunziata and C. Pellecchia, *Macromolecules*, 2009, **42**, 6056-6062.
123. N. Nomura, A. Akita, R. Ishii and M. Mizuno, *J. Am. Chem. Soc.*, 2010, **132**, 1750-1751.
124. A. Nakayama, N. Kawasaki, Y. Maeda, I. Arvanitoyannis, S. Aiba and N. Yamamoto, *J. Appl. Polym. Sci.*, 1997, **66**, 741-748.
125. D. J. Darensbourg, O. Karroonnirun and S. J. Wilson, *Inorg. Chem.*, 2011, **50**, 6775-6787.

Chapter 2

2. Titanium (IV) Homo/Piperazine Salan Complexes and Their Application for the ROP of *rac*-Lactide

2. Titanium (IV) Homo/Piperazine Salan Complexes and Their Application for the ROP of *rac*-Lactide

2.1 Introduction

Metal complexes derived from tetradentate amine bis(phenol) ligands (Figure 2.01) have been extensively utilised for the ROP of lactide.[1-7] Aluminium tetradentate imine bis(phenoxy) complexes containing flexible backbones have been used to produce highly isotactic enriched PLA from *rac*-lactide.[8, 9] Related aluminium tetradentate amine bis(phenoxy) complexes have also been reported for the ROP of *rac*-lactide, the stereoselectivity obtained was shown to be reliant upon the phenoxy substituents.[2] Although they were all slow, moderately isotactic biased PLA was reported ranging to highly heterotactic PLA.

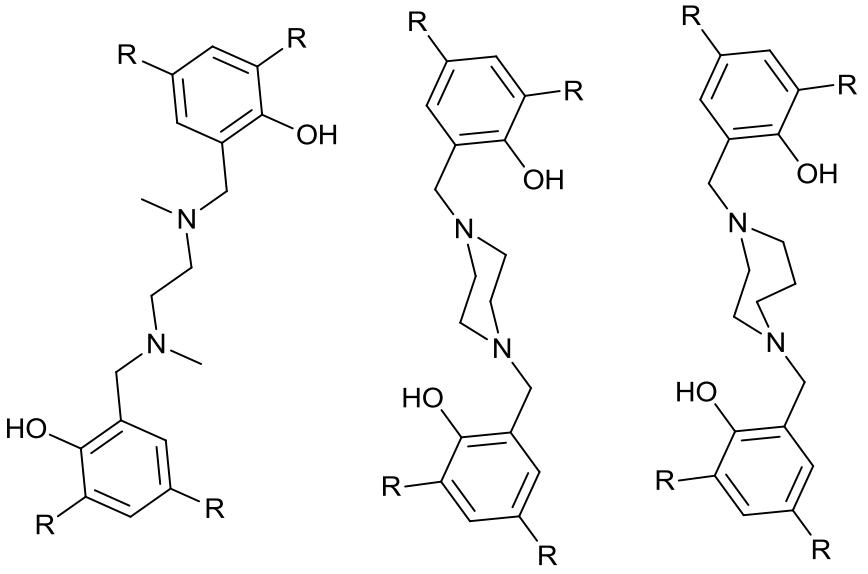

Figure 2.01: Examples of flexible tetradentate amine bis(phenol) ligands and ridged piperazine and homopiperazine bis(phenol) ligands.

Group 4 metals complexed to tetradentate imine bis(phenol) ligands have been reported for the polymerisation of lactide, these initiators produced atactic PLA from the ROP of *rac*-lactide.[10, 11] Although no stereoselectivity was obtained the initiators proved moderately active and resulted in well defined molecular weight PLA. The related group 4 tetradentate amine bis(phenoxy) complexes investigated by Davidson *et al.*[5] and Kol *et al.*[4] proved to be more stereoselective for the ROP of

rac-lactide. Limited activity was observed in the solution state but all the initiators proved to be moderately active initiators for the solvent free polymerisation of lactide. Moderate isotacticity was reported for these bis(phenoxy) complexes that contain a flexible bridging diamine.[5] Herein is reported the synthesis and polymerisation activity of related compounds where the flexible bridging diamine has been substituted with a ridged piperazine and homopiperazine diamines.

Piperazine salan ligands complexed to aluminium have previously been utilised for the ROP of *rac*-lactide with little success (Figure 2.01).[12] Bimetallic[13] and monometallic[14] complex coordination geometries have been reported and shown to be highly active initiators for the ROP of ε-caprolactone. Yao *et al.*[15, 16] have reported the synthesis of piperazine salan ligands for the coordination to lanthanides with various monometallic and bimetallic configurations being adopted. The formation of lanthanide-lithium multi-metallic piperazine salan complexes were also developed by Yao *et al.*[15, 16] The lanthanide metal complexes were shown to be highly active initiators for the ROP of lactide at > 1000:1 [monomer]:[initiator] ratios. Furthermore, the resulting PLA form *rac*-lactide exhibited moderate heterotactic selectivity. Mountford *et al.*[17] previously reported the coordination of similar piperazine bridged bis(phenylamino) ligands to titanium resulting in monometallic titanium imido structures.

2.2 Homo/Piperazine Salan Ligands

2.2.1 Synthesis of homo/piperazine salan ligands

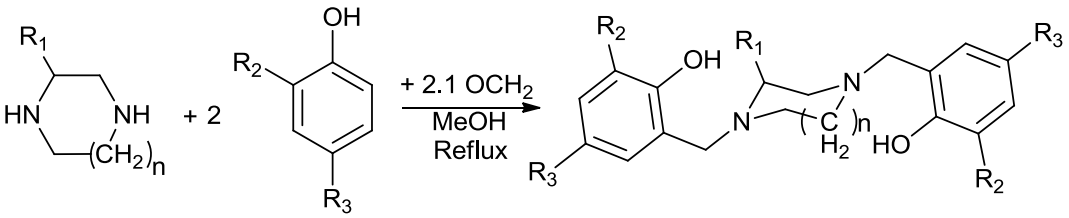

	n	R_1	R_2	R_3
1H_2 =	1	H,	Me,	Me
2H_2 =	1,	H,	Me,	^{t}Bu
3H_2 =	1,	H,	^{t}Bu,	^{t}Bu
4H_2 =	1,	H,	^{t}Bu,	Me
5H_2 =	1,	H,	Amyl,	Amyl

	n	R_1	R_2	R_3
6H_2 =	2	H,	Me,	Me
7H_2 =	2,	H,	Me,	^{t}Bu
8H_2 =	2,	H,	^{t}Bu,	^{t}Bu
9H_2 =	2,	H,	^{t}Bu,	Me
10H_2 =	2,	H,	Amyl,	Amyl
11H_2 =	2,	H,	H,	^{t}Bu

	n	R_1	R_2	R_3
12H_2 =	1,	Me,	^{t}Bu,	^{t}Bu
13H_2 =	1,	Me,	^{t}Bu,	Me
14H_2 =	1,	Me,	Amyl,	Amyl
15H_2 =	1,	Me,	Me,	tBu

Figure 2.02: Reaction pathway detailing the synthesis of piperazine and homopiperazine salan ligands.

The piperazine salan ligands were synthesised according to literature methods.[18] With the exception of **11**H_2, which was adapted from the synthesis procedure reported by Balakrishna *et al.*[19] The reaction is a one pot synthesis which requires heating (Figure 2.02), the pure ligands are obtained in good yields by filtration and washing with methanol. Specifically for **11**H_2 the reactive iminium ion is first produced then the phenol is introduced under less thermodynamic conditions. This method limits the probability of attack upon both *ortho*-positions of the 4-^{t}Bu-phenol.

2.2.2 Characterisation of homo/piperazine salan ligands

All the ligands isolated were fully characterised by ^{1}H and ^{13}C{^{1}H} NMR spectroscopy and high resolution ESI-TOF mass spectrometry. **1**H_2 (Figure 2.03) **3**H_2 and **8**H_2 (Figure 2.04) were characterised by X-ray crystallography. In all cases the solid-state structure showed the ligands adopt the chair configuration. A hydrogen bond exists between the phenol and the amine nitrogen, in all cases the hydrogen bond length was found to be between 1.8204 and 1.9954 Å.

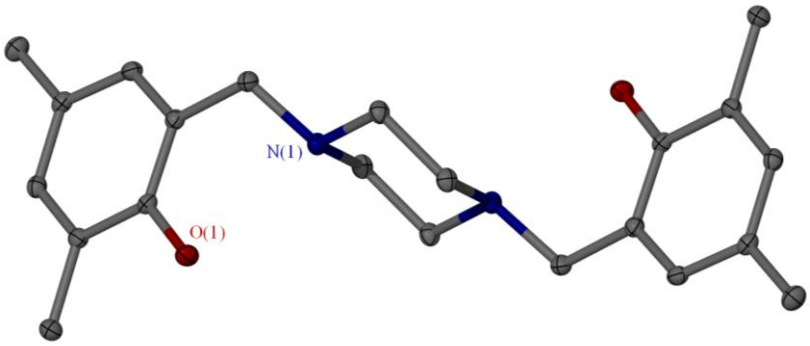

Figure 2.03: Solid-state structure for **1**H_2. Ellipsoids are shown at the 30 % probability level, hydrogens have been omitted for clarity.

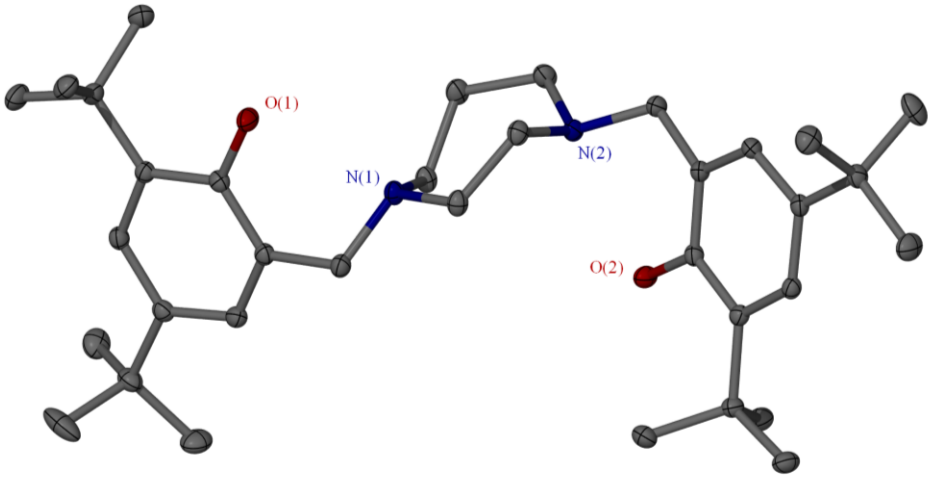

Figure 2.04: Solid-state structure for **8**H_2. Ellipsoids are shown at the 30 % probability level, hydrogens have been omitted for clarity.

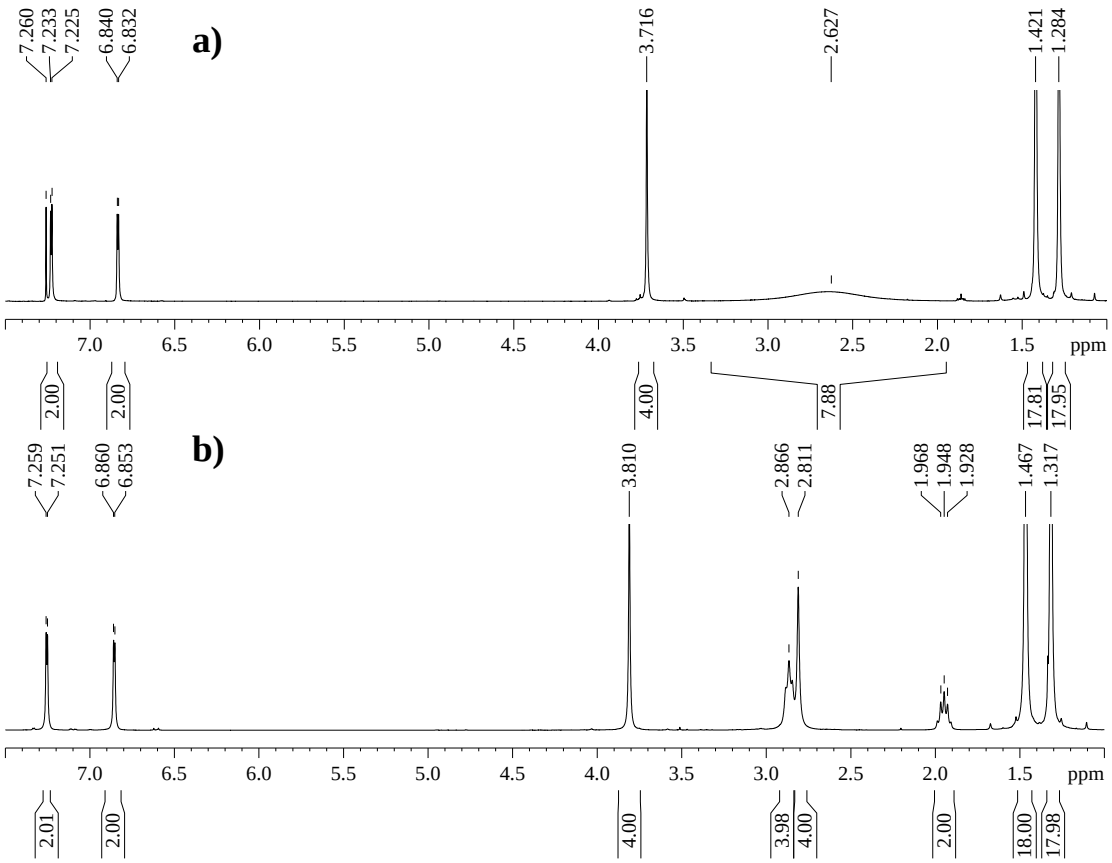

Figure 2.05: **a**) ^{1}H NMR spectrum of **3**H_2, **b**) ^{1}H NMR spectrum of **8**H_2

The ^{1}H and ^{13}C{^{1}H} NMR spectra for (**1-15**)H_2 were consistent with the solid-state structures. The ^{1}H NMR spectra for piperazine bridged salan **3**H_2 is shown in figure 2.05a. The aromatic proton region shows two proton resonances and a singlet for the N-C**H**$_2$-Ar protons at 3.72 ppm, these observations are consistent across ligands (**1-5**)H_2. The piperazine ring is fluxional on the NMR timescale where the equatorial and axial protons are interconverting, this is represented by the corresponding broad region between 2.20 – 3.10 ppm (Figure 2.05a).

The homopiperazine bridged salan ligands {(**6-11**)H_2} revealed similar trends, a representative ^{1}H NMR spectrum of **8**H_2 is given in figure 2.05b. The aromatic protons (6.70 – 7.30 ppm), N-C**H**$_2$-Ar (3.70 – 3.90 ppm), and the phenoxy substituent regions (~ 1.00 – 2.00 ppm) were well defined throughout compounds (**6-11**)H_2 (Figure 2.05b). For compounds (**6-11**)H_2 the homopiperazine ring proton region showed three resonances (2.87, 2.81, 1.95 ppm), this was attributed to a fast homopiperazine ring-flipping process on the ^{1}H NMR timescale. The fast

homopiperazine ring-flipping process causes the axial and equatorial ring protons to be observed as equivalent.

The ^{1}H NMR spectra for compounds (**12-15**)H_2 were more complex due to their unsymmetrical nature. Two phenol O-**H** environments were observed clearly indicating the two phenyl rings are not chemically equivalent. The N-C**H**$_2$-Ar protons were observed as a multiplet and a broad region, indicative of inequivalent proton environments alongside the influence of fluxionality. A broad region was observed for the methyl substituted piperazine ring –C**H**$_2$ protons. In contrast to the single broad resonance for **3**H_2 (Figure 2.05a), broad regions were observed at 2.10 - 2.60 ppm, and 2.60 - 3.00 ppm

2.3 Synthesis of Titanium Piperazine Salan complexes

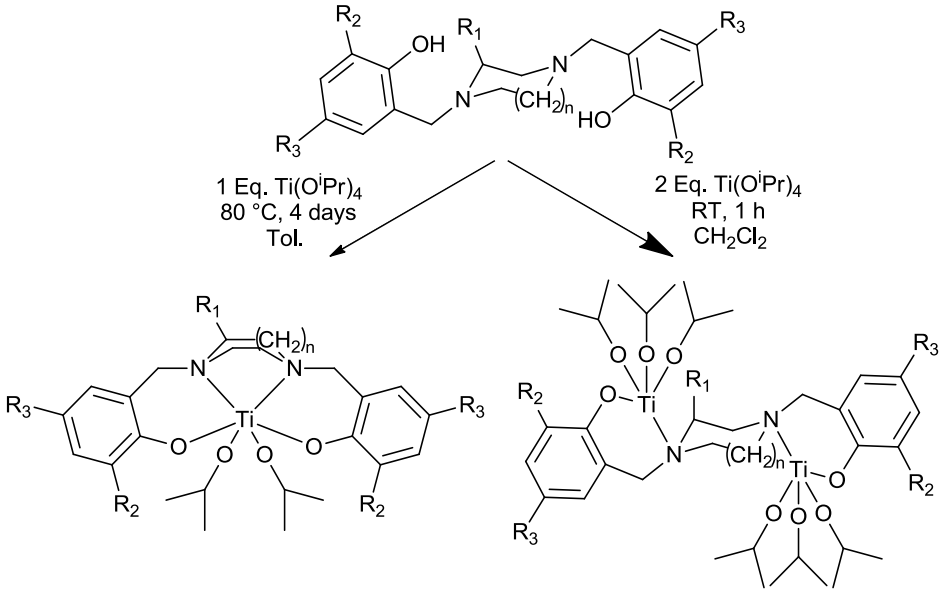

	n	R_1	R_2	R_3
Ti(**6**)$(O^iPr)_2$ =	2,	H,	Me,	Me
Ti(**7**)$(O^iPr)_2$ =	2,	H,	Me,	^{t}Bu
Ti(**8**)$(O^iPr)_2$ =	2,	H,	^{t}Bu,	^{t}Bu
Ti(**9**)$(O^iPr)_2$ =	2,	H,	^{t}Bu,	Me
Ti(**10**)$(O^iPr)_2$ =	2,	H,	Amyl,	Amyl
Ti(**11**)$(O^iPr)_2$ =	2,	H,	H,	^{t}Bu

	n	R_1	R_2	R_3
Ti_2(**1**)$(O^iPr)_6$ =	1	H,	Me,	Me
Ti_2(**2**)$(O^iPr)_6$ =	1,	H,	Me,	^{t}Bu
Ti_2(**3**)$(O^iPr)_6$ =	1,	H,	^{t}Bu,	^{t}Bu
Ti_2(**4**)$(O^iPr)_6$ =	1,	H,	^{t}Bu,	Me
Ti_2(**5**)$(O^iPr)_6$ =	1,	H,	Amyl,	Amyl
Ti_2(**8**)$(O^iPr)_6$ =	2,	H,	^{t}Bu,	^{t}Bu
Ti_2(**9**)$(O^iPr)_6$ =	2,	H,	^{t}Bu,	Me
Ti_2(**12**)$(O^iPr)_6$ =	1,	Me,	^{t}Bu,	^{t}Bu
Ti_2(**13**)$(O^iPr)_6$ =	1,	Me,	^{t}Bu,	Me

Figure 2.06: Reaction scheme detailing the synthesis of piperazine and homopiperazine titanium monometallic and bimetallic complexes.

2.4 Titanium Bimetallic Complexes

2.4.1 Synthesis

The room temperature complexation of $Ti(O^iPr)_4$ to piperazine salan ligands resulted in an incomplete reaction when a 1:1 ratio of ligand and metal was utilised. The species produced were not identified although it was clearly observed that unreacted ligands were still present in solution. Further attempts to isolate a pure complex were fruitful when two equivalents of $Ti(O^iPr)_4$ were introduced. The titanium metal centres were bound to each phenoxy resulting in the 2:1 metal to ligand complexes $\{Ti_2(\mathbf{1\text{-}5},\mathbf{8\text{-}9},\mathbf{12\text{-}13})(O^iPr)_6\}$ depicted in figure 2.06. These LM_2 style complexes have been previously reported for piperazine salan ligands by Fulton *et. al.*[12] who complexed them to aluminium and reported X-ray crystallographically determined structures. Attempts to isolate LM_2 complexes containing less steric bulk in the *ortho* phenoxy position and a homopiperazine ring $\{Ti_2(\mathbf{6},\mathbf{7},\mathbf{11})(O^iPr_6)\}$ or a methyl substituted piperazine ring $\{Ti_2(\mathbf{15})(O^iPr_6)\}$ were unsuccessful, the resulting complexes proved very soluble in all common organic solvents and purification was problematic. Ligands containing amyl phenol substituents with a homopiperazine ring and methylated piperazine ring (**10**,**14**H_2) were complexed to $Ti(O^iPr)_4$ under ambient conditions, NMR spectroscopy evidence suggests the formation of the LM_2 structural geometry but the enhanced solubility of said complexes caused difficulties in the separation from significant $Ti(O^iPr)_4$ impurities. All of the titanium complexes produced at room temperature in CH_2Cl_2 at a 2:1 ratio were recrystallised from hexane to yield a complex of the general formula, $LTi_2(O^iPr_6)$, in the solid state. The solid-state structure was confirmed by X-ray crystallography or supported by CHN analysis. Structures were determined for $Ti_2(\mathbf{2\text{-}5},\mathbf{8},\mathbf{12\text{-}13})(O^iPr)_6$ *via* X-ray diffraction studies. Additionally an isolated titanium 2:2 species $\{Ti_2(\mathbf{1})_2(O^iPr_4)\}$ was determined by X-ray crystallography, although further analysis showed this L_2M_2 structure was not consistent with the bulk material. The $Ti_2(\mathbf{1})(O^iPr)_6$ complex was isolated in a repeated reaction, as determined by CHN analysis. ^1H and $^{13}C\{^1H\}$ NMR spectroscopy was consistent with the stated LM_2 titanium complexes when the *ortho* phenoxy group substituents were sterically bulky ^{t}Bu or amyl groups. Where the *ortho* substituents were methyl groups the ^1H and $^{13}C\{^1H\}$ NMR spectra revealed

the presence of an equilibrium, which is later discussed in more depth (see section 2.4.3).

2.4.2 Solid-state characterisation by X-ray crystallography

At room temperature the titanium salan complexes synthesised primarily resulted in crystals of the LM_2 form, which were characterised by X-ray diffraction. Figure 2.07 displays a representative structure for the LM_2 titanium piperazine salan complexes that contain a 6 membered bridging piperazine ring {Ti_2(**2-5**)(O^iPr)$_6$}. These structures contain an inversion centre situated within the molecule as such the local environments around individual titanium metal centres are crystallographically equivalent. Selected bond lengths (Å) and angles (°) about the titanium metal centre are given in table 2.01. The piperazine ring adopts the favoured chair configuration. Each titanium metal centre resides in a distorted trigonal bipyramidal structure, with three isopropoxide groups, an amine nitrogen, and a phenoxy coordinating to the titanium. The axial-isopropoxide (1.7758 - 1.7838 Å) is shorter than the equatorial-isopropoxide groups (1.8003 - 1.8360 Å). The *cis*-phenoxy titanium bonds (Ti1-O4, 1.8649 - 1.8883 Å) are longer than the isopropoxide groups and as expected the axial nitrogen titanium bonds (2.3499 - 2.3567 Å) are longer than the alkoxide bonds. The angle between the two axial moieties (N1-Ti1-O1 = 173.06 - 177.20 °) deviates from the ideal trigonal bipramidal value of 180 °. Additionally the angle between equatorial oxygens and the axial nitrogen (79.86 - 84.62 °) deviates from the idealistic value of 90 °, this is consistent with the axial nitrogen titanium bond being longer than the axial isopropoxide causing all the equatorial oxygens to converge towards the nitrogen. An analogous LM_2 aluminium alkyl complex reported by Fulton *et al.*[12] has a shorter phenoxy-metal bond length {1.7586(12) Å} and a shorter nitrogen-metal bond length {2.0631(14) Å}.

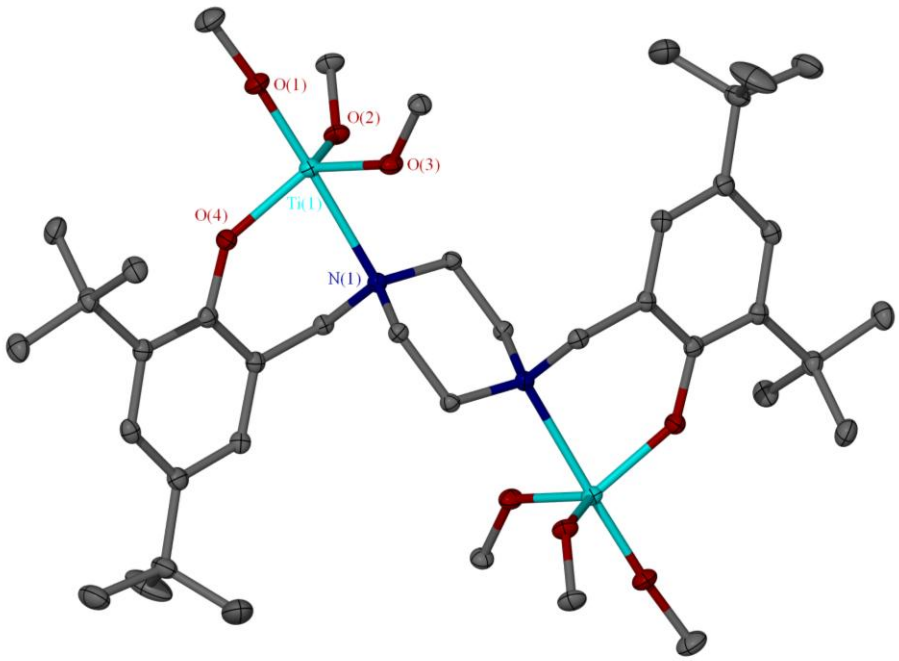

Figure 2.07: Solid-state structure for Ti_2(**3**)(O^iPr)$_6$. Ellipsoids are shown at the 30 % probability level, hydrogen atoms and isopropoxide –CH_3 moieties have been removed for clarity.

	Ti_2(**2**)(O^iPr)$_6$	Ti_2(**3**)(O^iPr)$_6$	Ti_2(**4**)(O^iPr)$_6$	Ti_2(**5**)(O^iPr)$_6$
Ti1-O1	1.7813(18)	1.7758(17)	1.7838(17)	1.7803(17)
Ti1-O2	1.8080(18)	1.8131(17)	1.8003(16)	1.8127(17)
Ti1-O3	1.8360(18)	1.8317(17)	1.8340(17)	1.8308(17)
Ti1-O4	1.8883(17)	1.8735(17)	1.8810(15)	1.8649(16)
Ti1-N1	2.3499(18)	2.3547(19)	2.3516(17)	2.3567(18)
N1-Ti1-O1	175.03(9)	177.20(8)	173.06(7)	176.55(7)
N1-Ti1-O2	84.39(7)	83.08(7)	84.62(7)	82.70(7)
N1-Ti1-O3	80.99(7)	81.00(7)	81.88(7)	80.85(7)
N1-Ti1-O4	79.86(7)	81.07(7)	79.29(6)	80.49(6)

Table 2.01: Selected bond lengths (Å) and angles (°) for LM_2 titanium salan complexes, as determined by X-ray crystallography.

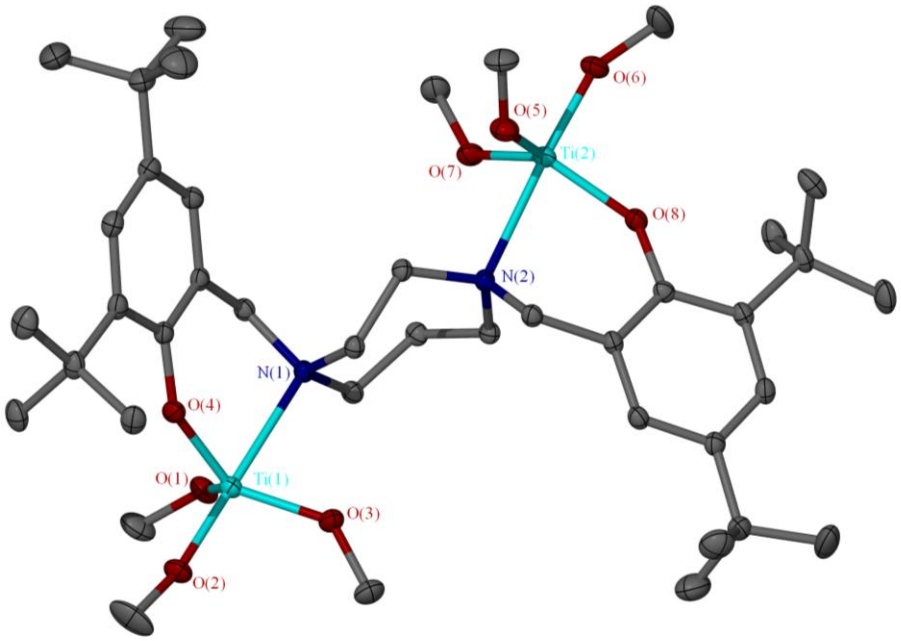

Figure 2.08: Solid-state structure for Ti_2(**8**)(O^iPr)$_6$. Ellipsoids are shown at the 30 % probability level, hydrogen atoms and isopropoxide –CH_3 moieties have been removed for clarity.

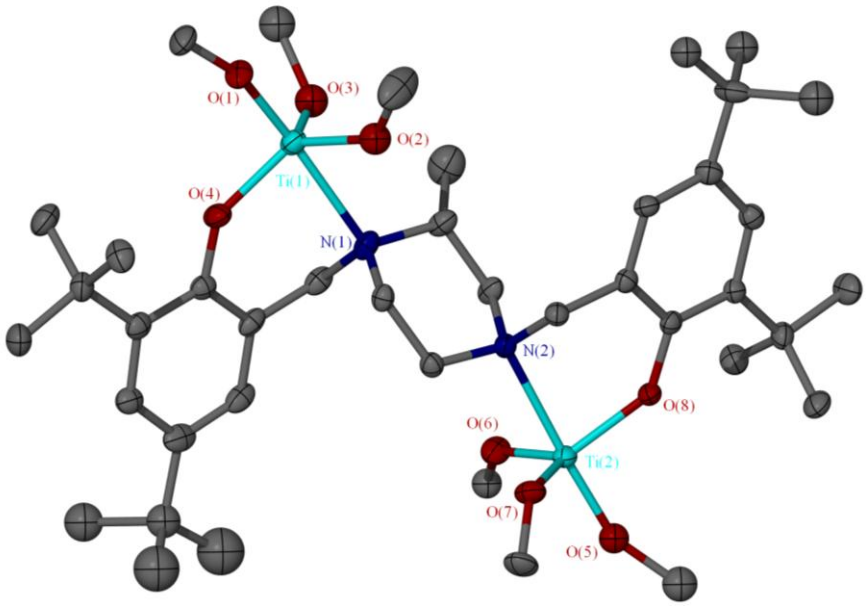

Figure 2.09: Solid-state structure for Ti_2(**12**)(O^iPr)$_6$. Ellipsoids are shown at the 30 % probability level, hydrogen atoms and isopropoxide –CH_3 moieties have been removed for clarity.

	Ti_2(**8**)(O^iPr)$_6$	Ti_2(**12**)(O^iPr)$_6$	Ti_2(**13**)(O^iPr)$_6$
Ti1-O1	1.7801(18)	1.789(3)	1.796(5)
Ti1-O2	1.8141(19)	1.816(3)	1.791(6)
Ti1-O3	1.8322(18)	1.817(3)	1.832(2)
Ti1-O4	1.8622(17)	1.869(3)	1.8691(19)
Ti1-N1	2.3775(19)	2.357(3)	2.357(2)
Ti2-O5	1.7890(18)	1.740(6)	-[a]
Ti2-O6	1.8076(19)	1.850(7)	-[a]
Ti2-O7	1.8396(18)	1.788(6)	-[a]
Ti2-O8	1.8823(17)	1.875(3)	-[a]
Ti2-N2	2.3525(19)	2.391(3)	-[a]
N1-Ti1-O1	173.81(8)	177.25(13)	165.3(8)
N1-Ti1-O4	80.26(7)	81.73(11)	79.80(7)
N2-Ti2-O5	175.12(8)	177.3(3)	-[a]
N2-Ti2-O8	81.28(7)	80.78(12)	-[a]

Table 2.02: Selected bond lengths (Å) and angles (°) for LM_2 titanium salan complexes, as determined by X-ray crystallography. [a] The piperazine ring methyl was located in the inverse symmetry position in a 50:50 ratio, values are the same due to an inversion centre.

Selected bond lengths (Å) and angles (º) for titanium salan complexes of the general structure LM_2 containing an unsymmetrical bridging piperazine ring is shown in table 2.02. A single homopiperazine based salan titanium complex was characterised by X-ray crystallography {Ti_2(**8**)(O^iPr)$_6$} (Figure 2.08). Both titanium salan complexes bridged by a methyl substituted piperazine ring were modelled with a degree of disorder. For Ti_2(**12**)(O^iPr)$_6$ (Figure 2.09) the piperazine methyl group was disordered over three positions in a 60:20:20 ratio, additionally the isopropoxide and *tert*-butyl substituents were disordered. Ti_2(**12**)(O^iPr)$_6$ was modelled with an inversion centre, although the piperazine methyl substituent was disordered over two positions in a 50:50 ratio, furthermore the isopropoxide groups were disordered. Akin to the symmetrical piperazine salan LM_2 titanium complexes (table 2.01) the

bridging homo/piperazine ring adopts a chair configuration and the titanium metal centres adopt a distorted trigonal bipyramidal structure. The titanium bond lengths and angles for unsymmetrical homo/piperazine salan titanium complexes (table 2.02) are similar to their analogous bond lengths and angles for symmetrical piperazine salan titanium complexes (table 2.01).

The titanium centres within the homopiperazine salan LM_2 titanium complex $\{Ti_2(\mathbf{8})(O^iPr)_6\}$ (Figure 2.08) are not in crystallography equivalent environments, albeit the differences are inconsequential. Notably, the titanium amine bonds are different, Ti1-N1 = 2.3775(19) Å, Ti2-N2 = 2.3525(19) Å. Also the phenoxy bonds are significantly different, Ti1-O4 = 1.8622(17) Å, Ti2-O8 = 1.8823(17) Å. Furthermore, there is a difference in the chelating phenoxy-titanium-nitrogen angle, N1-Ti1-O4 = 80.26(7) °, N2-Ti2-O8 = 81.28(7) °. The two titanium metal centres are not in equivalent environments for the methyl substituted piperazine ring derivative $\{Ti_2(\mathbf{12})(O^iPr)_6\}$. Markedly the chelating phenoxy-titanium-nitrogen angles {N1-Ti1-O4 = 81.73(11) °, N2-Ti2-O8 = 80.78(12) °} are also different.

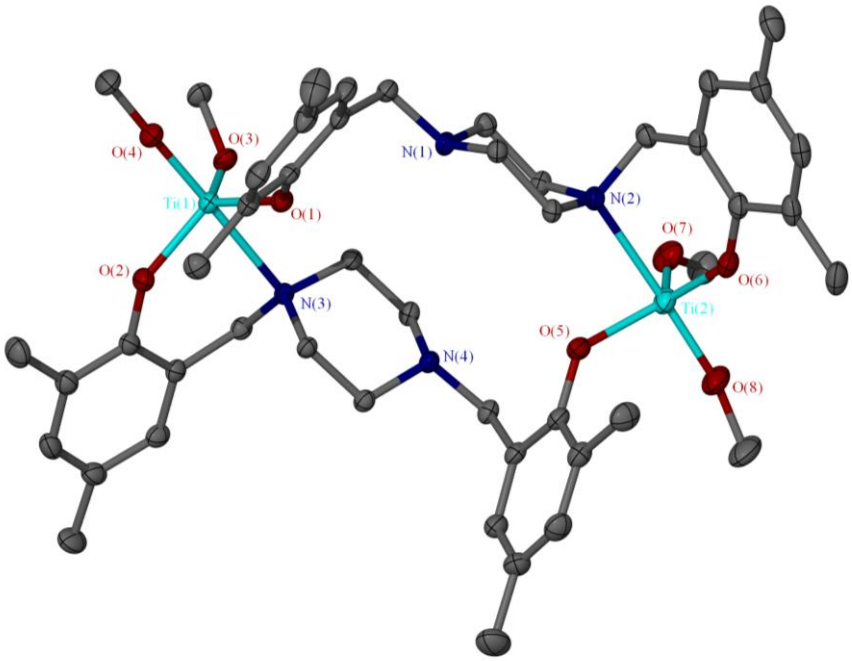

Figure 2.10: Solid-state structure for $Ti_2(\mathbf{1})_2(O^iPr)_4$. Ellipsoids are shown at the 30 % probability level, hydrogen atoms and isopropoxide $-CH_3$ moieties have been removed for clarity.

$Ti_2(\mathbf{1})_2(O^iPr)_4$			
Ti1–O1	1.7749(4)	**Ti2–O7**	1.8500(4)
Ti1–O2	1.8173(5)	**Ti2–O8**	1.8624(4)
Ti1–O3	1.8587(4)	**Ti2–N2**	2.3609(6)
Ti1–O4	1.8569(3)	**O1–Ti1–N1**	178.60(10)
Ti1–N1	2.3526(6)	**O5–Ti2–N2**	177.15(12)
Ti2–O5	1.7715(4)	**O4–Ti1–N1**	81.29(9)
Ti2–O6	1.7950(5)	**O8–Ti2–N2**	81.29(9)

Table 2.03: Selected bond lengths (Å) and angles (°) for $Ti_2(\mathbf{1})_2(O^iPr)_4$, as determined by X-ray crystallography.

An isolated $Ti_2(\mathbf{1})_2(O^iPr)_4$ crystal was characterised by X-ray diffraction (Figure 2.10) and selected bond length (Å) and angles (°) are given in table 2.03. This structure contains two titanium metal centres and two ligands, where each ligand coordinates to two titanium metals *via* independent phenols. Both ligands adopt a chair configuration and the ligands are significantly twisted in comparison to the ligands in the LM_2 structures, as a consequence of geometric strain. Each titanium metal adopts a distorted trigonal bipyramidal structure with two coordinating phenoxy groups, two coordinating isopropoxide groups, and one coordinating amine, also one amine per ligand is un-coordinated. The Ti-$O_{isopropoxide}$ bond lengths (1.8500 - 1.8624 Å) are similar to the bond lengths reported for LM_2 Ti-$O_{isopropoxide}$ (1.8003 - 1.8810 Å). When considering a single titanium metal centre the chelating phenoxy exhibited longer bond lengths (Ti1-O2 = 1.8173(5) Å, Ti2-O6 = 1.7950(5) Å) than the non-chelating phenoxy (Ti1-O1 = 1.7749(4) Å, Ti2-O5 = 1.7715(4) Å). The equatorial oxygen atoms are deviated towards the axial nitrogen with an angle below 90 ° {O4-Ti1-N1 = 81.29 (9), O8-Ti2-N2 = 81.29 (9)}. No evidence of this structure has been observed in further analysis when a more sterically bulky ^{t}Bu groups were present in the *ortho*-position of the phenol. It was proposed that the increased steric demands of ^{t}Bu groups make the L_2M_2 type structure geometrically unfavourable.

2.4.3 Characterisation by solution NMR spectroscopy

The titanium complexes {Ti_2(**1-5**,**8-9**,**12-13**)(O^iPr)$_6$} reported herein were characterised by ^{1}H NMR and ^{13}C{^{1}H} NMR spectroscopy. The solution state characterisation for Ti_2(**3-5**,**8-9**,**12-13**)(O^iPr)$_6$ was consistent with the solid state structures being maintained in solution. For Ti_2(**1-2**)(O^iPr)$_6$ the NMR spectroscopic characterisation was contradictory to a LM_2 or L_2M_2 structures being solely present.

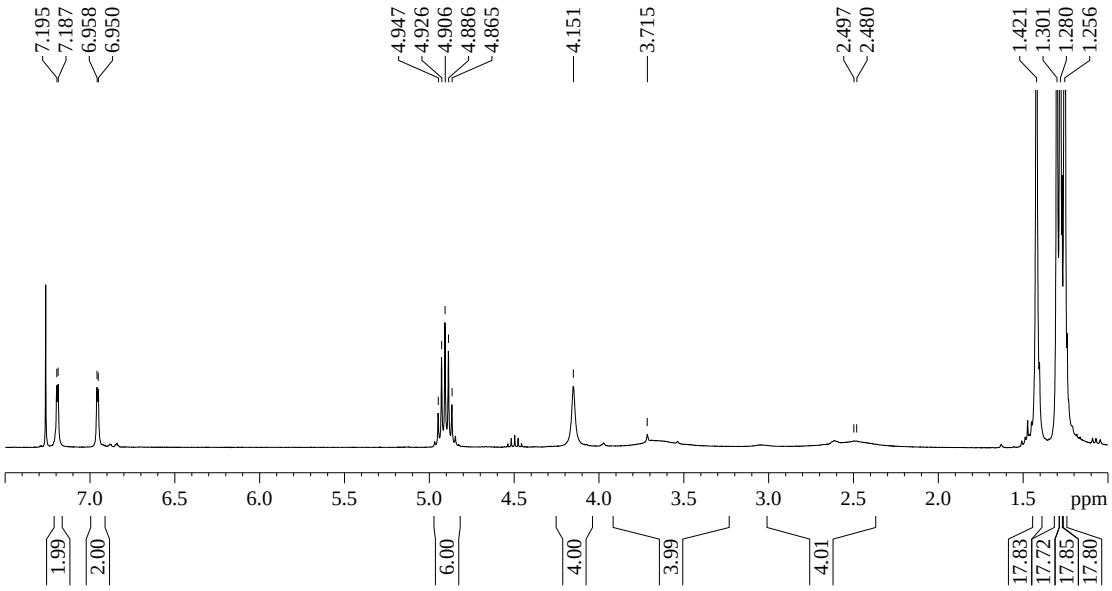

Figure 2.11: ^{1}H NMR spectrum for Ti_2(**3**)(O^iPr)$_6$ in $CDCl_3$.

A representative ^{1}H NMR spectrum for Ti_2(**3-5**)(O^iPr)$_6$ is given in figure 2.11. Only two aromatic proton environments are present, as two doublets (6.95, 7.19 ppm), showing the two phenoxy rings are in equivalent environments. The septet at 4.91 ppm corresponds to six methine isopropoxide protons, the fact only one environment is present is indicative of the isopropoxide groups being highly fluxional. The N-C**H$_2$**-Ar protons are associated with a singlet at 4.15 ppm, a slight broadening of this resonance indicates the presence of a fluxional process on the NMR timescale. The axial and equatorial protons of the piperazine ring are observed as two very broad regions between 2.00 – 4.00 ppm, further supporting a fluxional process on the NMR timescale.

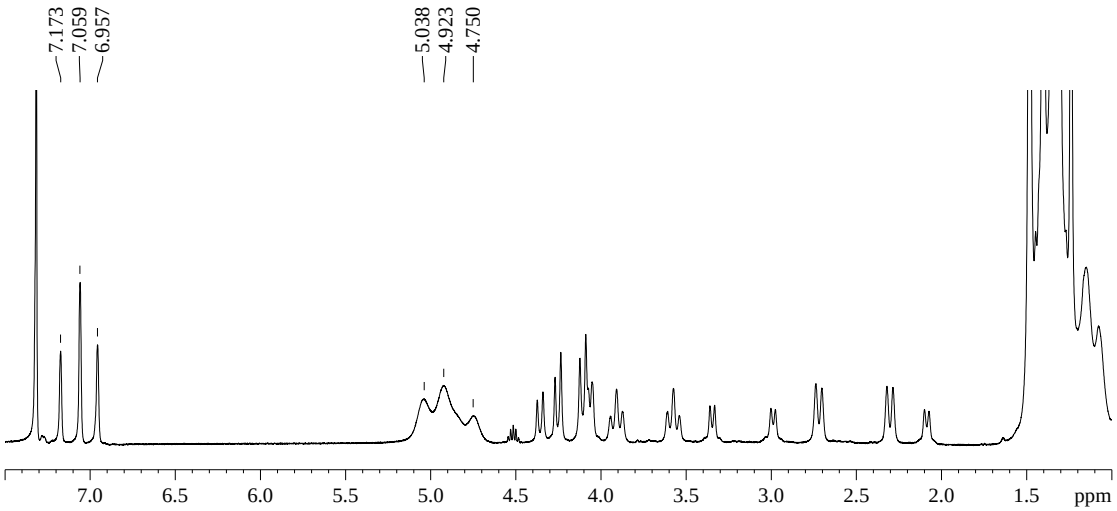

Figure 2.12: ^{1}H NMR spectrum for Ti_2(**3**)(O^iPr)$_6$ at 233 K in $CDCl_3$.

Upon cooling of the complexes in solution the fluxional processes become slower, the ^{1}H NMR spectrum for Ti_2(**3**)(O^iPr)$_6$ at 233 K is shown in figure 2.12 as a representative example for Ti_2(**3-5**)(O^iPr)$_6$ complexes. The aromatic region separates into four environments, it should be noted that in the example given an Ar resonance is located under the solvent. The single resonance assigned to the isopropoxide methine region (figure 2.11) separates into three broad methine resonances {5.04, 4.92, 4.75 ppm (figure 2.12)}. These observations show the complexes undergo conformational locking and reduced fluxionality at 233 K on the NMR timescale. The CH_2 ring protons display distinct resonances at lower temperature demonstrating a slower ring flipping mechanism on the NMR timescale.

The ^{1}H NMR spectra ($CDCl_3$) for titanium isopropoxide complexes supported by homopiperazine salan ligands {Ti_2(**8-9**)(O^iPr)$_6$} were consistent with the characterised solid-state structures. The solution NMR spectra revealed similar trends to those observed for Ti_2(**3**)(O^iPr)$_6$, a truncated representative ^{1}H NMR spectra ($CDCl_3$) for Ti_2(**8-9**)(O^iPr)$_6$ is given in figure 2.13a. The methine isopropoxide region septet, upon cooling (213 K, in d_8-toluene) this region separates into three broad resonances, demonstrating a similar fluxional process. The homopiperazine ring CH_2 protons are represented by three broad resonances, the resonances are more defined than the piperazine ring CH_2 protons of the Ti_2(**3**)(O^iPr)$_6$ complex (Figure 2.11). The homopiperazine based salan titanium complexes are more fluxional than the piperazine based salan titanium complexes, where the 7 membered

ring undergoes a faster ring inversion mechanism. The fluxional nature of the ring is reduced, upon cooling the ring CH_2 region of the ^1H NMR spectrum became more complex. The resonances were still less defined than analogous piperazine based LM_2 complexes, even under less thermodynamic conditions.

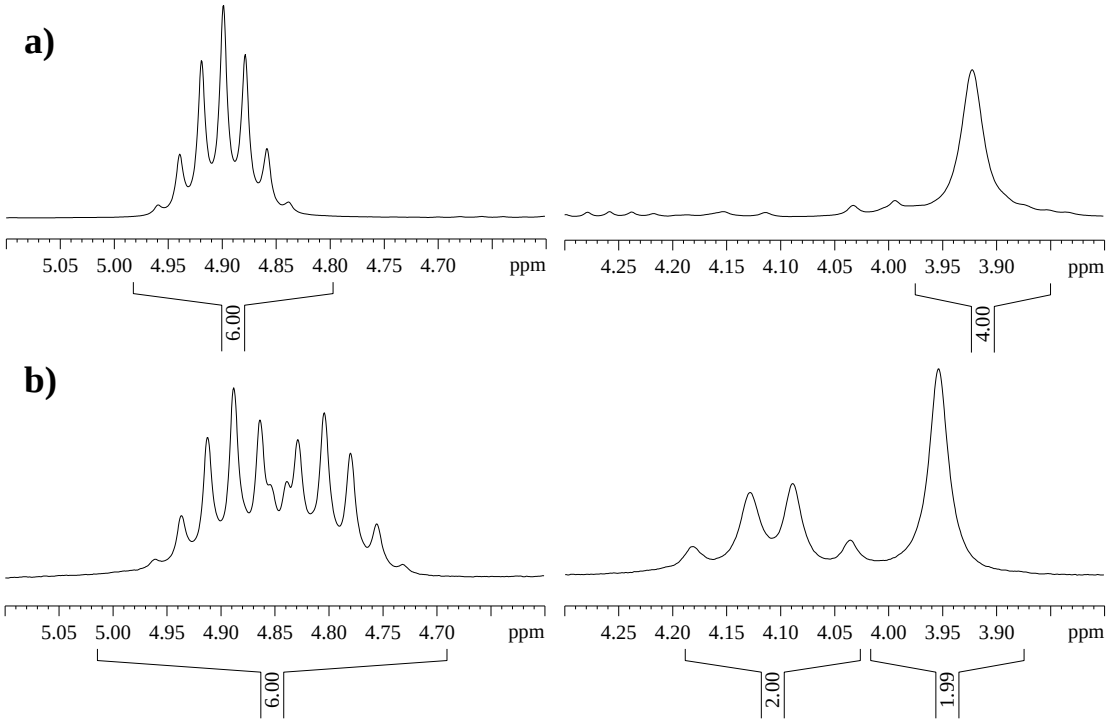

Figure 2.13: ^1H NMR spectrum showing the isopropoxide methine and N-CH_2-Ar regions for; **a**) Ti_2(**8**)(O^iPr)$_6$, **b**) Ti_2(**12**)(O^iPr)$_6$ in $CDCl_3$.

The methyl substituted piperazine ring salan ligands (**12-13**)H_2 are asymmetric, which is represented in their NMR spectra (previously discussed 2.1.2). The asymmetric nature is retained for the titanium complexes Ti_2(**12-13**)(O^iPr)$_6$, part of a representative ^1H NMR spectrum is given in figure 2.13b. The methine isopropoxide region contains two resonances, presumably three protons from the each titanium centre. A quartet and a singlet were observed for the N-C**H$_2$**-Ar region, both visual representations demonstrating asymmetry. Furthermore, four singlets are identifiable in the aromatic region of the ^1H NMR spectrum. As expected low temperature studies resulted in more complex spectra. The isopropoxide methine broadened and presumably the isopropoxide groups are fluxional on the ^1H NMR timescale.

When *ortho* methyl groups are present on the phenol ring (**1**-**2**)H_2 the resulting titanium complexes form an equilibrium system in solution. The Ti_2(**1**-**2**)(O^iPr)$_6$ structural motif was predominantly formed and isolated after a room temperature reaction, this was confirmed by CHN analysis and the structure demonstrated by X-ray diffraction {Ti_2(**2**)(O^iPr)$_6$}. An isolated crystal was obtained for the L_2M_2 motif but the structure was not consistent with the bulk solid material obtained from room temperature synthetic conditions. Equilibrium systems with titanium alkoxides have been previously reported by Sharpless[20] {titanium tartrate complexes} and Boyle[21] {titanium binaphtholate complexes}.

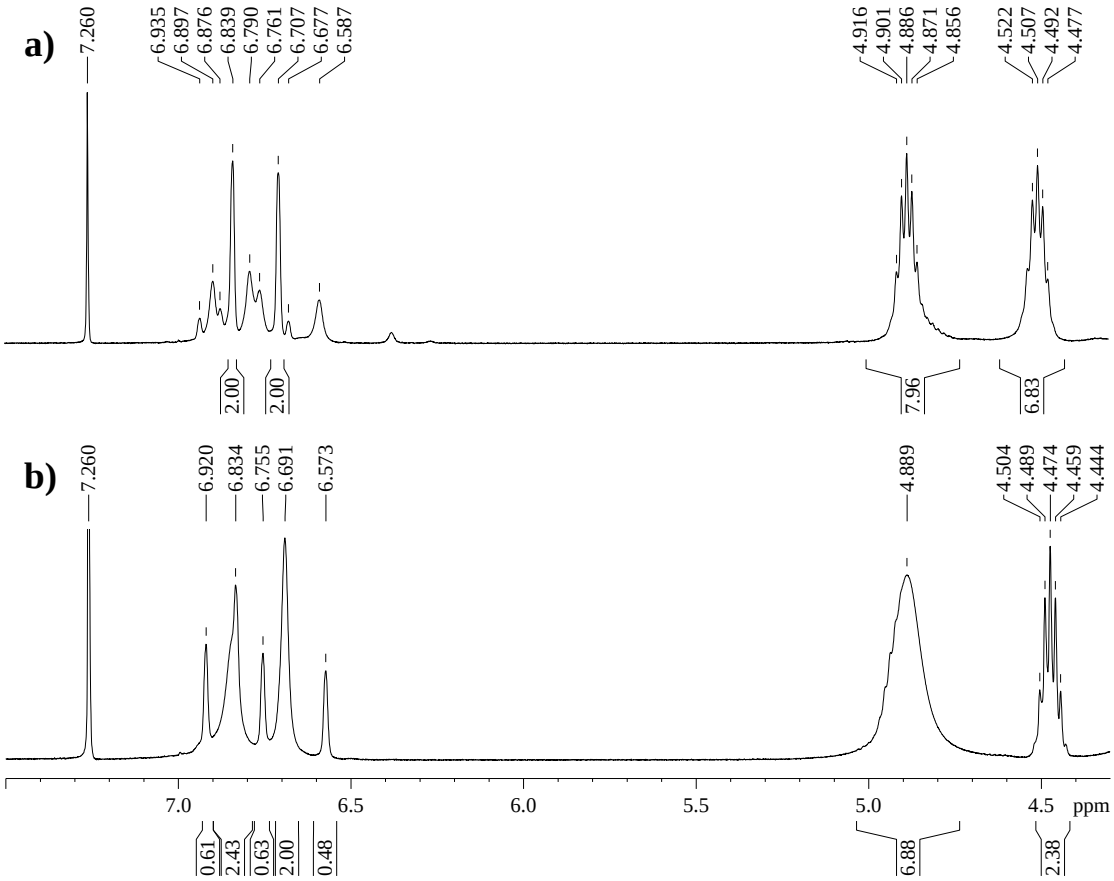

Figure 2.14: ^{1}H NMR spectrum showing the isopropoxide methine and aromatic regions for Ti_2(**1**)(O^iPr)$_6$ in $CDCl_3$ at a) 298 K, b) 233 K.

$$2\ LTi_2(O^iPr)_6 \rightleftharpoons 2\ Ti(O^iPr)_4 + L_2Ti_2(O^iPr)_4$$

Figure 2.15: Proposed equilibrium scheme for Ti_2(**1**-**2**)(O^iPr)$_6$ in solution.

The ^{1}H NMR spectrum for Ti_2(**1**)(O^iPr)$_6$ in $CDCl_3$ at 298 K is given in figure 2.14, the aromatic region shows two dominant singlets which correspond to the LM_2 structural motif. The aromatic region also shows a significant amount of broad/multiplets resonances, these were assigned to the L_2M_2 structural motif. The isopropoxide methine region shows a significant amount of free Ti(O^iPr)$_4$ (4.45 ppm) and titanium isopropoxide groups coordinated to the LM_2 complex. Upon cooling the isopropoxide methine region shows a clear shift in concentration of free Ti(O^iPr)$_4$ and ligand coordinated titanium isopropoxide groups, with the equilibrium shifted towards $LTi_2(O^iPr)_6$. At room temperature the complexed isopropoxide groups:titanium tetra-isopropoxide groups ratio is approximately 1:1 which changes to 3:1 when cooled to 233 K. Additionally the relative integral of the aromatic regions changed by a comparable degree when low temperature ^{1}H NMR spectroscopy was performed. Alongside a ratio change in relative integrals the resonances related to L_2M_2 structural motif became more defined at lower temperatures. From analysis of the NMR spectra under varying conditions the equilibrium given in figure 2.15 was proposed. Equilibrium constants of Ti_2(**1-2**)(O^iPr)$_6$ in $CDCl_3$ were calculated from ^{1}H NMR spectroscopy at different temperature intervals. The Van't Hoff equation (Figure 2.16) was used to quantitatively determine thermodynamic values (Table 2.04), from a plot of lnK against 1/T (Figure 2.17). The thermodynamic values are comparable to those reported for previous titanium equilibria.[20, 21] Higher temperatures favour the formation of multiple products, thus lower temperature entropically favour the Ti_2(**1-2**)(O^iPr)$_6$ structural motif.

$$lnK = -\frac{\Delta H^{\theta}}{RT} + \frac{\Delta S^{\theta}}{R}$$

Figure 2.16: Van't Hoff equation.[22]

	ΔG (kJ mol^{-1})	ΔH (kJ mol^{-1})	ΔS (J K^{-1} mol^{-1})
Ti_2(**1**)(O^iPr)$_6$	5.3(5)	37.3(20)	108(7)
Ti_2(**2**)(O^iPr)$_6$	11.0(3)	30.7(19)	66.2(7)

Table 2.04: Thermodynamic values determined by the Van't Hoff equation, ΔG calculated at 298 K

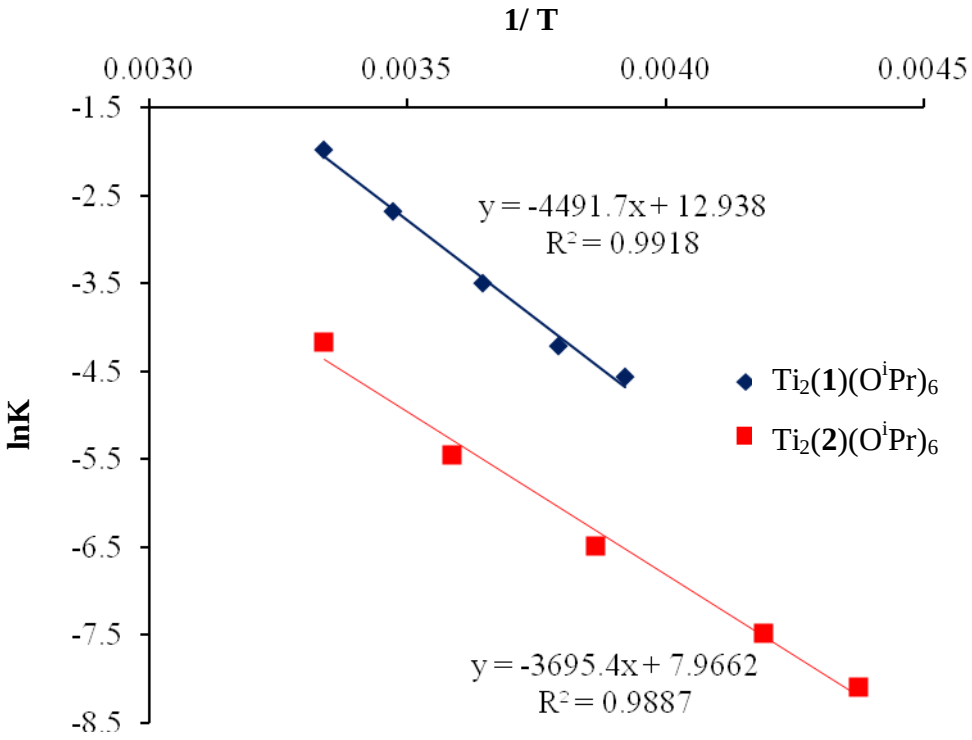

Figure 2.17: Van't Hoff plot for; Ti_2(**1**)(O^iPr)$_6$ and Ti_2(**2**)(O^iPr)$_6$ an NMR scale sample was used of concentration 0.022 mmol/ml in $CDCl_3$.

The addition of excess Ti(O^iPr)$_4$ to the equilibrium resulted in the almost exclusive formation of the LM_2 structural motif and Ti(O^iPr)$_4$ in the solution, in accordance with Le Chatelier's Principle. The location of the equilibrium was affected by changing the solvent with a preference for LM_2 structural motif in d_8-THF. The presence of Ti(O^iPr)$_4$ and ligand complexed species in solution was further confirmed by diffusion ordered spectroscopy (DOSY) NMR spectroscopic investigations.

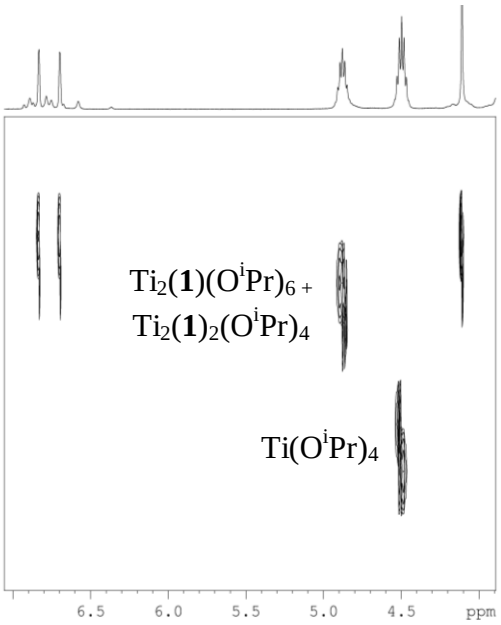

Figure 2.18: DOSY NMR spectrum for $Ti_2(\mathbf{1})(O^iPr)_6$

The synthesis of homopiperazine and methyl piperazine salan titanium complexes was attempted at room temperature, where the *ortho* phenoxy substituents were methyl groups. The ^1H NMR spectra for these complexes suggested the presence of an equilibrium system but the complexes could not be isolated to a degree of purity where conclusive characterisation could be conducted.

2.5 Elevated Temperature Synthesis of Titanium Piperazine Salan Compounds

2.5.1 Synthesis

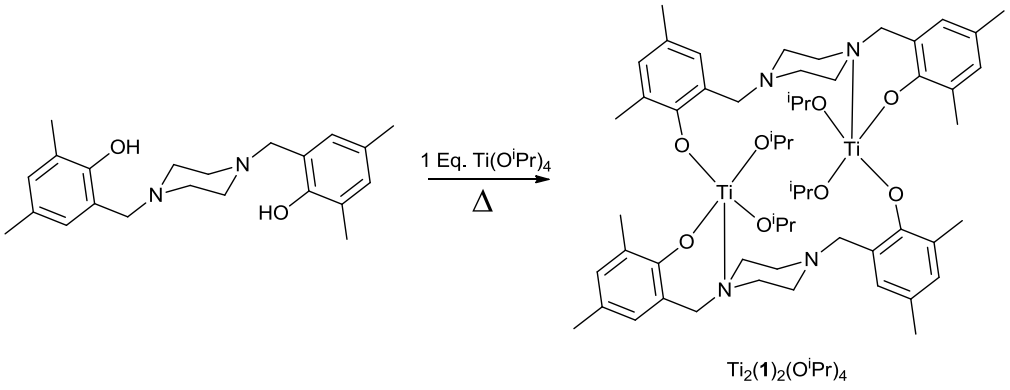

Figure 2.19: Reaction scheme depicting the synthesis of $Ti_2(\mathbf{1})_2(O^iPr)_4$

Further synthetic methods were trialled in an attempt to isolate 1:1 titanium piperazine salan complexes. Most reactions using a 1:1 titanium to ligand ratio yielded partially reacted products or mixtures, which often contained free ligands. Prolonged heating (80 °C) of $Ti(O^iPr)_4$ and **1**H_2 under a dynamic inert gas flow resulted in the exclusive formation and isolation of the L_2M_2 structural motif (Figure 2.19). Under these conditions any liberated isopropanol was gradually removed, therefore kinetically forcing the equilibrium. It was speculated that isopropanol groups dissociate the phenoxy groups from the titanium permitting the coordination of other phenoxy groups, allowing a dynamic system. This species was confirmed by CHN elemental analysis, ^1H and $^{13}C\{^1H\}$ NMR spectroscopy. Attempts to replicate this method for **2**H_2 proved unsuccessful and a mixture of products were still obtained, including Ti_2(**2**)$(O^iPr)_6$.

The same reaction method was utilised for homopiperazine salan ligands, (**6**-**11**)H_2. The removal of isopropanol from the reaction formed products with a 1:1 metal to ligand ratio. The additional heating (80 °C) allowed the homopiperazine ring backbone to adopt a boat type configuration and furthermore coordinate both phenols to a single titanium metal centre (Figure 2.20). These complexes were characterised by CHN elemental analysis, ^1H and $^{13}C\{^1H\}$ NMR spectroscopy. DOSY NMR spectroscopy was used to confirm the presence of the L_2M_2 and LM structural motifs in solution.

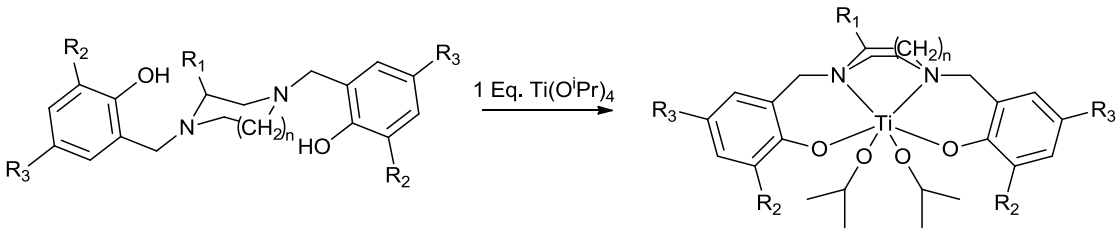

	n	R_1	R_2	R_3
Ti(**6**)$(O^iPr)_2$	2,	H,	Me,	Me
Ti(**7**)$(O^iPr)_2$	2,	H,	Me,	^{t}Bu
Ti(**8**)$(O^iPr)_2$	2,	H,	^{t}Bu,	^{t}Bu
Ti(**9**)$(O^iPr)_2$	2,	H,	^{t}Bu,	Me
Ti(**10**)$(O^iPr)_2$	2,	H,	Amyl,	Amyl
Ti(**11**)$(O^iPr)_2$	2,	H,	H,	^{t}Bu

Figure 2.20: Reaction scheme depicting the synthesis of titanium monometallic complexes supported by homopiperazine salan ligands

.

2.5.2 Solid-state characterisation by X-ray crystallography

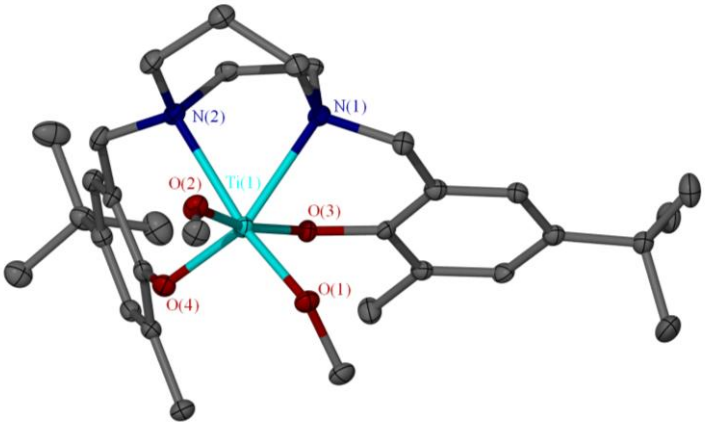

Figure 2.21: Solid-state structure for Ti(**7**)(O^iPr)$_2$ in the β-*cis* configuration. Ellipsoids are shown at the 30 % probability level, hydrogen atoms and isopropoxide –CH_3 moieties have been removed for clarity.

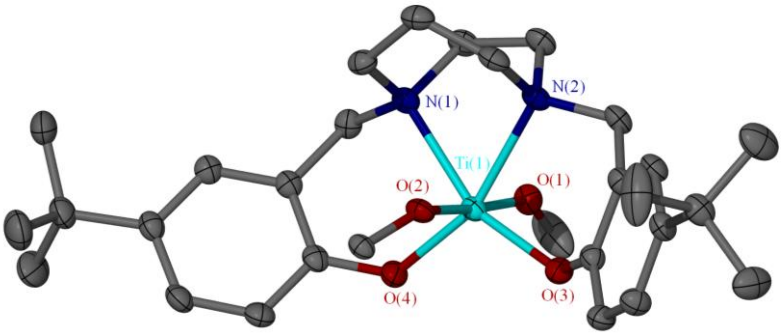

Figure 2.22: Solid-state structure for Ti(**11**)(O^iPr)$_2$ in the *trans*-configuration. Ellipsoids are shown at the 30 % probability level, hydrogen atoms and isopropoxide –CH_3 moieties have been removed for clarity.

X-ray crystallography was used to determine the structure of monometallic complexes Ti(**7**,**9**-**11**)(O^iPr)$_2$, while the Ti_2(**1**)$_2$(O^iPr)$_4$ structure is discussed previously (Figure 2.10). The titanium metal centres of complexes containing Me, ^{t}Bu, or Amyl *ortho*-phenol substituents were shown to adopt a *pseudo* octahedral configuration, contrasting to the prior determined titanium piperazine salan structures in this chapter. The structure obtained for Ti(**7**)(O^iPr)$_2$ is given as a representative example (Figure 2.21), these solid-state structures adopted a β-*cis* configuration

(Figure 2.23). Less steric bulk in the *ortho*-phenol position resulted in the isolation of a *pseudo trans*-octahedral titanium complex supported by a homopiperazine salan ligand, Ti(**11**)(O^iPr)$_2$ (figure 2.22).

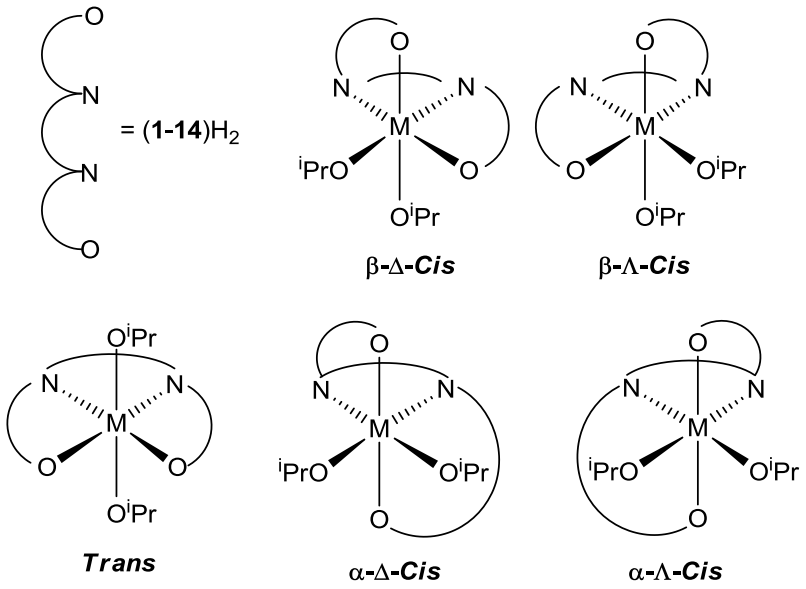

Figure 2.23: Binding modes of piperazine salan ligands.[23]

Selected bond length (Å) and angles (°) are given in table 2.05 for the crystallographically characterised titanium homopiperazine complexes. Those complexes which adopted a β-*cis* configuration {Ti(**7,9-11**)(O^iPr)$_2$} revealed similar bond length and angles. There was no significant difference in the isopropoxide metal (Ti1-O1, Ti1-O2) bond lengths, but phenoxy-metal bond lengths (Ti1-O3, Ti1-O4) were significantly different where the phenoxy *trans* to an isopropoxide exhibited a longer bond length. The two Ti-N bonds have different lengths; the nitrogen which is *trans* to an isopropoxide is longer. The amine bond length can be compared to the *trans* Ti-O bond, a longer phenoxy titanium bond (Ti1-O4) results in a shorter bond for the *trans* titanium nitrogen (Ti1-N1). The complexes adopted a distorted octahedral conformation, which is demonstrated by the deviation of the titanium angles from 90° or 180°, for *cis* or *trans* angles respectively. A high degree of variation from the idealistic 90° angle was observed between N1-Ti1-N2, giving angles between 67.90(13) - 68.08(7) ° (Table 2.05).

The less sterically hindered salan with a hydrogen at the *ortho* position adopted a distorted *trans*-octahedral structural configuration {Ti(**11**)(O^iPr)$_2$} (Figure 2.22). The two phenoxy-titanium bonds (Ti1-O1, Ti1-O2) are equivalent in length, additionally the two nitrogen-titanium bonds (Ti1-N1, Ti1-N2) are equivalent in length. This is indicative of the structures symmetrical nature. Similar to β-*cis* configurations the *trans*-octahedral structure deviates from an ideal octahedral environment.

	Ti(**7**)(O^iPr)$_2$	Ti(**9**)(O^iPr)$_2$	Ti(**10**)(O^iPr)$_2$	Ti(**11**)(O^iPr)$_2$
Ti1-O1	1.8310(17)	1.836(4)	1.812(3)	1.8490(18)
Ti1-O2	1.8375(16)	1.833(3)	1.838(3)	1.8323(17)
Ti1-O3	1.9568(16)	1.931(3)	1.939(3)	1.9175(19)
Ti1-O4	1.8834(17)	1.873(3)	1.892(3)	1.9106(18)
Ti1-N1	2.285(2)	2.293(4)	2.298(4)	2.255(2)
Ti1-N2	2.349(2)	2.346(4)	2.334(4)	2.268(2)
N1-Ti1-O1	101.94(7)	102.78(16)	103.54(15)	86.18(8)
N1-Ti1-O2	92.39(7)	89.46(16)	89.09(14)	90.87(8)
N2-Ti1-O1	168.57(8)	170.35(16)	171.26(14)	88.51(8)
N2-Ti1-O2	84.54(7)	86.07(15)	86.41(14)	87.99(8)
N1-Ti1-N2	68.08(7)	67.91(15)	67.90(13)	70.09(8)

Table 2.05: Selected bond lengths (Å) and angles (°) for Ti(**7,9-11**)(O^iPr)$_2$, as determined by X-ray crystallography.

2.5.3 Characterisation by solution NMR spectroscopy

Under these more thermodynamic forcing conditions Ti_2(**1**)$_2$(O^iPr)$_4$ was isolated as the bulk product. The ^{1}H NMR spectrum of this complex is given in figure 2.25b, a comparative ^{1}H NMR spectrum of Ti_2(**1**)(O^iPr)$_6$ and the resulting solution equilibrium is shown again in figure 2.25a. The isopropoxide -CH_3 resonances of Ti_2(**1**)$_2$(O^iPr)$_4$ are present in each spectrum as sets of doublets at 0.93 ppm, 0.96 ppm and 1.14 ppm respectively. It was assumed the doublet at

1.28 ppm (Figure 2.25b) is located under the broad resonance at a similar chemical shift in the equilibrium spectra (Figure 2.25a). Similarly the –CH isopropoxide septet resonances {4.47 ppm, 4.92 ppm (Figure 2.25b)} coincide almost directly with the isopropoxide –CH ^{1}H NMR resonances from both Ti_2(**1**)(O^iPr)$_6$ and Ti(O^iPr)$_4$ within the equilibrium spectra (4.47 ppm, 4.89 ppm) (Figure 2.14b), a subtle shoulder upon the broad resonance at 4.89 ppm supports this observation. It is difficult to distinguish resonances at 2.25 - 4.25 ppm as the -CH_2- region is inherently complex, due to ring flipping and fluxionality mechanisms. The aromatic region shows four singlets in both spectra, it should be noted a slight shoulder upon the resonance at 6.83 ppm is indicative of two overlapping resonances. Parallel observations are observed in variable temperature ^{1}H NMR spectra. The NMR spectrum of Ti_2(**1**)(O^iPr)$_6$ afforded two diffusion rates for the piperazine salan titanium complexes (Figure 2.18), the larger Ti_2(**1**)$_2$(O^iPr)$_4$ diffuses more slowly. The DOSY spectra for the isolated Ti_2(**1**)$_2$(O^iPr)$_4$ complex diffused at a rate of 5.09×10^{-10} m^2 s^{-1} and comparison to the determined diffusion rates for Ti_2(**1**)(O^iPr)$_6$ confirmed the presence of Ti_2(**1**)$_2$(O^iPr)$_4$ in each solution spectra. The Stokes-Einstein equation (Figure 2.24)[22] was used to obtain predicted radii of the molecules within solution (Table 2.06), although these complexes significantly deviate from the ideal spherical shape which is assumed for the Stokes-Einstein equation. While a perfect comparisons to the solid-state structures were difficult the radii shows the Ti_2(**1**)$_2$(O^iPr)$_4$ species is larger than the Ti_2(**1**)(O^iPr)$_6$ species in solution, therefore further supporting the formation of Ti_2(**1**)$_2$(O^iPr)$_4$ over Ti(**1**)(O^iPr)$_2$.

$$\text{Radius of the molecule} = \frac{kT}{6\pi\eta D}$$

Figure 2.24: Stokes-Einstein equation.[22]

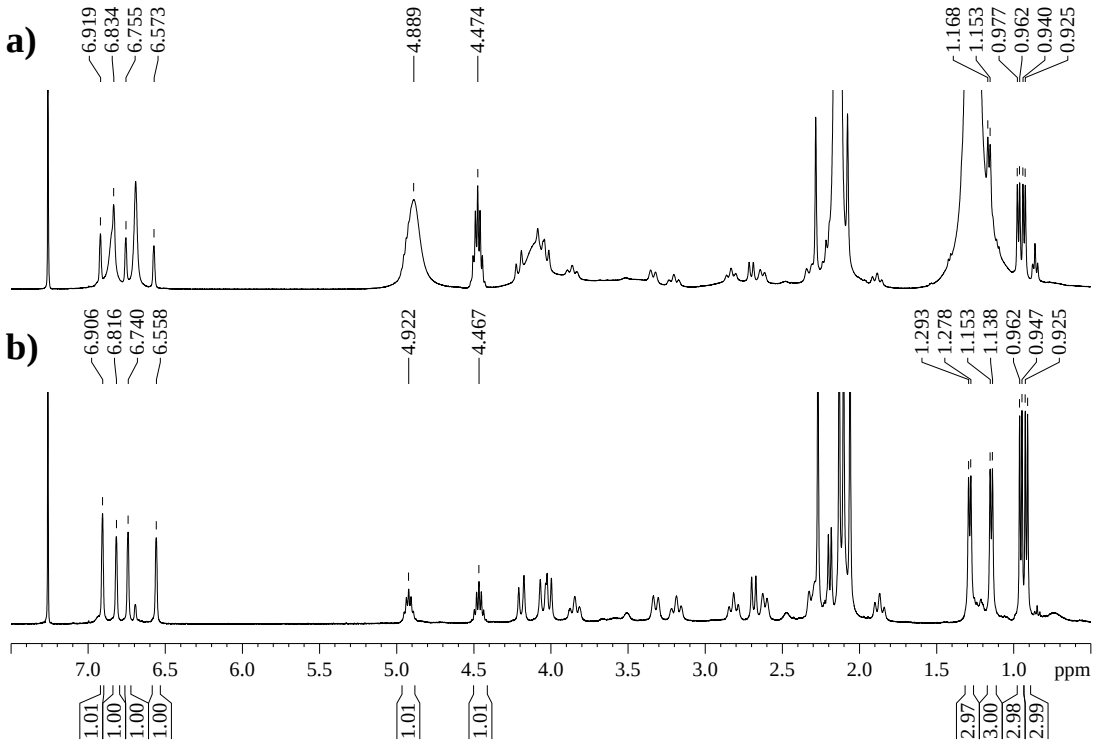

Figure 2.25: **a**) ^{1}H NMR spectrum of $Ti_2(\mathbf{1})(O^iPr)_6$, and resulting equilibrium in $CDCl_3$ (233 K). **b**) ^{1}H NMR spectrum of $Ti_2(\mathbf{1})_2(O^iPr)_4$ in $CDCl_3$ (233 K).

	Diffusion Rate (10^{-10} m^2 s^{-1})	**Calculated spherical radius (Å)**
$Ti_2(\mathbf{1})_2(O^iPr)_4$[a]	5.11	7.47
$Ti_2(\mathbf{1})(O^iPr)_6$[a]	5.65	6.76
$Ti_2(\mathbf{1})_2(O^iPr)_4$	5.09	7.50

Table 2.06: Diffusion rates obtained from DOSY spectra for titanium isopropoxide (**1**) complexes and spherical radii calculated from by the Stokes-Einstein equation[22] from the diffusion rates. [a] Data obtained from the solution ^{1}H NMR spectrum of $Ti_2(\mathbf{1})(O^iPr)_6$. Data obtained in $CDCl_3$ at 294 K.

The NMR spectra for the monometallic titanium piperazine salan complexes Ti(**6-10**)(O^iPr)$_2$ show that the complexes adopt multiple conformations, unlike the X-ray crystal structures where a single β-*cis* conformation was present. Representative ^{1}H NMR spectra for complexes Ti(**6-7**)(O^iPr)$_2$ are given in figure 2.26a, these *ortho* methyl containing complexes show two conformations in solution. One of the two species in solution is comparatively well defined where as the other is fluxional. For example isopropoxide –CH_3 resonances were located at 0.42 ppm and 1.16 ppm and a proportional quantity was identified as a broad region between 0.50 - 1.50 ppm (Figure 2.26a). The fluxional nature is supported by VT NMR spectroscopy (233 K) where the resonances become more defined at lower temperatures. These complexes can adopt the α-*cis*, β-*cis*, and *trans* octahedral conformations. Although the Δ and Λ forms of α-*cis* and β-*cis* conformations are possible they are indistinguishable by conventional NMR spectroscopy (Figure 2.23). It should be noted that although three octahedral conformations are present the orientation of the homopiperazine ring can further complicate the NMR spectra.

The more sterically hindered complexes Ti(**8-10**)(O^iPr)$_2$, with respect to the *ortho*-phenoxy positions, primarily adopted two conformations. The two conformations can be observed in their NMR spectra, a representative ^{1}H NMR spectrum example is given in figure 2.26b. The isopropoxide -CH_3 region shows two doublets at 0.39 ppm and 1.01 ppm which are related to one conformation. The analogous doublets resonances are present from different conformations at 0.55 ppm, 0.73 ppm, 0.94 ppm, and 0.97 ppm. The two species were present in an approximate 1:0.9 ratio. The same can be observed in the aromatic region where resonances at 6.88 ppm, and 7.25 ppm were attributed to the slightly dominant conformation. The ^{1}H NMR resonances are relatively well defined for each conformation at room temperature, it was speculated that the increased steric demands of the ligands reduce fluxionality within the complex when compared to Ti(**6-7**)(O^iPr)$_2$. The same conformations can be adopted as discussed above for Ti(**6-7**)(O^iPr)$_2$ (Figure 2.23).

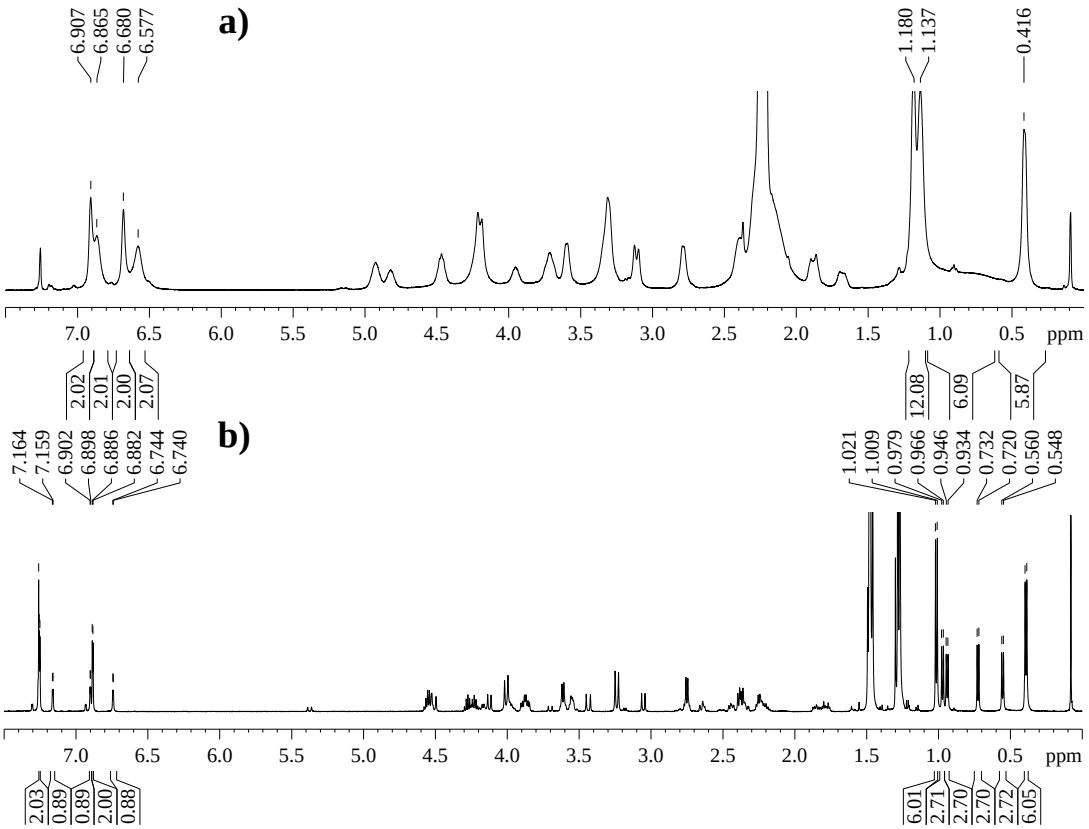

Figure 2.26: **a**) ^{1}H NMR spectrum of Ti(**6**)(O^{i}Pr)$_2$ in $CDCl_3$ (298 K). **b**) ^{1}H NMR spectrum of Ti(**8**)(O^{i}Pr)$_2$ in $CDCl_3$ (298 K).

The less sterically hindered Ti(**11**)(O^{i}Pr)$_2$ exclusively formed the *trans* octahedral conformation in solution and the solid-state, as determined by ^{1}H/^{13}C{^{1}H} NMR spectroscopy and X-ray crystallography. A truncated ^{1}H NMR spectrum for Ti(**11**)(O^{i}Pr)$_2$ is given in figure 2.27, specifically concentrating on the –CH_3 isopropoxide region, and the -CH_2/CH region. The isopropoxide –CH_3 protons afforded only two resonances at 0.63 ppm and 1.15 ppm thus consistent with a *trans* octahedral geometry being formed exclusively. This is further supported by the presence of two isopropoxide septets at 3.84 ppm and 4.82 ppm.

DOSY spectra mostly showed one diffusion rate, or 2 similar diffusion rates for Ti(**7**-**11**)(O^{i}Pr)$_2$. When considered alongside the X-ray crystallography evidence for these complexes it was concluded that the structures in solution adopt varying monometallic octahedral structures in preference to a dimeric (L_2M_2) structural motif.

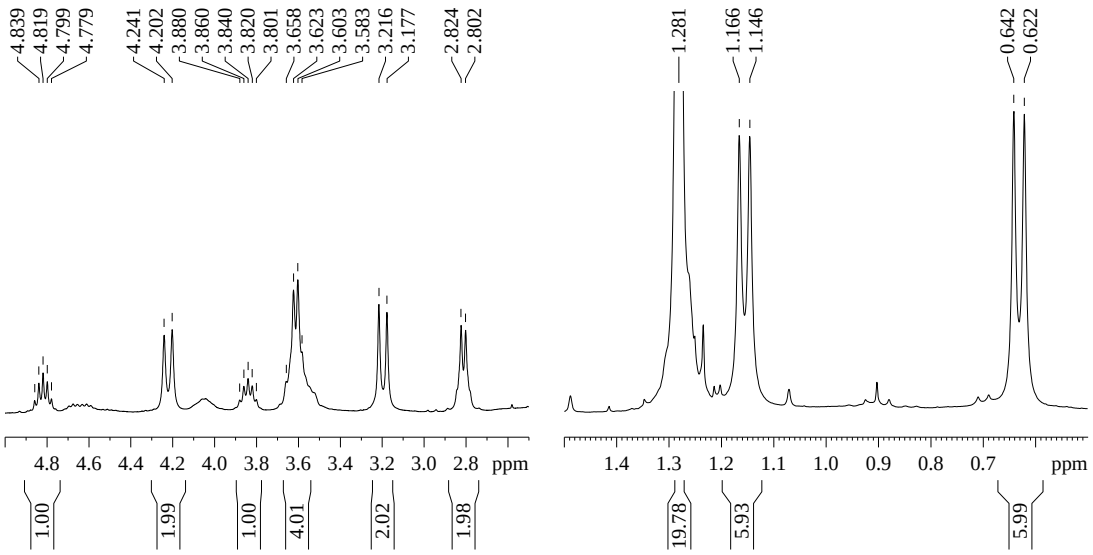

Figure 2.27: ^{1}H NMR spectra showing selected regions for Ti(**11**)(O^{i}Pr)$_2$ in $CDCl_3$ (298 K).

2.6 Ring-Opening-Polymerisation of *rac*-lactide

The titanium homo/piperazine based salan complexes {Ti$_2$(**1-5**,**8-9**,**12-13**)(O^{i}Pr)$_6$} were trialled for the ROP of *rac*-lactide in solvent and solvent free conditions. Conversion (%) was calculated by ^{1}H NMR spectroscopy from which the theoretical molecular weight was derived by equation shown in figure 2.28, which assumes the linear growth of one PLA chain per metal. Number average molecular weight (M_n) and polydispersity index (PDI) was determined by GPC in THF which was referenced to polystyrene standards. The probability of racemic enchainment (P_r) was calculated from the methine region of a methyl decoupled ^{1}H NMR spectra by Bernoullian statistics.[24]

$$M_{n(Theo.)} = \text{Conv.}(\%) \times 144.13 \times \frac{[\text{Lactide}]}{[\text{Metal}]} + 60.10$$

Figure 2.28: Equation showing the calculation of theoretical PLA molecular weight for titanium isopropoxide complexes.

2.6.1 Bimetallic titanium initiators for the solution ROP of *rac*-lactide

The ROP of *rac*-lactide was performed in toluene (10 ml) at 80 °C using 1.0 g of lactide. A 100:1 *rac*-lactide to initiator ratio was used, which equated to 50:1 *rac*-lactide to metal ratio. The mass of catalyst required was determined by the solid state LM_2 structure for consistency reasons, although the preservation of the LM_2 structure within solution at 80 °C was not assumed. The solution polymerisation data is given in table 2.07.

	Time (hours)	**Conv. (%)[a]**	M_n[b] *(theo)*	M_n[c]	**PDI[c]**	P_r[d]
Ti_2(**1**)$(O^iPr)_6$	24	96	7000	1750	1.72	0.50
Ti_2(**1**)$(O^iPr)_6$[e]	24	95	20600	12950	1.38	0.54
Ti_2(**2**)$(O^iPr)_6$	24	95	6900	5550	1.37	0.57
Ti_2(**3**)$(O^iPr)_6$	24	95	6900	5850	1.37	0.46
Ti_2(**3**)$(O^iPr)_6$[e]	24	96	20800	11300	1.48	0.55
Ti_2(**4**)$(O^iPr)_6$	24	96	7000	1500	1.51	0.51
Ti_2(**5**)$(O^iPr)_6$	24	94	6850	4200	1.34	0.57
Ti_2(**8**)$(O^iPr)_6$	24	94	6850	1200	2.31	0.49
Ti_2(**9**)$(O^iPr)_6$	24	95	6900	1400	1.36	0.52
Ti_2(**12**)$(O^iPr)_6$	24	91	6600	1200	2.21	0.54
Ti_2(**13**)$(O^iPr)_6$	24	96	7000	3750	1.28	0.53

Table 2.07: Solution ROP of *rac*-lactide for Ti_2(**1-5**,**8-10**,**12-14**)$(O^iPr)_6$ in 10 ml of toluene at 80 °C in a 100:1 [*rac*-lactide]:[initiator]. [a] Conversion ascertained by ^{1}H NMR spectroscopy. [b] Theoretical molecular weight calculated from conversion (Conv. × 100/2 × 144.13 + 60.10) (rounded to the nearest 50), [c] Molecular weight and PDI determined by GPC (THF) using polystyrene standards without applying a correction factor. [d] P_r as calculated from ^{1}H NMR homonuclear decoupled spectroscopy in $CDCl_3$. [e] 300:1 [*rac*-lactide]:[initiator].

High conversions were obtained after 24 h under solution conditions at 100:1 [*rac*-lactide]:[initiator] ratio for all initiators tested. The initiators Ti_2(**1**,**3**)$(O^iPr)_6$ were trialled at a 300:1 [rac-lactide]:[Initiator] ratio under the same conditions and resulted in high conversion. Generally the average molecular weight determined by GPC was lower than the theoretical molecular weight $M_{n(theo)}$. The reduced M_n values were attributed to the presence of more than one potentially initiating isopropoxide

group present on each metal centre, with a total of six possible initiating isopropoxide groups per complex. The large degree of possible polymerisation sites contributes to the high distribution of molecular chain lengths (PDI = 1.28 – 2.31). It was previously established that these complexes are not fixed in one geometric structure, notably Ti_2(**1-2**)(O^iPr)$_6$ forms an equilibrium system in solution. Furthermore Ti_2(**8-10**)(O^iPr)$_6$ were shown to form a monometallic structural motif under similar conditions. High temperature ^{1}H NMR spectroscopy scale analysis of the complexes showed these initiators in a contained system formed, to a small degree, the LM structural motif. Both the equilibrium and new structure formation contributes to the high PDI values observed. The initiators were shown to be highly fluxional complexes and there is evidence indicating high liability between titanium metals and ligands. As such a small degree of stereo-selectivity was observed with a very slight heterotactic bias being observed for the majority of initiators (see P_r in table 2.07).

2.6.2 Bimetallic titanium initiators for the solvent free ROP of *rac*-lactide

The ROP of *rac*-lactide was attempted in solvent free conditions using 1.0 g of lactide in a 300:1 [*rac*-lactide]:[initiator] ratio at 130 °C. As there are two metals per initiator the ratio of [*rac*-lactide]:[metal] is 150:1. The solvent free polymerisation data for Ti_2(**1-5**,**8-9**,**12-13**)(O^iPr)$_6$ is given in table 2.08.

At 130 °C high conversion was obtained after 30 mins for all of the titanium homo/piperazine salan complexes. The initiators Ti_2(**1**,**3**)(O^iPr)$_6$ also attained high conversion at a 300:1 [rac-lactide]:[Initiator] ratio under the same conditions. The molecular weights were more consistent with one PLA chain per metal centre than the analogous solvent polymerisation (Table 2.07). However, there was some reduction in number average molecular weights (M_n) when compared to the theoretical M_n values. This observation is similar to the solution polymerisations where the lower molecular weight were attributed to the presence of multiple isopropoxide groups on each metal, which are all potential PLA initiation sites. The PDI values were higher, and the P_r values were closer to atactic (P_r = 0.5) than observed for the solution polymerisations. These multiple possible initiating isopropoxide groups contribute to high PDI values. The true behaviour of these

initiators under these conditions is difficult to monitor, and it was further assumed that the initiating species was the LM_2 structural motif, although the possibility of other structures was also considered.

	Time (hours)	Conv. (%)[a]	M_n[b] *(theo)*	M_n[c]	PDI[c]	P_r[d]
Ti_2(**1**)$(O^iPr)_6$	0.5	96	20800	15950	1.86	0.52
Ti_2(**1**)$(O^iPr)_6$[e]	0.5	97	62900	55450	1.56	0.51
Ti_2(**2**)$(O^iPr)_6$	0.5	97	21050	23900	1.53	0.51
Ti_2(**3**)$(O^iPr)_6$	0.5	95	20600	20900	2.01	0.52
Ti_2(**3**)$(O^iPr)_6$[e]	0.5	97	62900	56750	1.57	0.52
Ti_2(**4**)$(O^iPr)_6$	0.5	99	21450	23650	2.01	0.51
Ti_2(**5**)$(O^iPr)_6$	0.5	95	20600	13200	1.56	0.52
Ti_2(**8**)$(O^iPr)_6$	0.5	99.9	21650	14200	2.03	0.51
Ti_2(**9**)$(O^iPr)_6$	0.5	96	20800	20400	1.63	0.53
Ti_2(**12**)$(O^iPr)_6$	0.5	96	20800	13600	1.52	0.52
Ti_2(**13**)$(O^iPr)_6$	0.5	97	21050	20400	1.63	0.54

Table 2.08: Solvent free ROP of *rac*-lactide for Ti_2(**1-5**,**8-10**,**12-14**)$(O^iPr)_6$ at 130 °C in a 300:1 [*rac*-lactide]:[initiator]. [a] Conversion ascertained by ^{1}H NMR spectroscopy. [b] Theoretical molecular weight calculated from conversion (Conv. × 300/2 × 144.13 + 60.10) (rounded to the nearest 50), [c] Molecular weight and PDI determined by GPC (THF) using polystyrene standards without applying a correction factor. [d] P_r as calculated from ^{1}H NMR homonuclear decoupled spectroscopy in $CDCl_3$. [e] 900:1 [*rac*-lactide]:[initiator].

2.6.3 Monometallic titanium initiators for the solution ROP of *rac*-lactide

The isolated Ti_2(**1**)$_2(O^iPr)_4$ and Ti(**6-11**)$(O^iPr)_2$ complexes were trialled for the ROP of *rac*-lactide in toluene (10 ml) at 80 °C at a 100:1 [rac-lactide]:[Initiator] ratio (Table 2.09). Limited activity was observed for this initiator series under these conditions typically achieving low conversions after 24 h. The molecular weights were consistent with one PLA chain per metal; additionally PDI values were lower indicating a more controlled polymerisation system than the LM_2 counterparts. The monometallic system is stable at 80 °C therefore it was assumed the monometallic species were initiating the polymerisation reaction. Due to the low activity of the

monometallic initiators it was concluded that the monometallic species potential contribution to the Ti_2(**1-5**,**8-10**,**12-14**)(O^iPr)$_6$ solution polymerisations (Table 2.07) was minor. Where the initiators were active enough to obtain reliable P_r values a slight isotactic bias was observed.

	Time (hours)	**Conv. (%)[a]**	M_n[b] *(theo)*	M_n[c]	**PDI[c]**	P_r[d]
Ti_2(**1**)$_2$(O^iPr)$_4$*	24	75	10850	15600	1.60	0.49
Ti(**6**)(O^iPr)$_2$	24	23	3400	1250	1.63	-[e]
Ti(**7**)(O^iPr)$_2$	24	8	1200	-	-	-[e]
Ti(**8**)(O^iPr)$_2$	24	27	3950	4700	1.17	-[e]
Ti(**9**)(O^iPr)$_2$	24	12	1800	700	1.01	-[e]
Ti(**10**)(O^iPr)$_2$	24	50	7250	8200	1.06	0.44
Ti(**11**)(O^iPr)$_2$	24	32	4650	6950	1.11	0.44

Table 2.09: Solution ROP of *rac*-lactide for Ti_2(**1**)(O^iPr)$_4$, Ti(**6-11**)(O^iPr)$_2$ in 10 ml of toluene at 80 °C in a 100:1 [*rac*-lactide]:[initiator] *200:1 [*rac*-lactide]:[initiator]. [a] Conversion ascertained by ^{1}H NMR spectroscopy. [b] Theoretical molecular weight calculated from conversion (Conv. × 100 × 144.13 + 60.10) (rounded to the nearest 50), [c] Molecular weight and PDI determined by GPC (THF) using polystyrene standards without applying a correction factor. [d] P_r as calculated from ^{1}H NMR homonuclear decoupled spectroscopy in $CDCl_3$.[e] P_r could not be accurately determined, strong tacticity was not observed.

2.6.4 Monometallic titanium initiators for the solvent free ROP of *rac*-lactide

Ti_2(**1**)$_2$(O^iPr)$_4$ and Ti(**6-11**)(O^iPr)$_2$ titanium salan complexes were trialled for the ROP of *rac*-lactide without solvent at 130 °C at a 300:1 [*rac*-lactide]:[Initiator] ratio (Table 2.10). Under solvent free conditions these initiators were comparatively slow, typically achieving 41 - 60 % conversion after 24 h, when compared to the Ti_2(**1-5**,**8-9**,**12-13**)(O^iPr)$_6$, which achieved > 94 % conversion after 30 mins. Molecular weights were consistent with two PLA chains propagating per metal centre. Despite the presence of two potentially initiating isopropoxide groups per metal the PDI values remained low (PDI < 1.25) at the elevated temperature. The more resolved structure permits the formation of controlled PLA chains but the lack of flexibility within the molecules causes the initiators to be more hindered thus leading to reduced activity. The Ti_2(**1**)$_2$(O^iPr)$_4$ and Ti(**6-11**)(O^iPr)$_2$ titanium

piperazine salan complexes produced PLA with a slight heterotactic bias (P_r = 0.51 - 0.63).

	Time (hours)	Conv. (%)[a]	M_n[b] *(theo)*	M_n[c]	PDI[c]	P_r[d]
Ti_2(**1**)$_2$(O^iPr)$_4$	24	74	32050	21250	1.25	0.51
Ti(**6**)(O^iPr)$_2$	24	54	23400	12050	1.07	0.56
Ti(**7**)(O^iPr)$_2$	24	50	21700	7900	1.19	0.63
Ti(**8**)(O^iPr)$_2$	24	42	18200	7050	1.14	0.53
Ti(**9**)(O^iPr)$_2$	24	41	17800	6750	1.10	0.63
Ti(**10**)(O^iPr)$_2$	24	60	26000	10900	1.14	0.61
Ti(**11**)(O^iPr)$_2$	24	51	22100	6850	1.23	0.55

Table 2.10: Solvent free ROP of *rac*-lactide for Ti_2(**1**)(O^iPr)$_4$, Ti(**6-11**)(O^iPr)$_2$ at 130 °C in a 300:1 [*rac*-lactide]:[initiator] *600:1 [*rac*-lactide]:[initiator]. [a] Conversion ascertained by ^{1}H NMR spectroscopy. [b] Theoretical molecular weight calculated from conversion (Conv. × 100/2 × 144.13 + 60.10) (rounded to the nearest 50), [c] Molecular weight and PDI determined by GPC (THF) using polystyrene standards without applying a correction factor. [d] P_r as calculated from ^{1}H NMR homonuclear decoupled spectroscopy in $CDCl_3$.

2.7 Titanium Homo/Piperazine Salan Catecholates

2.7.1 Introduction

Catechol is a bidentate, chelating ligand; the initial proposal was to observe the effect of a chelating agent upon the titanium piperazine salan equilibrium system. A series of monometallic piperazine salan catecholates complexes were isolated and characterised. Prior titanium catechol complexes were reported by Davidson *et al.*[25] the catecholate complexes form bimetallic structures {Ti(catechol)$_2$(HOiPr)$_2$}$_2$ where the catecholates both chelate to a single titanium and bridge two titanium metals. The titanium homo/piperazine catecholates reported herein proved ineffective for the ROP of *rac*-lactide this is presumably due to the lack of labile ligand to initiate the polymerisation.

Although inactive for the ROP of *rac*-lactide these titanium homo/piperazine catecholates were investigated for their cytotoxicity towards tumour cells. Cisplatin was the first metal compound to be utilised as an anticancer reagent, following this

derivatives have also been commercially used as anticancer treatments over the last decade.[26] While Cisplatin is an effective cancer treatment compound its effectiveness is limited to a small range of cancer types, particularly ovarian and testicular cancers. Additionally Cisplatin is a highly toxic compound, as such the dosage is limited to minimise adverse effects. Titanium compounds have been investigated for cytotoxicity with some promise towards different tumour cell lines which are either susceptible or resistant to treatment by Cisplatin (Figure 2.29, left) and its derivatives. Budotitane {*cis*-diethoxybis(1-phenylbutane-1,3-dionato)titanium(IV)} (Figure 2.29, centre) showed good toxicity towards tumour cells but the complex was proven to be unstable, as a consequence of the labile ligands, also the unsymmetrical ligands give rise to multiple geometric configurations.[27, 28] Titanocene dichloride (Cp_2TiCl_2) (Figure 2.29, right) was also investigated as an anticancer compound but it was deemed inefficient due to its high toxicity.[27, 28] Titanium compounds have a promising range of toxicity towards different cell lines but active compounds typically decompose quickly making it difficult to analyse and indentify the active species, or study the compound in mechanistic manner.[27, 28]

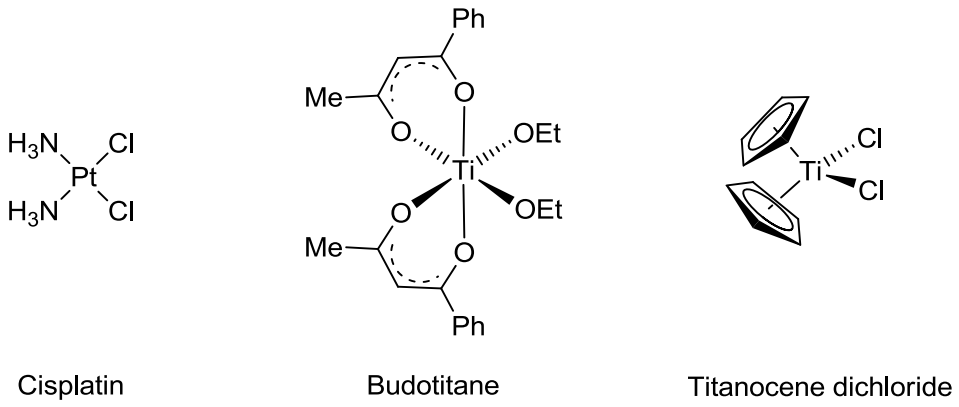

Figure 2.29: Notable anticancer compounds. left – Cisplatin, Centre – Butotitane, Right – Titanocene dichloride. [27, 28]

Cytotoxic salan titanium (IV) complexes have been investigated by Tshuva *et al.*[29] for their applicability as anticancer compounds (Figure 2.30a). These complexes proved to be more cytotoxic towards colon HT-29 and ovarian OVCAR-1 cell lines than Cisplatin and other reported titanium (IV) compounds (Budotitane / Titanocene dichloride) (Figure 2.29). The salan titanium complexes proved to be resilient

towards hydrolysis with a maximum half life of hydrolysis ($t_{½}$) of 32 h. The hydrolysis product, a trimer, was shown to be inactive by conventional *in-vitro* cell treatment. More recent studies revealed the trimeric hydrolysis product as active; the limiting factor is reported as cell penetration effects which were overcome by nano-particulate encapsulation of the complex.[30] Ligand lability is not essential, even detrimental,[31] for titanium complexes to be cytotoxic towards tumour cells[32] advocating the use of the relatively non-labile catecholates ligands. A titanium salan catecholate was synthesised and reported as cytotoxic for HT-29 and OVCAR-1 cell lines, albeit with slightly reduced activity than the isopropoxide containing analogue (Figure 2.30a).[29] The titanium salan catecholate was more stable towards hydrolytic degradation. Furthermore, a titanium salen catecholate has been investigated for the same cell lines (Figure 2.30b), negligible hydrolytic decomposition was observed, and the complex proved active towards the investigated cell lines, although the titanium salen isopropoxide analogue was more effective.[33]

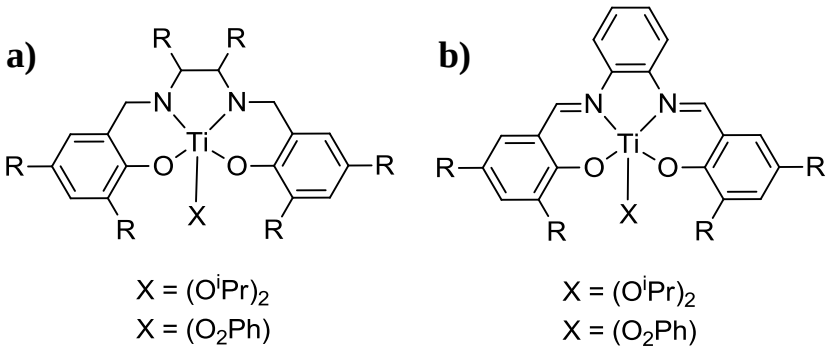

Figure 2.30: Titanium bis(phenoxy) complexes investigated as anti-tumour compounds **a**) Titanium salan isopropoxide/catecholate,[29] **b**) Titanium salen isopropoxide/catecholates.[33]

2.7.2 Synthesis

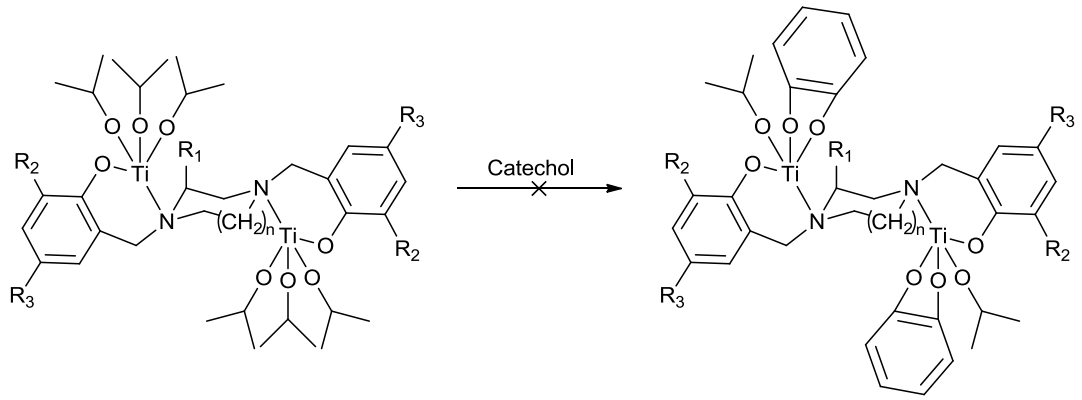

Figure 2.31: Reaction scheme detailing the initially desired homo/piperazine salan titanium catecholates.

The initial premise was the introduction of catechol to the titanium piperazine salan complexes would reduce the number of titanium coordinated isopropoxide groups. The ideal product would have resulted in one catechol per titanium thus leaving one lactide ROP initiating isopropoxide group per metal (Figure 2.31). It was anticipated that this would dictate the PLA chain growth leading to well defined molecular weights and PDI values. Additionally the effect of the chelating catechol upon the L_2M_2 titanium complexes and the equilibrium was an area of interest.

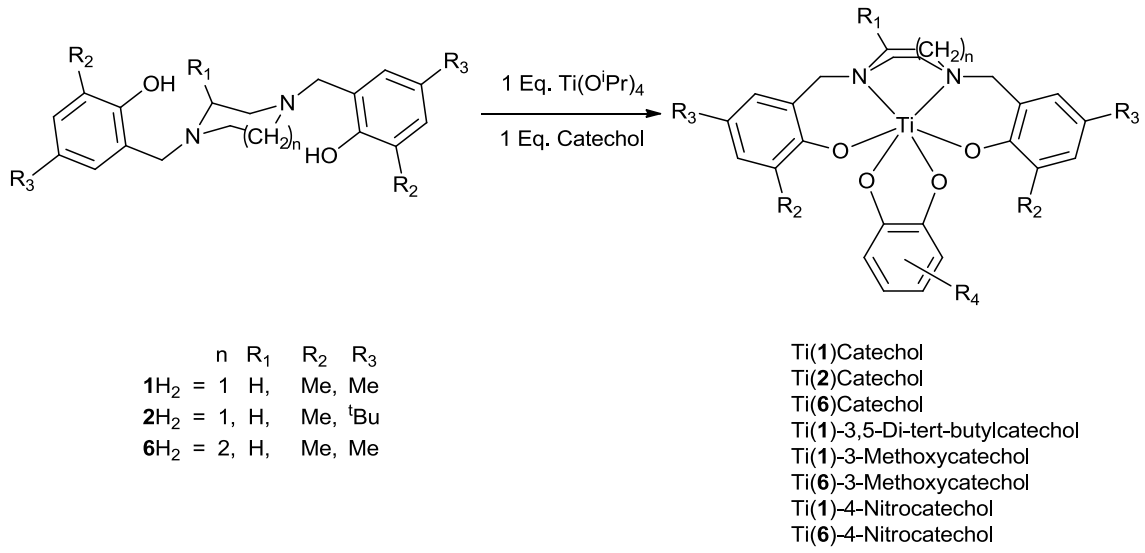

Figure 2.32: Reaction scheme detailing the synthesis of piperazine and homopiperazine salan titanium catecholates.

At room temperature the introduction of catechol, homo/piperazine salan ligand and $Ti(O^iPr)_4$ in a 1:1:1 ratio yielded monometallic complexes (Figure 2.32). The formation of a monometallic complex at lower temperature is presumably a consequence of the reduced steric demands of catechol when compared to two isopropoxide moieties. The investigation of this complex series was limited to methyl substituents as the presence of large alkyl groups is normally detrimental to water solubility, which is a consideration particularly in administration of a potential drug.[34] For comparison reasons a single complex was synthesised which contained ^{t}Bu groups in the *para* position of the phenoxy rings {Ti(**2**)Catechol}. Due to the limitations upon the piperazine salan phenoxy moieties a variety of readily available catechols with varying substituents were utilised for the synthesis. Additionally homopiperazine and piperazine complexes were investigated. Excess $Ti(O^iPr)_4$ or catechol still resulted in the formation of monometallic homo/piperazine salan titanium catecholates. The room temperature synthesis of piperazine salan titanium catecholates resulted in pure products and high yields which were characterised by ^{1}H NMR spectroscopy, $^{13}C\{^1H\}$ NMR spectroscopy, and CHN analysis. Recrystallisation from hot toluene or CH_2Cl_2 resulted in crystals suitable for X-ray crystallography, for Ti(**1**)Catechol, Ti(**1**)-3,5-di-*tert*-butylcatechol, Ti(**1**)-4-NO_2-catechol, and Ti(**6**)-4-NO_2-catechol. The isolation of Ti(**6**)-3,5-di-*tert*-butylcatechol was attempted but the complex could not be supported by NMR spectroscopy although the formation of multiple isomers was a possibility.

2.7.3 Solid-state characterisation by X-ray crystallography

A representative example {Ti(**1**)Catechol} of a modelled X-ray crystallography structure for the 6 membered piperazine bridged salan titanium catecholates {Ti(**1**)Catechol, Ti(**1**)-3,5-di-*tert*-butylcatechol, Ti(**1**)-4-NO_2-catechol} is given in figure 2.33. The solid-state structure for Ti(**6**)-4-NO_2-catechol is displayed in figure 2.34. All the structures were determined as six coordinate *pseudo* octahedral geometries, specifically β-*cis* geometric configurations are adopted (Figure 2.23). Both Λ and Δ forms are present according to the X-ray crystallography data as all the crystal structures contain centres of inversion.

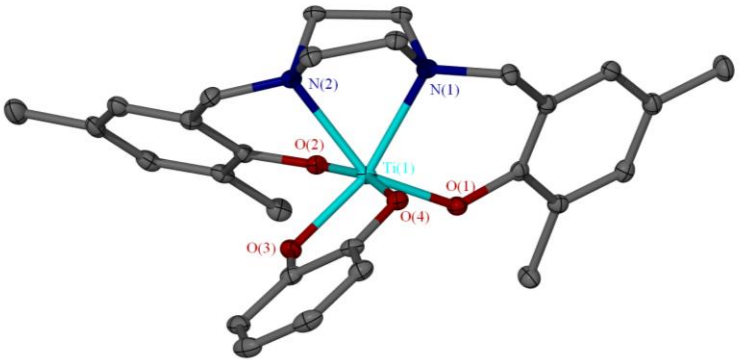

Figure 2.33: Solid-state structure for Ti(**1**)Catechol. Hydrogen atoms have been removed for clarity ellipsoids are shown at the 50 % probability.

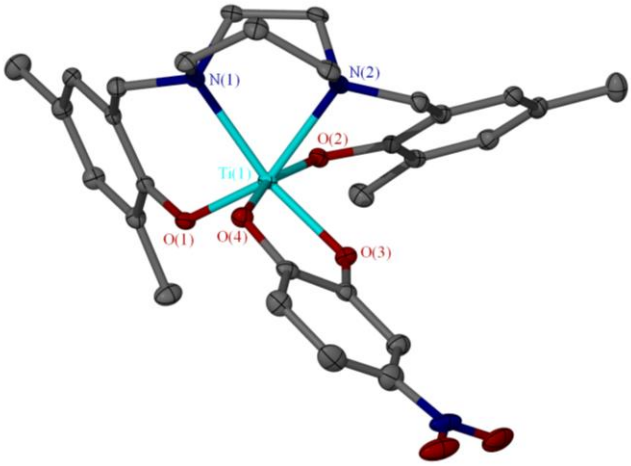

Figure 2.34: Solid-state structure for Ti(**6**)-4-NO_2-catechol. Hydrogen atoms have been removed for clarity ellipsoids are shown at the 50 % probability. The NO_2 group was found in the 4 and 5 positions of the catechol ring at a 50:50 ratio.

	Ti(**1**)Catechol	Ti(**1**)-3,5-di-*tert*-butylcatechol	Ti(**1**)-4-NO_2-catechol	Ti(**6**)-4-NO_2-catechol
Ti1-O1	1.934(3)	1.920(3)	1.939(2)	1.9607(15)
Ti1-O2	1.975(3)	1.944(3)	1.991(2)	1.9583(15)
Ti1-O3	1.864(3)	1.888(3)	1.8589(19)	1.8486(14)
Ti1-O4	1.855(3)	1.861(3)	1.8395(19)	1.8539(14)
Ti1-N1	2.207(3)	2.219(3)	2.206(2)	2.2514(17)
Ti1-N2	2.230(3)	2.232(3)	2.211(2)	2.2677(18)
N1-Ti1-O1	93.05(12)	95.63(12)	95.86(9)	94.00(6)
N1-Ti1-O2	98.47(12)	94.40(12)	97.49(9)	94.55(6)
N1-Ti1-O3	79.56(12)	78.84(12)	79.35(8)	80.55(6)
N1-Ti1-O4	146.30(12)	147.81(13)	146.54(9)	153.41(7)
N1-Ti1-N2	65.87(12)	65.32(13)	66.04(8)	69.92(6)

Table 2.11: Selected bond lengths (Å) and angles (°) for Ti_2(**1**)$_2$(O^iPr)$_4$, as determined by X-ray crystallography.

Selected bond lengths and angles for the homo/piperazine titanium catecholates are given in table 2.11. Typically the catechol Ti-O bonds (Ti-O1, Ti-O2) are longer than titanium phenoxy Ti-O bonds (Ti-O3, Ti-O4) with respective bond ranges of 1.920 – 1.991 Å and 1.854 – 1.888 Å. There is little effect upon bond length from the *trans* component, which is contrasting to the observation made for Ti(**6-11**)(O^iPr)$_2$ complexes. The N1-Ti1-O4 angle deviates from the idealist value of 180 ° giving angles between 146.30 - 153.41 °, the N1-Ti1-O3 angle deviates from the idealist value of 90 ° giving angles between 78.84 – 79.56 °. The homopiperazine complex allows for a larger bite angle between the two nitrogen groups where the N1-Ti1-N2 angles were 66.04 ° and 69.92 ° for Ti(**1**)-4-NO_2-catechol and Ti(**6**)-4-NO_2-catechol respectively.

2.7.4 Characterisation by solution NMR spectroscopy

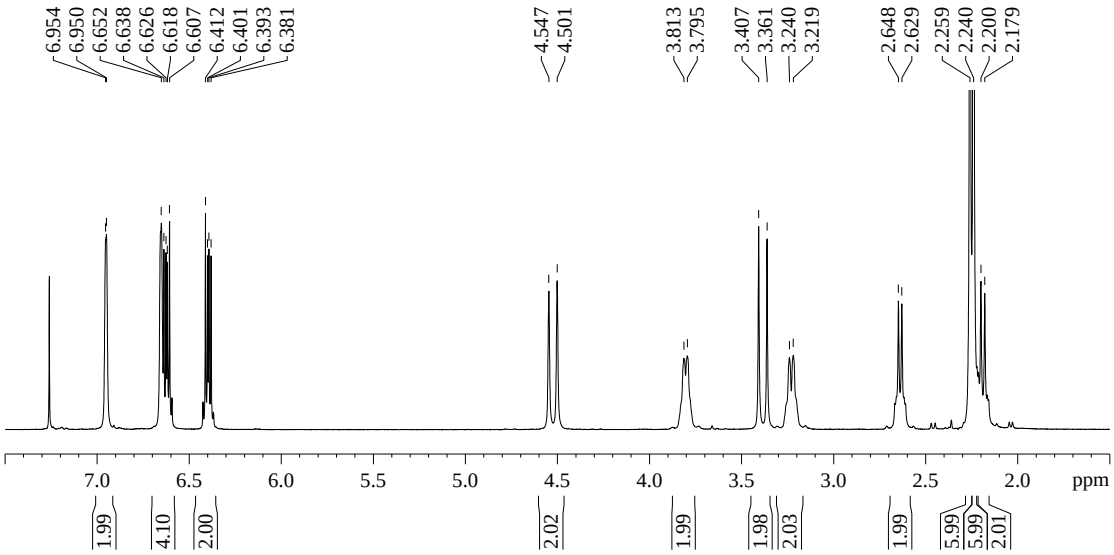

Figure 2.35: ^{1}H NMR spectrum of Ti(**1**)Catechol in $CDCl_3$ (298 K).

Without utilising forcing conditions the monometallic titanium catechols were isolated and the $^{1}H/^{13}C\{^{1}H\}$ NMR spectroscopy characterisation was consistent with the structures identified by X-ray crystallography and CHN analysis. A representative ^{1}H NMR spectrum for Ti(**1**)Catechol is given (Figure 2.35) for the piperazine salan catechols {Ti(**1**)Catechol, Ti(**1**)-3,5-di-*tert*-butylcatechol, Ti(**1**)-3-Methoxycatechol, Ti(**1**)-4-NO_2-catechol}. The ring $–CH_2$ protons were observed as discrete multiplets at 2.18, 2.63, 3.22, and 3.80 ppm. Two distinct doublets at 3.38 and 4.52 ppm were assigned to the N-C**H_2**-Ar protons. Although the aromatic region of the spectra is sharp the region was complicated by overlapping of the four proton resonances at 6.62 ppm.

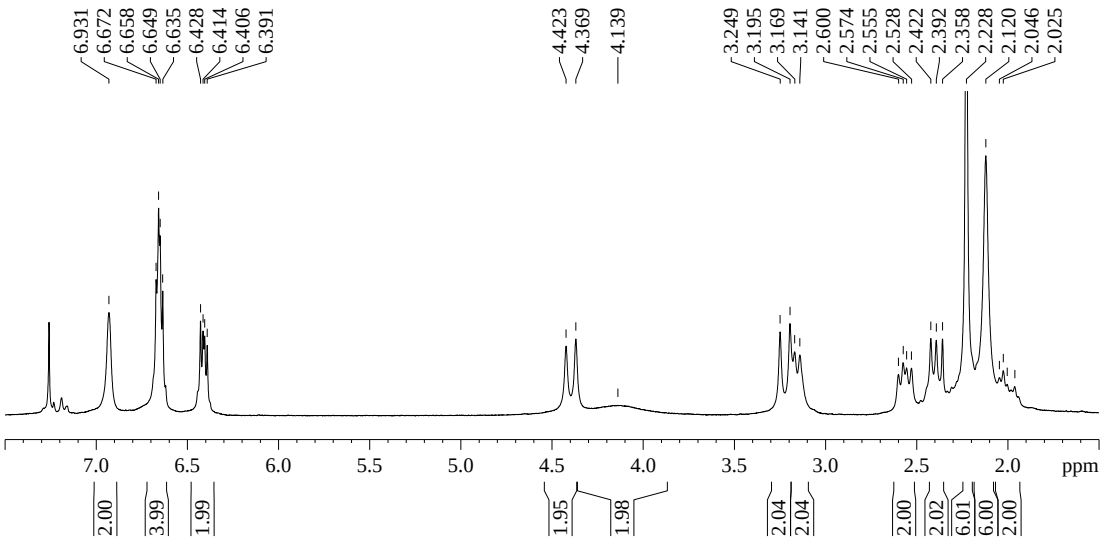

Figure 2.36: ^{1}H NMR spectrum of Ti(**6**)Catechol in $CDCl_3$ (298 K).

A representative ^{1}H NMR spectrum {Ti(**6**)Catechol} is shown in figure 2.36 for the homopiperazine based salan titanium catechols {Ti(**6**)Catechol, Ti(**6**)-3-Methoxycatechol, Ti(**6**)-4-NO_2-catechol}. The spectrum is consistent with the X-ray crystallography determined solid state structure (Figure 31). The ^{1}H NMR spectra for the homopiperazine salan titanium catecholates shows a distinct broadening of resonances when compared to their analogous piperazine complexes. The N-C**H$_2$**-Ar protons resulted in distinctive doublets at 3.22 and 4.38 ppm. The homopiperazine ring-CH_2 protons displayed a significant degree of complication (2.02, 2.39, 2.56, 3.15, and 4.14 ppm) including a noteworthy broadening of the resonance at 4.14 ppm. The aromatic region shows three resonances (6.40, 6.65, and 6.93 ppm) where four protons (two equivalent environments) are overlapping at 6.65 ppm. It was deduced that the broadening of the spectra is related to the higher degree of fluxionally typically observed for the homopiperazine compounds in comparison to the piperazine compounds.

2.7.5 Stability and cytotoxicity

Stability and cytotoxicity studies were performed by Dr. Edit Tshuva at The Hebrew University of Jerusalem, the investigation is currently ongoing at the date of writing. Preliminary cytotoxicity data was investigated with HT-29 and OVCAR-1 tumour cells lines, IC_{50} values are outlined in table 2.12. Stability of complexes towards hydrolysis was also investigated and the half lives ($t_{½}$) are given in

table 2.12. The titanium isopropoxide complex Ti_2(**1**)(O^iPr)$_6$ was investigated and the compound proved non-toxic towards the cell lines, additionally the equilibrium complicated half life studies. Ti(**1**)Catechol was evidently toxic towards the investigated cell line with IC_{50} values rivalling other titanium compounds and enhanced toxicity compared to Cisplatin, the stability was lower than previously investigated catecholates. The nitro subsistent upon the catechol ring enhanced the stability. The low stability of the compounds was attributed to the strained piperazine ring, as a boat configuration is less favourable. Upon introducing a homopiperazine ring the stability was significantly enhanced presumably due to the reduced steric strain of the 7 membered homopiperazine ring. Additionally Ti(**6**)-4-NO_2-catechol gave an increase toxicity towards the investigated cell lines.

	IC_{50} value for HT-29 (μM)	**IC_{50} value for** OVCAR-1 **(μM)**	**$t_{1/2}$(min)**
Ti_2(**1**)(O^iPr)$_6$	Inactive	Inactive	*
Ti(**1**)Catechol	21.9±4.6	27.8±4.6	16
Ti(**1**)-4-NO_2-catechol	20.7±7.3	25.6±3.0	25
Ti(**6**)-4-NO_2-catechol	11.5±4.3	7.2±3.4	92

Table 2.12: Preliminary IC_{50} values for HT-29 and OVCAR-1 cell lines, and half life stability of the complexes towards hydrolysis.

2.8 Conclusion

Tetradentate salan ligands containing homo/piperazine backbones were coordinated to titanium (IV) tetra-isopropoxide resulting in Ti_2(**1-5**,**8-9**,**12-13**)(O^iPr)$_6$ complexes. Their reliance upon backbone rigidity, reaction conditions, and steric requirements are discussed and their relevance in determining the structural motif obtained. Ti_2(**2-5**,**8**,**12**,**13**)(O^iPr)$_6$ were isolated as crystals and characterised as LM_2 structures by X-ray crystallography. From the same conditions a Ti_2(**1**)$_2$(O^iPr)$_4$ crystal was obtained and characterised by X-ray crystallography, although a bulk solid compound of Ti_2(**1**)(O^iPr)$_6$ was obtained in further synthesis. A titanium piperazine salan equilibrium based upon steric requirements was investigated for Ti_2(**1,2**)(O^iPr)$_6$. The equilibrium position was shown to vary upon temperature changes, solvent, and excess reagents. The more flexible homopiperazine structures

were complexed to $Ti(O^iPr)_4$ produce monometallic structures {Ti(**6-11**)$(O^iPr)_2$} after exposure to extended thermal conditions. X-ray crystallography characterisation was successfully conducted for Ti(**7,9-11**)$(O^iPr)_2$. ^1H NMR spectroscopy revealed titanium metal centres were present in solution as multiple *pseudo* octahedral conformations.

The titanium LM_2 complexes {Ti_2(**1-5**,**8-9**,**12-13**)$(O^iPr)_6$} were trialled for the ROP of *rac*-lactide and were shown to be active in both solvent and solvent free conditions. Ti_2(**1-5**,**8-9**,**12-13**)$(O^iPr)_6$ initiators achieved high conversion of *rac*-lactide to PLA within 24 h at 80 °C in toluene at 100:1 [*rac*-lactide]:[initiator] ratio. The solvent free polymerisation obtained high conversion within 30 mins at 130 °C at 300:1 [*rac*-lactide]:[initiator] ratio. The resulting PLA typically had lower molecular weights than expected and high PDI values were generally exhibited, it was speculated that more than one isopropoxide per metal was initiating the propagation of a PLA chain. The resulting PLA was generally atactic with slight variations of P_r about 0.5. The LM complexes {Ti(**6-11**)$(O^iPr)_2$} were poorly active under the same conditions for the ROP of *rac*-lactide. The solution ROP of *rac*-lactide required 24 h for low conversion to be obtained, the solvent free ROP required 24 h for moderate conversions to be obtained. The resulting PLA was predominantly atactic where slight deviations were observed towards isotactic or heterotactic lactide.

The favourable formation of monometallic catecholates is discussed along with their characterisation. The ligands (**1**,**2**,**6)**H_2 were investigated and four variants of catecholate were complexed to $Ti(O^iPr)_4$. Ti(**1**)Catechol, Ti(**1**) 3,5-di-*tert*-butylcatechol, Ti(**1**)-4-NO_2-catechol, and Ti(**6**)-4-NO_2-catechol solid-state structures were determined by X-ray crystallography. These catecholates did not display any activity towards the ROP of *rac*-lactide. These titanium piperazine salan catecholates have been preliminarily revealed as moderately promising compounds as anti tumour reagents by Dr. Edit Tshuva.

2.9 Future Work

The equilibrium observed for Ti_2(**1**,**2**)(O^iPr)$_6$ poses on interesting area, thus further investigation into the nature of the equilibrium under various conditions would be of interest. Other derivatives of these ligands could be investigated to better constitute the requirements for an equilibrium system. The mechanistic details of these titanium complexes could be investigated further, beginning with kinetic experiments at low monomer:initiator ratio. Further-work is being conducted on the anti-tumour properties of the titanium piperazine salan catecholates. Depending upon the trends observed other derivatives of these complexes could be investigated.

2.10 References

1. O. Dechy-Cabaret, B. Martin-Vaca and D. Bourissou, *Chem. Rev.*, 2004, **104**, 6147-6176.
2. P. Hormnirun, E. L. Marshall, V. C. Gibson, A. J. P. White and D. J. Williams, *J. Am. Chem. Soc.*, 2004, **126**, 2688-2689.
3. Z. Zhong, P. J. Dijkstra and J. Feijen, *J. Am. Chem. Soc.*, 2003, **125**, 11291-11298.
4. S. Gendler, S. Segal, I. Goldberg, Z. Goldschmidt and M. Kol, *Inorg. Chem.*, 2006, **45**, 4783-4790.
5. A. J. Chmura, M. G. Davidson, M. D. Jones, M. D. Lunn, M. F. Mahon, A. F. Johnson, P. Khunkamchoo, S. L. Roberts and S. S. F. Wong, *Macromolecules*, 2006, **39**, 7250-7257.
6. J. Wu, T.-L. Yu, C.-T. Chen and C.-C. Lin, *Coord. Chem. Rev.*, 2006, **250**, 602-626.
7. R. H. Platel, L. M. Hodgson and C. K. Williams, *Polym. Rev.*, 2008, **48**, 11-63.
8. N. Nomura, R. Ishii, M. Akakura and K. Aoi, *J. Am. Chem. Soc.*, 2002, **124**, 5938-5939.
9. N. Nomura, R. Ishii, Y. Yamamoto and T. Kondo, *Chem. Eur. J.*, 2007, **13**, 4433-4451.
10. C. K. A. Gregson, I. J. Blackmore, V. C. Gibson, N. J. Long, E. L. Marshall and A. J. P. White, *Dalton Trans.*, 2006, 3134-3140.
11. T. K. Saha, V. Ramkumar and D. Chakraborty, *Inorg. Chem.*, 2011, **50**, 2720-2722.
12. N. C. Johnstone, E. S. Aazam, P. B. Hitchcock and J. R. Fulton, *J. Organomet. Chem.*, 2010, **695**, 170-176.
13. W. Li, W. Wu, Y. Wang, Y. Yao, Y. Zhang and Q. Shen, *Dalton Trans.*, 2011, **40**, 11378-11381.
14. W. Li, Y. Yao, Y. Zhang and Q. Shen, *Chin. J. Chem.*, 2012, **30**, 609-615.
15. W. Li, Z. Zhang, Y. Yao, Y. Zhang and Q. Shen, *Organometallics*, 2012, **31**, 3499-3511.

16. Z. Zhang, X. Xu, S. Sun, Y. Yao, Y. Zhang and Q. Shen, *Chem. Commun.*, 2009, **0**, 7414-7416.
17. J. Lloyd, S. Z. Vatsadze, D. A. Robson, A. J. Blake and P. Mountford, *J. Organomet. Chem.*, 1999, **591**, 114-126.
18. E. Y. Tshuva, N. Gendeziuk and M. Kol, *Tetrahedron Lett.*, 2001, **42**, 6405-6407.
19. S. Mohanty, D. Suresh, M. S. Balakrishna and J. T. Mague, *J. Organomet. Chem.*, 2009, **694**, 2114-2121.
20. M. G. Finn and K. B. Sharpless, *J. Am. Chem. Soc.*, 1991, **113**, 113-126.
21. T. J. Boyle, D. L. Barnes, J. A. Heppert, L. Morales, F. Takusagawa and J. C. Connolly, *Organometallics*, 1992, **11**, 1112-1126.
22. P. W. Atkins and J. De Paula, *Élements of physical chemistry*, Oxford University Press, 2005.
23. K. Matsumoto, B. Saito and T. Katsuki, *Chem. Commun.*, 2007, **0**, 3619-3627.
24. B. M. Chamberlain, M. Cheng, D. R. Moore, T. M. Ovitt, E. B. Lobkovsky and G. W. Coates, *J. Am. Chem. Soc.*, 2001, **123**, 3229-3238.
25. M. G. Davidson, M. D. Jones, M. D. Lunn and M. F. Mahon, *Inorg. Chem.*, 2006, **45**, 2282-2287.
26. E. Wong and C. M. Giandomenico, *Chem. Rev.*, 1999, **99**, 2451-2466.
27. E. Y. Tshuva and J. A. Ashenhurst, *Eur. J. Inorg. Chem.*, 2009, **2009**, 2203-2218.
28. K. Strohfeldt and M. Tacke, *Chem. Soc. Rev.*, 2008, **37**, 1174-1187.
29. D. Peri, S. Meker, M. Shavit and E. Y. Tshuva, *Chem. Eur. J.*, 2009, **15**, 2403-2415.
30. S. Meker, K. Margulis-Goshen, E. Weiss, S. Magdassi and E. Y. Tshuva, *Angew. Chem., Int. Ed.*, 2012, **51**, 10515-10517.
31. M. Ravera, C. Cassino, E. Monti, M. Gariboldi and D. Osella, *J. Inorg. Biochem.*, 2005, **99**, 2264-2269.
32. M. Shavit, D. Peri, A. Melman and E. Tshuva, *J. Biol. Inorg. Chem.*, 2007, **12**, 825-830.
33. A. Tzubery and E. Y. Tshuva, *Inorg. Chem.*, 2011, **51**, 1796-1804.
34. M. F. Francis, M. Piredda and F. M. Winnik, *J. Controlled Release*, 2003, **93**, 59-68.

Chapter 3

3. Zirconium/Hafnium (IV) Homo/Piperazine Salan Complexes and Their Application for the ROP of *rac*-Lactide

3. Zirconium/Hafnium (IV) Homo/Piperazine Salan Complexes and Their Application for the ROP of *rac*-Lactide

3.1 Introduction

Group 4 tetradentate amine bis(phenoxy) complexes have been previously reported for the ROP of *rac*-lactide.[1-4] Zirconium and hafnium metals can form complexes in different manners with tetradentate -(ONNO)- ligands compared to titanium. For example, zirconium and hafnium metals have a stronger preference towards bridging to form dimers.[5, 6] Zirconium and hafnium complexes typically exhibit an enhancement for the ROP of lactide in terms of activity,[1, 7] and/or molecular weight control.[2, 7] Also stereoselectivity is often observed with zirconium and hafnium initiators over titanium initiators, due to the ability of lactide to chelate to the larger zirconium/hafnium metal. For example, isotactic enriched PLA was produced from *rac*-lactide by Davidson *et al*. with the -(ONNO)- initiators given in figure 3.01.[2] Furthermore, hafnium and zirconium trisphenolate initiators have resulted in strong heterotactic stereoselectivities (Figure 3.02).[1, 8] Reported herein is the synthesis of zirconium and hafnium piperazine and homopiperazine based salan complexes and their use as initiators for the ROP of *rac*-lactide. This follows prior titanium piperazine salan work (Chapter 2).[9]

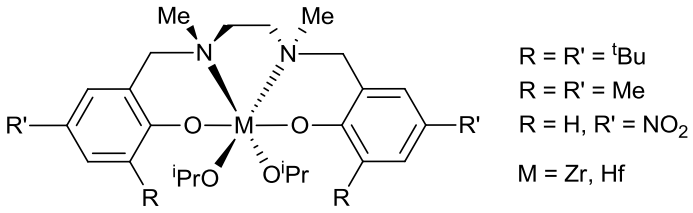

Figure 3.01: Zirconium and hafnium -{ONNO}- based bis(phenoxy) initiators.[2]

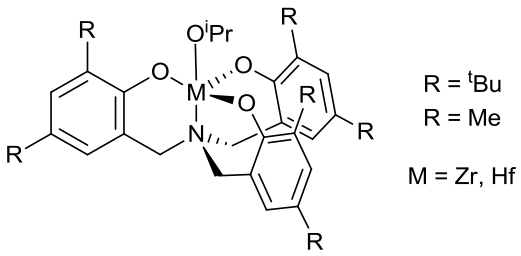

Figure 3.02: Zirconium and hafnium trisphenolate initiators.[1, 8]

3.2 Synthesis of Zirconium/Hafnium (IV) Homopiperazine Salan complexes

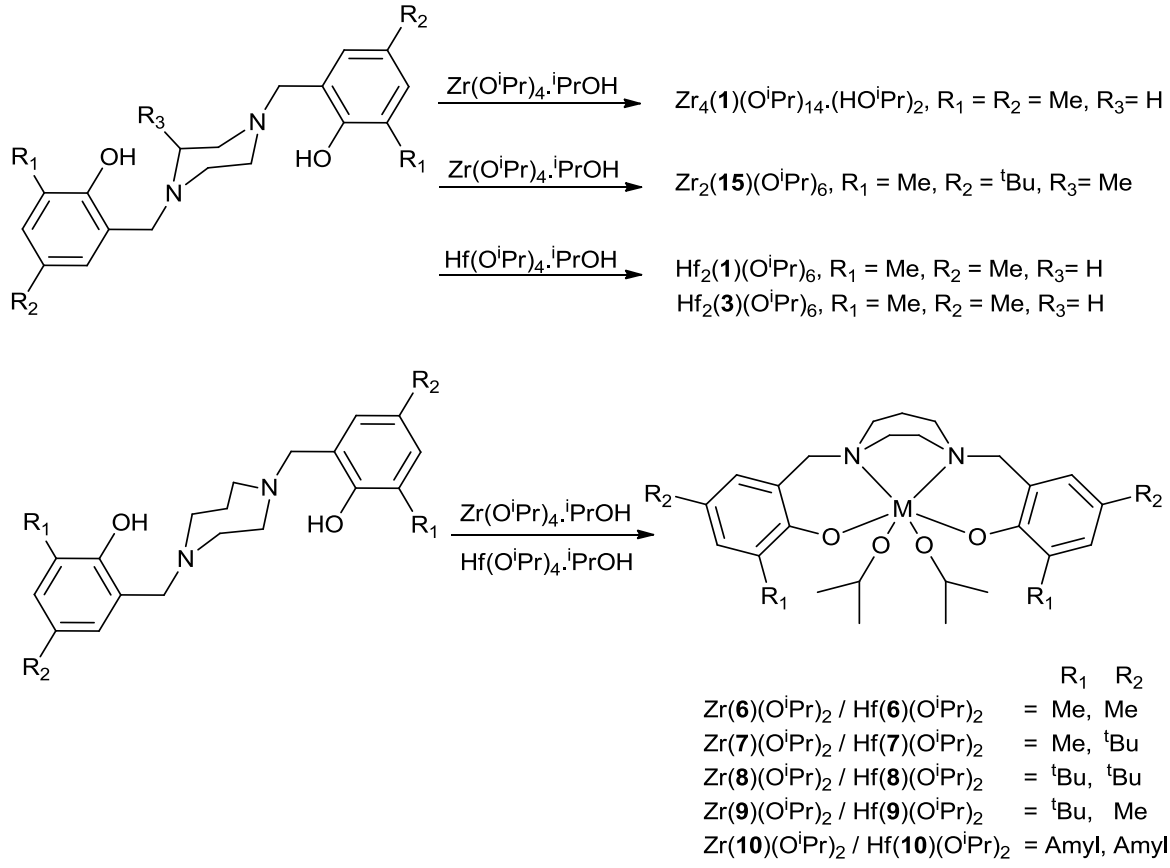

Figure 3.03: Reaction scheme for the synthesis of homo/piperazine salan zirconium/hafnium complexes.

The homo/piperazine salan ligands (**1-15**)H_2 discussed in chapter 2 (Figure 2.02) were complexed to Zr(O^{i}Pr)$_4$.HO^{i}Pr and Hf(O^{i}Pr)$_4$.HO^{i}Pr. The complexation of zirconium and hafnium isopropoxide to the piperazine based salan ligands (**1-5**,**12-15**H_2) was conducted with limited success (Figure 3.03). The

complexation of zirconium with (**1-5**,**12-15**)H_2 at elevated or ambient temperature, resulted in a plethora of species being observed; furthermore purification by recrystallisation either yielded mixed zirconium species and/or ligand. In two cases recrystallisation of zirconium piperazine salan complexes from hot hexane afforded crystals suitable for X-ray diffraction studies. A complex with a 4:1 metal to ligand ratio was isolated {(Zr_4(**1**)(O^iPr)$_{14}$.(HO^iPr)$_2$}. A 2:1 metal to ligand ratio complex was also observed {Zr_2(**15**)(O^iPr)$_6$}, with a differing structural motif than the previously discussed titanium complexes. The solution NMR spectroscopic analysis for these structures was not consistent with the structure being maintained in solution.

The complexation of Hf(O^iPr)$_4$.HO^iPr with (**1-5**,**12-15**)H_2 at room temperature also resulted in the production of a mixture of species (Figure 3.03). Recrystallisation attempts from small amounts of hexane yielded crystals for {Hf_2(**1,3**)(O^iPr)$_6$}, these complexes displayed the same structural motif. The bimetallic structure was observed in the solution state NMR spectra as the major product, but the high solubility of the all the products made purification difficult and any isolated material contained significant degrees of impurities. The synthesis of zirconium and hafnium six membered piperazine salan complexes lacked the repeatability required for systematic study.

The complexation of Zr/Hf(O^iPr)$_4$.HO^iPr to the homopiperazine salan ligands {(**6-10**)H_2} proved fruitful (Figure 3.03). Monometallic complexes were obtained at room temperature and furthermore recrystallisation from hexane resulted in crystals suitable for X-ray diffraction studies for Zr(**6-7,10**)(O^iPr)$_2$, and Hf(**6-8,10**)(O^iPr)$_2$. The synthetic methodology was repeatable and a pure product was consistently obtained, which was characterised by $^1H/^{13}C\{^1H\}$ NMR spectroscopy and CHN analysis. Analysis by $^1H/^{13}C\{^1H\}$ NMR spectroscopy and CHN analysis was consistent with the solid-state structure remaining in solution. Utilising heat and longer reaction times enhanced the obtained yields, presumably assisting to overcome the energy barrier between the chair and boat configurations of the bridging homopiperazine ring. The introduction of THF to the synthesis of Zr(**6**)(O^iPr)$_2$ lead to the determination of a crystal structure with a partially coordinated THF bound to the zirconium metal centre {Zr(**6**)(O^iPr)$_2$.0.5THF.0.5IPA}.

3.3 Characterisation by X-ray Crystallography

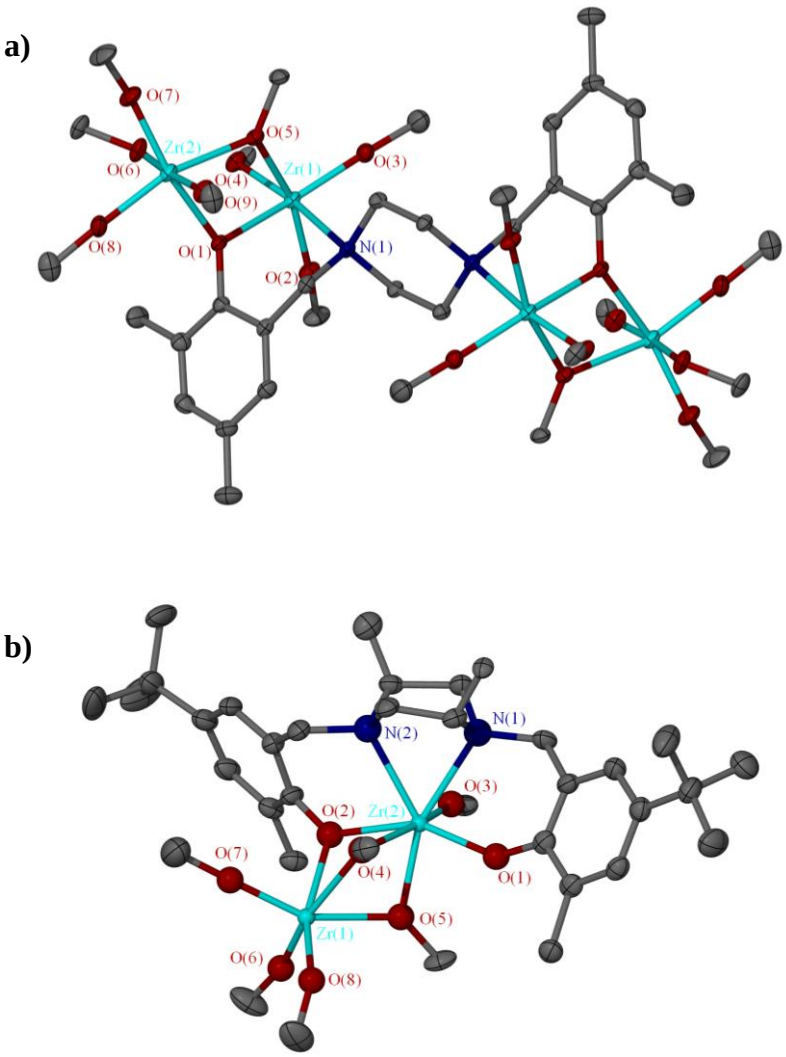

Figure 3.04: Solid-state structures of a) Zr_4(**1**)(O^iPr)$_{14}$.(HO^iPr)$_2$ b) Zr_2(**15**)(O^iPr)$_6$. Ellipsoids are shown at the 30 % probability level, hydrogen atoms and ^{i}Pr –CH_3 groups have been omitted for clarity.

Two structural motifs were obtained by X-ray crystallography for the zirconium piperazine salan complexes; Zr_4(**1**)(O^iPr)$_{14}$.(HO^iPr)$_2$ (Figure 3.04a), Zr_2(**15**)(O^iPr)$_6$ (Figure 3.04b). The tetramer Zr_4(**1**)(O^iPr)$_{14}$.(HO^iPr)$_2$ has two unique zirconium environments (Figure 3.04a), the complex has an inversion centre hence there are two pairs of equivalent zirconium centres. Both zirconium metals adopt a *pseudo* octahedral environment where both are bound to a bridging phenoxy group {Zr1-O1 = 2.168(3) Å, Zr2-O1 = 2.257(3) Å}, and a bridging isopropoxide moiety {Zr1-O1 = 2.184(3) Å, Zr2-O1 = 2.223(3) Å}. Zr1 is bound to three isopropoxide

groups with bond lengths ranging between 1.939(3) - 2.034(3) Å, and one chelating nitrogen {Zr1-N1 = 2.523(3) Å}. Zr2 also coordinated to three terminal isopropoxide groups with bond lengths ranging between 1.944(3) - 1.953(3) Å. An isopropanol was bound to Zr2 {Zr2-O6 = 2.287(3) Å}, the isopropanol hydrogen bonds to an isopropoxide oxygen (O6). The bridging groups favour binding to Zr1, which is an artefact from the stronger coordination of a neutral isopropoxide ligand to Zr2 over the coordination of a neutral nitrogen to Zr1. The bridging phenoxy oxygen (O1) is *trans* to two terminal isopropoxide groups of each Zr metal giving angles; O1-Zr1-O3 = 159.43(11) °, O1-Zr2-O7 = 160.89(12) °, both cases significantly deviate from the idealistic *trans* octahedral angle. Di(amine/imine) bridged bis(phenol) ligands have previously resulted in bimetallic zirconium complexes although examples typically include two ligands and two zirconium metals unlike Zr_2(**15**)(O^iPr)$_6$.[10, 11] No previous tetrametallic bis(phenoxy) complexes have been reported as a bulk material or crystallographically determined.

The bimetallic Zr_2(**15**)(O^iPr)$_6$ has two zirconium metal centres, the piperazine salan ligands adopt the boat configuration and coordinate as a tetradentate ligand to Zr2 (Figure 3.04b). The piperazine methyl substituents are disordered over two positions in a 50:50 ratio, which are shown in figure 3.04b. Zr1 adopt a six coordinate *pseudo* octahedral structure and is only directly bonded to the piperazine salan ligand by a single bridging phenoxy group {Zr1-O2 = 2.286(4) Å}. Three terminal isopropoxide groups are coordinated to Zr1 with bond lengths ranging between 1.931(6) – 1.959(4) Å. The two zirconium metals are bridged by two isopropoxide groups with bond lengths between 2.153(4) - 2.327(5) Å, with the bridging oxygen bonds to Zr2 being shorter. Zr2 coordinates to the piperazine salan ligand through two phenoxy groups {Zr2-O1 = 2.043(4) Å, Zr2-O2 = 2.199(4) Å} and two amine groups {Zr2-N1 = 2.481(5) Å, Zr2-N2 = 2.450(6) Å}. Zr2 is coordinated to a single terminal isopropoxide moiety to give a final seven coordinate metal centre which adopts a *pseudo* pentagonal bipyramidal structure. Seven coordinate zirconium complexes have been previously reported to adopt *pseudo* pentagonal bipyramidal conformations.[12, 13]

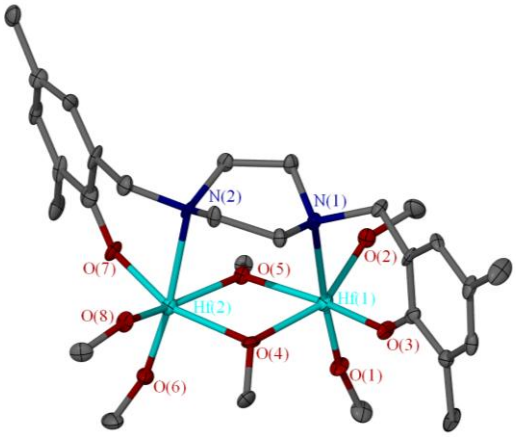

Figure 3.05: Solid-state structure of Hf_2(**1**)(O^iPr)$_6$. Ellipsoids are shown at the 30 % probability level, hydrogen atoms and ^iPr –CH_3 groups have been omitted for clarity.

Two hafnium piperazine salan structures {Hf_2(**1,3**)(O^iPr)$_6$} were characterised by X-ray crystallography and a representative structure for Hf_2(**1,3**)(O^iPr)$_6$ is given in figure 3.05. The piperazine ring adopts the boat configuration and each hafnium metal centre is bridged by two isopropoxide groups, selected bonds length are shown in table 3.01. Each hafnium metal adopts a *pseudo* octahedral structure chelating to one half of the piperazine salan ligand (a phenoxy and an amine) along with two terminal isopropoxide groups. The terminal isopropoxide Zr-O bonds are typically shorter, 1.891(11) – 1.964(9) Å, than the bridging isopropoxide Zr-O bonds, with bond lengths ranging between 2.122(9) -2.204(10) Å. A slight deviation from an idealistic octahedral structure was observed where the *trans* angles (N1-Hf1-O1), and *cis* angles (N1-Hf1-O2, N1-Hf1-O4) revealed deviations from 180 ° and 90 ° respectively. Bimetallic hafnium structures coordinated to diamine linked bis(phenol) ligands have been previously reported,[14] although they are not prevalent in the literature. Further bimetallic hafnium structures have been reported with -ON(N)O- based bis(phenol) ligands.[15]

	Hf_2(**1**)$(O^iPr)_6$	Hf_2(**3**)$(O^iPr)_6$
Hf1-O1	1.908(9)	1.917(7)
Hf1-O2	1.913(10)	1.929(9)
Hf1-O3	1.995(9)	2.009(6)
Hf1-O4	2.204(10)	2.152(10)
Hf1-O5	2.122(9)	2.180(11)
Hf1-N1	2.548(12)	2.534(9)
N1-Hf1-O1	173.9(4)	169.6(3)
N1-Hf1-O2	80.1(4)	87.1(3)
N1-Hf1-O4	80.9(4)	84.4(3)

Table 3.01: Selected bond lengths (Å) and angles (°) for piperazine salan hafnium complexes $\{Hf_2$(**1,3**)$(O^iPr)_6\}$, as determined by X-ray crystallography.

The homopiperazine salan ligands {(**6**-**10**)H_2} were complexed to zirconium which resulted in monometallic structures, a representative solid-state structure is displayed in figure 3.06a. Selected bond lengths (Å) and angles (°) for Zr(**6**)$(O^iPr)_2$, Zr(**7**)$(O^iPr)_2$, Zr(**10**)$(O^iPr)_2$, and Zr(**6**)$(O^iPr)_2$.0.5THF.0.5IPA are given in table 3.02. The zirconium metal centre adopts a *pseudo trans*-octahedral structure (Chapter 2.5.2, figure 2.23) where the homopiperazine salan ligand chelates equatorially, the phenoxy groups were orientated *cis* to each other, and the amines are also *cis* orientated. The two terminal isopropoxide ligands are *trans* to each other in the axial position with no significant difference in bond length between the two axial moieties. The axial isopropoxide groups revealed a slight deviation from 180 °, with O1-Zr-O2 angles between 173.5(2) - 175.9(2) °. A large deviation (from 90 °) between the two *cis* phenoxy groups was observed with the O3-Zr-O4 angles being ~120 °. The two phenyl rings are orientated towards the same isopropoxide, the angle between the planes of the phenyl rings ranges between 73.7 – 81.2 °.

A solid-state structure of Zr(**6**)$(O^iPr)_2$ with a coordinated THF/isopropanol group was determined by X-ray crystallography. The resulting structure is given in

figure 3.06b with selected bond lengths (Å) and angles (°) specified in table 3.02. The zirconium metal centre is seven coordinate and adopts a *pseudo* pentagonal bipyramidal structure, where the THF was found in a 50:50 ratio with an isopropanol moiety. The isopropoxide groups remains in the axial position of the complex although the *trans* isopropoxide angle was more acute {O1-Zr1-O2 = 169.18(7) °}. The introduction of the neutral coordinating oxygen group elongates the amine zirconium bonds (Zr1-N1 and Zr1-N2). The angle between the two phenoxy groups becomes more obtuse {O3-Zr1-O4 = 137.96(6)} to allow the introduction of an extra coordinating group.

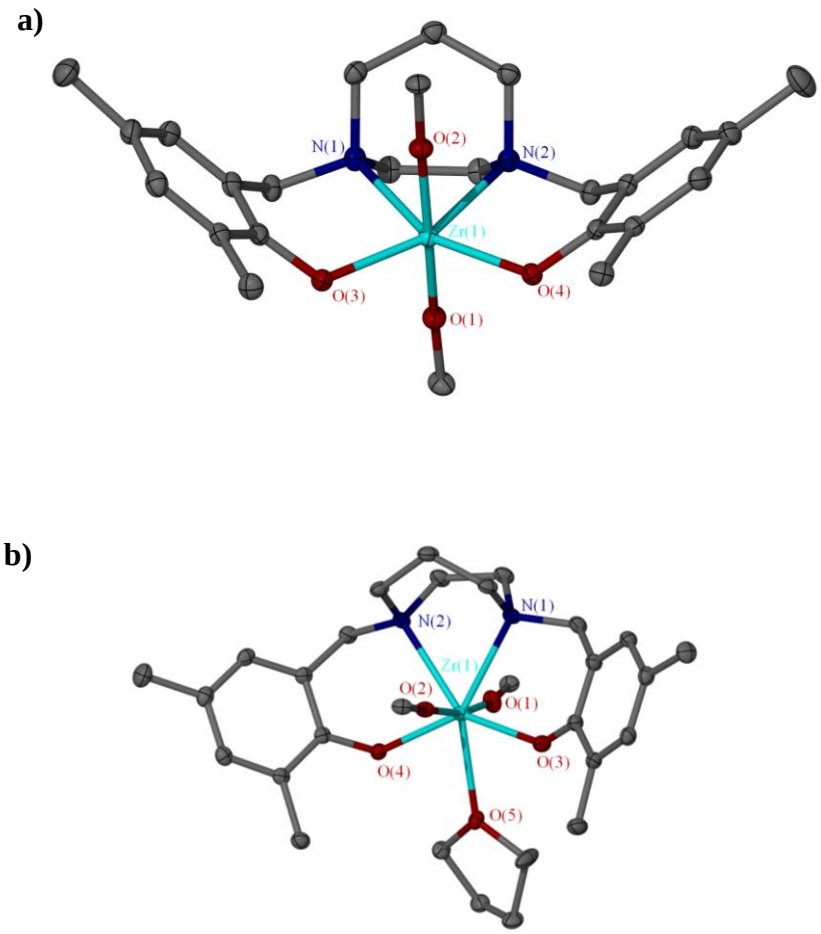

Figure 3.06: Solid-state structures of a) Zr(**6**)(O^iPr)$_2$ b) Zr(**6**)(O^iPr)$_2$.0.5THF.0.5IPA. Ellipsoids are shown at the 30 % probability level, hydrogen atoms and ^iPr –CH_3 groups have been omitted for clarity.

	Zr(**6**)(O^iPr)$_2$	Zr(**7**)(O^iPr)$_2$	Zr(**10**)(O^iPr)$_2$	Zr(**6**)(O^iPr)$_2$.0.5 THF.0.5IPA
Zr1-O1	1.9689(14)	1.968(4)	1.962(6)	1.9708(17)
Zr1-O2	1.9665(14)	1.964(4)	1.966(5)	1.9652(16)
Zr1-O3	2.0476(15)	2.041(2)	2.047(6)	2.0950(17)
Zr1-O4	2.0567(14)	-[a]	2.027(6)	2.1292(15)
Zr1-O5	-	-	-	2.469(10)[b]
Zr1-N1	2.3958(18)	2.387(3)	2.391(8)	2.4831(19)
Zr1-N2	2.3876(18)	-[a]	2.381(8)	2.4945(18)
N1-Zr1-O1	87.20(6)	86.25(14)	87.8(3)	84.05(7)
N1-Zr1-O4	152.67(6)	153.50(8)[a]	152.8(3)	142.89(6)
O1-Zr1-O2	174.71(6)	173.5(2)	175.9(2)	169.18(7)
O3-Zr1-O4	121.40(6)	119.57(13)	120.6(2)	137.96(6)

Table 3.02: Selected bond lengths (Å) and angles (°) for monometallic zirconium complexes, as determined by X-ray crystallography. [a] The molecule contains a mirror plane; Zr1-O3 = Zr1-O4, Zr1-N1 = Zr1-N2.

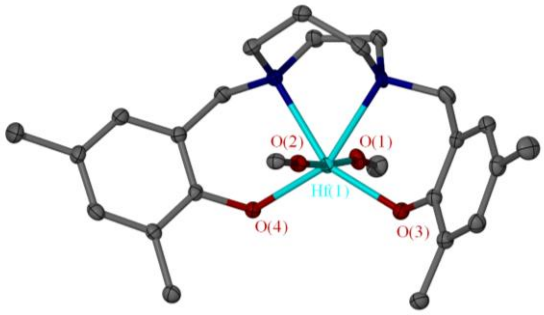

Figure 3.07: Solid-state structure of Hf(**6**)(O^iPr)$_2$. Ellipsoids are shown at the 30 % probability level, hydrogen atoms and ^iPr –CH_3 groups have been omitted for clarity.

Similar monometallic structures were identified by X-ray crystallography for the hafnium isopropoxide homopiperazine salan complexes {Hf(**6-8,10**)(O^iPr)$_2$}. The structures for Hf(**6**)(O^iPr)$_2$, Hf(**7**)(O^iPr)$_2$, Hf(**8**)(O^iPr)$_2$, and Hf(**10**)(O^iPr)$_2$ were obtained. The structure of Hf(**6**)(O^iPr)$_2$ is given in figure 3.07 as a representative example. Selected bond lengths (Å) and angles (°) determined by X-ray

crystallography can be found in table 3.03. These structures all adopt a *pseudo trans*-octahedral geometry (Chapter 2.5.2, figure 2.23) where the homopiperazine ligand coordinates *via* two amines and two phenoxy groups to the equatorial positions of the hafnium metal centre. The isopropoxide groups coordinates in the axial positions, while *trans* to each other a slight deviation from 180 ° was observed {O1-Hf1-O2 = 172.7(4) - 176.36(13) °}. Similarly the phenyl rings are both orientated towards the -$(CH_2)_3$- group of the homopiperazine ring, where the angle between planes of the two phenyl rings ranged between 71.8 – 81.1 °. The *trans* octahedral geometry is not prevalent in the literature for Zr(IV) or Hf(IV) (-ONNO-} bis(phenoxy) isopropoxide complexes. Titanium has been reported to adopt the *trans* octahedral configuration in solution.[16] However, the *trans* octahedral geometry is favourable in the presence of metal coordinated chloride moieties.[12, 17]

	Hf(**6**)(O^iPr)$_2$	Hf(**7**)(O^iPr)$_2$	Hf(**8**)(O^iPr)$_2$	Hf(**10**)(O^iPr)$_2$
Hf1-O1	1.960(4)	1.957(7)	1.982(3)	1.969(2)
Hf1-O2	1.955(4)	1.993(6)	1.966(3)	1.964(2)
Hf1-O3	2.030(4)	2.040(2)	2.037(3)	2.040(3)
Hf1-O4	2.041(4)	-[a]	2.037(3)	2.035(3)
Hf1-N1	2.364(5	2.363(3)	2.340(4)	2.355(4)
Hf1-N2	2.357(5)	-[a]	2.349(3)	2.359(3)
N1-Hf1-O1	87.14(16)	88.06(17)	87.95(12)	88.09(11)
N1-Hf1-O4	153.63(16)	155.00(9)[a]	153.88(12)	154.66(13)
O1-Hf1-O2	174.83(16)	172.7(4)	176.36(13)	175.55(11)
O3-Hf1-O4	119.17(15)	117.34(13)	119.36(12)	118.82(11)

Table 3.03: Selected bond lengths (Å) and angles (°) for homopiperazine salan hafnium complexes, as determined by X-ray crystallography. [a] The molecule contains a mirror plane; Zr1-O3 = Zr1-O4, Zr1-N1 = Zr1-N2.

3.4 Characterisation by NMR Spectroscopy

^{1}H NMR spectroscopy was utilised to analyse the products from the complexation reaction of zirconium and hafnium isopropoxide to piperazine salan ligands (**1-5**,**12-15**)H_2. The ^{1}H NMR spectra were typically indeterminable and acidic phenol protons were often observed indicating incomplete reactions. The isolated hafnium piperazine salan {Hf_2(**1**,**3**)(O^iPr)$_6$} product contained several impurities. These ^{1}H NMR spectra indicated the formation of structures with a metal-to-ligand ratio of 2:1, as determined by X-ray crystallography, but significant degrees of impurities were observed in the recrystallised product.

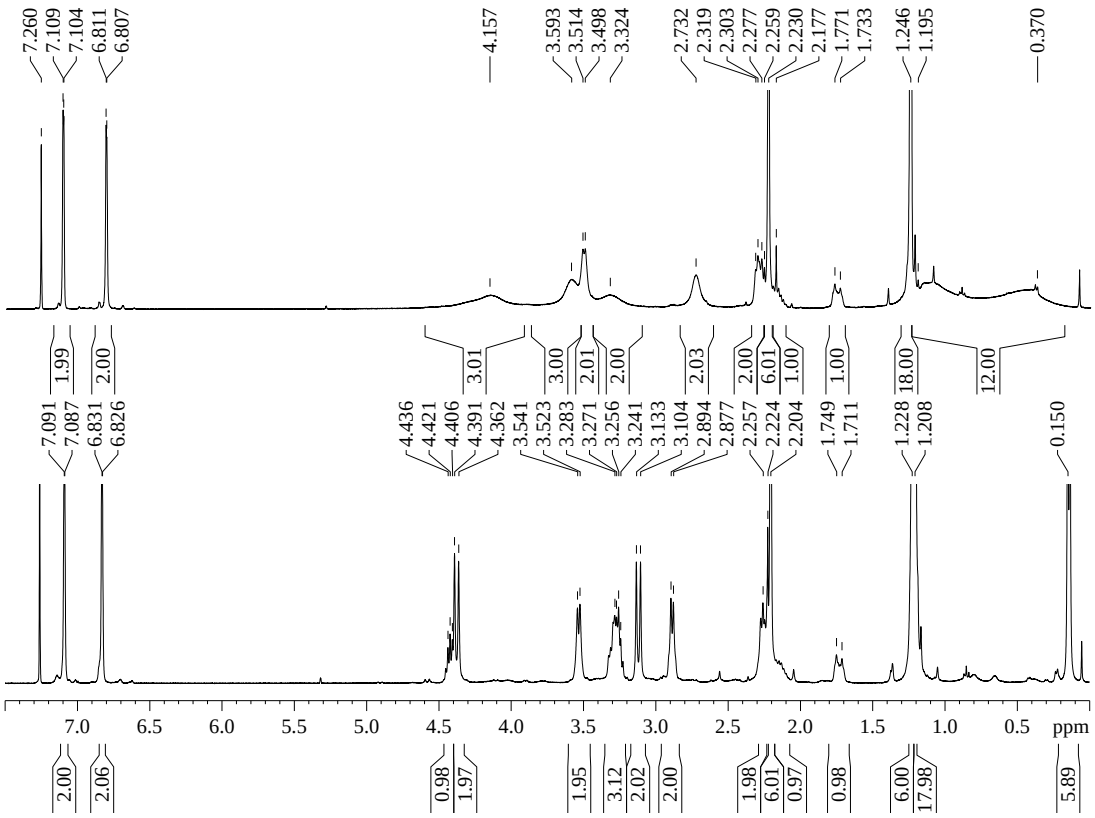

Figure 3.08: 1H NMR spectra for Zr(**7**)(O^iPr)$_2$, top 298 K, bottom 233 K.

The solution NMR spectra for Zr(**6-10**)(O^iPr)$_2$ were consistent with the X-ray crystallographically determined structures being maintained in solution. A representative room temperature ^{1}H NMR spectrum for Zr(**7**)(O^iPr)$_2$ is given in figure 3.08 alongside a low temperature ^{1}H NMR spectrum. The room temperature ^{1}H NMR spectra are typically broad around the CH_2 regions and the CH isopropoxide region (2.00 - 4.50 ppm). There are two broad isopropoxide CH_3

resonances at ~ 0.38 ppm and ~ 1.10 ppm, the broad regions are indicative of fluxionality in the isopropoxide moieties and the backbone of the homopiperazine salan ligand. Upon cooling (233 K) the aromatic region remains defined with two doublets at 6.83 ppm, and 7.11 ppm, whereas the lower chemical shift regions become more distinct. The homopiperazine ring system displays a significant sharpening of resonances at 3.53 ppm, 3.27 ppm, 2.88 ppm, 2.25 ppm, 2.18 ppm (partial overlap with the CH_3 resonances), and 1.73 ppm. A pronounced enhancement is observed for the isopropoxide moieties; both CH isopropoxide groups were located at 3.28 ppm and 4.43 ppm, although in this specific example (Figure 3.08) both resonances are located in the same region as the CH_2 group resonances. The CH_3 isopropoxide resonances are present at 0.15 ppm and 1.22 ppm, the resonance at 1.22 ppm coincides with resonances attributed to ^{t}Bu groups. The resonance at 0.15 ppm is significantly shifted upfield than typical zirconium bound isopropoxide CH_3 groups. It was deduced that this isopropoxide orientated towards the -$(CH_2)_3$- homopiperazine region and is profoundly shielded by the phenoxy aromatic rings orientated in the same direction.

Subsequent NMR spectroscopy investigations of the homopiperazine salan hafnium complexes {Hf(**6-10**)(O^iPr)$_2$} evidently proved the solution state structures were of the same *pseudo trans*-octahedral geometry as determined by X-ray crystallography (Figure 3.07). A representative ^{1}H NMR spectrum of Hf(**7**)(O^iPr)$_2$ under ambient conditions is provided, accompanied by a low temperature ^{1}H NMR spectrum of the same complex (Figure 3.09). Similar to the analogous zirconium complex {Zr(**7**)(O^iPr)$_2$} the ^{1}H NMR spectrum for Hf(**7**)(O^iPr)$_2$ revealed a broadening of the homopiperazine salan CH_2 resonances and the CH/CH_3 isopropoxide resonances. Upon cooling the phenoxy substituent resonances (1.21 ppm, 2.17 ppm) and aromatic resonances remain relatively unchanged. The CH_2 piperazine ring protons results in defined resonances, 1.17 ppm, 2.15 ppm (partial overlap with the CH_3 resonance), 2.35 ppm, 2.95 ppm, 3.35 ppm, and 3.54 ppm. The isopropoxide CH resonances become defined, 4.51 ppm and 3.35 ppm, although the latter resonance coincides with a CH_2 resonance. Similar to the Zr(**7**)(O^iPr)$_2$ ^{1}H NMR spectrum a single isopropoxide moiety reveals a significant upfield shift, as a consequence of the proximity of two phenoxy groups orientated towards a particular isopropoxide moiety.

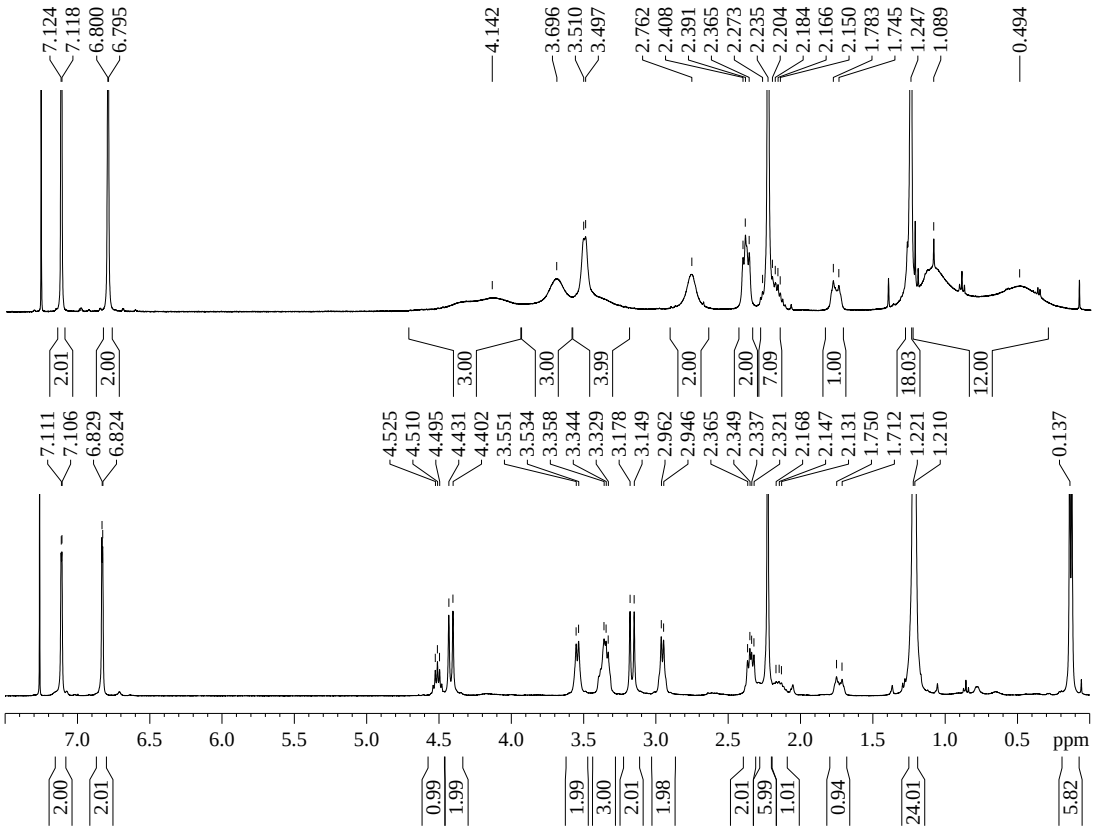

Figure 3.09: ^{1}H NMR spectra for Hf(**7**)($O^{i}Pr$)$_2$, top 298 K, bottom 233 K.

3.5 Ring-Opening-Polymerisation of *rac*-Lactide

The zirconium and hafnium homopiperazine salan complexes were trialled for the ring opening polymerisation (ROP) of *rac*-lactide in both solution and solvent free conditions. Furthermore no co-initiator was required and selected complexes were investigated at different monomer to initiator ratios.

3.5.1 Solution ROP of *rac*-lactide

The ROP of *rac*-lactide was investigated in toluene (10 ml) at 80 °C typically allowing 24 h reaction time. In all cases 1.0 g of *rac*-lactide was used and the initiator was added in a 100:1 [*rac*-lactide]:[initiator] ratio, no co-initiator was required for the ROP reaction to proceed. The polymerisation typically achieved high conversion after 24 h at which point the reaction was quenched with methanol (Table 3.04). Lower conversions were obtained for initiators that contain an *ortho*-^{t}Bu ring substituent {Zr(**8-9**)($O^{i}Pr$)$_2$, Hf(**8-9**)($O^{i}Pr$)$_2$}. This is presumably a

steric effect of the bulkier ^{t}Bu substituents hindering access to the zirconium or hafnium metal centre. The hafnium complexes containing ^{t}Bu groups on the *ortho*-position of the phenoxy ring {Hf(**8-9**)($O^{i}Pr$)$_2$} gave lower conversions than their zirconium counterparts. Complexes containing amyl phenoxy ring substituents did not show same degree of reduction in activity, it was speculated that the bulky amyl groups may destabilise the complex during the ROP reaction. Hence, higher conversions were observed despite the increased steric demands of amyl groups compared to ^{t}Bu moieties. It should be noted that erroneous CHN analysis of Zr/Hf(**10**)($O^{i}Pr$)$_2$ were obtained, although solution state and X-ray diffraction analysis supports the proposed structure.

Polylactide (PLA) molecular weights (M_n) were determined by GPC in THF (Table 3.04), the molecular weights were relatively consistent with the theoretical molecular weights, calculated from conversion, for the propagation of one PLA chain per metal centre. The majority of complexes investigated revealed narrow PDI values (PDI = 1.05 – 1.69). The zirconium complexes displayed increased molecular weight distributions in comparison to their hafnium analogues. *ortho*-Methyl substituents upon the phenoxy ring {Zr(**6-7**)($O^{i}Pr$)$_2$, Hf(**6-7**)($O^{i}Pr$)$_2$} resulted in higher PDI values, which was presumably a consequence of reduced steric hindrance, the effect was even more pronounced for the zirconium complexes.

The complexes {Zr(**6-10**)($O^{i}Pr$)$_2$} propagated *rac*-lactide to produce PLA, which revealed a slight to moderate isotactic bias (P_r = 0.38 – 0.45) (Table 3.04) as determined by homonuclear decoupled ^{1}H NMR spectroscopy. The zirconium complexes containing *ortho*-methyl phenoxy ring substituents {Zr(**6-7**)($O^{i}Pr$)$_2$} displayed the stronger isotactic selectivity. The hafnium homopiperazine salan complexes {Hf(**6-10**)($O^{i}Pr$)$_2$} also resulted in PLA with a slight to moderate isotactic bias (P_r = 0.35 – 0.5). Likewise the hafnium initiators with *ortho*-methyl phenoxy ring substituents {Hf(**6-7**)($O^{i}Pr$)$_2$)} revealed slightly enhanced isotactic selectivity (P_r = 0.35 – 0.37).

	Time (hours)	Conv. (%)[a]	M_n[b] *(theo)*	M_n[c]	PDI[c]	P_r[d]
Zr(**6**)(O^iPr)$_2$	24	96	13900	10000	1.69	0.38
Zr(**6**)(O^iPr)$_2$	24[e]	97[e]	42000[e]	45700[e]	1.59[e]	0.38
Zr(**7**)(O^iPr)$_2$	24	93	13450	10550	1.55	0.42
Zr(**8**)(O^iPr)$_2$	24	79	11450	7950	1.21	0.45
Zr(**9**)(O^iPr)$_2$	24	26	3800	4400	1.22	-
Zr(**10**)(O^iPr)$_2$	24	87	12600	10400	1.15	0.45
Hf(**6**)(O^iPr)$_2$	24	95	13750	12850	1.68	0.37
Hf(**6**)(O^iPr)$_2$	24	95[e]	41150[e]	52100[e]	1.20[e]	0.35
Hf(**7**)(O^iPr)$_2$	6	83	12000	9250	1.11	0.37
Hf(**8**)(O^iPr)$_2$	24	12	1800	1650	1.05	-
Hf(**9**)(O^iPr)$_2$	24	22	3250	2550	1.26	0.52
Hf(**10**)(O^iPr)$_2$	24	89	12900	9500	1.12	0.43

Table 3.04: Solution ROP of *rac*-lactide for Zr(**6**-**10**)(O^iPr)$_2$ and Hf(**6**-**10**)(O^iPr)$_2$ in 10 ml of toluene at 80 °C in a 100:1 [*rac*-lactide]:[initiator] ratio. [a] Conversion ascertained by ^{1}H NMR spectroscopy. [b] Theoretical molecular weight calculated from conversion (Conv. × 100 × 144.13 + 60.10) (rounded to the nearest 50), [c] Molecular weight and PDI determined by GPC (THF) using polystyrene standards without applying a correction factor. [d] P_r as calculated from ^{1}H NMR homonuclear decoupled spectroscopy in $CDCl_3$. [e] 300:1 [*rac*-lactide]:[initiator] ratio.

The homonuclear decoupled ^{1}H NMR spectrum of PLA synthesised from *rac*-lactide initiated by Hf(**6**)(O^iPr)$_2$ in a 300:1 [*rac*-lactide]:[Initiator] ratio after 24 h, in toluene, at 80 °C is displayed in figure 3.10. There is an enhancement of the [*iii*] tetrad resonance at 5.16 ppm. Alongside this is a decrease in intensity of the [*sis*] and [*isi*] tetrads resonances, at 5.22 ppm and 5.15 ppm respectively. The probability of racemic enchainment (P_r) was calculated using Bernoullian statistics[18] using the relative integrals fraction of the [*sis*] resonance against all the methine resonances, 1/15.99, gives a P_r = 0.35 from equation 1.06 (Figure 1.16). The homonuclear ^{1}H NMR spectrum given in figure 3.10 is a representative example for the isotactic bias determined for initiators given in table 3.04.

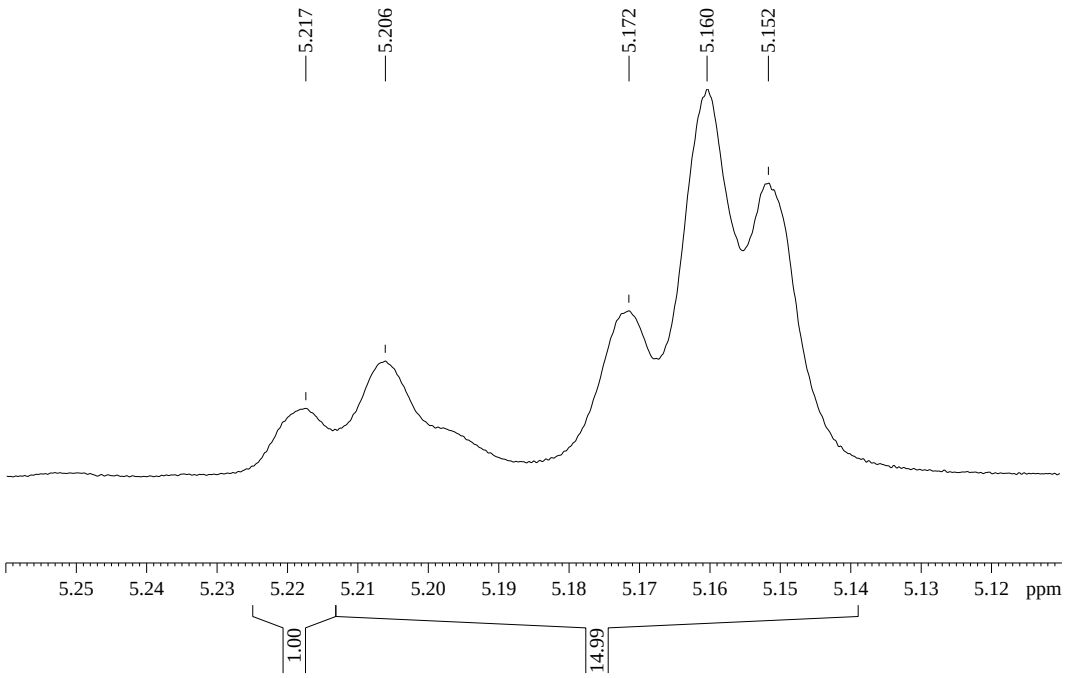

Figure 3.10: ^{1}H NMR homonuclear decoupled spectrum showing tetrad resonances for the ROP of *rac*-lactide by Hf(**6**)(O^{i}Pr)$_2$ in a 100:1 [*rac*-lactide]:[Initiator] ratio, after 24 h in toluene at 80 °C (Table 3.04).

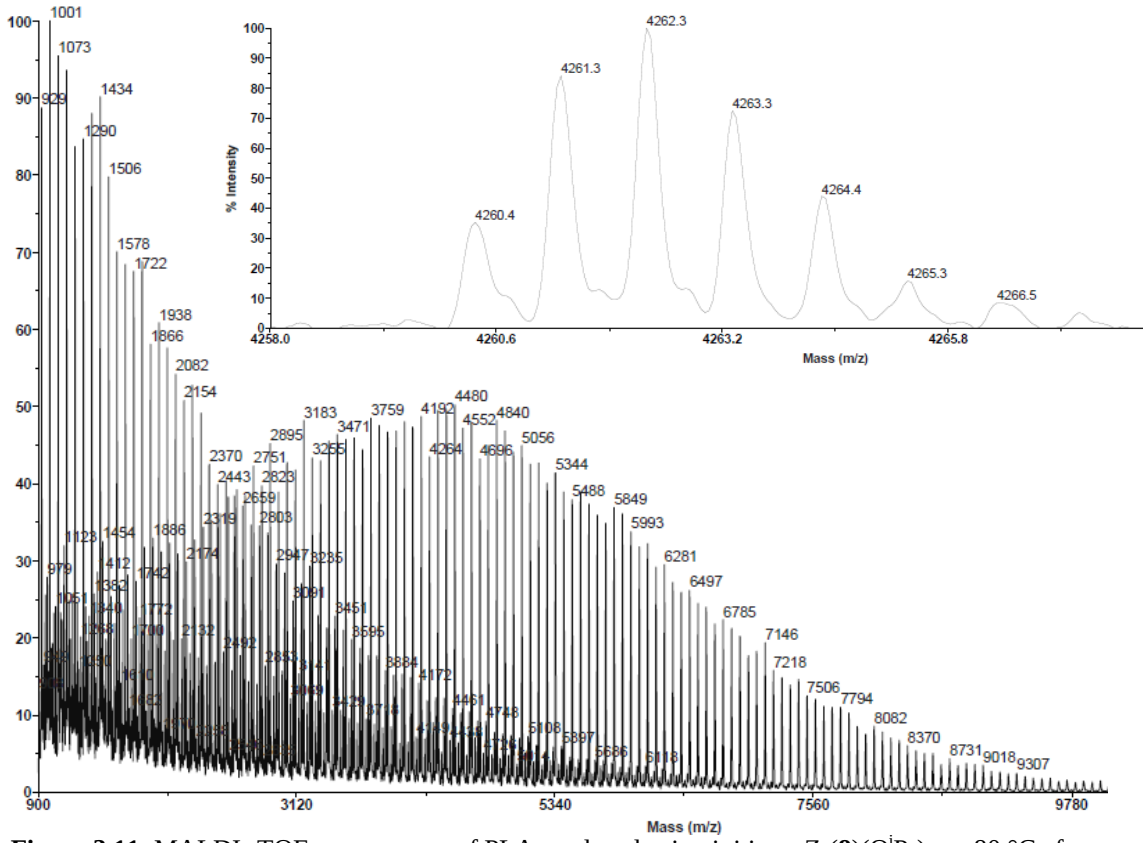

Figure 3.11: MALDI- TOF mass spectra of PLA produced using initiator Zr(**8**)(O^{i}Pr)$_2$, at 80 °C after 24 h.

The MALDI-TOF mass spectrum of polymer resulting from PLA produced by initiator Zr(**8**)(O^iPr)$_2$ is given in figure 3.11 for the major series of peaks. The spacing between signals was ~ 72 g mol^{-1}, this value is typical of half a lactide unit indicative of a degree of transesterification occurring during the ROP reaction. Analysis of peaks and splitting patterns allowed the identification of -H and -isopropoxide ends groups. The peak pattern at 4262.3 M_w (Figure 3.11) corresponded to the enchainment of 29 lactide units, a terminal hydrogen, a terminal isopropoxide and ionised with a sodium ion.

3.5.2 Solvent free ROP of *rac*-lactide

The homopiperazine salan zirconium {Zr(**6**-**10**)(O^iPr)$_2$} and hafnium {Hf(**6** **10**)(O^iPr)$_2$} complexes were trialled as initiators for the ROP of *rac*-lactide in solvent free conditions using 1.0 g of lactide at 130 °C. All initiators were used without a co-initiator at a 300:1 [*rac*-lactide]:[initiator] ratio, with selected trials at 900:1 [*rac*-lactide]:[initiator] ratio. High conversions were obtained for initiators containing *ortho* methyl or amyl phenoxy substituents {Zr(**6**-**7**,**10**)(O^iPr)$_2$, Hf(**6**-**7**,**10**)(O^iPr)$_2$} after 0.5 hours, whereas initiators with *ortho*-^{t}Bu phenoxy substituents {Zr(**8**-**9**)(O^iPr)$_2$, Hf(**8**-**9**)(O^iPr)$_2$} required 3 h to obtain high conversion (Table 3.04). At the higher *rac*-lactide to initiator ratios (900:1) the longer reaction time of 6 h resulted in partial conversion.

The Hf(**6**-**10**)(O^iPr)$_2$ initiators were relatively consistent with one PLA chain per metal. There was some deviation in molecular weight (M_n) from the conversion calculated theoretical molecular weights. Moderately low PDI (PDI = 1.12 – 1.39) values were obtained with little noted difference between initiators containing *ortho*-methyl and *ortho*-^{t}Bu phenoxy substituents, which is contrasting to the related solution ROP observations. The solvent free ROP of *rac*-lactide by Zr(**6**-**10**)(O^iPr)$_2$ and Hf(**8**-**10**)(O^iPr)$_2$ resulted in the production of predominantly atactic PLA (P_r = 0.44 – 0.56) (Table 3.05). Akin to the solution ROP reactions the *ortho*-methyl phenoxy substituted hafnium complexes {Hf(**6**-**7**)(O^iPr)$_2$} yielded PLA with a moderate isotactic bias (P_r = 0.37 – 0.39), to a similar degree to the lower temperature solution ROP of *rac*-lactide (P_r = 0.35 – 0.37) (Table 3.04).

	Time (hours)	Conv. (%)[a]	M_n[b] *(theo)*	M_n[c]	PDI[c]	P_r[d]
Zr(**6**)(O^iPr)$_2$	0.5	97	42000	45000	1.39	0.44
Zr(**7**)(O^iPr)$_2$	0.5	79	34200	15200	1.17	0.51
Zr(**8**)(O^iPr)$_2$	3	86	37250	20900	1.22	0.51
Zr(**8**)(O^iPr)$_2$[e]	6	48	62300	31950[e]	1.12[e]	0.56[e]
Zr(**9**)(O^iPr)$_2$	3	89	38550	19300	1.31	0.47
Zr(**10**)(O^iPr)$_2$	0.5	93	40250	34850	1.26	0.55
Hf(**6**)(O^iPr)$_2$	0.5	91	39400	47800	1.33	0.37
Hf(**7**)(O^iPr)$_2$	0.5	96	41550	37150	1.28	0.39
Hf(**8**)(O^iPr)$_2$	3	87	37700	26000	1.14	0.5
Hf(**8**)(O^iPr)$_2$[e]	6	41	53250	28850[e]	1.15[e]	0.56[e]
Hf(**9**)(O^iPr)$_2$	3	90	39000	35600	1.32	0.5
Hf(**10**)(O^iPr)$_2$	0.5	83	35950	27400	1.22	0.49

Table 3.05: Solvent free ROP of *rac*-lactide for Zr(**6**-**10**)(O^iPr)$_2$ and Hf(**6**-**10**)(O^iPr)$_2$ at 130 °C in a 300:1 [*rac*-lactide]:[initiator] ratio. [a] Conversion ascertained by ^{1}H NMR spectroscopy. [b] Theoretical molecular weight calculated from conversion (Conv. × 100 × 144.13 + 60.10) (rounded to the nearest 50), [c] Molecular weight and PDI determined by GPC (THF) using polystyrene standards without applying a correction factor. [d] P_r as calculated from ^{1}H NMR homonuclear decoupled spectroscopy in $CDCl_3$. [e] 900:1 [*rac*-lactide]:[initiator] ratio.

Independent ROP reactions were performed with Zr(**8**)(O^iPr)$_2$ and Hf(**8**)(O^iPr)$_2$ initiators in solvent free conditions. The individual polymerisations were allowed to achieve varying conversions, a dual plot of M_n against conversion and PDI against conversion is displayed in figure 3.12. The molecular weight growth shows a linear increase with conversion as expected for the controlled propagation of PLA chains. PDI was plotted against conversion, for the entire range the PDI values were low but a slight increase is present as conversion increases. The linear trend of molecular weight is indicative of a living polymerisation reaction, although transesterification and slowly increasing PDI values with conversion signify deviation from an idealistic living polymerisation.

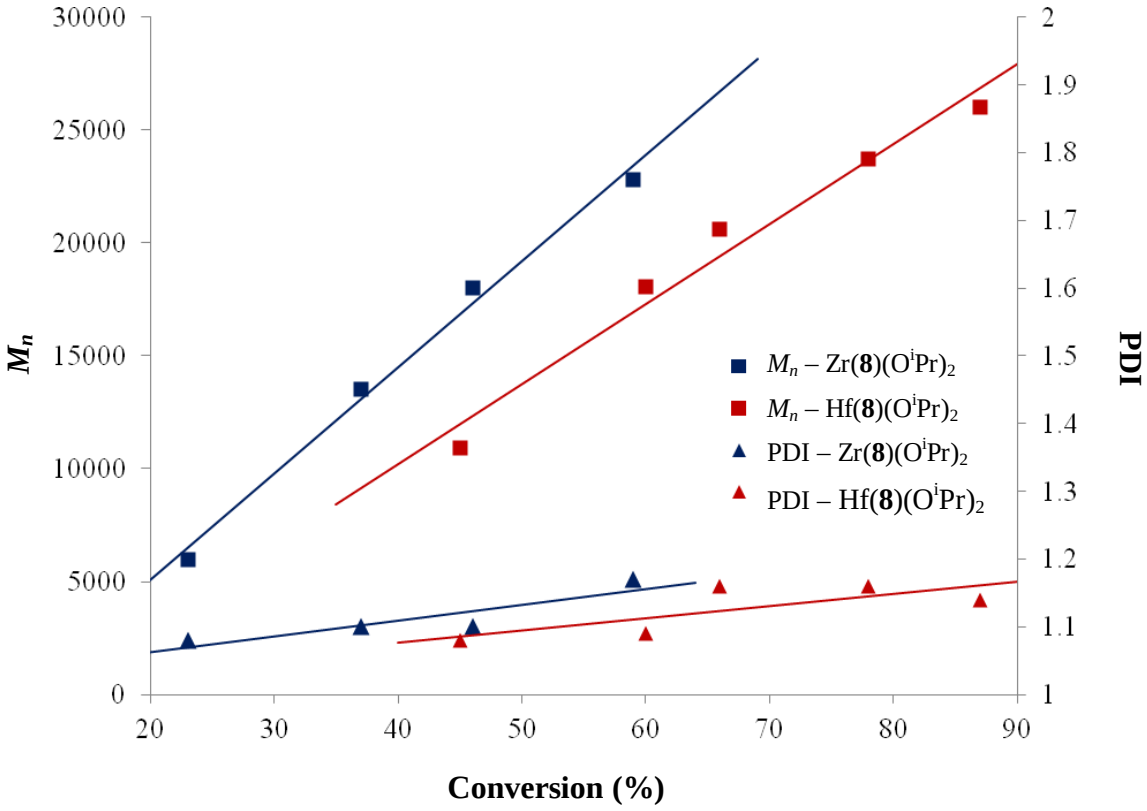

Figure 3.12: M_n (squares) and PDI (triangles) vs. conversion, from individual solvent free ROP reactions of *rac*-lactide, at 130 °C, 300:1 [*rac*-lactide]:[initiator] ratio. Initiators utilised; Zr(**8**)(O^{i}Pr)$_2$ (Blue), Hf(**8**)(O^{i}Pr)$_2$ (Red).

3.5.3 Kinetic investigation of the solution ROP of *rac*-lactide

NMR spectroscopy scale kinetic experiments were performed to investigate the apparent rate of propagation (k_{app}) for the ROP of *rac*-lactide using the homopiperazine salan initiators {Zr(**6**)(O^{i}Pr)$_2$, Hf(**6**)(O^{i}Pr)$_2$}. The NMR spectroscopy scale experiments were performed using 50 mg of *rac*-lactide in d_8-toluene (0.6 ml) at 80 °C, in both cases a 100:1 [*rac*-lactide]:[initiator] ratio was used. The kinetic experiments were allowed to run until high conversion was obtained. Spectra were recorded at 15 min intervals with the initiator Zr(**6**)(O^{i}Pr)$_2$, and at 30 min intervals with the initiator Hf(**6**)(O^{i}Pr)$_2$, both cases are truncated due to diffusion rate limitations at high conversions. ln([LA]$_0$/[LA]$_t$) was plotted against time (Figure 3.13) to present linear plots where the slope relates to the apparent *pseudo* first order rate constant (k_{app}) (Table 3.06). The zirconium catalyst was ~3 times more active towards the ROP of *rac*-lactide than the related hafnium complex. Zirconium

catalysts have been previously reported as more active than corresponding hafnium complexes for the ROP of *rac*-lactide.[6, 8, 19, 20]

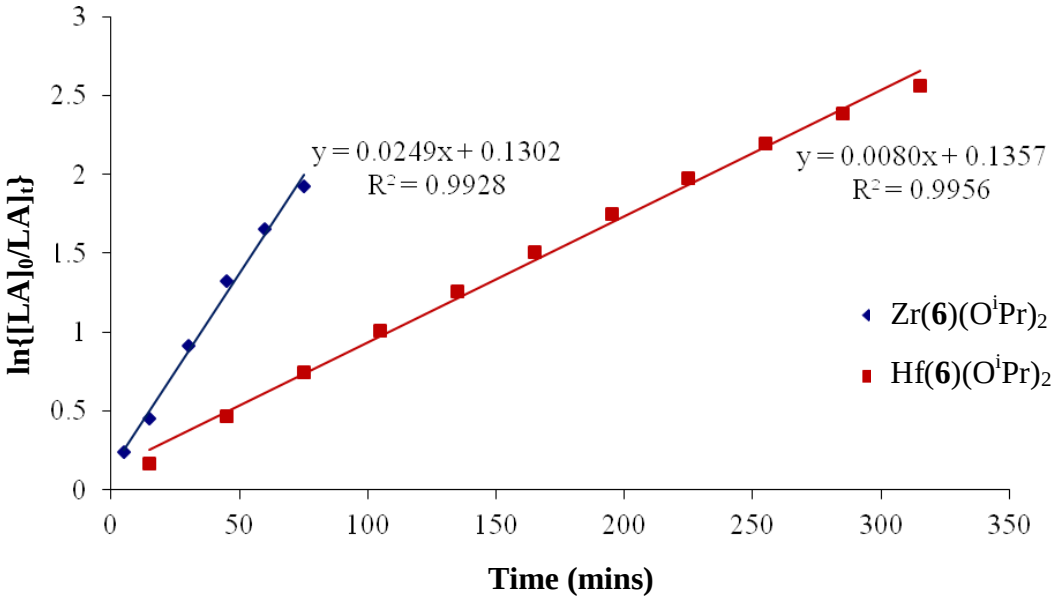

Figure 3.13: *Pseudo* first order plots for the ROP of *rac*-lactide by Zr(**6**)(O^iPr)$_2$ (Blue), and Hf(**6**)(O^iPr)$_2$ (Red), 50 mg of *rac*-lactide in 0.6 ml of d_8-toluene at 80 °C at 100:1 [*rac*-lactide]:[initiator] ratio.

	k_{app} × 10^{-3} (min^{-1})	R^2
Zr(**6**)(O^iPr)$_2$	24.9(11)	0.9928
Hf(**6**)(O^iPr)$_2$	8.00(2)	0.9956

Table 3.06: k_{app} values and R^2 values for ROP of *rac*-lactide by Zr(**6**)(O^iPr)$_2$ and Hf(**6**)(O^iPr)$_2$ initiators.

3.6 Conclusion

The synthesis and characterisation of zirconium and hafnium complexes bearing strained homopiperazine based salan ligands {Zr(**6-10**)(O^iPr)$_2$, Hf(**6-10**)(O^iPr)$_2$} is reported herein. Zr(**6-7,10**)(O^iPr)$_2$ and Hf(**6-8,10**)(O^iPr)$_2$ were isolated as crystals and characterised by X-ray crystallography, each structure was monometallic and adopted a *pseudo* octahedral *trans* configuration. An informative Zr(**6**)(O^iPr)$_2$.0.5THF.0.5IPA complex was characterised by X-ray crystallography

where this seven coordinate variant of Zr(**6**)(O^iPr)$_2$ demonstrated a possible coordination site a lactide unit could adopt. The synthesis of piperazine salan {(**1-5**,**12-15)**H_2} Zr(IV) and Hf(IV) complexes was attempted but generally a plethora of species was obtained and purification of a bulk material was unsuccessful. Isolated crystals of Zr_4(**1**)(O^iPr)$_{14}$.(HO^iPr)$_2$ and Zr_2(**15**)(O^iPr)$_6$ were characterised by crystallography showing a tetrametallic structure and an interesting bimetallic structure where the ligand chelates to one metal. Consistent bimetallic structures were observed for the X-ray determination of Hf_2(**1,3**)(O^iPr)$_6$ complexes. The difficultly in isolating a monometallic piperazine salan Zr(IV) or Hf(IV) structure was attributed to the increased conformational ring strain associated with the piperazine backbone in comparison to a homopiperazine backbone.

Zr(**6-10**)(O^iPr)$_2$ and Hf(**6-10**)(O^iPr)$_2$ were investigated as initiators for the ROP of *rac*-lactide in solvent free and solution conditions. High conversion was typically obtained after 24 h at 80 °C in toluene at a 100:1 [*rac*-lactide]:[initiator] ratio. Higher activity was observed for complexes containing *ortho*-methyl phenoxy substituents over the sterically bulky *ortho*-^{t}Bu phenoxy substituents. An isopropoxide moiety was identified by MALDI-TOF mass spectrometry as the chain end group, which supports a coordination insertion mechanism. Good molecular weight control was observed but a degree of transesterification was identified *via* MALDI-TOF mass spectrometry. An isotactic bias (P_r = 0.35 – 0.5) was generally observed for these complexes which was enhanced for complexes bearing *ortho*-methyl phenoxy substituents (P_r = 0.35 – 0.42). Hf(**6**,**7**)(O^iPr)$_2$ resulted in a small increase in stereoselectivity over Zr(**6**,**7**)(O^iPr)$_2$ complexes. The solvent free ROP was conducted at 130 °C at a 300:1 [*rac*-lactide]:[initiator] ratio. Zr(**6**,**7**,**10**)(O^iPr)$_2$ and Hf(**6**,**7**,**10**)(O^iPr)$_2$ achieved high conversion after 0.5 h, where as the *ortho*-^{t}Bu phenoxy containing complexes {Zr(**8**,**9**)(O^iPr)$_2$, Hf(**8**,**9**)(O^iPr)$_2$} required 3 h to obtain appreciable conversion. Lower molecular weights were obtained for the solvent free ROP of *rac*-lactide experiments where the increased thermal conditions activate both isopropoxides for the initiation of PLA chain growth. Controlled molecular weight growth was demonstrated with increasing conversion with minimal increase in PDI, this supports a chain-end control mechanism. NMR spectroscopy scale kinetic investigations resulted in *pseudo* first order apparent rate constants for Zr(**6**)(O^iPr)$_2$ and Hf(**6**)(O^iPr)$_2$ from which the zirconium complex was

demonstrated as approximately three times more active than its direct hafnium analogue for the ROP of *rac*-lactide.

3.7 Future Work

The piperazine hafnium solid-state structures $\{Hf_2(\mathbf{1},\mathbf{3})(O^iPr)_6\}$ show promise and further-work could be conducted into isolating these as pure materials, although extensive efforts were made. Variation of the homopiperazine salan ligands could be conducted particularly in the area of halide phenoxy substituents (Cl, Br) to ascertain their effect upon complexes and consequently the ROP of *rac*-lactide. Further-work into unsymmetrical homo/piperazine salan ligand sets could be attempted where substituents on each phenol are different. The effect of conformational hindered (6/7 membered ring backbones) diamine bridging groups upon salan complexes was conducted and future work could include 8 membered bridging ring groups (Figure 3.14).

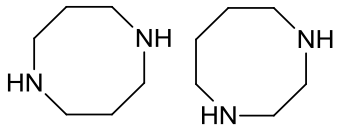

Figure 3.14: 8 membered ring diamines.

3.8 References

1. S. Gendler, S. Segal, I. Goldberg, Z. Goldschmidt and M. Kol, *Inorg. Chem.*, 2006, **45**, 4783-4790.
2. A. J. Chmura, M. G. Davidson, M. D. Jones, M. D. Lunn, M. F. Mahon, A. F. Johnson, P. Khunkamchoo, S. L. Roberts and S. S. F. Wong, *Macromolecules*, 2006, **39**, 7250-7257.
3. S. H. Kim, J. Lee, D. J. Kim, J. H. Moon, S. Yoon, H. J. Oh, Y. Do, Y. S. Ko, J.-H. Yim and Y. Kim, *J. Organomet. Chem.*, 2009, **694**, 3409-3417.
4. M. D. Jones, M. G. Davidson and G. Kociok-Kohn, *Polyhedron*, 2010, **29**, 697-700.
5. C. K. A. Gregson, I. J. Blackmore, V. C. Gibson, N. J. Long, E. L. Marshall and A. J. P. White, *Dalton Trans.*, 2006, 3134-3140.
6. T. K. Saha, V. Ramkumar and D. Chakraborty, *Inorg. Chem.*, 2011, **50**, 2720-2722.
7. A. J. Chmura, D. M. Cousins, M. G. Davidson, M. D. Jones, M. D. Lunn and M. F. Mahon, *Dalton Trans.*, 2008, 1437-1443.

8. A. J. Chmura, M. G. Davidson, C. J. Frankis, M. D. Jones and M. D. Lunn, *Chem. Commun.*, 2008, 1293-1295.
9. S. L. Hancock, M. F. Mahon and M. D. Jones, *Dalton Trans.*, 2011, **40**, 2033-2037.
10. P. D. Knight, P. N. O'Shaughnessy, I. J. Munslow, B. S. Kimberley and P. Scott, *J. Organomet. Chem.*, 2003, **683**, 103-113.
11. E. L. Whitelaw, M. D. Jones, M. F. Mahon and G. Kociok-Kohn, *Dalton Trans.*, 2009, 9020-9025.
12. F. Corazza, E. Solari, C. Floriani, A. Chiesi-Villa and C. Guastini, *J. Chem. Soc., Dalton Trans.*, 1990, 1335-1344.
13. M. Kettunen, C. Vedder, F. Schaper, M. Leskelä, I. Mutikainen and H.-H. Brintzinger, *Organometallics*, 2004, **23**, 3800-3807.
14. R. Cariou, V. C. Gibson, A. K. Tomov and A. J. P. White, *J. Organomet. Chem.*, 2009, **694**, 703-716.
15. M. Hu, M. Wang, H. Zhu, L. Zhang, H. Zhang and L. Sun, *Dalton Trans.*, 2010, **39**, 4440-4446.
16. A. L. Zelikoff, J. Kopilov, I. Goldberg, G. W. Coates and M. Kol, *Chem. Commun.*, 2009, 6804-6806.
17. M. Wang, H. Zhu, D. Huang, K. Jin, C. Chen and L. Sun, *J. Organomet. Chem.*, 2004, **689**, 1212-1217.
18. B. M. Chamberlain, M. Cheng, D. R. Moore, T. M. Ovitt, E. B. Lobkovsky and G. W. Coates, *J. Am. Chem. Soc.*, 2001, **123**, 3229-3238.
19. A. Sauer, J.-C. Buffet, T. P. Spaniol, H. Nagae, K. Mashima and J. Okuda, *Inorg. Chem.*, 2012, **51**, 5764-5770.
20. E. L. Whitelaw, M. D. Jones and M. F. Mahon, *Inorg. Chem.*, 2010, **49**, 7176-7181.

Chapter 4

4. Aluminium (III) Homopiperazine Salan Complexes and Their Application for the ROP of Cyclic Esters.

4. Aluminium (III) Homopiperazine Salan Complexes and Their Application for the ROP of Cyclic Esters.

4.1 Introduction

Aluminium tetradentate -(ONNO)- bis(phenoxy) complexes have been previously investigated as ROP initiators for lactide.[1] Specifically aluminium diimine bis(phenoxy) (salen) complexes have seen much use for the ROP of lactide throughout the past few decades,[2-6] many of which produce isotactic PLA or isotactic biased PLA. These stereoselective initiators typically required a time scale of days for appreciable conversion to be obtained. Whereas good control over molecular weight and stereoselectivity was observed in solution, a strong degree of isotactic stereoselectivity was retained in solvent free conditions for aluminium complexes supported by bis(phenol) ligands containing 1,2-diaminocyclohexane (1,2-DACH) and ($NCH_2CMe_2CH_2N$) linkers.[5]

Aluminium diamine bis(phenoxy) (salan) complexes have also been previously investigated as initiators for the ROP of lactide (Figure 4.01).[7, 8] Many aluminium salan complexes contain alkyl initiating groups and hence a co-initiator (typically an alcohol) is often introduced to the polymerisation. The aluminium salan complexes (Figure 4.01) gave varying stereoselectivities ranging between a strong isotactic bias to heterotactic (P_r = 0.21 – 0.96).[7] An isotactic bias was reported when R_2 = H and a heterotactic bias was reported when R_2 = Me, ^{t}Bu, or Cl, where the Cl subsistent resulted in the strongest heterotactic selectivity.

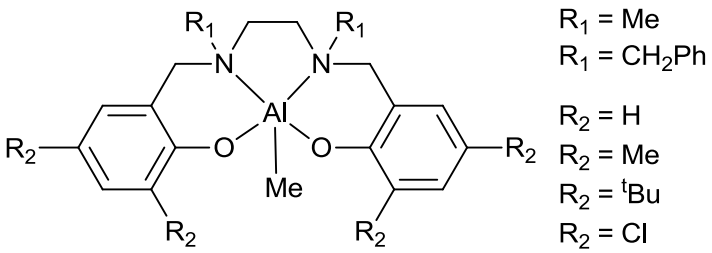

Figure 4.01: Aluminium diamine bis(phenoxy) (aluminium salan) complexes investigated for the ROP of lactide.[7]

Piperazine salan group 4 complexes for the ROP of *rac*-lactide have been previously reported and are discussed in chapters 3 and 4 of this thesis.[9, 10] Furthermore aluminium piperazine salan complexes were initially synthesised by Fulton *et al*.[11] who reported the synthesis of bimetallic and monometallic structures. The same piperazine ligand was utilised throughout the study and the monodentate aluminium substituents were varied.[11] The complexes were trialled as initiators for the ROP of lactide under solution conditions and were reported as inactive, although these complexes were reported as active initiators for the ROP of ε-caprolactone (Figure 4.02).[11] Yao *et al*.[12] reported similar bimetallic aluminium salan complexes and their high activity towards the ROP of ε-caprolactone at high monomer to initiator ratios. Molecular weights were shown to be dependent upon benzyl alcohol co-initiator concentration, whilst high molecular weights were obtained a range of PDI (distribution of molecular weights) values were also reported (PDI = 1.19 - 2.01). The ROP of ε-caprolactone was also investigated using monometallic aluminium piperazine salan derivatives developed by Yao *et al*.[13] While active initiators for the ROP of ε-caprolactone the monometallic aluminium initiators were significantly less active than their bimetallic counterparts. The monometallic aluminium piperazine salan initiators gave greater control over the ROP of ε-caprolactone resulting in lower PDI values (PDI = 1.17 - 1.52).

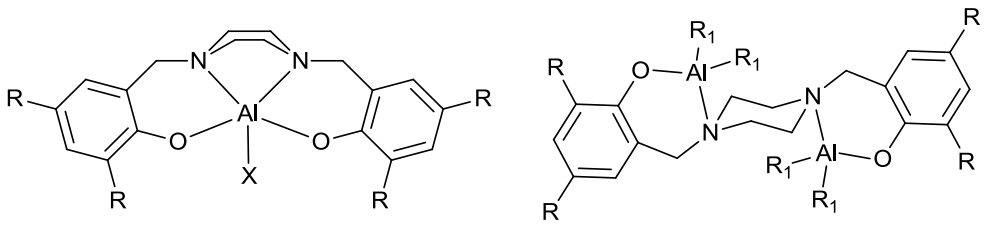

Figure 4.02: Aluminium piperazine salan complexes investigated for the ROP of cyclic esters.[11-13]

Prior investigations of piperazine salan and homopiperazine salan ligands complexed to group 4 metals (Chapter 2, and 3) revealed the two ligand sets can coordinate in differing manners.[9, 10] Herein the benzyloxy derivatives of aluminium methyl homopiperazine salan complexes were synthesised and their ROP activity for lactide, ε-caprolactone and δ-valerolactone is reported.

4.2 Synthesis of Aluminium Homopiperazine Salan Complexes

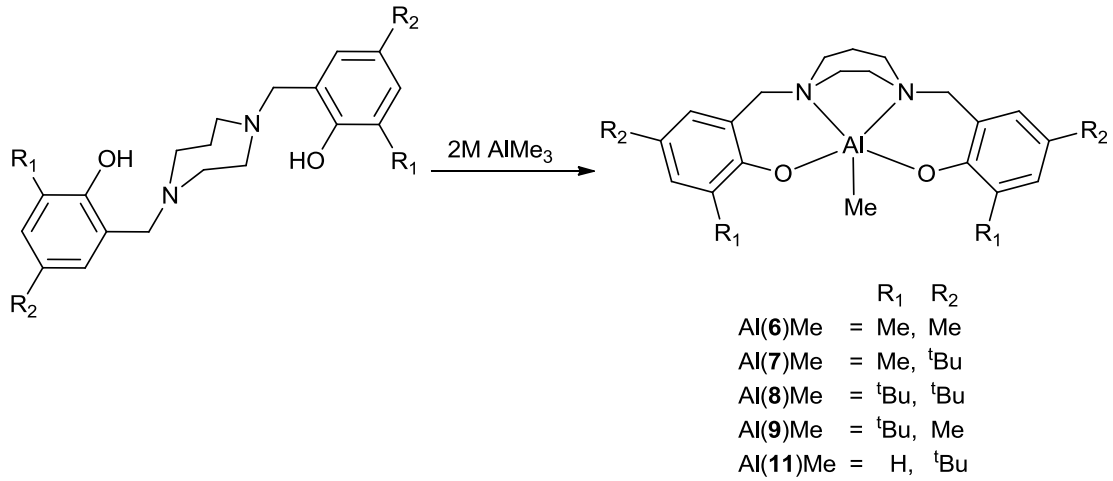

Figure 4.03: Reaction scheme for the synthesis of homopiperazine salan methyl aluminium complexes.

The homopiperazine ligands synthesised and discussed in chapter 2 (Figure 2.02) were complexed to $AlMe_3$, Conrad Langridge is acknowledged for his contribution to the development of these complexes.[14] The addition of aluminium was conducted at elevated temperature (50 °C) until the initial effervescence had slowed, at which point the temperature was increased (80 °C) to ensure complete reaction (Figure 4.03). The thermally energetic conditions were required to kinetically facilitate the homopiperazine ring formation of the boat type configuration. The aluminium complexes were recrystallised from toluene and hexane solvent mixtures, using thermal and diffusion based recrystallisation methods. Crystals suitable for X-ray diffraction were obtained for Al(**7**,**8**,**11**)Me. Attempts to synthesise aluminium complexes using **10**H_2 were unsuccessful presumably an artefact of the increased steric demands of the *ortho*-phenoxy ring amyl substituents. The complexes Al(**6**-**9**,**11**)Me were characterised by $^{1}H/^{13}C\{^{1}H\}$ NMR spectroscopy and CHN analysis, in all cases the complexes were consistent with the solid-sate structures.

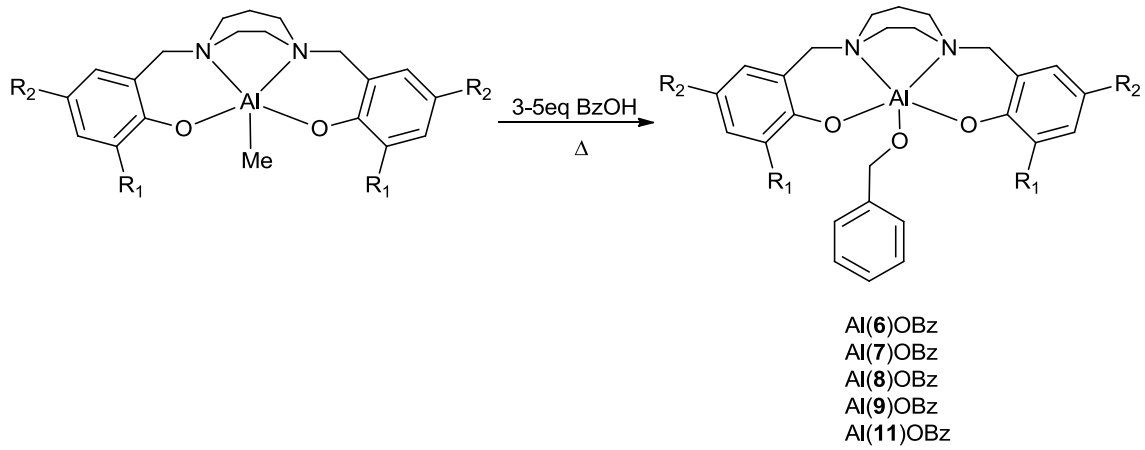

Al(**6**)OBz
Al(**7**)OBz
Al(**8**)OBz
Al(**9**)OBz
Al(**11**)OBz

Figure 4.04: Reaction scheme detailing the synthesis of homopiperazine salan benzyloxy aluminium complexes.

Aluminium methyl complexes typically require a co-initiator, normally an alkoxide, to enhance their properties as initiators for the ROP of cyclic esters. The direct incorporation of a co-initiating benzyl alcohol (BnOH) was attempted and the presumably active initiating species containing benzyloxy aluminium bound substituents were isolated. Firstly, the synthesis of a homopiperazine complex {Al(**6-9**,**11**)Me} was conducted and the complex rapidly purified by addition of hexane to a toluene solution. An excess of benzyl alcohol (3-5 equivalents) was required to fully substitute the aluminium bound methyl groups (Figure 4.04). Despite the use of excess benzyl alcohol at elevated temperature (70-80 °C) prolonged reaction times were required to ensure complete conversion of Al(**6-9**,**11**)Me to Al(**6-9**,**11**)OBn (Figure 4.04). High conversion was required as purification of Al(**6-9**,**11**)OBn in the presence of Al(**6-9**,**11**)Me impurities was difficult. The complexes were purified by recrystallisation from toluene and hexane mixes but no crystals suitable for X-ray diffraction were obtained. Hexane washes and toluene/hexane crystallisation was conducted to ensure the complete removal of benzyl alcohol. The complexes were isolated and characterised by $^{1}H/^{13}C\{^{1}H\}$ NMR spectroscopy and CHN analysis.

4.3 Solid-state characterisation by X-ray crystallography

Aluminium homopiperazine salan complexes Al(**7**)Me, Al(**8**)Me, and Al(**11**)Me were characterised by X-ray crystallography; Al(**8**)Me crystals were initially obtained by Conrad Langridge as part of the Jones group.[14] Similar aluminium piperazine based salan structures determined by X-ray crystallography were reported by Fulton *et al.*[11] and Yao *et al.*[13] The crystallographic determined structures are specifically compared with the literature structures; Al(**3**)Me ($R_1 = R_2 = {}^tBu$)[11] and Al(**4**)Et ($R_1 = {}^tBu$, $R_2 = Me$).[13]

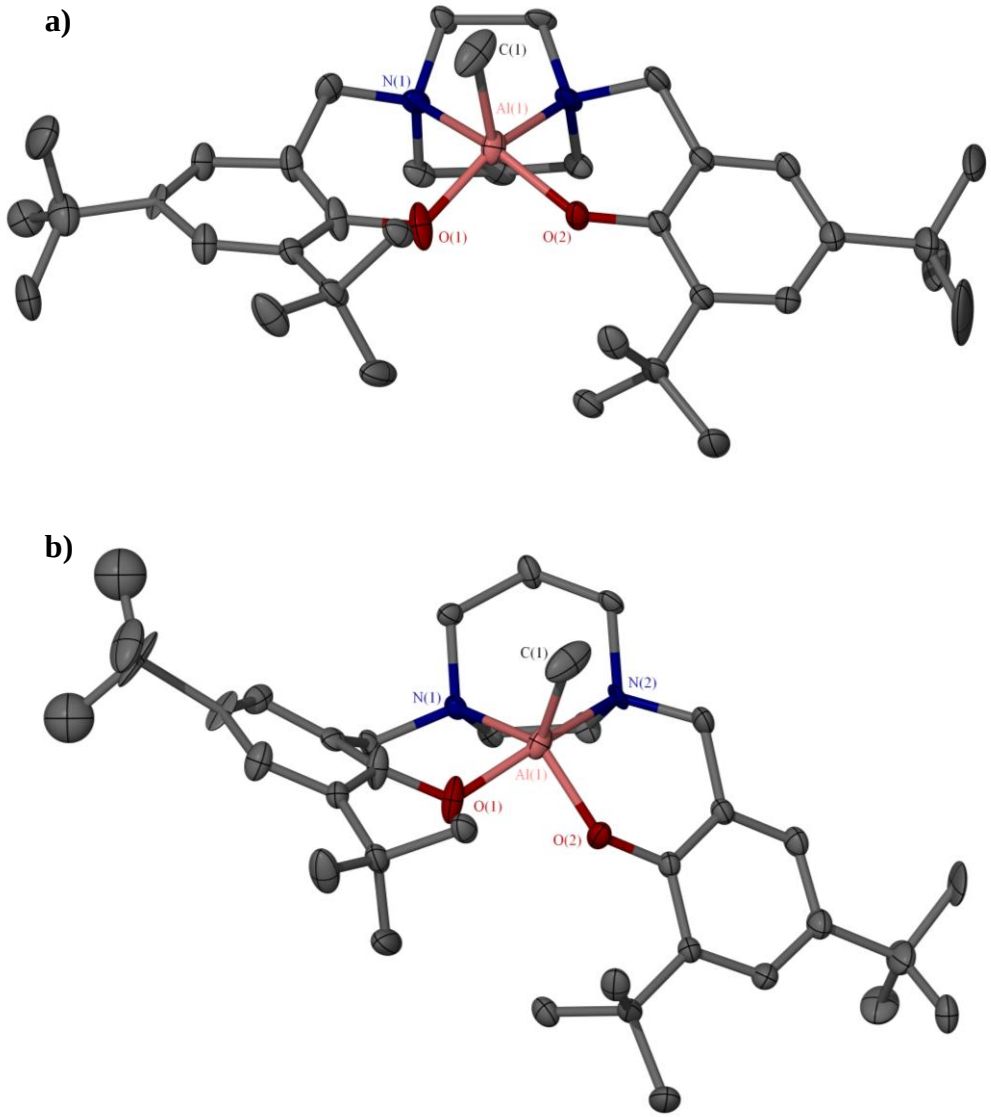

Figure 4.05: Solid-state structures for a single disordered crystal where two structures were obtained; **a**) Al(**8**)Me *cis*-(CH_2CH_2)-, **b**) Al(**8**)Me *cis*-($CH_2CH_2CH_2$)-. Ellipsoids are shown at the 30 % probability level, hydrogen atoms have been removed for clarity.[14]

The crystal structure for Al(**8**)Me was solved with a significant degree of disorder about the homopiperazine ring. The homopiperazine ring disorder could be extrapolated to generate two isomers which were present in the unit cell in a 50:50 ratio. One structure has the aluminium bound methyl orientated *cis* to the -(CH_2CH_2)- moiety of the homopiperazine ring (Figure 4.05a), the alternative structure has the aluminium bound methyl *cis* to the -($CH_2CH_2CH_2$)- homopiperazine ring moiety (Figure 4.05b). Selected bond lengths (Å) and angles (°) for both Al(**8**)Me structures alongside other aluminium homopiperazine salan structures are given in table 4.01. Both Al(**8**)Me isomers are five coordinate, the Al(**8**)Me *cis*-(CH_2CH_2)- structure adopts a *pseudo* square pyramidal structure with a τ value of 0.08[15] (square pyramidal $\tau = 0$, trigonal bipyramidal $\tau = 1$).[15] The Al(**8**)Me structure where the methyl was *cis* to the -($CH_2CH_2CH_2$)- homopiperazine moiety is indeterminate between a square pyramidal geometry and a trigonal bipyramidal structure with a τ value of 0.50.

	Al(**7**)Me	Al(**8**)Me[a]	Al(**8**)Me[b]	Al(**11**)Me
Al1-C1	1.980(3)	1.980(3)	1.960(5)	1.962(7)
Al1-O1	1.7873(19)	1.7873(19)	1.798(3)	1.784(4)
Al1-O2	1.7975(18)	1.7975(18)	1.768(2)	1.796(5)
Al1-N1	2.132(2)	2.188(7)	2.077(5)	2.108(5)
Al1-N2	2.108(2)	2.07(2)	2.171(18)	2.103(5)
O1-Al1-O1	91.79(9)	91.79(9)	89.90(13)	90.1(2)
N1-Al1-N2	73.74(8)	70.5(8)	76.1(7)	74.56(19)
O1-Al1-C1	114.29(13)	114.29(13)	104.6(2)	111.6(3)
O2-Al1-C1	106.86(12)	106.86(12)	116.85(16)	107.6(3)
N1-Al1-C1	100.09(12)	96.7(3)	117.6(2)	101.8(3)
N2-Al1-C1	103.63(12)	105.3(9)	99.2(7)	103.3(3)

Table 4.01: Selected bond lengths (Å) and angles (°) for piperazine salan aluminium complexes, as determined by X-ray crystallography. [a] methyl orientated *cis* to -$(CH_2)_2$- homopiperazine ring group, [b] methyl orientated *cis* to -$(CH_2)_3$- homopiperazine ring group.

Al(**8**)Me the Al1-C1 bonds (1.960 – 1.980 Å) are of a similar distance to the analogous bonds lengths reported for Al(**3**)Me {1.974(3) Å}[11] and Al(**4**)Et {2.004(4) Å}.[13] A significant difference in bond length can be observed between the two aluminium phenoxy bonds (Al1-O1, Al1-O2} of the Al(**8**)Me structures, additionally a distinct difference was observed between the aluminium amine bonds lengths (Al1-N1, Al1-N2). Similarly a significant difference between analogous bond lengths was reported for the literature structures Al(**3**)Me[11] and Al(**4**)Et.[13] This inherent asymmetry is supported through the bond angles between C1-Al1-O1/C1-Al1-O2 and C1-Al1-N1/C1-Al1-N2 (Table 4.01).

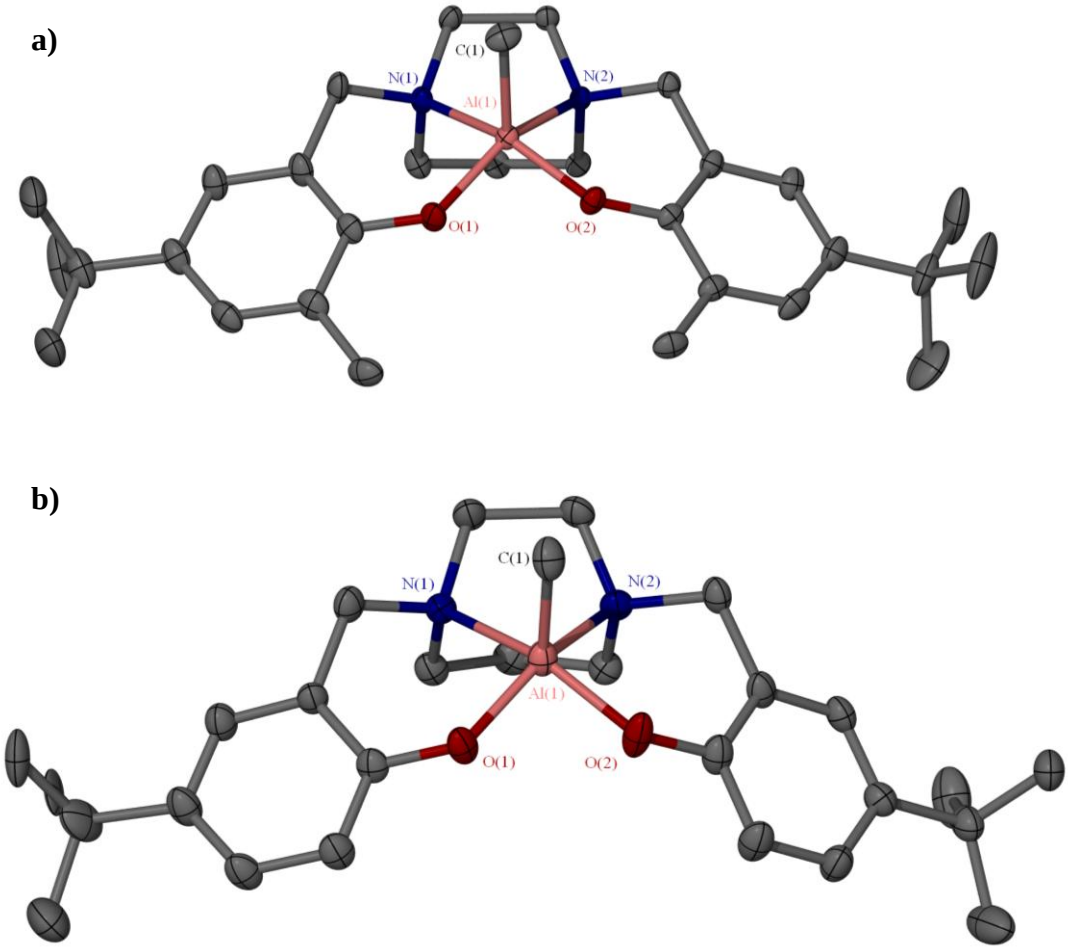

Figure 4.06: Solid-state structures **a**) Al(**7**)Me, and **b**) Al(**11**)Me Ellipsoids are shown at the 30 % probability level, hydrogen atoms have been removed for clarity.

The X-ray crystallographically determined structures for Al(**7**)Me and Al(**11**)Me are depicted in figure 4.06, selected bond lengths and angles are given in table 4.01. Both structures adopted the geometry where the aluminium bound methyl was orientated *cis* to the -(CH_2CH_2)- homopiperazine moiety. The complexes are five coordinate and adopt a distorted square pyramidal geometry {Al(**7**)Me; $\tau = 0.18$, Al(**11**)Me; $\tau = 0.09$}. The Al(**11**)Me structure was less distorted from the idealistic square pyramidal structure, presumably an artefact of the less sterically bulky *ortho*-phenoxy hydrogen substituents. The aluminium phenoxy bonds (Al1-O1, Al1-O2) and aluminium amine bonds (Al1-N1, Al1-N2) were significantly different for Al(**7**)Me, contrastingly the analogous bonds of Al(**11**)Me are statistically the same length. Both structures displayed significant variation between the C1-Al1-O1/C1-Al1-O2 and C1-Al1-N1/C1-Al1-N2 angles.

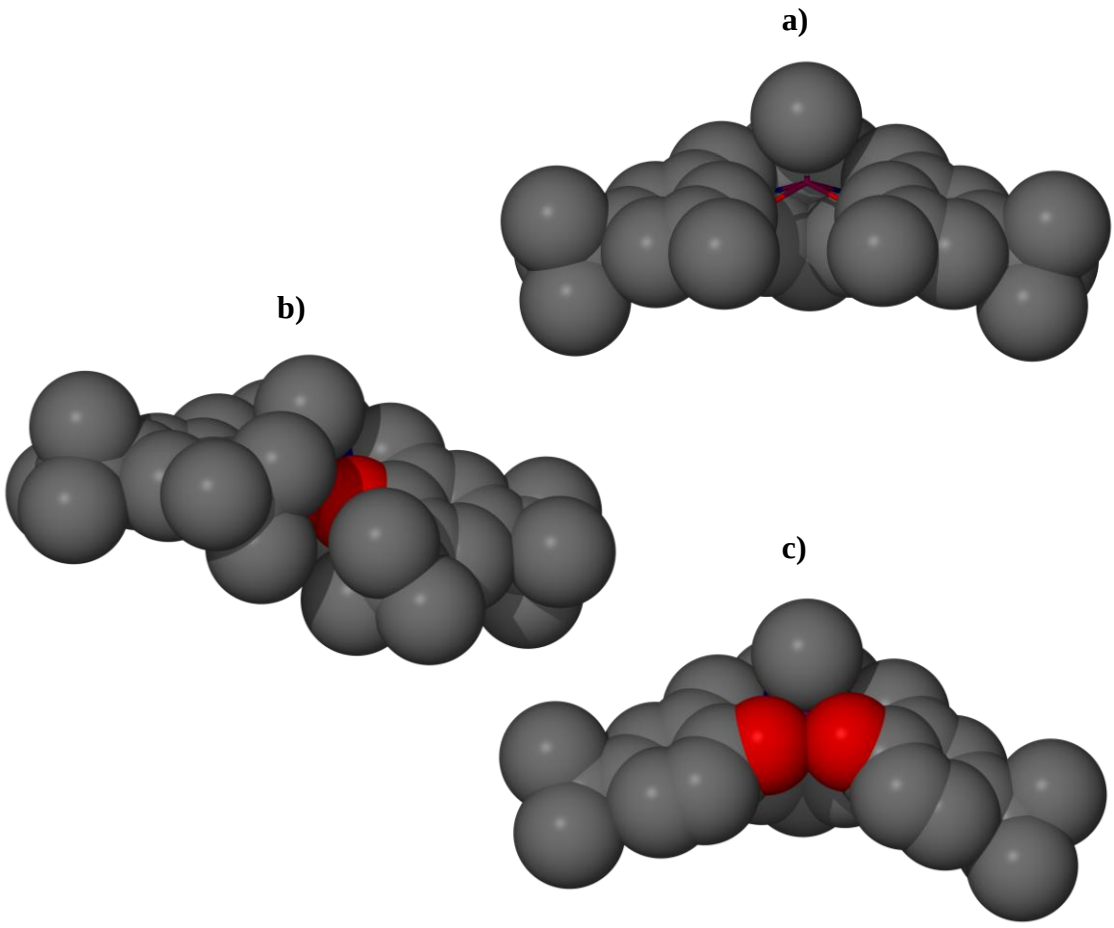

Figure 4.07: Solid-state space-filling structures showing van der Waals radii, **a**) Al(**7**)Me **b**) Al(**8**)Me (*cis* -(CH_2CH_2)-) **c**) Al(**11**)Me.

The two phenyl rings of Al(**7,11**)Me structures are both orientated away from the aluminium bound methyl moieties to a similar degree (Figure 4.07a,c). Whilst the Al(**8**)Me complex demonstrates a puckered orientation of the phenyl rings. This configuration is presumably a consequence of the sterically bulky *ortho*-^{t}Bu substituents, the puckered and steric nature is demonstrated by space filling diagrams based on van der Waals radii in figure 4.07. The aluminium metal centre is also appreciably contained by the coordinated substituents.

4.4 Computational Investigation

To investigate the two isomers for Al(**8**)Me, quantum mechanical calculations were performed using the ORCA electronic structure program.[16] The crystallographically determined structures for Al(**8**)Me *cis*-(CH_2CH_2)-, and Al(**8**)Me *cis*-($CH_2CH_2CH_2$)- were initially optimised *via* TightSCF conversion calculations. Initial calculations utilised the BP86[17, 18] functional with RI[19, 20] approximation using the def2-svp[21] basis set. The structures were further refined iteratively by the B3LYP[22, 23] functional with the RIJCOSX[24] algorithm; firstly using the def2-svp basis set and finally the def2-TZVPP[25] basis set. Empirical van der Waals corrections (VDW)[26] were applied alongside COSMO[27] solvent effects at infinite dielectric constant to more closely emulate solvated conditions. A 1.3 kcal mol^{-1} energy difference between the structurally optimised final single point energies was observed, at this degree of computational accuracy this energy disparity is not considered significant. The Al(**8**)Me (*cis* -(CH_2CH_2)-) complex was the favourable conformation although it is possible to isolate both structures in a crystal environment, which is consistent with a small energy disparity.

4.5 Characterisation by NMR Spectroscopy

The aluminium homopiperazine salan complexes Al(**6-9,11**)Me, and Al(**6-9,11**)OBn were characterised by ^{1}H and $^{13}C\{^{1}H\}$ NMR spectroscopy. Room temperature spectroscopy resulted in broad resonances in the CH_2 region of the Al(**6-9,11**)Me ^{1}H NMR spectra. A ^{1}H NMR spectrum for Al(**8**)Me is given in figure 4.08. The majority of CH_2 related resonances are shown in the truncated spectra of Al(**8**)Me where a distinctive sharpening of the resonances is observed

upon cooling of the complex in solution (d_8-toluene). At high temperature it is not possible to distinguish between axial and equatorial protons for the CH_2 ring groups, due to the highly fluxional nature on the NMR timescale. Axial and equatorial CH_2 proton resonances become independent signals upon cooling (Figure 4.08), an artefact of conformation locking of the complexes under less thermally energetic conditions. Al(**8**)Me was characterised by X-ray crystallography as two geometric configurations, where the aluminium bound methyl was either *cis* to the $-CH_2CH_2-$ or $-CH_2CH_2CH_2-$ homopiperazine ring groups (Figure 4.05). The isomers isolated are dependent upon the crystallisation conditions. The presence of two conformations in the solution-state was an isolated case for the Al(**8**)Me crystals. Further synthetic attempts of Al(**8**)Me synthesis resulted in the formation of a single isomer, best represented by a single Al-Me proton resonance. The two isomers do not appear to interconvert upon heating in solution. A single isomer was characterised by NMR spectroscopy for complexes Al(**7-9**)Me, however Al(**6**)Me was isolated as both isomers due to two Al-Me resonances being observed.

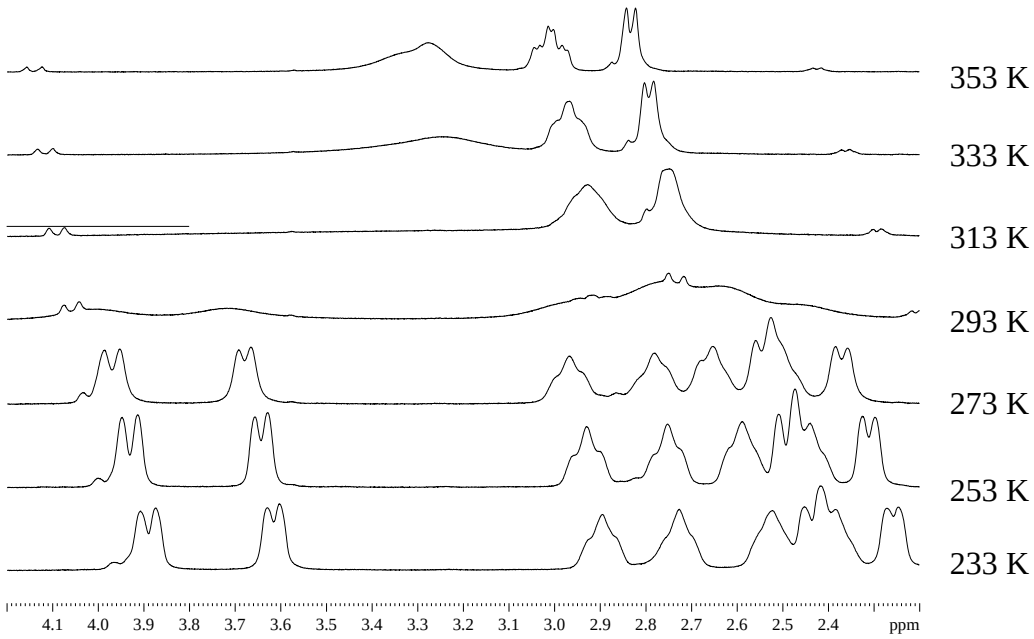

Figure 4.08: Variable temperature ^{1}H NMR spectra showing the methylene region for Al(**8**)Me 233K (bottom) ranging 20 K intervals to 353 K.

Benzyl alcohol derivatives Al(**6-9,11**)OBn of Al(**6-9,11**)Me were characterised by NMR spectroscopic methods. The complete disappearance of the aluminium bound methyl proton resonances required prolonged elevated temperature conditions and excess benzyl alcohol. Ambient conditions or stoichiometric

quantities of BnOH yielded mixtures of Al(**6-9,11**)OBn and Al(**6-9,11**)Me, unusual considering the high reactivity of aluminium methyl groups and the entropically favourable evolution of methane. A distinctive resonance at ~5 ppm was attributed to the CH_2 protons of an aluminium bound benzyloxy ligand. Stringent purification was required to ensure uncoordinated BnOH was removed from the compound. The complex Al(**8**)OBn (Figure 4.09) was significantly less fluxional at room temperature than the Al(**8**)Me complex. The aromatic region becomes more defined at reduced temperatures, overlap with solvent peaks complicated the analysis of this region.

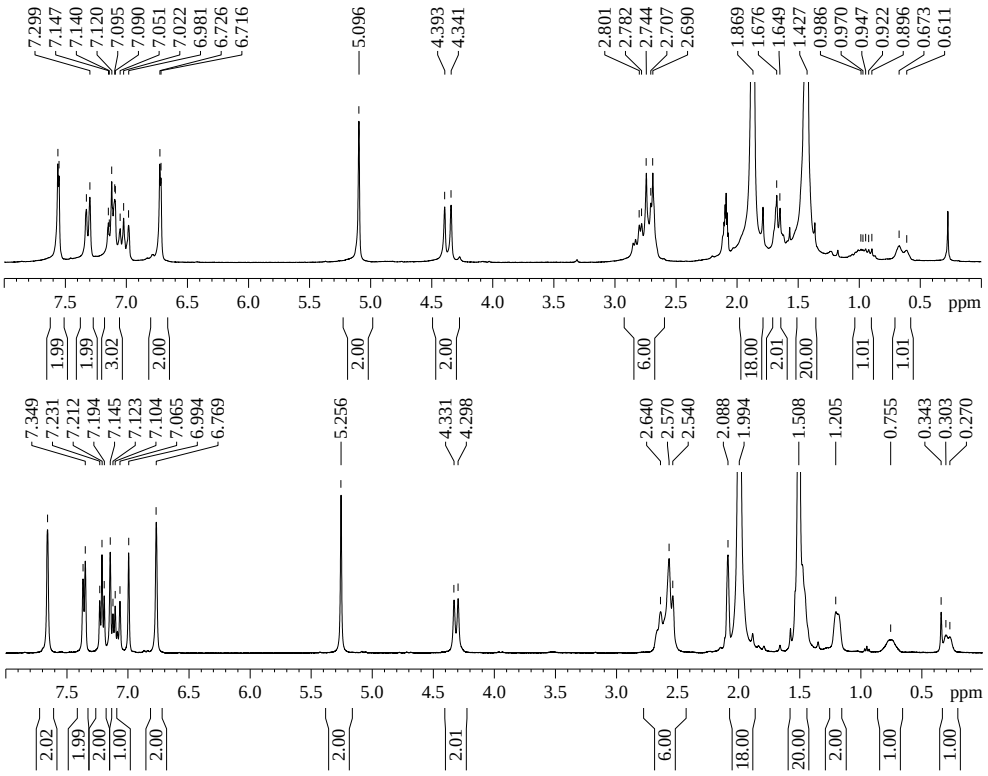

Figure 4.09: ^{1}H NMR spectra for Al(**8**)OBn, Top 298 K, Bottom 233 K.

4.6 Investigation of the ROP of Cyclic-Esters

Prior aluminium piperazine salan complexes have been investigated for solution ROP of *rac*-lactide and were shown to be unsuccessful initiators.[11] Further solution ROP reactions of ε-caprolactone have been conducted and aluminium piperazine salan complexes were proven to be active initiators.[11-13] The ROP of the cyclic esters; *rac*-lactide, ε-caprolactone, and δ-valerolactone (Figure 4.10) by

aluminium homopiperazine salan initiators Al(**6**-**9**,**11**)OBn is herein reported. A focus upon the environmentally favourable solvent free ROP conditions was conducted to complement the prior literature solution ROP reported for similar structures.[11-13] The initiators with coordinated benzyloxy derivatives {Al(**6**-**9**,**11**)OBn} were utilised in preference to the aluminium methyl analogues {Al(**6**-**9**,**11**)Me} to remove *in-situ* co-initiator complications. The synthesis of the benzyloxy aluminium complexes Al(**6**-**9**,**11**)OBn from Al(**6**-**9**,**11**)Me was challenging, hence the assumption of rapid coordination and generation of the active alkoxide species *in-situ* was not possible. Additionally these initiators were trialled for co-polymerisation reactions with the aforementioned cyclic-ester monomers.

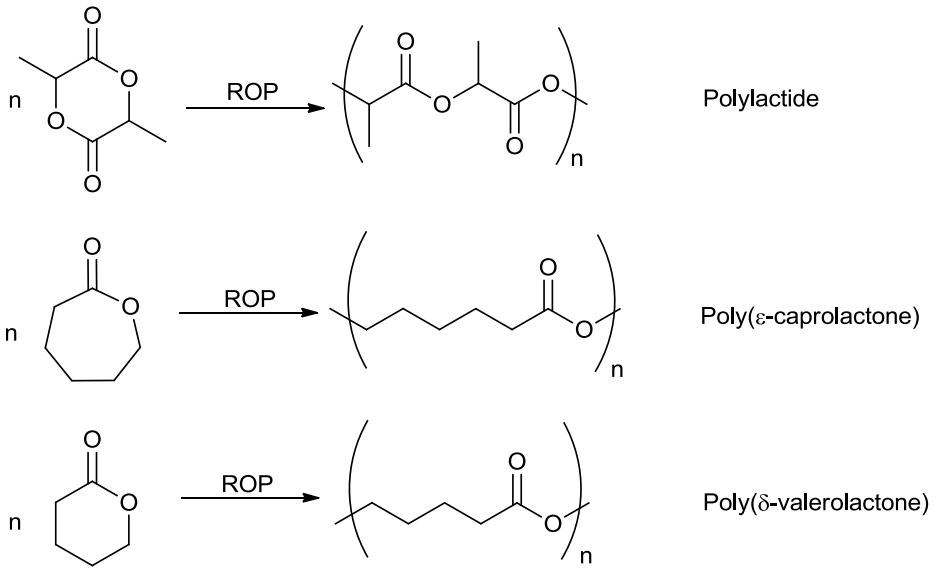

Figure 4.10: Synthetic schemes depicting the ROP of lactide, ε-caprolactone, and δ-valerolactone including their resulting polymers.

4.6.1 Investigation of the ROP of *rac*-lactide

The aluminium alkyl initiators Al(**6**-**9**,**11**)Me were initially trialled in solution (toluene) at 80 °C, with benzyl alcohol as a co-initiator, for the ROP of *rac*-lactide but no signs of the formation of polymer were observed. The low activity in solvent at 80 °C was thought to be linked to the difficultly of substituting a benzyl alcohol group into the aluminium coordination sphere, thus the formation the *in-situ* initiator is restricted. This observation was extrapolated as an indication of the difficult coordination of a *rac*-lactide monomer to the aluminium centre. The benzyloxy

aluminium complexes Al(**6-9**,**11**)OBn were investigated as initiators for the ROP of *rac*-lactide in solvent free conditions at 130 °C. Respectable conversions were obtained under these conditions after 2 h, although Al(**11**)OBn resulted in a reduced conversion (Table 4.02). Molecular weights (M_n) were typically higher than expected for the formation of one PLA chain per metal centre; this is supposedly a product of low rate of initiation relative to the rate of propagation. The exception is Al(**11**)OBn which resulted in lower molecular weight PLA than expected, a consequence of reduced steric demands about the metal centre. Only moderate control over the PLA molecular weights (M_n) was observed with PDI values ranging between 1.08 – 1.42. The resulting PLA was slightly heterotactic (P_r = 0.53 – 0.57) with a stronger bias observed for initiators with *ortho*-^{t}Bu substituents (P_r = 0.57).

	Time (hours)	**Conv. (%)[a]**	M_n [b] *(theo)*	M_n [c]	**PDI[c]**	P_r [d]
Al(**6**)OBn	2	87	37750	42100	1.42	0.54
Al(**7**)OBn	2	81	35150	56400	1.40	0.55
Al(**8**)OBn	2	87	37750	54400	1.31	0.57
Al(**9**)OBn	2	88	38150	58200	1.40	0.57
Al(**11**)OBn	2	56	24300	16800	1.08	0.53

Table 4.02: Solvent free ROP of *rac*-lactide for Al(**6-9**,**11**)OBn at 130 °C in a 300:1 [*rac*-lactide]:[initiator] ratio. [a] Conversion ascertained by ^{1}H NMR spectroscopy. [b] Theoretical molecular weight calculated from conversion (Conv. × 300 × 144.13 + 108.14) (rounded to the nearest 50), [c] Molecular weight and PDI determined by GPC (THF) using polystyrene standards without applying a correction factor. [d] P_r as calculated from ^{1}H NMR homonuclear decoupled spectroscopy in $CDCl_3$.

4.6.2 Investigation of the ROP of ε-caprolactone

The ROP of ε-caprolactone was conducted in solvent free conditions at 130 °C, in a 300:1 [ε-caprolactone]:[initiator] ratio using the benzyloxy aluminium initiators {Al(**6-9**,**11**)OBn}. High conversions were obtained after 30 mins, with the exception of Al(**9**)OBn (Table 4.03). Conversion was calculated from the ^{1}H NMR spectra methylene proton resonances H_a (monomer) and H_b (polymer) at 4.20 and 4.03 ppm respectively (Figure 4.11). The high relative activity when compared to *rac*-lactide is consistent with literature which reported inactivity of similar piperazine

aluminium complexes towards lactide and high activity towards ε-caprolactone.[11] The molecular weights (M_n) were consistent for high conversion polymers (Conv. > 90%), albeit higher then expected. This is indicative of a slow initiation step compared to the rate of propagation or not all of the aluminium centres initiate PCL chain growth. Al(**11**)OBn resulted in a lower molecular weight polymer, which was similarly observed for the ROP of *rac*-lactide investigation (See section 4.6.1). Similarly moderate molecular chain length control was observed with PDI values ranging from 1.15 – 1.63.

	Time (hours)	**Conv. (%)[a]**	M_n *(theo)*[b]	M_n[c]	**PDI[c]**
Al(**6**)OBn	0.5	94	32300	54100	1.42
Al(**7**)OBn	0.5	94	32300	71900	1.63
Al(**8**)OBn	0.5	97	33300	73100	1.54
Al(**9**)OBn	0.5	30	10400	11400	1.15
Al(**11**)OBn	0.5	83	28550	25800	1.48

Table 4.03: Solvent free ROP of ε-caprolactone for Al(**6-9**,**11**)OBn at 130 °C in a 300:1 [ε-caprolactone]:[initiator] ratio. [a] Conversion ascertained by ^{1}H NMR spectroscopy. [b] Theoretical molecular weight calculated from conversion (Conv. × 300 × 114.14 + 108.14) (rounded to the nearest 50), [c] Molecular weight and PDI determined by GPC (THF) using polystyrene standards without applying a correction factor.

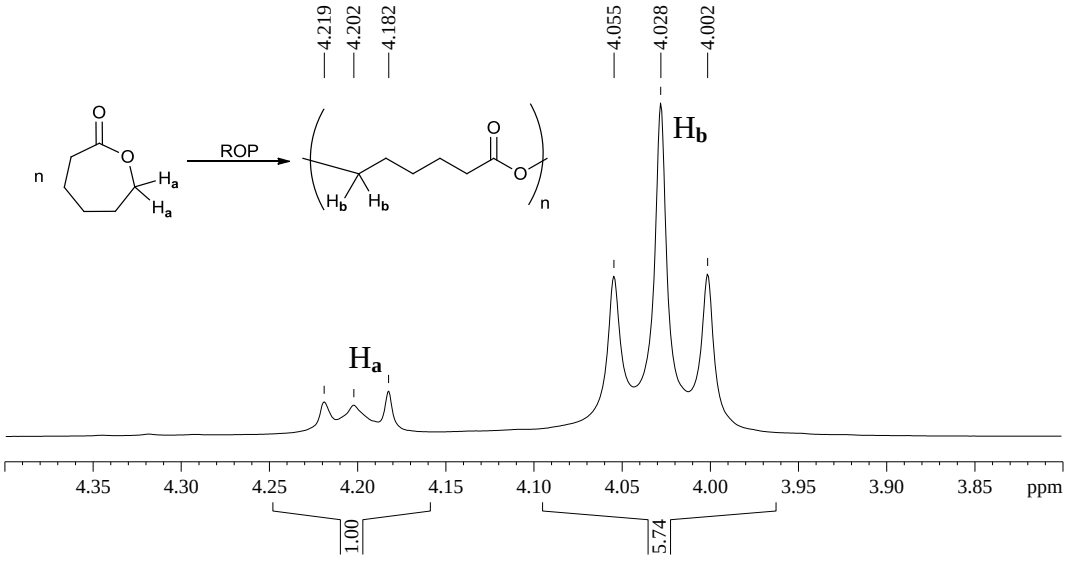

Figure 4.11: ^{1}H NMR spectra ($CDCl_3$) for the ROP conversion of ε-caprolactone to poly(ε-caprolactone) using the initiator Al(**11**)OBn.

4.6.3 Investigation of the ROP of δ-valerolactone

Homopiperazine salan aluminium benzyloxy initiators were utilised for the ROP of δ-valerolactone in solvent free conditions at 130 °C, at a 300:1 [δ-valerolactone]:[initiator] ratio (Table 4.04). High conversion was obtained for the majority of initiators after 1 h with Al(**9**)OBn yielding lower conversion, similarly observed with caprolactone. Also Al(**11**)OBn resulted in a slightly lower conversion, an observation consistent with the ROP of *rac*-lactide and caprolactone. The conversions are calculated from the ^{1}H NMR spectra methylene proton resonances H_a (monomer) and H_b (polymer) (Figure 4.12), 4.31 and 4.05 ppm respectively. The determined molecular weights (M_n) were consistent across Al(**6**-**9**)OBn initiators, the obtained molecular weight were somewhat consistent with one polymer chain being propagated by each metal centre. Similarly previously discussed ROP investigations of Al(**11**)OBn also resulted in lower than expected molecular weights. It was speculated that the lower steric demands of Al(**11**)OBn was allowing the propagation of more than one valerolactone chain. The molecular chain length distributions were moderately high with PDI values ranging between 1.12 – 1.77.

	Time (hours)	**Conv. (%)[a]**	M_n [b] *(theo)*	M_n [c]	**PDI[c]**
Al(**6**)OBn	1	90	27150	39600	1.50
Al(**7**)OBn	1	94	28350	33000	1.54
Al(**8**)OBn	1	88	26550	24800	1.77
Al(**9**)OBn	1	31	9400	10100	1.12
Al(**11**)OBn	1	81	24450	16000	1.25

Table 4.04: Solvent free ROP of δ-valerolactone for Al(**6**-**9**,**11**)OBn at 130 °C in a 300:1 [δ-valerolactone]:[initiator] ratio. [a] Conversion ascertained by ^{1}H NMR spectroscopy. [b] Theoretical molecular weight calculated from conversion (Conv. × 300 × 100.12 + 108.14) (rounded to the nearest 50), [c] Molecular weight and PDI determined by GPC (THF) using polystyrene standards without applying a correction factor.

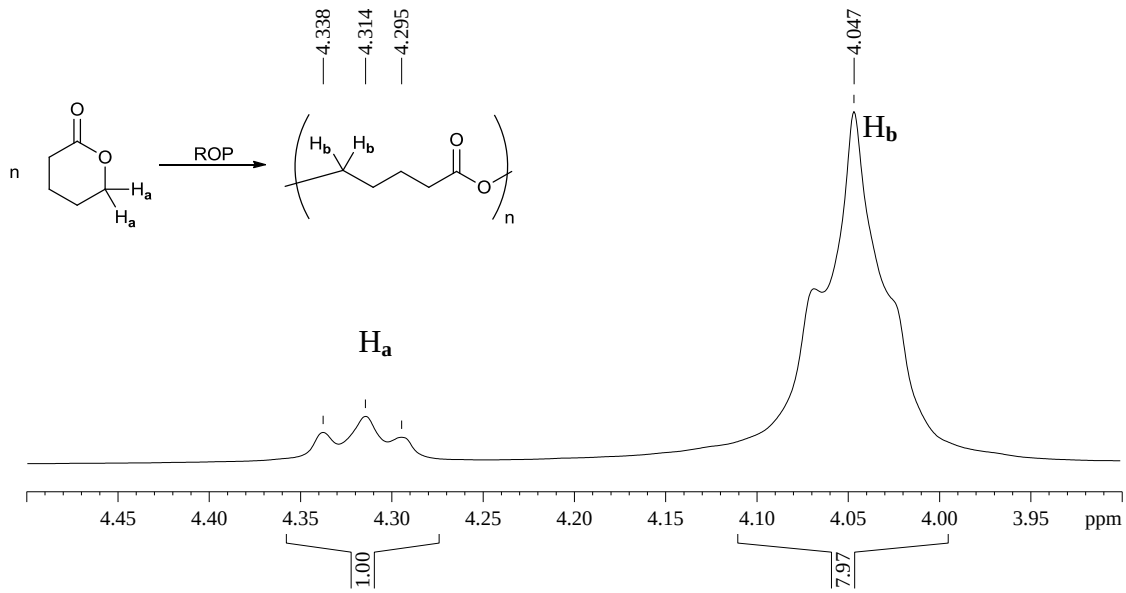

Figure 4.12: ^{1}H NMR spectra ($CDCl_3$) for the ROP conversion of δ-valerolactone to poly(δ-valerolactone) using the initiator Al(**8**)OBn.

4.6.4 Investigation of co-polymerisations of cyclic-esters

Co-polymer investigations were trialled using these aluminium benzyloxy homopiperazine salan complexes as initiators Al(**6-9**,**11**)OBn. All ROP reactions were conducted in an inert atmosphere environment at 130 °C in solvent free conditions. Direct ROP attempts of *rac*-lactide/ε-caprolactone or *rac*-lactide/δ-valerolactone mixes were not successful with no polymerisation being observed. The sequential addition of monomers to complete reactions led to high conversion of each sequential monomer given time for each monomer to polymerise. The insertion of a ε-caprolactone/δ-valerolactone monomer into an Al-PLA linkage did not occur hence the sequential polymerisations starting with *rac*-lactide were not successful. It should be noted that the presence of un-reacted monomer from the prior step has a detrimental effect upon the subsequent ROP steps.

Sequential tri-block poly-esters were synthesised using Al(**7-9**)OBn initiators, the polymer sequence followed ε-caprolactone/δ-valerolactone/*rac*-lactide. Each monomer was present in 100:1 ratio of [monomer]:[initiator] and the time allowed for each addition was 0.5 h/1 h/2 h to obtain high conversion for each subsequent step (Table 4.05). Al(**8**)OBn gave high conversion of each subsequent monomer, conversion was calculated from the ^{1}H NMR spectra ($CDCl_3$). The conversion of

rac-lactide was calculated by direct comparison of the monomer/polymer methine resonances. The poly(ε-caprolactone), and poly(δ valerolactone) resonances (4.03 ppm and 4.05 ppm respectively) used for calculation of conversion overlap, the conversion was calculated from the monomer and polymer integrals with the assumption that the total amount of methylene (H_a/H_b) protons of each monomer were in a 50:50 ratio. Al(**7**)OBn resulted in good conversion of both ε-caprolactone and δ-valerolactone but not *rac*-lactide. Al(**9**)OBn was comparatively poorly active towards caprolactone and valerolactone this is followed within the tri-block polymerisation results. The ROP of *rac*-lactide still proceeded with Al(**9**)OBn initiator with no detrimental effect observed for the presence of ε-caprolactone and δ-valerolactone monomer. The tri-block polyester molecular weights (M_n) were consistent with the expected values through comparison with homopolymer ROP data (table 4.02, 4.03, 4.04). The molecular weight values are much higher than expected for 100:1 homopolymer conversions indicative of the formation of co-polymers. The GPC traces were also unimodal demonstrating the formation of co-polymers over multiple homopolymers.

	Time (hours)	**Conv. (%)[a]**	M_n [b]	**PDI[b]**
Al(**7**)OBn	0.5/1/2	99/95/17	47800	1.76
Al(**8**)OBn	0.5/1/2	99/95/98	42400	1.66
Al(**9**)OBn	0.5/1/2	88/43/64	29500	1.63

Table 4.05: Sequential solvent free ROP of ε-caprolactone/δ-valerolactone/*rac*-lactide for Al(**7**-**9**)OBn at 130 °C in a 100:100:100:1 [ε-caprolactone]:[δ-valerolactone]:[*rac*-lactide]:[initiator] ratio. [a] Conversion ascertained by ^{1}H NMR spectroscopy. [b] Molecular weight and PDI determined by GPC (THF) using polystyrene standards without applying a correction factor.

4.7 Conclusion

Aluminium methyl homopiperazine salan complexes Al(**6**-**9**,**11**)Me have been synthesised and characterised by NMR spectroscopy, X-ray crystallography, and CHN elemental analysis. X-ray crystallography indentified *pseudo* square based pyramidal monometallic structures for Al(**7**,**8**,**11**)Me. Two configurations were

identified for Al(**8**)Me one where the aluminium bound methyl was *cis* to the -(CH_2CH_2)- homopiperazine group, and one where the aluminium bound methyl was *cis* to the -($CH_2CH_2CH_2$)- homopiperazine ring group. The majority of complexes were isolated where methyl was *cis* to the -(CH_2CH_2)- homopiperazine ring segment. Structural optimisation calculations were preformed and revealed a slight preference for the Al(**8**)Me *cis* -(CH_2CH_2)- structure, with a final point energy difference of 1.3 kCal mol^{-1}. The complexes were typically indentified in solution as a single isomer and were found to be structurally stable at higher temperatures.

Direct isolation of the commonly assumed *in-situ* aluminium benzyloxy complexes Al(**6-9**,**11**)OBn was achieved and their characterisation by NMR spectroscopy discussed. The Al(**6-9**,**11**)OBn complexes were shown to be highly active initiators for the production of homopolymers by a ROP mechanism for *rac*-lactide, ε-caprolactone, and δ-valerolactone. The ROP of the cyclic esters was conducted at 130 °C at a 300:1 [monomer]:[initiator] ratio in solvent free conditions. The ROP of *rac*-lactide achieved 56-88 % conversion after 2 h and resulted in predominantly atactic PLA. ε-Caprolactone attained 30-97 % conversion after 30 mins and δ-valerolactone attained 31-94 % conversion after 1 h. The molecular weights determined by GPC (THF) were typically higher than expected, presumably not all of the aluminium initiators were initiating a polymerisation. Investigations into co-polymer synthesis were conducted and the formation of sequential co-block polyesters was achieved, up to tri-block polyesters of poly(ε-caprolactone/ δ-valerolactone/*rac*-lactide).

4.8 Future Work

Further derivatives of homopiperazine salan ligands could be synthesised with an emphasis of varying the electronic effect of the phenol rings using halide substituents. Investigating an 8 membered diamine ring bridging group is another interesting variation upon this ligand set. Further investigations into solution polymerisations could be conducted to elucidate the ROP mechanism. Indium has proved a promising candidate for the ROP of lactide.[28-31] Indium is a promising metal for coordination to homo/piperazine salan ligands due to its relation to

aluminium. It would be interesting to compare the reactivity of indium piperazine salan complexes.

4.9 References

1. P. J. Dijkstra, H. Du and J. Feijen, *Polym. Chem.*, 2011, **2**, 520-527.
2. N. Spassky, M. Wisniewski, C. Pluta and A. Le Borgne, *Macromol. Chem. Phys.*, 1996, **197**, 2627-2637.
3. N. Nomura, R. Ishii, M. Akakura and K. Aoi, *J. Am. Chem. Soc.*, 2002, **124**, 5938-5939.
4. N. Nomura, R. Ishii, Y. Yamamoto and T. Kondo, *Chem. Eur. J.*, 2007, **13**, 4433-4451.
5. Z. Zhong, P. J. Dijkstra and J. Feijen, *Angew. Chem., Int. Ed.*, 2002, **41**, 4510-4513.
6. Z. Zhong, P. J. Dijkstra and J. Feijen, *J. Am. Chem. Soc.*, 2003, **125**, 11291-11298.
7. P. Hormnirun, E. L. Marshall, V. C. Gibson, A. J. P. White and D. J. Williams, *J. Am. Chem. Soc.*, 2004, **126**, 2688-2689.
8. H. Du, A. H. Velders, P. J. Dijkstra, J. Sun, Z. Zhong, X. Chen and J. Feijen, *Chem. Eur. J.*, 2009, **15**, 9836-9845.
9. S. L. Hancock, M. F. Mahon and M. D. Jones, *Dalton Trans.*, 2011, **40**, 2033-2037.
10. S. L. Hancock, M. F. Mahon, G. Kociok-Kohn and M. D. Jones, *Eur. J. Inorg. Chem.*, 2011, 4596-4602.
11. N. C. Johnstone, E. S. Aazam, P. B. Hitchcock and J. R. Fulton, *J. Organomet. Chem.*, 2010, **695**, 170-176.
12. W. Li, W. Wu, Y. Wang, Y. Yao, Y. Zhang and Q. Shen, *Dalton Trans.*, 2011, **40**, 11378-11381.
13. W. Li, Y. Yao, Y. Zhang and Q. Shen, *Chin. J. Chem.*, 2012, **30**, 609-615.
14. S. L. Hancock, M. D. Jones, C. J. Langridge and M. F. Mahon, *New J. Chem.*, 2012, **36**, 1891-1896.
15. M.-A. Munoz-Hernandez, T. S. Keizer, P. Wei, S. Parkin and D. A. Atwood, *Inorg. Chem.*, 2001, **40**, 6782-6787.
16. F. Neese, *ORCA, Version 2.8.0*, (2011) Universitaït Bonn.
17. A. D. Becke, *Phys. Rev. A*, 1988, **38**, 3098-3100.
18. J. P. Perdew, *Phys. Rev. B*, 1986, **33**, 8822-8824.
19. K. Eichkorn, O. Treutler, H. Ohm, M. Haser and R. Ahlrichs, *Chem. Phys. Lett.*, 1995, **240**, 283-289.
20. F. Weigend, M. Haser, H. Patzelt and R. Ahlrichs, *Chem. Phys. Lett.*, 1998, **294**, 143-152.
21. A. Schafer, H. Horn and R. Ahlrichs, *J. Chem. Phys.*, 1992, **97**, 2571-2577.
22. C. T. Lee, W. T. Yang and R. G. Parr, *Phys. Rev. B*, 1988, **37**, 785-789.
23. A. D. Becke, *J. Chem. Phys.*, 1993, **98**, 5648-5652.
24. F. Neese, F. Wennmohs, A. Hansen and U. Becker, *Chem. Phys.*, 2009, **356**, 98-109.
25. F. Weigend and R. Ahlrichs, *Phys. Chem. Chem. Phys.*, 2005, **7**, 3297-3305.
26. S. Grimme, *J. Comput. Chem.*, 2006, **27**, 1787-1799.

27. S. Sinnecker, A. Rajendran, A. Klamt, M. Diedenhofen and F. Neese, *J. Phys. Chem. A*, 2006, **110**, 2235-2245.
28. A. Pietrangelo, M. A. Hillmyer and W. B. Tolman, *Chem. Commun.*, 2009, 2736-2737.
29. A. F. Douglas, B. O. Patrick and P. Mehrkhodavandi, *Angew. Chem., Int. Ed.*, 2008, **47**, 2290-2293.
30. M. Normand, V. Dorcet, E. Kirillov and J.-F. Carpentier, *Organometallics*, 2013, **32**, 1694-1709.
31. M. P. Blake, A. D. Schwarz and P. Mountford, *Organometallics*, 2011, **30**, 1202-1214.

Chapter 5

5. Titanium (IV) and Aluminium (III) *trans*-1,4-DACH Salen Complexes and Their Application for the ROP of Lactide.

5. Titanium (IV) and Aluminium (III) *trans*-1,4-DACH Salen Complexes and Their Application for the ROP of Lactide.

5.1 Introduction

Aluminium imine bis(phenoxy) complexes have been investigated for the ring-opening-polymerisation (ROP) of lactide. Although active these initiators typically displayed low activity (see section 1.3.6).[1-3] These ROP investigations resulted in a high degree of molecular weight control alongside the production of highly isotactic PLA from the ROP of *rac*-lactide. Stereoselectivity observed for these complexes was retained under solvent free conditions for various aluminium imine bis(phenoxy) initiators. Imine mono(phenol) ligands have been coordinated to aluminium in monometallic structural motifs (Figure 5.01).[4, 5] Solution polymerisations using these monometallic aluminium imine mono(phenoxy) initiators required forcing conditions to attain high conversion (70 °C/14 h, 100 °C/48 h). Only moderate molecular weight control was observed (PDI = 1.12 - 1.69) and predominately atactic lactide was reported from the ROP of *rac*-lactide.[4, 5] Depending upon the substituents isotactic enriched PLA was obtained, although a direct probability of racemic enchainment (P_r) was not reported a ^{1}H NMR example was given showing slightly isotactic enriched PLA.[5]

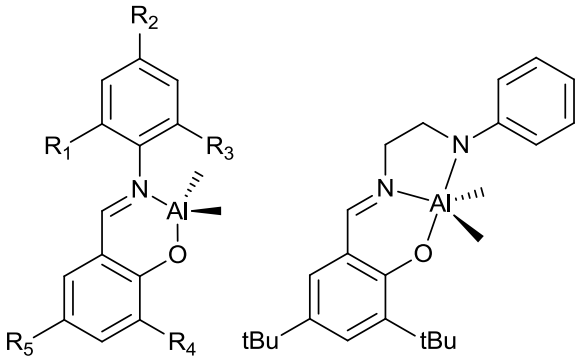

Figure 5.01: Monometallic aluminium imine mono(phenoxy) complexes trialled for the ROP of lactide.[4, 5]

Titanium imine bis(phenoxy) complexes (Figure 1.40, 1.41) have been utilised for the ROP of *rac*-lactide,[6] they were proven to be active initiators and resulted in a high degree molecular weight control. In comparison to the aluminium analogues atactic PLA was produced with perhaps a slight heterotactic bias. Imine mono(phenol) ligands have been coordinated to group 4 metals resulting in monometallic complexes with two chelating ligands (Figure 1.39).[7] These initiators resulted in a moderate heterotactic bias for zirconium based catalysts from *rac*-lactide. Similar monometallic titanium imine mono(phenoxy) complexes, containing coordinating chloride ligands have been reported as initiators for the ROP of lactide. Despite the lack of an alkoxide initiator group these titanium imine mono(phenoxy) complexes gave moderate molecular weight control and yielded predominately atactic lactide.[8]

1,2-Diaminocylohexane (1,2-DACH) bridged bis(phenol) ligands have been complexed to group 4 metals and aluminium, these complexes have been utilised for the ROP of lactide (Figure 5.02).[6, 9-11] Titanium 1,2-DACH bis(phenoxy) complexes were active for the ROP of *rac*-lactide albeit these initiators revealed low activity.[6, 9] They gave a good degree of molecular weight control but no significant stereoselectivity was reported. Aluminium 1,2-DACH bis(phenoxy) complexes were reported as poorly active initiators for the ROP of lactide.[10, 11] In contrast to their titanium analogues they resulted in the production of highly isotactic PLA. While 1,2-DACH bis(phenoxy) complexes have been synthesised and investigated as initiators for the ROP of lactide 1,4-DACH bis(phenoxy) complexes have not been previously synthesised. The following chapter discusses the synthesis and reactivity of various 1,4-DACH bis(phenoxy) complexes.

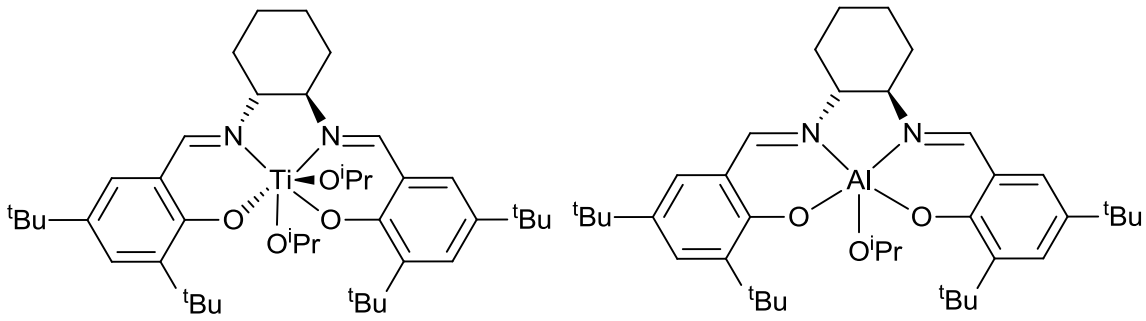

Figure 5.02: Previous DACH based complexes used for the ROP of lactide, Left - 1,2-DACH salen titanium complex,[6, 9] Right - 1,2-DACH salen aluminium complex.[10, 11]

5.2 Synthesis of *trans*-1,4-DACH Salen Ligands

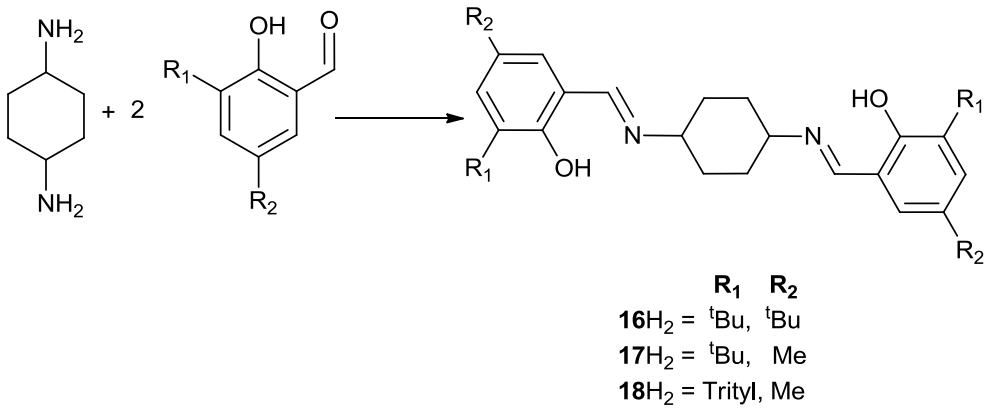

Figure 5.03: Scheme for the synthetic preparation of *trans*-1,4-DACH salen ligands.

trans-1,4-Diaminocyclohexane (1,4-DACH) salen ligands {(**16**-**18**)H_2} were synthesised *via* a condensation reaction of *trans*-1,4-DACH and two equivalents of 3,5-subsituted salicylaldehyde (Figure 5.03). The ligands {(**16**-**18**)H_2} were isolated as pure solid compounds from the reaction solvent (MeOH), at which point they were filtered and further washed (MeOH). The resulting ligands were characterised by $^{1}H/^{13}C\{^{1}H\}$ NMR spectroscopy and high resolution ESI-TOF mass spectrometry. *trans*-1,4-DACH and 3,5-^{t}Bu-salicylaldehyde were commercially obtained while 3-^{t}Bu-5-Me-salicylaldehyde and 3-trityl-5-Me-salicylaldehyde were synthesised before use. 3-^{t}Bu-5-Me-salicylaldehyde was synthesised by a less moisture sensitive deviation than reported in the literature.[12] 3-trityl-5-Me-phenol was first synthesised by literature methods and then converted to 3-trityl-5-Me-salicylaldehyde *via* a deviation of the Duff formylation reaction.[13]

5.3 *trans*-1,4-DACH Titanium Isopropoxide Complexes

5.3.1 Synthesis

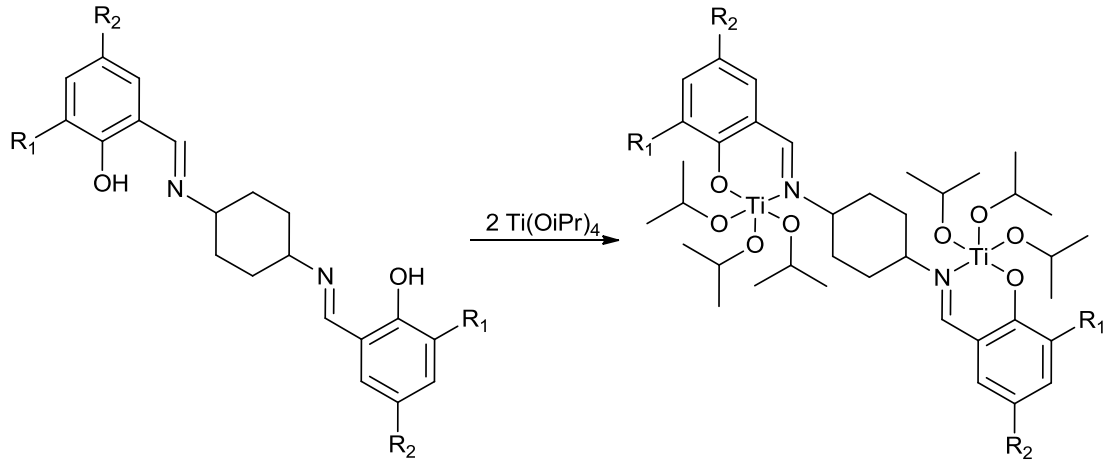

	R_1	R_2
Ti_2(**16**)(O^iPr)$_6$ =	^{t}Bu,	^{t}Bu
Ti_2(**17**)(O^iPr)$_6$ =	^{t}Bu,	Me
Ti_2(**18**)(O^iPr)$_6$ =	Trityl,	Me

Figure 5.04: Scheme depicting the synthesis of titanium isopropoxide *trans*-1,4-DACH salen complexes {Ti_2(**16-18**)(O^iPr)$_6$}.

Initial attempts to synthesise *trans*-1,4-DACH salen complexes using (**16-18**)H_2 ligands and Ti(O^iPr)$_4$ yielded different products dependent upon the *ortho*-phenol substituents. Following prior titanium work with hindered salan ligands (Chapter 2), the (**16-18**)H_2 ligands were reacted with two equivalents of Ti(O^iPr)$_4$ to yield a bimetallic complex (Figure 5.04). The complexation of less sterically hindered *ortho*-phenol substituted ligands (R_1 = Me, H) was attempted but these ligands resulted in insoluble titanium complexes. It was speculated the formation of polymeric material was occurring. Recrystallisation attempts from hexane or hexane/toluene mixes yielded crystals of Ti_2(**16-18**)(O^iPr)$_6$ suitable for X-ray crystallographic studies. Ti_2(**16-18**)(O^iPr)$_6$ were all obtained as pure products after recrystallisation and they were characterised by $^1H/^{13}C\{^1H\}$ NMR spectroscopy and CHN analysis.

5.3.2 Solid-state characterisation by X-ray crystallography

Crystals suitable for X-ray diffraction were obtained for Ti_2(**16-18**)(O^iPr)$_6$, a solid-state structure is given for Ti_2(**16**)(O^iPr)$_6$ in figure 5.05. These Ti_2(**16-18**)(O^iPr)$_6$ structures contained an inversion centre hence both titanium metal centres are in equivalent crystallographic environments. The DACH backbone adopts the favourable chair configuration. The titanium metals are five coordinate with three isopropoxide groups, and a chelating amine/phenoxy ligand. The titanium centres adopt distorted trigonal bipyramidal geometries where the imine and a single isopropoxide moiety assume axial positions.

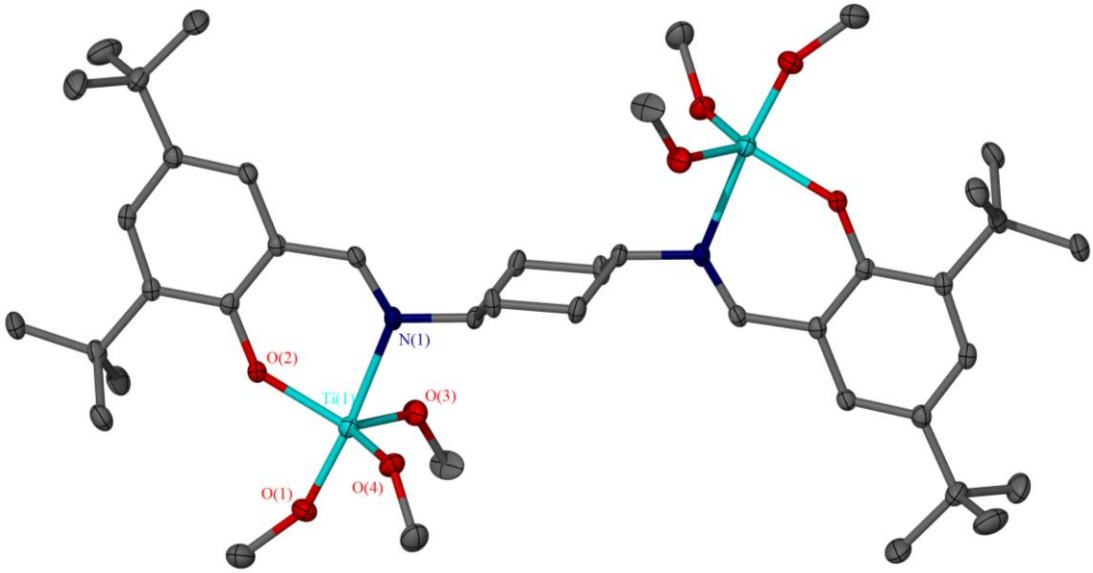

Figure 5.05: Solid-state structure for Ti_2(**16**)(O^iPr)$_6$. Ellipsoids are shown at the 30 % probability level, hydrogen atoms and isopropoxide –CH_3 moieties have been removed for clarity.

Selected bond lengths and angles for Ti_2(**16-18**)(O^iPr)$_6$ are given in table 5.01. The phenoxy-titanium (Ti1-O2) bond lengths are slightly longer {1.8932(17) - 1.901(2) Å} than previously reported Ti_2(**2-5**,**8**,**12**,**13**)(O^iPr)$_6$ complexes {1.8622(17) - 1.8883(17) Å} (see section 2.4.2).[14] The imine N1-Ti1 bond {2.224(2) - 2.239(2) Å} presented shorter lengths than similar amine N1-Ti1 bonds {2.3499(18) - 2.3567(18) Å}.[14] The shorter bond lengths are indicative of the stronger coordination of the imine justifying the formation of polymeric complexes when the *ortho* position is less sterically hindered. The equatorial substituents are distorted towards the axial nitrogen {80.76(9) - 84.33(8) °}. The bulky trityl (-CPh_3)

group in the *ortho*-phenoxy position causes the axial isopropoxide to converge towards 180 ° {179.48(8) °} in comparison to the same angle with ^{t}Bu *ortho*-phenoxy groups {174.29(8) - 174.63(10) °}. The equatorial isopropoxide groups of trityl substituted complexes are further slightly distorted towards the axial nitrogen {81.43(8) - 81.74(8) °} in comparison to complexes containing ^{t}Bu *ortho*-phenoxy groups {83.58(8) - 84.33(8) °}.

	Ti_2(**16**)$(O^iPr)_6$	Ti_2(**17**)$(O^iPr)_6$	Ti_2(**18**)$(O^iPr)_6$
Ti1-O1	1.787(2)	1.7915(19)	1.7815(18)
Ti1-O2	1.901(2)	1.8985(17)	1.8932(17)
Ti1-O3	1.811(2)	1.8059(19)	1.8394(18)
Ti1-O4	1.814(2)	1.8264(19)	1.8149(18)
Ti1-N1	2.225(3)	2.224(2)	2.239(2)
N1-Ti1-O1	174.63(10)	174.29(8)	179.48(8)
N1-Ti1-O2	80.76(9)	80.86(7)	80.79(7)
N1-Ti1-O3	84.17(10)	84.33(8)	81.74(8)
N1-Ti1-O4	83.88(10)	83.58(8)	81.43(8)

Table 5.01: Selected bond lengths (Å) and angles (°) for LM_2 titanium salen complexes {Ti_2(**16**-**18**)$(O^iPr)_6$}, as determined by X-ray crystallography.

5.3.3 Solution characterisation by NMR spectroscopy

Ti_2(**16**-**18**)$(O^iPr)_6$ were characterised by ^{1}H and ^{13}C{^{1}H} NMR spectroscopy the ^{1}H NMR spectrum for Ti_2(**17**)$(O^iPr)_6$ is given in figure 5.06. This spectrum is consistent with the ^{1}H NMR spectra obtained for Ti_2(**16**,**18**)$(O^iPr)_6$ and the solid-state structures. The fact that no uncoordinated ligand resonances were observed indicated full coordination of the ligands to titanium. The presence of six isopropoxide methine resonances (4.91 ppm) and corresponding CH_3 isopropoxide resonances (1.27 ppm) confirms the coordination of two -Ti$(O^iPr)_3$ groups to a single ligand, when integrated relative to one **17**H_2 ligand. The CH_2 groups are in equivalent environments which is best demonstrated by a single resonance (32.5 ppm) in the

$^{13}C\{^{1}H\}$ NMR spectra. Axial and equatorial CH_2 protons gave rise to two separate resonances (1.58, 2.25 ppm) indicating a locked chair configuration where ring flipping is significantly hindered.

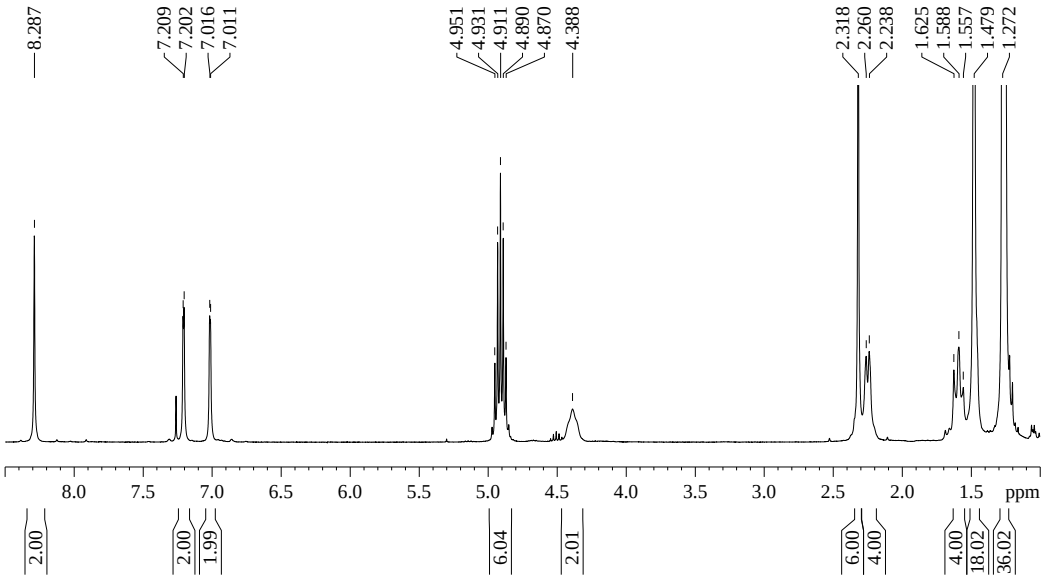

Figure 5.06: ^{1}H NMR spectrum for Ti_2(**17**)$(O^iPr)_6$ in $CDCl_3$ at 298 K.

5.4 *trans*-1,4-DACH Aluminium Methyl Complexes

5.4.1 Synthesis

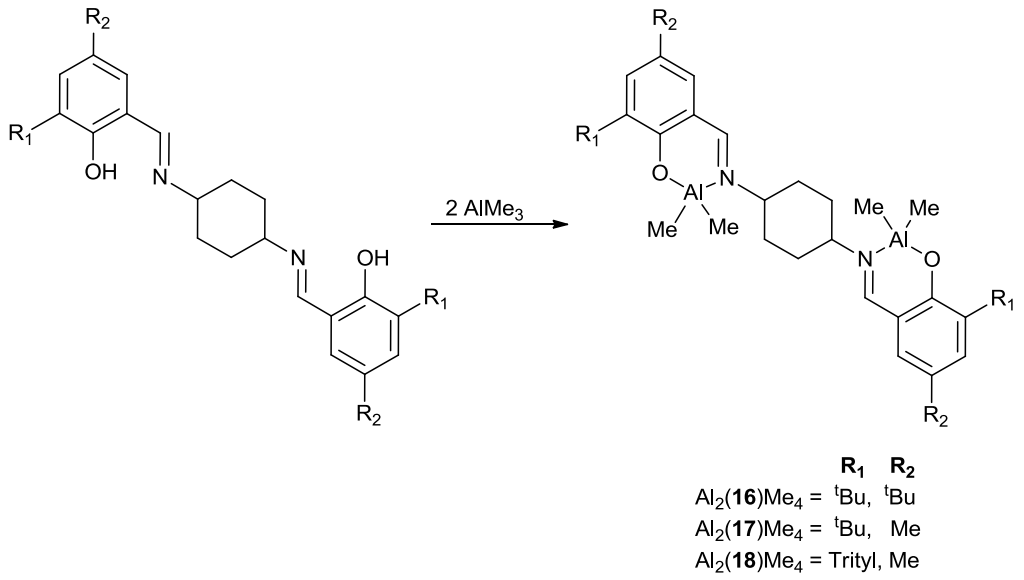

Figure 5.07: Scheme depicting the synthesis of aluminium methyl *trans*-1,4-DACH salen complexes {Al_2(**16**-**18**)Me_4}.

Similarly *trans*-1,4-DACH salen ligands {(**16**-**18**)H_2} were reacted with a 2M $AlMe_3$ solution in a 2:1 ratio of metal to ligand (Figure 5.07). The product was isolated by recrystallisation to yield pure Al_2(**16**-**18**)Me_4 complexes. The isolated Al_2(**16**-**18**)Me_4 complexes contained two aluminium metal centres where each was coordinated to a single ligand phenoxy group. Similar synthetic attempts under varying conditions were conducted with ligands containing less steric bulk about the *ortho*-phenol position but attempts resulted in undeterminable compounds. These complexes with less sterically hindered ligands yielded insoluble materials, additionally in some cases temperature and time caused more insoluble material to be produced. It was speculated that the possible formation of polymeric conglomerates of complexes and ligands was occurring. The Al_2(**16**-**18**)Me_4 complexes were characterised by $^1H/^{13}C\{^1H\}$ NMR spectroscopy and CHN analysis. Recrystallisation attempts resulted in crystals of Al_2(**16**)Me_4 and Al_2(**17**)Me_4 which were suitable for X-ray diffraction characterisation.

5.4.2 Solid-state characterisation by X-ray crystallography

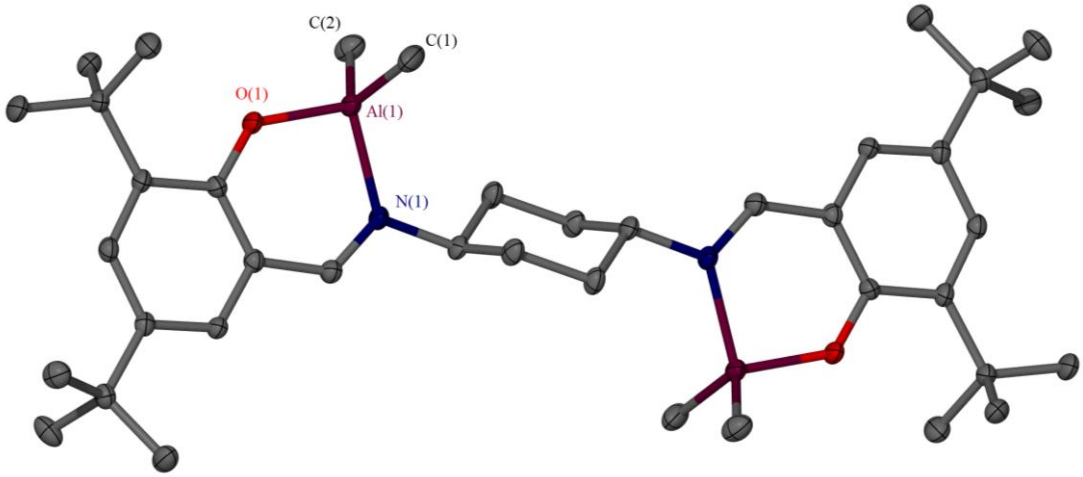

Figure 5.08: Solid-state structure for Al_2(**16**)Me_4. Ellipsoids are shown at the 30 % probability level, hydrogen atoms have been removed for clarity.

Recrystallisation of the aluminium *trans*-1,4-DACH salen complexes resulted in suitable crystals of Al_2(**16**,**17**)Me_4 for X-ray diffraction studies. The structure for Al_2(**16**)Me_4 is given in figure 5.08. The aluminium metal centres are four coordinate and only bound to a single phenoxy and a single imine of the *trans*-1,4-DACH salen

ligand, the other two coordination sites are occupied by methyl groups. The carbon aluminium bonds are similar in length to each other and are also of similar lengths to prior aluminium carbon bonds (see section 4.3) (Table 5.02).[15-17] Aluminium nitrogen imine bonds {Al1-N1 = 1.979(4) - 1.9783(12) Å} are shorter, as expected, than previously discussed aluminium nitrogen amine bonds {2.07(2) - 2.188(7) Å} (see 4.3).[15] The aluminium metal centres adopt *pseudo* tetrahedral geometries. Interestingly the nitrogen-aluminium-carbon angles {N1-Al1-C1/C2} are inequivalent within each structure despite their presumed similarity. The N1-Al-C1 and N1-Al-C2 angles are also significantly different between the crystal structures of Al_2(**16**)Me_4 and Al_2(**17**)Me_4. The N1-Al1-O1 chelate angle {94.39(5) - 94.69(14) °} significantly deviates from the ideal tetrahedral angle of 109 °.

	Al_2(**16**)Me_4	Al_2(**17**)Me_4
Al1-C1	1.946(5)	1.9497(17)
Al1-C2	1.952(5)	1.9637(17)
Al1-O1	1.763(3)	1.7684(11)
Al1-N1	1.979(4)	1.9783(12)
N1-Al1-C1	108.73(18)	109.05(7)
N1-Al1-C2	115.00(18)	113.43(7)
N1-Al1-O1	94.69(14)	94.39(5)

Table 5.02: Selected bond lengths (Å) and angles (°) for LM_2 aluminium salen complexes {Al_2(**16**-**17**)Me_4}, as determined by X-ray crystallography.

5.4.3 Solution characterisation by NMR spectroscopy

Al_2(**16**-**18**)Me_4 were characterised by ^{1}H and ^{13}C{^{1}H} NMR spectroscopy. The ^{1}H and ^{13}C{^{1}H} NMR spectra were consistent with the solid-state structures determined by X-ray diffraction. The ^{1}H NMR spectrum for Al_2(**17**)Me_4 is given in figure 5.09, the NMR spectra were consistent throughout the Al_2(**16**-**18**)Me_4 complexes. No ligand resonances were observed, confirming the full coordination of the (**16**-**18**)H_2 ligands. Twelve shielded aluminium bound methyl resonances (-0.19 ppm) were present, relative to a single ligand (**17**H_2), confirming four

aluminium bound methyl groups (Figure 5.09). The DACH ring CH_2 protons were located in a slightly broad resonance region at ~1.6 ppm, this region coincided with the ^{t}Bu-phenoxy substituent resonance at 1.65 ppm. The imine CH resonance and two phenoxy protons resonances also coincided at 7.40 ppm.

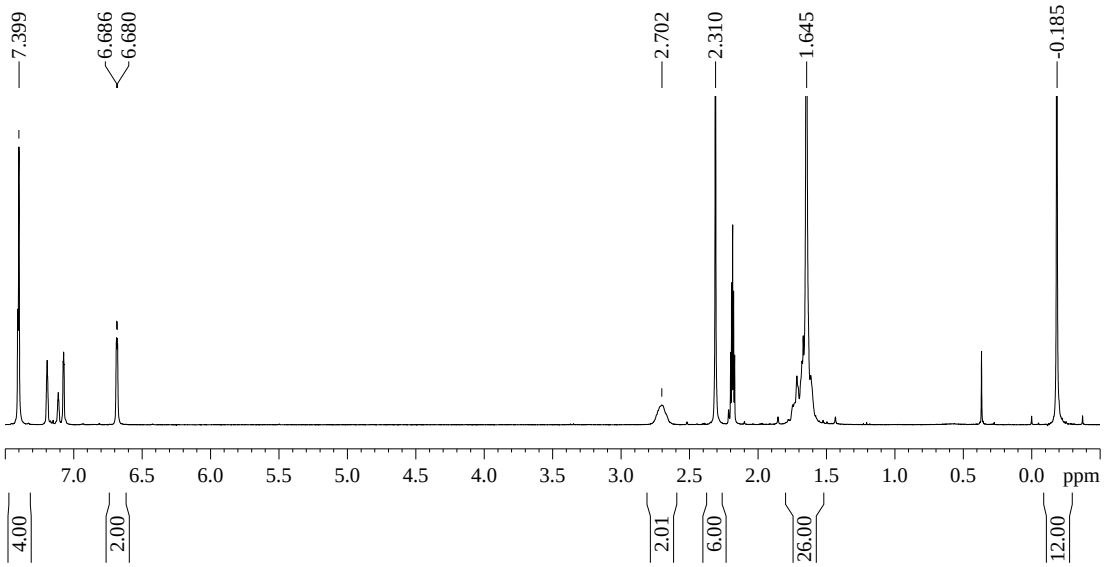

Figure 5.09: ^{1}H NMR spectrum for {Al_2(**17**)Me_4} in d_8-toluene at 298 K

5.5 Attempts to Coordinate *trans*-1,4-DACH Salen Ligands to Zirconium and Zinc.

5.5.1 Synthesis

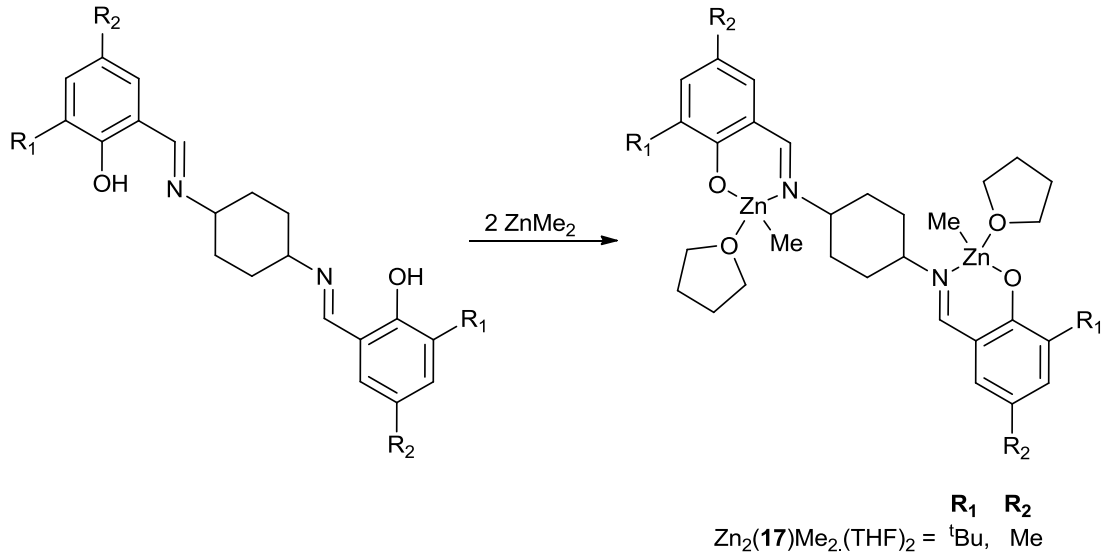

Figure 5.10: Scheme depicting the synthesis of zinc methyl *trans*-1,4-DACH salen complex Zn_2(**17**)$Me_2(THF)_2$.

The complexation of (**16**-**18**)H_2 to diethyl zinc was attempted and coordination occurred and various stoichiometries were investigated. Partial success was achieved with the complexation of (**16**-**18**)H_2 with a two equivalence of dimethyl zinc. The reaction of **17**H_2 with dimethyl zinc and purification by recrystallisation resulted in a mixture of zinc complexes. Exposure of the dimethyl zinc and **17**H_2 ligand products to THF prior to recrystallisation attempts from toluene and hexane yielded crystals of Zn_2(**17**)$Me_2(THF)_2$ suitable for X-ray diffraction studies (Figure 5.10). Although isolated as individual crystals the ^{1}H NMR spectrum revealed broad resonances at 298 K. ^{1}H NMR spectroscopy was inconclusive and CHN elemental analysis significantly deviated from the calculated values. Further attempts to synthesise Zn_2(**16**,**18**)Me_4 complexes either resulted in the production of a plethora of species identified by ^{1}H NMR spectroscopy or highly soluble products which could not be purified from common solvents. Attempts at the formation of zinc complexes using less sterically bulky ligands about the *ortho*-phenol position (R_1 = Me, H) were troublesome, typically resulting in insoluble material.

Attempts to synthesise LM_2 type structures using $Zr(O^iPr)_4.HO^iPr$ and (**16**-**18**)H_2 were unsuccessful. The resulting complexes were typically insoluble, a few cases of soluble complexes were isolated but the solubility of the complexes changed with time or heating. The zirconium products were indeterminate and any soluble product was presumed unstable in solution making analysis difficult. We speculated that formation of multiple products, where the increased size of the zirconium metal centre compared to titanium allows the coordination of more than one ligand. Furthermore zirconium complexes have been shown to bridge *via* phenoxy or isopropoxide groups (See section 3.2).

5.5.2 Solid-state characterisation by X-ray crystallography

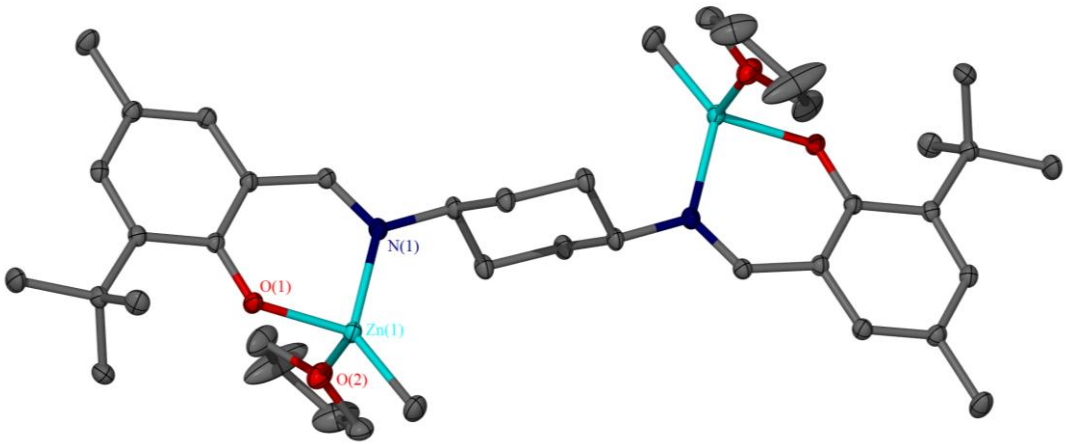

Figure 5.11: Solid-state structure for Zn_2(**17**)$Me_2(THF)_2$. Ellipsoids are shown at the 30 % probability level, hydrogen atoms have been removed for clarity.

Zn_2(**17**)$Me_2(THF)_2$ was isolated as crystals and determined by X-ray diffraction (Figure 5.11), selected bond lengths (Å) and angles (°) are given in table 5.03. Similar zinc complexes containing one phenoxy and one imine have been characterised by X-ray crystallography.[18-20] Comparison to the earliest reported imine phenoxy zinc complex showed similar Zn-C bonds {1.965(2) Å} and Zn-N_{imine} bonds {2.051(2) Å}.[20] The zinc centres within Zn_2(**17**)$Me_2(THF)_2$ are four coordinate; bound to an alkyl, phenoxy oxygen, imine nitrogen and a THF oxygen. As expected the THF Zn1-O2 bond {2.2029(15) Å} is significantly longer then the phenoxy Zn1-O1 bond {1.9312(13) Å}. The zinc centres adopt a *pseudo* tetrahedral

structure, where the degree of distortion is represented by the N1-Zn1-C1 angle {131.14(9) °}.

Zn_2(**17**)Me_2.$(THF)_2$			
Zn1-C1	1.961(2)	**O1-Zn1-O2**	95.86(6)
Zn1-O1	1.9312(13)	**N1-Zn1-C1**	131.14(9)
Zn1-O2	2.2029(15)	**N1-Zn1-O1**	93.53(6)
Zn1-N1	2.0356(16)	**N1-Zn1-O2**	93.11(6)

Table 5.03: Selected bond lengths (Å) and angles (°) for the zinc salen complex {Zn_2(**17**)Me_2.$(THF)_2$}, as determined by X-ray crystallography.

5.6 Ring-Opening-Polymerisation of Lactide

Ti_2(**16-18**)O^iPr_6 and Al_2(**16-18**)Me_4 were trialled as initiators for the ROP of *rac*-lactide. The titanium initiators {Ti_2(**16-18**)O^iPr_6} were investigated for the ROP of *rac*-lactide in toluene and solvent free conditions. The aluminium initiators were investigated for the solvent ROP of *rac*-lactide, benzyl alcohol was added as a co-initiator and its effect at different ratios was studied. Conversions were calculated by ^{1}H NMR spectroscopy by comparison of the monomer and polymer methine regions. Molecular weights (M_n) and PDI values were obtained from gel permeation chromatography (GPC). Stereoselectivity was calculated from homonuclear decoupled ^{1}H NMR spectroscopy and the probability of racemic enchainment was calculated by Bernoullian statistics.[21]

5.6.1 Titanium and aluminium initiators for the solution ROP of *rac*-lactide

Titanium and aluminium 1,4-DACH salen complexes {Ti_2(**16-18**)O^iPr_6, Al_2(**16-18**)Me_4} were trialled for the ROP of *rac*-lactide. The ROP using Ti_2(**16-18**)O^iPr_6 complexes was investigated at 80 °C in toluene at 100:1 [*rac*-lactide]:[initiator] ratio. The aluminium initiators utilised conditions of 80 °C in toluene, benzyl alcohol was added *in-situ* to promote the ROP reaction. The polymerisation data is given in table 5.04.

	Ratio [a]	Time (hours)	Conv. (%)[b]	M_n[c] (theo)	M_n[d]	PDI[d]	P_r[e]
Ti_2(**16**)O^iPr_6	100:1	24	91	6600	4850	1.50	0.53
Ti_2(**17**)O^iPr_6	100:1	24	92	6700	5450	1.33	0.55
Ti_2(**18**)O^iPr_6	100:1	24	94	6850	4800	1.32	0.44
Al_2(**16**)Me_4	100:1:2	24	96	7000	9000	1.24	0.42
Al_2(**16**)Me_4	100:1:4	24	99	3700	5400	1.24	0.42
Al_2(**16**)Me_4	100:1:8	24	99	1900	2700	1.27	0.40
Al_2(**17**)Me_4	100:1:2	24	96	7050	9250	1.22	0.35
Al_2(**17**)Me_4	100:1:4	24	99	3700	5500	1.23	0.35
Al_2(**17**)Me_4	100:1:8	24	96	1850	2650	1.22	0.38
Al_2(**18**)Me_4	100:1:2	24	73	5350	6750	1.08	0.43

Table 5.04: Solution ROP of *rac*-lactide for Ti_2(**16-18**)$(O^iPr)_6$ in 10 ml of toluene at 80 °. [a] ratio of [*rac*-lactide]:[initiator]:[benzyl alcohol]. [b] Conversion ascertained by ^{1}H NMR spectroscopy. [c] Theoretical molecular weight calculated from conversion (Ti = Conv. × 100/2 × 144.13 + 60.10) (Al = Conv. × 100/[co-initiator ratio] × 144.13 + 108.14) (rounded to the nearest 50), [d] Molecular weight and PDI determined by GPC (THF) using polystyrene standards without applying a correction factor. [e] P_r as calculated from ^{1}H NMR homonuclear decoupled spectroscopy in $CDCl_3$.

The titanium initiators Ti_2(**16-18**)$(O^iPr)_6$ resulted in high conversion after 24 h. Slightly lower molecular weights than expected were obtained which was attributed to multiple initiating isopropoxide groups per metal centre. Moderate chain length distributions were observed (PDI = 1.32 -1.50), this was also attributed to the potential to initiate multiple PLA chains per metal centre.

High conversions were obtained after 24 h when the aluminium initiators {Al_2(**16-18**)Me_4} were utilised. Molecular weight distributions were typically low (PDI = 1.08 – 1.27) and the molecular weights were dependent upon the ratio of benzyl alcohol utilised, this observation is indicative of an immortal polymerisation system. All the aluminium initiators {Al_2(**16-18**)Me_4} resulted in isotacticly biased PLA (P_r = 0.35 – 0.43), a stronger degree of stereocontrol was found for Al_2(**17**)Me_4 (P_r = 0.35) independent of the amount of benzyl alcohol co-initiator. MALDI-TOF mass spectrometry of PLA initiated by Al_2(**16**)Me_4 with eight equivalents of benzyl alcohol was performed (Figure 5.12). The unit spacing between peaks is ~72 g mol^{-1}

indicating transesterification reactions. Benzyl alcohol was identified as the end group supporting a chain exchange mechanism.

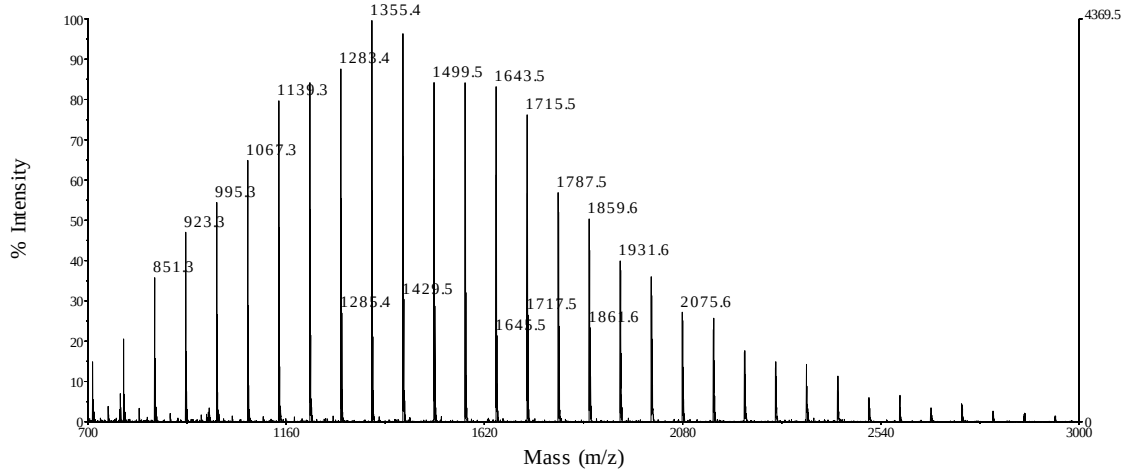

Figure 5.12: MALDI- TOF mass spectra (ionised with Na^+) of PLA produced using initiator Al_2(**16**)Me_4, at 80 C after 24 h at 100:1:8 [*rac*-lactide]:[initiator]:[benzyl alcohol] ratio.

5.6.2 Titanium initiators for the solvent free ROP of *rac*-lactide

Ti_2(**16-18**)O^iPr_6 were trialled for the ROP of *rac*-lactide in solvent free conditions of 130 °C at a 300:1 [*rac*-lactide]:[Initiator] ratio. The aluminium analogues {Al_2(**16-18**)Me_4} were not investigated under these condition due to complexities involved with co-initiator addition. High conversion of *rac*-lactide to PLA was achieved for Ti_2(**16-18**)O^iPr_6 initiators before methanol quenching after 1 h (Table 5.05). The molecular weights (M_n) were lower than the theoretical derived molecular weights ($M_{n\ (theo)}$), higher PDI values (PDI = 1.34 - 1.74) than the analogous solvated polymerisations were obtained. The high PDI and low M_n values were credited to multiple initiating isopropoxide groups per metal centre.

	Time (hours)	Conv. (%)[a]	M_n[b] (theo)	M_n[c]	PDI[c]	P_r[d]
Ti_2(**16**)O^iPr_6	1	95	20600	9,450	1.74	0.51
Ti_2(**17**)O^iPr_6	1	96	20800	15,500	1.60	0.51
Ti_2(**18**)O^iPr_6	1	94	20400	17,600	1.34	0.51

Table 5.05: Solvent free ROP of *rac*-lactide for Ti_2(**16-18**)$(O^iPr)_6$ at 130 °C in a 300:1 [*rac*-lactide]:[initiator] ratio. [a] Conversion ascertained by ^{1}H NMR spectroscopy. [b] Theoretical molecular weight calculated from conversion (Conv. × 300/2 × 144.13 + 60.10) (rounded to the nearest 50), [c] Molecular weight and PDI determined by GPC (THF) using polystyrene standards without applying a correction factor. [d] P_r as calculated from ^{1}H NMR homonuclear decoupled spectroscopy in $CDCl_3$.

5.7 Kinetic Studies of the Ring-Opening-Polymerisation of Lactide

The apparent rate of propagation (k_{app}) was determined by NMR spectroscopy scale ROP of lactide experiments using Al_2(**16**,**17**)Me_4 initiators with two equivalence of benzyl alcohol as a co-initiator. Both *rac*-lactide and *L*-lactide were investigated to quantitatively indentify any rate enhancement and stereoselective preferences of these isotactic biased initiators. The ROP reactions were performed in an NMR tube using 50 mg of lactide in 0.6 ml of d_8-toluene at 80 °C, the initiators {Al_2(**16**,**17**)Me_4} were in a 100:1:2 ratio of [lactide]:[initiator]:[benzyl alcohol]. By plotting *pseudo* first order graphs of $\ln([LA]_0/[LA]_t)$ against time the slope of the graph is equal to the apparent first order rate constant (k_{app}) {Figure 5.13 = Al_2(**16**)Me_4, Figure 5.14 = Al_2(**17**)Me_4}.

	Lactide	k_{app} (x 10^{-3}) (min^{-1})	R^2
Al_2(**16**)Me_4	*L*	2.09(1)	0.9987
Al_2(**16**)Me_4	*Rac*	1.96(1)	0.9994
Al_2(**17**)Me_4	*L*	2.31(1)	0.9996
Al_2(**17**)Me_4	*Rac*	1.37(1)	0.9996

Table 5.06: k_{app} values and R^2 values for ROP of *rac*-lactide and *L*-lactide by Al_2(**16-17**)Me_4 initiators.

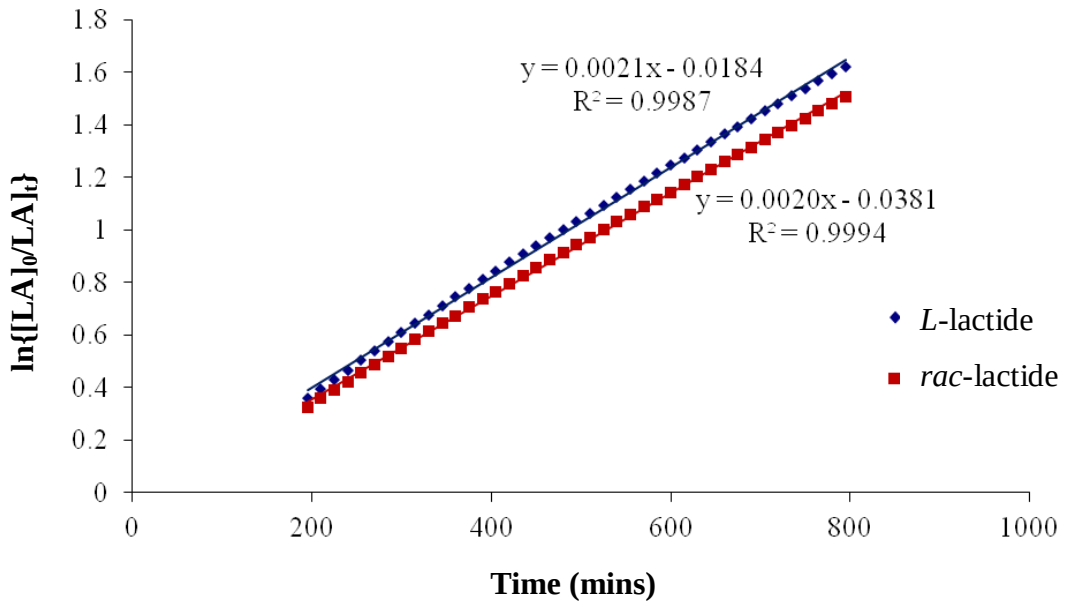

Figure 5.13 *Pseudo* first order plots for the ROP of *rac*-lactide (Red) and *L*-lactide (Blue) by Al_2(**16**)Me_4. For each case 50 mg of lactide was dissolved in 0.6 ml of d_8-touene at 80 °C at 100:1:2 [*rac*-lactide]:[initiator]:[benzyl alcohol] ratio.

The p*seudo* first order plots for the ROP of *rac*-lactide and *L*-lactide data were truncated as the rate did not equilibrate until ~200 mins (Figure 5.13, figure 5.14). Table 5.06 gives the k_{app} rates for *rac*-lactide and *L*-lactide using Al_2(**16**,**17**)Me_4 as the initiators. No significant difference between the k_{app} values for *L*-lactide and *rac*-lactide was observed using Al_2(**16**)Me_4 initiator. Al_2(**17**)Me_4 revealed an approximate 70 % increase in apparent rate (k_{app}) towards *L*-lactide over *rac*-lactide. Al_2(**17**)Me_4 resulted in a much larger k_{app} difference between the ROP of *L*-lactide and *rac*-lactide than Al_2(**16**)Me_4 (Table 5.06). This is consistent with the greater stereoselectivity observed for Al_2(**17**)Me_4 (P_r = 0.35) over Al_2(**16**)Me_4 (P_r = 0.42) (Table 5.04). The cause of the enhanced stereoselectivity upon substitution of the *para*-phenoxy subsistent is unresolved but the *para*-positioning is indicative of an electronic effect. It should be noted the N1-Al1-C1/C2 angles showed variance between the two structures Al_2(**16**,**17**)Me_4 indicating the likely lactide coordination sites upon the aluminium metal are not equivalent between the structures (Table 5.02).

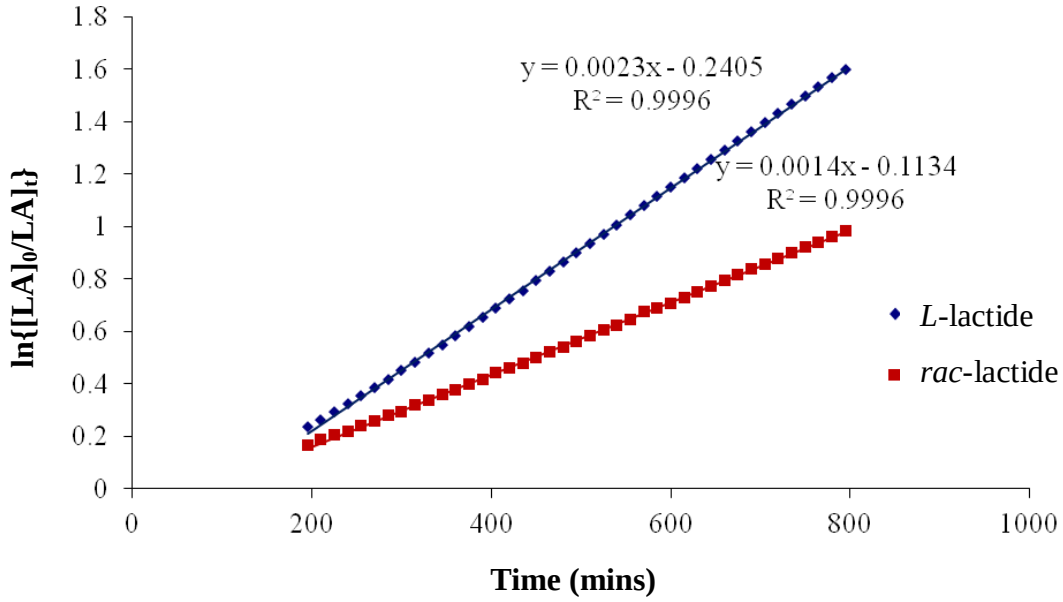

Figure 5.14: *Pseudo* first order plots for the ROP of *rac*-lactide (Red) and *L*-lactide (Blue) by Al_2(**17**)Me_4. For each case 50 mg of lactide was dissolved in 0.6 ml of d_8-toluene at 80 °C at 100:1:2 [*rac*-lactide]:[initiator]:[benzyl alcohol] ratio.

5.8 Conclusion

The synthesis of novel *trans*-1,4-DACH salen complexes {Ti_2(**16-18**)(O^iPr)$_6$, Al_2(**16-18**)Me_4} is reported herein with supporting characterisation by $^1H/^{13}C\{^1H\}$ NMR spectroscopy and CHN analysis. Ti_2(**16-18**)(O^iPr)$_6$ and Al_2(**16,17**)Me_4 were isolated as crystals and their structures determined by X-ray diffraction studies. Both metals were shown to coordinate to the ligands in a 2:1 metal-to-ligand ratio. The attempted synthesis of derivatives with ligands containing less sterically bulky groups (H, Me, or Cl) in the *ortho* position of the phenol rings resulted in highly insoluble complexes. The synthesis of various zirconium *trans*-1,4-DACH salen complexes was unsuccessful. The complexation of **17**H_2 to $ZnMe_2$ resulted in the formation of Zn_2(**17**)Me_4(THF)$_2$ as determined by X-ray crystallography, further analysis did not confirm this species as a pure bulk material. Attempts to synthesise further Zn(II) *trans*-1,4-DACH salen complexes with (**16**,**18**)H_2 were unsuccessful.

The titanium complexes {Ti_2(**16-18**)(O^iPr)$_6$} were investigated for the ROP of *rac*-lactide under solvent free conditions at 130 °C in a 300:1 [*rac*-lactide]:[initiator] ratio. Ti_2(**16-18**)(O^iPr)$_6$ and Al_2(**16,17**)Me_4 were trialled for the ROP of *rac*-lactide at 80 °C in toluene at a 100:1 [*rac*-lactide]:[initiator] ratio.

Two equivalents of benzyl alcohol were added to initiate the ROP of *rac*-lactide using Al_2(**16-18**)Me_4. Both aluminium {Al_2(**16-18**)Me_4} and titanium {Ti_2(**16-18**)(O^iPr)$_6$} initiators attained high conversion after 24 h. Moderate chain length control is observed for these initiators with lower molecular weight PLA being obtained due to multiple initiation sites per titanium metal centre. The aluminium initiators Al_2(**16-18**)Me_4 display some isotactic stereoselectivity for the ROP of *rac*-lactide, where Al_2(**17**)Me_4 is the most selective (P_r = 0.35). Comparative apparent rate constants (k_{app}) for the ROP of *rac*-lactide and *L*-lactide are determined by ^{1}H NMR spectroscopy and Al_2(**17**)Me_4 is 70 % more active towards *L*-lactide than *rac*-lactide, which is consistent with a chain-end control mechanism. The isotactic bias observed is dependent upon the *ortho/para*-phenoxy substituents. Altering the *para* subsistent to a ^{t}Bu has a detrimental effect on the isotactic stereoselectivity observed, this was speculatively attributed to electronic variations. The addition of excess benzyl alcohol to the ROP of *rac*-lactide by Al_2(**16,17**)Me_4 proportionally reduces the resulting PLA molecular weights without loss of stereoselectivity. This is indicative of an immortal polymerisation system where a chain-end exchange mechanism is in operation.[22]

5.9 Future Work

Smaller *ortho*-phenol substituents upon the *trans*-1,4-DACH salen ligands resulted in insoluble material after complexation to titanium or aluminium. Further work could be conducted to ascertain the structure of these complexes through further synthetic attempts and solution trails, such as monitoring the reaction *via* NMR spectroscopy. Solid-state characterisation techniques could also be used to identify the compounds. Further-work preparing zinc complexes could be conducted in an attempt to isolate more complexes as pure material and investigate these for the ROP of cyclic esters. Attempts with other metals such as zirconium, hafnium and indium could be conducted to expand the library of this series of initiators.

5.10 References

1. N. Spassky, M. Wisniewski, C. Pluta and A. Le Borgne, *Macromol. Chem. Phys.*, 1996, **197**, 2627-2637.
2. N. Nomura, R. Ishii, M. Akakura and K. Aoi, *J. Am. Chem. Soc.*, 2002, **124**, 5938-5939.
3. N. Nomura, R. Ishii, Y. Yamamoto and T. Kondo, *Chem. Eur. J.*, 2007, **13**, 4433-4451.
4. M. Bouyhayi, Y. Sarazin, O. L. Casagrande and J.-F. Carpentier, *Appl. Organomet. Chem.*, 2012, **26**, 681-688.
5. W. Zhang, Y. Wang, W.-H. Sun, L. Wang and C. Redshaw, *Dalton Trans.*, 2012, **41**, 11587-11596.
6. C. K. A. Gregson, I. J. Blackmore, V. C. Gibson, N. J. Long, E. L. Marshall and A. J. P. White, *Dalton Trans.*, 2006, 3134-3140.
7. A. J. Chmura, D. M. Cousins, M. G. Davidson, M. D. Jones, M. D. Lunn and M. F. Mahon, *Dalton Trans.*, 2008, 1437-1443.
8. J. Lee, Y. Kim and Y. Do, *Inorg. Chem.*, 2007, **46**, 7701-7703.
9. T. K. Saha, V. Ramkumar and D. Chakraborty, *Inorg. Chem.*, 2011, **50**, 2720-2722.
10. Z. Zhong, P. J. Dijkstra and J. Feijen, *Angew. Chem., Int. Ed.*, 2002, **41**, 4510-4513.
11. Z. Zhong, P. J. Dijkstra and J. Feijen, *J. Am. Chem. Soc.*, 2003, **125**, 11291-11298.
12. P. D. Knight, G. Clarkson, M. L. Hammond, B. S. Kimberley and P. Scott, *J. Organomet. Chem.*, 2005, **690**, 5125-5144.
13. A. I. Kochnev, I. I. Oleynik, I. V. Oleynik, S. S. Ivanchev and G. A. Tolstikov, *Russ. Chem. Bull.*, 2007, **56**, 1125-1129.
14. S. L. Hancock, M. F. Mahon and M. D. Jones, *Dalton Trans.*, 2011, **40**, 2033-2037.
15. S. L. Hancock, M. D. Jones, C. J. Langridge and M. F. Mahon, *New J. Chem.*, 2012, **36**, 1891-1896.
16. N. C. Johnstone, E. S. Aazam, P. B. Hitchcock and J. R. Fulton, *J. Organomet. Chem.*, 2010, **695**, 170-176.
17. W. Li, W. Wu, Y. Wang, Y. Yao, Y. Zhang and Q. Shen, *Dalton Trans.*, 2011, **40**, 11378-11381.
18. C. Zhang and Z.-X. Wang, *J. Organomet. Chem.*, 2008, **693**, 3151-3158.
19. W.-C. Hung, S.-L. Lai and C.-C. Lin, *Acta Crystallogr., Sect. E*, 2008, **64**, m129-m130.
20. D. Steinborn, M. Rausch, U. Baumeister, I. Potočňák, D. Mikloš and M. Dunaj-Jurčo, *Z. Anorg. Allg. Chem.*, 1996, **622**, 1941-1945.
21. B. M. Chamberlain, M. Cheng, D. R. Moore, T. M. Ovitt, E. B. Lobkovsky and G. W. Coates, *J. Am. Chem. Soc.*, 2001, **123**, 3229-3238.
22. T. M. Ovitt and G. W. Coates, *J. Polym. Sci., Part A: Polym. Chem.*, 2000, **38**, 4686-4692.

Chapter 6

6. Aluminium *trans*-1,2-DACH Salalen Complexes and Their Application for the ROP of *rac*-Lactide

6. Aluminium *trans*-1,2-DACH Salalen Complexes and Their Application for the ROP of *rac*-Lactide

6.1 Introduction

As discussed in chapter 1.3.6 imine and amine linked bis(phenoxy) aluminium complexes have been widely investigated for the ROP of lactide.[1-3] Aluminium imine bis(phenoxy) complexes are some of the most selective initiators for isotactic PLA. The aluminium *R*-(+)-1,1'-binaphthyl-2,2'-diamine linked bis(phenoxy) complex was reported by Spassky *et al*. and is one of the earliest examples of an aluminium imine bis(phenoxy) complex which resulted in isotactic stereoselectivity for the ROP of *rac*-lactide.[4] This was preceded by further aluminium salen bis(phenoxy) initiators, notably; alkane linked salen bis(phenoxy) complexes by Nomura *et al.*[5, 6] and 1,2-diaminocyclohexane (1,2-DACH) linked salen bis(phenoxy) complexes by Fiejen *et al.*[7, 8], which both result in isotactic PLA from *rac*-lactide.

Related amine bis(phenoxy) aluminium (aluminium salan) complexes were synthesised by Gibson *et al.*[9] who showed the stereoselectivity of such complexes could be inverted by changing the phenoxy substituents, where Me substituents gave isotactic biased PLA and Cl substituents resulted in heterotactic PLA. DACH linked salan bisphenoxy aluminium complexes were also synthesised by Fiejen *et al.*[10] and demonstrated high isotactic control. This has led to interest in salalen systems which contain both an imine phenol linked to an amine phenol.[11] The most pertinent study of an aluminium system of this type utilised for the ROP of *rac*-lactide was reported by Jones *et al.*[11] Only the imine phenol substituents were varied in the previous study and PLA stereoselectivity was predominately heterotactic biased. Investigation into varying the alkyl group on the nitrogen was conducted to reveal that the stereoselectivity bias could be inverted. Herein similar salalen aluminium complexes are reported using a *trans*-1,2-DACH linking group. The *trans*-1,2-DACH linked salen bis(phenoxy) complexes by Fiejen *et al*. produced highly isotactic PLA.[7, 8] It was anticipated that the more ridged and chiral DACH would form strongly defined initiator structures and induce stereocontrol. Additionally, investigation into the effect of phenol substituents of both the imine phenol and amine phenol groups was

conducted with respect to steric bulk and electronic effects. Kol *et. al.* reported the use of salalen titanium complexes for the selective polymerization of 1-hexene and propylene.[12] Prior aluminium DACH salalen complexes have been reported in the literature for the enantioselective hydrophosphonylation of aldehydes[13, 14] and aldimines.[14] Katsuki *et al.* was the first to report the enantioselective oxidation of sulphides by aluminium salalen complexes and has demonstrated high enantioselectivity in various systems.[15-17] The same complexes were shown to be active for the oxidation of cyclic dithioacetals and afforded high enantioselectivity alongside high diastereoselectivity.[18] Although their catalytic activity was studied in detail the aluminium salalen structural aspects and coordinated *N*-methyl chirality are discussed to a lesser degree by Katsuki and Saito.[14]

6.2 Synthesis of *trans*-1,2-DACH Salalen Ligands

The ligand synthesis shown in figure 6.01 is an adaptation of the procedures used by Katsuki *et al.*[19] The ligands were synthesised from *rac*-1,2-*trans*-DACH which was first protected with a Boc group and the mono-boc-protected *rac*-1,2-*trans*-DACH was isolated by acid/base extractions. The *mono*-boc-1,2-*trans*-DACH was reacted with a selected salicylaldehyde by an imine condensation reaction, which was then reduced. The boc-protected half salans {(**19-21**)HBoc} were then synthesised by reductive methylation and the crude mixture was analysed by NMR spectroscopy. The compound was then deprotected with acid and reacted with a second substituted salicylaldehyde *via* an imine condensation to produce the pure *trans*-1,2-DACH salalen ligands {(**22-30**)H_2}. All of the salalen ligands shown in figure 6.01 {(**22-30**)H_2} were isolated and characterised by $^{1}H/^{13}C\{^{1}H\}$ NMR spectroscopy, and high resolution ESI-TOF mass spectrometry. This method allows independent variation of the salan phenol substituents and the salen phenol substituents. Chirally resolved (*R*,*R*)-1,2-DACH was used for the synthesis of a chiral salalen ligand (*R*,*R*-**22**)H_2, by the same methodology. The steric and electronic effects of the phenol substituents were upon the salan and salen sections were investigated and consequently their effect upon the ROP of *rac*-lactide can be probed in detail.

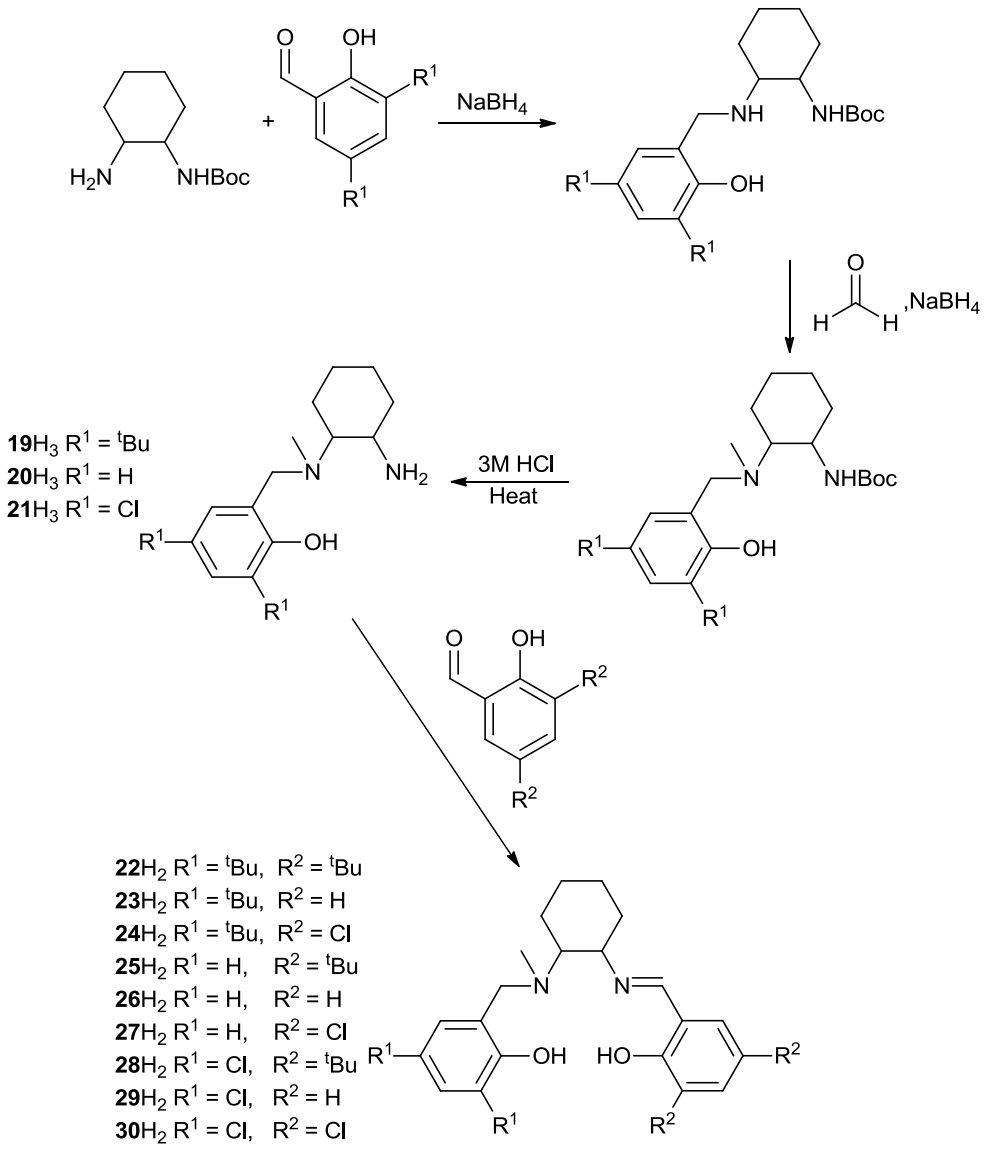

Figure 6.01: Reaction pathway detailing the synthesis of *trans*-1,2-DACH-salalen ligands.

6.3 Aluminium *trans*-1,2-DACH Salalen Complexes

6.3.1 Synthesis of aluminium *trans*-1,2-DACH salalen complexes

The aluminium methyl 1,2-DACH-salalen complexes {Al(**22**-**30**)Me} were isolated by reacting the ligands (**22**-**30**)H_2 with $AlMe_3$ (2M in hexanes) in a 1:1 ratio in toluene. The crude product was recrystallised from toluene/hexane mixes. The aluminium complexes Al(**22**-**25**,**28**)Me were characterised by $^{1}H/^{13}C\{^{1}H\}$ NMR spectrometry, and CHN analysis. While the Al(**22**-**30**)Me complexes can be isolated as solids Al(**26**-**27**)Me and Al(**29**-**30**)Me were insoluble in all suitable solvents for characterisation. As shown in previously discussed work (Chapter 4) Al(**6**-**9**,**11**)OBn

complexes can be isolated promoting solvent free and co-initiator free polymerisation studies. Aluminium complexes Al(**22**-**30**)Me were further reacted with 1.1 equivalence of benzyl alcohol (BnOH) in toluene (Figure 6.02), which were purified by recrystallisation in toluene/hexane mixes. The benzyl alcohol complexes Al(**22**-**30**)OBn are notably more soluble in organic solvents, and as such complexes Al(**22**-**28**)OBn and Al(**30**)OBn were characterised by $^{1}H/^{13}C\{^{1}H\}$ NMR spectroscopy, and CHN analysis. After multiple attempts Al(**29**)OBn could not be isolated in acceptable purity although the analysis revealed the major product as the desired Al(**29**)OBn complex.

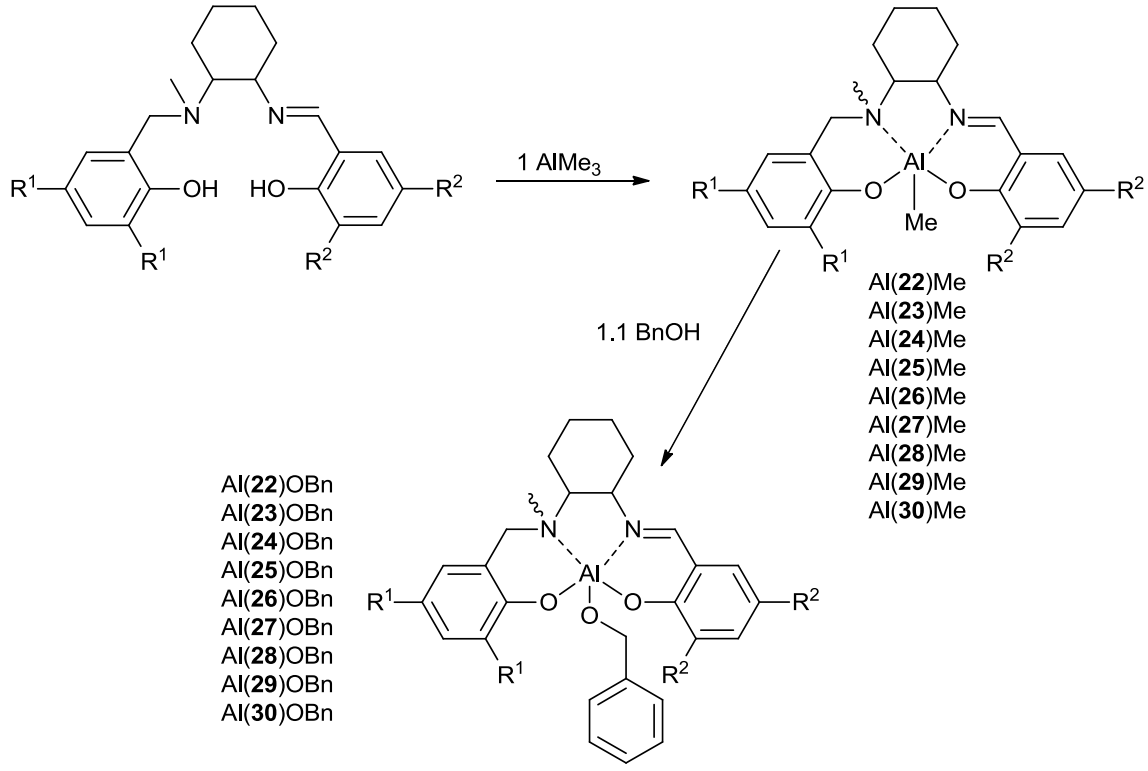

Figure 6.02: Reaction scheme for the synthesis of aluminium methyl and benzyloxy 1,2-DACH-salalen complexes.

6.3.2 Solid-state characterisation of aluminium *trans*-1,2-DACH salalen complexes

Few structures of aluminium salalen complexes have been characterised by X-ray crystallography. A chloro-aluminium 1,2-DACH-salalen complex was reported by Saito and Katsuki, the aluminium coordinated tertiary amine was shown

to be exclusively in the *S* configuration.[13] Jones *et al*. reported aluminium salalen structures which contained varying phenoxy substituents upon the salan and salen segments.[11] Suitable crystals for X-ray diffraction were obtained for Al(**22**)Me (Figure 6.03), Al(*R*,*R*-**22**)Me (Figure 6.04), and Al(**25**)OBn (Figure 6.05).

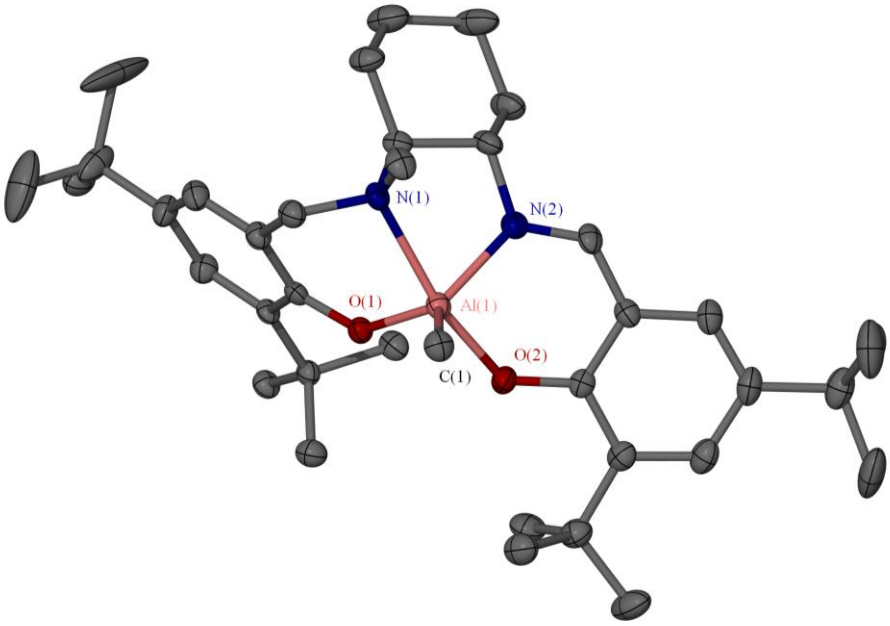

Figure 6.03: Solid-state structure for Al(**22**)Me. Ellipsoids are shown at the 30 % probability level, hydrogen atoms have been removed for clarity.

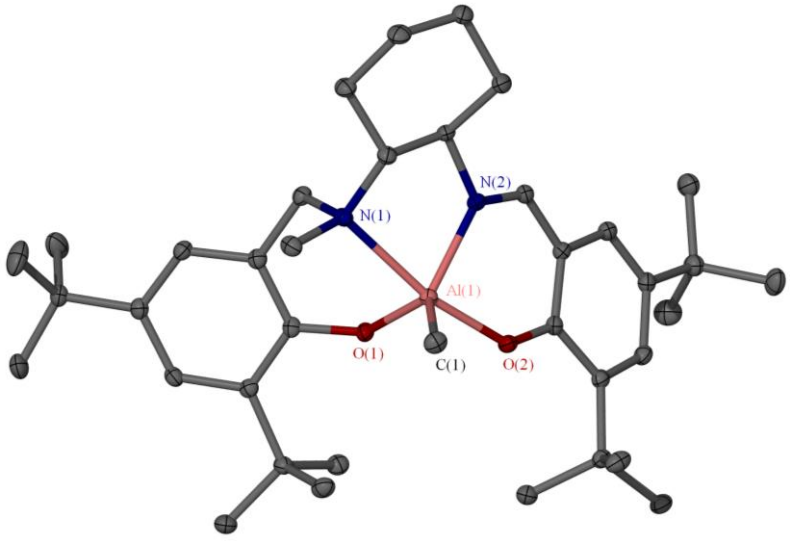

Figure 6.04: Solid-state structure for Al(*R*,*R*-**22**)Me. Ellipsoids are shown at the 30 % probability level, hydrogen atoms have been removed for clarity.

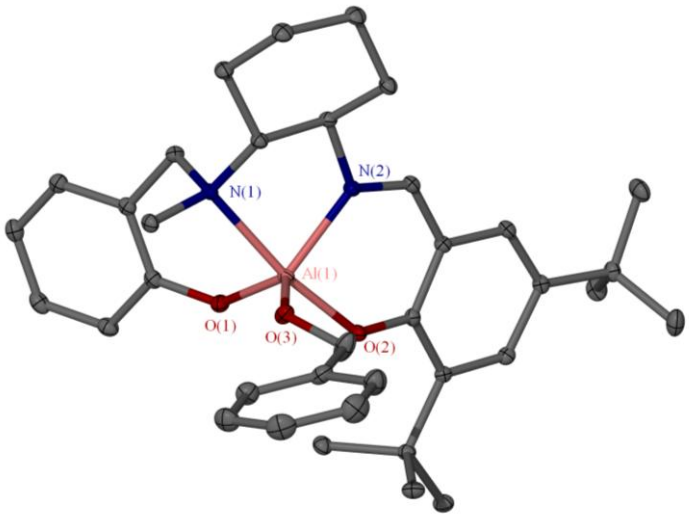

Figure 6.05: Solid-state structure for Al(**25**)OBn. Ellipsoids are shown at the 30 % probability level, hydrogen atoms have been removed for clarity.

All the aluminium 1,2-DACH salalen crystal structures obtained adopt *pseudo* trigonal bipyramidal geometries (Figure 6.03, 6.04, and 6.05). The N_{amine} and the O-Ph_{imine} adopt axial positions, which is consistent with prior literature Al salalen structures.[11, 13] Within the Al(**22**)Me structure the N_{amine} centre (N1) is illustrated in the *R* configuration, and the carbon centres of the 1,2-DACH in the *S*,*S* configuration. The crystal contains a centre of inversion which allows inversion of the structure to obtain the diastereomers configuration Al-(*S*)-N_{amine}, (*R*,*R*)-1,2-DACH. Conversely, the literature solid-state structure for Al(*R*,*R*-**22**)Cl exclusively adopted the Al-(*S*)-N_{amine}, (*R*,*R*)-1,2-DACH diastereomer,[13] due to chirality limitations within the synthetic procedure. Additionally the solid-state structure for the chirally resolved Al(*R*,*R*-**22**)Me was modelled as the exclusive Al-(*R*)-N_{amine}, (*R*,*R*)-1,2-DACH diastereomers (Figure 6.04). The identification of multiple stereo-isomers is pertinent to further characterisation. A benzyloxy aluminium salalen complex {Al(**25**)OBn} was structurally determined by X-ray crystallography and identified as the Al-(*R*)-N_{amine}, (*R*,*R*)-1,2-DACH diastereomers (Figure 6.05), a centre of inversion allows the Al-(*S*)-N_{amine}, (*S*,*S*)-1,2-DACH diastereomer. To our knowledge no solid-state structures of aluminium salalen complexes containing non-^{t}Bu phenoxy substituents upon the salan segment, or aluminium bound alkoxy groups have been previously reported.

The solid-state structures for all the salalen complexes discussed in table 6.01 show the same trends in bond lengths (Å) and angles (°). Al(**22**)Me and Al(*R*,*R*-**22**)Me show very similar bond lengths and angles. However, there is a clear twist of the amine phenoxy ring between the diastereomers, which is demonstrated through a torsion angle measured between $C_{1\text{-DACH}}$-N1-C_{amine}-$C_{phenoxy}$ (Table 6.02). Similar torsion angles are observed between Al(**22**)Me and Al(*R*,*R*-**22**)Cl[13] as they can both be the Al-(*S*)-N_{amine}, (*R*,*R*)-1,2-DACH diastereomer. Therefore, Al(*R*,*R*-**22**)Me and Al(**25**)OBn have comparable torsion angles as they can both be represented as the Al-(*R*)-N_{amine}, (*R*,*R*)-1,2-DACH diastereomer.

	Al(**22**)Me	Al(*R*,*R*-**22**)Me	Al(**25**)OBn	Al(*R*,*R*-**22**)Cl[13]	Al(Salen)Et[20]	Al(Salan)Et[10]
Al1-O1	1.768(4)	1.7665(15)	1.7714(11)	1.747(2)	1.802(4)	1.763(2)
Al1-O2	1.831(4)	1.8339(13)	1.8065(10)	1.800(2)	1.821(4)	1.793(2)
Al1-N1	2.179(5)	2.2083(16)	2.1192(12)	2.124(2)	2.046(5)	2.448(2)
Al1-N2	1.978(6)	1.9801(17)	1.9652(12)	1.960(2)	2.011(6)	2.039(2)
Al1-C1	1.966(7)	1.968(2)	1.7335(11)[a]	2.187(1)[b]	1.969(7)	1.972(3)
N1-C (Amine)	1.478(8)	1.492(3)	1.492(2)	1.500(3)	---	1.494(3)
	---	---	---	---	---	1.520(3)
N2=C (Imine)	1.303(8)	1.306(2)	1.298(2)	1.292(3)	1.291(7)	---
	---	---	---	---	1.292(8)	---
O1-Al1-N1	88.8(2)	87.73(6)	88.71(5)	91.24(9)	86.5(2)	84.89(7)
O2-Al1-N2	87.6(2)	88.62(6)	89.65(5)	88.66(9)	88.0(2)	91.53(8)
C1-Al1-N1	95.1(3)	94.27(8)	90.11(5)[a]	91.84(7)[b]	101.9(3)	88.59(9)
C1-Al1-N2	121.5(3)	121.87(9)	113.22(5)[a]	120.57(7)[b]	106.7(3)	119.7(1)
N1-Al1-N2	77.7 (2)	77.93(6)	80.49(5)	79.34(9)	77.6(2)	78.11(7)
O1-Al1-O2	93.0(2)	94.43(6)	90.68(5)	94.81(9)	89.4(2)	95.81(8)

Table 6.01: Selected bond lengths (Å) and angles (°) for aluminium salalen compounds and comparative literature complexes, Al(*R*,*R*-**22**)Cl[13], Al(Salen)Et,[20] Al(Salan)Et.[10] [a] O3 was substituted for C(1), [b] Cl was substituted for C(1).

	Torsion angle $C_{1\text{-DACH}}$-N1-C_{amine}-$C_{phenoxy}$
Al(**22**)Me	46.6(7)
Al(*R*,*R*-**22**)Me	178.4(1)
Al(**25**)OBn	177.9(1)
Al(*R*,*R*-**22**)Cl[13]	45.8(3)

Table 6.02: Selected torsion angles (°) for 1,2-DACH-Salalen structures.

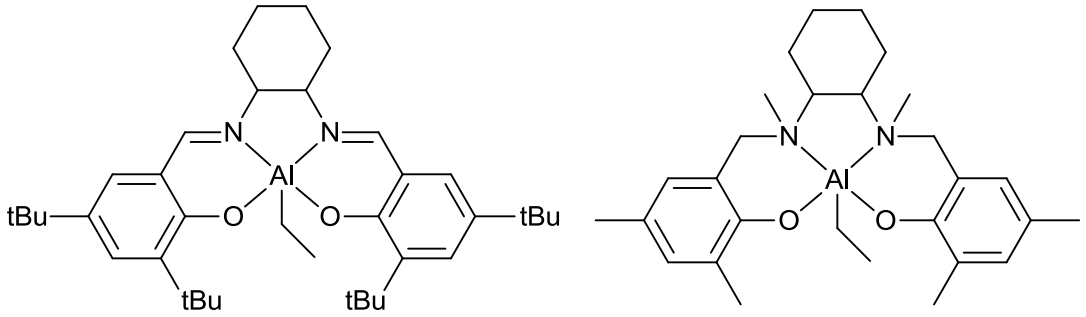

Figure 6.06: Depiction of Al(Salen)Et[20] and Al(Salan)Et[10] used for structural comparison (Table 6.01).

As expected there is a clear difference in imine and amine bond lengths. Imine bond lengths (C=N) in these complexes {Al(**22**)Me, Al(*R*,*R*-**22**)Me, Al(**25**)OBn} are between 1.298(2) - 1.306(2) Å, which are consistent with the literature solid-state salen complex {Al(Salen)Et} (Figure 6.06).[20] Moreover, amine-benzyl bond lengths {1.478(8) – 1.492(3) Å} are consistent with previously reported DACH salan complexes.[10] The Al-$N1_{amine}$ bonds are longer {2.1192(12) - 2.2083(16) Å} than Al-$N1_{imine}$ bonds {1.9652(12) - 1.9801(17) Å}. Furthermore, the Al-N_{imime} bonds in aluminium salalen complexes are similar to equivalent bonds within 1,2-DACH salen species {Al(Salen)Et} (Figure 6.06). Within the Al(salan)Et structure the Al-N_{amine} bonds are not equal indicating a bias to coordinate more strongly to one N_{amine} over the other.[10] The angles between equatorial and axial groups within the benzyloxy salalen complex Al(**25**)OBn converge towards 90 ° when compared to Al(**22**)Me or Al(*R*,*R*-**22**)Me. The reduced

steric demands of the amine phenoxy substituents possibly allow the ligands to orientate towards a less distorted trigonal bipyramidal structure.

6.3.3 Solution characterisation of aluminium *trans*-1,2-DACH salalen complexes

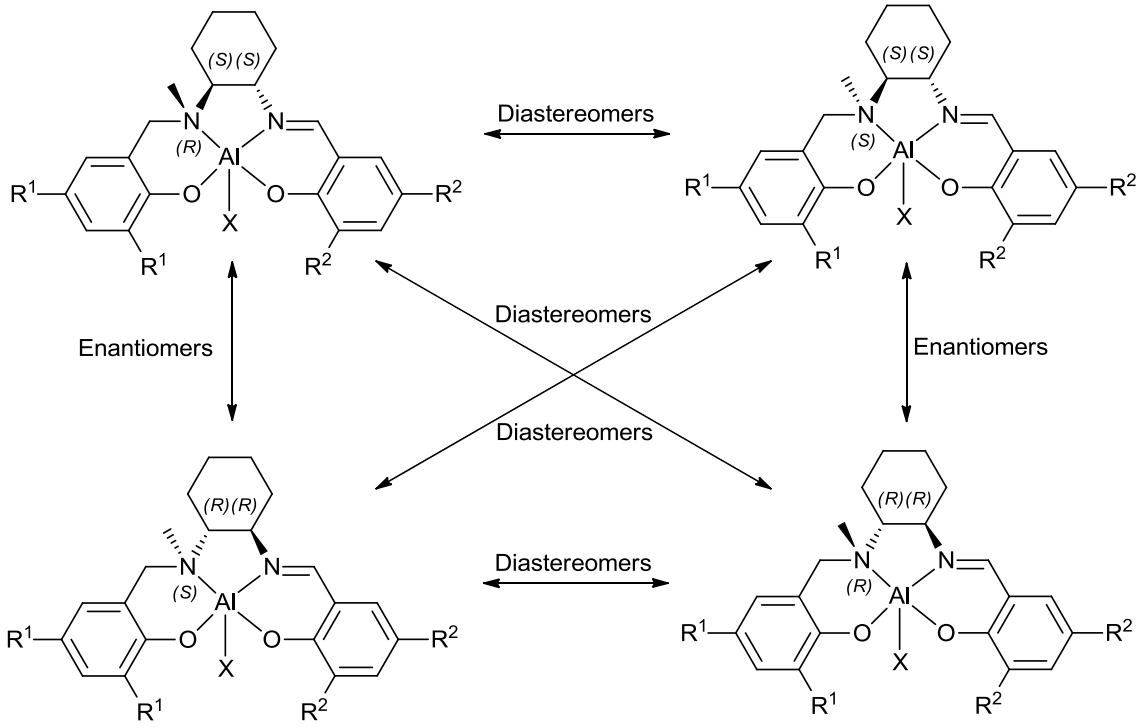

Figure 6.07: Depiction of the possible diastereomers and enantiomers that aluminium salalen complexes can adopt.

There are three chiral centres in the ligands when coordinated, with the *trans*-1,2-DACH ring locked in either *R*,*R* or *S*,*S* configurations, the amine becomes chiral once coordinated. The aluminium metal is also a chiral centre. There are four possible diastereomers configurations {Al-(*R*)-N_{amine}, (*S*,*S*)-1,2-DACH}, {Al-(*S*)-N_{amine}, (*S*,S)-1,2-DACH}, {Al-(*S*)-N_{amine}, (*R*,*R*)-1,2-DACH}, {Al-(*R*)-N_{amine}, (*R*,*R*)-1,2-DACH} (Figure 6.07). Due to the locked configurations (*R*,*R*, *S*,*S*) of the DACH ring the system can be considered as a diastereomer system. As discussed before two possible diastereomers are present in the solid-state structure for Al(**22**)Me, in this scenario the diastereomers are enantiomers. The solid-state structure was also supported by solution NMR spectroscopy.

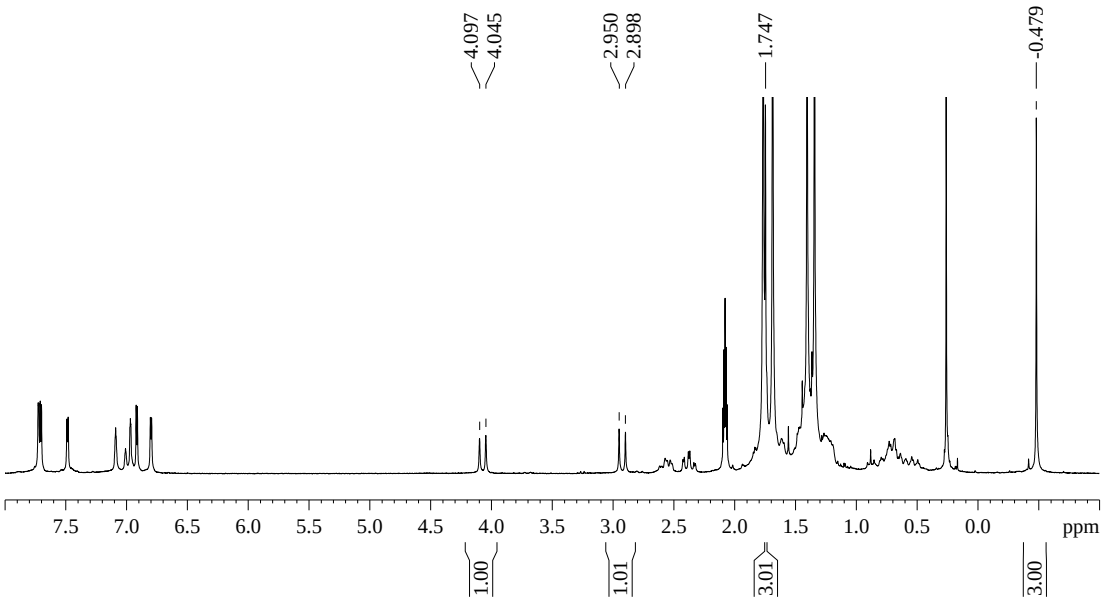

Figure 6.08: Al(**22**)Me ^{1}H NMR spectrum for the isolated enantiomers {Al-(*S*)-N_{amine}, (*R*,*R*)-1,2-DACH} and {Al-(*R*)-N_{amine}, (*S*,*S*)-1,2-DACH}.

A single pair of enantiomers, as opposed to diastereomers, is demonstrated by the ^{1}H NMR spectrum (Figure 6.08) of the X-ray crystallographically determined compound Al(**22**)Me. The two enantiomers present in the solution state are not distinguishable by conventional ^{1}H NMR spectroscopy. A single Al-Me resonance was identified at low chemical shift (-0.48 ppm), alongside a single N_{amine}-Me resonance, indicating a single diastereomer. Doublets at 2.92 ppm and 4.07 ppm are identified as inequivalent N_{amine}-C-$\mathbf{H}_2$ protons. Therefore, demonstrating structural rigidity around the N_{amine} region and reinforcing the presence of a single pair of enantiomers.

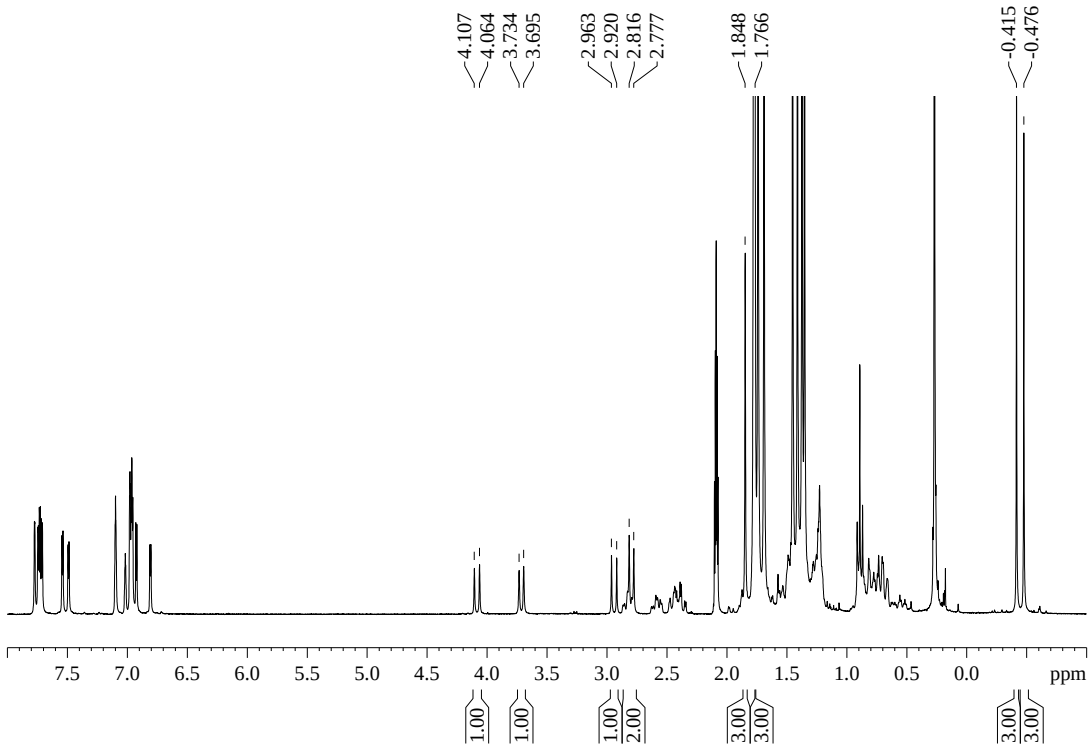

Figure 6.09: Al(*R*,*R*-**22**)Me ^{1}H NMR spectrum depicting the diastereomers {Al-(*S*)-N_{amine}, (*R*,*R*)-1,2-DACH} and {Al-(*R*)-N_{amine}, (*R*,*R*)-1,2-DACH}.

The ^{1}H NMR spectrum for Al(*R*,*R*-**22**)Me suggests the presence of two diastereomers in solution (Figure 6.09). This observation is not consistent with a single diastereomers in the solid-state as characterised by X-ray crystallography. Two Al-Me resonances are present in the ^{1}H NMR spectrum. The Al-Me resonance at -0.48 ppm is consistent with the previously discussed Al(**22**)Me structure and is attributed to the {Al-(*S*)-N_{amine}, (*R*,*R*)-1,2-DACH} isomer exclusively, due to (*R*,*R*)-1,2-DACH being used as the staring material disallowing its enantiomer {Al-(*R*)-N_{amine}, (*S*,*S*)-1,2-DACH}. Under the same principle the resonance at -0.42 ppm is attributed to the X-ray crystallography determined diastereomers {Al-(*R*)-N_{amine}, (*R*,*R*)-1,2-DACH}. The N-Me resonances at 1.76 and 1.84 ppm were assigned to the {Al-(*S*)-N_{amine}, (*R*,*R*)-1,2-DACH} and {Al-(*R*)-N_{amine}, (*R*,*R*)-1,2-DACH} respectively. The N_{amine}-C-$\mathbf{H}_2$ doublets at 2.94 ppm and 4.08 ppm confirm the presence of the {Al-(*S*)-N_{amine}, (*R*,*R*)-1,2-DACH} diastereomer. Two doublets at 2.80 ppm and 3.72 ppm were assigned to N_{amine}-C$\mathbf{H}_2$ protons from the {Al-(*R*)-N_{amine}, (*R*,*R*)-1,2-DACH}, the 4.08 ppm resonance is significantly shifted upfield from its analogous 3.72 ppm N_{amine}-C-$\mathbf{H}_2$ resonance.

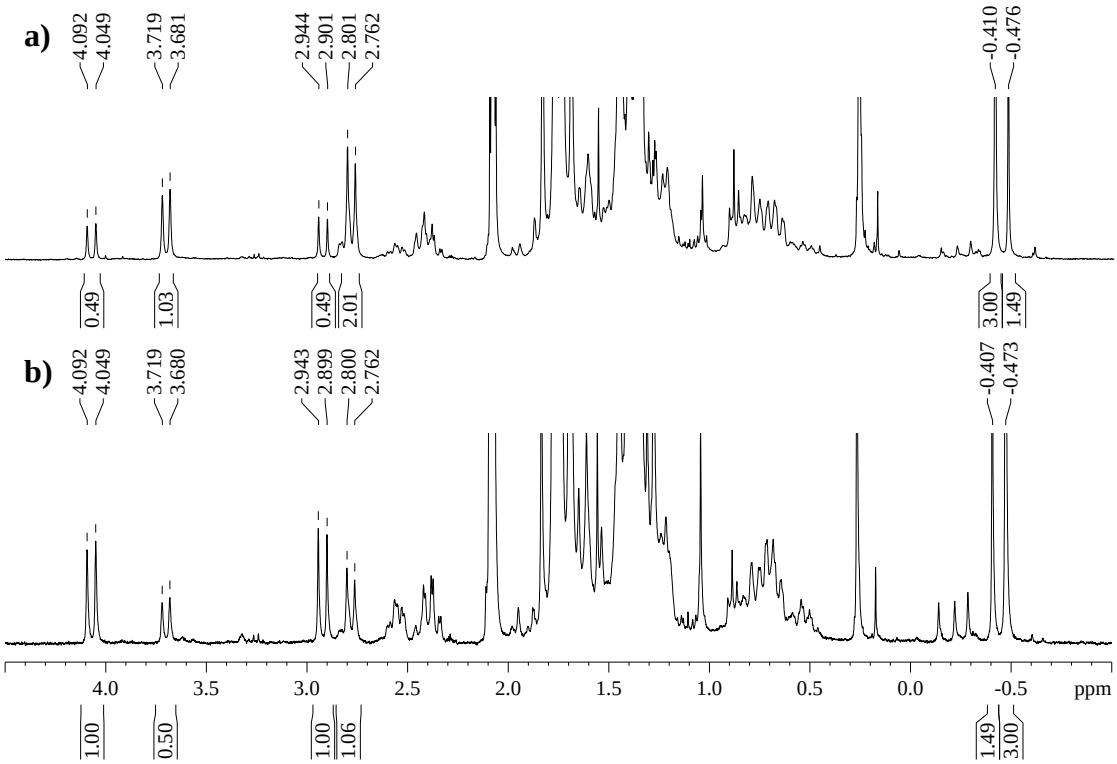

Figure 6.10: a) The ^{1}H NMR spectrum of the crystallised product of Al(**22**)Me showing a bias towards the {Al-(*S*)-N_{amine}, (*R*,*R*)-1,2-DACH} and {Al-(*R*)-N_{amine}, (*S*,*S*)-1,2-DACH} enantiomer pairing. b) The ^{1}H NMR spectrum for the further crystallised product from the same solution, resulting in a bias towards the {Al-(*R*)-N_{amine}, (*R*,*R*)-1,2-DACH} and {Al-(*S*)-N_{amine}, (*S*,*S*)-1,2-DACH} enantiomer pairing.

The exact diastereomers isolated is dependent upon the crystallisation conditions. A further attempt at synthesising Al(**22**)Me resulted in a mixture of diastereomers (Figure 6.10a), in this specific example the {Al-(*R*)-N_{amine}, (*R*,*R*)-1,2-DACH}/ {Al-(*S*)-N_{amine}, (*S*,*S*)-1,2-DACH} enantiomer pairing was isolated in a 2:1 majority. Further crystallisation of the resulting solution resulted in the opposite enantiomer pairing ({Al-(*S*)-N_{amine}, (*R*,*R*)-1,2-DACH}/{Al-(*R*)-N_{amine}, (*S*,*S*)-1,2-DACH}) as the major product in a 2:1 ratio (Figure 6.10b). This dependence on crystallisation conditions is not a unique phenomenon and the other aluminium complexes discussed here have also been isolated as mixtures of diastereomers or specific enantiomer pairs. All of the aluminium methyl salalen complexes {Al(**23-25,28**)Me} were isolated as the {Al-(*R*)-N_{amine}, (*R*,*R*)-1,2-DACH}/{Al-(*S*)-N_{amine}, (*S*,*S*)-1,2-DACH} enantiomer pairings with the exception of Al(**22**)Me (Figure 6.11).

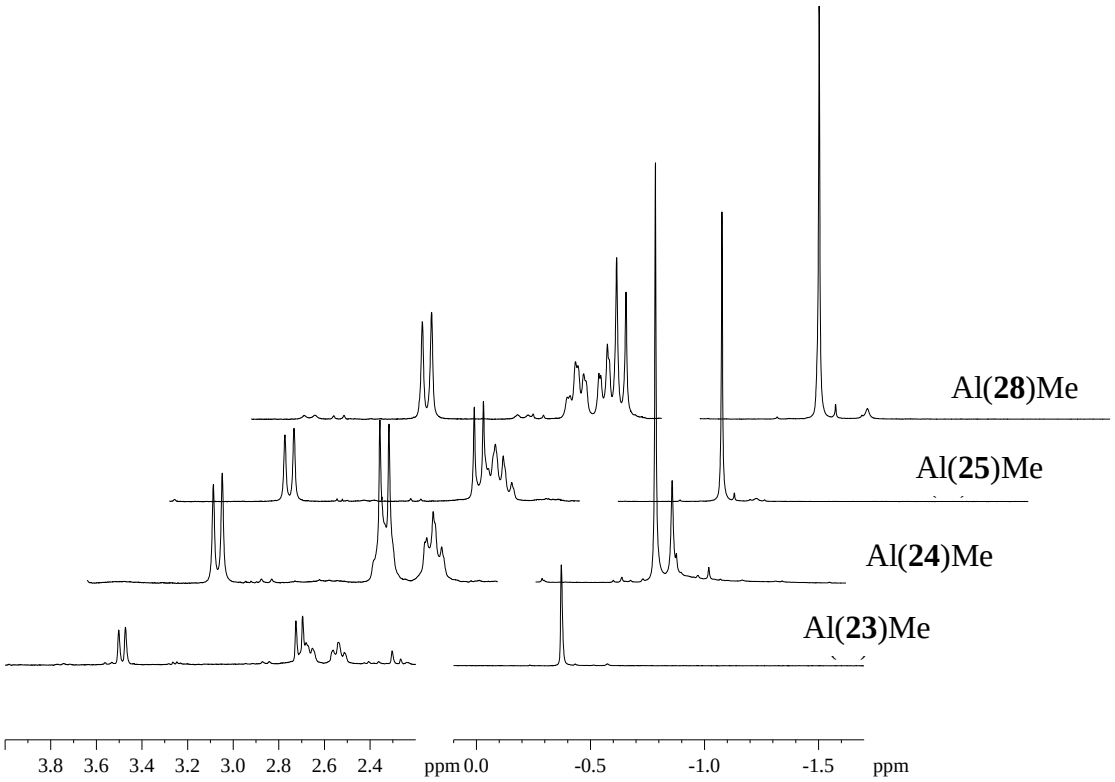

Figure 6.11: Truncated [1]H NMR spectrum showing aluminium methyl salalen complexes isolated enantiomer pairs.

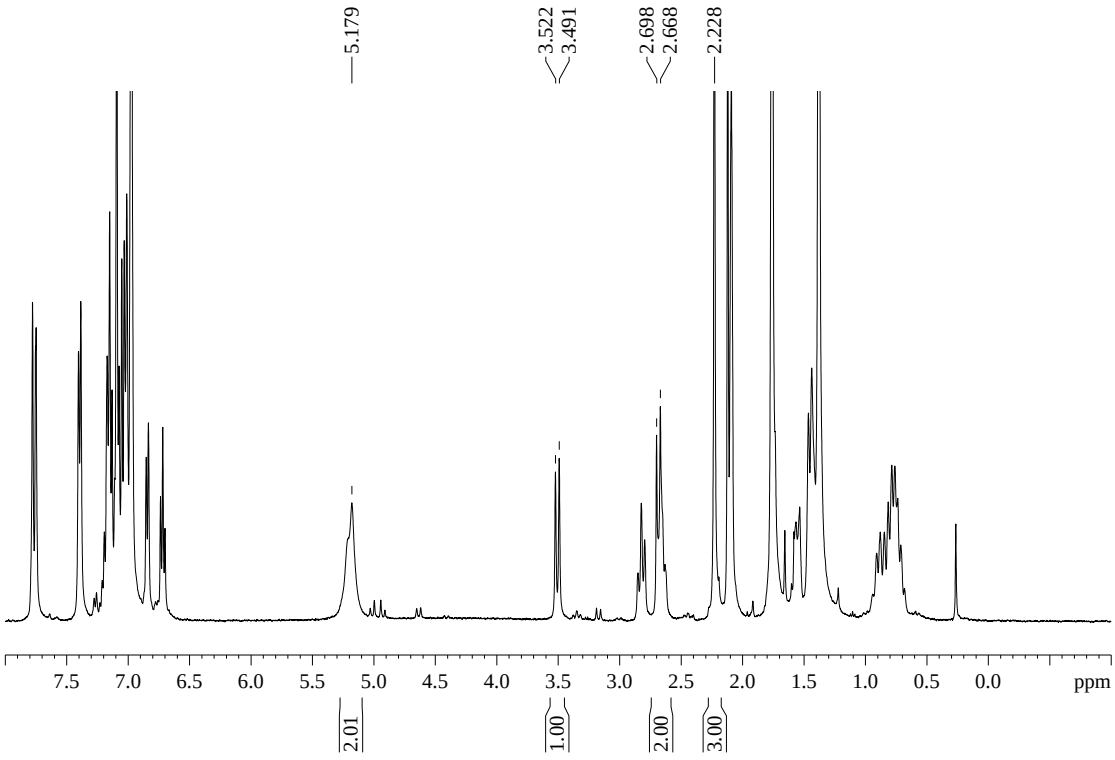

Figure 6.12: [1]H NMR spectrum for Al(**25**)OBn

The aluminium benzyloxy salalen complexes displayed similar characteristic to their aluminium methyl counterparts. The solid-state structure for the Al(**25**)OBn complex was identified as the {Al-(*R*)-N_{amine}, (*R*,*R*)-1,2-DACH}/{Al-(*S*)-N_{amine}, (*S*,*S*)-1,2-DACH} enantiomer pairing. Additionally one enantiomer pairing is observed in solution (Figure 6.12), the characteristic amine CH_2 protons are represented as two doublets at 3.51 ppm and 2.67 ppm. In this case the doublet at 2.67 ppm also coincides with a CH proton from the DACH ring. There is significant broadening of the CH_2 protons about the OBn moieties representing a degree of fluxionality about the OBn group.

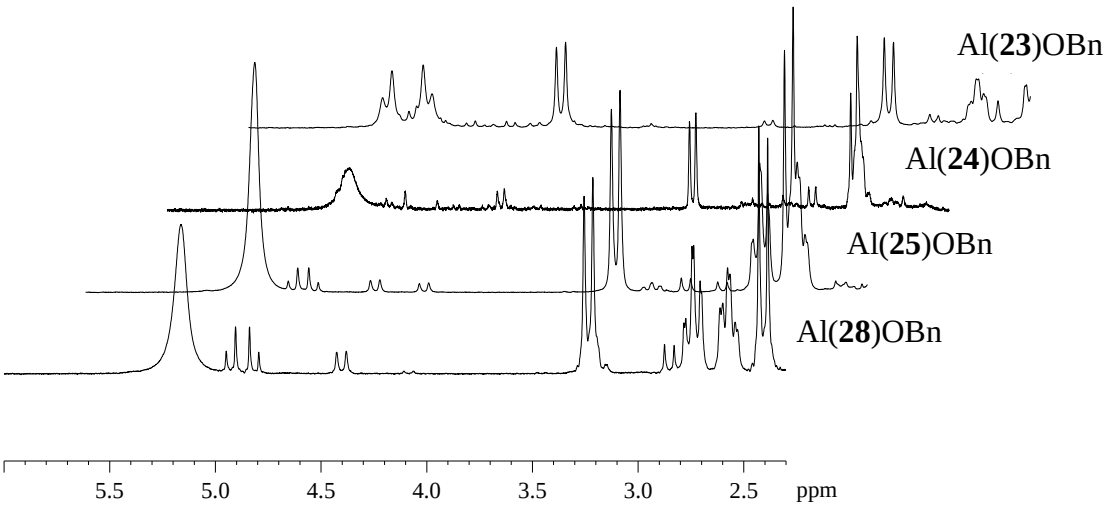

Figure 6.13: ^{1}H NMR spectra of Al(**23**-**25**,**28**)OBn salalen complexes isolated with an enantiomer pair as the major product.

Akin to the Al-Me salalen complexes the diastereomers isolated for the Al(**22**-**30**)OBn complexes is highly dependent upon crystallisation conditions. Al(**24,25,28**)OBn were obtained as the enantiomer pair {Al-(*R*)-N_{amine}, (*R*,*R*)-1,2-DACH}/{Al-(*S*)-N_{amine}, (*S*,*S*)-1,2-DACH} as the major product, as evident from the CH_2 proton resonances of the ^{1}H NMR spectra (Figure 6.13). Only Al(**23**)OBn formed the {Al-(*S*)-N_{amine}, (*R*,*R*)-1,2-DACH}/{Al-(*R*)-N_{amine}, (*S*,*S*)-1,2-DACH} enantiomer pair as the major product, indicated by the significant shift of the amine CH_2 protons (Figure 6.13). The other aluminium benzyloxy {Al(**22**,**26**,**27**,**29**,**30**)OBn} complexes were isolated as a mixtures of diastereomers in approximate 1:1 ratios.

Upon heating (80 °C, toluene) an aluminium salalen complex, which was isolated as a single enantiomer pairing, the alternate enantiomer pairing is formed. This observation is true for aluminium methyl salalen complexes and their benzyloxy derivatives. Significant inter-conversion occurs after exposure to elevated temperatures for 30 mins. This is clearly demonstrated by figure 6.14, Al(**22**)Me was heated (80 °C) for 4 hours and the resulting spectrum (figure 6.14) shows the presence of two diastereomers. The stereomeric mixture equilibrates at a 1:1 ratio so there is presumably little difference in energy between the various diastereomers in solution. This is of significant importance, as *rac*-lactide ROP was conducted above 80 °C. The complexes can be considered as mixtures of diastereomers within the polymerisations, irrelevant of the stereomeric form a specific aluminium salalen complex is isolated as.

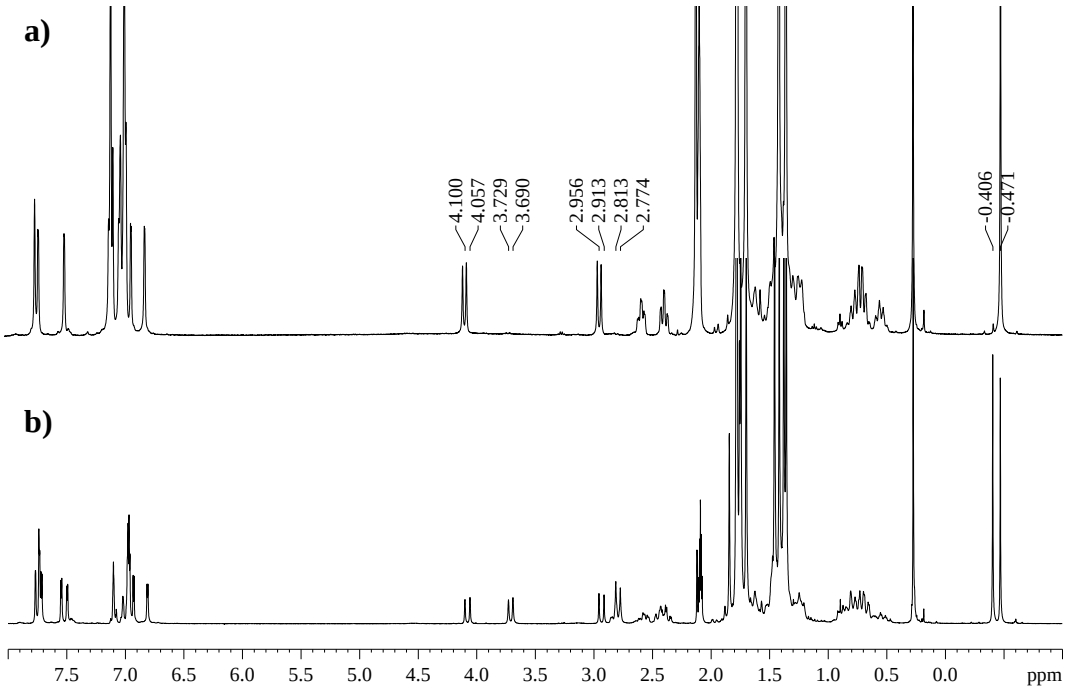

Figure 6.14: a) ^{1}H NMR spectrum of Al(**22**)Me at 20 °C. b) ^{1}H NMR spectrum of Al(**22**)Me after heating (4h, 80 °C).

6.4 Ring-Opening-Polymerisation of *rac*-Lactide

The aluminium salalen complexes were trialled as initiators for the ROP of *rac*-lactide in solution and solvent free conditions. The aluminium methyl salalen complexes require the addition of one equivalent of benzyl alcohol as a co-initiator to

form the presumed *in-situ* benzyloxy complex. The isolated aluminium benzyloxy complexes were utilised without the addition of a co-initiator. Only the aluminium salalen benzyloxy complexes were used for solvent free ROP reactions due to practical complications.

6.4.1 Solution ROP of *rac*-lactide

Solution polymerisations were performed in 10 ml of toluene at 80 °C using 1.0 g of *rac*-lactide in all cases. A 100:1 lactide to initiator ratio was utilised and one equivalent of benzyl alcohol was introduced as a co-initiator where required. Aluminium salen complexes are typically slow,[5, 6] particularly in the case of salen complexes with a 1,2-DACH bridging group where 12 days was required to achieve appreciable conversion at 70 °C.[7] Within this report a typical polymerisation required 4 days to reach acceptable conversions, the data is given in table 6.03. Polymerisations of *rac*-lactide using Al(**25**)OBn and Al(**28**)OBn initiators yielded low conversion and as such were repeated and allowed 10 days reaction time.

The reactions reached appreciable conversion although the presence of a ^{t}Bu group on the salen moiety significantly reduced conversion. This is presumably a steric effect although this is in conjunction with the orientation of the salen phenoxy, as the same effect is not observed to such a degree when considering the salan section. The effect of the salen phenoxy substituent upon rate is investigated later in this chapter (see figure 6.18). Molecular weight distributions are narrow with PDI values ranging between 1.06 - 1.67. The resulting tacticity of the PLA is defined by the phenoxy group substituents upon the Al salalen initiators. The initiators containing ^{t}Bu-phenoxy substituents on the imine and amine sections {Al(**22**)Me, Al(*R*,*R*-**22**)Me, Al(**22**)OBn} were the least active initiators investigated in this series. The molecular weights (M_n) were much higher than anticipated for the low conversion polymers produced by Al(**22**)Me and Al(*R*,*R*-**22**)Me initiators. It was speculated that not all of the Al(**22**)Me and Al(*R*,*R*-**22**)Me initiators initiated a growing polymer chain.

	Time (days)	Conv. (%)[a]	M_n[b] *(theo)*	M_n[c]	PDI[c]	P_r[d]
Al(**22**)Me	4	34	5000	8950	1.06	0.49
Al(*R*,*R*-**22**)Me	4	30	4400	10100	1.06	0.55
Al(**22**)OBn	4	26	3900	3750	1.08	0.54
Al(**23**)Me	4	71	10300	12200	1.07	0.65
Al(**23**)OBn	4	91	13200	19550	1.12	0.61
Al(**24**)Me	4	97	14100	17150	1.35	0.60
Al(**24**)OBn	4	99	14400	17000	1.18	0.69
Al(**25**)Me	4	83	12100	7700	1.06	0.57
Al(**25**)OBn	10	40	5900	6400	1.08	0.42
Al(**26**)OBn	4	96	13900	24600	1.12	0.56
Al(**27**)OBn	4	96	13900	19900	1.27	0.54
Al(**28**)Me	4	61	8900	7100	1.07	0.54
Al(**28**)OBn	10	49	7200	8300	1.06	0.31
Al(**29**)OBn	4	96	13900	14600	1.67	0.54
Al(**30**)OBn	4	99	14400	19350	1.15	0.73

Table 6.03: Solution ROP of *rac*-lactide for Al(**22-25**,**28**)Me and Al(**22-30**)OBn initiators. 10 ml of toluene, 80 °C, 100:1:1 [*rac*-lactide]:[initiator]:[benzyl alcohol]*where required. [a] Conversion ascertained by ^{1}H NMR spectroscopy. [b] Theoretical molecular weight calculated from conversion (Conv. × 100 × 144.13 + 108.14), [c] Molecular weight and PDI determined by GPC (THF) using polystyrene standards without applying a correction factor. [d] P_r as calculated from ^{1}H NMR homonuclear decoupling spectroscopy in $CDCl_3$.

A slight heterotactic bias was typically obtained when the salan phenoxy contained ^{t}Bu moieties Al(**23**,**24**)Me/OBn. Interestingly, the introduction of ^{t}Bu group upon the salen phenoxy resulted in the production of PLA with a slight isotactic bias for Al(**25**,**28**)OBn initiators (Figure 6.15), this was not observed for Al(**22**)OBn or analogous Al(**25**,**28**)Me initiators. Moreover, the *in-situ* reactions using Al(**22-25,28**)Me initiators with BnOH co-initiator gave different yields and selectivity than their Al(**22-25,28**)OBn analogues. It was postulated that multiple initiating species were being produced during the *in-situ* reactions, whereas the isolated Al(**22-25,28**)OBn initiators were comparatively well defined.

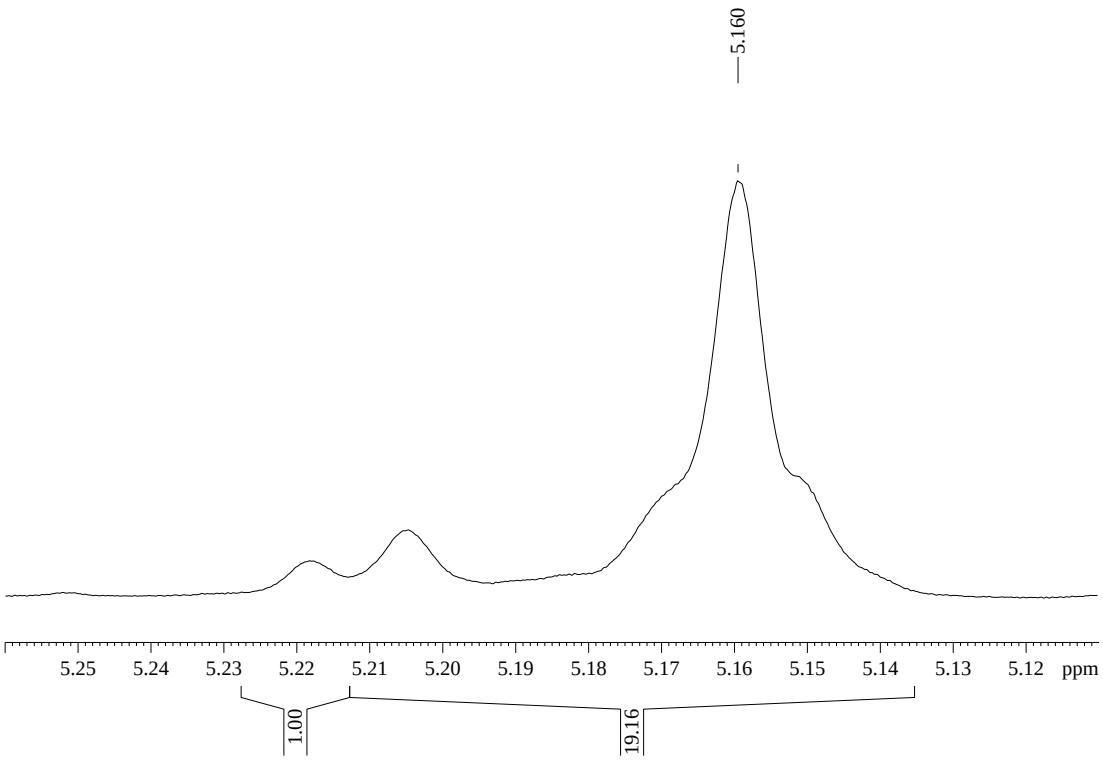

Figure 6.15: ^{1}H NMR homonuclear decoupled spectrum showing tetrad resonances for the ROP of *rac*-lactide by Al(**28**)OBn in toluene at 80 °C.

The introduction of chloro-substituents upon the salen phenoxy ring gave an increase in conversion all achieving > 96 % conversion after 4 days at 80 °C in toluene (See table 6.03; Al(**24**)Me, Al(**24**,**27**,**30**)OBn). Narrow molecular weight distributions were still obtained and the resulting PLA revealed some heterotactic selectivity (P_r = 0.54 – 0.73). The homonuclear decoupled ^{1}H NMR spectrum for PLA produced by Al(**30**)OBn is given in figure 6.16, a clear enhancement of the [*isi*] and [*sis*] tetrads at 5.15 ppm and 5.22 ppm is observed. This switch to a heterotactic preference and enhanced activity is presumably an electronic effect, a direct result of the chloro-phenoxy substituents. The 1,2-DACH salalen aluminium initiators series show enhanced rates when compared to prior 1,2-DACH salen aluminium initiators, although the stereoselectivity was not maintained.[7, 8]

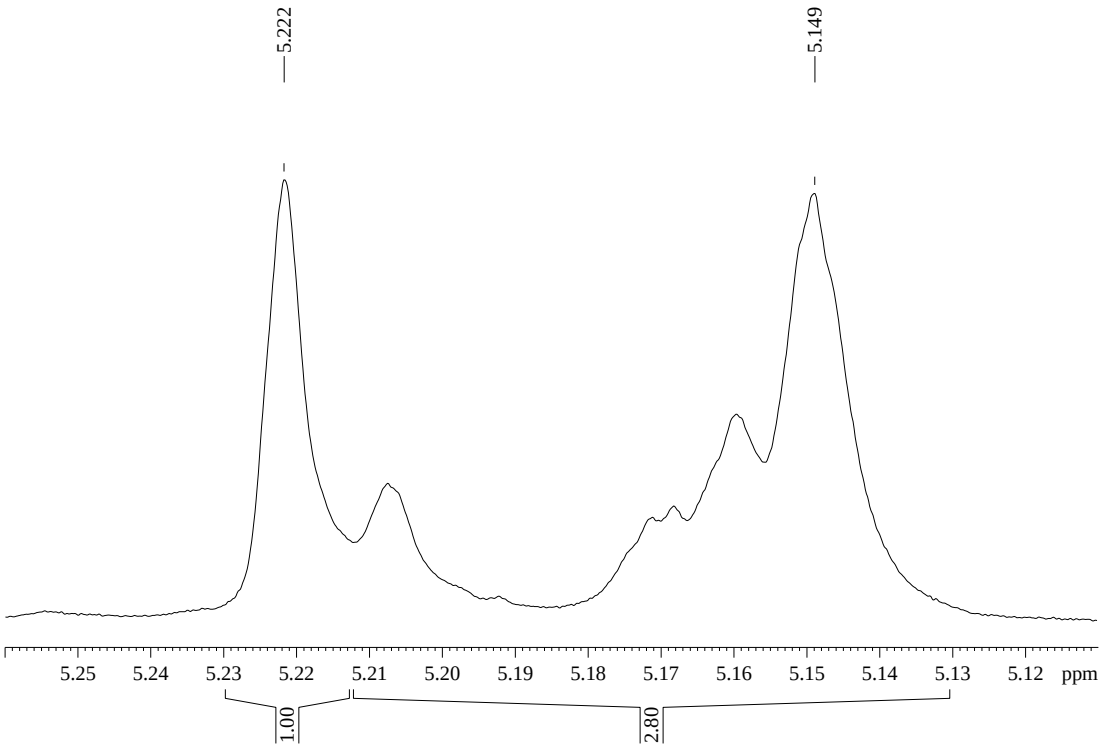

Figure 6.16: ^{1}H NMR homonuclear decoupled spectrum showing tetrad resonances for the ROP of *rac*-lactide by Al(**30**)OBn in toluene at 80 °C.

6.4.2 Solvent free ROP of *rac*-lactide

Solvent free polymerisations were performed at 130 °C where 1.0 g of *rac*-lactide was melted in the presence of Al(**22**-**30**)OBn initiators, the reaction was allowed to proceed for the amount of time given in table 6.04. The isolated benzyloxy initiators {Al(**22**-**30**)OBn} allowed the solvent free ROP reactions to be conducted. When the aluminium salalen initiator contained chloro or hydrogen substituents on both the salan and salen phenoxy groups good conversion is obtained in 2 h. On the other hand the steric bulk associated with the ^{t}Bu moieties of the initiator Al(**22**)OBn reduces activity, hence 48 hours is required for appreciable conversion to be obtained. It was speculated that isolated complex diastereomers interconvert at the higher temperatures in melt conditions, although direct analysis of the initiators under these condition is complicated.

	Time (h)	Conv. (%)[a]	M_n[b] *(theo)*	M_n[c]	PDI[c]	P_r[d]
Al(**22**)OBn	48	30	13100	7850	1.07	0.54
Al(**23**)OBn	24	85	36900	57600	1.51	0.58
Al(**24**)OBn	24	91	39500	48150	1.71	0.64
Al(**25**)OBn	24	27	11800	9100	1.06	0.41
Al(**26**)OBn	2	42	18300	28700	1.07	0.51
Al(**27**)OBn	2	94	40800	33350	1.10	0.57
Al(**28**)OBn	24	68	29500	14300	1.56	0.43
Al(**29**)OBn	2	98	42500	46550	1.47	0.61
Al(**30**)OBn	24	60	26100	23350	1.14	0.72

Table 6.04: Solvent free ROP of *rac*-lactide for initiators Al(**22-30**)OBn at 130 °C, 300:1 [*rac*-lactide]:[initiator] ratio. [a] Conversion ascertained by ^{1}H NMR spectroscopy. [b] Theoretical molecular weight calculated from conversion (Conv. × 300 × 144.13 + 108.14), [c] Molecular weight and PDI determined by GPC (THF) using polystyrene standards without applying a correction factor. [d] P_r as calculated from ^{1}H NMR homonuclear decoupling spectroscopy in $CDCl_3$.

The melt polymerisation data is shown in table 6.04, notably ^{t}Bu moieties on either the salan or salen phenoxy groups gave lower conversions. At elevated temperature narrow molecular weight distributions could still be obtained for Al(**22,25-27,30**)OBn (PDI = 1.06 - 1.14). Parallel to the solution ROP of *rac*-lactide heterotacticly biased PLA was obtained when chloro substituents were present on the salen phenoxy (P_r = 0.57 – 0.72), no loss in stereoselectivity was observed at the elevated temperature. The homonuclear decoupled ^{1}H NMR spectrum of PLA produced by Al(**30**)OBn used to determine PDI is given in figure 6.17, a significant enhancement of the [*isi*] and [*sis*] tetrads is shown. Analogous to the solution state polymerisations ^{t}Bu groups on the salen segment results in a slight isotactic bias (P_r = 0.41 – 0.43), with the exception of the Al(**22**)OBn initiator.

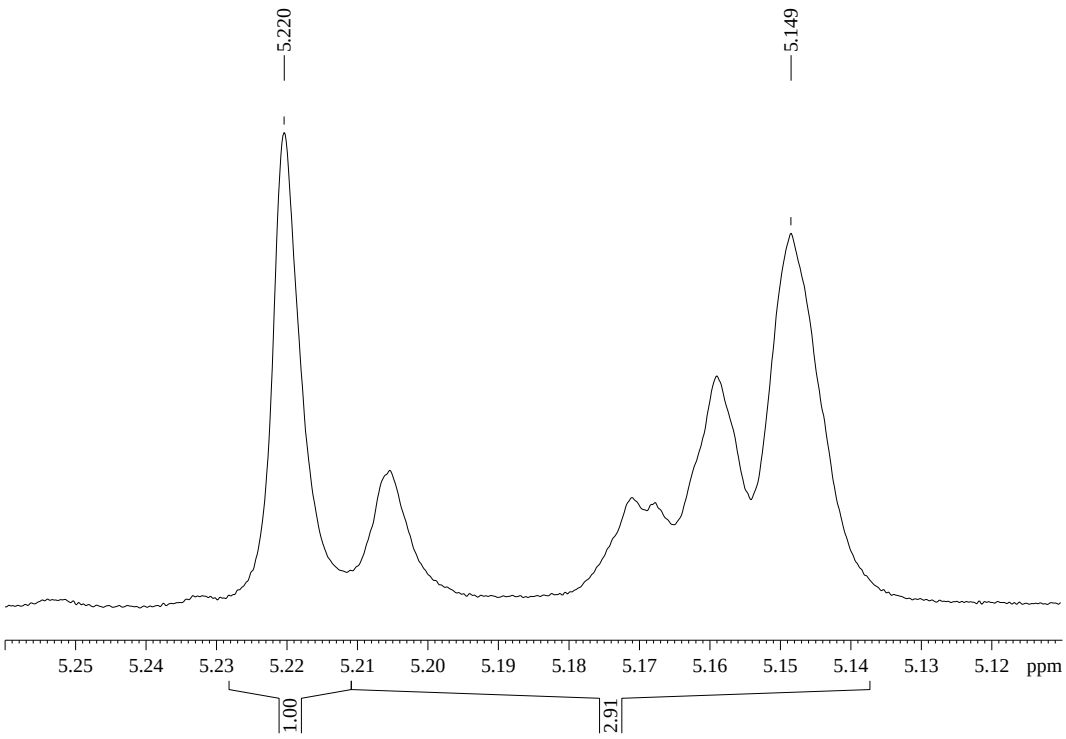

Figure 6.17: ^{1}H NMR homonuclear decoupled spectrum showing tetrad resonances for the ROP of *rac*-lactide by Al(**30**)OBn under solvent free conditions.

6.4.3 Kinetic investigation for the solution ROP of *rac*-lactide

Kinetic experiments were performed to analyse the apparent rate of propagation of the ROP of *rac*-lactide by 1,2-DACH aluminium salalen complexes. The effect of the changing the substituents on the salen phenoxy was investigated. The kinetic experiments were performed on an NMR scale using 0.05 g of *rac*-lactide in a 100:1 ratio with an aluminium initiator {Al(**25**-**27**)OBn} at 80 °C in d_8-toluene. The graph of $\ln([LA]_0/[LA]_t)$ versus time gave *pseudo* first order linear plots (Figure 6.18). The aluminium salalen complexes chosen for kinetic analysis contained hydrogen substituents on the salan phenoxy, ^{t}Bu, H, and Cl substituents were investigated on the salen phenoxy. The apparent first order rate constant was determined from the graph given in figure 6.18. When ^{t}Bu and H substituents are present upon the phenoxy ring long reaction times are required hence the spectra were recorded in greater than 24 h intervals. Contrastingly Cl substituents resulted in very high conversion after 24 h, hence a spectrum was recorded at 15 mins intervals.

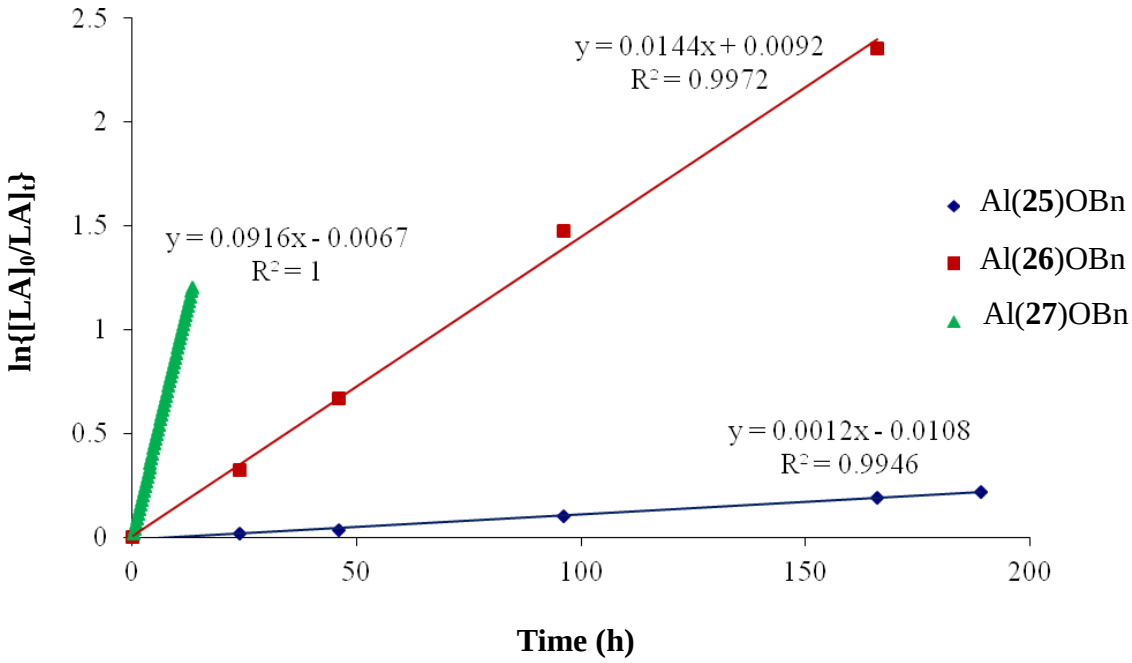

Figure 6.18: *Pseudo* first order plots for the ROP of *rac*-lactide by Al(**25-27**)OBn. 50 mg of *rac*-lactide in 0.6 ml of d_8-toluene at 80 °C at 100:1 [*rac*-lactide]:[initiator] ratio.

	k_{app} (min^{-1}) (× 10^{-5})	R^2
Al(**25**)OBn	2.00(7)	0.9946
Al(**26**)OBn	24.0(7)	0.9972
Al(**27**)OBn	153.7(1)	1.0000

Table 6.05: k_{app} values and R^2 values for ROP of *rac*-lactide by Al(**25-27**)OBn initiators

It can be clearly seen that ^{t}Bu salen phenoxy substituents hinder the ROP reaction rate, k_{app} = 2.00 × 10^{-5} min^{-1} (Table 6.05). A significant enhancement of around two orders of magnitude (152.71 × 10^{-5} min^{-1}) is observed when Cl moieties are present on the salen phenoxy ring. Previous salalen aluminium initiators trialled for the ROP of *rac*-lactide within the Jones group gave first order k_{app} between 13.80 × 10^{-5} - 33.53 × 10^{-5} min^{-1} for ^{t}Bu, Me, and H salan *ortho*-phenoxy substituents.[11] The 1,2-DACH salan complex synthesised by Feijen *et al.*[10] analogous to Al(**26**)OBn, containing hydrogen phenoxy substituents, gave a k_{app} = 448 × 10^{-5} min^{-1}. Feijen *et al.*[10] also reported that Cl substituents on salan phenoxy groups gave a reduction in apparent rate, k_{app} = 93.7 × 10^{-5} min^{-1}.

Previously reported salen *rac*-1,2-DACH complexes for the ROP of *rac*-lactide by Feijen *et al.*[8] gave k_{app} = 11.6 × 10^{-5} min^{-1} at 70 °C (62:1 *rac*-lactide to initiator ratio) this is comparable to the k_{app} reported for the ROP of *rac*-lactide by the salalen complex Al(**25**)OBn.

Kinetic investigations of the ROP of *rac*-lactide by Al(**28**)Me and Al(**28**)OBn was conducted. The experiments were performed at 80 °C in d_8-toluene using 0.05 g of *rac*-lactide in a 20:1 ratio, one equivalent of BnOH was added to the Al(**28**)Me initiated polymerisation. Apparent rates of propagation (k_{app}) were obtained from the gradient of *pseudo* first order rate plots (Figure 6.19). The *in-situ* Al(**28**)Me + BnOH initiator system was more than two times faster (k_{app} = 20.82 × 10^{-5} min^{-1}) than the less active Al(**28**)OBn initiator (k_{app} = 9.51 × 10^{-5} min^{-1}) (Table 6.06). The expected initiating species from the *in-situ* reaction of Al(**28**)Me + BnOH is Al(**28**)OBn. This rate difference indicated the active species from the *in-situ* reaction of Al(**28**)Me + BnOH were not identical to the isolated Al(**28**)OBn initiator. This demonstrates the formation of a discrete metal co-initiator species cannot always be assumed within *in-situ* ROP reactions.

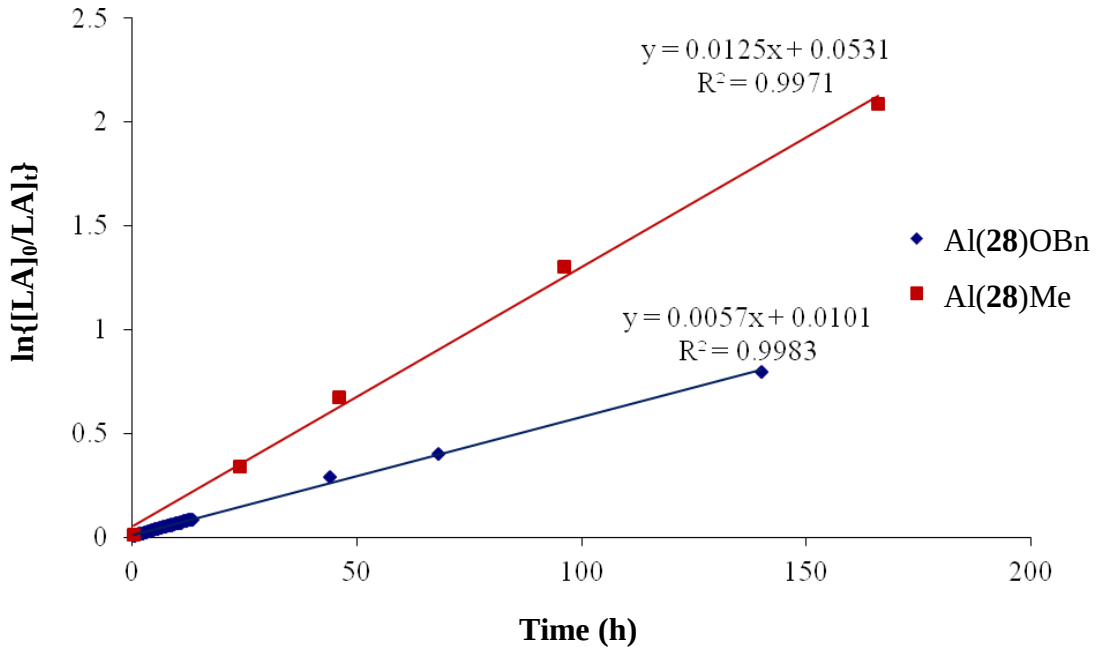

Figure 6.19: *Pseudo* first order plots for the ROP of *rac*-lactide by Al(**28**)Me with one equivalent of benzyl alcohol and Al(**28**)OBn at 80 °C in d_8-toluene. 50 mg of *rac*-lactide in 0.6 ml of d_8-toluene at 80 °C at 20:1 [*rac*-lactide]:[initiator] ratio, one equivalent of BnOH was added *in-situ* to the Al(**28**)Me initiator.

	k_{app} (min^{-1}) (×10^{-5})	R^2
Al(**28**)Me	20.8(6)	0.9971
Al(**28**)OBn	9.51(5)	0.9983

Table 6.06: k_{app} values and R^2 values for ROP of *rac*-lactide by Al(**28**)Me and Al(**28**)OBn initiators.

6.5 Conclusion

Further salalen ligands with a 1,2-DACH backbone {(**22**-**30**)H_2} were synthesised and characterised to expand the derivatives library for these ligands. Aluminium methyl complexes Al(**22**-**30**)Me were synthesised along with their benzyloxy derivatives Al(**22**-**30**)OBn. The majority of aluminium complexes {Al(**22**-**25,28**)Me, Al(**22**-**30**)OBn} were characterised by ^{1}H, $^{13}C\{^{1}H\}$ NMR spectroscopy and CHN analysis. Solid-state structures for Al(**22**)Me, Al(*R,R*-**22**)Me, and Al(**25**)OBn were determined by X-ray diffraction. X-ray diffraction demonstrated; Al(**22**)Me existed as the {Al-(*S*)-N_{amine}, (*R,R*)-1,2-DACH}/{Al-(*R*)-N_{amine}, (*S,S*)-1,2-DACH} diastereomers, Al(*R,R*-**22**)Me existed as the {Al-(*R*)-N_{amine}, (*R,R*)-1,2-DACH} diastereomer, Al(**25**)OBn existed as the {Al-(*R*)-N_{amine}, (*R,R*)-1,2-DACH}/{Al-(*R*)-N_{amine}, (*R,R*)-1,2-DACH} diastereomers. NMR spectroscopic investigations showed the isolation of isomers was possible with a dependence upon crystallisation conditions. However, in solution these isomers interconvert at high temperature (80 °C).

The ROP of *rac*-lactide was conducted using Al(**22**-**25,28**)Me, Al(*R,R*-**22**)Me, and Al(**22**-**30**)OBn initiators to investigate the effect of substituents (R = ^{t}Bu, H, and Cl) upon the imine (salen) side and amine (salan) side. Al(**22**-**25,28**)Me and Al(*R,R*-**22**)Me were investigated for the polymerisation of *rac*-lactide with benzyl alcohol as a co-initiator. The solution (toluene) ROP of *rac*-lactide attained appreciable conversion for the majority of cases in 4-10 days (80 ºC, 100:1 [*rac*-lactide]:[initiator] ratio). The solvent free ROP of *rac*-lactide resulted in appreciable conversion for Al(**22**-**30**)OBn initiators between 2-48 hours dependent upon the phenoxy substituents. Bulky ^{t}Bu phenoxy groups had a negative impact upon polymerisation rate, where rate follows Cl > H > ^{t}bu for Al(**25**-**27**)OBn

initiators. Selectivity ranged from moderately isotactic to moderately heterotactic (P_r = 0.31 - 0.73). Al(**25**,**28**)OBn initiators gave the strongest isotactic bias (P_r = 0.31 - 0.43) and Al(**30**)OBn revealed the strongest heterotactic bias (P_r = 0.72 - 0.73). A greater than two fold rate difference was observed between Al(**28**)Me + BnOH ($k_{app} = 20.82 \times 10^{-5}$ min^{-1}) and isolated Al(**28**)OBn initiator ($k_{app} = 9.51 \times 10^{-5}$ min^{-1}). This prompted speculation that the active species from Al(**28**)Me + BnOH contained other initiating complexes than just the Al(**28**)OBn species.

6.6 Future Work

Further derivatives of 1,2-DACH salalen ligands could be synthesised, firstly the phenol substituents could be varied. The amine-methyl group could also be varied as previous work on salalen complexes has shown this substituent region can affect the initiator properties.[11] Other metals can be trialled with this ligand set, e.g. group 4, indium, and lanthanides are possible candidates. The presence of one initiating benzyloxy group upon the aluminium metal makes these initiators candidates for initiating co-polymerisation reactions with other cyclic esters. Other salalen ligands could be synthesised with differing linking diamines, a notable candidate is based upon the salen ligands synthesised by Nomura *et. al.*,[6] the possible salalen variant is given in figure 6.20.

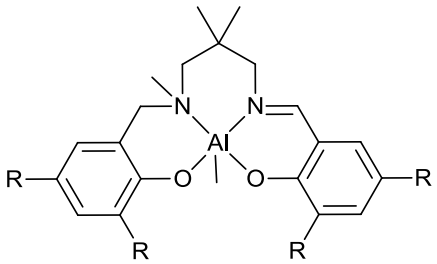

Figure 6.20: Potential aluminium salalen complex for the ROP of *rac*-lactide.

6.7 Final concluding remarks

The homo/piperazine based salan ligands gave 2:1 titanium to ligand complexes {Ti_2(**1-5**,**8-9**,**12-13**)(O^iPr)$_6$} with an interesting equilibrium based upon the steric demands of the *ortho*-phenoxy substituents. The bimetallic titanium

complexes were active for the ROP of lactide but lacked control over molecular weight and resulted in predominately atactic PLA. Homopiperaine salan group 4 monometallic complexes were formed and the titanium complexes {Ti(**6-11**)(O^iPr)$_2$} were poor initiators most likely due to hindrance about the titanium metal. The zirconium and hafnium homopiperazine salan complexes {Zr/Hf(**6-9,10**)(O^iPr)$_2$} resulted in mostly atactic lactide but the hafnium initiators {Hf(**6**,**7**)(O^iPr)$_2$} resulted in an isotactic biased PLA from *rac*-lactide in solvent and solvent free conditions. Aluminium benzyloxy and aluminium methyl homopiperazine salan complexes were synthesised as monometallic complexes. The aluminium benzyloxy homopiperazine salan complexes {Al(**6-9**,**11**)OBn} were shown to be active under solvent free conditions for the ROP of *rac*-lactide, ε-caprolactone, and δ-valerolactone. 1,4-DACH salen titanium and aluminium bimetallic complexes {Ti_2(**16-18**)(O^iPr)$_6$, Al_2(**16-18**)Me_4} were isolated with bulky *ortho*-phenoxy substituents and proven to be active initiators for the ROP of lactide. The aluminium 1,4-DACH based salen complexes {Al_2(**16-18**)Me_4} were shown to polymerise lactide in an immortal manner and resulted in isotactic biased PLA. A systematic study of 1,2-DACH salalen complexes {Al(**22-25**,**28**)Me, Al(**22-30**)OBn} was conducted and the phenoxy substituents on the imine and amine side were systematically investigated. Imine phenoxy substituents were shown to have the most prominent effect upon activity and stereoselectivity. Additionally isolated aluminium benzyloxy 1,2-DACH salalen complexes and aluminium benzyloxy 1,2-DACH salalen complexes formed *in-situ* within a polymerisation were compared, where the initiators formed *in-situ* resulted in reduced selectivity.

6.8 References

1. O. Dechy-Cabaret, B. Martin-Vaca and D. Bourissou, *Chem. Rev.*, 2004, **104**, 6147-6176.
2. J. Wu, T.-L. Yu, C.-T. Chen and C.-C. Lin, *Coord. Chem. Rev.*, 2006, **250**, 602-626.
3. R. H. Platel, L. M. Hodgson and C. K. Williams, *Polym. Rev.*, 2008, **48**, 11-63.
4. N. Spassky, M. Wisniewski, C. Pluta and A. Le Borgne, *Macromol. Chem. Phys.*, 1996, **197**, 2627-2637.
5. N. Nomura, R. Ishii, M. Akakura and K. Aoi, *J. Am. Chem. Soc.*, 2002, **124**, 5938-5939.

6. N. Nomura, R. Ishii, Y. Yamamoto and T. Kondo, *Chem. Eur. J.*, 2007, **13**, 4433-4451.
7. Z. Zhong, P. J. Dijkstra and J. Feijen, *Angew. Chem., Int. Ed.*, 2002, **41**, 4510-4513.
8. Z. Zhong, P. J. Dijkstra and J. Feijen, *J. Am. Chem. Soc.*, 2003, **125**, 11291-11298.
9. P. Hormnirun, E. L. Marshall, V. C. Gibson, A. J. P. White and D. J. Williams, *J. Am. Chem. Soc.*, 2004, **126**, 2688-2689.
10. H. Du, A. H. Velders, P. J. Dijkstra, J. Sun, Z. Zhong, X. Chen and J. Feijen, *Chem. Eur. J.*, 2009, **15**, 9836-9845.
11. E. L. Whitelaw, G. Loraine, M. F. Mahon and M. D. Jones, *Dalton Trans.*, 2011, **40**, 11469-11473.
12. K. Press, A. Cohen, I. Goldberg, V. Venditto, M. Mazzeo and M. Kol, *Angew. Chem., Int. Ed.*, 2011, **50**, 3529-3532.
13. B. Saito and T. Katsuki, *Angew. Chem., Int. Ed.*, 2005, **44**, 4600-4602.
14. B. Saito, H. Egami and T. Katsuki, *J. Am. Chem. Soc.*, 2007, **129**, 1978-1986.
15. K. Matsumoto, T. Yamaguchi and T. Katsuki, *Chem. Commun.*, 2008, 1704-1706.
16. T. Yamaguchi, K. Matsumoto, B. Saito and T. Katsuki, *Angew. Chem., Int. Ed.*, 2007, **46**, 4729-4731.
17. K. Matsumoto, T. Yamaguchi, J. Fujisaki, B. Saito and T. Katsuki, *Chem.--Asian J.*, 2008, **3**, 351-358.
18. J. Fujisaki, K. Matsumoto, K. Matsumoto and T. Katsuki, *J. Am. Chem. Soc.*, 2010, **133**, 56-61.
19. K. Suyama, Y. Sakai, K. Matsumoto, B. Saito and T. Katsuki, *Angew. Chem., Int. Ed.*, 2010, **49**, 797-799.
20. D. J. Darensbourg and D. R. Billodeaux, *Inorg. Chem.*, 2005, **44**, 1433-1442.

Chapter 7

7. Experimental

7. Experimental

7.1 General Experimental Considerations

Metal complex preparations and characterisations were performed under dry inert gas atmosphere (N_2 or Ar) using standard Schlenk line and glove box techniques. Dry solvents were collected from an MBraun solvent purification system (SPS) for the handling of and preparation of metal complexes. Laboratory reagent grade solvents were used for the preparation of ligands. All chemicals were purchased from Sigma-Aldrich and used without further purification unless stated. $Ti(O^iPr)_4$ (97 %, Aldrich) was purified by vacuum distillation and stored under inert atmosphere within a young's ampoule. *Rac*-lactide was crystallised from high purity toluene obtained from an MBraun SPS system and sequentially sublimed twice before glove-box storage under inert atmosphere. ε-caprolactone and δ-valereolactone were purified by vacuum distillation before storage under inert atmosphere.

^1H and $^{13}C\{^1H\}$ NMR spectra were recorded with a Bruker 250, 300, 400 or 500 MHz instrument and referenced to residual solvent peaks. NMR spectroscopy analysis was conducted in $CDCl_3$, $C_6D_5CD_3$, or C_4D_8O. $CDCl_3$ was dried by distillation from calcium hydride, before use with metal complexes. $C_6D_5CD_3$ and C_4D_8O were dried over molecular sieves before use. NMR tubes fitted with Young's taps were utilised for analysis of metal complexes, high temperature, and kinetic experiments. Ligands dissolved in acetonitrile were analysed by high resolution mass spectrometry on a micrOTOFQ (ESI-TOF) spectrometer in the positive mode. CHN elemental analysis data was recorded by either Mr. A. Craver (at the University of Bath, on an Exeter Analytical CE440 Elemental Analyzer) or by Mr Stephen Boyer (London Metropolitan University). X-ray diffraction data was collected on a Nonius Kappa CCD diffractometer using Mo-Kα radiation (λ = 0.71073 Å) at 150 K. X-ray diffraction data for $Ti_2(\mathbf{1})_2(O^iPr)_4$ was recorded at the diamond synchrotron facility using X-ray wavelength of λ = 0.6889 Å at 150 K by Dr Mary Mahon. All structures were solved by direct methods and refined on all F^2 data using the SHELXL-97 suite of programs. All hydrogen atoms were included in idealised positions and refined using the riding model.

7.2 General Polymerisation Procedures

^{1}H Homonuclear decoupled NMR spectroscopy was preformed on a Bruker 400 MHz spectrometer for determination of P_r (P_r = the probability of heterotactic linkages) values of *rac*-lactide polymers. This was found through analysis of the decoupled methine region of the spectra by Bernoulli statistics discussed by Coates et al.[1] Polymers were analysed by GPC on a Polymer Laboratories PL-GPC 50 integrated system using a PLgel 5 μm MIXED-D 300 × 7.5 mm column at 35°C with a flow rate of 1 ml min^{-1}. Samples were solubilised in THF and filtered through a PTFE 0.2 μm filter prior to auto-sampler injection. The polymers are analysed by refractive index which was referenced against 11 narrow molecular weight polystyrene polymer standards giving a calibrated range of M_w 615-568000 Da. The PDI is calculated from M_w/M_n (M_w = weight average molecular weight, M_n = number average molecular weight). MALDI-TOF mass spectrometry analysis of polymers was conducted by the EPSRC National Mass Spectrometry service Centre, Swansea, UK on the Applied Biosystems Voyager DE-STR instrument. The samples were dissolved in THF and analysed in positive-reflection mode using a dithranol matrix with a NaOAc additive to promote positive ionisation.

7.3 Homo/Piperazine Salan Ligand Preparation for Chapters 2-4

1H_2. 2,4-di-methylphenol (8.50 g, 69.6 mmol), piperazine anhydrous (3.00 g, 34.8 mmol), and formaldehyde (38% in H_2O) (5.78 ml, 2.35 g, 78.1 mmol) were refluxed in MeOH (40 ml) for 24 h. During which time a white precipitate was observed this was filtered and washed with cold MeOH and dried to yield a white solid (5.64 g, 15.9 mmol, 46 %). ^{1}H NMR ($CDCl_3$): δ 2.22 (6H, s, Me), 2.23 (6H, s, Me), 2.30 – 3.20 (8H, br, *ring*-CH_2), 3.67 (4H, s, N-CH_2-Ar), 6.65 (2H, d, J = 1.5 Hz, ArH), 6.85 (2H, d, J = 1.5 Hz, ArH), 10.54 (2H, br, OH). $^{13}C\{^1H\}$ NMR ($CDCl_3$): δ 15.7 (CH_3), 20.5 (CH_3), 52.4 (CH_2), 61.4 (CH_2), 119.9 (Ar), 124.7 (Ar), 126.9 (ArH), 127.9 (Ar), 138.8 (ArH), 153.4 (ArO). Calc. *m/z* $[C_{22}H_{30}N_2O_2 + H]^+$ 355.2385. Found 355.2488.

2H_2. 2-methyl-4-*tert*-butylphenol (3.97 g, 22.4 mmol), piperazine anhydrous (1.00 g, 11.6 mmol), and formaldehyde (38% in H_2O) (1.92 ml, 0.78 g, 26.0 mmol) were refluxed in MeOH (25 ml) for 24 h. During which time a white precipitate was

observed this was filtered and washed with cold MeOH and dried to yield a white solid (1.20 g, 2.7 mmol, 24 %). ^{1}H NMR ($CDCl_3$): δ 1.28 (18H, s, ^{t}Bu), 2.24 (6H, s, CH_3), 2.30 – 3.20 (8H, br, *ring*-CH_2), 3.71 (4H, s, N-CH_2-Ar), 6.84 (2H, d, J = 2.0 Hz, ArH), 7.08 (2H, d, J = 2.0 Hz, ArH), 10.67 (2H, br, OH). ^{13}C{^{1}H} NMR ($CDCl_3$): δ 16.1 (CH_3), 31.7 (CH_3), 33.9 (C), 52.5 (CH_2), 61.8 (CH_2), 119.5 (Ar), 123.2 (ArH), 124.2 (Ar), 127.1 (ArH), 141.6 (Ar), 153.4, (ArO). Calc. m/z $[C_{28}H_{42}N_2O_2 + H]^+$ 439.3325. Found 439.3306.

3H_2. 2,4-di-*tert*-butylphenol (14.37 g, 69.7 mmol), piperazine anhydrous (3.00 g, 34.8 mmol), and of formaldehyde (38% in H_2O) (5.78 ml, 2.35 g, 78.14 mmol) were refluxed in MeOH (40 ml) for 24 h. During which time a white precipitate was observed this was filtered and washed with cold MeOH and dried to yield a white solid (13.31 g, 25.5 mmol, 73 %). ^{1}H NMR ($CDCl_3$): δ 1.28 (18H, s, ^{t}Bu), 1.42 (18H, s, ^{t}Bu), 2.10 – 3.20 (8H, br, *ring*-CH_2), 3.72 (4H, s, N-CH_2-Ar), 6.84 (2H, d, J = 2.5 Hz , ArH), 7.23 (2H, d, J = 2.5 Hz, ArH), 10.68 (2H, br, OH). ^{13}C{^{1}H} NMR ($CDCl_3$): δ 29.7 (CH_3), 31.8 (CH_3), 34.3 (C), 35.0 (C), 52.3 (CH_2), 62.1 (CH_2), 120.4 (Ar), 123.2 (ArH), 123.7 (ArH), 135.7 (Ar), 140.9 (Ar), 154.2, (ArO). Calc. m/z $[C_{22}H_{30}N_2O_2 + H]^+$ 523.4263. Found 523.4366.

4H_2. 2-*tert*-butyl-4-methylphenol (7.63 g, 46.5 mmol), piperazine anhydrous (2.00 g, 23.2 mmol), and formaldehyde (38% in H_2O) (3.85 ml, 1.57 g, 52.1 mmol) were refluxed in MeOH (30 ml) for 24 h. During which time a white precipitate was observed this was filtered and washed with cold MeOH and dried to yield a white solid (5.66 g, 12.9 mmol, 56 %). ^{1}H NMR ($CDCl_3$): δ 1.41 (18H, s, ^{t}Bu), 2.25 (6H, s, Me), 2.30 – 3.20 (8H, b, *ring*-CH_2), 3.69 (4H, s, N-CH_2-Ar), 6.68, (2H, s, ArH), 7.01 (2H, s, ArH), 10.68 (2H, b, OH). ^{13}C{^{1}H} NMR ($CDCl_3$): δ 20.9 (CH_3), 29.6 (CH_3), 34.7 (C), 52.2 (CH_2), 61.3 (CH_2), 121.0 (Ar), 126.9, 127.5 (ArH), 127.1 (Ar), 136.4 (Ar), 154.2 (ArO). Calc. *m/z* $[C_{28}H_{42}N_2O_2 + H]^+$ 439.3325. Found 439.3308.

5H_2. 2,4-di-*tert*-amylphenol (5.44 g, 23.2 mmol), piperazine anhydrous (1.00 g, 11.6 mmol), and formaldehyde (38% in H_2O) (1.92 ml, 0.78 g, 26.0 mmol) were refluxed in MeOH (25 ml) for 24 h. During which time a white precipitate was observed this was filtered and washed with cold MeOH and dried to yield a white solid (1.84 g, 3.2

mmol, 28 %). ^{1}H NMR ($CDCl_3$): δ 0.62 (6H, t, J = 7.5 Hz, CH_3), 0.64 (6H, t, J = 7.5 Hz, CH_3), 1.24 (12H, s, CH_3), 1.36 (12H, s, CH_3), 1.57 (4H, q, J = 7.5 Hz, CH_2), 1.88 (4H, q, J = 7.5 Hz, CH_2), 2.30 – 3.20 (8H, br, *ring*-CH_2), 3.67 (4H, s, N-CH_2-Ar), 6.76 (2H, d, J = 2.0 Hz, ArH), 7.08 (2H, d, J = 2.0 Hz, ArH), 10.55 (2H, br, OH). ^{13}C{^{1}H} NMR ($CDCl_3$): δ 9.3 (CH_3), 9.7 (CH_3), 27.7 (CH_2), 28.7 (CH_3), 33.1 (CH_2), 37.3 (C), 38.5 (C), 52.2 (CH_2), 61.2 (CH_2), 120.1 (Ar), 124.3 (ArH), 125.3 (ArH), 133.9 (Ar), 139.0 (Ar), 153.9 (ArO). Calc. m/z $[C_{38}H_{63}N_2O_2 + H]^+$ 579.4890. Found 579.4906.

6H_2. 2,4-di-methyl-butylphenol (2.44 g, 20.0 mmol), homo-piperazine (1.00 g, 10.0 mmol), and formaldehyde (38% in H_2O) (1.67 ml, 0.68 g, 22.6 mmol) were refluxed in MeOH (20 ml) for 24 h. During which time a white precipitate was observed this was filtered and washed with cold MeOH and dried to yield a white solid (1.84 g, 5.0 mmol, 50 %). ^{1}H NMR ($CDCl_3$): δ 1.93 (2H, quin, J = 6.1 Hz, CH_2), 2.22 (12H, s, Me), 2.78 (4H, s, ring-CH_2), 2.83 (4H, t, J = 6.2 Hz, ring-CH_2), 3.74 (4H, s, N-CH_2-Ar), 6.62 (2H, s, ArH), 6.87 (2H, s, ArH), 10.82 (2H, br, OH). ^{13}C{^{1}H} NMR ($CDCl_3$): δ 15.7 (CH_3), 20.5 (CH_3), 26.7 (CH_2), 53.5 (CH_2), 54.6 (CH_2), 62.0 (CH_2), 120.1 (Ar), 124.7 (Ar), 126.7 (ArH), 127.7 (Ar), 130.7 (ArH), 153.7, (ArO). Calc. m/z $[C_{23}H_{32}N_2O_2 + H]^+$ 369.2542. Found 369.2530.

7H_2. 2-methyl-4-*tert*-butylphenol (3.28 g, 20.0 mmol), homo-piperazine (1.00 g, 10.0 mmol), and formaldehyde (38% in H_2O) (1.66 ml, 0.67 g, 22.5 mmol) were refluxed in MeOH (20 ml) for 24 h. During which time a white precipitate was observed this was filtered and washed with cold MeOH and dried to yield a white solid (1.68 g, 3.7 mmol, 37 %). ^{1}H NMR ($CDCl_3$): δ 1.28 (18H, s, ^{t}Bu), 1.95 (2H, quin, J = 6.0 Hz, CH_2), 2.25 (6H, s, CH_3), 2.80 (4H, s, ring-CH_2), 2.85 (4H, t, J = 6.0 Hz, ring-CH_2), 3.78 (4H, s, N-CH_2-Ar), 6.81 (2H, d, J = 2.3 Hz, ArH), 7.08 (2H, d, J = 2.3 Hz, ArH), 10.95 (2H, br, OH). ^{13}C{^{1}H} NMR ($CDCl_3$): δ 16.1 (CH_3), 26.8 (CH_2), 31.8 (CH_3), 34.0 (C), 53.6 (CH_2), 54.8 (CH_2), 62.5 (CH_2), 120.4 (Ar), 123.0 (ArH), 124.2 (Ar), 127.1 (ArH), 141.4 (Ar), 153.7, (ArO). Calc. m/z $[C_{29}H_{44}N_2O_2 + H]^+$ 453.3481. Found 453.3497.

8H_2. 2,4-di-*tert*-butylphenol (4.12 g, 20.0 mmol), homo-piperazine (1.00 g, 10.0 mmol), and formaldehyde (38% in H_2O) (1.66 ml, 0.67 g, 24.5 mmol) were refluxed in MeOH (20 ml) for 24 h. During which time a white precipitate was observed this was filtered and washed with cold MeOH and dried to yield a white solid (1.29 g, 2.4 mmol, 24 %). ^{1}H NMR ($CDCl_3$): δ 1.28 (18H, s, ^{t}Bu), 1.42 (18H, s, ^{t}Bu), 1.91 (2H, quintet, J = 6.0 Hz, ring-CH_2), 2.78 (4H, s, ring-CH_2), 2.83 (4H, t, J = 6.0 Hz, ring-CH_2), 3.77 (4H, s, N-CH_2), 6.84 (2H, d, J = 2.5 Hz, ArH), 7.23 (2H, d, J = 2.5 Hz, ArH), 10.68 (2H, br, OH). ^{13}C{^{1}H} NMR ($CDCl_3$): δ 26.9 (CH_2), 29.7 (CH_3), 31.8 (CH_3), 34.2 (C), 35.0 (C), 52.2 (CH_2), 54.6 (CH_2), 62.6 (CH_2), 121.4 (Ar), 123.1 (ArH), 123.6 (ArH), 135.8 (Ar), 140.7 (Ar), 154.4, (ArO). Calc. m/z [$C_{35}H_{56}N_2O_2$ + H]$^+$ 537.4420. Found 537.4442.

9H_2. 2-*tert*-butyl-4-methylphenol (3.28 g, 20.0 mmol), homo-piperazine (1.00 g, 10.0 mmol), and formaldehyde (38% in H_2O) (1.66 ml, 0.67 g, 22.5 mmol) were refluxed in MeOH (20 ml) for 24 h. During which time a white precipitate was observed this was filtered and washed with cold MeOH and dried to yield a white solid (1.56 g, 3.5 mmol, 35 %). ^{1}H NMR ($CDCl_3$): δ 1.42 (18H, s, ^{t}Bu), 1.89 (2H, quin, J = 6.1 Hz, CH_2), 2.24 (6H, s, CH_3), 2.77 (4H, s, ring-CH_2), 2.81 (4H, t, J = 6.0 Hz, ring-CH_2), 3.75 (4H, s, N-CH_2-Ar), 6.66 (2H, d, J = 1.9 Hz, ArH), 7.01 (2H, d, J = 2.3 Hz, ArH), 11.00 (2H, br, OH). ^{13}C{^{1}H} NMR ($CDCl_3$): δ 20.9 (CH_2), 26.9 (CH_3), 29.6 (CH_3), 34.7 (C), 53.2 (CH_2), 54.6 (CH_2), 62.1 (CH_2), 122.0 (Ar), 126.9 (ArH), 127.3 (Ar), 127.4 (ArH), 136.6 (Ar), 154.6, (ArO). Calc. m/z [$C_{29}H_{44}N_2O_2$ + H]$^+$ 453.3481. Found 453.3494.

10H_2. 2,4-di-*tert*-amylphenol (4.68 g, 20.0 mmol), homo-piperazine (1.00 g, 10.0 mmol), and formaldehyde (38% in H_2O) (1.67 ml, 0.68 g, 22.5 mmol) were refluxed in MeOH (20 ml) for 24 h. During which time a white precipitate was observed this was filtered and washed with cold MeOH and dried to yield a white solid (1.85 g, 3.1 mmol, 31 %). ^{1}H NMR ($CDCl_3$): δ 0.64 (12H, q, J = 7.6 Hz CH_3), 1.23 (12H, s, CH_3), 1.37 (12H, s, CH_3), 1.57 (4H, quart, J = 7.5 Hz, CH_2), 1.90 (4H, quart, J = 7.3 Hz, CH_2), 1.90 (2H, s, ring-CH_2), 2.74 (4H, s, ring-CH_2), 2.81 (4H, t, J = 5.8 Hz, ring-CH_2), 3.76 (4H, s, N-CH_2-Ar), 6.74 (2H, d, J = 2.3 Hz, ArH), 7.07 (2H, d, J = 2.5 Hz, ArH), 10.87 (2H, br, OH). ^{13}C{^{1}H} NMR ($CDCl_3$): δ 9.3 (CH_3), 9.7 (CH_3), 26.8

(CH_2), 27.8 (CH_3), 28.7 (CH_3), 33.2 (C), 37.3 (C), 37.4 (CH_2), 38.5 (CH_2), 53.1 (CH_2), 54.6 (CH_2), 62.6 (CH_2), 121.1 (Ar), 124.2 (ArH), 125.2 (ArH), 134.0 (Ar), 138.9 (Ar), 154.2 (ArO). Calc. m/z $[C_{39}H_{64}N_2O_2 + H]^+$ 593.5046. Found 593.4993.

11H_2. homopiperazine anhydrous (2.20 g, 25 mmol) and formaldehyde (38% in H_2O) (5.30 ml, 75.4 mmol) were refluxed (2 h) in MeOH (40 ml). The solution was then cooled to room temperature and 4-*tert*-butylphenol (7.51 g, 50.0 mmol) in methanol (60 ml) was added slowly then refluxed (16 h) and then cooled to room temperature. The solid was filtered, washed in cold MeOH then dried under vacuum to yield a white powder (2.31 g, 5.5 mmol, 22%). ^{1}H NMR ($CDCl_3$): δ 1.27 (18H, s, CH_3), 1.94 (2H, quintet, J = 6.0 Hz, CH_2), 2.79 (4H, s, CH_2), 2.84 (4H, t, J = 6.0 Hz, CH_2), 3.78 (4H, s, CH_2), 6.76 (2H, d, J = 8.50 Hz, ArH), 6.95 (2H, d, J = 2.5 Hz, ArH), 7.19 (2H, dd, J = 8.5 Hz, J = 2.5 Hz, ArH), 10.47 (2H, br, OH). ^{13}C{^{1}H} NMR ($CDCl_3$): δ 26.8 (CH_2), 31.6 (CH_3), 34.0 (C), 53.6 (CH_2), 54.7 (CH_2), 62.4 (CH_2), 115.5 (ArH), 121.0 (Ar), 125.4 (ArH), 125.6 (ArH), 141.9 (Ar), 155.4 (ArO). Calc. m/z $[C_{27}H_{40}N_2O_2 + H]^+$425.3168. Found 425.3233.

12H_2. 2,4-di-*tert*-butylphenol (4.11 g, 19.9 mmol), 2-methylpiperazine (1.00 g, 10.0 mmol), and formaldehyde (38 % in H_2O) (1.62 ml, 0.66 g, 21.9 mmol) were refluxed in MeOH (20 ml ml) for 24 h. During which time a white precipitate was observed this was filtered and washed with cold MeOH and dried to yield a white solid (2.71 g, 5.0 mmol, 51 %). ^{1}H NMR ($CDCl_3$): δ 1.23 (3H, d J = 6.5 Hz), 1.28 (9H, s, ^{t}Bu), 1.29 (9H, s, ^{t}Bu), 1.41 (18H, s, ^{t}Bu), 2.10 – 3.20 (7H, br, *ring*-CH_2/CH), 3.69 (4H, m, N-CH_2-Ar), 6.82, (2H, br ArH), 7.21 (1H, d, J = 2.5 Hz, ArH), 7.23 (1H, d, J = 2.5 Hz, ArH), 10.71 (1H, br, OH), 10.82 (1H, br, OH). ^{13}C{^{1}H} NMR ($CDCl_3$): δ 25.7 (CH_3), 29.7 (CH_3), 31.8 (CH_3), 34.2 (C), 35.0 (C), 52.5 (CH_2), 62.1 (CH_2), 120.8 (Ar), 122.9 (ArH), 123.0 (ArH), 123.5 (ArH), 123.6 (ArH), 135.6 (Ar), 135.7 (Ar), 140.9 (Ar), 140.9 (Ar), 154.1, (ArO). Calc. m/z $[C_{35}H_{56}N_2O_2 + H]$+ 537.4420. Found 537.4413.

13H_2. 2-*tert*-butyl-4-methylphenol (3.38 g, 20.5 mmol), 2-methylpiperazine (1.00 g, 10.0 mmol), and formaldehyde (38% in H_2O) (1.66 ml, 0.67 g, 22.5 mmol) were refluxed in MeOH (20 ml) for 24 h. During which time a white precipitate was

observed this was filtered and washed with cold MeOH and dried to yield a white solid (1.29 g, 2.8 mmol, 29 %). ^{1}H NMR ($CDCl_3$): δ 1.21 (3H, d J = 6.5 Hz, *ring*-CH_3), 1.42 (18H, s, ^{t}Bu), 2.26 (6H, s, Me), 2.30 – 3.20 (7H, br, *ring*-CH_2/CH), 3.30 (1H, br, N-CH_2), 3.65 (2H, m, N-CH_2), 4.27 (1H, br, N-CH_2), 6.68 (1H, s, ArH), 6.68 (1H, s, ArH), 7.01 (1H, d, J = 2.0 Hz, ArH), 7.02 (1H, d, J = 2.0 Hz, ArH), 10.67 (2H, br, OH). ^{13}C{^{1}H} NMR ($CDCl_3$): δ 20.9 (CH_3), 24.1 (CH_3), 29.5 (CH_3), 29.5 (CH_3), 34.6 (C), 34.6 (C), 52.6 (CH_2), 57.4 (CH_2), 61.7 (CH_2), 121.1 (Ar), 126.7 (ArH), 127.0 (ArH), 127.4 (ArH), 127.4 (Ar), 127.5 (ArH), 136.4 (Ar), 134.4 (Ar), 154.3 (ArO). Calc. *m/z* $[C_{29}H_{44}N_2O_2 + H]^+$ 453.3481. Found 453.3462.

14H_2. 2,4-di-*tert*-amylphenol (9.36 g, 40.0 mmol), 2-methylpiperazine (2.00 g, 20.0 mmol), and formaldehyde (38 % in H_2O) (3.31 ml, 1.35 g, 44.5 mmol) were refluxed in MeOH (30 ml) for 24 h. During which time a white precipitate was observed this was filtered and washed with cold MeOH and dried to yield a white solid (5.96 g, 10.3 mmol, 52 %). ^{1}H NMR ($CDCl_3$): δ 0.66 (12H, m, CH_3), 1.21 (3H, d, Me, J = 6.3 Hz), 1.25 (12H, s, CH_3), 1.36 (12H, s, CH_3), 1.56 (4H, q, CH_2), 1.89 (4H, m, CH_2), 2.10 – 3.20 (7H, b, ring-CH_2), 3.30 (1H, b, N-CH_2-Ar), 3.65 (2H, m, N-CH_2-Ar), 4.25 (1H, b, N-CH_2-Ar), 6.75 (2H, s, ArH), 7.07 (2H, m, ArH), 10.58 (2H, b, OH). ^{13}C{^{1}H} NMR ($CDCl_3$): δ 9.3 (CH_3), 9.7 (CH_3), 28.7 (CH_3), 33.1 (CH_2), 37.3 (C), 38.5 (C), 52.5 (ring-CH_2), 57.8 (ring-CH_2), 62.1 (N-CH_2), 120.1 (ArC), 120.2 (ArC), 124.2 (ArH), 124.3 (ArH), 125.1 (ArH), 125.3 (ArH), 133.9(Ar), 138.8 (Ar), 138.8 (Ar), 153.9 (ArO). Calc. m/z $[C_{39}H_{64}N_2O_2 + H]^+$ 593.5046. Found 593.5063.

15H_2. 2-methyl-4-*tert*-butylphenol (3.38 g, 20.5 mmol), 2-methylpiperazine (1.00 g, 10.0 mmol), and formaldehyde (38 % in H_2O) (1.66 ml, 0.67 g, 22.5 mmol) were refluxed in MeOH (20 ml, 65 °C) to yield a white solid (1.20 g, 2.7 mmol, 27 %). ^{1}H NMR ($CDCl_3$): δ 1.23 (3H, d, Me, J = 6.5 Hz), 1.31 (18H, s, ^{t}Bu), 2.25 (6H, s, Me), 2.30 – 3.20 (7H, b, ring-CH_2), 3.28 (1H, b, N-CH_2-Ar), 3.68 (2H, m, N-CH_2-Ar), 4.36 (1H, b, N-CH_2-Ar), 6.84 (4H, s, ArH), 7.08 (4H, s, ArH), 10.66 (2H, b, OH). ^{13}C{^{1}H} NMR ($CDCl_3$): δ 16.1 (CH_3), 31.7 (CH_3), 34.0 (C), 52.7 (CH_2), 61.7 (CH_2), 119.5 (Ar), 119.9 (Ar), 123.1 (ArH), 123.2 (ArH), 126.9 (ArH), 127.1 (ArH), 124.1 (Ar), 141.6 (Ar), 141.7 (Ar), 141.6 (Ar), 153.4, (ArO). Calc. m/z $[C_{29}H_{44}N_2O_2 + H]^+$ 453.3481. Found 453.3475.

7.4 Preparation of Complexes for Chapter 2

7.4.1 Preparation of titanium bimetallic homo/piperazine salan complexes

Ti_2(**1**)(O^iPr)$_6$. **1**H_2 (0.50 g, 1.41 mmol) and Ti(O^iPr)$_4$ (0.85 ml, 2.87 mmol) were dissolved in CH_2Cl_2 (30 ml) and stirred (16 h). The solvent was removed *in-vacuo* and recrystallised from hot hexane (40 ml) to yield pale yellow crystals (0.51 g, 0.64 mmol, 45 %). The NMR was a mixture of Ti_2(**1**)(O^iPr)$_6$ and Ti_2(**1**)$_2$(O^iPr)$_4$ and Ti(O^iPr)$_4$ in a 4:1:2 ratio as discussed in the text. The NMR spectrum for the individual components follows: Ti_2(**1**)(O^iPr)$_6$ ^{1}H NMR ($CDCl_3$) (233 K): δ 1.26 (36H, d, J = 6.0 Hz, CH_3), 2.13 (6H, s, CH_3), 2.15 (3H, s, CH_3), 2.16 (3H, s, CH_3), 2.30 – 3.90 (8H, br, *ring*-CH_2), 4.09 (4H, m, N-CH_2-Ar), 4.89 (6H, br, CH), 6.69 (2H, s ArH), 6.83 (2H, s, ArH). Ti_2(**1**)$_2$(O^iPr)$_4$ ^{1}H NMR (233 K): δ 0.94 (3H, d, J = 6.0 Hz, Me), 0.97 (3H, d, J = 6.0 Hz, Me), 1.16 (6H, d, J = 6.0 Hz, Me), 1.20 – 1.40 (12H, br, CH_3), 2.08 (3H, s, Me), 2.10 – 2.25 (18H, br, Me), 2.28 (3H, s, Me), 2.30 – 3.90 (16H, br, *ring*-CH_2), 4.09 (8H, m, N-CH_2-Ar), 4.89 (4H, b, CH), 6.57 (2H, ArH), 6.76 (2H, ArH), 6.84 (2H, ArH), 6.92 (2H, ArH). Ti(O^iPr)$_4$ ^{1}H NMR ($CDCl_3$) (233 K): δ 1.26 (24H, d, J = 6.0 Hz, CH_3), 4.47 (4H, sept, J = 6.0 Hz, CH). ^{13}C{^{1}H} NMR ($CDCl_3$): δ 16.8 (CH_3), 20.5 (CH_3), 26.7 (CH_3), 43.3 (CH_2), 52.0 (CH_2), 77.8 (CH), 122.7 (Ar), 124.8 (Ar), 127.0 (Ar), 127.7 (ArH), 130.8 (ArH), 158.2 (ArO). Calc. (%) for $C_{40}H_{70}N_2O_8Ti_2$: C 59.85, H 8.79, N 3.49. Found (%), C 59.3, H 8.80, N 3.72.

Ti_2(**2**)(O^iPr)$_6$. **2**H_2 (0.22g, 0.50 mmol) and Ti(O^iPr)$_4$ (0.30 ml, 1.01 mmol) were dissolved in CH_2Cl_2 (30 ml) and stirred (16 h). The solvent was removed *in-vacuo* and recrystallised from hot hexane (20 ml) to yield a pale yellow crystals (0.19 g, 0.20 mmol, 41 %). The NMR was a mixture of Ti_2(**2**)(O^iPr)$_6$ and Ti_2(**2**)$_2$(O^iPr)$_4$ and Ti(O^iPr)$_4$ in a 4:1:2 ratio as discussed in the text. The NMRs for the individual components are: Ti_2(**2**)(O^iPr)$_6$ ^{1}H NMR ($CDCl_3$) (233 K): δ 1.23 (18H, s, CH_3), 1.26 (36H, d, J = 6.0 Hz, CH_3), 2.18 (6H, br, CH_3), 2.30 – 4.00 (8H, br, *ring*-CH_2), 4.15 (4H, br, N-CH_2-Ar), 4.90 (6H, br, CH), 6.89 (2H, br, ArH), 7.10 (2H, br ArH), Ti_2(**2**)$_2$(O^iPr)$_4$ ^{1}H NMR ($CDCl_3$) (233 K): δ 0.85 (3H, d, J = 6.0 Hz, CH_3), 0.87 (3H, d, J = 6.0 Hz, CH_3), 0.97 (3H, d, J = 6.0 Hz, CH_3), δ 1.14 (18H, s, CH_3), 1.10 – 1.50 (15H, br, CH_3), 1.34 (18H, s, CH_3), 2.13 (3H, s CH_3), 2.20 (6H, s, CH_3), 2.26 (3H, s,

CH_3), 2.30 – 4.00 (16H, br, *ring*-CH_2), 4.15 (8H, m, N-CH_2-Ar), 4.90 (4H, br, CH), 6.70 (2H, s, ArH), 6.94 (2H, s, ArH), 7.05 (2H, s, ArH), 7.17 (2H, s, ArH). $Ti(O^iPr)_4$ ^1H NMR ($CDCl_3$) (233 K): δ 1.26 (24H, d, J = 6.0 Hz, CH_3), 4.47 (4H, sept, J = 6.0 Hz, CH). $^{13}C\{^1H\}$ NMR ($CDCl_3$): δ 17.2 (CH_3), 26.7 (CH_3), 31.8 (C), 43.3 (CH_2), 52.3 (CH_2), 77.8 (CH), 122.3 (Ar), 124.0 (ArH), 124.1 (Ar), 127.2 (ArH), 140.7 (Ar), 158.3 (ArO). Calc. (%) for $C_{46}H_{82}N_2O_8Ti_2$: C 62.30, H 9.32, N 3.16. Found (%), C 61.7, H 9.33, N 3.21.

Ti_2(**3**)$(O^iPr)_6$. **3**H_2 (0.49g, 0.94 mmol) and $Ti(O^iPr)_4$ (0.70 ml, 2.36 mmol) were dissolved in CH_2Cl_2 (30 ml) and stirred (16 h). The solvent was removed *in-vacuo* and recrystallised from hot hexane (30 ml) to yield yellow crystals (0.37 g, 0.38 mmol, 41 %). ^1H NMR ($CDCl_3$): δ 1.27 (18H, s, ^tBu), 1.30 (36H, d J = 6.0 Hz, CH_3), 1.43 (18H, s, CH_3), 2.10 – 3.80 (8H, br, *ring*-CH_2), 4.16 (4H, s, N-CH_2-Ar), 4.92 (6H, sept, J = 6.0 Hz, CH), 6.97 (2H, d = 2.3 Hz, ArH), 7.20 (2H, d = 2.3 Hz, ArH). $^{13}C\{^1H\}$ NMR ($CDCl_3$): δ 27.0 (CH_3), 29.7 (CH_3), 31.9 (CH_3), 34.3 (C), 35.1 (C), 52.2 (CH_2), 77.4 (CH), 123.2 (ArH), 123.7 (ArH), 124.5 (Ar), 135.5 (Ar), 140.1 (Ar), 154.7 (ArO). Calc. (%) for $C_{52}H_{94}N_2O_8Ti_2$: C 64.32, H 9.76, N 2.88. Found (%), C 63.8, H 9.76, N 2.78.

Ti_2(**4**)$(O^iPr)_6$. **4**H_2 (0.22g, 0.50 mmol) and $Ti(O^iPr)_4$ (0.30 ml, 1.01 mmol) were dissolved in CH_2Cl_2 (30 ml) and stirred (16 h). The solvent was removed *in-vacuo* and recrystallised from hot hexane (20 ml) to yield pale yellow crystals (0.23 g, 0.26 mmol, 52 %). ^1H NMR ($CDCl_3$): δ 1.31 (36H, d, J = 6.0 Hz, CH_3), 1.41 (18H, s, CH_3), 2.21 (6H, s, Me), 2.30 – 3.80 (8H, br, *ring*-CH_2), 4.12 (4H, s, N-CH_2-Ar), 4.93 (6H, sept, J = 6.0 Hz, CH), 6.78 (2H, d, J = 2.0 Hz, ArH), 6.97 (2H, d, J = 2.0 Hz, ArH). $^{13}C\{^1H\}$ NMR ($CDCl_3$): δ 20.9 (CH_3), 27.0 (CH_3), 29.6 (CH_3), 34.8 (C), 51.9 (N-CH_2), 77.6 (CH), 124.3 (Ar), 126.7 (Ar), 126.9 (ArH), 128.3 (ArH), 136.2 (Ar), 158.9 (ArO). Calc. (%) for $C_{46}H_{82}N_2O_8Ti_2$: C 62.30, H 9.32, N 3.16. Found (%), C 61.9, H 9.28, N 3.61.

Ti_2(**5**)$(O^iPr)_6$. **5**H_2 (0.50 g, 0.86 mmol) and $Ti(O^iPr)_4$ (0.80 ml, 2.70 mmol) were dissolved in CH_2Cl_2 (30 ml) and stirred (16 h). The solvent was removed *in-vacuo* and recrystallised from hot hexane (40 ml) to yield yellow crystals (0.18 g, 0.18

mmol, 20 %). ^{1}H NMR ($CDCl_3$): δ 0.61 (12H, m, CH_3), 1.20 – 1.25 (12H, m, CH_3), 1.28 (36H, d, J = 6.0 Hz, CH_3), 1.35 (12H, s, CH_3), 1.54 (4H, m, CH_2), 1.96 (4H, m, CH_2), 2.20 – 2.80 (4H, br, *ring*-CH_2), 3.30 – 3.80 (4H, br, *ring*-CH_2), 4.10 (4H, s, N-CH_2-Ar), 4.90 (6H, sept, J = 6.0 Hz, CH), 6.88 (2H, d, J = 2.0 Hz, ArH), 7.04 (2H, d, J = 2.0 Hz, ArH). ^{13}C{^{1}H} NMR ($CDCl_3$): δ 9.28 (CH_3), 9.81 (CH_3), 26.7 (CH_3), 26.8 (CH_3), 27.0 (CH_3), 27.8 (CH_2) 28.8 (CH_3) 32.8 (CH_2), 37.3 (C), 38.6 (C), 43.7 (CH_2), 77.5 (CH), 123.4 (Ar), 125.2 (ArH), 125.3 (ArH), 133.7 (Ar), 138.1 (Ar), 158.9 (ArO). Calc. (%) for $C_{56}H_{102}N_2O_8Ti_2$: (%), C 65.48, H 10.01, N 2.73. Found CHN (%), C 64.2, H 9.98, N 3.02.

Ti_2(**8**)(O^iPr)$_6$. **8**H_2 (0.48g, 0.89 mmol) and Ti(O^iPr)$_4$ (0.80 ml, 2.70 mmol) were dissolved in CH_2Cl_2 (30 ml) and stirred (16 h). The solvent was removed *in-vacuo* and recrystallised from hot hexane (30 ml) to yield pale yellow crystals (0.68 g, 0.69 mmol, 77 %). ^{1}H NMR ($CDCl_3$): δ 1.27 (36H, br, CH_3), 1.29 (18H, s, CH_3), 1.45 (18H, s, CH_3), 2.00 (2H, br, *ring*-CH_2), 2.98 (4H, br, *ring*-CH_2), 3.14 (4H, br, *ring*-CH_2), 3.92 (4H, s, N-CH_2-Ar), 4.90 (6H, sept, J = 6.0 Hz, CH), 6.86 (2H, d, J = 2.5 Hz, ArH), 7.19 (2H, d J = 2.5 Hz, ArH). ^{13}C{^{1}H} NMR ($CDCl_3$): δ 26.9 (CH_3), 31.8 (CH_3), 34.3 (C), 35.1 (C), 55.2 (CH_2), 64.3 (CH_2), 77.6 (CH), 123.2 (ArH), 124.1 (Ar), 124.6 (ArH), 135.5 (Ar), 140.0 (Ar), 159.9 (ArO). Calc. (%) for $C_{53}H_{96}N_2O_8Ti_2$, C 64.62, H 9.82, N 2.84. Found (%), C 64.4, H 9.61, N 2.95

Ti_2(**9**)(O^iPr)$_6$. **9**H_2 (0.51g, 1.13 mmol) and Ti(O^iPr)$_4$ (1.00 ml, 3.38 mmol) were dissolved in CH_2Cl_2 (30 ml) and stirred (16 h). The solvent was removed *in-vacuo* and recrystallised from hexane (10 ml) to yield yellow crystals (0.37 g, 0.24 mmol, 36 %). ^{1}H NMR ($CDCl_3$) (233 K): δ 1.26 (36H, b, CH_3-^{i}Pr), 1.42 (18H, d, ^{t}Bu), 2.24 (6H, m, Me), 2.41 (1H, b, *ring*-CH_2), 2.59 (1H, b, *ring*-CH_2), 2.80 (1H, b, *ring*-CH_2), 2.99 (1H, b, *ring*-CH_2), 3.20 (2H, b, *ring*-CH_2), 3.43 (2H, b, *ring*-CH_2), 3.62 (2H, b, *ring*-CH_2), 3.80-4.20 (4H, m, N-CH_2-Ar), 4.90 (6H, b, CH), 6.64 (1H, s, ArH), 6.72 (1H, s, ArH), 6.95 (1H, s, ArH), 7.04 (1H, s, ArH). ^{13}C{^{1}H} NMR ($CDCl_3$): δ 21.0 (CH_3), 26.9 (CH_3), 34.8 (C), 27.0 (CH_3), 21.2 (CH_2), 29.7 (CH_2), 30.0 (CH_2), 30.2 (CH_2), 30.6 (CH_2), 56.8 (N-CH_2), 77.6 (CH), 122.9 (Ar), 124.0 (Ar), 123.5 (ArH), 127.9 (ArH), 139.4 (Ar), 163.1 (ArO). Calc. (%) for $C_{47}H_{84}N_2O_8Ti_2$, C 62.66, H 9.40, N 3.11. Found (%), C 60.1, H 9.01, N 3.10.

Ti_2(**12**)(O^iPr)$_6$. **12**H_2 (0.60g, 1.11 mmol) and Ti(O^iPr)$_4$ (1.00 ml, 3.38 mmol) were dissolved in CH_2Cl_2 (30 ml) and stirred (16 h). The solvent was removed *in-vacuo* and recrystallised from hexane (2 ml) to yield yellow crystals (0.72 g, 0.73 mmol, 65 %). ^{1}H NMR ($CDCl_3$) (233 K): δ 0.97 (3H, d, J = 6.0 CH_3), 1.25 (9H, br, CH_3), 1.28 (36H, d J = 6.0 Hz, CH_3), 1.31 (9H, br, CH_3), 1.41 (9H, s, CH_3), 1.42 (9H, s, CH_3), 2.40 – 3.70 (7H, br, *ring*-CH_2), 3.95 (2H, br, N-CH_2-Ar), 4.12 (2H, m, N-CH_2-Ar), 4.80 (3H, sept, J = 6.0 Hz, CH), 4.89 (3H, sept, J = 6.0 Hz, CH), 6.90 (1H, d, J = 2.5 Hz, ArH), 7.14 (1H, d, J = 2.5 Hz, ArH), 7.18 (2H, br, ArH). ^{13}C{^{1}H} NMR ($CDCl_3$): δ 26.7 (CH_3), 26.8 (CH_3), 26.8 (CH_3), 26.9 (CH_3), 26.9 (CH_3), 29.7 (C), 29.8 (C), 31.8 (CH_3), 34.3 (C), 34.4 (C), 35.1 (CH_2), 76.5 (CH), 77.4 (CH), 77.8 (CH), 122.0 (ArH), 123.1 (ArH), 123.6 (ArH), 123.9 (Ar), 124.4 (ArH), 135.5 (Ar), 135.7 (Ar), 140.0 (Ar), 141.0 (Ar), 158.9 (ArO). Calc. (%) for $C_{53}H_{96}N_2O_8Ti_2$, C 64.62, H 9.82, N 2.84. Found (%), C 63.0, H 9.48, N 3.04

Ti_2(**13**)(O^iPr)$_6$. **13**H_2 (0.51g, 1.13 mmol) and Ti(O^iPr)$_4$ (1.00 ml, 3.38 mmol) were dissolved in CH_2Cl_2 (30 ml) and stirred (16 h). The solvent was removed *in-vacuo* and recrystallised from hexane (5 ml) to yield yellow crystals (0.59 g, 0.65 mmol, 58 %). ^{1}H NMR ($CDCl_3$): δ 1.07 (3H, d, J = 6.5, CH_3), 1.31 (18H, d, J = 6.0 Hz, CH_3), 1.33 (18H, d, J = 6.0 Hz, CH_3), 1.44 (9H, s, CH_3), 1.45 (9H, s, CH_3), 2.23 (3H, s, CH_3), 2.25 (3H, s, CH_3), 2.48 (1H, br, CH_2), 2.52 (1H, br, CH_2), 2.66, (1H, br, CH_2), 3.04 (1H, m, CH_2), 3.34 (1H, m, CH_2), 3.38 (1H, m, CH_2), 3.55 (1H, br, CH_2) 3.94 (2H, s, CH_2), 4.09 (2H, m, CH_2), 4.83 (3H, sept, J = 6.0 Hz, CH), 4.92 (3H, sept, J = 6.0 Hz, CH), 6.72 (1H, s, ArH), 6.95 (1H, s, ArH), 6.98 (1H, s, ArH), 7.01 (1H, s, ArH). ^{13}C{^{1}H} NMR ($CDCl_3$): δ 17.9 (CH_3), 21.0 (CH_3), 21.1 (CH_3), 26.8 (CH_3), 26.9 (CH_3), 29.7 (C), 30.0 (C), 34.8 (CH_2), 44.9 (CH_2), 49.5 (CH_1), 50.2 (CH_2), 53.4 (CH_2), 77.5 (CH), 77.9 (CH), 124.4 (Ar), 125.7 (ArH), 126.5 (Ar), 126.7 (ArH), 127.6 (ArH), 127.6 (Ar), 128.2 (ArH), 136.2 (Ar), 136.5 (Ar), 159.1 (ArO), 159.7 (ArO). Calc. (%) for $C_{47}H_{84}N_2O_8Ti_2$, C 62.66, H 9.40, N 3.11. Found (%), C 61.0, H 9.00, N 3.03

Ti_2(**1**)$_2$(O^iPr)$_4$. **1**H_2 (0.60 g, 1.69 mmol) and Ti(O^iPr)$_4$ (0.50 ml, 1.69 mmol) were dissolved in Tol. (30 ml) then heated (80 °C) and stirred (16 h). The solvent was removed *in-vacuo* and recrystallised from hexane to yield pale yellow crystals (0.27

g, 0.52 mmol, 31 %). ^{1}H NMR ($CDCl_3$) (233 K): δ 0.92 (6H, d, J = 6.0 Hz, CH_3), 0.95 (6H, d, J = 6.0 Hz, CH_3), 1.15 (6H, d, J = 6.0 Hz, CH_3), 1.29 (6H, d, J = 6.0 Hz, CH_3), 1.86 (2H, t, J = 12.5 Hz, CH_2), 2.06 (6H, s, CH_3), 2.10 (6H, s, CH_3), 2.13 (6H, s, CH_3), 2.19 (4H, d, J = 7.5 Hz, CH_2), 2.27 (6H, s, CH_3), 2.61 (2H, d, J = 11.5 Hz, CH_2), 2.69 (2H, d, J = 11.0 Hz, CH_2), 2.82 (2H, t, J = 11.5 Hz, CH_2), 3.19 (2H, t, J = 12.0 Hz, CH_2), 3.32 (2H, d, J = 12.0 Hz, CH_2), 3.85 (2H, t, J = 11.5 Hz, CH_2), 4.03 (4H, m, CH_2), 4.19 (2H, d, J = 13.5 Hz, CH_2), 4.47 (2H, septet, J = 12.0 Hz, CH), 4.92 (2H, septet, J = 12.0 Hz, CH), 6.56 (2H, s, ArH), 6.74 (2H, s, ArH), 6.82 (2H, s, ArH), 6.91 (2H, s, ArH). ^{13}C{^{1}H} NMR ($CDCl_3$): δ 16.5 (CH_3), 16.7 (CH_3), 17.4 (CH_3), 20.6 (CH_3), 25.8 (CH_3), 26.5 (CH_3), 26.7 (CH_3), 27.0 (CH_3), 44.9 (CH_2), 47.5 (CH_2), 48.8 (CH_2), 51.4 (br, CH_2), 52.8 (br, CH_2), 59.3 (CH_2), 78.5 (CH), 79.3 (CH), 123.3 (ArH), 123.7 (ArH), 124.7 (ArH), 126.0 (ArH), 126.9 (ArH), 127.6 (ArH), 127.9 (Ar), 129.6 (Ar), 130.5 (Ar), 130.9 (Ar), 158.5 (ArO), 163.2 (ArO). Calc. (%) for $C_{28}H_{42}N_2O_4Ti$: C 64.86, H 8.16, N 5.40. Found (%), C 64.67, H 8.16, N 5.56.

7.4.2 Preparation of titanium monometallic homopiperazine salan complexes

Ti(**6**)($O^{i}Pr$)$_2$. **6**H_2 (0.37 g, 1.00 mmol) and Ti($O^{i}Pr$)$_4$ (0.30 ml, 1.01 mmol) were dissolved in toluene (30 ml) then heated (80 °C) and stirred (16 h). The solvent was removed *in-vacuo* and recrystallised from hexane to yield pale yellow crystals (0.14 g, 0.26 mmol, 26 %). 2 species identified in the solution state NMR spectra. ^{1}H NMR ($CDCl_3$): δ 0.40 (3H, d, J = 5.5 Hz, CH_3), 1.14 (6H, br, CH_3), 1.19 (3H, d, J = 5.5 Hz, CH_3), 1.68 (1H, m, CH_2), 1.88 (1H, m, CH_2), 2.21 (9H, s, CH_3), 2.29 (3H, s, CH_3), 2.42 (2H, br, CH_2), 2.79 (1H, d, J = 6.0 Hz, CH_2), 3.11 (1H, d, J = 11.5 Hz, CH_2), 3.31 (2H, s, CH_2), 3.60 (1H, d, J = 6.5 Hz, CH_2), 3.72 (1H, m, CH_2), 3.95 (1H, m, CH_2), 4.20 (2H, d, J = 11.0 Hz, CH_2), 4.46 (1H, m, CH_2), 4.85 (1H, m, CH_2), 4.93 (1H, m, CH_2), 6.68 (2H, s, ArH), 6.91 (1H, s, ArH). 2nd species ^{1}H NMR ($CDCl_3$): δ 0.45 – 1.45 (12H, br, CH_3), 2.00 – 2.50 (12H, br, CH_3), 2.00 – 2.50 (4H, br, CH_2), 3.00 – 5.00 (10H, br, CH_2), 3.00 – 5.00 (2H, br, CH), 6.58 (2H, s, ArH), 6.87 (2H, s, ArH). ^{13}C{^{1}H} NMR ($CDCl_3$): δ 16.5 (CH_3), 16.9 (CH_3), 20.8 (CH_3), 23.0 (CH_2), 23.7 (CH_2), 25.9 (CH_3), 26.1 (CH_3), 26.3 (CH_3), 50.8 (br, CH_2), 55.6 (CH_2), 58.0 (CH_2), 59.2 (br, CH_2), 62.7 (br, CH_2), 64.1 (CH_2), 72.1 (CH), 73.2 (CH), 75.7 (CH), 75.9 (CH), 123.4 (ArH), 124.6 (ArH), 125.4 (ArH), 127.4 (Ar), 122.0 – 132.0 (Ar),

131.5 (Ar), 163.0 (ArO). Calc. (%) for $C_{29}H_{44}N_2O_4Ti$: C 65.41, H 8.33, N 5.26. Found (%), C 65.29, H 8.27, N 5.37

Ti(**7**)(O^iPr)$_2$. **7**H_2 (0.46 g, 1.02 mmol) and Ti(O^iPr)$_4$ (0.30 ml, 1.01 mmol) were dissolved in toluene (30 ml) then heated (80 °C) and stirred (16 h). The solvent was removed *in-vacuo* and recrystallised from hexane to yield pale yellow crystals (0.48 g, 0.78 mmol, 77 %). 2 species identified in the solution state NMR spectra. ^{1}H NMR ($CDCl_3$): δ 0.32 (3H, d, J = 6.0 Hz, CH_3), 0.87 (6H, br, CH_3), 1.65 (9H, d, J = 6.0 Hz, CH_3), 1.26 (36H, s, CH_3), 1.71 (1H, m, CH_2), 1.90 (2H, m, CH_2), 2.16 (4H, br, CH_2), 2.28 (12H, s, CH_3), 2.24 (2H, br, CH_2), 2.80 (1H, d, J = 6.5 Hz, CH_2), 3.16 (1H, d, J = 11.5 Hz, CH_2), 3.30 (4H, br, CH_2), 3.61 (1H, d, J = 6.5 Hz, CH_2), 3.71 (2H, m, CH_2), 3.97 (1H, m, CH), 4.20 (2H, d, J = 11.5 Hz, CH_2), 4.22 (1H, br, CH_2), 4.45 (1H, m, CH), 4.80 (1H, m, CH), 4.92 (1H, m, CH), 6.74 (2H, br, ArH), 6.86 (2H, s, ArH), 7.05 (2H, br, ArH), 7.11 (2H, s, ArH). ^{13}C{^{1}H} NMR ($CDCl_3$): δ 16.5 (CH_3), 16.9 (CH_3), 20.7 (CH_3), 23.0 (C), 23.7 (C), 25.8 (CH_3), 26.1 (CH_3), 26.3 (CH_3), 55.6 (CH_2), 58.0 (CH_2), 59.2 (br, CH_2), 62.7 (br, CH_2), 64.1 (CH_2), 72.1 (CH), 73.1 (CH), 75.7 (CH), 75.9 (CH), 122.9 (Ar), 123.4 (ArH), 124.0 (Ar), 126.7 (br, Ar), 127.9 (ArH), 139.1 (Ar), 163.0 (ArO). Calc. (%) for $C_{35}H_{56}N_2O_4Ti$: C 68.17, H 9.15, N 4.54. Found (%), C 68.29, H 9.28, N 4.57

Ti(**8**)(O^iPr)$_2$. **8**H_2 (0.54 g, 1.01 mmol) and Ti(O^iPr)$_4$ (0.30 ml, 1.01 mmol) were dissolved in toluene (30 ml) then heated (80 °C) and stirred (16 h). The solvent was removed *in-vacuo* and recrystallised from hexane to yield pale yellow crystals (0.24 g, 0.34 mmol, 34 %). 2 species identified in the solution state NMR spectra in a approximate 50:50 ratio, a third species is present in a negligible ratio. ^{1}H NMR ($CDCl_3$): δ 0.39 (3H, d, J = 6.0 Hz, CH_3), 0.55 (3H, d, J = 6.0 Hz, CH_3), 0.72 (3H, d, J = 6.0 Hz, CH_3), 0.94 (3H, d, J = 6.0 Hz, CH_3), 0.97 (3H, d, J = 6.0 Hz, CH_3), 0.98 (3H, d, J = 6.0 Hz, CH_3), 1.01 (6H, d, J = 6.0 Hz, CH_3), 1.26 (18H, s, ^{t}Bu), 1.28 (18H, s, ^{t}Bu), 1.46 (9H, s, ^{t}Bu), 1.47 (9H, s, ^{t}Bu), 1.48 (18H, s, ^{t}Bu), 1.82 (2H, m, CH_2), 2.23 (3H, m, CH_2), 2.38 (3H, m, CH_2), 2.45 (1H, m, CH_2), 2.72 (2H, m, CH_2), 3.05 (1H, d, J = 11.5 Hz, CH_2), 3.23 (2H, d, J = 11.5 Hz, CH_2), 3.44 (1H, d, J = 14.5 Hz, CH_2), 3.55 (2H, m, CH_2), 3.61 (2H, d, J = 6.5 Hz, CH_2), 3.88 (2H, m, CH_2), 3.97 (1H, br, CH_2), 4.01 (2H, d, J = 11.5 Hz, CH_2), 4.13 (1H, d, J = 11.5 Hz, CH_2), 4.17 (1H, m,

CH_2), 4.23 (1H, m, CH), 4.28 (1H, m, CH), 4.51 (1H, d, J = 11.5 Hz, CH_2), 4.55 (2H, m, CH), 6.74 (1H, d, J = 2.0 Hz, ArH), 6.88 (2H, d, J = 2.5 Hz, ArH), 6.90 (1H, d, J = 2.5 Hz, ArH), 7.16 (1H, d, J = 2.5 Hz, ArH), 7.25 (2H, d, J = 2.5 Hz, ArH), 7.27 (1H, br, ArH). $^{13}C\{^1H\}$ NMR ($CDCl_3$): δ 22.9 (CH_2), 23.3 (CH_2), 25.4 (CH_3), 25.5 (CH_3), 25.9 (CH_3), 26.1 (CH_3), 26.2 (CH_3), 26.7 (CH_3), 30.0 (CH_3), 30.3 (CH_3), 30.6 (CH_3), 32.0 (CH_3), 34.1 (C), 34.2 (C), 35.1 (C), 35.3 (C), 35.5 (C), 35.6 (C), 51.3 (CH_2), 52.6 (CH_2), 55.2 (CH_2), 55.3 (CH_2), 55.6 (CH_2), 57.7 (CH_2), 58.4 (CH_2), 59.0 (CH_2), 63.2 (CH_2), 64.4 (CH_2), 64.6 (CH_2), 72.7 (CH), 72.9 (CH), 74.9 (CH), 76.0 (CH), 121.5 (ArH), 122.2 (Ar), 122.9 (Ar), 123.5 (Ar), 123.7 (ArH), 123.8 (ArH), 123.9 (ArH), 123.9 (ArH), 124.0 (ArH), 124.4 (ArH), 124.6 (Ar), 134.1 (Ar), 134.3 (Ar), 136.7 (Ar), 136.8 (Ar), 138.3 (Ar), 138.5 (Ar), 139.4 (Ar), 139.5 (Ar), 159.1 (ArO), 160.0 (ArO), 163.5 (ArO), 164.3 (ArO). Calc. (%) for $C_{41}H_{68}N_2O_4Ti$: C 70.26, H 9.78, N 4.00. Found (%), C 70.19, H 9.69, N 4.12.

Ti(**9**)(O^iPr)$_2$. **9**H_2 (0.46 g, 1.02 mmol) and Ti(O^iPr)$_4$ (0.30 ml, 1.01 mmol) were dissolved in toluene (30 ml) then heated (80 °C) and stirred (16 h). The solvent was removed *in-vacuo* and recrystallised from hexane to yield pale yellow crystals (0.16 g, 0.26 mmol, 26 %). 2 species identified in the solution state NMR spectra in a approximate 50:50 ratio. ^1H NMR ($CDCl_3$): δ 0.41 (3H, br, CH_3), 0.55 (3H, d, J = 6.0 Hz, CH_3), 0.72 (3H, d, J = 6.0 Hz, CH_3), 0.98 (3H, d, J = 6.0 Hz, CH_3), 1.02 (3H, d, J = 6.0 Hz, CH_3), 1.00 (3H, s, CH_3), 0.98 (6H, br, CH_3), 1.43 (54H, s, ^{t}Bu), 1.81 (3H, m, CH_2), 2.15 – 2.30 (7H, br, CH_2), 2.22 (6H, s, CH_3), 2.24 (6H, s, CH_3), 2.25 (6H, s, CH_3), 2.30-2.45 (6H, m, CH_2), 2.54 (1H, m, CH_2), 2.66 (2H, m, CH_2), 2.78 (1H, br, CH_2), 3.05 (2H, d, J = 12.0 Hz, CH_2), 3.22 (2H, d, J = 11.5 Hz, CH_2), 3.41 (2H, t, J = 13.0 Hz, CH_2), 3.43 (2H, br, CH_2), 3.54 (2H, br, CH_2), 3.68 (2H, d, J= 3.5 Hz, CH_2), 3.82 (2H, br, CH), 3.98 (3H, br, CH_2), 4.05 (2H, d, J = 12.0 Hz, CH_2), 4.12 (2H, m, CH_2), 4.24 (2H, m, CH), 4.51 (2H, d, J = 14.0 Hz, CH_2), 4.61 (2H, m, CH), 5.31 (1H, d, J = 13.0 Hz, CH_2), 6.61 (1H, s, ArH), 6.75 (2H, s, ArH), 6.77 (2H, s, ArH), 6.81 (1H, s, ArH), 6.97 (1H, s, ArH), 7.01 (4H, s, ArH), 7.09 (1H, s, ArH). $^{13}C\{^1H\}$ NMR ($CDCl_3$): δ 20.9 (CH_3), 21.0 (CH_3), 21.1 (CH_3), 22.9 (CH_3), 23.4 (CH_3), 25.8 (CH_3), 25.9 (CH_3), 26.0 (CH_3), 26.3 (CH_3), 26.4 (CH_3), 26.9 (CH_3), 29.9 (CH_3), 30.2 (CH_3), 30.6 (CH_3), 34.8 (C), 35.0 (C), 35.2 (C), 35.3 (C), 50.9 (CH_2), 52.6 (CH_2), 55.2 (CH_2), 55.5 (CH_2), 55.7 (CH_2), 57.8 (CH_2), 58.4 (CH_2), 59.1 (CH_2), 62.9 (CH_2), 64.3

(CH_2), 64.4 (CH_2), 64.7 (CH_2), 72.7 (CH), 73.0 (CH), 75.1 (CH), 75.9 (CH), 121.8 (Ar), 122.9 (Ar), 124.2 (Ar), 124.6 (Ar), 124.9 (Ar), 125.3 (Ar), 125.7 (ArH), 125.9 (Ar), 126.0 (Ar), 126.9 (ArH), 127.4 (ArH), 127.7 (ArH), 127.8 (ArH), 128.0 (ArH), 128.2 (ArH), 134.8 (Ar), 135.0 (Ar), 137.5 (Ar), 137.6 (Ar), 134.8 (Ar), 159.1 (ArO), 159.9 (ArO), 163.5 (ArO), 164.3 (ArO). Calc. (%) for $C_{35}H_{56}N_2O_4Ti$: C 68.17, H 9.15, N 4.54. Found (%), C 66.45, H 8.85, N 4.58.

Ti(**10**)(O^iPr)$_2$. **10**H_2 (0.60 g, 1.01 mmol) and Ti(O^iPr)$_4$ (0.30 ml, 1.01 mmol) were dissolved in toluene (30 ml) then heated (80 °C) and stirred (16 h). The solvent was removed *in-vacuo* and recrystallised from hexane to yield pale yellow crystals (0.13 g, 0.17 mmol, 17 %). 2 species identified in the solution state NMR spectra in a approximate 50:50 ratio. ^{1}H NMR ($CDCl_3$): δ 0.33 (3H, d, J = 6.0 Hz, CH_3), 0.55 (3H, d, J = 6.0 Hz, CH_3), 0.67 (15H, m, CH_3), 0.76 (12H, m, CH_3), 0.99 (3H, d, J = 6.0 Hz, CH_3), 1.01 (3H, d, J = 6.0 Hz, CH_3), 1.12 (6H, d, J = 6.0 Hz, CH_3), 1.23 (6H, s, CH_3), 1.26 (12H, s, CH_3), 1.29 (6H, s, CH_3), 1.39 (3H, s, CH_3), 1.41 (3H, s, CH_3), 1.45 (9H, s, CH_3), 1.47 (9H, s, CH_3), 1.60 (8H, m, CH_2), 1.60 (8H, m, CH_2), 1.75 – 1.95 (6H, m, CH_2), 2.07 (3H, m, CH_2), 2.22 (4H, m, CH_2), 2.30 – 2.50 (4H, m, CH_2), 2.66 (1H, m, CH_2), 2.78 (2H, m, CH_2), 3.06 (1H, d, J = 11.5 Hz, CH_2), 3.20 (2H, d, J = 11.5 Hz, CH_2), 3.44 (1H, d, J = 14.5 Hz, CH_2), 3.53 (2H, d, J = 7.5 Hz, CH_2), 3.62 (2H, d, J = 6.5 Hz, CH_2), 3.90 (2H, m, CH_2), 4.00 (1H, br, CH_2), 4.10 (3H, d, J = 11.5 Hz, CH_2), 4.22 (1H, m, CH_2), 4.25 (1H, m, CH), 4.34 (1H, m, CH), 4.54 (1H, d, J = 13.5 Hz, CH_2), 4.59 (1H, m, CH), 4.68 (1H, m, CH), 6.68 (1H, d, J = 2.0 Hz, ArH), 6.83 (2H, d, J = 2.5 Hz, ArH), 6.85 (1H, d, J = 2.0 Hz, ArH), 7.05 (1H, d, J = 2.0 Hz, ArH), 7. 14 (2H, d, J = 2.5 Hz, ArH), 7.16 (1H, br, ArH). ^{13}C{^{1}H} NMR ($CDCl_3$): δ 9.3 (CH_3), 9.4 (CH_3), 9.7 (CH_3), 9.9 (CH_3), 22.9 (CH_2), 23.4 (CH_2), 25.7 (CH_3), 25.8 (CH_3), 26.2 (CH_3), 26.3 (CH_3), 26.4 (CH_3), 27.0 (CH_3), 27.4 (CH_3), 27.8 (CH_3), 27.8 (CH_3), 28.0 (CH_3), 28.1 (CH_3), 28.2 (CH_3), 28.3 (CH_3), 28.7 (CH_3), 28.7 (CH_3), 28.9 (CH_3), 29.0 (CH_3), 29.1 (CH_3), 29.2 (CH_3), 29.3 (CH_3), 32.9 (C), 33.3 (C), 33.8 (C), 37.2 (CH_2), 37.2 (CH_2), 37.3 (CH_2), 37.4 (CH_2), 37.6 (C), 38.3 (C), 38.5 (C), 38.9 (C), 38.9 (C), 51.1 (CH_2), 52.5 (CH_2), 55.4 (CH_2), 55.6 (CH_2), 57.6 (CH_2), 58.2 (CH_2), 59.0 (CH_2), 63.2 (CH_2), 64.7 (CH_2), 64.8 (CH_2), 65.2 (CH_2), 72.7 (CH), 73.0 (CH), 74.8 (CH), 75.9 (CH), 120.9 (Ar), 121.9 (Ar), 123.3 (Ar), 123.4 (ArH), 123.8 (ArH), 124.5 (ArH), 124.6 (ArH), 125.3 (ArH), 125.9 (ArH), 126.5

(ArH), 132.9 (Ar), 133.0 (Ar), 134.9 (Ar), 135.1 (Ar), 136.1 (Ar), 136.2 (Ar), 137.2 (Ar), 137.4 (Ar), 158.8 (ArO), 159.7 (ArO), 163.5 (ArO), 164.1 (ArO). CHN Calc. (%) for $C_{45}H_{76}N_2O_4Ti$: C 71.40, H 10.12, N 3.70. Found (%), C 71.38, H 9.97, N 3.78.

Ti(**11**)(O^iPr)$_2$. **11**H_2 (0.43 g, 1.01 mmol) and Ti(O^iPr)$_4$ (0.30 ml, 1.01 mmol) were dissolved in toluene (30 ml) then heated (80 °C) and stirred (16 h). The solvent was removed *in-vacuo* and recrystallised from hexane to yield pale yellow crystals (0.39 g, 0.66 mmol, 65 %). ^{1}H NMR ($CDCl_3$): δ 0.63 (6H, d, J = 6.0 Hz, CH_3), 1.61 (6H, d, J = 6.0 Hz, CH_3), 1.28 (18H, s, ^{t}Bu), 1.72 (1H, m, CH_2), 1.72 (1H, m, CH_2), 2.19 (1H, m, CH_2), 2.28 (2H, m, CH_2), 2.81 (2H, d, J = 6.5 Hz, CH_2), 3.20 (2H, d, J = 11.5 Hz, CH_2), 3.61 (2H, d, J = 6.0 Hz, CH_2), 3.61 (2H, br, CH_2), 3.84 (1H, m, CH), 4.22 (2H, d, J = 11.5 Hz, CH_2), 4.82 (1H, m, CH), 6.79 (1H, s, ArH), 6.82 (1H, s, ArH), 7.02 (2H, d, J = 2.0 Hz, ArH), 7.18 (1H, s, ArH), 7.27 (1H, s, ArH). ^{13}C{^{1}H} NMR ($CDCl_3$): δ 23.0 (CH_2), 26.1 (CH_3), 26.2 (CH_3), 31.9 (CH_3), 34.0 (C), 55.3 (CH_2), 58.0 (CH_2), 64.1 (CH_2), 72.0 (CH), 73.0 (CH), 116.6 (ArH), 123.6 (Ar), 125.9 (ArH), 126.5 (ArH), 139.7 (Ar), 164.1 (ArO). CHN Calc. (%) for $C_{33}H_{52}N_2O_4Ti$: C 67.33, H 8.90, N 4.76. Found (%), C 67.42, H 8.89, N 4.70.

7.4.3 Preparation of titanium catechol homo/piperazine salan complexes

Ti(**1**)Catechol. **1**H_2 (0.60 g, 1.69 mmol) and Ti(O^iPr)$_4$ (0.50 ml, 1.69 mmol) were dissolved in CH_2Cl_2 (30 ml) and stirred (1 h). Catechol (0.185 g, 1.68 mmol) was added to the yellow solution and the resulting dark red solution was stirred (16 h) before the solvent was removed *in-vacuo* and recrystallised from hot toluene (30 ml) to yield orange crystals (0.71 g, 1.39 mmol, 83 %). ^{1}H NMR ($CDCl_3$): δ 2.18 (2H, d, J = 6.5 Hz, CH_2), 2.25 (6H, s, CH_3), 2.26 (6H, s, CH_3), 2.63 (2H, d, J = 5.5 Hz, CH_2), 3.23 (2H, d, J = 6.5 Hz, CH_2), 3.38 (2H, d, J = 14.0 Hz, CH_2), 3.80 (2H, d, J = 5.5 Hz, CH_2), 4.51 (2H, d, J = 13.5 Hz, CH_2), 6.40 (1H, d, J = 3.5 Hz, ArH), 6.42 (1H, d, J = 3.5 Hz, ArH), 6.62 (1H, d, J = 3.5 Hz, ArH), 6.64 (1H, d, J = 3.5 Hz, ArH), 6.65 (2H, s, ArH), 6.96 (2H, s, ArH). ^{13}C{^{1}H} NMR ($CDCl_3$): δ 16.7 (CH_3), 20.7 (CH_3), 49.7 (CH_2), 50.1 (CH_2), 58.5 (CH_2), 111.2 (ArH), 119.1 (ArH), 121.9 (Ar), 126.1 (Ar), 126.8 (ArH), 129.0, (Ar), 131.4, (ArH), 157.3, (ArO), 158.7, (ArO). Calc. (%) for $C_{28}H_{32}N_2O_4Ti$: C 66.14, H 6.34, N 5.51. Found (%), C 66.28, H 6.20, N 5.55.

Ti(**1**)-3,5-Di-*tert*-butylcatechol. **1**H_2 (0.36 g, 1.02 mmol) and Ti(O^iPr)$_4$ (0.30 ml, 1.01 mmol) were dissolved in CH_2Cl_2 (30 ml) and stirred (1 h). 3,5-Di-*tert*-butylcatechol (0.225 g, 1.01 mmol) was added to the yellow solution and the resulting dark red solution was stirred (16 h) before the solvent was removed *in-vacuo* and recrystallised from hot toluene (30 ml) to yield orange crystals (0.42 g, 0.68 mmol, 67 %). ^{1}H NMR ($CDCl_3$): δ 1.12 (9H, s, ^{t}Bu), 1.26 (9H, s, ^{t}Bu), 2.19 (2H, d, J = 6.0 Hz, CH_2), 2.24 (6H, s, CH_3), 2.27 (6H, s, CH_3), 2.65 (2H, d, J = 5.5 Hz, CH_2), 3.24 (2H, d, J = 6.0 Hz, CH_2), 3.40 (2H, d, J = 13.5 Hz, CH_2), 3.91 (2H, d, J = 5.5 Hz, CH_2), 4.51 (2H, d, J = 13.5 Hz, CH_2), 6.34 (1H, d, J = 2.5 Hz, ArH), 6.62 (1H, d, J = 4.5 Hz, ArH), 6.61 (2H, s, ArH), 6.96 (2H, s, ArH). ^{13}C{^{1}H} NMR ($CDCl_3$): δ 16.5 (CH_3), 20.7 (CH_3), 29.6 (CH_3), 32.1 (CH_3), 34.3 (C), 34.5 (C), 49.8 (CH_2), 55.1 (CH_2), 58.6 (CH_2), 106.9 (ArH), 112.9 (ArH), 121.7 (Ar), 126.2 (Ar), 126.6 (ArH), 128.5 (Ar), 131.1 (ArH), 131.3 (Ar), 141.1 (Ar), 154.8, (ArO), 157.6, (ArO), 158.8, (ArO). Calc. (%) for $C_{36}H_{48}N_2O_4Ti$: C 69.67, H 7.80, N 4.51. Found (%), C 64.47, H 7.25, N 4.23.

Ti(**1**)-3-Methoxycatechol. **1**H_2 (0.36 g, 1.02 mmol) and Ti(O^iPr)$_4$ (0.30 ml, 1.01 mmol) were dissolved in CH_2Cl_2 (30 ml) and stirred (1 h). 3-Methoxycatechol (0.142 g, 1.01 mmol) was added to the yellow solution and the resulting dark red solution was stirred (16 h) before the solvent was removed *in-vacuo* and recrystallised from hot toluene (30 ml) to yield orange crystals (0.25 g, 0.46 mmol, 46 %). ^{1}H NMR ($CDCl_3$): δ 2.19 (2H, d, J = 6.5 Hz, CH_2), 2.23 (6H, s, CH_3), 2.25 (6H, s, CH_3), 2.63 (2H, d, J = 5.5 Hz, CH_2), 3.22 (2H, d, J = 6.0 Hz, CH_2), 3.38 (2H, d, J = 13.5 Hz, CH_2), 3.69 (3H, s, CH_3), 3.83 (2H, d, J = 5.5 Hz, CH_2), 4.53 (2H, d, J = 13.5 Hz, CH_2), 6.12 (1H, dd, J = 8.0 Hz, J = 1.0 Hz, ArH), 6.33 (1H, dd, J = 8.5 Hz, J = 1.5 Hz, ArH), 6.54 (1H, t, J = 8.0 Hz, ArH), 6.64 (2H, s, ArH), 6.94 (2H, s, ArH).^{13}C{^{1}H} NMR ($CDCl_3$): δ 16.6 (CH_3), 20.7 (CH_3), 49.7 (CH_2), 55.2 (CH_2), 56.9 (CH_3), 58.6 (CH_2), 115.7 (ArH), 115.9 (ArH), 118.3 (ArH), 122.0 (Ar), 126.1 (Ar), 126.7 (ArH), 128.9 (Ar), 131.3 (ArH), 144.1 (Ar), 146.7 (ArO), 157.4 (ArO), 160.0 (ArO). Calc. (%) for $C_{29}H_{34}N_2O_5Ti$: C 64.69, H 6.36, N 5.20. Found (%), C 64.74, H 6.29, N 5.39.

Ti(**1**)-4-Nitrocatechol. **1**H_2 (0.36 g, 1.02 mmol) and Ti(O^iPr)$_4$ (0.30 ml, 1.01 mmol) were dissolved in CH_2Cl_2 (30 ml) and stirred (1 h). 4-Nitrocatechol (0.16 g, 1.03

mmol) was added to the yellow solution and the resulting dark red solution was stirred (16 h) before the solvent was removed *in-vacuo* and recrystallised from hot toluene (30 ml) to yield orange crystals (0.44 g, 0.80 mmol, 78 %). ^{1}H NMR ($CDCl_3$): δ 2.25 (6H, s, CH_3), 2.27 (6H, s, CH_3), 2.31 (2H, d, J = 7.0 Hz, CH2), 2.75 (2H, d, J = 5.5 Hz, CH_2), 3.32 (2H, d, J = 6.0 Hz, CH_2), 3.47 (2H, d, J = 14.0 Hz, CH_2), 3.79 (2H, d, J = 6.0 Hz, CH_2), 4.48 (2H, d, J = 14.0 Hz, CH_2), 6.38 (1H, d, J = 8.5 Hz, ArH), 6.70 (2H, s, ArH), 6.98 (2H, s, ArH), 7.25 (1H, s, ArH), 7.70 (1H, dd, J = 8.5 Hz, J = 2.5 Hz, ArH). ^{13}C{^{1}H} NMR ($CDCl_3$): δ 16.5 (CH_3), 20.8 (CH_3), 49.8 (CH_2), 55.2 (CH_2), 58.5 (CH_2), 106.2 (ArH), 110.0 (ArH), 117.5 (ArH), 121.7 (Ar), 125.9 (Ar), 126.8 (ArH), 130.1 (Ar), 131.7 (ArH), 144.5 (Ar), 157.1 (ArO), 158.2 (ArO), 166.3 (ArO). Calc. (%) for $C_{28}H_{31}N_3O_6Ti$: C 60.77, H 5.65, N 7.59. Found (%), C 60.81, H 5.79, N 7.49.

Ti(**2**)Catechol. **2**H_2 (0.74 g, 1.69 mmol) and Ti($O^{i}Pr$)$_4$ (0.50 ml, 1.69 mmol) were dissolved in CH_2Cl_2 (30 ml) and stirred (1 h). Catechol (0.186 g, 1.69 mmol) was added to the yellow solution and the resulting dark red solution was stirred (16 h) before the solvent was removed *in-vacuo* and recrystallised from hot toluene (30 ml) to yield orange crystals (0.72 g, 1.22 mmol, 72 %). ^{1}H NMR ($CDCl_3$): δ 1.29 (18H, s, ^{t}Bu), 2.17 (2H, d, J = 6.5 Hz, CH_2), 2.29 (6H, s, CH_3), 2.23 (6H, s, CH_3), 2.64 (2H, d, J = 5.5 Hz, CH_2), 3.22 (2H, d, J = 6.5 Hz, CH_2), 3.40 (2H, d, J = 13.5 Hz, CH_2), 3.79 (2H, d, J = 5.5 Hz, CH_2), 4.53 (2H, d, J = 13.5 Hz, CH_2), 6.39 (1H, d, J = 3.5 Hz, ArH), 6.41 (1H, d, J = 4.0 Hz, ArH), 6.61 (1H, d, J = 4.0 Hz, ArH), 6.63 (1H, d, J = 3.5 Hz, ArH), 6.83 (2H, d, J = 2.5, ArH), 7.14 (2H, d, J = 2.5, ArH). ^{13}C{^{1}H} NMR ($CDCl_3$): δ 17.0 (CH_3), 31.8 (CH_3), 34.1 (C), 49.6 (CH_2), 55.1 (CH_2), 58.8 (CH_2), 111.1 (ArH), 119.0 (ArH), 121.5 (Ar), 123.0 (ArH), 125.3 (Ar), 127.7 (ArH), 142.4 (Ar), 144.5 (Ar), 157.2 (ArO), 158.9 (ArO). Calc. (%) for $C_{34}H_{44}N_2O_4Ti$: C 68.91, H 7.48, N 4.73. Found (%), C 68.87, H 7.57, N 4.71.

Ti(**6**)Catechol. **6**H_2 (0.37 g, 1.00 mmol) and Ti($O^{i}Pr$)$_4$ (0.30 ml, 1.01 mmol) were dissolved in CH_2Cl_2 (30 ml) and stirred (1 h). Catechol (0.11 g, 1.00 mmol) was added to the yellow solution and the resulting dark red solution was stirred (16 h) before the solvent was removed *in-vacuo* and recrystallised from hot toluene (30 ml) to yield orange crystals (0.33 g, 0.63 mmol, 62 %). ^{1}H NMR ($CDCl_3$): δ 2.00 (2H, m,

CH_2), 2.12 (6H, s, CH_3), 2.23 (6H, s, CH_3), 2.41 (2H, d, J = 7.5 Hz, CH_2), 2.54 (1H, d, J = 7.0 Hz, CH_2), 2.58 (1H, d, J = 6.5 Hz, CH_2), 3.16 (2H, d, J = 7.0 Hz, CH_2), 3.22 (2H, d, J = 13.5 Hz, CH_2), 4.14 (2H, br, CH_2), 4.39 (2H, d, J = 13.0 Hz, CH_2), 6.40 (1H, d, J = 3.5 Hz, ArH), 6.42 (1H, d, J = 3.5 Hz, ArH), 6.62 (1H, d, J = 3.5 Hz, ArH), 6.64 (1H, d, J = 3.5 Hz, ArH), 6.65 (2H, s, ArH), 6.96 (2H, s, ArH). $^{13}C\{^1H\}$ NMR ($CDCl_3$): δ 16.5 (CH_3), 20.8 (CH_3), 23.2 (CH_2), 49.3 (CH_2), 58.7 (CH_2), 63.1 (CH_2), 111.6 (ArH), 119.5 (ArH), 123.1 (ArH), 125.5 (Ar), 127.0 (ArH), 129.1 (Ar), 131.5 (ArH), 158.2 (br, ArO), 158.8 (br, ArO). Calc. (%) for $C_{29}H_{34}N_2O_4Ti$: C 66.67, H 6.56, N 5.36. Found (%), C 66.28, H 6.20, N 5.55.

Ti(**6**)-3-Methoxycatechol. **6**H_2 (0.37 g, 1.00 mmol) and Ti(O^iPr)$_4$ (0.30 ml, 1.01 mmol) were dissolved in CH_2Cl_2 (30 ml) and stirred (1 h). 3-Methoxycatechol (0.142 g, 1.01 mmol) was added to the yellow solution and the resulting dark red solution was stirred (16 h) before the solvent was removed *in-vacuo* and recrystallised from hot toluene (30 ml) to yield orange crystals (0.50 g, 0.91 mmol, 89 %). ^1H NMR ($CDCl_3$): δ 2.01 (2H, d, J = 6.5 Hz, CH2), 2.12 (6H, br, CH_3), 2.36 (6H, s, CH_3), 2.40 (2H, d, J = 7.5 Hz, CH_2), 2.56 (2H, m, CH_2), 3.15 (2H, d, J = 7.0 Hz, CH_2), 3.22 (2H, d, J = 13.5 Hz, CH_2), 3.75 (3H, s, CH_3), 3.80 – 4.40 (2H, br, CH_2) 4.41 (2H, d, J = 13.5 Hz, CH_2), 6.14 (1H, dd, J = 8.0 Hz, J = 1.5 Hz, ArH), 6.37 (1H, dd, J = 8.0 Hz, J = 1.5 Hz, ArH), 6.58 (1H, t, J = 8.0 Hz, ArH), 6.65 (1H, br, ArH), 6.92 (1H, br, ArH). $^{13}C\{^1H\}$ NMR ($CDCl_3$) (328 K): δ 16.4 (CH_3), 20.7 (CH_3), 23.5 (CH_2), 49.6 (CH_2), 57.2 (CH_3), 58.9 (CH_2), 63.3 (CH_2), 106.3 (ArH), 106.7 (ArH), 118.9 (ArH), 123.2 (Ar), 125.6 (Ar), 126.9 (ArH), 129.1 (Ar), 131.6 (ArH), 144.5 (Ar), 158.4, (ArO), 160.4, (ArO), 177.6, (ArO). Calc. (%) for $C_{30}H_{36}N_2O_5Ti$: C 65.22, H 6.57, N 5.07. Found (%), C 65.18, H 6.65, N 5.16.

Ti(**6**)-4-Nitrocatechol. **6**H_2 (0.50 g, 1.36 mmol) and Ti(O^iPr)$_4$ (0.40 ml, 1.35 mmol) were dissolved in CH_2Cl_2 (30 ml) and stirred (1 h). 4-Nitrocatechol (0.21 g, 1.35 mmol) was added to the yellow solution and the resulting dark red solution was stirred (16 h) before the solvent was removed *in-vacuo* and recrystallised from hot toluene (30 ml) to yield orange crystals (0.34 g, 0.60 mmol, 44 %). ^1H NMR ($CDCl_3$): δ 2.06 (2H, m, CH_2), 2.15 (6H, s, CH_3), 2.27 (6H, s, CH_3), 2.32 (2H, m, CH_2), 2.37 (Toluene-CH_3), 2.53 (2H, d, J = 7.5 Hz, CH_2), 2.63 (2H, m, CH_2), 3.26 (2H, d, J =

7.0 Hz, CH_2), 3.37 (2H, d, J = 14.0 Hz, CH_2), 4.30 (2H, d, J = 13.5 Hz, CH_2), 6.41 (1H, d, J = 9.0 Hz, ArH), 6.72 (2H, s, ArH), 6.98 (2H, s, ArH), 7.15-7.30 (m, Toluene-ArH) 7.27 (1H, s, ArH), 7.74 (1H, dd, J = 8.5 Hz, J = 2.5 Hz, ArH). $^{13}C\{^1H\}$ NMR ($CDCl_3$): δ 16.4 (CH_3), 20.8 (CH_3), 23.1 (CH_2), 58.6 (CH_2), 58.9 (CH_2), 63.3 (CH_2), 106.6 (ArH), 110.4 (ArH), 117.7 (ArH), 122.5 (Ar), 125.1 (Ar), 127.1 (ArH), 130.2 (Ar), 131.8 (ArH) 140.8, (ArO), 157.5 (ArO), 166.8 (ArO). Calc. (%) for $C_{29}H_{33}N_2O_6Ti$: C 61.38, H 5.86, N 7.40. Found (%), C 61.47, H 6.00, N 7.11.

7.5 Preparation of Complexes for Chapter 3

7.5.1 Preparation of zirconium homopiperazine salan complexes

Zr(**6**)(O^iPr)$_2$. **6**H_2 (0.48 g, 1.29 mmol) and Zr(O^iPr)$_4$.^{i}PrOH (0.5 g, 1.29 mmol) were dissolved in CH_2Cl_2 (30 ml) and stirred (16 h). The solvent was removed *in-vacuo* and recrystallised from hot hexane (40 ml) to yield colourless crystals (0.34 g, 0.59 mmol, 46 %). ^1H NMR ($CDCl_3$) (233 K): δ 0.27 (6H, d, J = 6.8 Hz, Me), 1.24 (6H, d, J = 6.8 Hz, Me), 1.41 (1H, d, J = 5.8 Hz, CH_2), 1.68 (1H, br, CH_2), 2.17 (6H, s, Me), 2.19 (6H, s, Me), 2.24 (2H, m, CH_2), 2.88 (2H, d, J = 6.8 Hz, CH_2), 3.07 (2H, d, J = 11.6 Hz, CH_2), 3.30 (1H, br, CH_2), 3.30 (2H, br CH_2), 3.55 (2H, d, J = 6.8 Hz, CH_2), 4.37 (2H, d, J = 11.6 Hz, N-CH_2-Ar), 4.50 (1H, m, CH), 6.67 (2H, s, ArH), 6.90 (2H, s, ArH) $^{13}C\{^1H\}$ NMR ($CDCl_3$) (253 K): δ 17.1 (CH_3), 20.6 (CH_3), 22.5 (CH_2), 26.4 (CH_3), 27.2 (CH_3), 54.2 (CH_2), 56.0 (CH_2), 63.2 (CH_2), 67.5 (CH), 69.2 (CH), 122.4 (Ar), 124.8 (Ar), 126.3 (Ar), 127.8 (ArH) 131.9 (ArH) 159.8 (ArO). Calc. (%) for $C_{29}H_{44}N_2O_4Zr$: C 60.48, H 7.70, N 4.86. Found (%), C 60.54, H 7.66, N 4.71.

Zr(**7**)(O^iPr)$_2$. **7**H_2 (0.58 g, 1.29 mmol) and Zr(O^iPr)$_4$.^{i}PrOH (0.5 g, 1.29 mmol) were dissolved in CH_2Cl_2 (30 ml) and stirred (16 h). The solvent was removed *in-vacuo* and recrystallised from hot hexane (40 ml) to yield colourless crystals (0.49 g, 0.74 mmol, 58 %). ^1H NMR ($CDCl_3$) (233 K): δ 0.15 (6H, d , J = 5.8 Hz, Me), 1.21 (18H, s, ^{t}Bu), 1.23 (6H, s, Me), 1.73 (1H, br, CH_2), 2.15 (1H, br, CH_2), 2.20 (6H, s, Me), 2.26 (2H, br, CH_2), 2.89 (2H, d, J = 6.6 Hz, CH_2), 3.12 (2H, d, J = 11.6 Hz, CH_2), 3.27 (2H, m, CH_2), 3.27 (1H, m, CH), 3.53 (2H, d, J = 6.8 Hz, N-CH_2-Ar), 4.38 (2H, d, J = 11.4 CH), 4.43 (1H, s, J = 6.1 Hz, CH), 6.83 (2H, s, ArH), 7.09 (2H, s, ArH) $^{13}C\{^1H\}$ NMR ($CDCl_3$) (233 K): δ 17.4 (CH_3), 22.5 (CH_2), 26.0 (CH_3), 27.1 (CH_3),

31.7 (CH_3), 33.7 (C), 54.2 (CH_2), 55.8 (CH_2), 63.4 (CH_2), 67.6 (CH), 69.9 (CH), 121.7 (Ar), 123.8 (ArH), 125.7 (Ar), 128.4 (ArH), 138.4 (Ar), 159.8, (ArO). Calc. (%) for $C_{35}H_{56}N_2O_4Zr$: C 63.69, H 8.55, N 4.24. Found (%), C 62.7, H 8.55, N 4.65.

Zr(**8**)(O^iPr)$_2$. **8**H_2 (0.67 g, 1.25 mmol) and Zr(O^iPr)$_4$.^{i}PrOH (0.5 g, 1.29 mmol) were dissolved in CH_2Cl_2 (30 ml) and stirred (16 h). The solvent was removed *in-vacuo* and recrystallised from hot hexane (40 ml) to yield colourless crystals (0.31 g, 0.42 mmol, 33 %). ^{1}H NMR ($CDCl_3$) (253 K): δ 0.01 (6H, s, CH_3), 1.23 (18H, s, ^{t}Bu), 1.23 (6H, br, CH_3), 1.42 (18H, s, ^{t}Bu), 1.80 (1H, br, CH_2), 2.21 (1H, br, CH_2), 2.35 (2H, br, CH_2), 2.88 (2H, d, J = 6.3 Hz, CH_2), 3.14 (2H, d, J = 10.4 Hz, CH_2), 3.53 (2H, d, J = 7.1 Hz, CH_2), 3.60 (2H, br, N-CH_2-Ar), 3.60 (1H, br, CH), 4.30 (2H, br, N-CH_2-Ar), 4.32 (1H, br, CH), 6.88 (2H, s, ArH), 7.24 (2H, s, ArH) ^{13}C{^{1}H} NMR ($CDCl_3$): δ 23.1 (CH_2) 26.0 (CH_3), 27.1 (CH_3), 30.2 (CH_3), 31.9 (CH_3), 34.1 (C), 35.3 (C), 56.5 (CH_2), 63.9 (CH_2), 68.6 (CH), 69.6 (CH), 122.8 (Ar), 124.4 (Ar), 136.3 (Ar), 138.0 (Ar). due to poor solubility 2 Ar resonances were not detected. Calc. (%) for $C_{41}H_{68}N_2O_4Zr$: C 66.17, H 9.21, N 3.76. Found (%), C 66.1, H 9.30, N 4.16.

Zr(**9**)(O^iPr)$_2$. **9**H_2 (0.58 g, 1.29 mmol) and Zr(O^iPr)$_4$.^{i}PrOH (0.5 g, 1.29 mmol) were dissolved in CH_2Cl_2 (30 ml) and stirred (16 h). The solvent was removed *in-vacuo* and recrystallised from hot hexane (40 ml) to yield colourless crystals (0.19 g, 0.29 mmol, 22 %). ^{1}H NMR ($CDCl_3$) (233 K): δ 0.07 (6H, d, J = 5.1 Hz, Me), 1.21 (6H, d, J = 5.8 Hz, Me), 1.39 (18H, s, ^{t}Bu), 1.42 (1H, br, CH_2), 1.74 (1H, br, CH_2), 2.19 (6H, s, CH_3), 2.32 (2H, m, CH_2), 2.89 (2H, d, J = 6.3 Hz, CH_2), 3.10 (2H, d, J = 11.6 Hz, CH_2), 3.50 (2H, d, J = 6.6 Hz, CH_2), 3.59 (2H, br, N-CH_2-Ar), 3.59 (1H, br, CH), 4.27 (2H, br, N-CH_2-Ar), 4.27 (1H, br, CH), 6.72 (2H, s, ArH), 7.00 (2H, s, ArH) ^{13}C{^{1}H} NMR ($CDCl_3$) (233 K): δ 20.9 (CH_3), 22.5 (CH_2), 26.0 (CH_3), 27.2 (CH_3), 29.8 (CH_3), 34.9 (C), 54.3 (CH_2), 56.0 (CH_2), 63.5 (CH_2), 67.9 (CH), 69.1 (CH), 123.4 (Ar), 123.8 (ArH), 128.0 (Ar), 128.7 (ArH), 136.1 (Ar), 161.3, (ArO). Calc. (%) $C_{35}H_{56}N_2O_4Zr$: C 63.69, H 8.55, N 4.24. Found (%), C 63.68, H 8.66, N 4.24.

Zr(**10**)(O^iPr)$_2$. **10**H_2 (0.61 g, 1.03 mmol) and Zr(O^iPr)$_4$.^{i}PrOH (0.4 g, 1.03 mmol) were dissolved in CH_2Cl_2 (30 ml) and stirred (16 h). The solvent was removed *in-*

vacuo and recrystallised from hot hexane (40 ml) to yield colourless crystals (0.37 g, 0.46 mmol, 45 %). ^{1}H NMR ($CDCl_3$) (233 K): δ 0.02 (6H, br, CH_3), 0.52 (6H, t, J = 7.2 Hz, CH_3), 0.72 (6H, t, J = 7.2 Hz, CH_3), 1.16 (6H, br, CH_3), 1.19 (12H, s, CH_3), 1.34 (6H, s, CH_3), 1.36 (6H, s, CH_3), 1.50 (4H, m, CH_2), 1.65 (2H, m, CH_2), 1.79 (1H, br, CH_2), 2.11 (2H, m, CH_2), 2.19 (1H, br, CH_2), 2.33 (2H, m, CH_2), 2.88 (2H, d, J = 6.6 Hz, CH_2), 3.13 (2H, d, J = 11.4 Hz, CH_2), 3.49 (2H, d, J = 7.1 Hz, CH_2), 3.66 (1H, br, CH), 3.66 (2H, br, N-CH_2-Ar), 4.24 (1H, br, CH), 4.28 (2H, d, J = 11.6 Hz, CH_2), 6.80 (2H, s, ArH), 7.10 (2H, s, ArH) $^{13}C\{^{1}H\}$ NMR ($CDCl_3$) (253 K): δ 9.2 (CH_3), 9.8 (CH_3), 22.7 (CH_2), 26.0 (CH_3), 27.0 (CH_3), 27.2 (CH_3), 27.7 (CH_3), 28.6 (CH_3), 29.4 (CH_3), 33.1 (C), 37.0 (C), 37.1 (CH_2), 38.3 (CH_2), 54.4 (CH_2), 56.1 (CH_2), 64.0 (CH_2), 68.2 (CH), 69.1 (CH), 123.5 (Ar), 125.4 (ArH), 126.2 (ArH), 134.7 (Ar), 135.2 (Ar), 161.4 (ArO). Calc. (%) for $C_{45}H_{76}N_2O_4Zr$: C 67.53, H 9.57, N 3.50. Found (%), C 64.38, H 9.22, N 3.11.

7.5.2 Preparation of hafnium homopiperazine salan complexes

Hf(**6**)($O^{i}Pr$)$_2$. **6**H_2 (0.39 g, 1.05 mmol) and Hf($O^{i}Pr$)$_4$.^{i}PrOH (0.5 g, 1.05 mmol) were dissolved in CH_2Cl_2 (30 ml) and stirred (16 h). The solvent was removed *in-vacuo* and recrystallised from hot hexane (40 ml) to yield colourless crystals (0.30 g, 0.45 mmol, 43 %). ^{1}H NMR ($CDCl_3$) (233 K): δ 0.25 (6H, d, J = 5.8 Hz, Me), 1.23, (6H, d, J = 5.8 Hz, Me), 1.68 (1H, br, CH_2), 2.15 (1H, br, CH_2), 2.17 (6H, s, Me), 2.20 (6H, s, Me), 2.34 (2H, m, CH_2), 2.95 (2H, d, J = 6.3 Hz, CH_2), 3.12 (2H, d, J = 11.6 Hz, CH_2), 3.37 (1H, br, CH_2), 3.37 (2H, br CH_2), 3.56 (2H, d, J = 6.8 Hz, CH_2), 4.31 (2H, d, J = 11.6 Hz, N-CH_2-Ar), 4.57 (1H, sept, J = 5.8 Hz, CH), 6.66 (2H, s, ArH), 6.92 (2H, s, ArH) $^{13}C\{^{1}H\}$ NMR ($CDCl_3$) (233 K): δ 17.1 (CH_3), 20.6 (CH_3), 22.5 (CH_2), 26.6 (CH_3), 27.4 (CH_3), 54.3 (CH_2), 56.3 (CH_2), 63.1 (CH_2), 67.3 (CH), 69.0 (CH), 122.4 (Ar), 124.9 (Ar), 126.9 (Ar), 127.8 (ArH) 131.9 (ArH) 159.6 (ArO). Calc. (%) for $C_{29}H_{44}N_2O_4Hf$: C 52.52, H 6.69, N 4.22. Found (%), C 52.4, H 6.71, N 4.28.

Hf(**7**)($O^{i}Pr$)$_2$. **7**H_2 (0.48 g, 1.05 mmol) and Hf($O^{i}Pr$)$_4$.^{i}PrOH (0.5 g, 1.05 mmol) were dissolved in CH_2Cl_2 (30 ml) and stirred (16 h). The solvent was removed *in-vacuo* and recrystallised from hot hexane (40 ml) to yield colourless crystals (0.42 g, 0.56 mmol, 54 %). ^{1}H NMR ($CDCl_3$) (233 K): δ 0.13 (6H, d, J = 6.1 Hz, Me), 1.21 (18H, s, ^{t}Bu), 1.22 (6H, s, ^{t}Bu), 1.73 (1H, br, CH_2), 2.16 (1H, br, CH_2), 2.23 (6H, s, Me),

2.35 (2H, m, CH_2), 2.95 (2H, d, J = 6.6 Hz, CH_2), 3.16 (2H, d, J = 11.6 Hz, CH_2), 3.36 (2H, br, CH_2), 3.36 (1H, br, CH), 3.55 (2H, d, J = 6.8 Hz, N-CH_2-Ar), 4.42 (2H, d, J = 11.4 Hz, N-CH_2-Ar), 4.51 (1H, sept, J = 6.0 Hz, CH), 6.83 (2H, d, J = 2.3 Hz, ArH), 7.11 (2H, d, J = 2.0 Hz, ArH) $^{13}C\{^1H\}$ NMR ($CDCl_3$) (233 K): δ 17.4 (CH_3), 22.5 (CH_2), 26.2 (CH_3), 27.3 (CH_3), 31.7 (CH_3), 33.7 (C), 54.3 (CH_2), 56.1 (CH_2), 63.4 (CH_2), 67.4 (CH), 69.0 (CH), 121.7 (Ar), 123.7 (ArH), 126.3 (Ar), 128.4 (ArH), 138.5 (Ar), 159.7 (ArO). Calc. (%) $C_{35}H_{56}N_2O_4Hf$: C 56.25, H 7.55, N 3.75. Found (%), C 56.24, H 7.48, N 3.63.

Hf(**8**)(O^iPr)$_2$. **8**H_2 (0.53 g, 0.99 mmol) and Hf(O^iPr)$_4$.^{i}PrOH (0.47 g, 0.99 mmol) were dissolved in CH_2Cl_2 (30 ml) and stirred (16 h). The solvent was removed *in-vacuo* and recrystallised from hot hexane (40 ml) to yield colourless crystals (0.14 g, 0.17 mmol, 17 %). ^1H NMR ($CDCl_3$) (233 K): δ -0.02 (6H, d, J = 4.5 Hz, Me), 1.18 (6H, d, J = 5.7 Hz, ^{t}Bu), 1.20 (18H, s, ^{t}Bu), 1.40 (18H, s, ^{t}Bu), 1.79 (1H, br, CH_2), 2.19 (1H, br, CH_2), 2.44 (2H, br, CH_2), 2.95 (2H, d, J = 6.1 Hz, CH_2), 3.17 (2H, d, J = 11.6 Hz, CH_2), 3.52 (2H, d, J = 6.8 Hz, CH_2), 3.63 (2H, br, N-CH_2-Ar), 3.63 (1H, br, CH), 4.32 (2H, d, J = 11.6 Hz, N-CH_2-Ar), 4.32 (1H, br, CH), 6.86 (2H, s, ArH), 7.24 (2H, s, ArH) $^{13}C\{^1H\}$ NMR ($CDCl_3$) (258 K): δ 22.6 (CH_2), 25.8 (CH_3), 27.5 (CH_3), 30.0 (CH_3), 31.8 (CH_3), 34.0 (C), 35.1 (C), 54.5 (CH_2), 56.3 (CH_2), 63.7 (CH_2), 68.0 (CH), 69.0 (CH), 122.6 (Ar), 124.5 (ArH), 124.6 (ArH), 136.3 (Ar), 136.3 (Ar), 137.6 (Ar), 161.3 (ArO). Calc. (%) for $C_{41}H_{68}N_2O_4Hf$: C 59.22, H 8.24, N 3.37. Found (%), C 59.8, H 8.26, N 3.68.

Hf(**9**)(O^iPr)$_2$. **9**H_2 (0.48 g, 1.05 mmol) and Hf(O^iPr)$_4$.^{i}PrOH (0.5 g, 1.05 mmol) were dissolved in CH_2Cl_2 (30 ml) and stirred (16 h). The solvent was removed *in-vacuo* and recrystallised from hot hexane (40 ml) to yield colourless crystals (0.50 g, 0.67 mmol, 64 %). ^1H NMR ($CDCl_3$) (233 K): δ 0.07 (6H, s, Me), 1.20 (6H, d, J = 5.3 Hz, Me), 1.40 (18H, s, ^{t}Bu), 1.41 (1H, br, CH_2), 1.74 (1H, br, CH_2), 2.20 (6H, s, CH_3), 2.42 (2H, m, CH_2), 2.95 (2H, d, J = 6.8 Hz, CH_2), 3.13 (2H, d, J = 11.6 Hz, CH_2), 3.52 (2H, d, J = 7.1 Hz, CH_2), 3.65 (2H, br, N-CH_2-Ar), 3.67 (1H, br, CH), 4.31 (2H, d, J = 11.6 Hz, N-CH_2-Ar), 4.38 (1H, br, CH), 6.72 (2H, s, ArH), 7.03 (2H, s, ArH). $^{13}C\{^1H\}$ NMR ($CDCl_3$) (233 K): δ 20.8 (CH_3), 22.5 (CH_2), 26.3 (CH_3), 27.5 (CH_3), 29.9 (CH_3), 34.8 (C), 54.5 (CH_2), 56.2 (CH_2), 63.4 (CH_2), 67.7 (CH), 68.9 (CH),

123.4 (Ar), 123.9 (ArH), 128.0 (Ar), 128.6 (ArH), 136.6 (Ar), 161.2 (ArO). Calc. (%) for $C_{35}H_{56}N_2O_4Hf$: C 56.25, H 7.55, N 3.75. Found (%), C 56.35, H 7.43, N 3.64.

Hf(**10**)(O^iPr)$_2$. **10**H_2 (0.62 g, 1.05 mmol) and Hf(O^iPr)$_4$.^{i}PrOH (0.5 g, 1.05 mmol) were dissolved in CH_2Cl_2 (30 ml) and stirred (16 h). The solvent was removed *in-vacuo* and recrystallised from hot hexane (40 ml) to yield colourless crystals (0.30 g, 0.34 mmol, 32 %). ^{1}H NMR ($CDCl_3$) (233 K): δ 0.03 (6H, s, CH_3), 0.52 (6H, t, J = 7.3 Hz, CH_3), 0.72 (6H, t, J = 7.3 Hz, CH_3), 1.16 (12H, s, CH_3), 1.20 (6H, s, CH_3), 1.35 (6H, s, CH_3), 1.37 (6H, s, CH_3), 1.50 (4H, m, CH_2), 1.69 (2H, m, CH_2), 1.78 (1H, br, CH_2), 2.09 (2H, m, CH_2), 2.20 (1H, br, CH_2), 2.43 (2H, m, CH_2), 2.95 (2H, d, J = 6.3 Hz, CH_2), 3.16 (2H, d, J = 11.4 Hz, CH_2), 3.51 (2H, d, J = 7.3 Hz, CH_2), 3.74 (2H, br, N-CH_2-Ar), 3.74 (1H, br, CH), 4.32 (2H, d, J = 11.4 Hz, N-CH_2-Ar), 4.33 (1H, br, CH), 6.80 (2H, s, ArH), 7.12 (2H, s, ArH). ^{13}C{^{1}H} NMR (233 K): δ 9.2 (CH_3), 9.8 (CH_3), 22.9 (CH_2), 26.3 (CH_3), 27.1 (CH_3), 27.6 (CH_3), 27.7 (CH_3), 28.4 (CH_3), 29.8 (CH_3), 33.0 (C), 37.1 (C), 37.2 (CH_2), 38.2 (CH_2), 54.6 (CH_2), 56.4 (CH_2), 63.8 (CH_2), 68.0 (CH_2), 68.9 (CH_2), 122.5 (Ar), 125.4 (ArH), 126.3 (ArH), 135.1 (Ar), 135.1 (Ar), 161.2 (ArO). Calc. (%) for $C_{45}H_{76}N_2O_4Hf$: C 60.89, H 8.63, N 3.16. Found (%), C 51.99, H 7.82, N 2.50.

7.6 Preparation of Complexes for Chapter 4

7.6.1 Preparation of methyl aluminium homopiperazine salan complexes

Al(**6**)Me. A solution of **6**H_2 (0.69 g, 1.87 mmol) in toluene (30 ml) was heated to 50°C and 2M $AlMe_3$ (0.93 ml, 1.86 mmol) was added slowly while stirring (30 mins, 50°C), after which the solution was further heated and stirred (3 h, 80°C). The crude mixture was recrystallised from a toluene:hexane mix to yield a white powder (0.45 g, 1.1 mmol, 59 %). ^{1}H NMR (298 K) ($C_6D_5CD_3$): δ −0.59 (1.5H, s, Al-Me), −0.43 (1.5H, s, Al-Me), 0.50 (0.5H, d, J = 15.5 Hz, CH_2), 0.89 (1H, m, CH_2), 1.04 (0.5H, br, CH_2), 1.22 (1H, m, CH_2), 1.35 (2H, m, CH_2), 1.51 (1H, m, CH_2), 1.68 (1H, m, CH_2), 2.28 (3H, s, CH_3), 2.30 (3H, s, CH_3), 2.43 (3H, s, CH_3), 2.58 (2H, m, CH_2), 2.62 (3H, s, CH_3), 2.66 (2H, m, CH_2), 2.92 (1H, m, CH_2), 3.68 (1H, d, J = 13.0 Hz, CH_2), 4.04 (1H, d, J = 13.0 Hz, CH_2), 6.45 (2H, d, J = 4.5 Hz, ArH), 6.95 (2H, s, ArH). ^{13}C{^{1}H} NMR ($C_6D_5CD_3$): δ 16.7 (CH_3), 17.0 (CH_3), 20.8 (CH_3), 22.0 (CH_2), 22.4 (CH_2),

46.2 (CH_2), 49.5 (CH_2), 51.1 (CH_2), 55.5 (CH_2), 61.7 (CH_2), 62.8 (CH_2), 119.0 (Ar), 120.5 (Ar), 123.6 (Ar), 124.3 (Ar), 126.5 (ArH), 126.7 (ArH), 128.0 (Ar), 128.9 (Ar), 131.7 (ArH), 131.9 (ArH), 157.7 (ArO), 157.9 (ArO). Calc. (%) for $C_{24}H_{33}N_2O_2Al$, C 70.56, H 8.14, N 6.86. Found (%), C 70.68, H 8.08, N 6.69.

Al(**7**)Me. A solution of **7**H_2 (0.91 g, 2.01 mmol) in toluene (40 ml) was heated to 50°C and 2M $AlMe_3$ (1.0 ml, 1.00 mmol) was added slowly while stirring (30 mins, 50°C), after which the solution was further heated and stirred (3 h, 80°C). The crude mixture was recrystallised from a toluene:hexane mix to yield a white powder (0.25 g, 0.51 mmol, 25 %). ^{1}H NMR (233 K) ($C_6D_5CD_3$): δ −0.45 (3H, s, Al-Me), 0.18 (1H, br, CH_2), 0.73 (1H, br, CH_2), 1.12 (2H, d, J = 7.5 Hz, CH_2), 1.39 (2H, d, J = 7.0 Hz, CH_2), 1.51 (18H, s, CH_3), 2.06 (1H, m, CH_2), 2.45 (2H, d, J = 13.0 Hz, CH_2), 2.54 (2H, br, CH_2), 2.64 (1H, br, CH_2), 2.82 (6H, s, CH_3), 3.97 (2H, d, J = 13.0 Hz, CH_2), 6.80 (2H, d, J= 2.0 Hz, ArH), 7.40 (2H, d, J = 2.0 Hz, ArH). ^{13}C{^{1}H} NMR ($C_6D_5CD_3$): δ 17.3 (CH_3), 21.9 (C), 32.2 (CH_3), 40.0 (CH_2), 49.4 (CH_2), 52.1 (CH_2), 63.2 (CH_2), 118.5 (Ar), 122.3 (ArH), 127.8 (Ar), 127.9 (ArH), 137.5 (Ar), 157.6 (ArO). Calc. (%) for $C_{30}H_{45}N_2O_2Al$, C 73.14, H 9.21, N 5.69. Found (%), C 72.99, H 9.09, N 5.78.

Al(**8**)Me. A solution of **8**H_2 (0.54 g, 1.01 mmol) in toluene (30 ml) was heated to 50°C and 2M $AlMe_3$ (0.5 ml, 1.00 mmol) was added slowly while stirring (30 mins, 50°C), after which the solution was further heated and stirred (3 h, 80°C). The crude mixture was recrystallised from a toluene:hexane mix to yield clear crystals suitable for X-ray diffraction (0.25 g, 0.43 mmol, 43 %). ^{1}H NMR (233 K) (C_4D_8O): δ −0.87 (3H, s, Al-Me), 1.26 (18H, s, CH_3), 1.44 (9H, s, CH_3), 1.50 (9H, s, CH_3), 1.86 (1H, br, CH_2), 2.33 (2H, br, CH_2), 2.41 (1H, br, CH_2), 2.62 (1H, br, CH_2), 3.15 (2H, br, CH_2), 3.23 (2H, m, CH_2), 3.32 (2H, m, CH_2), 3.41 (1H, br, CH_2), 4.06 (1H, d, J = 11.5 Hz, CH_2), 4.27 (1H, d, J = 14.0 Hz, CH_2), 6.79 (1H, s, ArH), 6.86 (1H, s, ArH), 7.16 (1H, s, ArH), 7.20 (1H, s, ArH). ^{13}C{^{1}H} NMR (233 K) (C_4D_8O): δ 21.9 (CH_2), 29.8 (CH_3), 29.1 (CH_3), 31.3 (CH_3), 31.4 (CH_3), 33.7 (C), 33.8 (C), 34.8 (C), 35.1 (C), 43.9 (CH_2), 51.9 (CH_2), 54.2 (CH_2), 55.6 (CH_2), 59.4 (CH_2), 65.0 (CH_2), 120.5 (Ar), 121.8 (Ar), 122.4 (Ar), 122.7 (Ar), 123.2 (Ar), 123.5 (Ar), 135.8 (Ar), 136.4

(Ar), 137.3 (Ar), 137.8 (Ar), 155.7 (ArO), 159.7 (ArO). Calc. (%) for $C_{36}H_{57}N_2O_2Al$, C 74.96, H 9.96, N 4.86. Found (%), C 74.96, H 9.90, N 4.81.

Al(**9**)Me. A solution of **9**H_2 (0.45 g, 1.00 mmol) in toluene (30 ml) was heated to 50°C and 2M $AlMe_3$ (0.5 ml, 1.00 mmol) was added slowly while stirring (30 mins, 50°C), after which the solution was further heated and stirred (3 h, 80°C). The crude mixture was recrystallised from a toluene:hexane mix to yield a white powder (0.21 g, 0.43 mmol, 43 %). ^{1}H NMR (233 K) ($C_6D_5CD_3$): δ −0.59 (3H, s, Al-Me), 0.54 (1H, d, J = 13.5 Hz, CH_2), 0.92 (1H, br, CH_2), 1.08 (1H, br, CH_2), 1.16 (2H, br, CH_2), 1.30 (1H, d, J = 7.5 Hz, CH_2), 1.55 (1H, br, CH_2), 1.92 (9H, s, CH_3), 1.95 (9H, s, CH_3), 2.27 (1H, d, J = 11.5 Hz, CH_2), 2.40 (1H, d, J = 14.5 Hz, CH_2), 2.43 (1H, br, CH_2), 2.43 (3H, s, 2.76), 2.48 (3H, s, 2.76), 2.57 (1H, br, CH_2), 2.87 (1H, br, CH_2), 3.63 (1H, d, J = 11.5 Hz, CH_2), 3.81 (1H, d, J = 14.0 Hz, CH_2), 6.54 (1H, s, ArH), 6.60 (1H, s, ArH), 7.36 (1H, s, ArH), 7.41 (1H, s, ArH). ^{13}C{^{1}H} NMR (233 K) (C_4D_8O): δ 21.3 (CH_3), 21.4 (CH_3), 22.9 (CH_2), 30.2 (CH_3), 30.9 (CH_3), 35.6 (C), 35.9 (C), 44.8 (CH_2), 52.7 (CH_2), 55.3 (CH_2), 56.8 (CH_2), 60.2 (CH_2), 65.6 (CH_2), 122.1 (Ar), 123.3 (Ar), 123.4 (Ar), 124.8 (Ar), 127.4 (Ar), 127.5 (Ar), 128.1 (Ar), 128.5 (Ar), 138.2 (Ar), 139.4 (Ar), 156.8 (ArO), 161.0 (ArO). Calc. (%) for $C_{30}H_{45}N_2O_2Al$, C 73.14, H 9.21, N 5.69. Found (%), C 73.02, H 9.25, N 5.73.

Al(**11**)Me. A solution of **11**H_2 (0.85 g, 2.00 mmol) in toluene (40 ml) was heated to 50°C and 2M $AlMe_3$ (1.0 ml, 2.00 mmol) was added slowly while stirring (30 mins, 50°C), after which the solution was further heated and stirred (3 h, 80°C). The crude mixture was recrystallised from a toluene:hexane mix to yield a white powder (0.55 g, 1.18 mmol, 59 %). ^{1}H NMR (233 K) (C_4D_8O): δ −0.53 (3H, s, Al-Me), 1.23 (18H, s, CH_3), 1.23 (2H, br, CH_2), 2.30 (2H, m, CH_2), 2.94 (2H, br, CH_2), 3.04 (2H, br, CH_2), 3.13 (2H, br, CH_2), 3.40 (2H, d, J = 13.5 Hz, CH_2), 4.30 (2H, d, J = 13.0 Hz, CH_2), 6.58 (2H, d, J = 8.5 Hz, ArH), 6.87 (2H, d, J = 2.0 Hz, ArH), 7.07 (2H, dd, J = 8.5 Hz, J = 2.0 Hz, ArH). ^{13}C{^{1}H} NMR (C_4D_8O): δ 22.5 (CH_2), 31.6 (CH_3), 33.7 (C), 50.2 (CH_2), 52.7 (CH_2), 63.1 (CH_2), 119.3 (ArH), 119.7 (Ar), 124.6 (ArH), 126.0 (ArH), 137.5 (Ar), 159.4 (ArO). Calc. (%) for $C_{28}H_{41}N_2O_2Al$, C 72.38, H 8.89, N 6.03. Found (%), C 72.35, H 8.88, N 6.17.

7.6.2 Preparation of benzoxy aluminium homopiperazine salan complexes

Al(**6**)OBn. A solution of **6**H_2 (0.37 g, 1.00 mmol) in toluene (30 ml) was heated to 50°C and 2M $AlMe_3$ (0.5 ml, 1.00 mmol) was added slowly while stirring (30 mins, 50°C), after which the solution was further heated and stirred (3 h, 80°C). Excess benzyl alcohol (0.52 ml, 5.02 mmol) was carefully added to the hot solution and allowed to stir (3 h, 80 °C) the reaction was then cooled and the solvent removed under vacuum. The crude mixture was recrystallised from a toluene:hexane mix to yield a white powder (0.22 g, 0.44 mmol, 44 %). ^{1}H NMR (233 K) ($C_6D_5CD_3$): δ 0.22 (1H, d, J = 13.5 Hz, CH_2), 0.75 (1H, br, CH_2), 1.10 (2H, br, CH_2), 1.45 (2H, br, CH_2), 2.40 (6H, s, CH_3), 2.45 (4H, m, CH_2), 2.71 (2H, br, CH_2), 2.81 (6H, s, CH_3), 4.30 (2H, d, J = 12.5 Hz, CH_2), 5.25 (2H, s, CH_2), 6.51 (2H, s, ArH), 7.15 (1H, br, ArH), 7.15 (2H, br, ArH), 7.23 (2H, m, ArH), 7.41 (2H, d, J = 7.5 Hz, ArH). ^{13}C{^{1}H} NMR ($C_6D_5CD_3$): δ 16.8 (CH_3), 20.8 (CH_3), 21.9 (C), 22.4 (C), 45.6 (CH_2), 50.0 (CH_2), 52.5 (CH_2), 55.7 (CH_2), 61.9 (CH_2), 62.4 (CH_2), 64.9 (CH_2), 66.4 (CH_2), 119.6 (Ar), 120.5 (Ar), 124.3 (Ar), 124.7 (Ar), 126.1 (ArH), 126.5 (ArH), 126.6 (ArH), 127.3 (ArH), 126.8 (ArH), 128.1 (Ar), 128.1 (ArH), 128.3 (ArH), 128.8 (Ar), 131.8 (ArH), 132.0 (ArH), 157.4 (ArO), 157.3 (ArO). Calc. (%) for $C_{30}H_{37}N_2O_3Al$, C 71.98, H 7.45, N 5.60. Found (%), C 72.12, H 7.50, N 5.52.

Al(**7**)OBn. A solution of **7**H_2 (0.45 g, 0.99 mmol) in toluene (30 ml) was heated to 50°C and 2M $AlMe_3$ (0.5 ml, 1.00 mmol) was added slowly while stirring (30 mins, 50°C), after which the solution was further heated and stirred (3 h, 80°C). Excess benzyl alcohol (0.52 ml, 5.02 mmol) was carefully added to the hot solution and allowed to stir (3 h, 80°C) the reaction was then cooled and the solvent removed under vacuum. The crude mixture was recrystallised from a toluene:hexane mix to yield a white powder (0.47 g, 0.81 mmol, 81 %). ^{1}H NMR (233 K) ($C_6D_5CD_3$): δ 0.11 (1H, d, J = 12.0 Hz, CH_2), 0.70 (1H, br, CH_2), 1.10 (2H, d, J= 8.0 Hz, CH_2), 1.47 (2H, br, CH_2), 1.50 (18H, s, CH_3), 2.43 (4H, m, CH_2), 2.71 (2H, d, J = 6.5 Hz, CH_2), 2.85 (6H, s, CH_3), 4.31 (2H, d, J = 12.5 Hz, CH_2), 5.29 (2H, s, CH_2), 6.79 (2H, s, ArH), 7.15 (1H, br, ArH), 7.24 (2H, t, J = 7.5 Hz, ArH), 7.40 (4H, m, ArH). ^{13}C NMR ($C_6D_5CD_3$): δ 17.6 (CH_3), 22.3 (CH_2), 32.5 (C), 32.6 (CH_3), 34.5 (CH_2), 50.4 (CH_2), 52.9 (CH_2), 63.2 (CH_2), 66.7 (CH_2), 119.5 (Ar), 122.7 (ArH), 126.5 (ArH), 127.2 (ArH), 128.1 (Ar), 128.4 (ArH), 128.5 (ArH), 138.4 (Ar), 147.3 (Ar), 157.7

(ArO). Calc. (%) for $C_{36}H_{49}N_2O_3Al$, C 73.94, H 8.45, N 4.79. Found (%), C 73.91, H 8.50, N 4.72.

Al(**8**)OBn. A solution of **8**H_2 (0.54 g, 1.00 mmol) in toluene (40 ml) was heated to 50°C and 2M $AlMe_3$ (0.5 ml, 1.00 mmol) was added slowly while stirring (30 mins, 50°C), after which the solution was further heated and stirred (3 h, 80°C). Excess benzyl alcohol (0.31 ml, 3.0 mmol) was carefully added to the hot solution and allowed to stir (3 h, 80°C) the reaction was then cooled and the solvent removed under vacuum. The crude mixture was recrystallised from a toluene:hexane mix to yield a white powder (0.24 g, 0.36 mmol, 36 %). ^{1}H NMR (233 K) ($C_6D_5CD_3$): δ 0.29 (1H, br, CH_2), 0.76 (1H, br, CH_2), 1.48 (4H, br, CH_2), 1.51 (18H, s, CH_3), 2.00 (18H, s, CH_3), 2.56 (4H, m, CH_2), 2.64 (2H, m, CH_2), 4.32 (2H, d, J = 13.5 Hz, CH_2), 5.26 (2H, s, CH_2), 6.77 (2H, s, ArH), 7.15 (1H, s, ArH), 7.21 (2H, t, J = 7.5 Hz, ArH), 7.36 (2H, d, J = 7.5 Hz, ArH), 7.66 (2H, s, ArH). ^{13}C{^{1}H} NMR ($C_6D_5CD_3$): δ 22.1 (CH_2), 30.1 (CH_3), 32.1 (CH_3), 34.2 (C), 36.1 (C), 50.7 (CH_2), 52.3 (CH_2), 63.7 (CH_2), 65.9 (CH_2), 119.8 (Ar), 122.8 (ArH), 124.0 (ArH), 126.1 (ArH), 126.7 (ArH), 128.1 (ArH), 137.9 (Ar), 139.0 (Ar), 147.0 (Ar), 157.6 (ArO). Calc. (%) for $C_{42}H_{61}N_2O_3Al$, C 75.41, H 9.19, N 4.19. Found (%), C 75.37, H 9.04, N 4.12.

Al(**9**)OBn. A solution of **9**H_2 (0.45 g, 0.99 mmol) in toluene (30 ml) was heated to 50°C and 2M $AlMe_3$ (0.5 ml, 1.00 mmol) was added slowly while stirring (30 mins, 50°C), after which the solution was further heated and stirred (3 h, 80°C). Excess benzyl alcohol (0.52 ml, 5.02 mmol) was carefully added to the hot solution and allowed to stir (5 h, 80°C) the reaction was then cooled and the solvent removed under vacuum. The crude mixture was recrystallised from a toluene:hexane mix to yield a white powder (0.20 g, 0.34 mmol, 34 %). ^{1}H NMR (233 K) ($C_6D_5CD_3$): δ 0.40 (1H, d, J = 13.5 Hz, CH_2), 0.76 (1H, br, CH_2), 1.20 (2H, d, J = 9.0 Hz, CH_2), 1.40 (2H, br, CH_2), 1.96 (18H, s, CH_3), 2.43 (6H, s, CH_3), 2.51 (4H, m, CH_2), 2.66 (2H, m, CH_2), 4.27 (2H, d, J = 13.0 Hz, CH_2), 5.25 (2H, s, CH_2), 6.48 (2H, s, ArH), 7.14 (1H, s, ArH), 7.21 (2H, t, J = 7.5 Hz, ArH), 7.40 (4H, m, ArH). ^{13}C{^{1}H} NMR ($C_6D_5CD_3$): δ 21.0 (CH_3), 22.1 (CH_2), 30.9 (CH_3), 35.7 (C), 50.6 (CH_2), 52.2 (CH_2), 63.2 (CH_2), 65.9 (CH_2), 120.3 (Ar), 124.3 (Ar), 126.1 (ArH), 126.7 (ArH), 126.9

(ArH), 127.8 (ArH), 128.1 (ArH), 139.4 (Ar), 146.7 (Ar), 157.6 (ArO). Calc. (%) for $C_{36}H_{49}N_2O_3Al$, C 73.94, H 8.45, N 4.79. Found (%), C 73.86, H 8.51, N 4.75.

Al(**11**)OBn. A solution of **11**H_2 (0.43 g, 1.01 mmol) in toluene (30 ml) was heated to 50°C and 2M $AlMe_3$ (0.5 ml, 1.00 mmol) was added slowly while stirring (30 mins, 50°C), after which the solution was further heated and stirred (3 h, 80°C). Excess benzyl alcohol (0.31 ml, 3.00 mmol) was carefully added to the hot solution and allowed to stir (16 h, 70°C) the reaction was then cooled and the solvent removed under vacuum. The crude mixture was recrystallised from a toluene:hexane mix to yield a white powder (0.41 g, 0.74 mmol, 74 %). ^{1}H NMR ($C_6D_5CD_3$): δ 0.80 (1H, m, CH_2), 1.14 (1H, m, CH_2), 1.35 (18H, s, CH_3), 1.50 (4H, m, CH_2), 2.59 (2H, d, J = 7.5 Hz, CH_2), 3.22 (2H, d, J = 12.5 Hz, CH_2), 3.36 (2H, m, CH_2), 3.58 (2H, m, CH_2), 5.16 (2H, s, CH_2), 6.85 (2H, d, J = 2.5 Hz, ArH), 7.04 (1H, m, ArH), 7.12 (2H, m, ArH), 7.14 (1H, s, ArH), 7.14 (1H, br, ArH), 7.22 (1H, d, J = 2.5 Hz, ArH), 7.25 (1H, d, J = 2.5 Hz, ArH), 7.29 (1H, m, ArH), 7.32 (1H, br, ArH). ^{13}C{^{1}H} NMR ($C_6D_5CD_3$): δ 22.1 (CH_2), 32.0 (CH_3), 34.0 (C), 46.8 (CH_2), 50.1 (CH_2), 52.4 (CH_2), 55.2 (CH_2), 62.6 (CH_2), 66.3 (CH_2), 120.9 (ArH), 121.4 (Ar), 125.3 (ArH), 126.3 (ArH), 127.6 (ArH), 127.7 (ArH), 128.4 (ArH), 139.3 (Ar), 147.3 (Ar), 159.6 (ArO). Calc. (%) for $C_{34}H_{45}N_2O_3Al$, C 73.35, H 8.15, N 5.03. Found (%), C 73.45, H 8.14, N 4.89.

7.7 Preparation of Ligands and Complexes for Chapter 5

7.7.1 Preparation of *trans*-1,4-DACH salen ligands

3-(*tert*-butyl)-2-hydroxy-5-methylbenzaldehyde. 2-(*tert*-butyl)-4-methylphenol (15 g, 91.3 mmol) was dissolved in dry acetonitrile (150 ml) in an argon charged vessel. Then triethylamine (36.96 g, 365.3 mmol) and $MgCl_2$ (17.39 g, 182.6 mmol) were added and allowed to stir (15 mins). At which point paraformaldehyde (19.20 g, 639.4 mmol) was added and the mixture was stirred (15 mins) before refluxing (4 h) in an inert atmosphere. The solution was allowed to cool to room temperature before addition of 5% HCl (100ml). The product was extracted into diethyl ether (50 ml x 6), the organic layers were washed with saturated brine (20 ml x 3) and dried with $MgSO_4$. The $MgSO_4$ was removed by filtration and the solvent removed *in-vacuo*,

the solid was dissolved in hexane (10 ml) and run through a silica plug before crystallisation yielding beige solid (5.61 g, 29.2 mmol, 32 %). ^{1}H NMR ($CDCl_3$): δ 1.32 (9H, s, CH_3), 2.23 (3H, s, CH_3), 7.06 (1H, s, ArH), 7.24 (1H, s, ArH), 9.73 (1H, s, CH), 11.51 (1H, s, OH).

4-methyl-2-tritylphenol. *p*-Cresol (39.00 g, 360.6 mmol) was melted (100 °C) under an inert atmosphere and sodium metal (2.14 g, 93.1 mmol) was slowly added while vigorously stirring (1 h). Trityl chloride (20 g, 71.7 mmol) was added and the reaction was further heated (140 °C) and stirred (5 h). The reaction was cooled (~25 °C) then NaOH solution (1 M, 100 ml) and diethyl ether (100 ml) was added, the organic layer was isolated and washed with NaOH solution (1 M, 50 ml x 5). The organic phase was washed with water (50 ml x 2) then saturated brine (50 ml) before drying with $MgSO_4$. $MgSO_4$ was filtered and the solvent removed *in-vacuo*, the product was recrystallised from ethanol to yield a solid (16.45 g, 46.9 mmol, 65 %). ^{1}H NMR ($CDCl_3$): δ 2.16 (3H, s, CH_3), 2.80 (1H, s, OH), 6.71 (1H, d, J =8 Hz, ArH), 6.84 (1H, s, ArH), 7.01 (1H, d, J = 6.6 Hz, ArH), 7.15 – 7.30 (15H, m, ArH).

2-hydroxy-5-methyl-3-tritylbenzaldehyde. 4-methyl-2-tritylphenol (12.0 g, 34.2 mmol), hexamethylenetetramine (9.60 g, 68.5 mmol), and trifluoroacetic acid (35 ml) were added to a vessel and heated while stirring (120 °C, 4 h). The reaction was cooled (~75 °C) before addition of H_2SO_4 (33 % aq, 50 ml), the mixture was heated (125 °C) and further stirred (2 h). The reaction was then cooled to ambient conditions then water (50 ml) and ethyl acetate (50 ml) was added. The organic phase was isolated and the aqueous phase was further extracted with ethyl acetate (30 ml x 3) at which point the organic layers were combined and washed with water (50 ml) and brine (20 ml). The organic layer was dried with $MgSO_4$ then filtered, the solvent was removed *in-vacuo* and recrystallised from ethanol to yield a white solid (9.04 g, 23.9 mmol, 70 %). ^{1}H NMR ($CDCl_3$): δ 2.20 (3H, s, CH_3), 7.05 – 7.35 (17H, m, ArH), 9.72 (1H, s, CH), 11.10 (1H, s, OH).

16H_2 3,5-di-*tert*-butyl-2-hydroxybenzaldehyde (1.03 g, 4.4 mmol) and *trans*-1,4-diaminocyclohexane (0.25 g, 2.2 mmol) were stirred in MeOH (40 ml) for 4 h. The resulting yellow precipitate was filtered and washed with cold MeOH and dried in

vacuo to yield a white solid (1.16 g, 2.1 mmol, 97 %). ^{1}H NMR ($CDCl_3$): δ 1.32 (18H, s, ^{t}Bu), 1.47 (18H, s, ^{t}Bu), 1.74 (4H, m, ring-CH_2), 1.98 (4H, m, ring-CH_2), 3.28 (2H, br, ring-CH), 7.12 (2H, d, J = 2.0 Hz, ArH), 7.40 (2H, d, J = 2.0 Hz, ArH), 8.45 (2H, s, N=CH) 13.88 (2H, br, OH). ^{13}C{^{1}H} NMR ($C_6D_5CD_3$): δ 29.6 (CH_3), 31.7 (CH_3), 32.7 (CH_2), 34.3 (C), 35.2 (C), 67.2 (CH), 118.0 (Ar), 129.6 (ArH), 126.9 (ArH), 136.7 (Ar), 140.1 (Ar), 158.2 (ArO), 164.3 (N=CH). Calc. m/z $[C_{36}H_{54}N_2O_2 + H]^+$ 547.4258. Found 547.4320.

17H_2 3-(*tert*-butyl)-2-hydroxy-5-methylbenzaldehyde (1.88 g, 9.8 mmol) and *trans*-1,4-diaminocyclohexane (0.56 g, 4.9 mmol) were stirred in MeOH (40 ml) for 4 h. The resulting yellow precipitate was filtered and washed with cold MeOH and dried in vacuo to yield a white solid (2.17 g, 4.7 mmol, 96 %). ^{1}H NMR ($CDCl_3$): δ 1.45 (18H, s, ^{t}Bu), 1.74 (4H, m, ring-CH_2), 1.98 (4H, m, ring-CH_2), 2.30 (6H, s, CH_3), 3.27 (2H, br, ring-CH), 6.94 (2H, br, ArH), 7.14 (2H, d, J = 2.0 Hz, ArH), 8.39 (2H, s, N=CH) 13.80 (2H, br, OH). ^{13}C{^{1}H} NMR ($C_6D_5CD_3$): δ 20.8 (CH_3), 29.5 (CH_3), 32.6 (CH_2), 34.9 (C), 67.1 (CH), 118.5 (Ar), 126.8 (Ar), 129.5 (ArH), 130.6 (ArH), 137.3 (Ar), 158.2 (ArO), 164.0 (N=CH). Calc. m/z $[C_{30}H_{42}N_2O_2 + H]^+$ 463.3319. Found 463.3362.

18H_2 2-hydroxy-5-methyl-3-tritylbenzaldehyde (3.0 g, 7.9 mmol) and *trans*-1,4-diaminocyclohexane (0.45 g, 3.9 mmol) were stirred in MeOH (40 ml) for 4 h. The resulting yellow precipitate was filtered and washed with cold MeOH and dried in vacuo to yield a white solid (2.64 g, 3.2 mmol, 80 %) ^{1}H NMR ($CDCl_3$): δ 1.54 (4H, br, ring-CH_2), 1.76 (4H, br, ring-CH_2), 2.22 (6H, s, CH_3), 3.08 (2H, br, ring-CH), 7.09 (2H, s, ArH), 7.22 (32H, br, ArH), 8.30 (2H, s, N=CH) 13.34 (2H, br, OH). ^{13}C{^{1}H} NMR ($CDCl_3$) (333 K): δ 20.9 (CH_2), 30.9 (CH_2), 32.6 (CH_3), 63.6 (CH), 67.1 (C), 119.1 (Ar), 125.6 (ArH), 127.3 (ArH), 127.5 (Ar), 130.9 (ArH), 131.2 (Ar), 131.3 (ArH), 134.5 (ArH), 134.7 (Ar), 146.0 (Ar), 158.2 (ArO), 163.3 (N=CH). Calc. m/z $[C_{60}H_{54}N_2O_2 + H]^+$ 835.4264. Found 835.4267.

7.7.2 Preparation of titanium *trans*-1,4-DACH salen complexes

Ti_2(**16**)($O^{i}Pr$)$_6$. $Ti(O^{i}Pr)_4$ (0.31 ml, 1.03 mmol) was added to a solution of **16H$_2$** (0.28 g, 0.51 mmol) in CH_2Cl_2 (30 ml) and stirred (16 h). The solvent was removed *in-*

vacuo and recrystallised from hexane to yield yellow crystals (0.22 g, 0.22 mmol, 43 %). ^{1}H NMR ($CDCl_3$): δ 1.26 (36H, d, J = 6.0 Hz, ^{t}Bu), 1.36 (18H, s, ^{t}Bu), 1.49 (18H, s, ^{t}Bu), 1.61 (4H, m, ring-CH_2), 2.26 (4H, d, J = 7.0 Hz, ring-CH_2), 4.39 (2H, br, ring-CH), 4.91 (6H, Sept, J = 6.0 Hz, CH), 7.17 (2H, d, J = 2.5 Hz, ArH), 7.47 (2H, d, J = 2.5 Hz, ArH), 8.32 (2H, s, N=CH). ^{13}C{^{1}H} NMR ($CDCl_3$): δ 26.8 (CH_3), 29.6 (CH_3), 31.7 (CH_3), 32.6 (CH_2), 34.3 (C), 35.4 (C), 62.6 (CH), 77.3 (CH), 121.5 (Ar), 127.6 (ArH), 128.5 (ArH), 138.0 (Ar), 140.0 (Ar), 159.7 (ArO), 162.7 (N=CH). Calc. (%) for $C_{54}H_{94}Ti_2N_2O_8$, C 65.18, H 9.52, N 2.82. Found (%), C 63.5, H 9.37, N 2.78.

Ti_2(**17**)($O^{i}Pr$)$_6$. $Ti(O^{i}Pr)_4$ (0.0.5 ml, 1.69 mmol) was added to a solution of **17**H_2 (0.39 g, 0.84 mmol) in CH_2Cl_2 (30 ml) and stirred (16 h). The solvent was removed *in-vacuo* and recrystallised from hexane to yield yellow crystals (0.19 g, 0.21 mmol, 25 %). ^{1}H NMR ($CDCl_3$): δ 1.26 (36H, d, J = 6.0 Hz, CH_3), 1.48 (18H, s, ^{t}Bu), 1.59 (4H, m, ring-CH_2), 2.25 (4H, d, J = 8.0 Hz ring-CH_2), 2.32 (6H, s, Me), 4.39 (2H, br, ring-CH), 4.91 (6H, Sept, J = 6.0 Hz, CH), 7.02 (2H, d, J = 1.5 Hz, ArH), 7.20 (2H, d, J = 2.0 Hz, ArH), 8.29 (2H, s, N=CH). ^{13}C{^{1}H} NMR ($CDCl_3$): δ 20.8 (CH_3), 26.8 (CH_3), 29.6 (CH_3), 32.5 (CH_2), 35.1 (C), 62.5 (CH), 77.3 (CH), 122.0 (Ar), 126.6 (Ar), 131.3 (ArH), 132.2 (ArH), 138.4 (Ar), 159.8 (ArO), 162.3 (N=CH). Calc. (%) for $C_{48}H_{82}N_2O_8Ti_2$, C 63.29, H 9.07, N 3.08. Found (%), C 63.15, H 8.94, N 3.23.

Ti_2(**18**)($O^{i}Pr$)$_6$. $Ti(O^{i}Pr)_4$ (0.30 ml, 1.01 mmol) was added to a solution of **18H$_2$** (0.42 g, 0.50 mmol) in CH_2Cl_2 (30 ml) and stirred (16 h). The solvent was removed *in-vacuo* and recrystallised from hexane to yield yellow crystals (0.31 g, 0.24 mmol, 48 %). ^{1}H NMR ($CDCl_3$) (328 K): δ 0.98 (36H, d, J = 5.5 Hz, ^{t}Bu), 1.47 (4H, br, ring-CH_2), 2.13 (4H, br, ring-CH_2), 2.19 (2H, s, CH_3), 4.22 (2H, br, ring-CH), 4.42 (6H, br, CH), 7.00 – 7.30 (34H, br, ArH), 8.17 (2H, s, N=CH). ^{13}C{^{1}H} NMR ($CDCl_3$) (328 K): δ 20.8 (CH_3), 26.6 (CH_3), 32.8 (CH_2), 62.4 (CH), 63.9 (C), 77.1 (CH), 122.9 (Ar), 125.5 (ArH), 126.2 (Ar), 127.2 (ArH), 131.5 (ArH), 133.0 (ArH), 136.2 (ArH), 136.3 (ArH), 159.7 (ArO), 161.7 (N=CH). Calc. (%) for $C_{78}H_{94}N_2O_8Ti_2$, C 73.00, H 7.38, N 2.18. Found (%), C 72.85, H 7.25, N 2.20.

7.7.3 Preparation of aluminium *trans*-1,4-DACH salen complexes

Al_2(**16**)Me_4. 2M $AlMe_3$ (0.84 ml, 1.68 mmol) in heptane was added to a solution of **16**H_2 (0.46 g, 0.84 mmol) in toluene (40 ml) and stirred (16 h). The solvent was removed *in-vacuo* and recrystallised from hexane to yield yellow crystals (0.19 g, 0.29 mmol, 34 %). ^{1}H NMR (D_8-Tol): δ -0.27 (12H, s, Al-Me) 1.37 (18H, s, ^{t}Bu), 1.57 (18H, s, ^{t}Bu), 1.45 – 1.70 (8H, m, ring-CH_2), 2.60 (2H, br, ring-CH), 6.94 (2H, d, J = 2.5 Hz, ArH), 7.40 (2H, s, N=CH), 7.69 (2H, d, J = 2.5 Hz, ArH). ^{13}C{^{1}H} NMR (D_8-Tol): δ -5.7 (Al-Me), 30.6 (CH_3), 32.6 (CH_3), 33.4 (CH_2), 35.3 (C), 36.3 (CH_2), 69.5 (CH), 119.8 (Ar), 130.1 (ArH), 133.2 (ArH), 138.5 (Ar), 140.1 (Ar), 163.3 (ArO), 172.7 (N=CH). Calc. (%) for $C_{40}H_{64}Al_2N_2O_2$, C 72.91, H 9.79, N 4.25. Found (%), C 73.03, H 9.66, N 4.19.

Al_2(**17**)Me_4. 2M $AlMe_3$ (0.60 ml, 1.20 mmol) in heptane was added to a solution of **17**H_2 (0.28 g, 0.61 mmol) in toluene (40 ml) and stirred (16 h). The solvent was removed *in-vacuo* and recrystallised from a hexane:toluene mixture to yield yellow crystals (0.13 g, 0.23 mmol, 37 %). ^{1}H NMR (D_8-Tol): δ -0.28 (12H, s, Al-Me) 1.55 (18H, s, ^{t}Bu), 1.45 – 1.70 (8H, m, ring-CH_2), 2.22 (6H, s, CH_3), 2.59 (2H, br, ring-CH), 6.59 (2H, d, J = 1.5 Hz, ArH), 7.29 (2H, s, N=CH), 7.39 (2H, d, J = 2.5 Hz, ArH). ^{13}C{^{1}H} NMR (D_8-Tol): δ -7.0 (Al-Me), 20.6 (CH_3), 29.5 (CH_3), 32.6 (CH_2), 32.3 (C), 35.2 (CH_2), 68.5 (CH), 119.2 (Ar), 125.5 (Ar), 132.7 (ArH), 135.7 (ArH), 141.2 (Ar), 162.3 (ArO), 171.2 (N=CH). Calc. (%) for $C_{34}H_{52}Al_2N_2O_2$, C 71.05, H 9.12, N 4.87. Found (%), C 70.95, H 9.13, N 5.09.

Al_2(**18**)Me_4. 2M $AlMe_3$ (0.50 ml, 1.00 mmol) in heptane was added to a solution of **18**H_2 (0.42 g, 0.50 mmol) in toluene (40 ml) and stirred (16 h). The solvent was removed *in-vacuo* and recrystallised from a hexane:toluene mixture to yield yellow crystals (0.22 g, 0.17 mmol, 34 %). ^{1}H NMR (D_8-Tol): δ -0.70 (12H, s, Al-Me) 1.39 (8H, br, ring-CH_2), 2.10 (6H, s, CH_3), 2.46 (2H, br, ring-CH), 6.61 (2H, d, J = 2.0 Hz, ArH), 6.95 – 7.15 (18H, m, ArH), 7.12 (2H, s, N=CH), 7.40 (6H, s, ArH), 7.43 (6H, s, ArH), 7.58 (2H, d, J = 2.5 Hz, ArH). ^{13}C{^{1}H} NMR (D_8-Tol): δ -6.9 (Al-Me), 20.6 (CH_3), 32.3 (CH_2), 63.9 (C), 68.1 (CH), 119.4 (Ar), 125.8 (ArH), 127.5 (ArH), 131.6 (ArH), 139.3 (Ar), 139.4 (ArH), 146.1 (Ar), 161.8 (ArO), 170.6 (N=CH). Calc. (%) for $C_{64}H_{64}Al_2N_2O_2$, C 81.16, H 6.81, N 2.96. Found (%), C 81.01, H 6.78, N 3.04.

7.8 Preparation of Ligands and Complexes for Chapter 6

7.8.1 Preparation of *trans*-1,2-DACH salalen ligands

tert-Butyl (2-aminocyclohexyl)carbamate. A solution of di-*tert*-butyl dicarbonate (9.61 g, 44.04 mmol) in CH_2Cl_2 (50 ml) was added dropwise to a cooled (0 °C) solution of *trans*-1,2-diaminecyclohexane (15.08 g, 70.47 mmol) in CH_2Cl_2 (50 ml) over a period of 30 mins while stirring. The solution was allowed to warm to room temperature and stirred overnight. CH_2Cl_2 (50 ml) and water (50 ml) were added to the resulting suspension to dissolve the precipitate and the organic phase was separated then the solvent was removed *in-vacuo*. The residue was dissolved in ethyl ether (50 ml) and water (50 ml) and the solution was acidified to pH 5 with 4M HCl, the mixture was separated and the aqueous layer was washed with ethyl ether (3 x 50 ml). 2M NaOH was added to the aqueous layer until pH 10.5 was reached, at which point the product was extracted with AcOEt (3 x 50 ml). The organic phase was washed with saturated brine (20 ml) and dried with anhydrous $MgSO_4$. After filtration the solvent was removed *in-vacuo* to yield a pale beige solid (7.17 g, 33.46 mmol, 47 %). ^{1}H NMR ($CDCl_3$): δ 1.00 – 1.30 (4H, m, CH_2), 1.38 (2H, s, NH_2), 1.41 (9H, s, ^{t}Bu), 1.65 (2H, m, CH_2), 1.95 (2H, m, CH_2), 2.29 (1H, td, J = 10 Hz, J = 4.0 Hz, CH), 3.08 (1H, br, CH), 4.52 (1H, br, NH).

19HBoc. *tert*-Butyl (2-aminocyclohexyl)carbamate (2.00 g, 9.33 mmol) was added to a solution of 3,5-di-*tert*-butyl-2-hydroxybenzaldehyde (2.18 g, 9.30 mmol) in MeOH (30 ml) / THF (30 ml) and stirred for 1 h. Sodium borohydride (2.12 g, 56.03 mmol) was added slowly to the yellow solution and then stirred for 5 h until the solution became colourless. The reaction was quenched with water (10 ml) and the solvent partially removed *in-vacuo*. Water (50 ml) was then used to precipitate a white solid, which was then filtered and washed with water (3 x 50 ml). The resulting solid was dissolved in MeOH (30 ml) and formaldehyde solution (37 % in H_2O, 2.12 ml, 26.74 mmol) was slowly added and allowed to stir for 1 h. The solvent was removed *in-vacuo* and the residue was dissolved in MeOH (30 ml) / THF (30 ml) and cooled (0 °C), then sodium borohydride (2.12 g, 56.03 mmol) was slowly added and the solution was stirred for 2 h. The reaction was quenched with water (10 ml) and the solvent partially removed *in-vacuo*. Water (50 ml) was then used to precipitate a

white solid, which was then filtered and washed with water (3 x 50 ml) and dried to yield a white solid (3.40 g, 7.61 mmol, 82 %). ^{1}H NMR ($CDCl_3$): δ 1.00 – 1.20 (2H, m, CH_2), 1.28 (9H, s, ^{t}Bu), 1.43 (9H, s, ^{t}Bu), 1.48 (9H, s, ^{t}Bu), 1.60 – 2.10 (6H, m, CH_2), 2.29 (3H, s, CH_3), 2.36 (1H, m, CH), 3.62 (1H, m, CH), 3.75 (1H, m, NH), 3.79 (1H, d, J = 4.5 Hz, CH_2), 4.55 (1H, d, J = 10.0 Hz, CH_2), 6.81 (1H, d, J = 2.5 Hz, ArH), 7.21 (1H, d, J = 2.5 Hz, ArH), 11.10 (1H, br, ArOH).

19H_3. **19**HBoc (2.40 g, 5.37 mmol) was dissolved in methanol (30 ml) and 3M HCl (30 ml) then heated to 60 °C and allowed to stir (16 h). The mixture was neutralised with 3M NaOH and the white precipitate was extracted with AcOEt (20 ml x 4). The organic phase was washed with saturated brine (20 ml) then dried with $MgSO_4$, the solid was removed by filtration and the solvent removed *in-vacuo* to yield an oily residue which was used without further purification (1.80 g, 5.19 mmol, 97 %) ^{1}H NMR ($CDCl_3$): δ 1.10 – 1.30 (4H, m, CH_2), 1.28 (9H, s, ^{t}Bu), 1.48 (9H, s, ^{t}Bu), 1.65 - 2.05 (4H, m, CH_2), 2.25 (3H, s, CH_3), 2.35 (1H, m, CH), 2.79 (1H, m, CH), 3.72 (1H, d, J = 13.5 Hz, CH_2), 3.86 (1H, d, J = 13.5 Hz, CH_2), 4.12 (1H, q, J = 7.5 Hz, NH) 3.50 – 4.00 (3H, br, NH_2, ArOH), 6.83 (1H, d, J = 2.5 Hz, ArH), 7.21 (1H, d, J = 2.5 Hz, ArH).

20HBoc. *tert*-Butyl (2-aminocyclohexyl)carbamate (2.43 g, 11.34 mmol) was added to a solution of 2-hydroxybenzaldehyde (1.39 g, 11.38 mmol) in MeOH (30 ml) / THF (30 ml) and stirred for 1 h. Sodium borohydride (1.29 g, 34.10 mmol) was added slowly to the yellow solution and then stirred for 5 h until the solution became colourless. The reaction was quenched with water (10 ml) and the solvent partially removed *in-vacuo*. Water (50 ml) was then used to precipitate a white solid, which was then filtered and washed with water (3 x 50 ml). The resulting solid was dissolved in MeOH (30 ml) and formaldehyde solution (37 % in H_2O, 2.58 ml, 31.79 mmol) was slowly added and allowed to stir for 1 h. The solvent was removed *in-vacuo* and the residue was dissolved in MeOH (30 ml) / THF (30 ml) and cooled (0 °C), then sodium borohydride (2.00 g, 52.87 mmol) was slowly added and the solution was stirred for 2 h. The reaction was quenched with water (10 ml) and the solvent partially removed *in-vacuo*. Water (50 ml) was then used to precipitate a white solid, which was then filtered and washed with water (3 x 50 ml) and dried to

yield a white solid (3.33 g, 9.96 mmol, 81 %). ^{1}H NMR ($CDCl_3$): δ 1.00 – 1.30 (4H, m, CH_2), 1.41 (9H, s, ^{t}Bu), 1.60 – 2.05 (4H, m, CH_2), 2.21 (3H, s, CH_3), 2.34 (1H, td, J = 11.0 Hz, J = 3.5 Hz, CH), 3.60 (1H, m, CH), 3.75 (1H, q, J = 14.0 Hz, CH_2), 4.40 (1H, br, NH), 6.71 (2H, m, ArH), 6.88 (1H, dd, J = 7.5 Hz, J = 1.5 Hz, ArH), 7.08 (1H, td, J = 7.5 Hz, J = 1.5 Hz, ArH), 10.88 (1H, br, ArOH).

20H_3. **20**HBoc (3.25g, 9.72 mmol) was dissolved in methanol (30 ml) and 3M HCl (30 ml) then heated to 60 °C and allowed to stir (16 h). The mixture was neutralised with 3M NaOH and the white precipitate was extracted with AcOEt (30 ml x 4). The organic phase was washed with saturated brine (20 ml) then dried with $MgSO_4$, the solid was removed by filtration and the solvent removed *in-vacuo* to yield a white solid (1.85, 7.89 mmol, 81 %). ^{1}H NMR ($CDCl_3$): δ 1.10 – 1.35 (4H, m, CH_2), 1.65 – 2.05 (4H, m, CH_2), 2.22 (3H, s, CH_3), 2.34 (1H, td, J = 10.0 Hz, J = 3.5 Hz, CH), 2.78 (1H, td, J = 10.0 Hz, J = 4.5 Hz, CH), 3.61 (1H, d, J = 13.5 Hz, CH_2), 3.89 (1H, d, J = 13.5 Hz, CH_2), 4.39 (3H, br, NH_2, ArOH), 6.76 (1H, td, J = 7.5 Hz, J = 1.0 Hz, ArH), 6.82 (1H, dd, J = 8.0 Hz, J = 1.0 Hz, ArH), 6.97 (1H, dd, J = 7.5 Hz, J = 1.5 Hz, ArH), 7.15 (1H, td, J = 7.5 Hz, J = 1.5 Hz, ArH).

21HBoc. *tert*-Butyl (2-aminocyclohexyl)carbamate (3.00 g, 14.00 mmol) was added to a solution of 3,5-dichloro-2-hydroxybenzaldehyde (2.67 g, 13.98 mmol) in MeOH (30 ml) / THF (30 ml) and stirred for 1 h. Sodium borohydride (1.60 g, 42.29 mmol) was added slowly to the yellow solution and then stirred for 16 h until the solution became colourless. The reaction was quenched with water (10 ml) and the solvent partially removed *in-vacuo*. Water (50 ml) was then used to precipitate a white solid, which was then filtered and washed with water (3 x 50 ml). The resulting solid was dissolved in MeOH (30 ml) and formaldehyde solution (37 % in H_2O, 3.18 ml, 39.18 mmol) was slowly added and allowed to stir for 1 h. The solvent was removed *in-vacuo* and the residue was dissolved in MeOH (30 ml) / THF (30 ml) and cooled (0 °C), then sodium borohydride (2.50 g, 66.09 mmol) was slowly added and the solution was stirred for 2 h. The reaction was quenched with water (10 ml) and the solvent partially removed *in-vacuo*. Water (50 ml) was then used to precipitate a white solid, which was then filtered and washed with water (3 x 50 ml) and dried to yield a white solid (4.30 g, 10.66 mmol, 76 %). ^{1}H NMR ($CDCl_3$): δ 1.10 – 1.35 (4H,

m, CH_2), 1.48 (9H, s, ^{t}Bu), 1.70 – 2.10 (4H, m, CH_2), 2.27 (3H, s, CH_3), 2.40 (1H, td, J = 11.0 Hz, J = 3.5 Hz, CH), 3.69 (1H, m, CH), 3.71 (1H, d, J = 14.0 Hz, CH_2), 3.87 (1H, d, J = 14.0 Hz, CH_2), 4.48 (1H, d, J = 10.0 Hz, NH), 6.82 (1H, d, J = 2.5 Hz, ArH), 7.22 (1H, d, J = 2.5 Hz, ArH), 9.87 (1H, br, ArOH).

21H_3. **21**HBoc (4.20 g, 10.41 mmol) was dissolved in methanol (30 ml) and 3M HCl (30 ml) then heated to 60 °C and allowed to stir (16 h). The mixture was neutralised with 3M NaOH and the white precipitate was extracted with AcOEt (30 ml x 4). The organic phase was washed with saturated brine (20 ml) then dried with $MgSO_4$, the solid was removed by filtration and the solvent removed *in-vacuo* to yield a white solid (2.66, 8.77 mmol, 84 %). ^{1}H NMR ($CDCl_3$): δ 1.00 – 1.25 (4H, m, CH_2), 1.61 (1H, br, CH_2), 1.71 (1H, br, CH_2), 1.85 (2H, br, CH_2), 2.21 (3H, s, CH_3), 2.25 (1H, br, CH), 2.84 (1H, br, CH), 3.08 (1H, d, J = 12.0 Hz, CH_2), 3.79 (1H, d, J = 12.5 Hz, CH_2), 4.92 (3H, br, NH_2, ArOH), 6.80 (1H, d, J = 2.5 Hz, ArH), 7.14 (1H, d, J = 2.5 Hz, ArH).

22H_2. **19**HBoc (1.00 g, 2.24 mmol) was dissolved in methanol (20 ml) and 3M HCl (20 ml) then heated to 60 °C and allowed to stir (16 h). The mixture was neutralised with 3M NaOH and the white precipitate was extracted with AcOEt (15 ml x 4). The organic phase was washed with saturated brine (10 ml) then dried with $MgSO_4$, the solid was removed by filtration and the solvent removed *in-vacuo*. The oily residue was dissolved in MeOH (30 ml) and 3,5-di-*tert*-butyl-2-hydroxybenzaldehyde (0.52 g, 2.24 mmol) was added. The solution was stirred for 2 h then the solid was filtered and further dried *in-vacuo* to yield a yellow solid (0.50 g, 0.89 mmol, 40 %). ^{1}H NMR ($CDCl_3$): δ 1.15 (9H, s, ^{t}Bu), 1.28 (9H, s, ^{t}Bu), 1.32 (9H, s, ^{t}Bu), 1.35 – 1.45 (3H, m, ring-CH_2), 1.51 (9H, s, ^{t}Bu), 1.63 – 2.07 (5H, m, ring-CH_2), 2.26 (3H, s, CH_3), 3.00 (1H, m, ring-CH), 3.33 (1H, m, ring-CH), 3.75 (1H, d, J = 13.0 Hz, CH_2), 3.91 (1H, d, J = 13.0 Hz, CH_2), 6.83 (1H, d, J = 2.5 Hz, ArH), 7.06 (1H, d, J = 2.5 Hz, ArH), 7.14 (1H, d, J = 2.5 Hz, ArH), 7.41 (1H, d, J = 2.5 Hz, ArH), 8.40 (1H, s, CH), 10.61 (1H, br, OH), 13.59 (1H, s, OH). ^{13}C{^{1}H} NMR ($CDCl_3$): δ 24.8 (CH_2), 25.3 (CH_2), 29.5 (CH_3), 29.8 (CH_3), 31.7 (CH_3), 31.9 (CH_3), 34.2 (C), 34.9 (C), 35.2 (CH_2), 35.4 (CH_2), 66.6 (CH), 70.3 (CH), 118.1 (Ar), 121.0 (Ar), 122.5 (ArH), 123.3 (ArH), 125.8 (ArH), 126.9(ArH), 135.4 (Ar), 136.6 (Ar), 139.8 (Ar), 139.8 (Ar),

154.7 (Ar), 158.2 (Ar), 165.8 (CH). Calc. m/z $[C_{37}H_{58}N_2O_2 + Na]^+$ 585.4396. Found 585.4398

(***R,R*-22**)H_2. *tert*-butyl (1S,2S)-2-aminocyclohexyl)carbamate (0.375 g, 1.75 mmol) was added to a solution of 3,5-di-*tert*-butyl-2-hydroxybenzaldehyde (0.41 g, 1.75 mmol) in MeOH (15 ml) / THF (15 ml) and stirred for 1 h. Sodium borohydride (0.30 g, 9.99 mmol) was added slowly to the yellow solution and then stirred for 5 h until the solution became colourless. The reaction was quenched with water (10 ml) and the solvent partially removed *in-vacuo*. Water (30 ml) was then used to precipitate a white solid, which was then filtered and washed with water (3 x 30 ml). The resulting solid was dissolved in MeOH (30 ml) and formaldehyde solution (37 % in H_2O, 0.40 ml, 4.93 mmol) was slowly added and allowed to stir for 1 h. The solvent was removed *in-vacuo* and the residue was dissolved in MeOH (15 ml) / THF (15 ml) and cooled (0 °C), then sodium borohydride (0.30 g, 9.99 mmol) was slowly added and the solution was stirred for 16 h. The reaction was quenched with water (10 ml) and the solvent partially removed *in-vacuo*. Water (30 ml) was then used to precipitate a white solid, which was then filtered and washed with water (3 x 30 ml) and dried to yield a white solid. The white solid was dissolved in methanol (20 ml) and 3M HCl (20 ml) then heated to 60 °C and allowed to stir (16 h). The mixture was neutralised with 3M NaOH and the white precipitate was extracted with AcOEt (10 ml × 4). The organic phase was washed with saturated brine (10 ml) then dried with $MgSO_4$, the solid was removed by filtration and the solvent removed *in-vacuo*. The residue was dissolved in MeOH (20 ml) and 3,5-di-*tert*-butyl-2-hydroxybenzaldehyde (0.41 g, 1.75 mmol) was added. The solution was stirred for 16 h then the solid was filtered and further dried *in-vacuo* to yield a pale yellow solid (0.49 g, 0.87 mmol, 50 %). ^{1}H NMR ($CDCl_3$): δ 1.12 (9H, s, ^{t}Bu), 1.25 (9H, s, ^{t}Bu), 1.29 (9H, s, ^{t}Bu), 1.35 – 1.45 (3H, m, ring-CH_2), 1.48 (9H, s, ^{t}Bu), 1.63 – 2.07 (5H, m, ring-CH_2), 2.23 (3H, s, CH_3), 2.98 (1H, m, ring-CH), 3.31 (1H, m, ring-CH), 3.72 (1H, d, J = 12.0 Hz, CH_2), 3.88 (1H, d, J = 12.0 Hz, CH_2), 6.80 (1H, d, J = 2.5 Hz, ArH), 7.03 (1H, d, J = 2.5 Hz, ArH), 7.11 (1H, d, J = 2.5 Hz, ArH), 7.38 (1H, d, J = 2.5 Hz, ArH), 8.38 (1H, s, CH), 10.61 (1H, br, OH), 13.58 (1H, s, OH). ^{13}C{^{1}H} NMR ($CDCl_3$): δ 24.8 (CH_2), 25.3 (CH_2), 29.5 (CH_3), 29.7 (CH_3), 31.6 (CH_3), 31.9 (CH_3), 34.2 (C), 34.8 (C), 35.2 (CH_2), 35.5 (CH_2), 66.7 (CH), 70.4 (CH), 118.2 (Ar),

121.0 (Ar), 122.6 (ArH), 123.4 (ArH), 125.9 (ArH), 126.9 (ArH), 135.5 (Ar), 136.6 (Ar), 139.9 (Ar), 154.8 (Ar), 158.2 (Ar), 165.8 (CH). Calc. m/z $[C_{37}H_{57}N_2O_2]^-$ 561.4410. Found 561.4415

23H_2. **19**H_3 (1.00 g, 2.89 mmol) was dissolved in MeOH (30 ml) and 2-hydroxybenzaldehyde (0.31 ml, 2.91 mmol) was added. The solution was stirred for 2 h then the solid was filtered and further dried *in-vacuo* to yield a yellow solid (0.98 g, 2.17 mmol, 75 %). ^{1}H NMR ($CDCl_3$): δ 1.11 (9H, s, ^{t}Bu), 1.25 (9H, s, ^{t}Bu), 1.31 – 1.53 (3H, m, ring-CH_2), 1.63 – 2.08 (5H, m, ring-CH_2), 2.20 (3H, s, CH_3), 2.97 (1H, m, ring-CH), 3.36 (1H, m, ring-CH), 3.70 (1H, br, CH_2), 3.80 (1H, d, J = 13.0 Hz, CH_2), 6.77 (1H, d, J = 2.0 Hz, ArH), 6.86 (1H, t, J = 7.5 Hz, ArH), 6.99 (1H, d, J = 8.0 Hz, ArH), 7.11 (1H, br, ArH), 7.23 (1H, d, J = 7.5 Hz, ArH), 7.42(1H, t of d, J = 8.0 Hz, , J = 2.0 Hz, ArH), 8.38 (1H, s, CH), 10.62 (1H, br, OH), 13.15 (1H, s, OH). ^{13}C{^{1}H} NMR ($CDCl_3$): δ 23.1 (CH_2), 24.6 (CH_2), 25.1 (CH_2), 29.3 (CH_3), 31.7 (CH_3), 34.1 (C), 34.6 (C), 34.9 (CH_2), 58.5 (CH_2), 67.2 (CH), 70.1 (CH), 117.0 (ArH), 118.4 (ArH), 119.1 (Ar), 120.7 (Ar), 122.5 (ArH), 123.1 (ArH), 131.3 (ArH), 132.1 (ArH), 135.4 (Ar), 139.8 (Ar), 154.6 (ArO), 161.2 (ArO), 164.7 (CH). Calc. m/z $[C_{29}H_{42}N_2O_2 + Na]^+$ 473.3144. Found 473.3166

24H_2. **19**H_3 (0.80 g, 2.31 mmol) was dissolved in MeOH (30 ml) and 2-hydroxybenzaldehyde (0.44 ml, 2.30 mmol) was added. The solution was stirred for 2 h then the solid was filtered and further dried *in-vacuo* to yield a yellow solid (0.77 g, 1.48 mmol, 64 %). ^{1}H NMR ($CDCl_3$): δ 1.10 (9H, s, ^{t}Bu), 1.25 (9H, s, ^{t}Bu), 1.28 – 1.50 (3H, m, ring-CH_2), 1.64 – 2.08 (5H, m, ring-CH_2), 2.18 (3H, s, CH_3), 2.94 (1H, m, ring-CH), 3.36 (1H, m, ring-CH), 3.70 (1H, d, J = 13.0 Hz, CH_2), 3.81 (1H, d, J = 13.0 Hz, CH_2), 6.76(1H, d, J = 2.0 Hz, ArH), 7.10 (1H, br, ArH), 7.14 (1H, d, J = 2.0 Hz, ArH), 7.42 (1H, d, J = 2.5 Hz, ArH), 8.29 (1H, s, CH), 10.50 (1H, br, OH), 14.20 (1H, s, OH). ^{13}C{^{1}H} NMR ($CDCl_3$): δ 22.5 (CH_2), 24.5 (CH_2), 25.1 (CH_2), 29.3 (CH_3), 31.8 (CH_3), 34.2 (C), 34.6 (C), 34.7 (CH_3), 67.8 (CH), 69.5 (CH), 120.2 (Ar), 120.4 (Ar), 122.7 (Ar), 122.8 (Ar), 122.8 (ArH), 123.2 (ArH), 129.2 (ArH), 132.0 (ArH), 135.5 (Ar), 140.2 (Ar), 154.5 (ArO), 156.6 (ArO), 163.2 (CH). Calc. m/z $[C_{29}H_{40}Cl_2N_2O_2 + H]^+$ 519.2545. Found 519.2564

25H_2. **20**H_3 (0.60 g, 2.56 mmol) was dissolved in MeOH (30 ml) and 3,5-di-*tert*-butyl-2-hydroxybenzaldehyde (0.60 g, 2.56 mmol) was added. The solution was stirred for 2 h then the solid was filtered and further dried *in-vacuo* to yield a yellow solid (0.92 g, 2.04 mmol, 80 %). ^{1}H NMR ($CDCl_3$): δ 1.20 – 1.44 (3H, m, ring-CH_2), δ 1.33 (9H, s, ^{t}Bu), 1.49 (9H, s, ^{t}Bu), 1.60 – 2.06 (5H, m, ring-CH_2), 2.30 (3H, s, CH_3), 3.03 (1H, m, ring-CH), 3.36 (1H, td, J = 10.5 Hz, J = 4.5, Hz, ring-CH), 3.92 (2H, m, CH_2), 6.69 – 6.77 (2H, m, ArH), 6.94 (1H, m, ArH), 7.09 (1H, d, J = 2.5 Hz, ArH), 7.13 (1H, m, ArH), 7.41 (1H, d, J = 2.5 Hz, ArH), 8.42 (1H, s, CH), 9.6 – 11.8 (1H, br, OH), 12.1 – 14.2 (1H, br, OH). ^{13}C{^{1}H} NMR ($CDCl_3$): δ 24.7 (CH_2), 25.3 (CH_2), 25.5 (CH_2), 29.6 (CH_3), 31.7 (CH_3), 34.3 (C), 35.2 (C), 35.6 (CH_3), 35.7 (CH_2), 58.7 (CH_2), 66.1 (CH), 70.1 (CH), 116.5 (ArH), 118.0 (Ar), 119.7 (ArH), 121.9 (Ar), 126.1 (ArH), 127.3 (ArH), 128.8 (ArH), 128.8 (ArH), 136.7 (Ar), 140.1 (Ar), 158.2 (ArO), 158.4 (ArO), 165.8 (CH). Calc. m/z $[C_{29}H_{42}N_2O_2 + Na]^+$ 473.3144. Found 473.3154

26H_2. **20**H_3 (0.60 g, 2.56 mmol) was dissolved in MeOH (30 ml) and 2-hydroxybenzaldehyde (0.31 g, 2.54 mmol) was added. The solution was stirred for 2 h then the solid was filtered and further dried *in-vacuo* to yield a yellow solid (0.70 g, 2.07 mmol, 81 %). ^{1}H NMR ($CDCl_3$): δ 1.19 – 1.43 (3H, m, ring-CH_2), 1.48 – 1.63 (1H, m, ring-CH_2), 1.68 (1H, br, ring-CH_2), 1.72 (1H, br, ring-CH_2), 1.80 (1H, m, ring-CH_2), 1.92 (1H, m, ring-CH_2), 2.16 (3H, s, CH_3), 2.88 (1H, m, ring-CH), 3.25 (1H, td, J = 10.5 Hz, J = 4.5, Hz, ring-CH), 3.61 (1H, d, J = 13.5 Hz, CH_2), 3.70 (1H, d, J = 13.5 Hz, CH_2), 6.60 – 6.68 (2H, m, ArH), 6.78 – 6.88 (2H, m, ArH), 6.94 (1H, d, J = 8.0 Hz, ArH), 7.02(1H, td, J = 7.5 Hz, J = 2.0 Hz ArH), 7.18 (1H, m, ArH), 7.25 (1H, m, ArH), 8.31 (1H, s, CH), 9.5 – 14.0 (2H, br, OH). ^{13}C{^{1}H} NMR ($CDCl_3$): δ 23.8 (CH_2), 24.7 (CH_2), 25.1 (CH_2), 35.6 (CH_2), 35.6 (CH_3), 58.1 (CH_2), 66.5 (CH), 70.0 (CH), 116.3 (ArH), 117.2 (ArH), 118.7 (ArH), 118.8 (ArH), 119.0 (Ar), 121.8 (Ar), 128.5 (ArH), 128.6 (ArH), 131.5 (ArH), 132.4 (ArH), 158.3 (ArO), 161.2 (ArO), 164.7 (CH). Calc. m/z $[C_{21}H_{26}N_2O_2 + Na]^+$ 361.1892. Found 361.1895

27H_2. **20**H_3 (0.60 g, 2.56 mmol) was dissolved in MeOH (30 ml) and 3,5-dichloro-2-hydroxybenzaldehyde (0.49 g, 2.57 mmol) was added. The solution was stirred for 2 h then the solid was filtered and further dried *in-vacuo* to yield a yellow solid (0.79 g,

1.91 mmol, 75 %). ^{1}H NMR ($CDCl_3$): δ 1.25 – 1.50 (3H, m, ring-CH_2), 1.62 (1H, m, ring-CH_2), 1.70 (2H, br, ring-CH_2), 1.90 (1H, br, ring-CH_2), 2.02 (1H, m, ring-CH_2), 2.24 (3H, s, CH_3), 2.92 (1H, m, ring-CH), 3.38 (1H, td, J = 10.5 Hz, J = 4.5, Hz, ring-CH), 3.72 (1H, d, J = 13.5 Hz, CH_2), 3.87 (1H, d, J = 13.5 Hz, CH_2), 6.63 – 6.77 (2H, m, ArH), 6.92 (1H, d, J = 7.0 Hz, ArH), 7.10 (1H, td, J = 8.0 Hz, J = 1.5 Hz, ArH), 7.17 (1H, d, J = 2.5 Hz, ArH), 7.41 (1H, d, J = 2.5 Hz, ArH), 8.28 (1H, s, CH), 9.0 – 11.5 (1H, br, OH), 12.5 – 15.0 (1H, br, OH). ^{13}C{^{1}H} NMR ($CDCl_3$): δ 23.0 (CH_2), 24.5 (CH_2), 25.0 (CH_2), 35.2 (CH_2), 36.3 (CH_3), 57.4 (CH_2), 66.7 (CH), 69.2 (CH), 116.4 (ArH), 118.9 (ArH), 119.9 (Ar), 121.5 (Ar), 122.7 (Ar), 122.8 (Ar), 128.6 (ArH), 128.8 (ArH), 129.3 (ArH), 132.3 (ArH), 156.6 (ArO), 158.0 (ArO), 163.3 (CH).Calc. m/z $[C_{21}H_{24}Cl_2N_2O_2 + Na]^+$ 429.1113. Found 429.1119

28H_2. **21**H_3 (0.75 g, 2.47 mmol) was dissolved in MeOH (30 ml) and 3,5-di-*tert*-butyl-2-hydroxybenzaldehyde (0.58 g, 2.48 mmol) was added. The solution was stirred for 2 h then the solid was filtered and further dried *in-vacuo* to yield a yellow solid (1.08 g, 2.08 mmol, 84 %). ^{1}H NMR ($CDCl_3$): δ 1.24 – 1.44 (3H, m, ring-CH_2), δ 1.32 (9H, s, ^{t}Bu), 1.48 (9H, s, ^{t}Bu), 1.60 – 2.00 (5H, m, ring-CH_2), 2.28 (3H, s, CH_3), 3.01 (1H, m, ring-CH), 3.36 (1H, td, J = 10.5 Hz, J = 4.5, Hz, ring-CH), 3.85 (1H, d, J = 14.5 Hz, CH_2), 3.95 (1H, d, J = 14.5 Hz, CH_2), 6.83 (1H, d, J = 2.5 Hz, ArH), 7.09 (1H, d, J = 2.5 Hz, ArH), 7.19 (1H, d, J = 2.5 Hz, ArH), 7.42 (1H, d, J = 2.5 Hz, ArH), 8.43 (1H, s, CH), 11.4 – 14.7 (1H, br, OH). ^{13}C{^{1}H} NMR ($CDCl_3$): δ 24.7 (CH_2), 25.2 (CH_2), 29.6 (CH_3), 31.6 (CH_3), 34.3 (C), 35.2 (C), 35.3 (CH_3), 35.7 (CH_2), 59.5 (CH_2), 66.5 (CH), 70.1 (CH), 117.9 (Ar), 121.5 (Ar), 123.1 (Ar), 124.0 (Ar), 126.1 (ArH), 126.8 (ArH), 127.5 (ArH), 128.6 (ArH), 137.1 (Ar), 140.3 (Ar), 153.3 (ArO), 158.1 (ArO), 166.1 (CH).Calc. m/z $[C_{29}H_{40}Cl_2N_2O_2 + Na]^+$ 541.2365. Found 541.2393

29H_2. **21**H_3 (0.75 g, 2.47 mmol) was dissolved in MeOH (30 ml) and 2-hydroxybenzaldehyde (0.30 g, 2.46 mmol) was added. The solution was stirred for 2 h then the solid was filtered and further dried *in-vacuo* to yield a yellow solid (0.63 g, 1.55 mmol, 63 %). ^{1}H NMR ($CDCl_3$): δ 1.23 – 2.05 (8H, m, ring-CH_2), 2.27 (3H, s, CH_3), 2.97 (1H, m, ring-CH), 3.35 (1H, td, J = 10.5 Hz, J = 4.5, Hz, ring-CH), 3.79 (1H, d, J = 14.5 Hz, CH_2), 3.90 (1H, d, J = 14.5 Hz, CH_2), 6.80 (1H, d, J = 2.5 Hz,

ArH), 6.91 (1H, td, J = 7.5 Hz, J = 1.0 Hz, ArH), 7.01 (1H, m, ArH), 7.18 (1H, d, J = 2.5 Hz, ArH), 7.26 (1H, dd, J = 7.5 Hz, J = 1.5 Hz, ArH), 7.35 (1H, ddd, J = 8.5 Hz, J = 7.5 Hz, J = 1.5 Hz, ArH), 8.41 (1H, s, CH), 10.5 – 14.0 (2H, br, OH). $^{13}C\{^{1}H\}$ NMR ($CDCl_3$): δ 24.5 (CH_2), 25.1 (CH_2), 25.7 (CH_2), 35.4 (CH_2), 35.7 (CH_3), 58.6 (CH_2), 66.9 (CH), 70.0 (CH), 117.2 (ArH), 118.8 (ArH), 118.8 (Ar), 121.6 (Ar), 123.1 (Ar), 123.9 (Ar), 126.7 (ArH), 128.6 (ArH), 131.6 (ArH), 132.7 (ArH), 153.1 (ArO), 161.2 (ArO), 165.0 (CH). Calc. m/z $[C_{21}H_{24}Cl_2N_2O_2 + Na]^+$ 429.1113. Found 429.1102

30H_2. **21**H_3 (0.75 g, 2.47 mmol) was dissolved in MeOH (30 ml) and 3,5-dichloro-2-hydroxybenzaldehyde (0.46 g, 2.46 mmol) was added. The solution was stirred for 2 h then the solid was filtered and further dried *in-vacuo* to yield a yellow solid (0.94 g, 1.97 mmol, 80 %). ^{1}H NMR ($CDCl_3$): δ 1.23 – 2.06 (8H, m, ring-CH_2), 2.25 (3H, s, CH_3), 2.91 (1H, m, ring-CH), 3.37 (1H, td, J = 10.5 Hz, 4.5 Hz, ring-CH), 3.73 (1H, d, J = 14.5 Hz, CH_2), 3.86 (1H, d, J = 14.5 Hz, CH_2), 6.80 (1H, d, J = 2.5 Hz, ArH), 7.18 (1H, m, ArH), 7.42 (1H, d, J = 2.5 Hz, ArH), 8.30 (1H, s, CH), 11.0 – 14.5 (1H, br, OH). $^{13}C\{^{1}H\}$ NMR ($CDCl_3$): δ 24.0 (CH_2), 24.4 (CH_2), 25.0 (CH_2), 35.1 (CH_2), 36.1 (CH_3), 57.8 (CH_2), 67.0 (CH), 69.4 (CH), 119.8 (Ar), 121.8 (Ar), 122.8 (Ar), 123.0 (Ar), 123.3 (Ar), 123.6 (Ar), 126.6 (ArH), 128.8 (ArH), 129.3 (ArH), 132.4 (ArH), 152.9 (ArO), 156.3 (ArO), 163.5 (CH). Calc. m/z $[C_{21}H_{22}Cl_4N_2O_2 + Na]^+$ 497.0333. Found 497.0350

7.8.2 Preparation of aluminium *trans*-1,2-DACH salalen complexes

Al(**22**)Me. **22**H_2 (0.45 g, 0.80 mmol) was dissolved in toluene (30 ml) then 2M $AlMe_3$ in heptane (0.40 ml, 0.80 mmol) was slowly added and stirred (16 h). The solvent was removed *in-vacuo* and the crude mixture was recrystallised from hexane to yield yellow crystals (0.29 g, 0.48 mmol, 60 %). ^{1}H NMR (D_8-Tol) (233 K): δ -0.35 (3H, s, Al-Me), 0.50 (2H, m, ring-CH_2), 0.63 (2H, br, ring-CH_2), 1.05 – 1.30 (4H, m, ring-CH_2), 1.40 (9H, s, ^{t}Bu), 1.49 (9H, s, ^{t}Bu), 1.60 (3H, s, CH_3), 1.82 (9H, s, ^{t}Bu), 1.86 (9H, s, ^{t}Bu), 2.35 (2H, m, ring-CH), 2.78 (1H, d, J = 13.0 Hz, CH_2), 3.98 (1H, d, J = 13.0 Hz, CH_2), 6.84 (1H, s, ArH), 6.98 (1H, s, ArH), 7.52 (1H, s, ArH), 7.58 (1H, s, ArH), 7.76 (1H, s, CH). ^{13}C NMR (D_8-Tol): δ 21.5 (CH_2), 24.1 (CH_2), 24.8 (CH_2), 30.0 (CH_3), 30.1 (CH_3), 31.5 (CH_3), 32.1 (CH_3), 33.1 (CH_2), 34.1 (C),

34.3 (C), 35.6 (C), 35.7 (C), 36.3 (CH_3), 58.5 (CH_2), 60.2 (CH), 60.3 (CH), 118.1 (Ar), 120.9 (Ar), 123.6 (ArH), 123.7 (ArH), 127.5 (ArH), 131.7 (ArH), 136.7 (Ar), 138.1 (Ar), 138.4 (Ar), 141.7 (Ar), 157.1 (ArO), 166.0 (ArO), 171.4 (N=CH). Despite significant efforts elemental analysis could not be obtained for complexes containing ligand **1**H_2, clean NMRs and the single crystal data supports the complex.

Al(***R,R*-22**)Me. ***R,R*-22**H_2 (0.225 g, 0.80 mmol) was dissolved in toluene (30 ml) then 2M $AlMe_3$ in heptane (0.20 ml, 0.40 mmol) was slowly added and stirred (16 h). The solvent was removed *in-vacuo* and the crude mixture was recrystallised from hexane to yield yellow crystals (0.08 g, 0.13 mmol, 33 %). The following analysis shows a diastereomeric compound in an approximate 1:1 ratio. ^{1}H NMR (d_8-Tol): δ -0.48 (3H, s, Al-Me), -0.41 (3H, s, Al-Me), 0.50 - 0.85 (8H, m, ring-CH_2), 1.15 – 1.35 (8H, m, ring-CH_2), 1.35 (9H, s, ^{t}Bu), 1.37 (9H, s, ^{t}Bu), 1.41 (9H, s, ^{t}Bu), 1.45 (9H, s, ^{t}Bu), 1.69 (9H, s, ^{t}Bu), 1.74 (9H, s, ^{t}Bu), 1.76 (3H, s, CH_3), 1.77 (9H, s, ^{t}Bu), 1.78 (9H, s, ^{t}Bu), 1.85 (3H, s, CH_3), 2.35 – 2.50 (2H, m, ring-CH), 2.59 (1H, m, ring-CH), 2.80 (1H, d, J = 12.0 Hz, CH_2), 2.83 (1H, m, ring-CH), 2.94 (1H, d, J = 13.0 Hz, CH_2), 2.71 (1H, d, J = 12.0 Hz, CH_2), 4.08 (1H, d, J = 13.0 Hz, CH_2), 6.81 (1H, d, J = 2.5 Hz, ArH), 6.92 (1H, d, J = 2.5 Hz, ArH), 6.96 (2H, t, J = 2.5 Hz, ArH), 7.49 (1H, d, J = 2.5 Hz, ArH), 7.54 (1H, d, J = 2.5 Hz, ArH), 7.71 (1H, d, J = 2.5 Hz, ArH), 7.73 (1H, d, J = 2.5 Hz, ArH), 7.74 (1H, d, J = 1.0 Hz, ArH), 7.77 (1H, d, J = 1.0 Hz, ArH).^{13}C{^{1}H} NMR (d_8-Tol): δ 21.2 (CH_2), 21.6 (CH_2), 23.1 (CH_2), 24.2 (CH_2), 24.8 (CH_2), 25.0 (CH_2), 30.0 (CH_3), 30.2 (CH_3), 30.4 (CH_3), 30.5 (CH_3), 31.5 (CH_3), 31.6 (CH_3), 32.0 (CH_2), 32.1 (CH_3), 32.2 (CH_3), 32.6 (CH_2), 33.1 (C), 34.1 (C), 34.3 (C), 34.3 (C), 35.6 (C), 35.7 (C), 35.8 (C), 35.8 (C), 36.3 (CH_3), 41.1 (CH_3), 52.3 (CH_2), 58.6 (CH_2), 60.3 (CH), 61.2 (CH), 66.4 (CH), 118.1 (Ar), 120.9 (Ar), 122.2 (Ar), 123.7 (ArH), 123.7 (ArH), 123.8 (ArH), 123.9 (ArH), 127.5 (ArH), 127.8 (ArH), 131.7 (ArH), 132.0 (ArH), 136.7 (Ar), 136.8 (Ar), 138.0 (Ar), 138.2 (Ar), 138.4 (Ar), 141.4 (Ar), 141.8 (Ar), 157.1 (ArO), 157.4 (ArO), 166.1 (ArO), 166.5 (ArO), 171.4 (N=CH), 171.7 (N=CH). CHN analysis - see comment for Al(**21**)Me

Al(**22**)OBn. **22**H_2 (0.45 g, 0.80 mmol) was dissolved in toluene (30 ml) then 2M $AlMe_3$ in heptane (0.40 ml, 0.80 mmol) was slowly added and stirred (16 h). The solvent was removed *in-vacuo* and the crude mixture was briefly washed with

hexane to remove any traces of $AlMe_3$. The residue was dissolved in toluene (30 ml) then benzyl alcohol (0.092 ml, 0.89 mmol) was slowly added and the reaction was stirred (16 h). The solvent was removed *in-vacuo* and the crude mixture was recrystallised from hexane to yield a yellow solid (0.06 g, 0.09 mmol, 11 %). The following analysis shows a diastereomeric compound in an approximate 1:1 ratio. ^{1}H NMR (D_8-Tol): δ 0.45 – 0.9 (8H, m, ring-CH_2), 1.10 – 1.55 (8H, m, ring-CH_2), 1.35 (9H, s, ^{t}Bu), 1.37 (9H, s, ^{t}Bu), 1.39 (9H, s, ^{t}Bu), 1.44 (9H, s, ^{t}Bu), 1.62 (9H, s, ^{t}Bu), 1.73 (9H, s, ^{t}Bu), 1.74 (9H, s, ^{t}Bu), 1.78 (9H, s, ^{t}Bu), 2.18 (3H, s, CH_3), 2.23 (3H, s, CH_3), 2.30 (1H, td, J = 11.5 Hz, J = 3.0 Hz, ring-CH), 2.60 – 2.80 (3H, m, ring-CH), 2.83 (1H, d, J = 12.0 Hz, CH_2), 3.00 (1H, d, J = 13.0 Hz, CH_2), 3.71 (1H, d, J = 12.0 Hz, CH_2), 4.50 (1H, d, J = 13.0 Hz, CH_2), 5.20 (4H, br, CH_2), 6.80 (1H, d, J = 2.5 Hz, ArH), 6.93 (1H, d, J = 2.5 Hz, ArH), 6.96 (1H, s, ArH), 7.00 (1H, d, J = 2.5 Hz, ArH), 7.04 (2H, br, ArH), 7.15 – 7.40 (8H, br, ArH), 7.47 (1H, d, J = 2.5 Hz, ArH), 7.54 (1H, d, J = 2.5 Hz, ArH), 7.71 (1H, s, N=CH), 7.74 (1H, d, J = 2.5 Hz, ArH), 7.78 (1H, d, J = 2.5 Hz, ArH), 7.80 (1H, s, N=CH). ^{13}C NMR (D_8-Tol): δ 24.1 (CH_2), 24.8 (CH_2), 30.0 (CH_3), 30.4 (CH_3), 30.5 (CH_3), 30.7 (CH_3), 31.5 (CH_3), 31.5 (CH_3), 32.0 (CH_2), 32.1 (CH_3), 32.2 (CH_3), 32.2 (CH_2), 34.1 (C), 34.2 (C), 34.3 (C), 34.3 (C), 35.5 (C), 35.7 (C), 35.8 (C), 35.9 (C), 37.6 (CH_3), 41.7 (CH_3), 52.1 (CH_2), 59.2 (CH_2), 60.2 (CH), 60.2 (CH), 60.7 (CH), 66.2 (CH), 118.4 (Ar), 121.2 (Ar), 122.1 (Ar), 123.6 (ArH), 123.7 (ArH), 123.8 (ArH), 123.9 (ArH), 126.8 (ArH), 127.8 (ArH), 128.0 (ArH), 128.2 (ArH), 132.1 (ArH), 132.3 (ArH), 137.3 (Ar), 137.3(Ar), 138.5 (Ar), 141.4 (Ar), 141.5 (Ar), 156.9 (ArO), 157.3 (ArO), 166.4 (ArO), 171.2 (N=CH), 171.5 (N=CH). CHN analysis - see comment for Al(**21**)Me

Al(**23**)Me. **23**H_2 (0.45 g, 1.00 mmol) was dissolved in toluene (30 ml) then 2M $AlMe_3$ in heptane (0.50 ml, 1.00 mmol) was slowly added and stirred (16 h). The solvent was removed *in-vacuo* and the crude mixture was recrystallised from toluene to yield yellow crystals (0.10 g, 0.20 mmol, 20 %). ^{1}H NMR (D_8-Tol): δ -0.36 (3H, s, Al-Me), 0.70 - 1.00 (4H, br, ring-CH_2), 1.30 – 1.60 (4H, m, ring-CH_2), 1.45 (9H, s, ^{t}Bu), 1.75 (9H, s, ^{t}Bu), 1.86 (3H, s, CH_3), 2.45 – 2.65 (2H, m, ring-CH), 2.72 (1H, d, J = 12.0 Hz, CH_2), 3.49 (1H, d, J = 12.0 Hz, CH_2), 6.53 (1H, ddd, J = 8.0 Hz, J = 6.5 Hz, J = 1.5 Hz, ArH), 6.90 (1H, d, J = 1.5 Hz, ArH), 6.93 (1H, d, J = 2.0 Hz, ArH), 7.14 (1H, d, J = 1.5 Hz, ArH), 7.18 (1H, dd, J = 6.5 Hz, J = 2.0 Hz, ArH), 7.52 (1H, d,

J = 2.5 Hz, ArH), 7.69 (1H, s, CH). ^{13}C NMR (D_8-Tol): δ 29.7 (CH_2), 29.8 (CH_2), 34.8 (CH_3), 37.1 (CH_3), 38.0 (C), 39.1 (C), 40.3 (CH_2), 45.5 (CH_3), 57.2 (CH_2), 66.7 (CH), 70.9 (CH), 120.1 (ArH), 123.4 (Ar), 126.4 (Ar), 127.8 (ArH), 128.3 (ArH), 128.6 (ArH), 138.7 (ArH), 142.1 (ArH), 142.7 (Ar), 143.3 (Ar), 162.1 (ArO), 173.9 (ArO), 176.3 (N=CH). Calc. (%) for $C_{30}H_{43}AlN_2O_2$, C 73.44, H 8.83, N 5.71. Found (%), C 73.57, H 8.83, N 5.80.

Al(**23**)OBn. **23**H_2 (0.36 g, 0.80 mmol) was dissolved in toluene (30 ml) then 2M $AlMe_3$ in heptane (0.40 ml, 0.80 mmol) was slowly added and stirred (16 h). The solvent was removed *in-vacuo,* then the residue was dissolved in toluene (30 ml). Benzyl alcohol (0.083 ml, 0.80 mmol) was slowly added to the reaction and allowed to stir (16 h). The solvent was removed *in-vacuo* and the crude mixture was recrystallised from hexane to yield a yellow solid (0.06 g, 0.09 mmol, 11 %). ^{1}H NMR (D_8-Tol) (233 K): δ 0.40 – 0.65 (4H, m, ring-CH_2), 1.05 – 1.30 (4H, m, ring-CH_2), 1.46 (9H, s, ^{t}Bu), 1.74 (9H, s, ^{t}Bu), 2.21 (3H, s, CH_3), 2.29 (2H, br, ring-CH), 2.88 (1H, d, J = 13.5 Hz, CH_2), 4.56 (1H, d, J = 13.5 Hz, CH_2), 5.31 (1H, d, J = 14.0 Hz, CH_2), 5.57 (1H, d, J = 14.0 Hz, CH_2), 6.56 (1H, t, J = 7.5 Hz, ArH), 6.82 (1H, s, ArH), 6.87 (1H, d, J = 7.5 Hz, ArH), 7.04 (1H, s, ArH), 7.20 (1H, s, ArH), 7.23 (1H, s, ArH), 7.29 (2H, t, J = 7.5 Hz, ArH), 7.41 (1H, s, ArH), 7.56 (1H, s, ArH), 7.60 (1H, s, ArH), 7.62 (1H, s, CH). ^{13}C NMR (D_8-Tol): δ 25.0 (CH_2), 25.6 (CH_2), 30.9 (CH_3), 32.7 (C), 33.2 (CH_3), 36.4 (C), 38.6 (CH_3), 60.3 (CH_2), 60.7 (CH), 60.9 (CH), 67.5 (CH_2), 116.9 (ArH), 118.9 (Ar), 121.3 (Ar), 122.0 (Ar), 123.1 (ArH), 124.0 (ArH), 126.0 (ArH), 126.2 (ArH), 127.3 (ArH), 128.4 (ArH), 129.7 (ArH), 134.2 (ArH), 137.5 (ArH), 138.7 (Ar), 138.8 (Ar), 143.3 (Ar), 157.2 (ArO), 168.1 (ArO), 170.6 (N=CH). Calc. (%) for $C_{36}H_{47}AlN_2O_3$, C 74.20, H 8.13, N 4.81. Found (%), C 72.31, H 7.86, N 4.47.

.

Al(**24**)Me. **24**H_2 (0.41 g, 0.79 mmol) was dissolved in toluene (30 ml) then 2M $AlMe_3$ in heptane (0.40 ml, 0.80 mmol) was slowly added and stirred (16 h). The solvent was removed *in-vacuo* and the crude mixture was recrystallised from a toluene:hexane mix to yield a yellow solid (0.34 g, 0.61 mmol, 77 %).^{1}H NMR (D_8-Tol) (233 K): δ -0.41 (3H, s, Al-Me), 0.70 – 0.95 (4H, br, ring-CH_2), 1.30 – 1.50 (4H, m, ring-CH_2), 1.43 (9H, s, ^{t}Bu), 1.73 (9H, s, ^{t}Bu), 1.81 (3H, s, CH_3), 2.50 (1H, m,

ring-CH), 2.70 (1H, br, ring-CH), 2.71 (1H, d, J = 12.0 Hz, CH_2), 3.44 (1H, d, J = 12.0 Hz, CH_2), 6.65 (1H, d, J = 2.5 Hz, ArH), 6.92 (1H, d, J = 2.5 Hz, ArH), 7.34 (1H, s, ArH), 7.35 (1H, s, CH), 7.52 (1H, d, J = 2.5 Hz, ArH). ^{13}C NMR (D_8-Tol): δ 24.7 (CH_2), 24.9 (CH_2), 30.0 (CH_3), 32.2 (CH_3), 33.0 (C), 34.3 (C), 35.5 (CH_2), 40.8 (CH_3), 52.3 (CH_2), 62.2 (CH), 60.9 (CH), 66.0 (CH_2), 116.5 (ArH), 117.9 (Ar), 120.7 (ArH), 122.2 (Ar), 127.4 (ArH), 128.8 (ArH), 130.0 (ArH), 131.9 (ArH), 136.8 (Ar), 141.6 (Ar), 161.5 (ArO), 166.4 (ArO), 172.1 (N=CH). Calc. (%) for $C_{30}H_{41}AlCl_2N_2O_2$, C 64.40, H 7.39, N 5.01. Found (%), C 64.39, H 7.46, N 5.18.

Al(**24**)OBn. **24**H_2 (0.42 g, 0.81 mmol) was dissolved in toluene (30 ml) then 2M $AlMe_3$ in heptane (0.40 ml, 0.80 mmol) was slowly added and stirred (16 h). The solvent was removed *in-vacuo* and the crude mixture was briefly washed with hexane to remove any traces of $AlMe_3$. The residue was dissolved in toluene (30 ml) then benzyl alcohol (0.091 ml, 0.88 mmol) was slowly added and the reaction was stirred (16 h). The solvent was removed *in-vacuo* and the crude mixture was recrystallised from hexane to yield a yellow solid (0.22 g, 0.34 mmol, 42 %). ^{1}H NMR (D_8-Tol) (K): δ 0.65 – 0.85 (4H, br, ring-CH_2), 1.30 – 1.55 (4H, m, ring-CH_2), 1.42 (9H, s, ^{t}Bu), 1.74 (9H, s, ^{t}Bu), 2.23 (3H, s, CH_3), 2.74 (2H, br, CH_2), 2.77 (1H, br, CH), 3.51 (1H, d, J = 12.0 Hz, CH), 5.14 (2H, br, CH_2), 6.64 (1H, d, J = 2.0 Hz, ArH), 6.93 (1H, s, ArH), 7.03 (1H, s, ArH), 7.12 (1H, s, ArH), 7.13 (1H, s, CH), 7.30 (1H, s, ArH), 7.33 (1H, s, ArH), 7.35 (1H, s, ArH), 7.53 (1H, d, J = 2.5 Hz, ArH). ^{13}C NMR (D_8-Tol): δ 24.6 (CH_2), 24.7 (CH_2), 30.0 (CH_3), 31.8 (CH_2), 32.2 (C), 34.3 (C), 35.5 (CH_2), 41.6 (CH_3), 52.3 (CH_2), 61.0 (CH), 65.9 (CH_2), 66.2 (CH), 118.8 (Ar), 119.1 (Ar), 121.1 (Ar), 123.4 (ArH), 124.0 (ArH), 126.0 (ArH), 127.1 (ArH), 128.0 (ArH), 130.9 (ArH), 135.8 (ArH), 138.7 (Ar), 138.9 (Ar), 156.8 (ArO), 162.0 (ArO), 169.7 (N=CH). Calc. (%) for $C_{36}H_{45}AlCl_2N_2O_3$, C 66.35, H 6.96, N 4.30. Found (%), C 66.20, H 7.08, N 4.28

Al(**25**)Me. **25**H_2 (0.36 g, 0.80 mmol) was dissolved in toluene (30 ml) then 2M $AlMe_3$ in heptane (0.40 ml, 0.80 mmol) was slowly added and stirred (16 h). The solvent was removed *in-vacuo* and the crude mixture was recrystallised from a toluene:hexane mix to yield a yellow solid (0.18 g, 0.37 mmol, 46 %). ^{1}H NMR (D_8-Tol) (233 K): δ -0. 35 (3H, s, Al-Me), 0.70 – 0.90 (4H, br, ring-CH_2), 1.35 – 1.55

(4H, m, ring-CH_2), 1.40 (9H, s, ^{t}Bu), 1.79 (9H, s, ^{t}Bu), 1.86 (3H, s, CH_3), 2.55 (1H, m, ring-CH), 2.66 (1H, d, J = 12.0 Hz, CH_2), 3.49 (1H, d, J = 12.0 Hz, CH_2), 6.73 (1H, t, J = 7.0 Hz, ArH), 6.86 (1H, d, J = 7.0 Hz, ArH), 6.94 (1H, d, J = 2.5 Hz, ArH), 7.05 (1H, d, J = 8.0 Hz, ArH), 7.19 (1H, t, J = 7.5 Hz, ArH), 7.72 (1H, s, ArH), 7.73 (1H, s, CH). ^{13}C NMR (D_8-Tol): δ 24.9 (CH_2), 25.0 (CH_2), 29.7 (CH_3), 31.6 (CH_3), 33.4 (C), 34.2 (C), 35.7 (CH_2), 40.8 (CH_3), 51.7 (CH_2), 61.5 (CH), 66.3 (CH), 118.9 (Ar), 119.0 (Ar), 121.3 (Ar), 123.5 (ArH), 124.0 (ArH), 128.1 (Ar), 130.9 (ArH), 135.9 (ArH), 138.4 (Ar), 138.9 (Ar), 156.9 (ArO), 162.0 (ArO), 170.4 (N=CH). Calc. (%) for $C_{30}H_{43}AlN_2O_2$, C 73.44, H 8.83, N 5.71. Found (%), C 73.37, H 8.90, N 5.82.

Al(**25**)OBn. **25**H_2 (0.36 g, 0.80 mmol) was dissolved in toluene (30 ml) then 2M $AlMe_3$ in heptane (0.40 ml, 0.80 mmol) was slowly added and stirred (16 h). The solvent was removed *in-vacuo* and the crude mixture was briefly washed with hexane to remove any traces of $AlMe_3$. The residue was dissolved in toluene (30 ml) then benzyl alcohol (0.083 ml, 0.80 mmol) was slowly added and the reaction was stirred (16 h). The solvent was removed *in-vacuo* and the crude mixture was recrystallised from a toluene:hexane mix to yield a yellow solid (0.23 g, 0.39 mmol, 49 %). ^{1}H NMR (D_8-Tol) (233 K): δ 0.40 – 0.80 (4H, m, ring-CH_2), 1.15 – 1.55 (4H, m, ring-CH_2), 1.48 (9H, s, ^{t}Bu), 1.88 (9H, s, ^{t}Bu), 2.24 (3H, s, CH_3), 2.25 (1H, br, ring-CH), 2.59 (1H, d, J = 12.0 Hz, CH_2), 2.77 (1H, t, J = 11.0 Hz, ring-CH), 3.39 (1H, d, J = 12.0 Hz, CH_2), 5.34 (1H, d, J = 13.0 Hz, CH_2), 5.44 (1H, d, J = 13.0 Hz, CH_2), 6.86 (1H, t, J = 7.0 Hz, ArH), 6.93 (1H, d, J = 7.5 Hz, ArH), 7.15 – 7.30 (5H, m, ArH), 7.48 (2H, d, J = 7.5 Hz, ArH), 7.60 (1H, s, ArH), 7.85 (1H, s, ArH). ^{13}C NMR (D_8-Tol): δ 24.9 (CH_2), 25.0 (CH_2), 30.0 (CH_3), 31.6 (CH_3), 32.4 (C), 34.2 (C), 35.8 (CH_2), 41.4 (CH_3), 51.5 (CH_2), 60.7 (CH), 66.1 (CH), 66.2 (CH_2), 116.9 (ArH), 118.2 (Ar), 120.6 (ArH), 122.1 (Ar), 125.9 (ArH), 127.3 (ArH), 128.0 (ArH), 128.7 (ArH), 130.0 (ArH), 132.1 (ArH), 137.3 (Ar), 141.8 (Ar), 161.3 (ArO), 166.6 (ArO), 171.8 (N=CH). Calc. (%) for $C_{36}H_{47}AlN_2O_3$, C 74.20, H 8.13, N 4.81. Found (%), C 74.29, H 8.11, N 4.72.

Al(**26**)OBn. **26**H_2 (0.34 g, 1.00 mmol) was dissolved in toluene (30 ml) then 2M $AlMe_3$ in heptane (0.50 ml, 1.00 mmol) was slowly added and stirred (16 h). The solvent was removed *in-vacuo* and the crude mixture was briefly washed with

hexane to remove any traces of $AlMe_3$. The residue was dissolved in toluene (30 ml) then benzyl alcohol (0.11 ml, 1.06 mmol) was slowly added and the reaction was stirred (16 h). The solvent was removed *in-vacuo* and the crude mixture was recrystallised from a toluene:hexane mix to yield a yellow solid (0.27 g, 0.57 mmol, 57 %). The following analysis shows a diastereomeric compound in an approximate 1:1 ratio. ^{1}H NMR (D_8-Tol): δ 0.45 – 0.90 (8H, m, ring-CH_2), 1.15 – 1.55 (8H, m, ring-CH_2), 2.16 (3H, s, CH_3), 2.22 (3H, s, CH_3), 2.39 (1H, td, J = 12.0 Hz, J = 2.5 Hz, ring-CH), 2.52 (1H, t, J = 11.0 Hz, ring-CH), 2.64 (1H, br, ring-CH), 2.67 (1H, d, J = 12.0 Hz, CH_2), 2.74 (1H, t, J = 11.0 Hz, ring-CH), 2.99 (1H, d, J = 13.5 Hz, CH_2), 3.50 (1H, d, J = 12.5 Hz, CH_2), 4.51 (1H, d, J = 12.5 Hz, CH_2), 5.09 (4H, br, CH_2), 6.54 (2H, t, J = 6.5 Hz, ArH), 6.70 (2H, m, ArH), 6.76 (1H, d, J = 7.5 Hz, ArH), 6.86 (2H, t, J = 8.0 Hz, ArH), 6.92 (1H, d, J = 7.5 Hz, ArH), 7.03 – 7.09 (5H, m, ArH), 7.16 (8H, m, ArH), 7.38 (4H, br, ArH), 7.56 (1H, s, ArH), 7.67 (1H, s, ArH). ^{13}C NMR (D_8-Tol): δ 21.3 (CH_2), 23.9 (CH_2), 24.6 (CH_2), 24.7 (CH_2), 24.8 (CH_2), 31.0 (CH_2), 32.0 (CH_2), 37.4 (CH_3), 41.6 (CH_3), 51.6 (CH_2), 58.3 (CH_3), 59.7 (CH), 59.8 (CH), 60.5 (CH), 66.1 (CH), 66.2 (CH_2), 115.7 (ArH), 115.7 (ArH), 117.0 (ArH), 117.2 (ArH), 118.6 (Ar), 118.7 (Ar), 120.4 (ArH), 120.5 (ArH), 121.1 (Ar), 122.2 (Ar), 122.6 (ArH), 122.8 (ArH), 125.9 (ArH), 127.1 (ArH), 128.1 (ArH), 130.1 (ArH), 130.2 (ArH), 133.9 (ArH), 134.0 (ArH), 137.1 (ArH), 137.2 (ArH), 160.9 (ArO), 161.3 (ArO), 168.4 (ArO), 168.8 (ArO), 170.8 (N=CH), 171.1 (N=CH). Calc. (%) for $C_{28}H_{31}AlN_2O_3$, C 71.47, H 6.64, N 5.95. Found (%), C 71.38, H 6.65, N 6.02.

Al(**27**)OBn. **27**H_2 (0.41 g, 1.00 mmol) was dissolved in toluene (30 ml) then 2M $AlMe_3$ in heptane (0.50 ml, 1.00 mmol) was slowly added and stirred (16 h). The solvent was removed *in-vacuo* and the crude mixture was briefly washed with hexane to remove any traces of $AlMe_3$. The residue was dissolved in toluene (30 ml) then benzyl alcohol (0.11 ml, 1.06 mmol) was slowly added and the reaction was stirred (16 h). The solvent was removed *in-vacuo* and the crude mixture was recrystallised from a toluene:hexane mix to yield a yellow solid (0.20 g, 0.37 mmol, 37 %). The following analysis shows a diastereomeric compound in an approximate 1:1 ratio. ^{1}H NMR (D_8-Tol): δ 0.30 – 0.80 (8H, m, ring-CH_2), 1.30 – 1.50 (8H, m, ring-CH_2), 1.66 (1H, m, CH_2), 2.12 (3H, s, CH_3), 2.16 (3H, s, CH_3), 2.36 (1H, m, ring-CH), 2.57 (1H, m, ring-CH), 2.65 (1H, d, J = 12.5 Hz, CH_2), 2.72 (1H, d, J =

12.5 Hz, ring-CH), 2.79 (1H, m, ring-CH), 2.96 (1H, d, J = 13.5 Hz, CH_2), 3.51 (1H, d, J = 12.5 Hz, CH_2), 4.45 (1H, d, J = 13.5 Hz, CH_2), 5.13 (4H, br, CH_2), 6.50 – 6.85 (7H, m, ArH), 7.03 (2H, m, ArH), 7.14 (5H, m, ArH), 7.25 – 7.40 (7H, m, ArH), 7.51 (1H, s, N=CH). ^{13}C NMR (D_8-Tol): δ 21.3 (CH_2), 23.8 (CH_2), 24.5 (CH_2), 24.7 (CH_2), 24.8 (CH_2), 30.9 (CH_2), 32.0 (CH_2), 37.5 (CH_3), 41.7 (CH_3), 51.6 (CH_2), 58.3 (CH_3), 59.5 (CH), 60.2 (CH), 60.9 (CH), 65.9 (CH_2), 66.1 (CH), 117.3 (ArH), 117.5 (ArH), 118.9 (Ar), 119.0 (Ar), 119.2 (Ar), 119.3 (Ar), 120.4 (ArH), 120.6 (ArH), 120.8 (Ar), 121.9 (Ar), 126.2 (ArH), 127.0 (ArH), 128.1 (ArH), 130.2 (ArH), 130.3 (ArH), 131.0 (ArH), 131.1 (ArH), 135.7 (ArH), 135.82 (ArH), 160.5 (ArO), 160.8 (ArO), 161.3 (ArO), 161.8 (ArO), 169.7 (N=CH), 170.3 (N=CH). Calc. (%) for $C_{28}H_{29}AlCl_2N_2O_3$, C 62.34, H 5.42, N 5.19. Found (%), C 62.28, H 5.46, N 5.07.

Al(**28**)Me. **28**H_2 (0.41 g, 0.79 mmol) was dissolved in toluene (30 ml) then 2M $AlMe_3$ in heptane (0.40 ml, 0.80 mmol) was slowly added and stirred (16 h). The solvent was removed *in-vacuo* and the crude mixture was recrystallised from a toluene:hexane mix to yield a yellow solid (0.32 g, 0.57 mmol, 72 %). ^{1}H NMR (D_8-Tol): δ -0.43 (3H, s, Al-Me), 0.60 – 1.00 (4H, m, ring-CH_2), 1.20 – 1.60 (4H, br, ring-CH_2), 1.37 (9H, s, ^{t}Bu), 1.63 (3H, s, CH_3), 1.78 (9H, s, ^{t}Bu), 2.42 (2H, m, ring-CH), 2.61 (1H, m, CH), 3.26 (1H, d, J = 11.5 Hz, CH_2), 6.65 (1H, s, ArH), 6.94 (1H, s, ArH), 7.34 (1H, s, ArH), 7.72 (1H, s, ArH), 7.73 (1H, s, CH). ^{13}C NMR (D_8-Tol): δ 24.8 (CH_2), 24.9 (CH_2), 29.9 (CH_3), 31.5 (CH_3), 32.2 (C), 34.2 (C), 35.7 (CH_2), 40.7 (CH_3), 51.0 (CH_2), 61.3 (CH), 66.3 (CH), 117.8 (Ar), 120.2 (Ar), 124.7 (Ar), 125.4 (Ar), 127.1 (ArH), 127.4 (ArH), 129.8 (ArH), 127.5 (ArH), 132.3 (ArH), 137.3 (Ar), 141.9 (Ar), 155.7 (ArO), 166.2 (ArO), 172.3 (N=CH). Calc. (%) for $C_{30}H_{41}AlCl_2N_2O_2$, C 64.40, H 7.39, N 5.01. Found (%), C 64.47, H 7.51, N 5.13.

Al(**28**)OBn. **28**H_2 (0.42 g, 0.81 mmol) was dissolved in toluene (30 ml) then 2M $AlMe_3$ in heptane (0.40 ml, 0.80 mmol) was slowly added and stirred (16 h). The solvent was removed *in-vacuo* and the crude mixture was briefly washed with hexane to remove any traces of $AlMe_3$. The residue was dissolved in toluene (30 ml) then benzyl alcohol (0.083 ml, 0.80 mmol) was slowly added and the reaction was stirred (16 h). The solvent was removed *in-vacuo* and the crude mixture was recrystallised from a toluene:hexane mix to yield a yellow solid (0.34 g, 0.52 mmol,

65 %). ^{1}H NMR (D_8-Tol): δ 0.65 – 0.95 (4H, m, ring-CH_2), 1.30 – 1.55 (4H, br, ring-CH_2), 1.37 (9H, s, ^{t}Bu), 1.75 (9H, s, ^{t}Bu), 2.00 (3H, s, CH_3), 2.41 (1H, d, J = 12.5 Hz, CH_2), 2.58 (1H, m, ring-CH), 2.74 (1H, m, ring-CH), 3.23 (1H, d, J = 12.5 Hz, CH_2), 5.16 (2H, br, CH_2), 6.64 (1H, d, J = 2.5 Hz, ArH), 6.97 (1H, s, ArH), 7.06 (1H, d, J = 7.0 Hz, ArH), 7.19 (2H, t, J = 7.5 Hz, ArH), 7.34 (1H, d, J = 2.5 Hz, ArH), 7.41 (2H, J = 7.5 Hz, ArH), 7.75 (1H, m, ArH), 7.77 (1H, m, CH). ^{13}C NMR (D_8-Tol): δ 24.8 (CH_2), 24.9 (CH_2), 30.2 (CH_3), 31.5 (CH_3), 32.3 (C), 34.2 (C), 37.8 (CH_2), 41.4 (CH_3), 60.5 (CH), 65.5 (CH_2), 66.2 (CH), 118.1 (Ar), 120.8 (Ar), 124.6 (Ar), 125.6 (Ar), 126.1 (ArH), 127.0 (ArH), 127.4 (ArH), 127.5 (ArH), 128.1 (ArH), 129.3 (ArH), 129.8 (ArH), 132.5 (ArH), 137.8 (Ar), 142.1 (Ar), 146.7 (Ar), 155.5 (ArO), 166.4 (ArO), 172.1 (N=CH). Calc. (%) for $C_{36}H_{45}AlCl_2N_2O_3$, C 66.35, H 6.96, N 4.30. Found (%), C 66.45, H 7.02, N 4.40.

Al(**29**)OBn. **29**H_2 (0.33 g, 0.81 mmol) was dissolved in toluene (30 ml) then 2M $AlMe_3$ in heptane (0.40 ml, 0.80 mmol) was slowly added and stirred (16 h). The solvent was removed *in-vacuo* and the crude mixture was briefly washed with hexane to remove any traces of $AlMe_3$. The residue was dissolved in toluene (30 ml) then benzyl alcohol (0.091 ml, 0.88 mmol) was slowly added and the reaction was stirred (16 h). The solvent was removed *in-vacuo* and the crude mixture was recrystallised twice from a toluene / hexane mix to yield a yellow solid (0.19 g, 0.35 mmol, 43 %). The following analysis shows a diastereomeric compound in an approximate 1:1 ratio. Analysis also shows impurities were present in this sample despite extensive efforts to isolate a pure product. ^{1}H NMR (d_8-Tol): δ 0.30 – 0.90 (8H, m, ring-CH_2), 1.10 – 1.65 (8H, m, ring-CH_2), 2.07 (3H, s, CH_3), 1.95 – 2.15 (3H, m, CH_3), 2.30 – 2.70 (4H, m, CH), 2.73 (1H, d, J = 13.5 Hz, CH_2), 3.10 – 4.10 (2H, m, CH_2), 4.24 (1H, d, J = 13.5 Hz, CH_2), 4.90 - 5.30 (4H, br, CH_2), 6.45 – 6.75 (4H, m, ArH), 6.80 – 6.90 (2H, m, ArH), 7.05 (1H, s, ArH), 7.07 (1H, s, ArH), 7.10 – 7.23 (6H, m, ArH), 7.29 (2H, m, ArH), 7.35 (2H, s, ArH), 7.38 (2H, s, ArH), 7.48 (1H, br, ArH), 7.54 (1H, s, N=CH), 7.55 – 7.90 (2H, m, ArH, N=CH). ^{13}C{^{1}H} NMR (d_8-Tol): δ 21.2 (CH_2), 23.7 (CH_2), 24.4 (CH_2), 24.6 (CH_2), 24.7 (CH_2), 30.7 (CH_2), 31.8 (CH_2), 37.4 (CH_3), 41.5 (CH_3), 50.8 (CH_2), 57.4 (CH_2), 59.6 (CH), 60.2 (CH), 60.3 (CH), 66.1 (CH_2), 66.1 (CH), 116.0 (ArH), 118.4 (Ar), 118.5 (Ar), 120.8 (Ar), 120.9 (Ar), 122.7 (ArH), 122.7 (ArH), 123.5 (Ar), 124.2 (Ar), 24.6 (Ar), 126.2 (ArH),

126.9 (ArH), 127.1 (ArH), 127.1 (ArH), 128.1 (ArH), 129.8 (ArH), 129.9 (ArH), 133.8 (ArH), 133.9 (ArH), 137.4 (ArH), 137.6 (ArH), 155.3 (ArO), 155.5 (ArO), 168.3 (ArO), 168.8 (ArO), 170.9 (N=CH), 171.1 (N=CH). Calc. (%) for $C_{28}H_{29}AlCl_2N_2O_3$, C 62.34, H 5.42, N 5.19. Found (%), C 57.91, H 5.78, N 4.39.

Al(**30**)OBn. **30**H_2 (0.38 g, 0.80 mmol) was dissolved in toluene (30 ml) then 2M $AlMe_3$ in heptane (0.40 ml, 0.80 mmol) was slowly added and stirred (16 h). The solvent was removed *in-vacuo* and the crude mixture was briefly washed with hexane to remove any traces of $AlMe_3$. The residue was dissolved in toluene (30 ml) then benzyl alcohol (0.091 ml, 0.88 mmol) was slowly added and the reaction was stirred (16 h). The solvent was removed *in-vacuo* and the crude mixture was recrystallised from a toluene:hexane mix to yield a yellow solid (0.16 g, 0.26 mmol, 33 %). The major diastereomer is characterised, the minor diastereomer is present at an approximate 3:1 ratio. ^{1}H NMR (D_8-Tol): δ 0.25 – 0.40 (2H, m, ring-CH_2), 0.50 – 0.75 (2H, m, ring-CH_2), 1.17 (2H, m, ring-CH_2), 1.32 (1H, m, ring-CH_2), 1.44 (1H, m, ring-CH_2), 2.09 (3H, s, CH_3), 2.45 (1H, m, ring-CH), 2.68 (1H, m, ring-CH), 3.22 (1H, d, J = 12.5 Hz, CH_2), 4.18 (1H, d, J = 12.5 Hz, CH_2), 5.11 (2H, br, CH_2), 6.56 (2H, m, ArH), 7.05 (1H, d, J = 7.5 Hz, ArH), 7.17 (2H, t, J = 7.5 Hz, ArH), 7.25 (1H, s, ArH), 7.29 (2H, m, ArH), 7.37 (1H, s, ArH), 7.39 (1H, s, CH). Calc. (%) for $C_{28}H_{27}AlCl_4N_2O_3$, C 55.28, H 4.47, N 4.61. Found (%), C 55.17, H 4.54, N 4.64. $^{13}C\{^1H\}$ NMR analysis was not possible due to solubility.

7.9 References

1. B. M. Chamberlain, M. Cheng, D. R. Moore, T. M. Ovitt, E. B. Lobkovsky and G. W. Coates, *J. Am. Chem. Soc.*, 2001, **123**, 3229-3238.

8.0 Appendix

X-ray diffraction data

8.1 X-ray diffraction data

8.1.1 Chapter 2

1H_2

Empirical formula	$C_{22}H_{30}N_2O_2$
Formula weight	354.48
Temperature	150(2) K
Wavelength	0.71073 Å
Crystal system, space group	Monoclinic, $P2_1/n$
Unit cell dimensions	a = 8.4960(3) Å α = 90 ° b = 12.8830(3) Å β = 102.393(2) ° c = 8.9960(3) Å γ = 90 °
Volume	961.70(5) $Å^3$
Z, Calculated density	2, 1.224 Mg/m^3
Absorption coefficient	0.078 mm^{-1}
F(000)	384
Crystal size	0.30 x 0.30 x 0.30 mm
Theta range for data collection	4.04 to 27.53 °
Limiting indices	-11≤h≤11, -15≤k≤16, -11≤l≤11
Reflections collected / unique	17655 / 2199 [R(int) = 0.0443]
Completeness to theta = 27.53	99.2 %
Absorption correction	None
Refinement method	Full-matrix least-squares on F^2
Data / restraints / parameters	2199 / 0 / 124
Goodness-of-fit on F^2	1.040
Final R indices [I>2σ(I)]	R_1 = 0.0440, wR_2 = 0.1186
R indices (all data)	R_1 = 0.0600, wR_2 = 0.1293
Largest diff. peak and hole	0.234 and -0.253 $eÅ^{-3}$

3H$_2$

Empirical formula	$C_{19}H_{31}NO$
Formula weight	289.41
Temperature	150(2) K
Wavelength	0.68890 Å
Crystal system, space group	Triclinic, *P*-1
Unit cell dimensions	a = 7.229(7) Å α = 102.458 (14) ° b = 9.916(9) Å β = 96.862(5) ° c = 14.129(12) Å γ = 104.919(11) °
Volume	939.1(14) Å^3
Z, Calculated density	2, 1.24 Mg/m^3
Absorption coefficient	0.062 mm^{-1}
F(000)	320
Crystal size	0.07 x 0.06 x 0.02 mm
Theta range for data collection	2.13 to 22.50 °
Limiting indices	-8≤h≤8, -9≤k≤11, -15≤l≤15
Reflections collected / unique	6488 / 2639 [R(int) = 0.0334]
Data Completeness	0.984
Absorption correction	Semi-empirical from equivalents
Refinement method	Full-matrix least-squares on F^2
Data / restraints / parameters	2639 / 0 / 200
Goodness-of-fit on F^2	1.653
Final R indices [I>2σ(I)]	R_1 = 0.1211, wR_2 = 0.3648
R indices (all data)	R_1 = 0.1391, wR_2 = 0.3898
Largest diff. peak and hole	1.226 and -0.367 eÅ^{-3}

8H_2

Empirical formula	$C_{35}H_{56}N_2O_2$
Formula weight	536.82
Temperature	150(2) K
Wavelength	0.71073 Å
Crystal system, space group	Triclinic, *P*-1
Unit cell dimensions	a = 10.0750(2) Å α = 65.7700(10) ° b = 13.3950(3) Å β = 88.2360(10) ° c = 14.3470(3) Å γ = 71.9810(10) °
Volume	1668.67(6) $Å^{-3}$
Z, Calculated density	2, 1.068 Mg/m^{-3}
Absorption coefficient	0.065 mm^{-1}
F(000)	592
Crystal size	0.12 x 0.10 x 0.10 mm
Theta range for data collection	3.53 to 27.48 °
Limiting indices	-13≤h≤13, -17≤k≤17, -18≤l≤18
Reflections collected / unique	31839 / 7601 [R(int) = 0.0633]
Completeness to theta = 27.48	99.3 %
Absorption correction	None
Max. and min. transmission	0.9935 and 0.9923
Refinement method	Full-matrix least-squares on F^2
Data / restraints / parameters	7601 / 0 / 364
Goodness-of-fit on F^2	1.041
Final R indices [I>2σ(I)]	R_1 = 0.0549, wR_2 = 0.1391
R indices (all data)	R_1 = 0.0796, wR_2 = 0.1577
Largest diff. peak and hole	0.268 and -0.372 $eÅ^{-3}$

$Ti_2(\mathbf{1})_2(OiPr)_4$

Empirical formula	$C_{59}H_{91}N_4O_8Ti_2$
Formula weight	1080.16
Temperature	150(2) K
Wavelength	0.68890 Å
Crystal system, space group	Monoclinic, *P*21/*c*
Unit cell dimensions	a = 23.224(6) Å α = 90 ° b = 16.478(5) Å β = 96.782(3) ° c = 31.844(9) Å γ = 90 °
Volume	12101(6) $Å^3$
Z, Calculated density	8, 1.186 Mg/m^3
Absorption coefficient	0.317 mm^{-1}
F(000)	4648
Crystal size	0.08 x 0.05 x 0.02 mm
Theta range for data collection	2.83 to 25.17 °
Limiting indices	$-22 \leq h \leq 28$, $-20 \leq k \leq 20$, $-39 \leq l \leq 38$
Reflections collected / unique	102329 / 23430 [R(int) = 0.0710]
Data Completeness	0.982
Absorption correction	Semi-empirical from equivalents
Refinement method	Full-matrix least-squares on F^2
Data / restraints / parameters	23430 / 0 / 1365
Goodness-of-fit on F^2	1.061
Final R indices [I>2σ(I)]	R_1 = 0.0727, wR_2 = 0.1813
R indices (all data)	R_1 = 0.1017, wR_2 = 0.2020
Largest diff. peak and hole	0.646 and -0.471 $eÅ^{-3}$

Ti_2(**2**)$(OiPr)_6$

Empirical formula	$C_{23}H_{41}NO_4Ti$
Formula weight	443.47
Temperature	150(2) K
Wavelength	0.71073 Å
Crystal system, space group	Monoclinic, $P2_1/c$
Unit cell dimensions	a = 9.5960(5) Å α = 90 ° b = 23.1890(14) Å β = 91.398(3) ° c = 11.4210(8) Å γ = 90 °
Volume	2540.7(3) $Å^3$
Z, Calculated density	4, 1.159 Mg/m^3
Absorption coefficient	0.362 mm^{-1}
F(000)	960
Crystal size	0.20 x 0.15 x 0.10 mm
Theta range for data collection	3.68 to 27.48 °
Limiting indices	$-12 \leq h \leq 12$, $-28 \leq k \leq 30$, $-14 \leq l \leq 14$
Reflections collected / unique	27064 / 5764 [R(int) = 0.0931]
Completeness to theta = 27.48	98.9 %
Absorption correction	Semi-empirical from equivalents
Max. and min. transmission	0.9647 and 0.9311
Refinement method	Full-matrix least-squares on F^2
Data / restraints / parameters	5764 / 0 / 303
Goodness-of-fit on F^2	1.049
Final R indices [I>2σ(I)]	R_1 = 0.0572, wR_2 = 0.1373
R indices (all data)	R_1 = 0.0852, wR_2 = 0.1525
Largest diff. peak and hole	0.575 and -0.539 e. $Å^{-3}$

Ti_2(**3**)$(OiPr)_6$

Empirical formula	$C_{52}H_{94}N_2O_8Ti_2$
Formula weight	971.09
Temperature	150(2) K
Wavelength	0.71073 Å
Crystal system, space group	Monoclinic, $P2_1/n$
Unit cell dimensions	a = 10.8260(6) Å α = 90 ° b = 18.8930(9) Å β = 104.050(2) ° c = 14.5330(10) Å γ = 90 °
Volume	2883.6(3) $Å^3$
Z, Calculated density	2, 1.118 Mg/m^3
Absorption coefficient	0.324 mm^{-1}
F(000)	1056
Crystal size	0.10 x 0.05 x 0.05 mm
Theta range for data collection	3.54 to 24.00 °
Limiting indices	$-12 \leq h \leq 12$, $-21 \leq k \leq 21$, $-16 \leq l \leq 16$
Reflections collected / unique	42193 / 4506 [R(int) = 0.1040]
Completeness to theta = 24.00	99.7 %
Absorption correction	None
Refinement method	Full-matrix least-squares on F^2
Data / restraints / parameters	4506 / 0 / 301
Goodness-of-fit on F^2	1.064
Final R indices [I>2σ(I)]	R_1 = 0.0434, wR_2 = 0.0873
R indices (all data)	R_1 = 0.0682, wR_2 = 0.0985
Largest diff. peak and hole	0.233 and -0.354 $eÅ^{-3}$

Ti_2(**4**)$(OiPr)_6$

Empirical formula	$C_{52}H_{96}N_2O_8Ti_2$
Formula weight	973.11
Temperature	150(2) K
Wavelength	0.71073 Å
Crystal system, space group	Triclinic, *P*-1
Unit cell dimensions	a = 9.4410(3) Å α = 79.5090(10) ° b = 10.0110(3) Å β = 84.6760(10) ° c = 15.1580(5) Å γ = 87.7970(10) °
Volume	1402.28(8) $Å^3$
Z, Calculated density	1, 1.152 Mg/m^3
Absorption coefficient	0.334 mm^{-1}
F(000)	530
Crystal size	0.20 x 0.20 x 0.15 mm
Theta range for data collection	3.72 to 27.53 °
Limiting indices	$-12 \leq h \leq 12$, $-12 \leq k \leq 12$, $-18 \leq l \leq 19$
Reflections collected / unique	19702 / 6423 [R(int) = 0.0458]
Completeness to theta = 27.53	99.2 %
Absorption correction	Semi-empirical from equivalents
Max. and min. transmission	0.9517 and 0.9363
Refinement method	Full-matrix least-squares on F^2
Data / restraints / parameters	6423 / 0 / 350
Goodness-of-fit on F^2	1.025
Final R indices [I>2σ(I)]	R_1 = 0.0541, wR_2 = 0.1354
R indices (all data)	R_1 = 0.0735, wR_2 = 0.1509
Largest diff. peak and hole	0.951 and -0.932 $eÅ^{-3}$

Ti_2(**5**)$(OiPr)_6$

Empirical formula	$C_{31}H_{58}NO_4Ti$
Formula weight	556.68
Temperature	150(2) K
Wavelength	0.71073 Å
Crystal system, space group	Triclinic, *P*-1
Unit cell dimensions	a = 11.0450(10) Å α = 115.990(5) ° b = 13.2550(11) Å β = 109.683(5) ° c = 13.9140(14) Å γ = 91.805(5) °
Volume	1685.0(3) $Å^3$
Z, Calculated density	2, 1.097 Mg/m^3
Absorption coefficient	0.285 mm^{-1}
F(000)	610
Crystal size	0.10 x 0.10 x 0.10 mm
Theta range for data collection	4.09 to 27.52 °
Limiting indices	-14≤h≤14, -16≤k≤17, -18≤l≤18
Reflections collected / unique	33515 / 7641 [R(int) = 0.0614]
Completeness to theta = 27.52	98.8 %
Absorption correction	None
Max. and min. transmission	0.9720 and 0.9720
Refinement method	Full-matrix least-squares on F^2
Data / restraints / parameters	7641 / 0 / 347
Goodness-of-fit on F^2	1.017
Final R indices [I>2σ(I)]	R_1 = 0.0590, wR_2 = 0.1504
R indices (all data)	R_1 = 0.0903, wR_2 = 0.1713
Largest diff. peak and hole	0.761 and -0.626 $eÅ^{-3}$

Ti_2(**8**)($OiPr$)$_6$

Empirical formula	$C_{56}H_{103}N_2O_8Ti_2$
Formula weight	1028.20
Temperature	150(2) K
Wavelength	0.71073 Å
Crystal system, space group	Triclinic, *P*-1
Unit cell dimensions	a = 14.2220(3) Å α = 69.6250(10) ° b = 15.3740(4) Å β = 89.943(2) ° c = 17.4080(4) Å γ = 62.8660(10) °
Volume	3118.09(13) Å^3
Z, Calculated density	2, 1.095 Mg/m^3
Absorption coefficient	0.303 mm^{-1}
F(000)	1122
Crystal size	0.20 x 0.10 x 0.10 mm
Theta range for data collection	3.75 to 27.50 °
Limiting indices	-18≤h≤18, -19≤k≤19, -22≤l≤22
Reflections collected / unique	53817 / 14138 [R(int) = 0.0624]
Completeness to theta = 27.50	98.7 %
Absorption correction	None
Refinement method	Full-matrix least-squares on F^2
Data / restraints / parameters	14138 / 0 / 717
Goodness-of-fit on F^2	1.007
Final R indices [I>2σ(I)]	R_1 = 0.0576, wR_2 = 0.1516
R indices (all data)	R_1 = 0.0942, wR_2 = 0.1780
Largest diff. peak and hole	0.706 and -0.519 eÅ^{-3}

Ti_2(**12**)$(OiPr)_6$

Empirical formula	$C_{53}H_{96}N_2O_8Ti_2$
Formula weight	985.12
Temperature	150(2) K
Wavelength	0.71073 Å
Crystal system, space group	monoclinic, $P2_1/n$
Unit cell dimensions	a = 9.24600(10) Å α = 90 ° b = 24.3060(3) Å β = 91.5990(10) ° c = 26.2840(3) Å γ = 90 °
Volume	5904.59(12) $Å^3$
Z, Calculated density	4, 1.108 Mg/m^3
Absorption coefficient	0.318 mm^{-1}
F(000)	2144
Crystal size	0.20 x 0.15 x 0.10 mm
Theta range for data collection	3.53 to 24.99 °
Limiting indices	-10≤h≤10, -28≤k≤28, -31≤l≤31
Reflections collected / unique	67951 / 10306 [R(int) = 0.0726]
Completeness to theta = 24.99	99.4 %
Absorption correction	None
Max. and min. transmission	0.9689 and 0.9392
Refinement method	Full-matrix least-squares on F^2
Data / restraints / parameters	10306 / 93 / 589
Goodness-of-fit on F^2	1.150
Final R indices [I>2σ(I)]	R_1 = 0.0822, wR_2 = 0.2120
R indices (all data)	R_1 = 0.1025, wR_2 = 0.2276
Largest diff. peak and hole	0.867 and -0.505 $eÅ^{-3}$

Ti_2(**13**)$(OiPr)_6$

Empirical formula	$C_{23.50}H_{41.50}NO_4Ti$
Formula weight	449.98
Temperature	150(2) K
Wavelength	0.71073 Å
Crystal system, space group	Triclinic, *P*-1
Unit cell dimensions	a = 9.4140(4) Å α = 92.550(2) ° b = 9.9250(4) Å β = 94.4870(10) ° c = 13.9710(12) Å γ = 92.879(3) °
Volume	1298.18(13) $Å^3$
Z, Calculated density	2, 1.151 Mg/m^3
Absorption coefficient	0.355 mm^{-1}
F(000)	487
Crystal size	0.20 x 0.10 x 0.10 mm
Theta range for data collection	4.35 to 27.51 °
Limiting indices	$-12 \le h \le 12$, $-12 \le k \le 12$, $-18 \le l \le 18$
Reflections collected / unique	18880 / 5909 [R(int) = 0.0247]
Completeness to theta = 27.51	99.1 %
Absorption correction	None
Max. and min. transmission	0.9653 and 0.9323
Refinement method	Full-matrix least-squares on F^2
Data / restraints / parameters	5909 / 3 / 299
Goodness-of-fit on F^2	1.056
Final R indices [I>2σ(I)]	R_1 = 0.0643, wR_2 = 0.1731
R indices (all data)	R_1 = 0.0720, wR_2 = 0.1823
Largest diff. peak and hole	0.912 and -0.754 $eÅ^{-3}$

Ti(**7**)$(OiPr)_2$

Empirical formula	$C_{35}H_{56}N_2O_4Ti$
Formula weight	616.72
Temperature	150(2) K
Wavelength	0.71073 Å
Crystal system, space group	Triclinic, *P*-1
Unit cell dimensions	a = 11.234(1) Å α =83.037(7) ° b = 12.431(2) Å β = 71.297(6) ° c = 13.347(1) Å γ = 89.540(5) °
Volume	1751.5(4) $Å^3$
Z, Calculated density	2, 1.169 Mg/m^3
Absorption coefficient	0.282 mm^{-1}
F(000)	668
Crystal size	0.20 x 0.15 x 0.10 mm
Theta range for data collection	3.75 to 27.52 °
Limiting indices	$-14 \leq h \leq 14$, $-16 \leq k \leq 16$, $-17 \leq l \leq 17$
Reflections collected / unique	36743 / 7965 [R(int) = 0.0877]
Completeness to theta = 27.52	98.8 %
Absorption correction	None
Refinement method	Full-matrix least-squares on F^2
Data / restraints / parameters	7965 / 0 / 391
Goodness-of-fit on F^2	1.034
Final R indices [I>2σ(I)]	R_1 = 0.0564, wR_2 = 0.1265
R indices (all data)	R_1 = 0.1066, wR_2 = 0.1497
Largest diff. peak and hole	0.299 and -0.473 $eÅ^{-3}$

Ti(**9**)$(OiPr)_2$

Empirical formula	$C_{35}H_{56}N_2O_4Ti$
Formula weight	616.72
Temperature	150(2) K
Wavelength	0.71073 Å
Crystal system, space group	Monoclinic, $P2_1/a$
Unit cell dimensions	a = 19.3720(7) Å α = 90 ° b = 9.6520(4) Å β = 116.015(2) ° c = 20.3950(10) Å γ = 90 °
Volume	3427.0(3) $Å^3$
Z, Calculated density	4, 1.195 Mg/m^3
Absorption coefficient	0.288 mm^{-1}
F(000)	1336
Crystal size	0.10 x 0.10 x 0.10 mm
Theta range for data collection	3.61 to 24.17 °
Limiting indices	-22≤h≤22, -10≤k≤11, -23≤l≤23
Reflections collected / unique	21094 / 5422 [R(int) = 0.1729]
Completeness to theta = 27.52	99.0 %
Absorption correction	Sortav
Refinement method	Full-matrix least-squares on F^2
Data / restraints / parameters	5422 / 0 / 391
Goodness-of-fit on F^2	1.079
Final R indices [I>2σ(I)]	R_1 = 0.0837, wR_2 = 0.1960
R indices (all data)	R_1 = 0.1272, wR_2 = 0.2254
Largest diff. peak and hole	1.219 and -0.422 $eÅ^{-3}$

Ti(**10**)$(OiPr)_2$

Empirical formula	$C_{45}H_{69}N_2O_4Ti$
Formula weight	749.92
Temperature	150(2) K
Wavelength	0.71073 Å
Crystal system, space group	Orthorhombic, $P2_12_12_1$
Unit cell dimensions	a = 10.9250(7) Å α = 90 ° b = 14.7200(12) Å β = 90 ° c = 27.1040(14) Å γ = 90 °
Volume	4358.8(5) $Å^3$
Z, Calculated density	4, 1.143 Mg/m^3
Absorption coefficient	0.238 mm^{-1}
F(000)	1628
Crystal size	0.10 x 0.10 x 0.10 mm
Theta range for data collection	3.66 to 24.10 °
Limiting indices	$-12 \leq h \leq 12$, $-16 \leq k \leq 16$, $-31 \leq l \leq 31$
Reflections collected / unique	52730 / 6899 [R(int) = 0.1339]
Completeness to theta = 24.10	99.4 %
Absorption correction	None
Max. and min. transmission	0.9766 and 0.9766
Refinement method	Full-matrix least-squares on F^2
Data / restraints / parameters	6899 / 4 / 514
Goodness-of-fit on F^2	1.039
Final R indices [I>2σ(I)]	R_1 = 0.0607, wR_2 = 0.1452
R indices (all data)	R_1 = 0.0918, wR_2 = 0.1651
Absolute structure parameter	-0.03(4)
Largest diff. peak and hole	0.344 and -0.350 $eÅ^{-3}$

Ti(**11**)$(OiPr)_2$

Empirical formula	$C_{40}H_{60}N_2O_4Ti$
Formula weight	680.80
Temperature	150(2) K
Wavelength	0.71073 Å
Crystal system, space group	Monoclinic, $P2_1/n$
Unit cell dimensions	a = 14.0530(2) Å α = 90 ° b = 13.5820(2) Å β = 91.528(1) ° c = 20.1480(4) Å γ = 90 °
Volume	3844.24(11) $Å^3$
Z, Calculated density	4, 1.176 Mg/m^3
Absorption coefficient	0.263 mm^{-1}
F(000)	1472
Crystal size	0.1 x 0.1 x 0.1 mm
Theta range for data collection	3.58 to 25.00 °
Limiting indices	$-16 \leq h \leq 16$, $-16 \leq k \leq 16$, $-23 \leq l \leq 23$
Reflections collected / unique	66001 / 6743 [R(int) = 0.1218]
Completeness to theta = 25.00	99.6 %
Absorption correction	Multi-scan
Refinement method	Full-matrix least-squares on F^2
Data / restraints / parameters	6743 / 15 / 563
Goodness-of-fit on F^2	1.027
Final R indices [I>2σ(I)]	R_1 = 0.0503, wR_2 = 0.1156
R indices (all data)	R_1 = 0.0830, wR2 = 0.1348
Largest diff. peak and hole	0.298 and -0.371 $eÅ^{-3}$

Ti(**1**)(catechol)

Empirical formula	$C_{58}H_{68}C_{14}N_4O_8Ti_2$
Formula weight	1186.76
Temperature	150(2) K
Wavelength	0.71073 Å
Crystal system, space group	Monoclinic, $P2_1/a$
Unit cell dimensions	a = 12.2350(4) Å α = 90 ° b = 17.2330(8) Å β = 96.642(2) ° c = 13.4000(5) Å γ = 90 °
Volume	2806.37(19) $Å^3$
Z, Calculated density	2, 1.404 Mg/m^3
Absorption coefficient	0.533 mm^{-1}
F(000)	1240
Crystal size	0.10 x 0.10 x 0.10 mm
Theta range for data collection	3.52 to 26.76 °
Limiting indices	$-15 \leq h \leq 15$, $-21 \leq k \leq 21$, $-16 \leq l \leq 16$
Reflections collected / unique	48977 / 5929 [R(int) = 0.1302]
Completeness to theta = 26.76	99.1 %
Absorption correction	None
Max. and min. transmission	0.9486 and 0.9486
Refinement method	Full-matrix least-squares on F^2
Data / restraints / parameters	5929 / 0 / 347
Goodness-of-fit on F^2	1.069
Final R indices [I>2σ(I)]	R_1 = 0.0684, wR_2 = 0.1672
R indices (all data)	R_1 = 0.1199, wR_2 = 0.2017
Largest diff. peak and hole	0.556 and -1.231 $eÅ^{-3}$

Ti(**1**)(3,5-di-*tert*-butylcatechol)

Empirical formula	$C_{37}H_{50}C_{12}N_2O_4Ti$
Formula weight	705.59
Temperature	150(2) K
Wavelength	0.71073 Å
Crystal system, space group	Monoclinic, $P2_1/c$
Unit cell dimensions	a = 19.8000(2) Å α = 90 ° b = 12.5740(2) Å β = 103.8080(10) ° c = 30.7360(5) Å γ = 90 °
Volume	7431.05(18) $Å^3$
Z, Calculated density	8, 1.261 Mg/m^3
Absorption coefficient	0.414 mm^{-1}
F(000)	2992
Crystal size	0.50 x 0.30 x 0.10 mm
Theta range for data collection	3.53 to 27.52 °
Limiting indices	-25≤h≤25, -16≤k≤16, -39≤l≤39
Reflections collected / unique	98628 / 16983 [R(int) = 0.1423]
Completeness to theta = 27.52	99.2 %
Absorption correction	None
Refinement method	Full-matrix least-squares on F^2
Data / restraints / parameters	16983 / 6 / 874
Goodness-of-fit on F^2	1.050
Final R indices [I>2σ(I)]	R_1 = 0.0867, wR_2 = 0.2228
R indices (all data)	R_1 = 0.1194, wR_2 = 0.2455
Largest diff. peak and hole	1.155 and -1.307 $eÅ^{-3}$

Ti(**1**)(4-NO_2-catechol)

Empirical formula	$C_{28.50}H_{32}ClN_3O_6Ti$
Formula weight	595.92
Temperature	150(2) K
Wavelength	0.71073 Å
Crystal system, space group	Monoclinic, $P2_1/n$
Unit cell dimensions	a = 12.7780(2) Å α = 90 ° b = 13.3090(2) Å β = 101.097(1)° c = 16.4640(3) Å γ = 90 °
Volume	2747.56(8) $Å^3$
Z, Calculated density	4, 1.441 Mg/m^3
Absorption coefficient	0.457 mm^{-1}
F(000)	1244
Crystal size	0.20 x 0.10 x 0.10 mm
Theta range for data collection	3.58 to 27.49 °
Limiting indices	$-16 \leq h \leq 16$, $-17 \leq k \leq 17$, $-21 \leq l \leq 21$
Reflections collected / unique	40787 / 6270 [R(int) = 0.0700]
Completeness to theta = 27.49	99.2 %
Absorption correction	None
Max. and min. transmission	0.9557 and 0.9141
Refinement method	Full-matrix least-squares on F^2
Data / restraints / parameters	6270 / 0 / 366
Goodness-of-fit on F^2	1.012
Final R indices [I>2σ(I)]	R_1 = 0.0638, wR_2 = 0.1590
R indices (all data)	R_1 = 0.0785, wR_2 = 0.1733
Largest diff. peak and hole	1.766 and -1.588 $eÅ^{-3}$

Ti(**6**)(4-NO_2-catechol)

Empirical formula	$C_{43}H_{49}N_3O_6Ti$
Formula weight	751.75
Temperature	150(2) K
Wavelength	0.71073 Å
Crystal system, space group	Monoclinic, $P2_1/c$
Unit cell dimensions	a = 20.0540(5) Å α = 90 ° b = 18.6670(5) Å β = 113.361(2)° c = 22.6240(6) Å γ = 90 °
Volume	7775.0(4) $Å^3$
Z, Calculated density	8, 1.284 Mg/m^3
Absorption coefficient	0.272 mm^{-1}
F(000)	3184
Crystal size	0.10 x 0.10 x 0.10 mm
Theta range for data collection	3.51 to 27.49 °
Limiting indices	-26≤h≤25, -24≤k≤24, -29≤l≤29
Reflections collected / unique	153642 / 17723 [R(int) = 0.0657]
Completeness to theta = 27.49	99.3 %
Absorption correction	None
Max. and min. transmission	0.9734 and 0.9734
Refinement method	Full-matrix least-squares on F^2
Data / restraints / parameters	17723 / 0 / 1021
Goodness-of-fit on F^2	1.054
Final R indices [I>2σ(I)]	R_1 = 0.0507, wR_2 = 0.1190
R indices (all data)	R_1 = 0.0829, wR_2 = 0.1357
Largest diff. peak and hole	0.351 and -0.450 $eÅ^{-3}$

8.1.2 Chapter 3

$Zr(\mathbf{6})(OiPr)_2$

Empirical formula	$C_{29}H_{44}N_2O_4Zr$
Formula weight	575.88
Temperature	150(2) K
Wavelength	0.71073 Å
Crystal system, space group	Monoclinic, $P2_1/n$
Unit cell dimensions	a = 8.5750(6) Å α = 90 ° b = 16.5030(14) Å β = 99.220(5) ° c = 20.7000(15) Å γ = 90 °
Volume	2891.5(4) $Å^3$
Z, Calculated density	4, 1.323 Mg/m^3
Absorption coefficient	0.415 mm^{-1}
F(000)	1216
Crystal size	0.10 x 0.10 x 0.05 mm
Theta range for data collection	3.53 to 27.49 °
Limiting indices	$-11 \leq h \leq 10$, $-21 \leq k \leq 21$, $-26 \leq l \leq 26$
Reflections collected / unique	45579 / 6603 [R(int) = 0.0584]
Completeness to theta = 27.49	99.5 %
Absorption correction	Semi-empirical from equivalents
Max. and min. transmission	0.9795 and 0.9597
Refinement method	Full-matrix least-squares on F^2
Data / restraints / parameters	6603 / 0 / 333
Goodness-of-fit on F^2	1.107
Final R indices [I>2σ(I)]	R_1 = 0.0349, wR_2 = 0.0789
R indices (all data)	R_1 = 0.0524, wR_2 = 0.0897
Largest diff. peak and hole	0.417 and -0.700 $eÅ^{-3}$

Zr(**6**)$(OiPr)_2$.0.5THF.0.5IPA

Empirical formula	$C_{32.50}H_{52}N_2O_5Zr$
Formula weight	641.98
Temperature	150(2) K
Wavelength	0.71073 Å
Crystal system, space group	Monoclinic, $P2_1/n$
Unit cell dimensions	a = 14.3840(2) Å α = 90 ° b = 10.8140(2) Å β = 95.0460(10) ° c = 20.7480(3) Å γ = 90 °
Volume	3214.81(9) $Å^3$
Z, Calculated density	4, 1.326 Mg/m^3
Absorption coefficient	0.383 mm^{-1}
F(000)	1364
Crystal size	0.25 x 0.20 x 0.10 mm
Theta range for data collection	3.88 to 27.46 °
Limiting indices	-18≤h≤18, -14≤k≤14, -26≤l≤26
Reflections collected / unique	59866 / 7319 [R(int) = 0.0617]
Completeness to theta = 27.46	99.6 %
Absorption correction	Semi-empirical from equivalents
Max. and min. transmission	0.9627 and 0.9103
Refinement method	Full-matrix least-squares on F^2
Data / restraints / parameters	7319 / 0 / 445
Goodness-of-fit on F^2	1.085
Final R indices [I>2σ(I)]	R_1 = 0.0392, wR_2 = 0.0989
R indices (all data)	R_1 = 0.0573, wR_2 = 0.1108
Largest diff. peak and hole	0.473 and -0.942 $eÅ^{-3}$

$Zr(\mathbf{7})(OiPr)_2$

Empirical formula	$C_{35}H_{56}N_2O_4Zr$
Formula weight	660.04
Temperature	150(2) K
Wavelength	0.71073 Å
Crystal system, space group	*Cm*, monoclinic
Unit cell dimensions	a = 11.7950(5) Å α = 90 ° b = 24.3760(10)Å β = 124.476(2) ° c = 7.6360(4) Å γ = 90 °
Volume	1809.86(14) $Å^3$
Z, Calculated density	2, 1.211 Mg/m^3
Absorption coefficient	0.340 mm^{-1}
F(000)	704
Crystal size	0.10 x 0.10 x 0.10 mm
Theta range for data collection	4.19 to 25.04 °
Limiting indices	$-13 \leq h \leq 14$, $-28 \leq k \leq 28$, $-9 \leq l \leq 9$
Reflections collected / unique	7278 / 3018 [R(int) = 0.0452]
Completeness to theta = 25.04	99.3 %
Absorption correction	None
Max. and min. transmission	0.9668 and 0.9668
Refinement method	Full-matrix least-squares on F^2
Data / restraints / parameters	3018 / 2 / 206
Goodness-of-fit on F^2	1.029
Final R indices [I>2σ(I)]	R_1 = 0.0360, wR_2 = 0.0799
R indices (all data)	R_1 = 0.0394, wR2 = 0.0816
Absolute structure parameter	-0.01(4)
Largest diff. peak and hole	0.462 and -0.579 $eÅ^{-3}$

Zr(10)(OiPr)$_2$

Empirical formula	$C_{45}H_{76}N_2O_4Zr$
Formula weight	800.30
Temperature	150(2) K
Wavelength	0.71073 Å
Crystal system, space group	Orthorhombic, $P2_12_12_1$
Unit cell dimensions	a = 12.0070(4) Å α = 90 ° b = 14.6590(5) Å β = 90 ° c = 25.1760(10) Å γ = 90 °
Volume	4431.2(3) Å^3
Z, Calculated density	4, 1.200 Mg/m^3
Absorption coefficient	0.289 mm^{-1}
F(000)	1728
Crystal size	0.10 x 0.10 x 0.10 mm
Theta range for data collection	3.52 to 24.09 °
Limiting indices	-13≤h≤13, -16≤k≤16, -28≤l≤28
Reflections collected / unique	34743 / 6996 [R(int) = 0.1963]
Completeness to theta = 24.09	99.3 %
Absorption correction	Semi-empirical from equivalents
Max. and min. transmission	0.9717 and 0.9717
Refinement method	Full-matrix least-squares on F^2
Data / restraints / parameters	6996 / 0 / 485
Goodness-of-fit on F^2	1.054
Final R indices [I>2σ(I)]	R_1 = 0.0825, wR_2 = 0.1712
R indices (all data)	R_1 = 0.1264, wR_2 = 0.1972
Absolute structure parameter	-0.10(9)
Largest diff. peak and hole	1.783 and -0.723 eÅ^{-3}

Hf(**6**)$(OiPr)_2$

Empirical formula	$C_{29}H_{44}HfN_2O_4$
Formula weight	663.15
Temperature	150(2) K
Wavelength	0.71073 Å
Crystal system, space group	Monoclinic, $P2_1/n$
Unit cell dimensions	a = 8.5680(3) Å α = 90 ° b = 16.4690(7) Å β = 99.410(3) ° c = 20.6830(7) Å γ = 90 °
Volume	2879.23(19) $Å^3$
Z, Calculated density	4, 1.530 Mg/m^3
Absorption coefficient	3.658 mm^{-1}
F(000)	1344
Crystal size	0.20 x 0.10 x 0.10 mm
Theta range for data collection	3.52 to 27.50 °
Limiting indices	$-11 \leq h \leq 11$, $-21 \leq k \leq 21$, $-26 \leq l \leq 26$
Reflections collected / unique	50883 / 6592 [R(int) = 0.0760]
Completeness to theta = 27.50	99.6 %
Absorption correction	Semi-empirical from equivalents
Max. and min. transmission	0.7112 and 0.5282
Refinement method	Full-matrix least-squares on F^2
Data / restraints / parameters	6592 / 0 / 333
Goodness-of-fit on F^2	1.185
Final R indices [I>2σ(I)]	R_1 = 0.0414, wR_2 = 0.0888
R indices (all data)	R_1 = 0.0614, wR_2 = 0.0977
Largest diff. peak and hole	1.963 and -1.601 $eÅ^{-3}$

$Hf(7)(OiPr)_2$

Empirical formula	$C_{17.50}H_{26}Hf_{0.50}NO_2$
Formula weight	371.64
Temperature	150(2) K
Wavelength	0.71073 Å
Crystal system, space group	Monoclinic, *Cm*
Unit cell dimensions	a = 11.7460(2) Å α = 90 ° b = 24.2790(5) Å β = 124.5040(10) ° c = 7.6000(2) Å γ = 90 °
Volume	1786.10(7) $Å^3$
Z, Calculated density	4, 1.382 Mg/m^3
Absorption coefficient	2.957 mm^{-1}
F(000)	760
Crystal size	0.20 x 0.15 x 0.10 mm
Theta range for data collection	3.58 to 27.49 °
Limiting indices	$-15 \le h \le 15$, $-31 \le k \le 31$, $-9 \le l \le 9$
Reflections collected / unique	17045 / 4042 [R(int) = 0.0338]
Completeness to theta = 27.49	99.6 %
Absorption correction	Semi-empirical from equivalents
Max. and min. transmission	0.7564 and 0.5893
Refinement method	Full-matrix least-squares on F^2
Data / restraints / parameters	4042 / 2 / 204
Goodness-of-fit on F^2	1.065
Final R indices [I>2σ(I)]	R_1 = 0.0201, wR_2 = 0.0491
R indices (all data)	R_1 = 0.0201, wR_2 = 0.0491
Absolute structure parameter	0.000(8)
Largest diff. peak and hole	0.789 and -1.438 $eÅ^{-3}$

Hf(**8**)$(OiPr)_2$

Empirical formula	$C_{23.50}H_{41}Hf_{0.50}NO_2$
Formula weight	458.82
Temperature	150(2) K
Wavelength	0.71073 Å
Crystal system, space group	Triclinic, *P*-1
Unit cell dimensions	a = 8.7915(3) Å α = 66.874(3) ° b = 16.8368(6) Å β = 79.532(3) ° c = 17.6504(6) Å γ = 84.196(3) °
Volume	2361.41(14) $Å^3$
Z, Calculated density	4, 1.291 Mg/m^3
Absorption coefficient	2.250 mm^{-1}
F(000)	964
Crystal size	0.50 x 0.20 x 0.03 mm
Theta range for data collection	2.88 to 27.48 °
Limiting indices	$-11 \leq h \leq 11$, $-21 \leq k \leq 21$, $-22 \leq l \leq 22$
Reflections collected / unique	23772 / 10822 [R(int) = 0.0696]
Completeness to theta = 27.48	99.8 %
Absorption correction	None
Max. and min. transmission	0.9356 and 0.3992
Refinement method	Full-matrix least-squares on F^2
Data / restraints / parameters	10822 / 0 / 505
Goodness-of-fit on F^2	0.980
Final R indices [I>2σ(I)]	R_1 = 0.0492, wR_2 = 0.0745
R indices (all data)	R_1 = 0.0792, wR2 = 0.0830
Largest diff. peak and hole	1.101 and -1.352 $eÅ^{-3}$

Hf(**10**)$(OiPr)_2$

Empirical formula	$C_{45}H_{76}HfN_2O_4$
Formula weight	887.57
Temperature	150(2) K
Wavelength	0.71073 Å
Crystal system, space group	Orthorhombic, $P2_12_12_1$
Unit cell dimensions	a = 12.00200(10) Å α = 90 ° b = 14.66100(10) Å β = 90 ° c = 25.1240(2) Å γ = 90 °
Volume	4420.85(6) $Å^3$
Z, Calculated density	4, 1.334 Mg/m^3
Absorption coefficient	2.401 mm^{-1}
F(000)	1856
Crystal size	0.10 x 0.10 x 0.10 mm
Theta range for data collection	3.53 to 27.49 °
Limiting indices	$-15 \leq h \leq 15$, $-19 \leq k \leq 19$, $-32 \leq l \leq 32$
Reflections collected / unique	71328 / 10103 [R(int) = 0.0771]
Completeness to theta = 27.49	99.6 %
Absorption correction	None
Max. and min. transmission	0.7953 and 0.7953
Refinement method	Full-matrix least-squares on F^2
Data / restraints / parameters	10103 / 0 / 493
Goodness-of-fit on F^2	1.080
Final R indices [I>2σ(I)]	R_1 = 0.0332, wR_2 = 0.0643
R indices (all data)	R_1 = 0.0504, wR_2 = 0.0693
Absolute structure parameter	-0.034(8)
Largest diff. peak and hole	1.319 and -1.303 $eÅ^{-3}$

Zr_4(**1**)$(OiPr)_6(HOiPr)_2$

Empirical formula	$C_{76}H_{156}N_2O_{18}Zr_4$
Formula weight	1750.91
Temperature	150(2) K
Wavelength	0.71073 Å
Crystal system, space group	Monoclinic, *C*2/*c*
Unit cell dimensions	a = 21.8419(4) Å α = 90 ° b = 15.0338(3) Å β = 104.8290(10) ° c = 29.6284(5) Å γ = 90 °
Volume	9404.9(3) $Å^3$
Z, Calculated density	4, 1.237 Mg/m^3
Absorption coefficient	0.488 mm^{-1}
F(000)	3720
Crystal size	0.1 x 0.1 x 0.15 mm
Theta range for data collection	3.68 to 25.03 °
Limiting indices	-25≤h≤25, -17≤k≤17, -34≤l≤35
Reflections collected / unique	42398 / 7991 [R(int) = 0.0794]
Completeness to theta = 25.03	96.1 %
Absorption correction	None
Refinement method	Full-matrix least-squares on F^2
Data / restraints / parameters	7991 / 8 / 489
Goodness-of-fit on F^2	1.046
Final R indices [I>2σ(I)]	R_1 = 0.0541, wR_2 = 0.1022
R indices (all data)	R_1 = 0.0916, wR_2 = 0.1170
Largest diff. peak and hole	0.508 and -0.653 $eÅ^{-3}$

Zr_2(**15**)$(OiPr)_6$

Empirical formula	$C_{47}H_{84}N_2O_8Zr_2$
Formula weight	987.60
Temperature	150(2) K
Wavelength	0.71073 Å
Crystal system, space group	orthorhombic, *C*2*cb*
Unit cell dimensions	a = 14.3530(6) Å α = 90 ° b = 39.3260(15) Å β = 90 ° c = 19.3250(7) Å γ = 90 °
Volume	10907.9(7) $Å^3$
Z, Calculated density	8, 1.203 Mg/m^3
Absorption coefficient	0.428 mm^{-1}
F(000)	4192
Crystal size	0.20 x 0.10 x 0.10 mm
Theta range for data collection	3.76 to 25.02 °
Limiting indices	$-17 \leq h \leq 17$, $-46 \leq k \leq 46$, $-22 \leq l \leq 22$
Reflections collected / unique	64279 / 9549 [R(int) = 0.0949]
Completeness to theta = 25.02	99.4 %
Absorption correction	None
Max. and min. transmission	0.9585 and 0.9193
Refinement method	Full-matrix least-squares on F^2
Data / restraints / parameters	9549 / 2 / 563
Goodness-of-fit on F^2	1.098
Final R indices [I>2σ(I)]	R_1 = 0.0536, wR_2 = 0.1273
R indices (all data)	R_1 = 0.0889, wR_2 = 0.1513
Absolute structure parameter	0.00(5)
Largest diff. peak and hole	0.665 and -0.561 $eÅ^{-3}$

Hf_2(**1**)$(OiPr)_6$

Empirical formula	$C_{80}H_{140}Hf_4N_4O_{16}$
Formula weight	2127.92
Temperature	150(2) K
Wavelength	0.71073 Å
Crystal system, space group	Triclinic, *P*-1
Unit cell dimensions	a = 12.8800(6) Å α = 108.912(2) ° b = 17.1940(9) Å β = 93.491(3) ° c = 21.3410(10) Å γ = 93.019(3) °
Volume	4449.6(4) $Å^3$
Z, Calculated density	2, 1.588 Mg/m^3
Absorption coefficient	4.711 mm^{-1}
F(000)	2128
Crystal size	0.10 x 0.05 x 0.05 mm
Theta range for data collection	4.74 to 24.00 °
Limiting indices	-14≤h≤13, -19≤k≤19, -23≤l≤24
Reflections collected / unique	34810 / 13794 [R(int) = 0.1529]
Completeness to theta = 24.00	98.7 %
Absorption correction	Semi-empirical from equivalents
Max. and min. transmission	0.7986 and 0.6502
Refinement method	Full-matrix least-squares on F^2
Data / restraints / parameters	13794 / 0 / 908
Goodness-of-fit on F^2	1.023
Final R indices [I>2σ(I)]	R_1 = 0.0655, wR_2 = 0.1120
R indices (all data)	R_1 = 0.1482, wR_2 = 0.1420
Largest diff. peak and hole	1.145 and -1.315 $eÅ^{-3}$

Hf_2(**3**)$(OiPr)_6$

Empirical formula	$C_{26}H_{47}HfNO_4$
Formula weight	616.14
Temperature	150(2) K
Wavelength	0.71073 Å
Crystal system, space group	Monoclinic, *Pn*
Unit cell dimensions	a = 10.3720(5) Å α = 90 ° b = 17.1010(9) Å β = 105.698(3) ° c = 16.7140(7) Å γ = 90 °
Volume	2854.0(2) $Å^3$
Z, Calculated density	4, 1.434 Mg/m^3
Absorption coefficient	3.683 mm^{-1}
F(000)	1256
Crystal size	0.10 x 0.10 x 0.10 mm
Theta range for data collection	3.79 to 25.37 °
Limiting indices	-12≤h≤12, -20≤k≤20, -20≤l≤18
Reflections collected / unique	28088 / 10193 [R(int) = 0.0707]
Completeness to theta = 25.37	99.1 %
Absorption correction	Semi-empirical from equivalents
Max. and min. transmission	0.7096 and 0.7096
Refinement method	Full-matrix least-squares on F^2
Data / restraints / parameters	10193 / 8 / 602
Goodness-of-fit on F^2	1.047
Final R indices [I>2σ(I)]	R_1 = 0.0414, wR_2 = 0.0812
R indices (all data)	R_1 = 0.0752, wR2 = 0.0957
Absolute structure parameter	-0.034(14)
Largest diff. peak and hole	1.258 and -0.748 $eÅ^{-3}$

8.1.3 Chapter 4

Al(**7**)Me

Empirical formula	$C_{33.50}H_{49}AlN_2O_2$
Formula weight	538.73
Temperature	150(2) K
Wavelength	0.71073 Å
Crystal system, space group	Orthorhombic, $P2_12_12_1$
Unit cell dimensions	a = 14.7810(2) Å α = 90 ° b = 15.1010(2) Å β = 90 ° c = 29.1190(4) Å γ = 90 °
Volume	6499.59(15) $Å^3$
Z, Calculated density	8, 1.101 Mg/m^3
Absorption coefficient	0.092 mm^{-1}
F(000)	2344
Crystal size	0.30 x 0.20 x 0.20 mm
Theta range for data collection	3.69 to 27.44 °
Limiting indices	-19≤h≤19, -19≤k≤19, -37≤l≤37
Reflections collected / unique	81419 / 14759 [R(int) = 0.0780]
Completeness to theta = 27.44	99.3 %
Absorption correction	Multi-scan
Max. and min. transmission	0.9818 and 0.9729
Refinement method	Full-matrix least-squares on F^2
Data / restraints / parameters	14759 / 0 / 733
Goodness-of-fit on F^2	1.091
Final R indices [I>2σ(I)]	R_1 = 0.0619, wR_2 = 0.1606
R indices (all data)	R_1 = 0.0676, wR2 = 0.1651
Absolute structure parameter	0.06(14)
Largest diff. peak and hole	0.450 and -0.264 $eÅ^{-3}$

Al(**8**)Me

Empirical formula	$C_{36}H_{57}AlN_2O_2$
Formula weight	576.82
Temperature	150(2) K
Wavelength	0.71073 Å
Crystal system, space group	Monoclinic, *C*2/*c*
Unit cell dimensions	a = 35.6710(9) Å α = 90 ° b = 10.4360(3) Å β = 116.4370(10) ° c = 24.9340(8) Å γ = 90 °
Volume	8311.3(4) $Å^3$
Z, Calculated density	8, 0.922 Mg/m^3
Absorption coefficient	0.075 mm^{-1}
F(000)	2528
Crystal size	0.30 x 0.30 x 0.25 mm
Theta range for data collection	3.64 to 27.49 °
Limiting indices	-45≤h≤46, -13≤k≤13, -32≤l≤32
Reflections collected / unique	70559 / 9479 [R(int) = 0.0411]
Completeness to theta = 27.49	99.3 %
Absorption correction	None
Max. and min. transmission	0.9814 and 0.9777
Refinement method	Full-matrix least-squares on F^2
Data / restraints / parameters	9479 / 9 / 514
Goodness-of-fit on F^2	1.112
Final R indices [I>2σ(I)]	R_1 = 0.1139, wR_2 = 0.3087
R indices (all data)	R_1 = 0.1264, wR2 = 0.3178
Largest diff. peak and hole	0.630 and -0.523 $eÅ^{-3}$

Al(**11**)Me

Empirical formula	$C_{34.30}H_{47.70}AlN_2O_2$
Formula weight	547.02
Temperature	150(2) K
Wavelength	0.71073 Å
Crystal system, space group	Monoclinic, *C*2/*c*
Unit cell dimensions	a = 32.935(3) Å α = 90 ° b = 7.0560(10) Å β = 114.289(5) ° c = 31.375(4) Å γ = 90 °
Volume	6645.8(14) $Å^3$
Z, Calculated density	8, 1.093 Mg/m^3
Absorption coefficient	0.091 mm^{-1}
F(000)	2372
Crystal size	0.10 x 0.10 x 0.10 mm
Theta range for data collection	3.53 to 24.98 °
Limiting indices	$-38 \leq h \leq 38$, $-8 \leq k \leq 8$, $-35 \leq l \leq 37$
Reflections collected / unique	24788 / 5755 [R(int) = 0.1342]
Completeness to theta = 24.98	98.5 %
Absorption correction	None
Max. and min. transmission	0.9909 and 0.9909
Refinement method	Full-matrix least-squares on F^2
Data / restraints / parameters	5755 / 10 / 394
Goodness-of-fit on F^2	1.078
Final R indices [I>2σ(I)]	R_1 = 0.1279, wR_2 = 0.3141
R indices (all data)	R_1 = 0.1946, wR2 = 0.3564
Largest diff. peak and hole	0.722 and -0.458 $eÅ^{-3}$

8.1.4 Chapter 5

Ti_2(**16**)$(OiPr)_6$

Empirical formula	$C_{60}H_{108}N_2O_8Ti_2$
Formula weight	1081.28
Temperature	150(2) K
Wavelength	0.71073 Å
Crystal system, space group	Monoclinic, $P2_1/n$
Unit cell dimensions	a = 17.1370(12) Å α = 90 ° b = 11.4570(16) Å β = 95.355(5) ° c = 17.2330(15) Å γ = 90 °
Volume	3368.7(6) $Å^3$
Z, Calculated density	2, 1.066 Mg/m^3
Absorption coefficient	0.284 mm^{-1}
F(000)	1180
Crystal size	0.10 x 0.10 x 0.10 mm
Theta range for data collection	3.52 to 25.03 °
Limiting indices	-20≤h≤19, -12≤k≤13, -20≤l≤20
Reflections collected / unique	26382 / 5924 [R(int) = 0.1132]
Completeness to theta = 25.03	99.3 %
Absorption correction	None
Max. and min. transmission	0.9722 and 0.9722
Refinement method	Full-matrix least-squares on F^2
Data / restraints / parameters	5924 / 0 / 401
Goodness-of-fit on F^2	1.022
Final R indices [I>2σ(I)]	R_1 = 0.0576, wR_2 = 0.1211
R indices (all data)	R_1 = 0.1157, wR_2 = 0.1481
Largest diff. peak and hole	0.530 and -0.357 $eÅ^{-3}$

Ti_2(**17**)$(OiPr)_6$

Empirical formula	$C_{24}H_{41}NO_4Ti$
Formula weight	455.48
Temperature	150(2) K
Wavelength	0.71073 Å
Crystal system, space group	Monoclinic, *P*21/*c*
Unit cell dimensions	a = 10.4230(2) Å α = 90 ° b = 22.8100(5) Å β = 114.617(1) ° c = 12.5010(2) Å γ = 90 °
Volume	2701.97(9) $Å^3$
Z, Calculated density	4, 1.120 Mg/m^3
Absorption coefficient	0.342 mm^{-1}
F(000)	984
Crystal size	0.40 x 0.20 x 0.20 mm
Theta range for data collection	3.59 to 27.54 °
Limiting indices	$-13 \leq h \leq 13$, $-29 \leq k \leq 29$, $-16 \leq l \leq 16$
Reflections collected / unique	39062 / 6195 [R(int) = 0.1081]
Completeness to theta = 27.54	99.4 %
Absorption correction	Semi-empirical from equivalents
Max. and min. transmission	0.9347 and 0.8753
Refinement method	Full-matrix least-squares on F^2
Data / restraints / parameters	6195 / 6 / 323
Goodness-of-fit on F^2	1.110
Final R indices [I>2σ(I)]	R_1 = 0.0691, wR_2 = 0.1764
R indices (all data)	R_1 = 0.0892, wR_2 = 0.1912
Largest diff. peak and hole	0.901 and -0.656 $eÅ^{-3}$

Ti_2(**18**)$(OiPr)_6$

Empirical formula	$C_{40}H_{49}Cl_2NO_4Ti$
Formula weight	726.60
Temperature	150(2) K
Wavelength	0.71073 Å
Crystal system, space group	Triclinic, *P*-1
Unit cell dimensions	a = 8.8350(2) Å α = 95.5030(10) ° b = 10.7560(3) Å β = 90.5850(10) ° c = 20.4880(7) Å γ = 97.9200(10) °
Volume	1918.96(10) $Å^3$
Z, Calculated density	2, 1.258 Mg/m^3
Absorption coefficient	0.402 mm^{-1}
F(000)	768
Crystal size	0.20 x 0.20 x 0.10 mm
Theta range for data collection	3.52 to 25.07 °
Limiting indices	-10≤h≤10, -12≤k≤12, -24≤l≤23
Reflections collected / unique	25157 / 6767 [R(int) = 0.0538]
Completeness to theta = 25.07	99.1 %
Absorption correction	None
Refinement method	Full-matrix least-squares on F^2
Data / restraints / parameters	6767 / 0 / 440
Goodness-of-fit on F^2	1.046
Final R indices [I>2σ(I)]	R_1 = 0.0493, wR_2 = 0.1165
R indices (all data)	R_1 = 0.0685, wR_2 = 0.1291
Largest diff. peak and hole	0.579 and -0.593 $eÅ^{-3}$

Al_2(**16**)Me_4

Empirical formula	$C_{48}H_{80}Al_2N_2O_4$
Formula weight	803.10
Temperature	150(2) K
Wavelength	0.71073 Å
Crystal system, space group	triclinic, *P*-1
Unit cell dimensions	a = 9.5690(10) Å α = 109.497(5) ° b = 11.6000(7) Å β = 96.776(4) ° c = 11.8190(13) Å γ = 93.635(5) °
Volume	1220.6(2) $Å^3$
Z, Calculated density	1, 1.093 Mg/m^3
Absorption coefficient	0.101 mm^{-1}
F(000)	440
Crystal size	0.20 x 0.10 x 0.05 mm
Theta range for data collection	3.56 to 24.16 °
Limiting indices	-11≤h≤11, -13≤k≤11, -13≤l≤13
Reflections collected / unique	7936 / 3792 [R(int) = 0.0831]
Completeness to theta = 24.16	96.9 %
Absorption correction	None
Refinement method	Full-matrix least-squares on F^2
Data / restraints / parameters	3792 / 6 / 261
Goodness-of-fit on F^2	1.013
Final R indices [I>2σ(I)]	R_1 = 0.0782, wR_2 = 0.1813
R indices (all data)	R_1 = 0.1313, wR_2 = 0.2188
Largest diff. peak and hole	0.490 and -0.615 $eÅ^{-3}$

Al_2(**17**)Me_4

Empirical formula	$C_{34}H_{52}Al_2N_2O_2$
Formula weight	574.74
Temperature	150(2) K
Wavelength	0.71073 Å
Crystal system, space group	Triclinic, *P*-1
Unit cell dimensions	a = 6.4870(6) Å α = 98.515(5) ° b = 7.6680(7) Å β = 90.729(5) ° c = 17.3850(14) Å γ = 94.709(5) °
Volume	852.08(13) $Å^3$
Z, Calculated density	1, 1.120 Mg/m^3
Absorption coefficient	0.116 mm^{-1}
F(000)	312
Crystal size	0.20 x 0.20 x 0.20 mm
Theta range for data collection	3.85 to 27.50 °
Limiting indices	-8≤h≤8, -9≤k≤9, -22≤l≤22
Reflections collected / unique	13796 / 3854 [R(int) = 0.0423]
Completeness to theta = 27.50	98.4 %
Absorption correction	None
Max. and min. transmission	0.9772 and 0.9772
Refinement method	Full-matrix least-squares on F^2
Data / restraints / parameters	3854 / 0 / 187
Goodness-of-fit on F^2	1.040
Final R indices [I>2σ(I)]	R_1 = 0.0429, wR_2 = 0.1084
R indices (all data)	R_1 = 0.0571, wR_2 = 0.1198
Largest diff. peak and hole	0.238 and -0.294 $eÅ^{-3}$

Zn_2(**17**)Me_2

Empirical formula	$C_{46}H_{68}N_2O_4Zn_2$
Formula weight	843.76
Temperature	150(2) K
Wavelength	0.71073 Å
Crystal system, space group	Monoclinic, *P*21/*n*
Unit cell dimensions	a = 14.2740(2) Å α = 90 ° b = 7.98300(10) Å β = 101.4560(10) ° c = 20.1200(4) Å γ = 90 °
Volume	2246.98(6) Å ^3
Z, Calculated density	2, 1.247 Mg/m^3
Absorption coefficient	1.109 mm^{-1}
F(000)	900
Crystal size	0.20 x 0.10 x 0.10 mm
Theta range for data collection	4.02 to 27.45 °
Limiting indices	-18≤h≤18, -10≤k≤10, -26≤l≤26
Reflections collected / unique	37316 / 5113 [R(int) = 0.0670]
Completeness to theta = 27.45	99.2 %
Absorption correction	Semi-empirical from equivalents
Max. and min. transmission	0.8972 and 0.8086
Refinement method	Full-matrix least-squares on F^2
Data / restraints / parameters	5113 / 0 / 275
Goodness-of-fit on F^2	1.028
Final R indices [I>2σ(I)]	R_1 = 0.0363, wR_2 = 0.0869
R indices (all data)	R_1 = 0.0538, wR_2 = 0.0950
Largest diff. peak and hole	0.283 and -0.389 $eÅ^{-3}$

8.1.5 Chapter 6

Al(**22**)Me

Empirical formula	$C_{38}H_{59}AlN_2O_2$
Formula weight	602.85
Temperature	150(2) K
Wavelength	0.71073 Å
Crystal system, space group	Monoclinic, $P2_1/n$
Unit cell dimensions	a = 11.8730(6) Å α = 90 ° b = 10.6560(7) Å β = 94.668(5) ° c = 28.8840(18) Å γ = 90 °
Volume	3642.2(4) $Å^3$
Z, Calculated density	4, 1.099 Mg/m^3
Absorption coefficient	0.089 mm^{-1}
F(000)	1320
Crystal size	0.10 x 0.10 x 0.02 mm
Theta range for data collection	3.72 to 23.80 °
Limiting indices	-13≤h≤13, -12≤k≤12, -29≤l≤32
Reflections collected / unique	18682 / 5538 [R(int) = 0.1690]
Completeness to theta = 23.80	99.2 %
Absorption correction	Multi-scan
Max. and min. transmission	0.9982 and 0.9912
Refinement method	Full-matrix least-squares on F^2
Data / restraints / parameters	5538 / 0 / 402
Goodness-of-fit on F^2	1.065
Final R indices [I>2σ(I)]	R_1 = 0.1076, wR_2 = 0.2127
R indices (all data)	R_1 = 0.2002, wR_2 = 0.2528
Largest diff. peak and hole	0.275 and -0.246 $eÅ^{-3}$

Al(*R*,*R*-**22**)Me

Identification code	h12mdj15
Empirical formula	$C_{44}H_{73}AlN_2O_2$
Formula weight	689.02
Temperature	150(2) K
Wavelength	0.71073 Å
Crystal system, space group	Monoclinic, $P2_1$
Unit cell dimensions	a = 14.159(2) Å α = 90 ° b = 10.235(4) Å β = 92.574(7) ° c = 14.801(2) Å γ = 90 °
Volume	2142.8(10) $Å^3$
Z, Calculated density	2, 1.068 Mg/m^3
Absorption coefficient	0.083 mm^{-1}
F(000)	760
Crystal size	0.30 x 0.10 x 0.10 mm
Theta range for data collection	4.08 to 27.49 °
Limiting indices	-18≤h≤18, -13≤k≤13, -19≤l≤18
Reflections collected / unique	38513 / 9665 [R(int) = 0.0612]
Completeness to theta = 27.49	99.4 %
Absorption correction	None
Refinement method	Full-matrix least-squares on F^2
Data / restraints / parameters	9665 / 1 / 458
Goodness-of-fit on F^2	1.033
Final R indices [I>2σ(I)]	R_1 = 0.0457, wR_2 = 0.0993
R indices (all data)	R_1 = 0.0691, wR_2 = 0.1097
Absolute structure parameter	-0.01(13)
Largest diff. peak and hole	0.308 and -0.317 $eÅ^{-3}$

Al(**25**)OBn

Identification code	k12mdj12
Empirical formula	$C_{39.50}H_{51}AlN_2O_3$
Formula weight	628.80
Temperature	150(2) K
Wavelength	0.71073 Å
Crystal system, space group	Monoclinic, *C*2/*c*
Unit cell dimensions	a = 25.7960(3) Å α = 90 ° b = 12.55700(10) Å β = 100.521(1) ° c = 21.7940(2) Å γ = 90 °
Volume	6940.84(12) $Å^3$
Z, Calculated density	8, 1.203 Mg/m^3
Absorption coefficient	0.098 mm^{-1}
F(000)	2712
Crystal size	0.20 x 0.20 x 0.15 mm
Theta range for data collection	3.62 to 27.45 °
Limiting indices	-33≤h≤30, -16≤k≤16, -28≤l≤28
Reflections collected / unique	55806 / 7910 [R(int) = 0.0619]
Completeness to theta = 27.45	99.5 %
Absorption correction	None
Max. and min. transmission	0.9854 and 0.9806
Refinement method	Full-matrix least-squares on F^2
Data / restraints / parameters	7910 / 0 / 420
Goodness-of-fit on F^2	1.033
Final R indices [I>2σ(I)]	R_1 = 0.0422, wR_2 = 0.0903
R indices (all data)	R_1 = 0.0634, wR_2 = 0.1006
Largest diff. peak and hole	0.330 and -0.293 $eÅ^{-3}$